

For Reference

NOT TO BE TAKEN FROM THIS ROOM

Ex LIBRIS
UNIVERSITATIS
ALBERTAENSIS



THE UNIVERSITY OF ALBERTA
GEOLOGY AND GEOCHEMISTRY OF STRATABOUND ORE DEPOSITS IN
SOUTH-CENTRAL YUKON TERRITORY AND SOUTHWESTERN DISTRICT OF
MACKENZIE, NORTHWEST TERRITORIES

by



SAY LEE KUO

A THESIS

SUBMITTED TO THE FACULTY OF GRADUATE STUDIES AND RESEARCH
IN PARTIAL FULFILMENT OF THE REQUIREMENTS FOR THE DEGREE
OF DOCTOR OF PHILOSOPHY

DEPARTMENT OF GEOLOGY

EDMONTON, ALBERTA

FALL, 1976

ABSTRACT

Detailed studies have been carried out on the geology and geochemistry of six Cambrian and Ordovician stratabound ore deposits in the Anvil Range, Frances Lake and Howard's Pass districts in the southern Yukon and southwestern District of Mackenzie, N.W.T.

From a reinterpretation of the regional geological setting and chemical evidence on some conformable volcanic sequences in the western part of the region, the writer concludes that there existed a passive (e.g. Atlantic type) continental margin geosyncline in which initial continental separation occurred over an extended period of time from Late Proterozoic to Lower Paleozoic in the western part of the geosyncline. Interruption or termination of the initial continental separation took place in the Lower Paleozoic while the Atlantic type geosyncline continued to develop with a prograding sedimentary wedge building oceanward (westward). Major subsidence of buried marginal escarpments or basins beyond the continental slope occurred during this period.

Chemical compositions, fluid inclusions and isotope compositions of sulfur, oxygen and lead of ore and gangue minerals, and country rock sulfides and bulk ores provide a firm basis for understanding ore-forming or metamorphic conditions of the deposits.

Massive pyritic ore deposits in the Anvil Range district (Faro, Grum, Vangorda and Swim Lakes) were formed in the western part of the geosyncline as a consequence of mixing of recharging heated connate brine (recycled seawater) with overlying seawater. The following physico-chemical features characterize the Anvil ore fluids: temperature - $170 \sim 250^{\circ}\text{C}$; pH - $4 \sim 6$; δS^{34} of total dissolved sulfur - 25‰; f_{O_2} - 10^{-34} to $10^{-41.5}$; seawater depth $\geq 400 \sim 1230$ meters; confining pressure $\geq 45 \sim 140$ bars;

Digitized by the Internet Archive
in 2023 with funding from
University of Alberta Library

<https://archive.org/details/Kuo1976>

total aqueous sulfur content (H_2S , $\text{SO}_4^{=}$, HS^-) - $0.01 \sim 0.001$ mole/kg water; NaCl equiv. wt. % - $2.3 \sim 9.2$ (averaging 6.5); immiscible CO_2 - 5 wt. %; density - $0.8 \sim 0.9$ gm/cc; Fe - 19.4 ppm; Zn - 3 ppm; Pb - 0.6 ppm; Ba - 0.13 ppm; Cu - 0.12 ppm; Mn - 0.07 ppm; Ag - 0.002 ppm. During regional and/or thermal metamorphism of the Anvil ore deposits up to about 300°C , the estimated fugacities of gaseous phases and metamorphic pressure as follows: $f_{\text{S}_2} - 10^{-10}$ to $10^{-11.7}$; $f_{\text{O}_2} - 10^{-30}$ to $10^{-34.5}$; $f_{\text{CO}_2} - 10^{1.5}$; $f_{\text{CO}} - 10^{-2.2}$; pressure - 1.9 to 4.4 Kb (averaging 2.5 Kb). Lead isotopes of Anvil ore minerals display an anomalous and apparent multistage lead pattern which probably was caused by "heterogeneous" circulation and/or interaction of heated seawater through a large volume of rocks. The age of the first stage (integrated source age) is 1400 m.y. and the age of the second stage (mineralization age) is between $410 \sim 500$ m.y.. Th/U ratio in the integrated source system is estimated to be 3.05, indicating an overall crustal environment.

Stratabound As-Zn-Ag deposits at Thompson Creek, Frances Lake district (occurring in the "central" deeper basin or escarpment) was probably formed by diagenetic-epigenetic stratabound replacement of deep basin sediments as a consequence of boiling of ascending ore fluids which originated from waters equilibrated with sediments during burial and/or sub-seafloor geothermal metamorphism. Physico-chemical conditions and properties of the ore fluids are as follows: temperature - $194\text{--}345^\circ\text{C}$; salinity - $5 \sim 20$ wt. % NaCl (averaging 12 wt. %); CO_2 - 4.4 wt. %; density - $0.81 \sim 0.94$ gm/cc; $f_{\text{O}_2} - 10^{-37.3}$ to $10^{-40.3}$; $f_{\text{S}_2} - 10^{-8.5}$ to $10^{-10.8}$; pH - 5.5 to 7.5; $\delta\text{O}^{18} - 4.6\text{‰}$; δS^{34} of total aqueous sulfide species - 14.6‰ ; confining pressure - $100 \sim 170$ bars; water depth - $874 \sim 1485$ meters; total dissolved aqueous sulfide species (H_2S and HS^-) - 35 ppm; Fe - 0.07 ppm; Zn - 0.07 ppm;

Pb - 0.02 ppm; Ag - 0.005 ppm; Mn - 0.003 ppm; Sb - 0.002 ppm; Cu - 0.001 ppm. Studies of Fe-S, Fe-Zn-S and Fe-C-O-S systems indicate the following conditions prevailed during regional and/or thermal metamorphism up to about 350°C: $f_{S_2} - 10^{-7}$ to $10^{-7.7}$; $f_{O_2} - 10^{-22}$ to 10^{-27} ; $f_{CO_2} - 10^2$; and metamorphic pressure - 2.5 to 6.2 Kb (averaging about 4 Kb). Lead isotope data of ore and sedimentary pyrite are linearly related and a two-stage calculation for the secondary isochron indicates an integrated source age of 1380 m.y. and a mineralization age of 400 ~ 500 m.y.. The ore lead was probably a mixing product of underlying Helikian basement rocks and the Cambro-Ordovician sediments (reworked basement ?).

The deposits in the Howard's Pass district were formed in a near-shelf region and are typically well-laminated to disseminated, very fine-grained sulfides in silty-calcareous siltstones occurring over a wide area. Metal-bearing fluids were most probably derived from updip migration of intraformational brines from adjacent basins but might also through thermal spring activity. Physico-chemical properties and conditions of the ore fluids are: temperature - 60 ~ 180°C; salinity - 4.2 ~ 13.8 wt. % NaCl; density - 0.93 ~ 1.0 gm/cc; pH - 7 ~ 8; dissolved sulfate in pore waters < 0.005 to 0.01 mole/kg water; confining pressure - 50 bars; water depth - 464 meters. The depositional environment was probably a restricted shallow marine basin with relatively quiet deposition in an anaerobic, iron oxide-carbonate-inert sediment-bearing system; ore formation in siltstone took place through mainly non-biological, chemical reduction of dissolved sulfate in pore waters or seawater without significant isotope fractionation due to "closed-system" effect or complete sulfate reduction. Ore and sedimentary pyrite lead isotope data display a short-period anomalous pattern, and two stage calculation gives an integrated source age of 1960 - 2015 m.y.

and a mineralization age of 350 - 450 m.y.. Th/U ratios in source rocks were variable and mixing of several heterogeneous source materials was suspected. The ore leads were probably derived from sources where sediment accumulation approximates single-cycled, closed-basin conditions in Precambrian terrains.

Characteristic features of ore deposits forming in distinctive sedimentary-tectonic settings across a passive continental margin geosyncline (of former divergent plate margin) may be significant and have general application in similar geological settings in both ancient and modern environments.

ACKNOWLEDGEMENTS

The writer wishes to express his sincere gratitude to Dr. Robert Folinsbee for the continuous and persisting enthusiasm and support he gave during the entire course of the thesis project. Dr. Folinsbee also visited the writer in the field in 1971 and 1974, provided advice to research approaches, and reviewed the first draft of the thesis; all this help is gratefully acknowledged.

The writer is grateful to Drs. Roger Morton, Halfdan Baadsgaard, Dorian Smith, George Cumming, John Gray of the Departments of Geology and Physics for their interest and assistance in the course of laboratory research. Drs. Morton, Baadsgaard and Cumming provided interesting discussions on various aspects of the thesis topics.

The writer is also grateful to the following persons in the Government and mineral industry for their cooperation and help: Drs. Dirk Tempelman-Kluit and Steward Blusson of the Geological Survey of Canada in Vancouver, B.C.; Dr. David Jennings of Cyprus Anvil Mining Corp.; Drs. Aaron Aho and Stanley Reamsbottom of Canadian Natural Resources Ltd.; Mr. Bruce Nicols of Kerr Addison Mines Ltd.; Mr. Leon LaPrairie of Matt Berry Mines Ltd.; Dr. Henry Thalenhorst of Metallgesellschaft Canada Ltd.; Messr. Anthony Rich and John Greig of Vestor Explorations Ltd.; and Mr. A.D. Drummond of Canex Placer Ltd.

The writer has been benefitted from oral or written communications with Drs. Hiroshi Ohmoto, Yoshimichi Kajiwara, Akira Sasaki, Donald Sangster and Steven Scott. Cooperation and discussion with fellow graduate students, among others, Messr. Steven Burnie and Karl Schimann, during laboratory research have been both interesting and beneficial.

Able assistance in laboratory work was provided by the following persons: Messr. David Tomlinson and Steven Launspach of the Electron Microprobe Laboratory, Messr. Hugh McCullough and Dragan Krstic of the Mass Spectrometry Laboratory, and Dr. Roger Morton of the Fluid Inclusions Laboratory, all at the Departments of Geology and Physics, University of Alberta.

The writer received financial assistance in the form of Teaching Assistantship and N.R.C. Grant from the Department of Geology and Dr. Robert Folinsbee during 1973-74, 1974-75 and part of 1975-76 sessions.

The thesis has been critically reviewed by Drs. Robert Folinsbee, Roger Morton, Halfdan Baadsgaard, Ernest Kanasewich, Bruce Doe and Robert Rye.

TABLE OF CONTENTS

	PAGE
ABSTRACT	iv
ACKNOWLEDGEMENTS	viii
CHAPTER	
I. INTRODUCTION	1
A. OBJECTIVES OF STUDY	1
B. OUTLINE OF WORK COMPLETED	3
C. PREVIOUS WORK	5
1. Regional Work	5
2. Local Work	6
II. REGIONAL GEOLOGY	9
A. GENERAL SETTING OF LATE PROTEROZOIC ROCKS . .	9
B. REGIONAL CORRELATION OF PALEOZOIC SEQUENCE . .	14
1. General Facies Distribution	14
2. Regional Stratigraphic Correlation	14
3. Igneous Activity, Metamorphism and Tectonism	32
C. REINTERPRETATION OF REGIONAL GEOLOGY	32
1. Late Proterozoic to Cambrian	32
2. Cambrian to Middle Devonian	36
3. Upper Devonian to Mississippian	37
4. Mississippian to Triassic	40
III. ORE DEPOSITS AND THEIR IMMEDIATE SETTINGS	45
A. INTRODUCTION	45
B. ANVIL RANGE DISTRICT	45
1. Location and Access	45
2. Physiography	47
3. Fieldwork and Exploration History	47
4. General Geology	49

TABLE OF CONTENTS (cont'd)

CHAPTER	PAGE
5. Structural Geology	53
6. Ore Deposits	53
(a) Faro Deposit	54
Immediate Mine Geology	54
Ore and Gangue Minerals	62
Ore Texture	65
(b) Grum Deposit	67
Immediate Mine Geology	68
Ore and Gangue Minerals	71
Ore Texture	72
(c) Vangorda Deposit	73
Immediate Mine Geology	74
Ore and Gangue Minerals	76
Ore Texture	77
(d) Swim Lakes Deposit	78
Immediate Mine Geology	78
Ore and Gangue Minerals	80
Ore Texture	82
C. FRANCES LAKE DISTRICT	107
1. Location and Access	107
2. Physiography	107
3. Fieldwork and Exploration History	109
4. General Geology	110
5. Structural Geology and Regional Metamorphism	110

TABLE OF CONTENTS (cont'd)

CHAPTER	PAGE
(a) Internal Structures	110
(b) Faults	115
(c) Regional Metamorphism	115
6. Ore Deposits	116
(a) Immediate Mine Geology	116
(b) Ore and Gangue Minerals	124
Ore Minerals	124
Gangue Minerals	125
(c) Ore Texture	126
D. HOWARD'S PASS DISTRICT	133
1. Location and Access	133
2. Physiography	133
3. Fieldwork and Exploration History	135
4. General Geology	136
5. Structural Geology	140
(a) Folding	140
(b) Faulting	144
6. Ore Deposits	145
(a) Immediate Mine Geology	145
(b) Ore and Gangue Minerals	150
(c) Ore Texture	152
IV. CHEMICAL PETROLOGY	158
A. INTRODUCTION	158
B. ANVIL RANGE DISTRICT	159

TABLE OF CONTENTS (cont'd)

CHAPTER	PAGE
1. Lower Paleozoic Volcanic Rocks	159
(a) Chemical Correlations	164
(b) Normative Compositions	171
(c) Petrogenetic Discussion	178
C. FRANCES LAKE DISTRICT	185
1. Lower Paleozoic Volcanic Rocks	185
V. CHEMICAL COMPOSITIONS OF ORES AND GANGUES	196
A. INTRODUCTION	196
B. ANVIL RANGE DISTRICT	196
1. Pyrrhotite	196
2. Sphalerite	201
(a) Pressure and Fugacity Estimate	208
(b) Equilibrium Temperature	211
3. Barite	213
4. Carbonate Minerals	218
(a) Carbonate-oxide System	227
(b) Sulfide-carbonate System	230
5. Bulk Ores	234
C. FRANCES LAKE DISTRICT	244
1. Pyrrhotite	244
2. Sphalerite	248
3. Carbonate Minerals	252
4. Sb-Pb Sulfosalt Minerals	259
5. Bulk Ores	266

TABLE OF CONTENTS (cont'd)

CHAPTER	PAGE
D. HOWARD'S PASS DISTRICT	270
1. Ore-bearing Sediments	270
2. Sphalerite	280
VI. FLUID INCLUSION STUDIES	295
A. INTRODUCTION	295
B. EXPERIMENTS	297
C. ANVIL RANGE DISTRICT	298
1. Types of Inclusions	298
2. Results	300
(a) Freezing Reactions and Products	300
(b) Salinity	301
(c) Filling Temperatures	302
(d) CO ₂ Contents	306
(e) Fluid Densities	309
3. Discussion	311
(a) Density-Salinity-Temperature Variation	311
(b) Pressure and Water Depth During Ore Deposition	314
(c) Nature of Immiscible CO ₂ -rich Fluids .	319
D. FRANCES LAKE DISTRICT	321
1. Types of Inclusions	322
2. Results	323
(a) Reactions and Products Formed During Freezing or Crushing	323
(b) Salinity	323

TABLE OF CONTENTS (cont'd)

CHAPTER	PAGE
(c) Filling Temperatures	325
(d) CO ₂ Contents	325
(e) Fluid Densities	325
3. Discussion	328
E. HOWARD'S PASS DISTRICT	334
1. Types of Inclusions	334
2. Results	335
(a) Salinity and Filling Temperatures . . .	335
(b) Fluid Densities	337
3. Discussion	337
F. SUMMARY	339
VII. ISOTOPE GEOCHEMISTRY OF ORE DEPOSITS	350
A. INTRODUCTION	350
B. STUDY OF STABLE ISOTOPES	351
1. General Statement	351
(a) Sulfur Isotopes	351
(b) Oxygen Isotopes	352
2. Experiments and Calibrations	353
(a) Mineral Separation and Purification . .	353
(b) Conversion to Ag ₂ S	354
(c) Collection of SO ₂ Gasses	355
(d) Calibration of Standards	356
(e) Mass Spectrometer Measurement	356
(f) Collection of CO ₂ Gasses	358

TABLE OF CONTENTS (cont'd)

CHAPTER	PAGE
3. Anvil Range District	360
(a) Results	360
(b) Sulfur Isotope Fractionation	365
(c) Chemical Environment of Ore Deposition	371
4. Frances Lake District	384
(a) Results	384
(b) Sulfur Isotope Fractionation and Chemical Environment	388
(c) Oxygen Isotope Composition of Ore Solution	397
5. Howard's Pass District	402
(a) Results	402
(b) Sulfur Diagenesis in Sediments	405
(c) Interpretation of Sulfur Isotope Data	408
6. Summary	412
C. STUDY OF LEAD ISOTOPES	414
1. General Statement	414
2. Experiments and Calibrations	416
(a) Lead Extraction	416
(b) Lead Mounting on Filaments	417
(c) Mass Spectrometer Measurement	417
(d) Experimental Errors and Calibration of Standards	418
3. Results and Discussion	420
(a) Anvil Range District	420
(b) Frances Lake District	430

TABLE OF CONTENTS (cont'd)

CHAPTER		PAGE
	(c) Howard's Pass District	434
	(d) Discussion	438
VIII.	CHEMICAL COMPOSITION OF ORE SOLUTIONS	446
	A. INTRODUCTION	446
	B. ANVIL ORE DEPOSITS	446
	C. THOMPSON CREEK ORE DEPOSIT	452
IX.	CONCLUSIONS	456

	BIBLIOGRAPHY	460
	APPENDICES	
II-1	GENERAL FACIES DISTRIBUTION OF PALEOZOIC STRATA IN THE SELWYN FOLD BELT AND RELATED AREAS	489
II-2	IGNEOUS ACTIVITY, METAMORPHISM AND TECTONISM IN THE SELWYN FOLD BELT AND RELATED AREAS	500
III-1	GENERAL GEOLOGY, ANVIL RANGE DISTRICT	511
III-2	IDENTIFICATION AND DATING OF FOSSILS	527
III-3	STRUCTURAL GEOLOGY, ANVIL RANGE DISTRICT	529
III-4	GENERAL GEOLOGY, FRANCES LAKE DISTRICT	533
III-5	GENERAL GEOLOGY, HOWARD'S PASS DISTRICT	542
IV-1	ECLOGITES AND THEIR MINERALS, ANVIL RANGE DISTRICT.	549
V-1	EXPERIMENTAL CONDITION AND RELATED DETAILS OF ELECTRON MICROPROBE ANALYSES OF SULFIDES, CARBONATES AND SULFOSALTS	581
V-2	APL COMPUTER PROGRAM MOL FOR ESTIMATING MOLE PERCENTS OF SOLID SOLUTIONS IN SULFIDES, CARBONATES AND SULFOSALTS	583
VII-1	PREFERENTIAL CHEMICAL DISSOLUTION AND PURIFICATION PROCEDURES FOR SULFIDE AND SULFATE MINERALS	587

TABLE OF CONTENTS (cont'd)

APPENDICES		PAGE
VII-2	APL COMPUTER PROGRAM XS1 FOR ESTIMATING MOLE FRACTIONS OF AQUEOUS SULFUR SPECIES	589
VII-2	APL COMPUTER PROGRAM DSI FOR ESTIMATING ISOTOPE COMPOSITION OF AQUEOUS SULFUR SPECIES	593
VII-3	LABORATORY PROCEDURES FOR LEAD ISOTOPE WORKS	595

LIST OF FIGURES

Figure		Page
I-1	Three ore districts under study, south-central Yukon Territory and southwestern District of Mackenzie, Northwest Territories	2
II-1	Main tectonic elements of northern Canadian Cordillera	10
II-2	Distribution of Proterozoic rocks in northern Canadian Cordillera (A) Purcell, (B) Windermere	15
II-3	Map areas of southeastern Yukon and southwestern District of Mackenzie	16
II-4	Distribution of Lower Cambrian rocks in the northern Canadian Cordillera	490
II-5	Facies distribution of Middle Cambrian rocks in the northern Canadian Cordillera	493
II-6	Facies distribution of Upper Cambrian rocks in the northern Canadian Cordillera	494
II-7	Facies distribution of Lower and Middle Ordovician rocks in the northern Canadian Cordillera	495
II-8	Facies distribution of Upper Ordovician and Silurian rocks in the northern Canadian Cordillera	498
II-9	Distribution of Upper Ordovician to early Middle Devonian rocks in the northern Canadian Cordillera	499
II-10	Facies distribution of Proterozoic to Devonian rocks in Selwyn Basin and related areas	18
II-11a	Stratigraphic correlation of Paleozoic strata (southern traverse)	27
II-11b	Stratigraphic correlation of Paleozoic strata (northern traverse)	28
II-12	Diagrammatic restored sections of Proterozoic-Paleozoic rocks in the northern Canadian Cordillera	31
II-13	Main structural elements of the northern Canadian Cordillera	504

LIST OF FIGURES (cont'd)

Figure		Page
II-14	Structural section across Selwyn, Mackenzie, and Franklin Mountains	505
II-15	Tectonic map of northern Canadian Cordillera	508
II-16	Upper Devonian to early Mississippian sedimentation and tectonism in the northern Canadian Cordillera	39
II-17	Mississippian to Middle Triassic sedimentation and tectonism in the Canadian Cordillera	42
III-1	Location map of the Anvil Range district, Yukon Territory, with locations of major ore deposits	46
III-2	Geological map of the Anvil Range district, Yukon	51
III-3	Isopach map of the Faro deposit	55
III-4a	Longitudinal section of the Faro deposit	56
III-4b	Cross sections of the Faro deposit	57
III-5	Geological map of the Faro No. 1 open pit	60
III-6	Drill hole plan of the Grum deposit (Kerr claims); the known boundary of the orebody is also shown	69
III-7	Cross section of the Grum deposit	70
III-8	Isopach map and cross sections of the Vangorda deposit	75
III-9	Cross sections and map of the Swim Lakes deposit	79
III-10	Location map of the Frances Lake district	108
III-11	Geological map of the Frances Lake district, Yukon	112
III-12	Geological map of the Thompson Creek deposit, Frances Lake district, Yukon	119
III-12a	Locations of drill holes from which samples are analyzed and studied in this thesis	120

LIST OF FIGURES (cont'd)

Figure		Page
III-13	Cross sections of the Thompson Creek deposit, Frances Lake district	121
III-14	Location map of the Howard's Pass district and the Summit Lake region	134
III-15	Geological map of the Summit Lake region, Yukon Territory - N.W.T.	138
III-16	Geological map of an area in the southeastern part of the Howard's Pass district	142
III-17	Geological map of an area in the northwestern part of the Howard's Pass district	143
III-18	Geological map of the Canex Placer's main zone (XY claims), Howard's Pass district	147
III-19	Cross sections of the Canex Placer's main ore zone, Howard's Pass district	148
IV-1	Locations of Lower Paleozoic volcanic rock specimens, Anvil Range district, Yukon	163
IV-2	Discrimination diagrams of ΣFeO , TiO_2 , Ni and V vs. $\Sigma\text{FeO}/\text{MgO}$	166
IV-3	Correlations of Ni and Cr versus solidification index (S.I.)	168
IV-4	Correlations of SiO_2 versus Cr and $\Sigma\text{FeO}/\text{MgO}$	168
IV-5	Plots of Anvil volcanics in an AFM diagram	169
IV-6	Discrimination diagrams of Ti-Zr-Y, Ti-Zr-Sr, Ti-Zr and Ti-Cr	170
IV-7	Discrimination diagrams of TiO_2 - K_2O - P_2O_5 and P_2O_5 - TiO_2	172
IV-8	Normative compositions of Anvil volcanics	177
IV-9	Al_2O_3 , Zr, and Y versus atomic ratio $\text{Mg}/(\text{Mg}+\text{Fe}^{++})$	183
IV-10	Comparison of Anvil eclogites with other rocks	562

LIST OF FIGURES (cont'd)

Figure		Page
IV-11	Composition diagrams of garnets, omphacites and amphiboles from Anvil eclogites	566
IV-12	CFM plots of coexisting garnet-pyroxene pairs from eclogites	570
IV-13	Comparison of Fe^{++}/Mg ratios in garnets and pyroxenes in eclogites and temperature estimates	573
IV-14	Pressure - X_{Jd} diagram for Di-Ac-Jd pyroxenes	576
IV-15	Locations of volcanic rock samples, Frances Lake district	186
IV-16	$\text{Na}_2\text{O} + \text{K}_2\text{O}$ versus SiO_2 plot showing various undersaturated differentiation trends and Frances Lake volcanic data	190
IV-17	Discrimination diagrams of Ti-Zr, Ti-Zr-Sr and Ti-Cr	191
IV-18	Discrimination diagrams of ΣFeO , TiO_2 , Ni and V vs. $\Sigma\text{FeO}/\text{MgO}$	192
IV-19	P_2O_5 vs. TiO_2	193
V-1	Temperature vs. atomic % Fe diagram showing phase relationships in the central portion of Fe-S system below 350°C (after Kissin, 1974)	199
V-2	Sulfur fugacity vs. temperature diagram showing variations of the activity of FeS in pyrrhotite and pyrite at 2.5 Kb	202
V-3	Electron microprobe x-ray scanning traces of sphalerite grains, Anvil Range district	207
V-4	Sphalerite-pyrite-pyrrhotite solvus isobars as functions of temperature and mole % FeS in sphalerite	209
V-5	Sulfur fugacity-temperature diagram showing mole % FeS in sphalerite at 2.5 Kb	212
V-6	Phase assemblages of Fe-Zn-S system below 300°C as functions of temperature and mole percent FeS in sphalerite	212

LIST OF FIGURES (cont'd)

Figure		Page
V-7	Activity isopleths of $(\text{PbSO}_4)_{\text{Barite}}$ and $(\text{BaS})_{\text{Galena}}$ as functions of oxygen fugacity and temperature	217
V-8	Partition of major elements in the Anvil carbonates	224
V-9	(a) Compositions of carbonates with subsolidus relations at 450°C (after Rosenberg, 1967). (b) Extrapolated subsolidus relations at 300°C for the Anvil carbonates	225
V-10	Stability fields of magnetite, hematite, siderite, and graphite as functions of oxygen fugacity and temperature (modified after Yui, 1966b)	229
V-11	FeS contents of sphalerites vs. FeCO_3 contents of carbonates from Anvil ore deposits	231
V-12	Activity isopleths of FeS and FeCO_3 as functions of fugacities of oxygen and sulfur	233
V-13	(a) Variation of Ag contents with depths, Faro deposit. (b) Correlation of Cu with Pb + Zn in drill holes, Faro deposit	243
V-14	Sulfur fugacity vs. temperature diagram showing variation of the activity of FeS in pyrrhotite and pyrite at 4 Kb	247
V-15	Electron microprobe x-ray scanning traces of sphalerite grains, Thompson Creek deposit	249
V-16	Sulfur fugacity vs. temperature diagram showing mole % FeS in sphalerite at 4 Kb, Thompson Creek deposit	253
V-17	Partition of major elements in the Thompson Creek carbonates	255
V-18	FeS contents of sphalerites vs. FeCO_3 contents of carbonates from Thompson Creek deposit	257
V-19	Activity isopleths of FeS and FeCO_3 as functions of fugacities of oxygen and sulfur	258

LIST OF FIGURES (cont'd)

Figure		Page
V-20	Phase relations in the system $\text{PbS-Cu}_2\text{S-Sb}_2\text{S}_3$	264
V-21	Sulfur fugacity vs. temperature diagram showing sulfidation curves of meneghinite and boulangerite at 1 Kb	265
V-22	Molecular ratios of Pb, Ag, Sb in Thompson Creek ore deposit, Frances Lake district (a) Pb vs. Ag. (b) Sb vs. Ag.	269
V-23	Molecular ratios of Pb, Zn, Cu in Thompson Creek ore deposit, Frances Lake district (a) Pb vs. Zn. (b) Pb-Zn-Cu	271
V-24	Molecular ratios of Pb and Zn in ore-bearing siltstones, Howard's Pass district	276
V-25	Comparison of elements in ore-bearing siltstones, Howard's Pass district	278
V-26	Comparison of elements in ore-bearing siltstones, Howard's Pass district	279
V-27	Distribution of elements in ore-bearing siltstones as compared with that in the background, Howard's Pass district	281
V-28	Electron microprobe x-ray scanning traces of sphalerite grains, Howard's Pass district	283
V-29	Sulfur fugacity vs. temperature diagram showing mole % FeS in sphalerite at 1 Kb	285
VI-1	A diagram for estimating CO_2 wt. % by volume ratios of phases in fluid inclusions	307
VI-2	Correlation of salinity, density, and temperature data of fluid inclusions in Anvil minerals	313
VI-3	Fluid pressure vs. temperature diagram as functions of salinity and density	315
VI-4	Dissociation curves of CO_2 hydrate at low pressures	320
VI-5	P-T diagram for $\text{H}_2\text{O-CO}_2\text{-NaCl}$	330

LIST OF FIGURES (cont'd)

Figure		Page
VI-6	Correlation of salinity, density and temperature data of fluid inclusions in Thompson Creek minerals	332
VII-1	Variation of sulfur isotope compositions in galena, sphalerite, pyrite, barite and mill concentrates from Anvil deposits	366
VII-2	Sulfur isotope fractionations among sulfur species and sulfide minerals plotted with respect to pyrite (after Rye and Ohmoto, 1974)	367
VII-3	Comparison of the mole fractions of aqueous sulfur species with the stability fields of Fe-S-O minerals and barite (a) T = 250°C; I = 1.0. (b) T = 200°C; I = 1.0	373
VII-4	Comparison of the positions of δS^{34} contours of pyrite and barite with stability fields of minerals (a) T = 250°C; I = 1.0; $\delta S^{34}_{\Sigma S} = 25\%$ (b) T = 200°C; I = 1.0; $\delta S^{34}_{\Sigma S} = 25\%$	378
VII-5	Sulfur isotope fractionations between pyrite-galena and sphalerite-galena pairs, Thompson Creek deposit, Frances Lake district	387
VII-6	Variation of sulfur isotope compositions in sulfide minerals, Thompson Creek deposit	387
VII-7	Stability fields of mineral assemblages as functions of T, f_{O_2} and f_{S_2}	390
VII-8	Comparison of the positions of stability fields of Fe-S-O minerals, chalcopyrite, bornite, graphite and sericite (muscovite).	391
VII-9	(a) Comparison of the effect of change in pH on the $\ln \alpha_{\Sigma H_2S-py}$ at different temperatures. (b) Comparison of the effect of change in pH on the $\delta S^{34}_{H_2S}$ values at different f_{O_2} values. (c) Stability fields of mineral assemblages as functions of pH and temperatures	394
VII-10	δS^{34} vs. T diagram showing fractionation curves of sulfide minerals and aqueous sulfide species	396
VII-11	Relationship among temperature and δO^{18} of quartz and δO^{18} of fluids from hydrothermal ore deposits	401

LIST OF FIGURES (cont'd)

Figure		Page
VII-12	Calibration of lead isotope standards	421
VII-13	Lead isotope ratios for galena, sphalerite, pyrite and barite from massive ores and vein galena in Anvil batholith	426
VII-14	Lead isotope ratios for ores and pyrite in host rocks, Thompson Creek deposit, Frances Lake district	433
VII-15	Lead isotope ratios for ores, sedimentary pyrite and barites in siltstones, Howard's Pass district	437
VII-16	Modern and ancient stratiform ore deposits as examples of anomalous leads or isotope heterogeneities	442
VIII-1	(a) Calculated solubility of complex ions of zinc as a function of T and pH at 1 m NaCl and 0.001 m Σ S. (b) Experimental solubility of ZnS as a function of T° and m _{NaCl} at a pH of 5.5 (after Hennig, 1971)	450

LIST OF TABLES

Table		Page
II-1	Stratigraphic succession of Late Proterozoic rocks underlying Lower-Middle Paleozoic sequence of the Selwyn Fold Belt	11
II-2	Lower-Middle Paleozoic stratigraphic sections of selected areas in the Selwyn Fold Belt and adjacent regions	20
II-3	Classification of sedimentary facies distribution, SE Selwyn Fold Belt	33
III-1	Stratigraphic section of the Anvil Range district, Yukon	52
III-2	Stratigraphic section of the Frances Lake district, Yukon	113
III-3	Stratigraphic section of the Summit Lake region, Yukon Territory - N.W.T.	139
IV-1	Chemical analyses of Cambro-Ordovician volcanic rocks, Anvil Range district, Yukon	160
IV-2	Normative compositions of Cambro-Ordovician volcanic rocks, Anvil Range district, Yukon	173
IV-3	Comparison of Cambro-Ordovician basalts in Anvil Range District with basalts from other regions	179
IV-4	Chemical and normative compositions of eclogites, Anvil Range district	550
IV-5	Electron microprobe analyses of minerals in eclogites. (a) garnets; (b) omphacites; (c) amphiboles; (d) white micas; (e) chlorites	552
IV-6	Estimation of minimum and maximum X_{H_2O} in fluid based on calculations from experimental phase equilibria	577
IV-7	Chemical and normative compositions of greenstones of the Frances Lake district	187
V-1	Chemical composition of pyrrhotites from the Anvil ore deposits	197
V-2	Chemical composition of sphalerites from the Anvil ore deposits	204
V-3	Pressure estimates of Anvil ore deposits by sphalerite geobarometry	210

LIST OF TABLES (cont'd)

Table		Page
V-4	Chemical composition of barites from Faro and Grum ore deposits, Anvil Range district	214
V-5	Comparison of chemical composition of barites from Anvil ores, Kuroko, hot springs and marine basin (in wt. %)	219
V-6	Chemical composition of carbonate minerals from Anvil ore deposits	220
V-7	Structural formula and stoichiometry of carbonates from Anvil ore deposits	221
V-8	Estimated fugacities of gaseous phases (in log unit) during metamorphism of Anvil ore deposits	235
V-9	Average grades of Faro, Vangorda, Grum and Swim Lakes ore deposits	236
V-10	Chemical analyses of drill hole ore specimens, Faro deposit	237
V-11	Mineral compositions of Anvil ore deposits (volume percents)	239
V-12	Metallic compositions of the Anvil ore deposits	241
V-13	Atomic ratios of metals in Anvil ore deposits; copper in Faro is taken to be 1	242
V-14	Chemical compositions of pyrrhotites from Thompson Creek deposit	246
V-15	Chemical compositions of sphalerites from Thompson Creek deposit	250
V-16	Chemical compositions of carbonate minerals from Thompson Creek deposit	254
V-17	Chemical composition of sulfosalt minerals from Thompson Creek deposit	261
V-18	Chemical analyses of bulk sulfide ores from Thompson Creek deposit	267
V-19	Relative atomic ratios of metals in Thompson Creek deposit; antimony is taken to be 1	268

LIST OF TABLES (cont'd)

Table		Page
V-20	Chemical analyses of cherty and calcareous siltstones with lead-zinc mineralization, Howard's Pass district	272
V-21	Ore grade of siltstones from drill holes and trench, Howard's Pass district	273
V-22	Average element content of rocks in Ordovician strata, Howard's Pass district	274
V-23	Chemical compositions of sphalerites from Placer's main zone, Howard's Pass district	282
VI-1	Salinity and filling temperature data of fluid inclusions in barite, quartz and sphalerite, Anvil ore deposits	304
VI-2	Volumes and concentrations of CO ₂ in fluid inclusions from Swim Lakes barites	308
VI-3	Density estimates of type I inclusion fluids in barite and quartz, Anvil ore deposits	310
VI-4	Vapor pressures and minimum depths of seawater to permit solution to reach seafloor without boiling	317
VI-5	Salinity and filling temperature data of fluid inclusions in quartz, Thompson Creek deposit	324
VI-6	Volumes and concentrations of CO ₂ in fluid inclusions from Thompson Creek quartz	326
VI-7	Fluid densities of type I inclusions in quartz, Thompson Creek deposit	327
VI-8	Salinity, filling temperature and density data of fluid inclusions in calcite, Howard's Pass district	336
VI-9	Density estimate of inclusion fluids in calcite, Howard's Pass district	338
VII-1	Calibration of mass spectrometer SO ₂ line standard against other artificial SO ₂ standards, 1974-1975	357
VII-2	Calibration of CO ₂ line standard, April 1975	359
VII-3	Sulfur isotope compositions (δS^{34} in %) and calculated isotope fractionation temperatures of minerals and mill concentrates from Anvil ore deposits, Yukon	361

LIST OF TABLES (cont'd)

Table		Page
VII-4	Estimates of $\delta S_{\Sigma S}^{34}$ in ore solution, Anvil Range district	376
VII-5	Proportions of aqueous sulfur species during ore deposition, Anvil Range district	381
VII-6	Simple mixing model of seawater sulfate with magmatic sulfur in a vent fluid system	383
VII-7	Sulfur isotope compositions (δS^{34} in %) and calculated temperatures of galena, sphalerite and pyrite, Thompson Creek deposit	385
VII-8	Sulfur isotope compositions and estimated temperatures of sulfides, Howard's Pass district	403
VII-9	Calibration of lead isotope standards NBS #981 Equal Atom Lead and Broken Hill #1 Galena	419
VII-10	Normalized lead isotope ratios of ore minerals, Anvil ore deposits, Yukon	422
VII-11	Normalized lead isotope ratios of ore minerals and host rock pyrites, Thompson Creek deposit	431
VII-12	Normalized lead isotope ratios of ore minerals, sedimentary pyrite and barite from siltstones, Howard's Pass district	435
VIII-1	Initial concentrations of major ions in Anvil ore solutions (ppm)	451
VIII-2	Comparison of chemical composition of Kuroko ore solution, Red Sea brines and Anvil ore solution (ppm)	453
VIII-3	Chemical composition of the Thompson Creek ore solution as compared with other replacement type deposits (unit in ppm)	455

LIST OF PHOTOGRAPHIC PLATES

Plate		Page
III-1	Photomicrographs of rock specimens (transmitted light)	84
III-2	Photomicrographs of rock specimens (transmitted light, open nicol)	86
III-3	Photomicrographs of rock specimens (transmitted light)	88
III-4	Photomicrographs of ore specimens (reflected plane light)	90
III-5	Photographs of ore specimens (reflected plane light)	92
III-6	Photographs of ore specimens (reflected plane light)	94
III-7	Photomicrographs of ore specimens (reflected plane light)	96
III-8	Photographs of ore specimens (reflected plane light)	98
III-9	Photographs of ore specimens (reflected plane light)	100
III-10	Photomicrographs of ore specimens (reflected plane light)	102
III-11	Photographs of ore specimens (reflected plane light)	104
III-12	Photographs of ore specimens (reflected plane light)	106
III-13	Photomicrographs of rock specimens (transmitted light)	128
III-14	Photomicrographs of ore specimens (reflected plane light)	130
III-15	Photographs of ore specimens (reflected plane light)	132
III-16	Photomicrographs of ore specimens (reflected light, open nicol)	155

LIST OF PHOTOGRAPHIC PLATES (cont'd)

Plate		Page
III-17	Photographs of ore specimens (reflected plane light)	157
V-1	Electron microprobe x-ray photomicrographs of ore specimens, Anvil Range district, Yukon	287
V-2	Electron microprobe x-ray photomicrographs of sphalerites, Thompson Creek deposit, Yukon	289
V-3	Electron microprobe x-ray photomicrographs of sulfosalt minerals, Thompson Creek deposit, Yukon	291
V-4	Electron microprobe x-ray photomicrographs of ore specimens, Howard's Pass district	294
VI-1	Photomicrographs of fluid inclusions in quartz and barite, Anvil ore deposits (transmitted light)	343
VI-2	Photomicrographs of fluid inclusions in quartz and barite, Anvil ore deposits (transmitted light)	345
VI-3	Photomicrographs of fluid inclusions in quartz, Thompson Creek deposit (transmitted light)	347
VI-4	Photomicrographs of fluid inclusions in calcite, Howard's Pass district (transmitted light)	349

Chapter I

INTRODUCTION

A. OBJECTIVES OF STUDY

This study originated from the writer's interest and curiosity about the variations in geological setting and mineral assemblages in "stratabound" ore occurrences in the southeastern Yukon Territory. The writer started his involvement in the region by working in the Frances Lake district in 1971. In the following two years, he became familiar with conditions of ore formation and variation in ore deposits of similar age in the Anvil Range near Ross River and Howard's Pass on the Yukon Territory - Northwest Territories border (Fig. I-1). Equipped with the knowledge gained while working in the three districts, he set out to pursue a new type of study in an attempt to resolve certain questions. The study is new because it is the first time a systematic study has been carried out on a number of ore deposits of essentially similar age in a geological setting analogous to a continental margin environment. The basic objectives of this study are:

(1) to understand the variations in features observed in essentially coeval ore deposits in terms of an ancient continental margin environment;

(2) to estimate, through extensive isotopic and other geochemical studies, the physico-chemical conditions under which these ore deposits formed;

(3) to establish and compare working models for the ore-forming processes involved in these ore deposits;

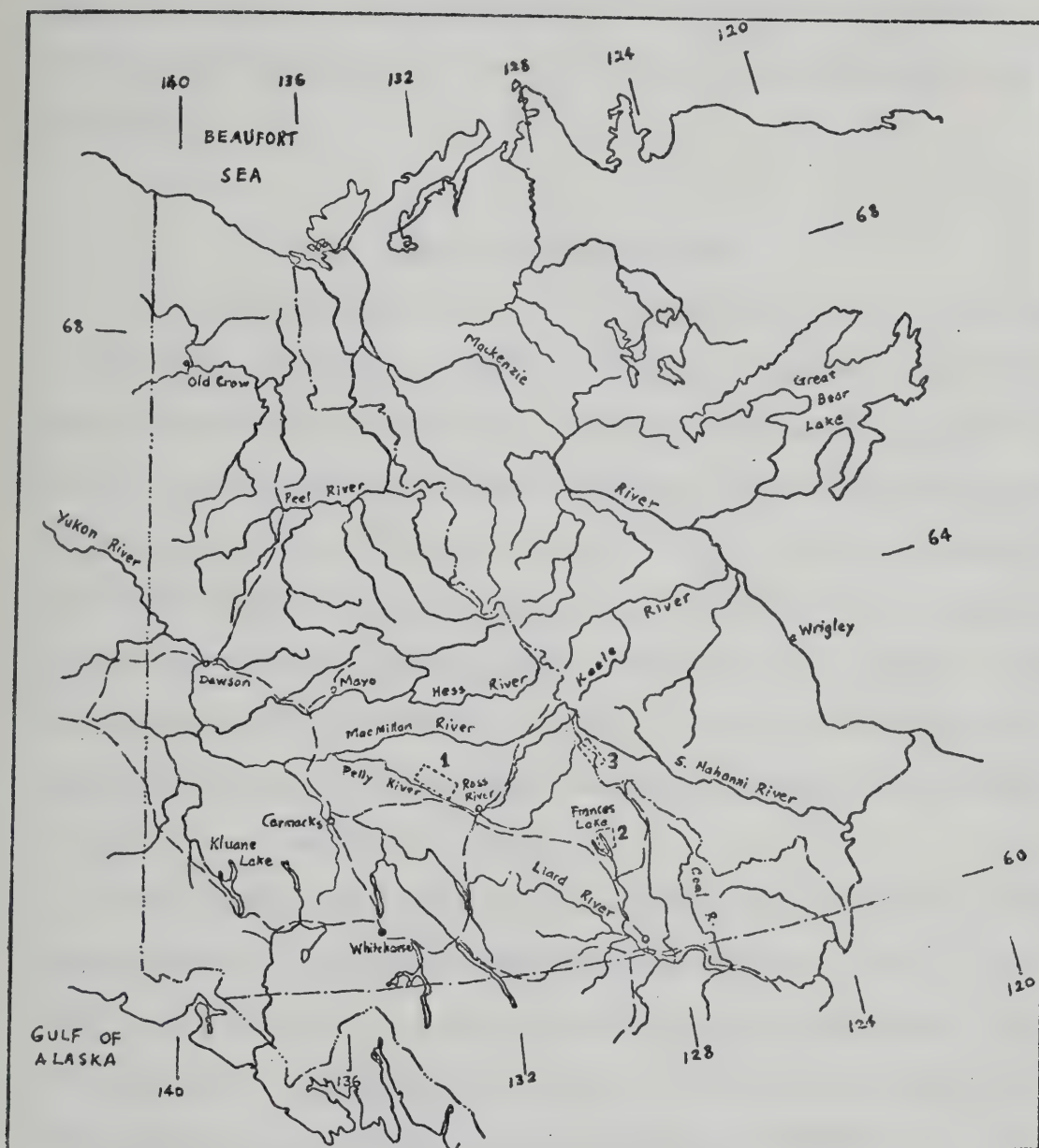


Fig. I-1. Three ore districts under study, south-central Yukon Territory and southwestern District of Mackenzie, Northwest Territories.

1. Anvil Range
2. Frances Lake
3. Howard's Pass

(4) to indicate, through the relative success and limitation of the working models, the significance of the conclusion on similar stratiform/stratabound ore deposition forming on a continental margin geosyncline.

B. OUTLINE OF WORK COMPLETED

A total of 10 months was spent in the field in the three districts in 1971, 1973, and 1974. Geological mapping was carried out by the writer in the Frances Lake district in detail, and also in part of the Howard's Pass district. Geological mapping of the Anvil Range district has been carried out by Tempelman-Kluit of the G.S.C. and Jennings of Cyprus-Anvil Mining Corporation in detail; the writer's field observation in this district adds only minor amendment to the geology. Through the cooperation of the Canex Placer Ltd. of Vancouver, the writer was permitted to make use of the local geological information on the main ore zone of the Howard's Pass district.

Regional geological mapping in the related areas within the southeastern Yukon Territory has been carried out in recent years by the G.S.C. and selectively by various mining exploration companies. The writer attempts, in Chapter II, to piece together available information in a reinterpretation of the regional geological setting.

Local geology immediate to the deposits under study is presented in Chapter III together with other information on ore mineralogy, ore grade, nature of mineralization, and textural features. This Chapter constitutes the basis for interpreting geochemical data and setting up working models.

Chemical analyses and petrogenetic interpretations are made for certain Lower Paleozoic volcanic rocks and some eclogite rocks and minerals in Chapter IV.

In Chapter V, chemical compositions of ore and gangue minerals and bulk ores are presented and interpretations on the metamorphic or ore-forming conditions under which these minerals or ores formed are suggested.

Fluid inclusions in quartz, barite, calcite and sphalerite were studied in Chapter VI to obtain important physico-chemical data on inclusion fluids as a first approximation to the ore solutions *sensu stricto*.

In Chapter VII, isotope study was conducted on ore and gangue minerals. Stable isotope data of sulfur and/or oxygen are presented to define isotopic variations and characteristics within each deposit, and adequate interpretations on the chemistry of ore solutions were derived. Lead isotope compositions were determined for sulfides and sulfates from the ore deposits to characterize the ore lead patterns and to estimate mineralization ages; pertinent anomalous lead mixing model was discussed and a compilation of new lead data on major stratiform deposits in the world was presented to show that generation of ore leads was largely a heterogeneous process in crustal environment.

Chapter VIII provides estimates on the initial concentrations of major elements in ore solutions responsible for the formation of ore deposits in the Anvil Range and Frances Lake districts.

In Chapter IX, the writer compares the derived information on the ore-forming conditions in the three groups of ore deposits and discusses the significance and the general implication on other similar types of ore deposition occurring in a continental margin environment.

Methods and techniques of the research experiments, computational procedures (programs) for constructing certain diagrams, fossil identifications, and various background information pertinent to the thesis, are given in the Appendices.

C. PREVIOUS WORK

1. Regional Work

Regional geological mapping (scale 1 inch = 4 miles) in selected areas (Fig. I-1) in or adjacent to the three districts was initiated in 1960 by geologists of the G.S.C. Green et al. (1960b) mapped in the Finlayson Lake map-area; Roddick and Green (1961a, b) in the Sheldon Lake and Tay River map-areas; Green and Roddick (1961) and Blusson (1967) in the Nahanni map-area; Blusson (1966) in the Frances Lake map-area; Blusson (1968) and Gabrielse et al. (1965) in the Cantung district and Flat River map-areas; Tempelman-Kluit (1968, 1972) in the Anvil Range district; and Gabrielse and Blusson (1969) in the Coal River map-area (for location of map-areas, see Fig. II-2).

Review of regional geological settings within or pertinent to the southeastern Yukon including the three districts was also made by the geologists of the G.S.C. Bostock (1948) reviewed the physiography of Canadian Cordillera north of 55° parallel; Gabrielse and Wheeler (1961) discussed the tectonic framework of southern Yukon and northwestern B.C.; Gabrielse (1967b) discussed tectonic evolution of the northern Canadian Cordillera in a general manner; Roddick (1964) and Tempelman-Kluit (1972) put forward their suggestions on the movement of the Tintina Trench; Roddick et al. (1967) reviewed the age and nature of the Canadian part of the Circum-Pacific orogenic belt, again in a general manner; Gabrielse

and Wheeler (1970) touched on the geology of the northern Canadian Cordillera in a general review of the Western Canadian Orogeny; Monger et al. (1972) put forward a plate-tectonic model for the evolution of the Canadian Cordillera in which the region of interest was included.

Mineral exploration activities in the region by various mining companies and individuals can be dated back as early as the 19th century. It is beyond the scope of this section to review all activities and mineral occurrences in the southeastern Yukon; however, those pertinent to the immediate districts will be reviewed in the next section on local geology. Consecutive and follow-up coverage of important activities and mineral occurrences is incorporated in a series of publications under the title "Mineral Industry of Yukon Territory and District of Mackenzie" followed by the year of review. The following authors made significant contributions to the accounts of mining activities: Green and Godwin (1963, 1964); Skinner (1962); Findlay (1967). In 1972, the G.S.C. published an open file map (scale 1:100,000 = 10 miles) on geology and mineral occurrences (both active and inactive) of Yukon and part of southwestern District of Mackenzie, N.W.T.

2. Local Work

Local geological studies in the Anvil Range district were made by Roddick and Green (1961b) and Tempelman-Kluit (1968, 1972) and the immediate geological setting to one producing Anvil Mine (Faro deposit) was reviewed by Gondi (1972). Detailed investigation of structural geology in the immediate vicinity of Faro deposit is currently being undertaken by the geologists of the Cyprus Anvil Mining Corp. Geological mapping in the vicinity of two other potential ore deposits (Vangorda and Swim Lakes) was made by geologists of Kerr Addison Mines Ltd..

Reconnaissance mapping in the Frances Lake map-area was carried out by Blusson (1966) on a scale of 1 inch = 4 miles. Detailed geological mapping (scale 1 inch = 1500 feet) in the immediate vicinity of the Frances Lake deposit was made by Thalenhorst (1971), Kuo and Thalenhorst (1972) for a joint project by Canadian Nickel Co. Ltd.-Metallgesellschaft Canada-Matt Berry Mines Ltd.

Geological mapping in the Nahanni map-area was conducted by Green and Roddick (1961) and Blusson (1967). Since the discovery and staking of the Howard's Pass ore deposit in the western Nahanni map-area, geologists working for various mining companies have carried out more detailed geological mapping in the immediate areas. Those known to the writer include: Canex Placer Ltd. (House in 1973, Morganti in 1973-75), Vestor Exploration Ltd. (Kuo in 1973, Badham in 1973), Noranda Exploration Co. Ltd. (McAndless in 1973), and Dynasty Explorations Ltd. (Adamson in 1974).

Research work conducted on the ore deposits in the Anvil Range district includes:

(a) Correlation of grain size of sulfides and metamorphic grade of host rocks in Faro, Vangorda, and Swim Lakes (Tempelman-Kluit, 1970);

(b) Lead isotope study of galena from Faro, Vangorda, and Swim Lakes deposits (LeCouteur, 1973);

(c) Sulfur isotope study and iron content analyses in sphalerite in Faro deposit (Campbell and Ethier, 1974).

Geological mapping and mineral exploration in areas related to Frances Lake district include:

(a) Fortin Lake (in northeastern Finlayson Lake map-area, 45 miles NW of Frances Lake district); unpublished report and maps (1967), by Dynasty Explorations Ltd.

(b) McEvoy Lake (in northeastern Finlayson Lake map-area, 37 miles WNW of Frances Lake district); unpublished report and map (Kuo, 1973) of Vestor Explorations Ltd.

(c) Quartz Lake (in westernmost Coal River map-area, 40 miles NE of Watson Lake); unpublished geological and drill hole information (1968), by American Smelting and Refining Co. Ltd., Vancouver.

Chapter II

REGIONAL GEOLOGY

In this chapter, a comprehensive review and interpretation of the geological history of Lower and Middle Paleozoic in the related areas is given. Igneous activity, metamorphism and structural styles imposing on the Lower and Middle Paleozoic sequence are discussed. Due to the extensive areas under review, only type sections or those known to the writer are presented for correlation.

A. GENERAL SETTING OF LATE PROTEROZOIC ROCKS

The region in which the three districts are situated belongs to the Selwyn Fold Belt (or Selwyn Basin in physiographic nomenclature) of the eastern Canadian Cordillera (Fig. II-1). The region is usually included in the northern extension of the Omineca Crystalline Belt. The region is truncated by a major tectonic lineament, the Tintina Trench or fault zone, to the southwest, and is flanked by Mackenzie Fold Belt to the north, northeast, and east.

The stratigraphic succession of Late Proterozoic rocks underlying the Lower and Middle Paleozoic sequence in the region is highly summarized in Table II-1, mainly after Gabrielse (1967b) and Gabrielse et al. (1973).

The Helikian rocks are a thick sequence of apparently conformable clastic and carbonate strata best exposed in northern Rocky Mountains (Bell, 1968) and in a great arc through Mackenzie, Wernecke, and Ogilvie Mountains (Green and Roddick, 1962; Gabrielse et al., 1965; Gabrielse, 1967b; Gabrielse et al., 1973). These rocks are correlative with the

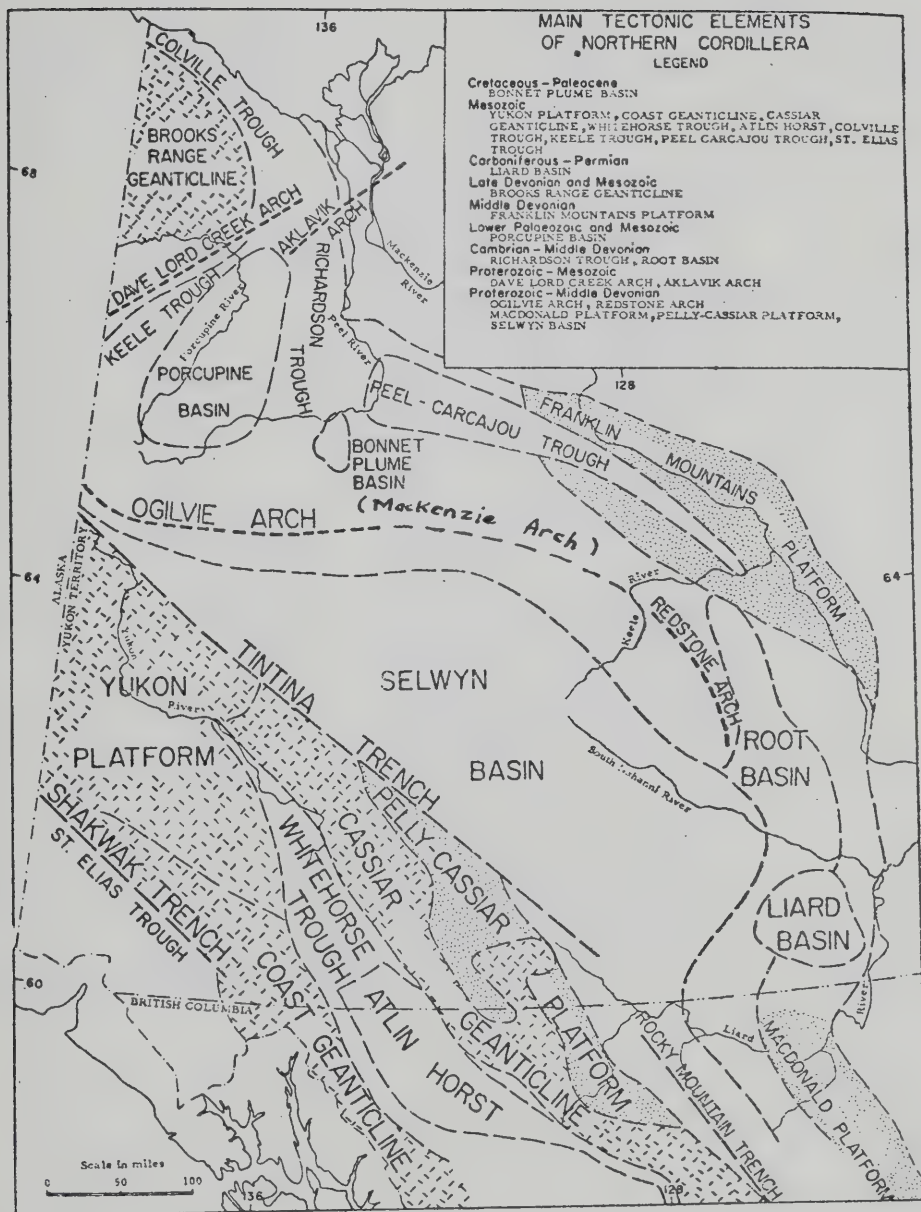


Fig. II-1. Main tectonic elements of northern Canadian Cordillera (after Gabrielse, 1967b).

TABLE II-1

Stratigraphic Succession of Late Proterozoic Rocks Underlying
Lower-Middle Paleozoic Sequence of the Selwyn Fold Belt

ERA	PERIOD	FORMATION	LITHOLOGY	THICKNESS (feet)
P R O T E R O Z O I C	Hadrynian	"Grit unit"	Phyllites, slates, siltstones, quartzites, calcarenite, feldspathic pebble conglomerates, gritty feldspathic sandstone, minor limestone	~ 5,000
		Rapitan Group	Upper Rapitan-shales and sandstone interbeds	5,000+
			Middle Rapitan-poorly sorted conglomerate mudstones	
			Lower Rapitan-chert-hematite iron formation, volcanoclastics, poorly sorted conglomerate, conglomerate mudstones	
C	Helikian		Sandy dolomites, stromatolitic limestones, siltstones, quartzites, minor conglomerates, anhydrite and gypsum	~ 15,000

Purcell System and Belt Series of southeastern B.C., southwestern Alberta and adjoining Montana. Price (1964) considered that the predominantly shallow water, fine-grained clastic and carbonate sediments of the Purcell sequence were deposited on and near the floodplain of a large subsiding delta along the western margin of the craton. A similar origin can also be suggested for the Helikian rocks now exposed on the mountains flanking the Selwyn Fold Belt.

An angular unconformity exists at the base of the Rapitan Group and indicates that Rapitan sedimentation followed a period of uplift, tilting, folding, and erosion. This period is generally referred to as the Racklan Orogeny which brought to a close the distinctive miogeosynclinal sedimentation in the eastern part of the northern Canadian Cordillera.

The Rapitan Group represents various disrupted cycles of sedimentation, volcanism, tectonism and erosion. Gabrielse et al. (1973) considered that the generally fine grain of Lower Rapitan strata, graded bedding of the coarser sediments (conglomerate), a lack of evidence for significant current action suggest deep-water deposition. Conglomerate material was introduced into this environment possibly by mudflows or turbidity currents; volcanoclastics in the Lower Rapitan sediments may have been derived from erosion of older volcanic rocks or from explosive volcanism; following uplift and tilting, deposition of widespread, thick, poorly sorted and bedded conglomeratic mudstones of the Middle Rapitan took place. These conglomeratic mudstones contain partly faceted and striated boulders (termed diamictite by Stewart, 1972) whose origin is debatable. Ziegler (1959) and Stewart (1972) consider them to be of glacial origin. Gabrielse (1967b) and Gabrielse et al. (1973) favored

the idea that they were derived from uplifted regions, subsequently rounded in streams or along beaches, and carried into the deposition site by periodic mudflows or flash floods and subaqueous slumping and turbid flows. Diamictite has been found extensively in the Hadrynian sequence in western North America and is used as a marker for stratigraphic correlation. Upper Rapitan time witnessed a return to normal sedimentation.

The "Grit unit" is correlative with the Windermere, Kaza, Miette strata of the southern Canadian Cordillera. The base of the unit has not been observed and no definite break with Lower Cambrian strata has been recognized. The coarse sediments of the Grit unit and the Upper Rapitan contain significant amounts of potash feldspar (orthoclase) and point to a source area of granitic and metamorphic rocks on the Canadian Shield. Doubt remains as to whether the source was mainly the craton to the east or a crystalline area to the west that was uplifted following the Racklan (and East Kootenay) orogeny. Age of the Grit unit and its correlation with the Rapitan Group are not established conclusively at present, but certain common features (both are thick, clastic units, partly poorly sorted; both contain significant amount of potash feldspar; both units occupy similar stratigraphic positions relative to the Lower Cambrian strata) might indicate that they are correlative with the "Windermere" sequence and could have had a westerly source.

Much of the lower part of the Windermere sequence is believed to represent deposition in relatively deep water with periodic introduction of coarse-grained material by turbidity currents. The fairly widespread carbonates in the upper part, on the other hand, reflect a shallow-water

environment. The site of maximum depositional thickness of Windermere rocks was generally to the west of that for the Purcell (Fig. II-2), suggesting that these sedimentary rocks were building out the western margin of the continent.

B. REGIONAL CORRELATION OF PALEOZOIC SEQUENCE

The Paleozoic sequence in the three districts is described in more detail in Chapter III. Generalized facies distribution, stratigraphic correlation and regional cross section of the Paleozoic are presented for the three districts (coincide with the Tay River, the Frances Lake, and the Nahanni map-areas of the G.S.C.) and related areas (the Sheldon Lake, the Finlayson Lake and the Flat River map-areas) (Fig. II-3).

1. General Facies Distribution

The details on facies distribution of strata from Lower Cambrian to Middle Devonian are treated in Appendix II-1.

A generalized facies distribution map of Late Proterozoic to Middle Devonian for the Selwyn Fold Belt and related areas is summarized in Fig. II-10. -

2. Regional Stratigraphic Correlation

Stratigraphic correlation of the Paleozoic sequence in various areas in the Selwyn Fold Belt itself is tedious and hazardous, if not impossible, mainly because mapping in several map-areas was of a reconnaissance nature and also because of relatively poor exposures. More detailed and accurate mapping was achieved in the Anvil Range district (Tempelman-Kluit, 1968,

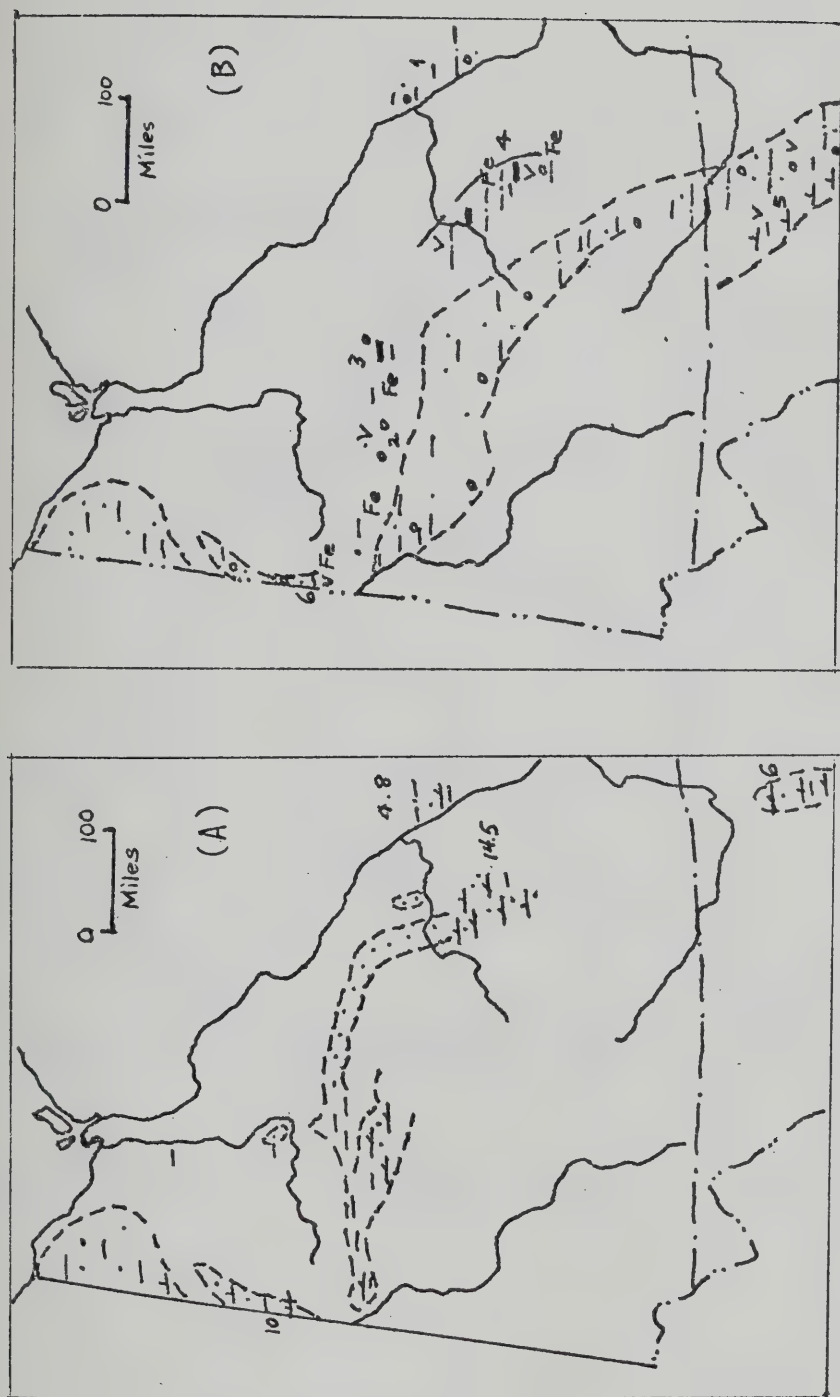


Fig. II-2. Distribution of Proterozoic rocks in northern Canadian Cordillera.
(A) Purcell, (B) Windermere.

- | | | | | | |
|--|--------------|--|---------------------|--|------------------|
| | Sandstone | | Limestone | | Limit of Outcrop |
| | Siltstone | | Dolomite | | |
| | Shale | | Volcanics | | Truncate edge |
| | Conglomerate | | Iron Formation | | |
| | Chert | | Thickness (x 1000') | | |

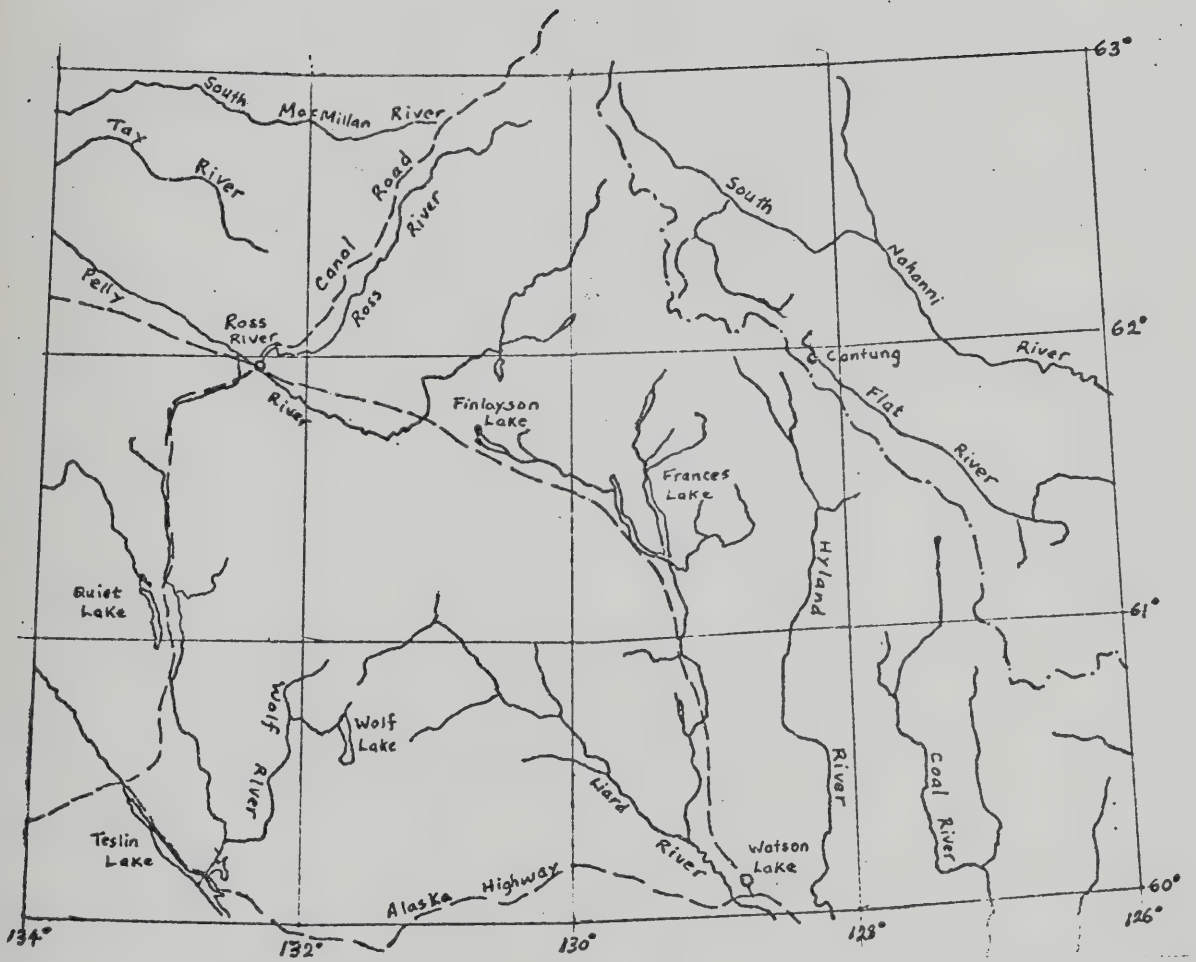


Fig. II-3. Map areas of southeastern Yukon and southwestern District of Mackenzie.

LEGEND FOR FIG. II-10

Ordovician-Silurian-Devonian



Shale



Dolomite

Cambrian



Sandstone, shale, conglomerate, dolomite

Hadrynian



Dolomite, shale

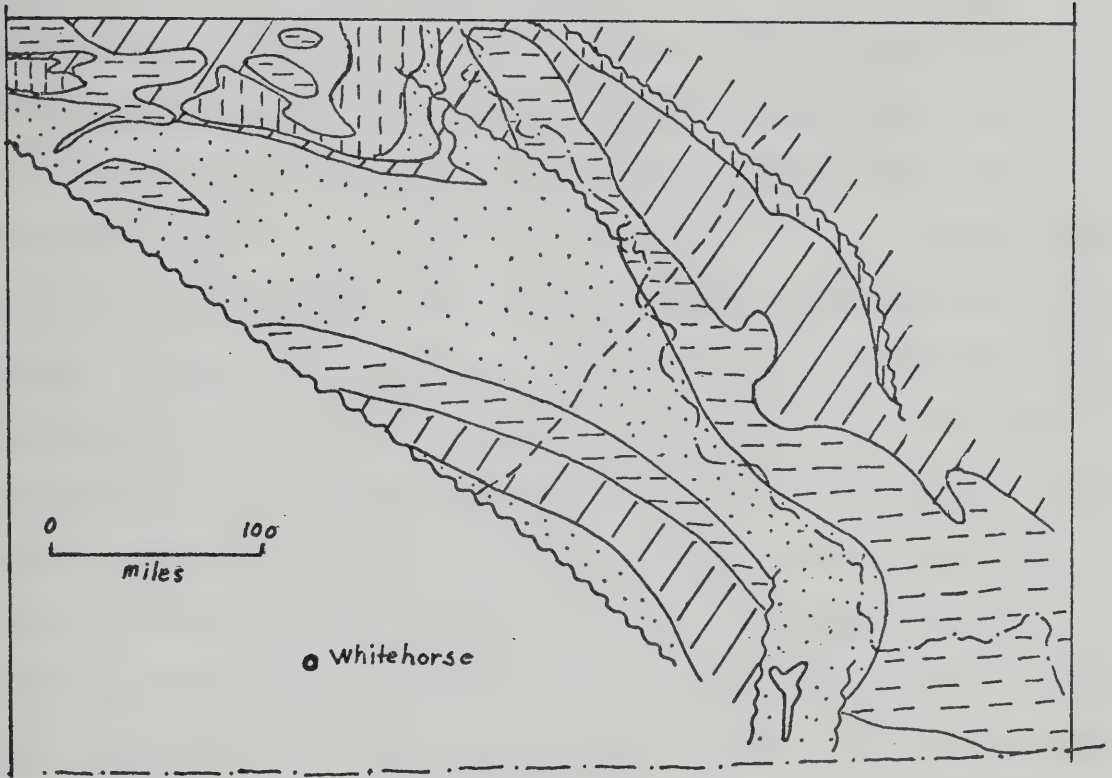


Fig. II-10. Facies distribution of Proterozoic to Devonian rocks in Selwyn Basin and related areas (after Blusson, 1973, personal communication).

1972) and the Cantung Mine district (Blusson, 1968). Based on the stratigraphic information of the Paleozoic sequence in the Flat River and Glacier Lake map-areas (Gabrielse et al., 1973; Blusson, 1968), the Nahanni map-area (Green and Roddick, 1960; Blusson, 1967) and the Howard's Pass district in particular, the Frances Lake map-area (Blusson, 1966; Frances Lake district in particular, Kuo and Thalenhorst, 1972), the Sheldon Lake map-area (Roddick and Green, 1961), the northeastern Finlayson Lake map-area (Green et al., 1960b; and Fortin Lake and McEvoy Lake district in particular), and the Tay River map-area (Roddick and Green, 1961; Anvil Range district in particular, Tempelman-Kluit, 1968, 1972; Gondi, 1972), the writer has compiled in this section a new stratigraphic section of the Lower-Middle Paleozoic sequence for the above-mentioned map-areas and particular districts. Original sediment types were reinterpreted for some metasediment units. These stratigraphic sections are shown in Table II-2; those for Anvil Range, Frances Lake, and Howard's Pass districts are presented in Table III-1, Table III-2 and Table III-3, respectively, in Chapter III.

Careful comparison of the Paleozoic strata was made for two regional traverses, from east to west-north-west, namely, a southern traverse from Flat River map-area → Frances Lake map-area → northeastern Finlayson Lake map-area, and a northern traverse from Nahanni map-area (northeast to southwest from Broken Skull River → South Nahanni River → Summit Lake region) → Sheldon Lake (central and south) map-area → Anvil Range district. These two traverses represent a regional cross section from the eastern flank of the southern Selwyn Fold Belt to its western part, and include the three districts under study. The result of the comparison is summarized in the stratigraphic correlation charts shown in Fig. II-

TABLE II-2

Lower-Middle Paleozoic Stratigraphic Sections of Selected Areas in the
Selwyn Fold Belt and Adjacent Regions

Flat River map-area

PERIOD	FORMATION	LITHOLOGY	SPECIAL FEATURES	THICKNESS (feet)
Silurian	Road River	Dark grey, calcareous, graptolitic shale	In South Central Flat River area graded bedding	max. 2,200
Upper Ordovician		Thin-bedded, grey-grey cherty-silty dolomite containing black chert		
		Black, pyritic graptolitic, calcareous shale		
Middle-Lower Ordovician	Rabbitkettle	~~~~~ Grey, thin-bedded, shaly limestones and calcareous shale and slate		4,000+
Upper Cambrian		Dolomitic, shaly limestone		
		Wavy banded silty limestone		
Middle Cambrian		Fine-grained, silty-dolomitic limestone ~~~~~		
Lower Cambrian	Sekwi	~~~~~ Brown to black, partly pyritic, calcareous siltstone, slate and shale; locally minor thin-bedded limestone		1,500
	Backbone Ranges	Sandstone, siltstone, minor quartz pebble conglomerate		≥2,000
		Sandy to silty dolomite		
Lower Cambrian and Hadrynian	"Phyllite unit"	Sandstone, minor siltstone and sandy dolomite		2,000
	"Grit unit"	Phyllite, slate, fine-grained quartzite, dark siltstone Black-grey slate, shale, quartzite, quartz pebble conglomerate, sandstone, siltstone, minor limestone, phyllite		5,000

TABLE II-2 (cont'd)

Cantung District

PERIOD	FORMATION	LITHOLOGY	SPECIAL FEATURES	THICKNESS (feet)
Middle-Upper Ordovician	Road River	Dark fine-grained shaly siltstone with chert intercalations Black, graptolitic, partly calcareous slate, shale <i>~~~~~</i>		4,000
Upper Cambrian	Rabbitkettle	Black silty lime- stone, calcareous shale Wavy banded, platy limestone, siltstone <i>~~~~~?</i>		4,000
Lower Cambrian	Avalanche and/or Rockslide	Massive dolomite Thin-bedded to flaggy dolomite, sandy dolomite, silty limestone and dolo- mitic sandstone		2,000
	Sekwi	Orange weathering silty dolomite Massive dolomite Sandy dolomite, dolomitic sandstone Lower dolomite, silty and dolomitic limestone Brown shale and silty shale		
		Calcareous shale, slate, minor lime- stone Light grey coarse dolomite "Ore limestone" (fine-grained lime- stone and coarse- grained marble) Interbedded dolo- mitic siltstone and impure limestone		≥2,500
				≥ 800
	"Phyllite unit"	Grey-greenish slate, phyllite, siltstone, fine-grained quartz- ite		9,000 ?

TABLE II-2 (cont'd)

Nahanni map-area							
		(SW)	(NE)				
PERIOD	FORMATION	LITHOLOGY		SPECIAL FEATURES	THICKNESS (feet)		
Lower-Middle Devonian	Nahanni	Limestone, partly bioclastic and dolomitic		Crinoid, algal and coral forms in limestone	2,000		
	Headless, Funeral	Dolomite, limestone, minor calcareous shale, chert and red hematite laminations			3,000		
Upper Ordovician and Silurian	Road River (Whittaker)	Black graptolitic shale	Black flaggy silty limestone interbedded black chert, minor black dolomite		1,000		
Middle Ordovician and Silurian	Whittaker Sunblood	Thick bedded dolomite Black chert Minor sandy dolomite, bioclastic limestone and quartzite near base	Thin bedded impure limestone	Oolitic and pisolitic dolomite beds near lower part	2600-5000		
Upper Cambrian and Lower Ordovician	Rabbitkettle	Wavy banded limestone, dolomitic sandstone, minor silty dolomite, locally sandy dolomite and quartzite near base				Red bed	500
		Red sandstone, sandy dolomite and quartzite					
Middle Cambrian		Limestone			?		
Middle & Lower Cambrian			Thin bedded silty dolomite, siltstone				
		ABSENT		Silty dolomite, laminated siltstone tuffaceous siltstone	Mudcracks, ripple marks, cross-bedding, abrupt facies change	700	
			Quartzite, dolomitic sandstone				
	Interbedded dolomite and siltstone Silty limestone and interbedded siltstone						
Lower Cambrian and Hadrynian		Varicolored slate and phyllite	Interbedded siltstone, quartzite and slate Massive dolomite		4,000		
Lower Cambrian and Hadrynian		Grey slate, shale and phyllite minor dark grey impure limestone			6,000		
		Grey gritty feldspathic sandstone, quartz-feldspar pebble conglomerate, interbedded sandstone and siltstone			3,000		

TABLE II-2 (cont'd)

Sheldon Lake map-area

PERIOD	FORMATION	LITHOLOGY	SPECIAL FEATURES	THICKNESS (feet)
Upper Devonian and Mississippian		Black slate, shale, sandstone, minor chert pebble con- glomerate, greywacke, phyllite		7,000
Silurian and Devonian		Sandy limestone, dolomite, dolomitic siltstone and quartz- ite ~~~~~		?
Lower Ordovician and Silurian	Road River	Black and varicolored chert, with inter- bedded black shale Graptolitic shale, minor platy limestone, quartzite and chert pebble conglomerate ~~~~~		10,000 ?
Upper & Middle Cambrian		ABSENT ~~~~~		
Lower Cambrian and Hadrynian		Light grey quartzite, minor chert, banded hornfels, skarn Massive, coarse crystalline lime- stone, locally lam- inated chert Interbedded limy shale and silty limestone Shale, slate, phyllite, minor greenstone ande- site Gritty, quartz pebble quartzite, with inter- bedded shale and slate; locally impure quartz- ite		2000-3000

TABLE II-2 (cont'd)

Frances Lake map-area

(W)		(E)		
PERIOD	FORMATION	LITHOLOGY	SPECIAL FEATURES	THICKNESS (feet)
Devonian and Mississippian	Anvil Range Group	Limestone and minor dolomite Andesite greenstone, serpen- tinite and serpentinized peridotite Black shale, chert, gritty quartzite, greywacke and chert pebble conglomerate	Absent in most areas except along NE corner (Flat River	4,000 ?
Silurian and Devonian		Dolomite and quartzite, minor dolomitic quartzite, sandy to silty dolomite		1,000
Middle Ordovician and Silurian	Road River	Black shale, slate, minor chert, siltstone, and dark limestone		1000-2000
Upper-Middle Cambrian		Silty shale, laminated siltstone, slate, sand- stone, minor hornfels		≥4,000
Middle & Lower Cambrian		Black, partly pyritic, cal- careous shale, slate and phyl- lite, minor silty limestone		800-2,500
Lower Cambrian and Hadrynian		"Swiss- cheese" lime- stone, dolo- mitic silt- stone, silty limestone	Only in NE corner	200
		Shale, slate, phyllite, minor fine-grained quartzite		≥10,000
		Gritty feldspathic quartzite, quartz-feldspar pebble con- glomerate, sandstone		≥10,000

TABLE II-2 (cont'd)

Northeastern Finlayson Lake map-area

PERIOD	FORMATION	LITHOLOGY	SPECIAL FEATURES	THICKNESS (feet)
Upper Devonian and Mississippian	Anvil Range Group	Massive limestone Foliated greenstone volcanic flows with minor serpentinite Black chert, shale, greywacke, minor chert pebble con- glomerate		?
Middle Devonian and Silurian		Interbedded dolomite and quartzite, sandy and silty dolomite	Quartzite shows current bedding & ripple marks	≥3,500
Upper Ordovician and Silurian		RARE or ABSENT		
Upper & Middle Cambrian		Lustrous sericite phyllite partly calcareous, minor greenstone volcanics in upper part; also limestone, chert and greywacke	Phyllites locally change into spotted hornfels	?
Lower Cambrian and Hadrynian	"Grit unit"	(Base not seen) Phyllite, quartzite, limestone (Base not seen) Gritty quartzite, quartz and feldspar pebble conglomerate, interbedded sandstone		1,800 ?

LEGENDS FOR FIG. II-11



Conformity



Unconformity



Disconformity



Correlation



Facies change
or
break of strata



Direction of thinning of strata



Absent or not exposed

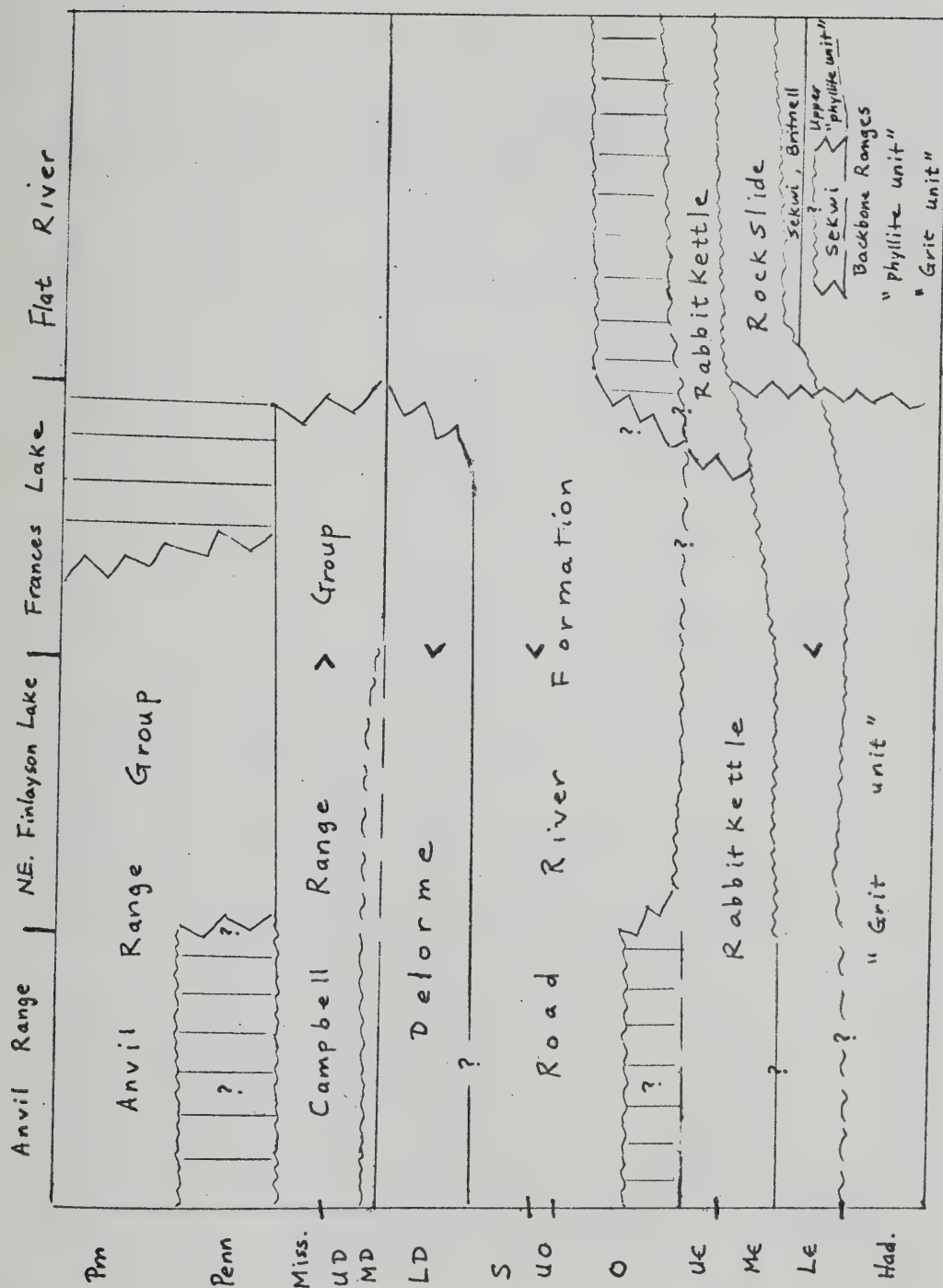


Fig. II-11a. Stratigraphic correlation of Paleozoic strata (southern traverse).

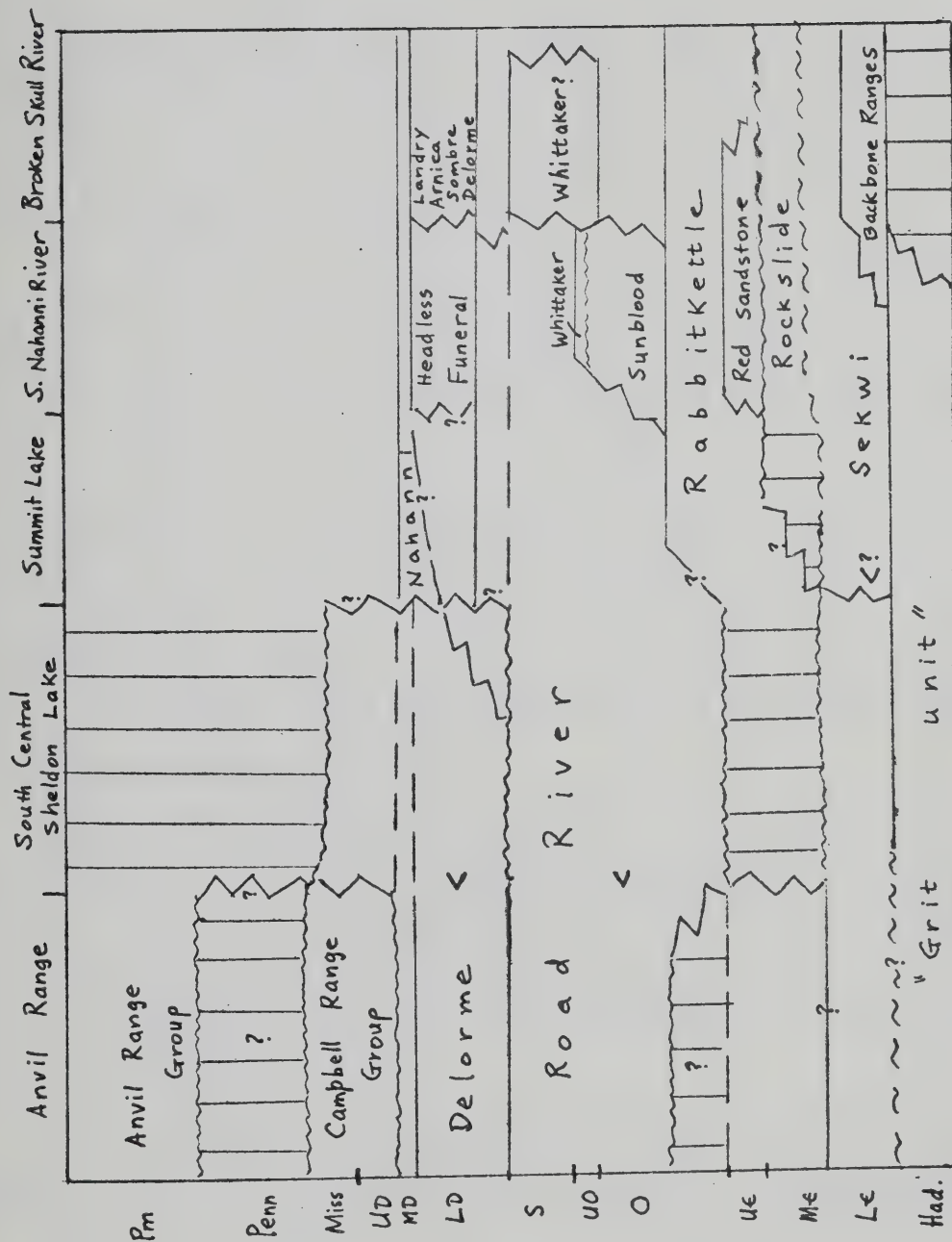


Fig. II-11b. Stratigraphic correlation of Paleozoic strata (northern traverse).

11a,b. Some uncertainties exist in correlating facies change, thickness and temporal relationship of a few strata. However, the general agreement in lateral correlation among Summit Lake, Flat River, Frances Lake and northeastern Finlayson Lake, and among Frances Lake, northeastern Finlayson Lake and Anvil Range is good. Depositional environment deduced from lithofacies for at least Lower-Middle Cambrian and Middle Cambrian-Lower Ordovician time is that:



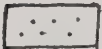

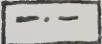

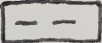
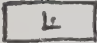


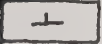

(a) shallow-water, probably shelf to near shore, in the eastern flank of the Selwyn Fold Belt (northeastern Nahanni map-area and the eastern Flat River map-area) characterized by red beds, oolitic carbonates, and shallow-water quartzite and sandstone.

(b) deep-water, probably off-slope and basinal, in the area starting from west and southwestern part of the Nahanni map-area (also of the Cantung district), most of the Frances Lake map-area, to the northeastern part of the Finlayson Lake map-area characterized by fine-grained black graphitic, pyritic shale and chert.

(c) in the area from northeastern Finlayson Lake map-area to Anvil Range district, water depth was probably shallower than or similar to the central part, but deeper than the shelf and near shore environment; submarine volcanism and associated clastic sedimentation were more pronounced here than to the east.

Coupled with regional interpretation for the Selwyn Fold Belt suggested by Douglas and Gabrielse (1970) and Blusson (personal communication, 1973) (see Fig. II-12a,b), it is thought that most of the Lower and Middle Paleozoic sequence in the Selwyn Fold Belt was deposited in an eugeosyncline separated from a miogeosyncline further to the east by a miogeanticline. A more detailed reinterpretation and discussion on

LEGENDS FOR FIG. II-12

	Conglomerate		Carbonate breccia
	Sandstone		Anhydrite
	Siltstone		Chert
	Shale		Salt, halite
	Dolomite		Volcanic rocks
	Limestone		Unconformity

Lithological Distribution for Fig. II-12b

Selwyn Basin - shale (graptolitic, calcareous near shelf), siltstone, chert, minor volcanic rocks

Transition zone between Selwyn Basin & Redstone Arch - sandstone, thick carbonates (in part reefoid)

Redstone Arch - Lagoonal laminites, dolomites, limestone, evaporites

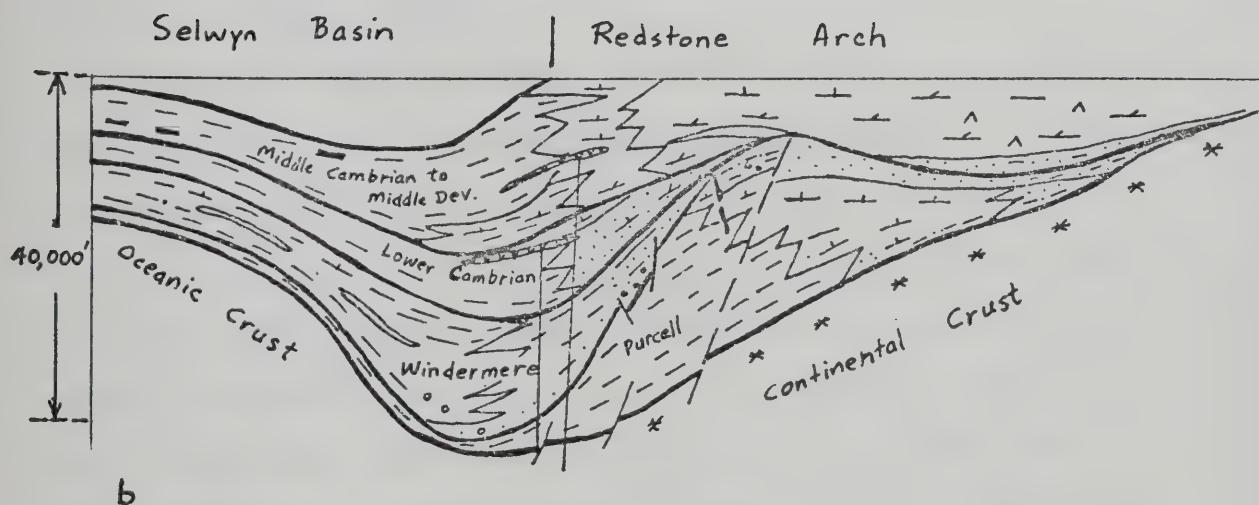
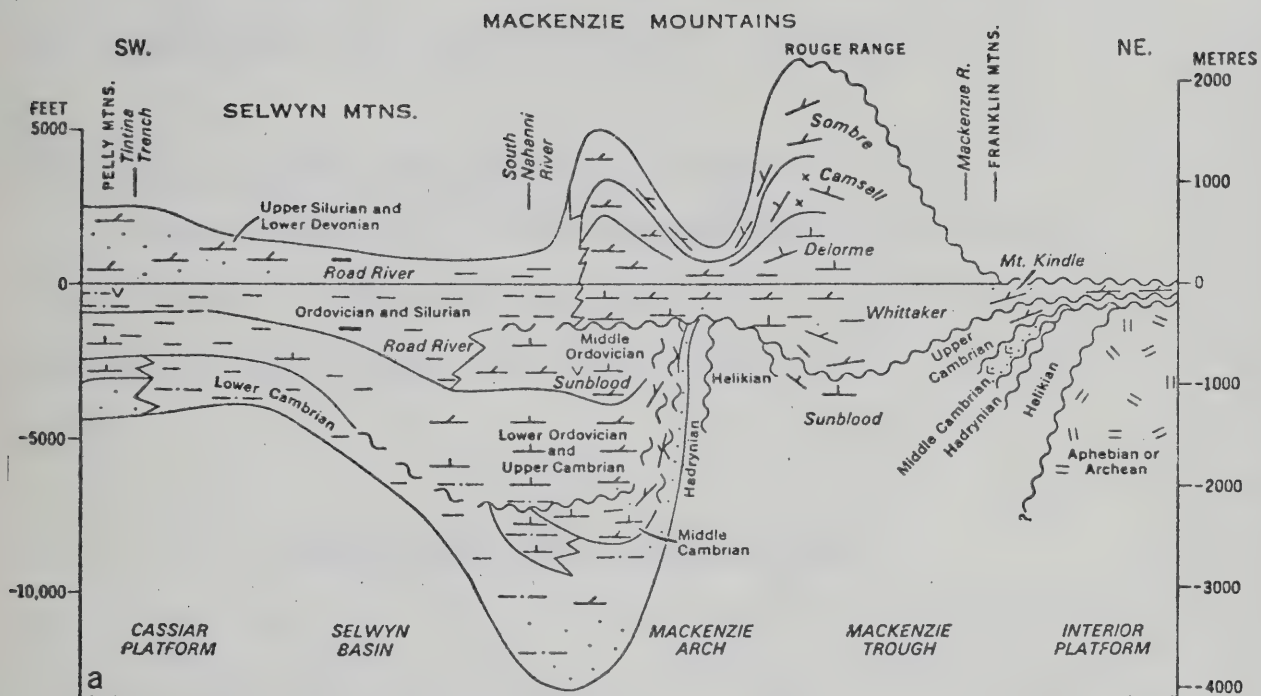


Fig. II-12. Diagrammatic restored sections of Proterozoic-Paleozoic rocks in the northern Canadian Cordillera. (a: after Douglas and Gabrielse, 1970; b: after Blusson, 1973, personal communication).

the nature and possible evolution of this eugeosyncline during most of the Paleozoic time will be made following the next section.

3. Igneous Activity, Metamorphism and Tectonism

Interested readers are referred to Appendix II-2 for details on the occurrences of Paleozoic volcanic and plutonic rocks, regional metamorphism and structural style of the Selwyn Fold Belt and related areas.

C. REINTERPRETATION OF REGIONAL GEOLOGY

A reinterpretation of the geological history of the southeastern Selwyn Fold Belt during Paleozoic period is presented below; periods immediately preceding and after Paleozoic are also discussed and correlated in the overall geological history.

1. Late Proterozoic to Cambrian

During this period, the western continental margin of the region (encompassing the eastern part of Selwyn Fold Belt, Redstone Arch, Mackenzie Mountains and Franklin Mountains) was broadly similar to the present-day Atlantic type continental margin geosyncline (Table II-3); a prograding sediment wedge was forming oceanward (westward) from the continent. Miogeosyncline sedimentation on the shelf side built up mainly shallow-water carbonate and a westwardly transgressive sand (orthoquartzite) suite represented by the carbonate clastic and arenite sequence of this period; simultaneously on the continental rise and abyssal plain beyond the continental slope, mainly lutite and minor turbidite sedimentation occurred above deeply buried (subsided escarpment ?) basin or trough containing a thick sequence of Late Proterozoic

TABLE II-3

Classification of Sedimentary Facies Distribution, S.E. Selwyn Fold Belt

	FLYSCH		PREFLYSCH		CARBONATE AND ORTHOQUARTZITE	
	Tholeiitic Volcanic Turbidites	Mature Sandstone Turbidites	Pelagic Sediments	Tholeiitic Lavas	Ultrabasics	Carbonate Carbonate Clastics
Nahanni map-area	a) -	-	rare (locally common)	-	-	abundant
	b) -	-	"	-	-	abundant
Flat River map-area	a) -	-	"	-	-	abundant
	b) -	-	"	-	-	abundant
Sheldon Lake map-area	a) -	-	common (locally abundant)	rare	-	common
	b) -	-	abundant	rare	-	locally common
Western Frances Lake & north central Finlay- son Lake map- areas	a) -	-	common	locally common	-	common
	b) -	-	common	locally common	locally common	common
Anvil Range District	a) -	-	common	common	-	common
	b) common	common	abundant	abundant	abundant	common
Atlantic type Geosynclines	a) -	-	common	common	-	rare
	b) common	common	abundant	abundant	abundant	rare
(Miogeosyncline) shelf, coast plains	-	-	-	-	-	abundant
	-	-	-	-	-	abundant
(Eugeosyncline) continental rise, abyssal plain, oceanic rise	-	-	-	-	-	abundant
	-	-	-	-	-	abundant
a) Late Proterozoic and Lower Paleozoic	-	-	-	-	-	abundant
	-	-	-	-	-	abundant
b) Middle to Upper Paleozoic	-	-	-	-	-	abundant
	-	-	-	-	-	abundant

to Lower Cambrian, coarser clastics and minor volcanics (see Fig. II-12a,b). An impure carbonate clastic and orthoquartzite "tongue" formed at the inner (eastern) side of the slope-rise region. This carbonate-orthoquartzite sequence has a complex relationship with the lutite and minor turbidite sequence - as interfingers or intercalations but regionally underlying the latter. The base of the western part of the subsided basin and overlying sequence probably was shallower than that of the central part and represented a transition to an "outer ridge" broadly analogous to an oceanic rise or an "eugeosynclinal ridge" of Aubouin. Locally subsided basins (at the base of the Windermere sequence) on the shelf-slope region (as shown in Fig. II-12b) contain coarse-grained clastics (partly red clastics) displaying cross bedding, ripple marks, sometimes mudcracks and minor intraformational slumping features; locally they contain minor occurrence of volcanic flows or sills, oolitic and/or stromatolitic carbonates, and salt clasts (Gabrielse et al., 1973). Examples are: Upper Helikian strata, Middle to Upper Rapitan Group, and Upper Hadrynian to Lower Cambrian strata. The "outer ridge" was probably a region of thick accumulation of fine-grained clastics and turbidites and subordinate volcanics. Anvil Range district, westernmost Frances Lake map-area and northeastern Finlayson Lake map-area probably coincided with this "outer ridge".

Generally speaking, volcanic flows and/or sills appear to be progressively younger from east to west. In the eastern part (southern Mackenzie Mountains and Sekwi Mountains, including Nahanni and Flat River map-areas), volcanics appear mainly in the Late Hadrynian to Lower Cambrian strata; in the central and western part (Sheldon Lake map-area, Frances Lake map-area, northeastern Finlayson Lake map-area,

and Anvil Range district), volcanics are mainly in the Middle to Upper Cambrian strata and more abundant.

An initial continental separation (Hadrynian ?) is proposed here to account for the following features observed in the Hadrynian-Cambrian rocks.

(i) Subsided escarpments or basins and thick sediment accumulation - they were probably formed as a result of block-faulting and graben development and could not have been produced by sedimentation on the continental rise (Dewey and Bird, 1971).

(ii) Coarse red clastics, volcanics and salt deposits are common - these deposits are characteristic of subsided grabens in the Atlantic type continental margin; e.g., Bay of Fundy, Connecticut; the Newark Graben; Gulf of Mexico (Ewing and Antoine, 1966; Ewing et al., 1962); and the Senegal Salt Basin of African Continental margin (Ayme, 1965).

(iii) Basic volcanic flows and sills appear to occur in progressively younger strata oceanward - the strata considered here represent a time span of close to 200 m.y.; many of the volcanic rocks appear to form in the subsided basin below which a continental-oceanic crustal transition zone (fracture-set zone) exists (Talwani and Eldholm, 1973; Dewey and Bird, 1971). Some volcanics probably generated as dike swarm through fracture zones in continental crust (R.A. Burwash, personal communication, 1975) and extruded/intruded into strata above crystalline basement. The observed younger strata probably represent a younger subsidence-graben event.

(iv) The general north-south trend of the Late Proterozoic (mainly Windermere) and Lower Cambrian (together with younger strata) sequence from Alaska down to northern Mexico has been convincingly demonstrated

by Stewart (1972) as cutting across the grain of several sedimentary troughs in underlying rocks (Belt series and equivalent rocks), indicating that tectonic setting changed before this sequence was deposited. A continental separation cutting across trends of underlying sedimentary rocks seems a likely mechanism for the initial development of our Atlantic type geosyncline.

2. Cambrian to Middle Devonian

The early part of this period probably witnessed an interrupted or terminated continental separation due to factors described by Osmaston (1971). Atlantic type geosyncline continued to develop along the continental margin. Major subsidence of the "buried marginal escarpments" or basins probably occurred during this period as thick sediments with minor volcanics accumulated. The early deformation observed in the thick sediments in Selwyn Mountains and Watson Lake map-area and Frances Lake map-area probably occurred during this period.

Development of Lower-Middle Paleozoic island arc has been reported in southeastern Alaska (Monger et al., 1972). Its significance and influence on the southern Yukon (such as possible development of margin basin) cannot be resolved at present. However, it is the general consensus (Monger et al., 1972; Gabrielse and Wheeler, 1972) that the Atlantic type geosyncline continued to prevail and no significant change in sedimentary-tectonic pattern occurred at least till the end of this period.

This period also witnessed the following events:

(i) Progressively westward building of miogeosynclinal terrace wedge; i.e., shelf front was migrating oceanward by the end of this period.

(ii) A constant polarity of sediment facies indicating a single (east) cratonic source.

(iii) Continuing occurrence of basic volcanic flows and sills of oceanic tholeiite compositions (see Chapter IV) in strata in the outer edge of the terrace wedge, i.e., in and around abyssal plain - "outer ridge" sediments above the deeply subsided basins. Occurrences of volcanic rocks in Cambro-Ordovician strata in western Frances Lake and northeastern Finlayson Lake map-areas and Anvil Range district are good examples.

(iv) Occurrence of stratabound orebodies in Lower Paleozoic strata across the entire outer part of the terrace wedge.

3. Upper Devonian to Mississippian

Allochthonous ultramafic intrusions and associated basic volcanic rocks of this age occur in the Pelly and Cassiar Platforms southwest of Tintina Trench (see Fig. II-16). Clastic sediments (conglomerates, sandstones, and siltstones) lying north and northeast of these platforms are considered to have been shed from the basic-ultramafic complex. No calc-alkalic volcanic rocks are found in this complex and it probably represents a fossil upthrust oceanic crust onto the western edge of a continental margin geosyncline (Monger et al., 1972; Gabrielse and Wheeler, 1972). The only requirement for this overthrust (obduction) to occur is the consumption of marginal basin and subsequent collision of either an island arc or an upthrust ridge with the continental margin (Dewey and Bird, 1970). Lack of associated arc volcanics with this complex suggests that a collision of upthrust ridge of marginal basin oceanic crust onto the continental margin geosyncline was a more likely

LEGEND FOR FIG. II-16



Mainly carbonate and shale



Sandstone and local conglomerate



Mixed siltstone, shale, limestone, volcanics



Basalt, chert, ultramafics



Deformation and/or metamorphism



Probable thrust faults



Direction of sedimentary transport

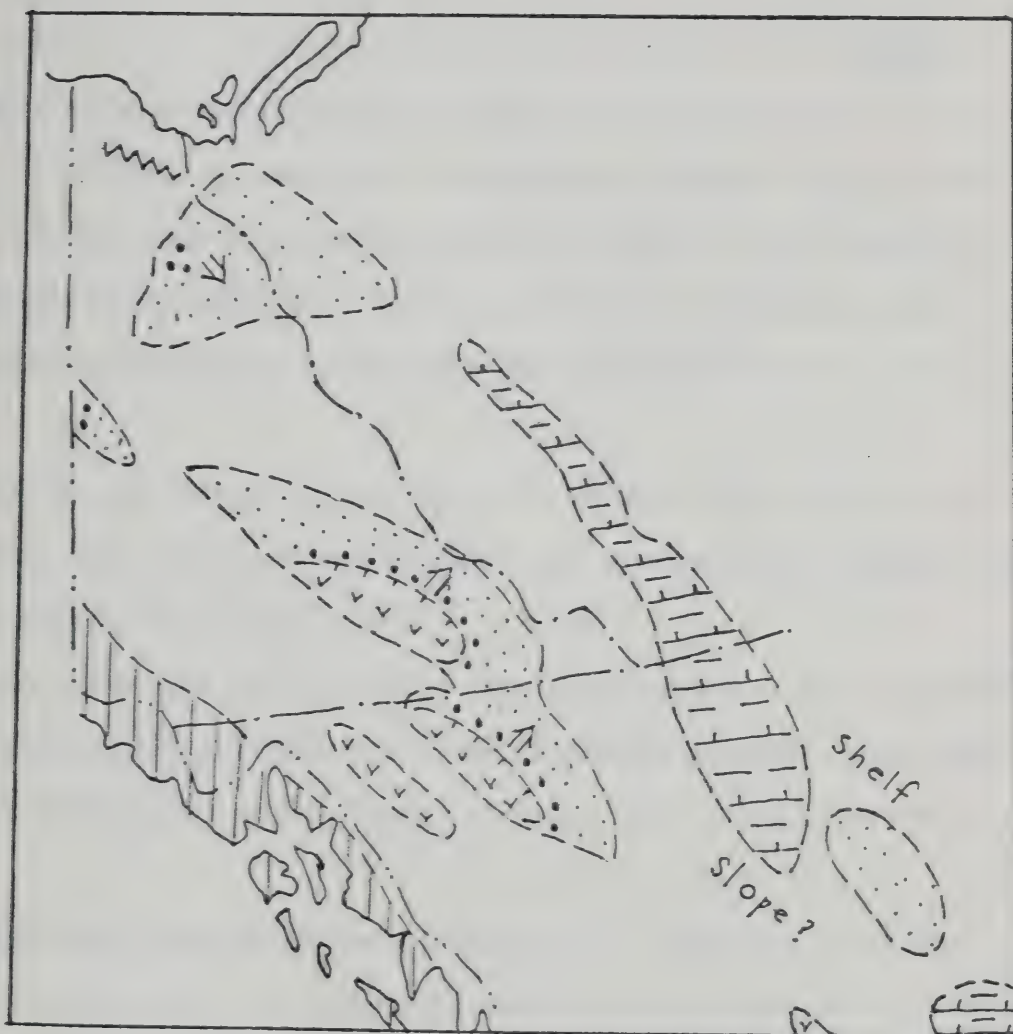


Fig. II-16. Upper Devonian to early Mississippian sedimentation and tectonism in the northern Canadian Cordillera.

mechanism. This situation occurred following a subduction zone initially developed near the continental margin (dipping away (?) from continent as suggested by Dewey and Bird, 1971) so that relatively undeformed oceanic crust wedges with some basic volcanics were obducted.

There is some field evidence in favor of this mechanism:

(i) Tectonic deformation of sediments in central Finlayson Lake and Frances Lake map-areas during Ellesmerian Orogeny could possibly have resulted from adjustment of upper portion of continental margin geosyncline sediment pile to the continuing overthrust of the oceanic crust.

(ii) No calc-alkalic volcanics are associated with the complex - thus making the island arc-continental margin geosyncline collision very unlikely during this period.

(iii) Structures of the Cassiar Thrust and Fold Belt are characterized by northeasterly-directed, locally folded thrusts that bring Lower Paleozoic rocks onto Upper Paleozoic clastics (Gabrielse and Wheeler, 1961).

(iv) Coarse clastic sediments lying at the eastern side of the complex are the result of erosion and shedding from the complex, indicating a westerly source.

4. Mississippian to Triassic

Occurrence of ultramafic and basic volcanic rocks grossly resembling ophiolite suite in the Anvil Range and possibly northeastern Finlayson Lake and western Frances Lake map-areas again suggests a similar situation. There is a discrepancy in estimates of ages for the rocks in this area. Tempelman-Kluit (1972) suggested a Pennsylvanian-Permian age for

the basic volcanics and Lower Triassic for the serpentinized peridotite (and presumably associated pyroxenite and gabbro ?). To the southeast and to the southwest of Tintina Trench, an older age (Devonian to Mississippian) was suggested (see section 3) (Gabrielse, 1963, 1967b; Monger et al., 1972), although a Permian age has been suggested for the ultramafic-basic complex of Atlin Horst in northern B.C. and southernmost Yukon (Aitken, 1959).

Gabrielse and Wheeler (1972) considered that two "mix volcanic zones" with occurrence of ultramafics were separated from a belt of "basalt" with ultramafics in the southern and southwestern Yukon during this period. They suggested that the eastern "mix volcanic zone" with ultramafics was an island arc with similarities to the western one (see Fig. II-17), and the central basalt + ultramafic belt an oceanic crust. It is very difficult, however, to picture a geological setting in which a previously obducted (Devonian to Mississippian) oceanic crust could have preserved in a double arc and interarc basin environment in roughly the same geographic location. Besides, except for the western "mix volcanic zone" which probably was an island arc, no conclusive evidence in favor of a typical island arc with preserved ophiolite suite can be given for the eastern "mix volcanic zone".

At least in the Anvil Range district, available petrographic and chemical data suggest that the Upper Paleozoic basic volcanics have an affinity with oceanic tholeiite, and no calc-alkalic trend could be detected. It is only fair to point out that some tholeiitic basalts, developed in an incipient or immature island arc, were found to closely resemble oceanic tholeiites in chemical characteristics. Furthermore, arc tholeiites may have been mixed with the pre-existing oceanic tho-

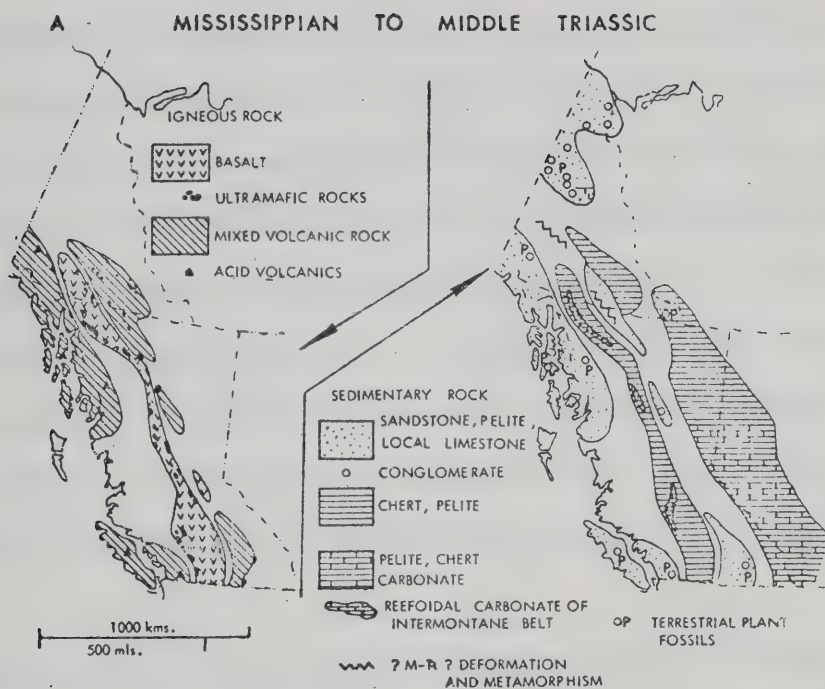


Fig. II-17. Mississippian to Middle Triassic sedimentation and tectonism in the Canadian Cordillera.

leites on the deep ocean floor, thus making it more difficult to identify the two different types of tholeiites (Miyashiro, 1974). Ultramafic rocks in the Anvil Range district include serpentized peridotite with minor pyroxenite and gabbro; the basic volcanics are mainly pillow flows with associated radiolarian chert and pyroclastics. The whole complex grossly resembles an ophiolite suite typical of oceanic ridge region. Most of the peridotite belts are either fault-bounded or very steeply dipping, and outcrops of pyroxenite and gabbro are generally poor and lack sheeted or layered structure. Therefore it is not possible to relate the complex to a typical allochthonous sheet-like ophiolite suite at present. For an ultramafic complex containing no rocks of calc-alkalic series, demonstration of its island arc origin is even more difficult.

However, based on the occurrence of eclogite and blue-amphibole rock (blueschist ?) in the Anvil Range district, a Middle Triassic deformation in some sediments, and the close resemblance of the complex to an ophiolite suite, it is suggested here that this complex formed by a tectonic process essentially similar to that of the Devonian-Mississippian complexes to the southwest. The overthrust (obduction) probably extended till at least the end of Paleozoic when younger (Pennsylvanian-Permian) basic volcanics and ultramafics were formed. If the complex is similar in age to other complexes southwest of Tintina Trench, then the overthrust would have been a continuous and persistent process.

Accumulation of coarse clastics derived from the complex and surrounding terrane (i.e., flysch type deposit) in the Anvil Range district completed the tectonic cycle of uplift and erosion for this period.

The unstable crustal configuration in the continental margin in Early Triassic times probably facilitated an isostatic readjustment with

the following consequences:

(i) Buoyancy or uplift of a thick sedimentary pile in the northeast and corresponding subsidence of oceanic crust and trench deposits to the southwest.

(ii) Deep seated normal block-faulting occurred in a fracture zone developed along the transition zone of the unstable crustal contact; transcurrent movement of Tintina fault system reactivated subsequently in the same zone in Cretaceous.

Chapter III

ORE DEPOSITS AND THEIR IMMEDIATE SETTINGS

A. INTRODUCTION

In this Chapter, the writer summarizes all the available information resulting from field and laboratory work on local geology, ore deposits, host rocks and ore and gangue minerals. The ore deposits under study are described in terms of districts for convenience and consistency.

Various rock units in local districts are described mainly in mesoscopic scale (outcrops and hand specimens); due to the extensive nature of the present study, petrographic description will be presently only for immediate host rock units, and whenever available, other rock units not hosting ore deposits.

B. ANVIL RANGE DISTRICT

1. Location and Access

Anvil Range district, in south-central Yukon, contains several important massive sulfide orebodies one of which is a large producing mine (Faro deposit). The district is about 35 miles northwest of Ross River and 125 miles northeast of Whitehorse, and located approximately at longitude $132^{\circ}30'$ to $134^{\circ}00'$ west and latitude $62^{\circ}00'$ to $62^{\circ}40'$ north. It is bounded by Tintina Trench on the south and west, Tay River on the north, and Ross River on the southwest (Fig. III-1).

The district is accessible from Watson Lake or Carmacks by road; the mining town Faro is connected both by road and by air. Faro open pit, situated about 9 miles due north of the town, can be reached by

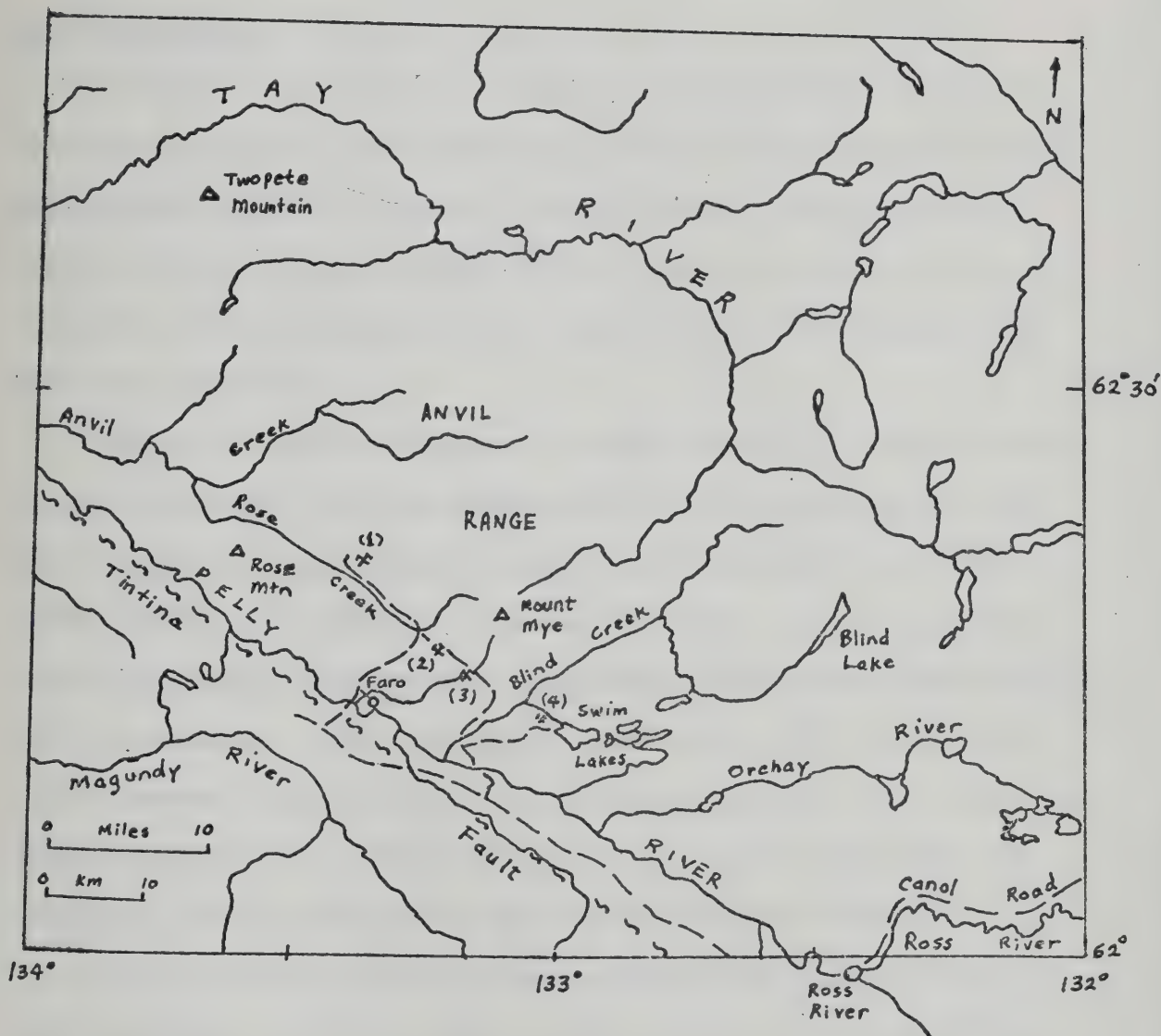


Fig. III-1. Location map of the Anvil Range district, Yukon Territory, with locations of major ore deposits. (1) Faro; (2) Grum; (3) Vangorda; (4) Swim Lakes.

road. Other important orebodies, situated about 5 to 10 miles northeast or east of the town, are connected by road.

2. Physiography

The district belongs to the Yukon Plateau physiographic province (Bostock, 1948) and is characterized by moderate relief and open valleys. Anvil Range, composed of several northwest-trending, dissected smooth rounded ridges, occupies the major part of the district and controls the topography and drainage system. The highest ridge is Mount Mye, 6,763 feet above sea level.

Valleys of dissected ridges are drained by mainly northeast to east flowing creeks with branching tributaries from topographic highs. Numerous rock-basin ponds generally formed near the headwaters. These creeks combined into northwest to southwest flowing main creeks south of the Anvil Range, and into east to northeast flowing main creeks north of the Anvil Range. The latter flow into Tay River which joins Pelly River northwest of the district; the southern creeks enter the Pelly River at their mouths. Pelly River, which flows in a broad valley delineated by Tintina Trench fault zone, is host to many sandbars.

Most of the district was probably covered by ice during the last glacial advance; some of the highest peaks may have escaped glaciation during this stage (Tempelman-Kluit, 1972).

3. Fieldwork and Exploration History

The earliest work in the district dated back to G.M. Dawson, who in 1887 descended Pelly River to its mouth. His topographic map and

geological notes described the district briefly. In 1935, J.R. Johnston produced the first geological map.

Systematic and modern mapping of the Tay River and adjacent map-areas was begun in 1958 by J.A. Roddick of the G.S.C., and completed in 1960 by Roddick and L.H. Green as part of the G.S.C.'s "Operation Pelly". D.J. Tempelman-Kluit (1968, 1970, 1972) conducted detailed geological mapping (scale: 1 inch = 2 miles) of the Anvil Range district and a study of the three orebodies (Faro, Vangorda, and Swim Lakes).

The district has been prospected intermittently since 1843, when Pelly River was "discovered" by R. Campbell of the Hudson's Bay Company. The Vangorda deposit was discovered and staked in 1953 by A. Kulan and associates of Ross River, and was optioned by Prospector's Airways who carried out an extensive drilling and exploration program between 1953 and 1956. Kerr Addison Mines Ltd., the current owner of the property, staked the Swim Lakes deposits in 1963, following an airborne magnetometer survey. The mineralized zone was discovered by drilling in 1965 and 1966. Dynasty Explorations Ltd. began a prospecting program in the district in 1965 using a combination of geophysical and geochemical prospecting techniques. The Faro deposit was drilled in 1965 and 1966 by Anvil Mining Corporation Ltd. (Dynasty Explorations was amalgamated with Cyprus Anvil Mining Corporation Ltd. in 1975), and the combined company is now the current owner of the deposit and related claims. Production from the deposit started in late 1969. Intensive exploration of the district by companies and individuals followed Dynasty's discovery and died down by 1968. In 1973-1974, AEX Minerals Corporation Ltd., headed by A.E. Aho (renamed Canadian Natural Resources Ltd. in

1975), on a farm out from Kerr Addison Mines Ltd., succeeded in finding a highly potential deposit (Grum) near Doal Lake, less than 2 miles northwest of the Vangorda deposit. Extensive drilling and underground exploration is still underway and a production plan has not yet been disclosed.

4. General Geology

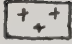
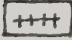
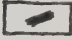
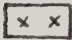

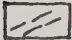
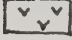
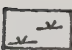
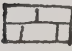
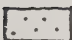

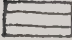


The general geology of the district and three deposits has been excellently reported by Tempelman-Kluit (1972). The following account constitutes a brief summary from his observations. Only minor addition and/or ammendment will be made, especially on the immediate geological setting of the Faro deposit, new information on AEX (Doal Lake or Grum) deposit, and some observations by the writer on local areas north of Mount Mye and northeast of Swim Lakes.

A general geological map of the Anvil Range district showing major rock units and related structures is presented in Fig. III-2 (modified after Tempelman-Kluit, 1972). Due to general scarcity of outcrops, correlation of some geological boundaries is uncertain.

Table III-1 summarizes the major rock units in the district. For correlation of Paleozoic stratigraphy with adjacent areas, see Chapter II.

Cretaceous intrusives, largely granodiorite and quartz monzonite in composition, underlie most of the Anvil Range and form the Anvil Batholith. Flanking the Batholith in the valleys and low-lying areas, a sequence of Proterozoic and Paleozoic strata is exposed. The Proterozoic and Lower Paleozoic (Cambrian to Mississippian) rocks are largely

LEGENDS FOR FIG. III-2

-  Quartz feldspar porphyry, rhyolite ignimbrite, olivine basalt, minor sandstone, shale and conglomerate
-  Saussuritized hornblende diorite porphyry
-  Pyroxenite, gabbro, hornblende diorite
-  Biotite quartz monzonite, muscovite biotite granodiorite
-  Cobble and pebble conglomerate, minor sandstone, slate and silty limestone
-  Serpentinite and serpentinized peridotite
-  Basalt flows and pyroclastics, varicolored radiolarian chert and tuff
-  Recrystallized limestone
-  Grey slate, chert, greywacke, chert-pebble conglomerate and limestone
- LD** Fetid crinoidal limestone and dolomite (too small to map)
-  Orthoquartzite
-  Black graptolitic slate, minor black chert
-  Chlorite muscovite quartz phyllite, locally graphitic and calcareous, staurolite-garnet-biotite-muscovite schist, foliated greenstone amphibolite
-  Biotite-garnet-diopside-quartz skarn, staurolite-garnet-biotite-muscovite-schist, foliated amphibolite, minor crystalline marble
-  Muscovite-quartz schist, micaceous quartzite, graphitic quartzite, all containing quartz and feldspar clasts and pebbles.
- E** Eclogite occurrences

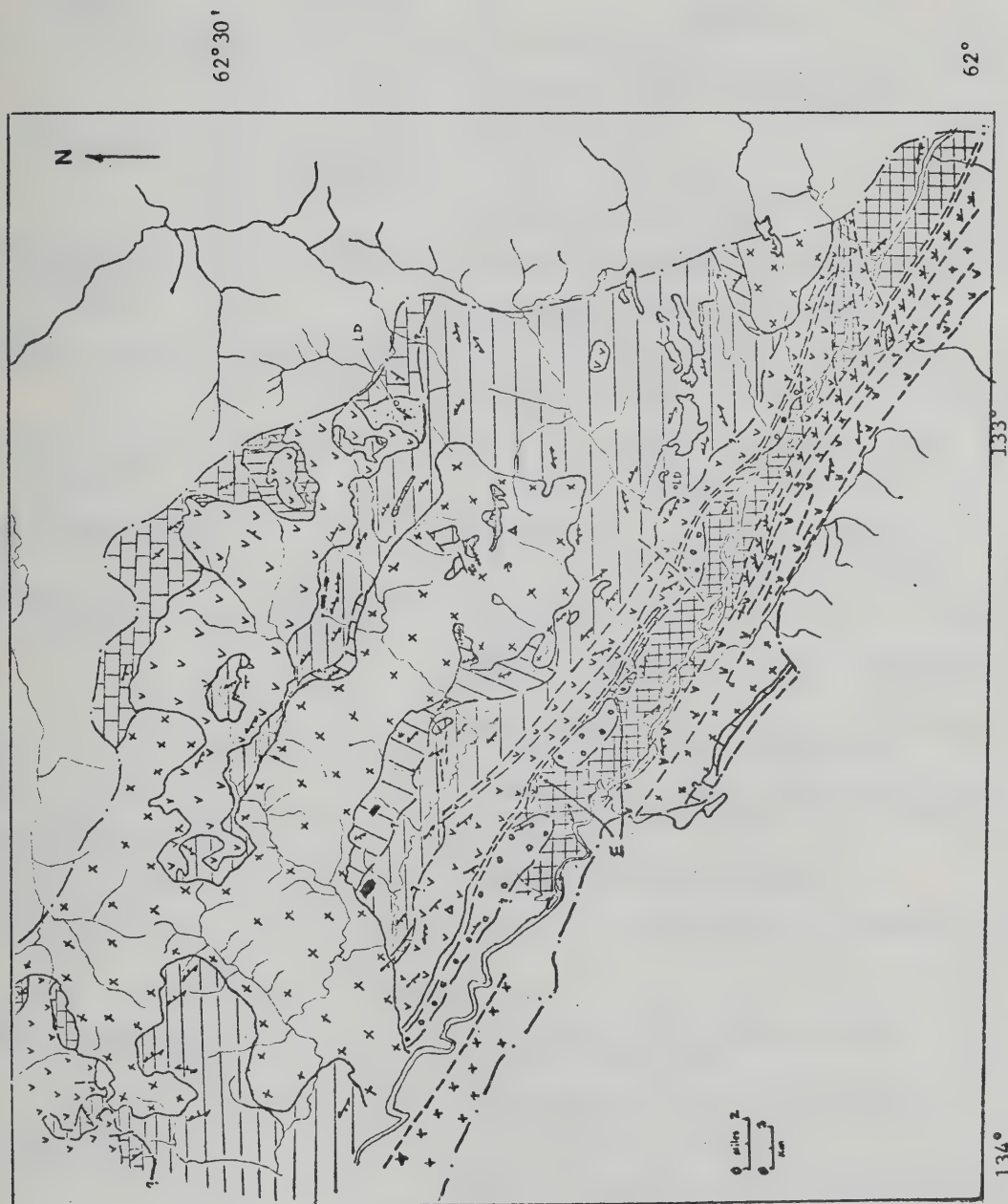


Fig. III-2. Geological map of the Anvil Range district, Yukon.

TABLE III-1

Stratigraphic Section of the Anvil Range District, Yukon

PERIOD	FORMATION	LITHOLOGY	THICKNESS (feet)
Tertiary	South Fork Volcanics	Sandstone, shale and conglomerate Olivine basalt Rhyolite ignimbrite	?
Cretaceous or Tertiary Age Unknown		Quartz feldspar porphyry (relations unknown)	
Middle Cretaceous	Anvil Batholith	Saussuritized hornblende diorite porphyry Pyroxenite, gabbro, hornblende diorite Porphyritic biotite quartz monzonite	
Middle & Upper Triassic		Muscovite biotite granodiorite (intrusive contact)	
Upper Permian and Lower Triassic		Cobble and pebble conglomerate, minor siltstone, slate and limestone near top ("Flysch" sediment)	2,000
Pennsylvanian to Permian	Anvil Range Group	Serpentinite, serpentized peridotite (fault bounded or intrusive contact)	
		Massive recrystallized limestone, locally minor tuff	~ 300
		Basalt amygdaloidal flows, pyroclastics and pillowed lavas	
		Varicolored massive to laminated "radio- larian" chert and siliceous tuff	~2,000
Upper Devonian and Mississippian		Graphitic chert and siltstone, minor inter- bedded limestone, greywacke and pebble conglomerate	10,000
Middle Devonian		Fetid limestone and dolomite	~ 100
Silurian and Devonian		Massive orthoquartzite, minor graphite	100
Middle Ordovician		Black graptolitic slate and shale, locally black chert	≥ 400
Middle & Upper Cambrian		Grey mica phyllite, containing layers of andesite greenstone, chert, tuf- fite and minor limestone	3,000
		Grey chlorite-mica quartz, phyllite, locally calcareous and graphitic, staurolite garnet mica schist	1,000
Lower & Middle Cambrian		Biotite muscovite schist, quartz diopside skarn, minor crystalline marble and amphibolite (base not seen)	
Hadrynian	Grit Unit	Muscovite quartz schist, mica quartzite, minor graphite, quartzite, locally containing quartz and feld- spar pebbles and clasts. Occurrence of eclogite and blue amphibole rocks (base not seen)	?

metasediments with minor metavolcanics, whereas the Pennsylvanian-Triassic rocks are largely unmetamorphosed volcanics and ultramafic intrusives and minor clastics. A total of 25,000 feet is estimated as the average thickness for rocks from Cambrian to Triassic. A thick sequence of Middle Triassic coarse clastics (flysch type) lies to the southwest of the Upper Paleozoic volcanic and ultramafic rocks, just north of Pelly River. Cretaceous basic intrusive and Tertiary volcanic and minor clastics occur locally and their thicknesses are unknown.

Field and petrographic (wherever available) descriptions of each rock unit from Hadrynian to Tertiary in the Anvil Range district are summarized in Appendix III-1.

5. Structural Geology

The internal structural styles of rock units in the Anvil Range district are mainly the cumulative results of two deformations, one in the Lower Paleozoic associated with regional metamorphism, the other in Early to Middle Cretaceous associated with the doming of Anvil Batholith. This structural cumulation is truncated in the southwestern part of the district by the Vangorda fault, which together with a number of other NW-trending faults defines a zone of major faulting - the Tintina fault zone or Tintina Trench.

Details on the internal structural styles of rock units, doming of Anvil Batholith, and major faults are given in Appendix III-3.

6. Ore Deposits

There are currently four major known ore deposits in the Anvil Range district, namely, the Faro, Doal Lake (Grum), Vangorda, and Swim

Lakes deposits (Fig. III-2). The Faro deposit is a large open pit mine with an average daily production of 6,600 tons of lead-zinc ore. The other three deposits are still under planning and development.

(a) Faro Deposit. The deposit is located northwest of Mount Mye and east of Ross Mountain. It consists of three orebodies, namely Faro No. 1, Faro No. 2 and Faro No. 3, with a total original reserve of 63.5 million tons and an average grade of 3.4% Pb, 5.7% Zn, 0.16% Cu and 1.196 oz/ton Ag. The No. 1 orebody covers a width of 1,100 feet, and extends for a length (along major axis) of 2,400 feet where it is met by a NE-trending fault; No. 3 orebody continues southeasterly for another 2,300 feet; No. 2 orebody is located 500 feet southeast of Faro No. 3 and lies along the same trend covering a width of 1,000 feet and a length of 1,200 feet as now known (Fig. III-3). The present study focuses on the No. 1 and No. 3 orebodies which together constitute the Faro Main Zone or orebody.

(i) Immediate Mine Geology. The Faro Main orebody, as understood from drill hole logging and open-pit exposure, has a NW-trending major axis of about 4,800 feet, a width of 1,200 feet, and an average thickness of about 120 feet. The thickest section of the orebody is about 300 feet in the central part, thinning gradually towards the margins along major and minor axes. An isopach map, a longitudinal (major axis) section and four latitudinal (minor axis) cross sections of the Faro Main orebody are shown in Fig. III-3 and Fig. III-4a,b, respectively (Tempelman-Kluit, 1972). A slightly different longitudinal section has been presented by Gondi (1972), but the general outline of the orebody remains the same. Generally speaking, the orebody is a regular and continuous, SW-dipping (18° - 25°) to flat-lying tabular lens, about 600

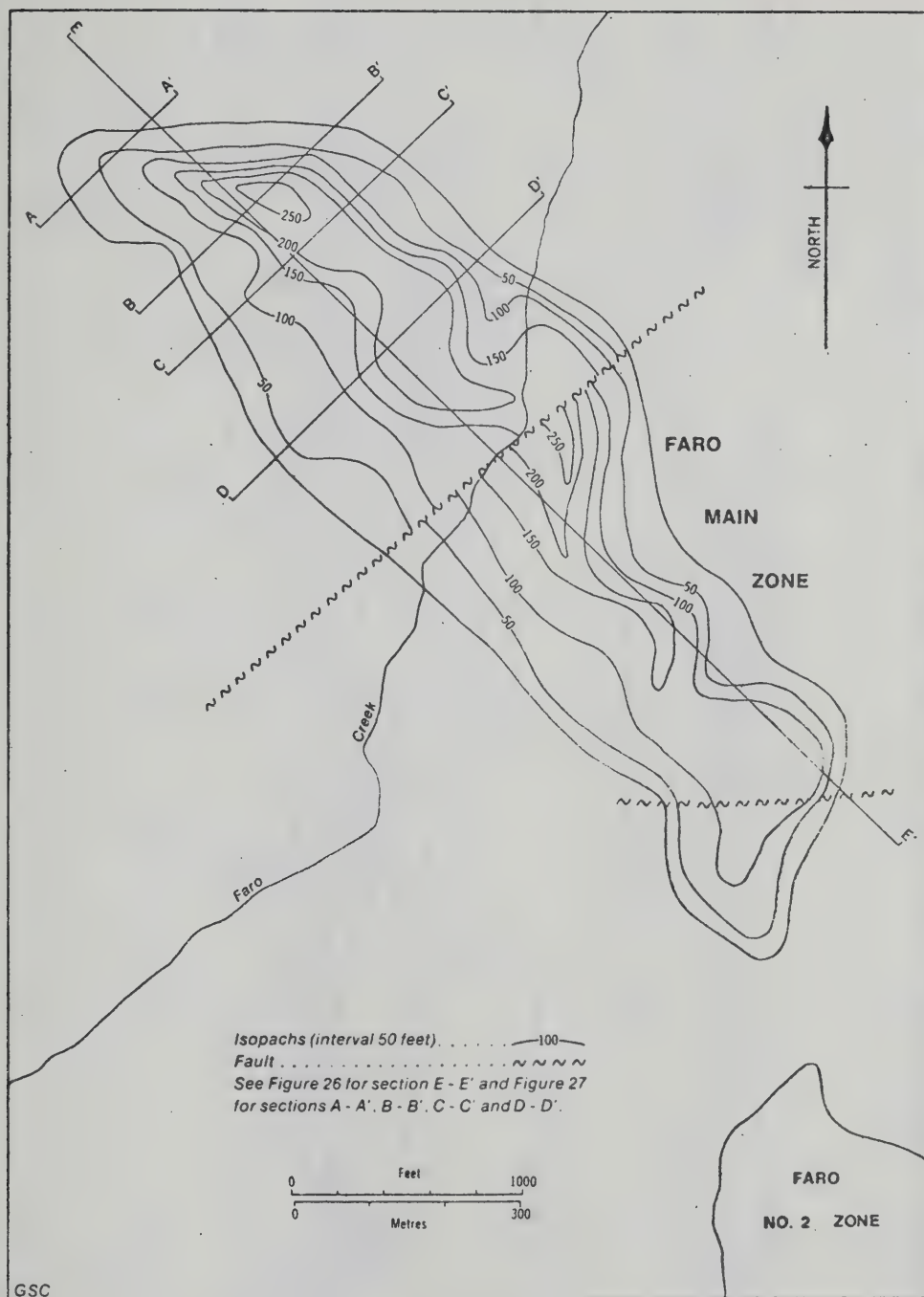


Fig. III-3. Isopach map of the Faro deposit (after Tempelman-Kluit, 1972).

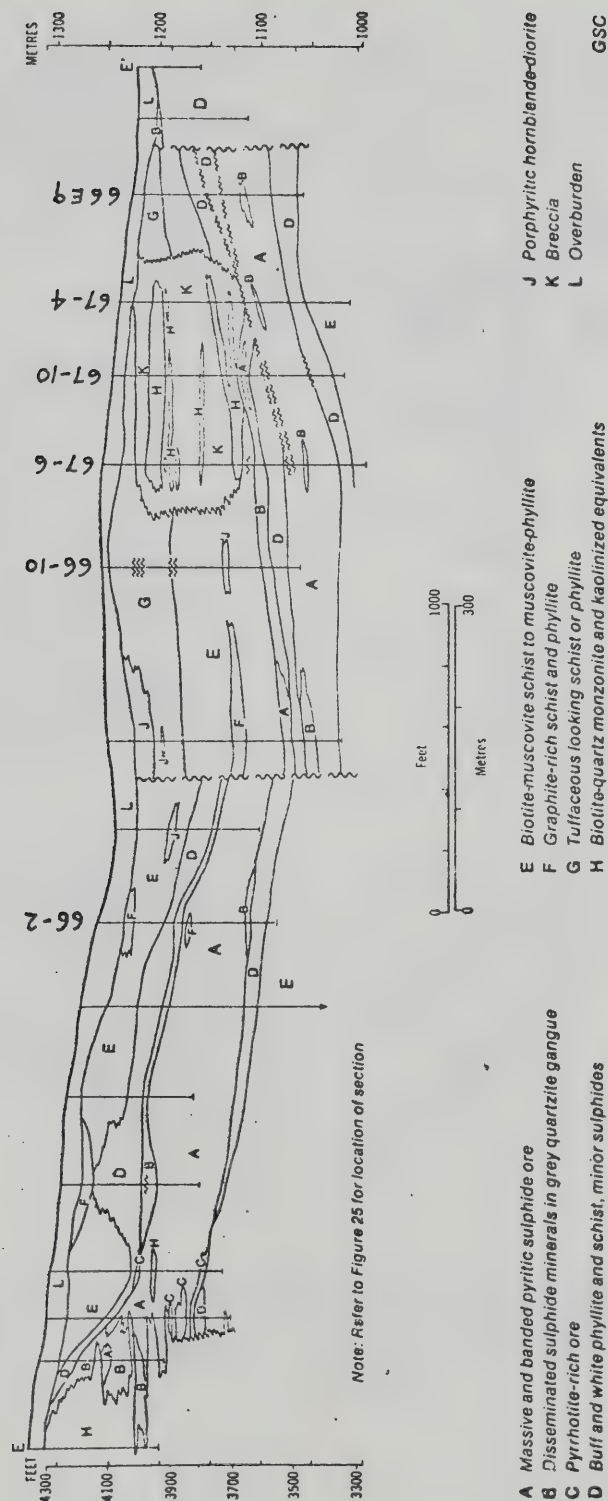


Fig. III-4a. Longitudinal section of the Faro deposit (after Tempelman-Kluit, 1972).

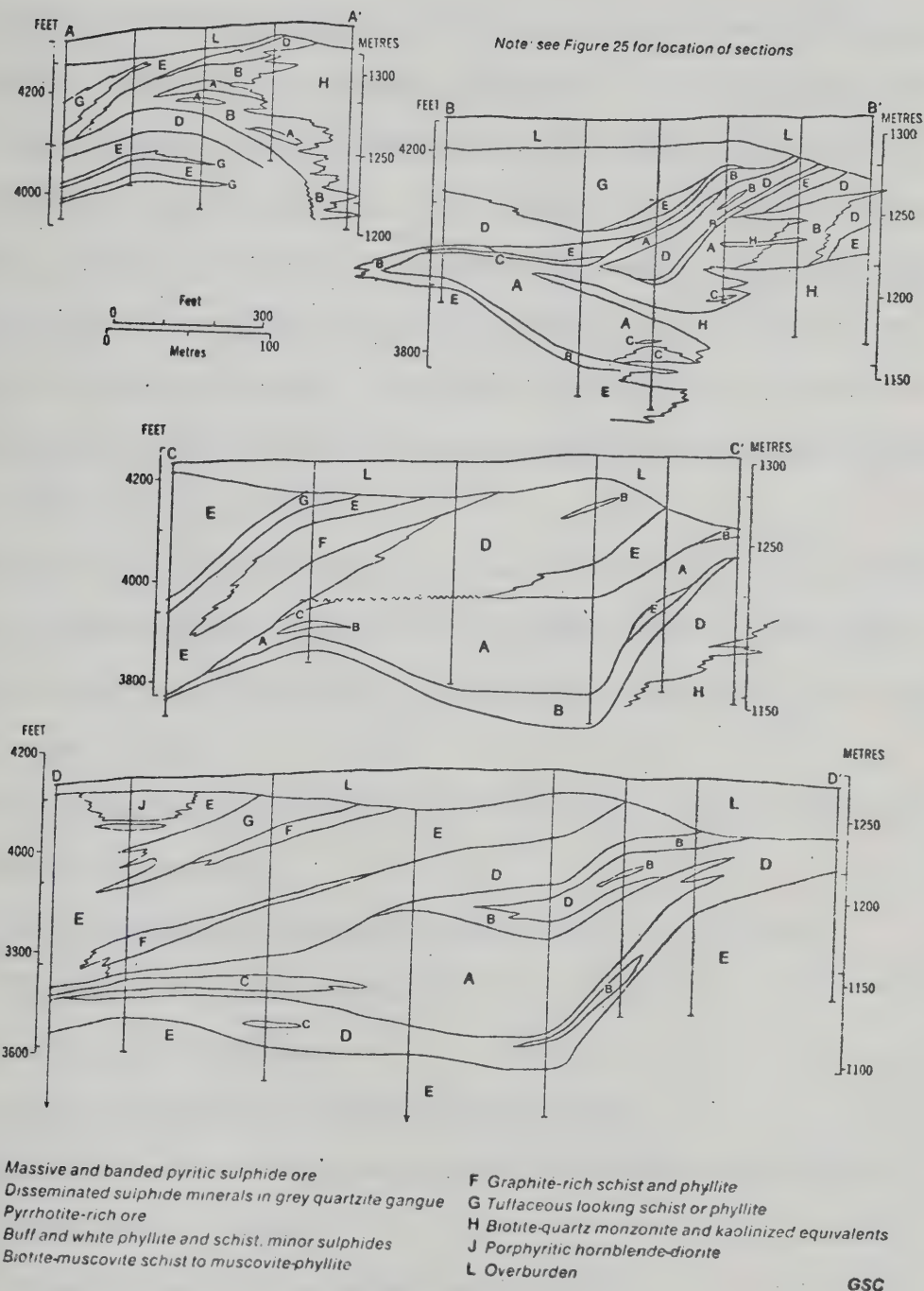


Fig. III-4b. Cross sections of the Faro deposit (after Tempelman-Kluit, 1972).

feet below surface at the central part and about 200 feet at the NW and SE margins.

At the northwestern margin the orebody abuts and terminates against acid granitic rocks and was strongly disturbed. It interfingers with the intrusive and bends upwards and occasionally forms small pods in the intrusive. A geological map of the open-pit area in the vicinity of intrusive is shown in Fig. III-5 to exhibit the extreme complexity of the contact zone. Away from the intrusive contact, especially in the central and southeastern parts, the orebody is believed to be much less disturbed and distorted, the thickness more uniform and the relationship to host rocks more distinctive.

The host rocks of the orebody, as indicated in Fig. III-4, include a series of metasediments belonging to the lower member of the Cambro-Ordovician strata described before. An apparent stratigraphy from top to base is as follows:

- (a) Chlorite-graphite-bearing quartz sericite phyllite, generally with tuffaceous components.
- (b) Quartz-chlorite-biotite-muscovite phyllite or schist.
- (c) Graphitic phyllite or schist.
- (d) Buff sericite schist.
- (e) Grey quartzite with disseminated sulfides.
- (f) Massive sulfides and their thermal metamorphic equivalent.
- (g) Buff sericite schist.
- (h) Quartz-chlorite mica schist and phyllite.

At its northwestern contact with the orebody, the intrusive contains an alteration zone composed of rocks made up of altered biotite, quartz, and a very fine-grained mixture of clay minerals pseudomorphous after feldspar. Biotite is altered to a mixture of siderite and seri-

LEGENDS FOR FIG. III-5

Dioritic Intrusive Rocks



Hornblende biotite diorite



Leucocratic hornblende diorite

Calc-silicate Rocks



Calc-silicate gneiss, minor amphibolite

Biotite Schist and Intercalated Units



Biotite schist



Graphite schist



Muscovite schist



Quartzite



Massive sulfides



Rhyolitic tuff

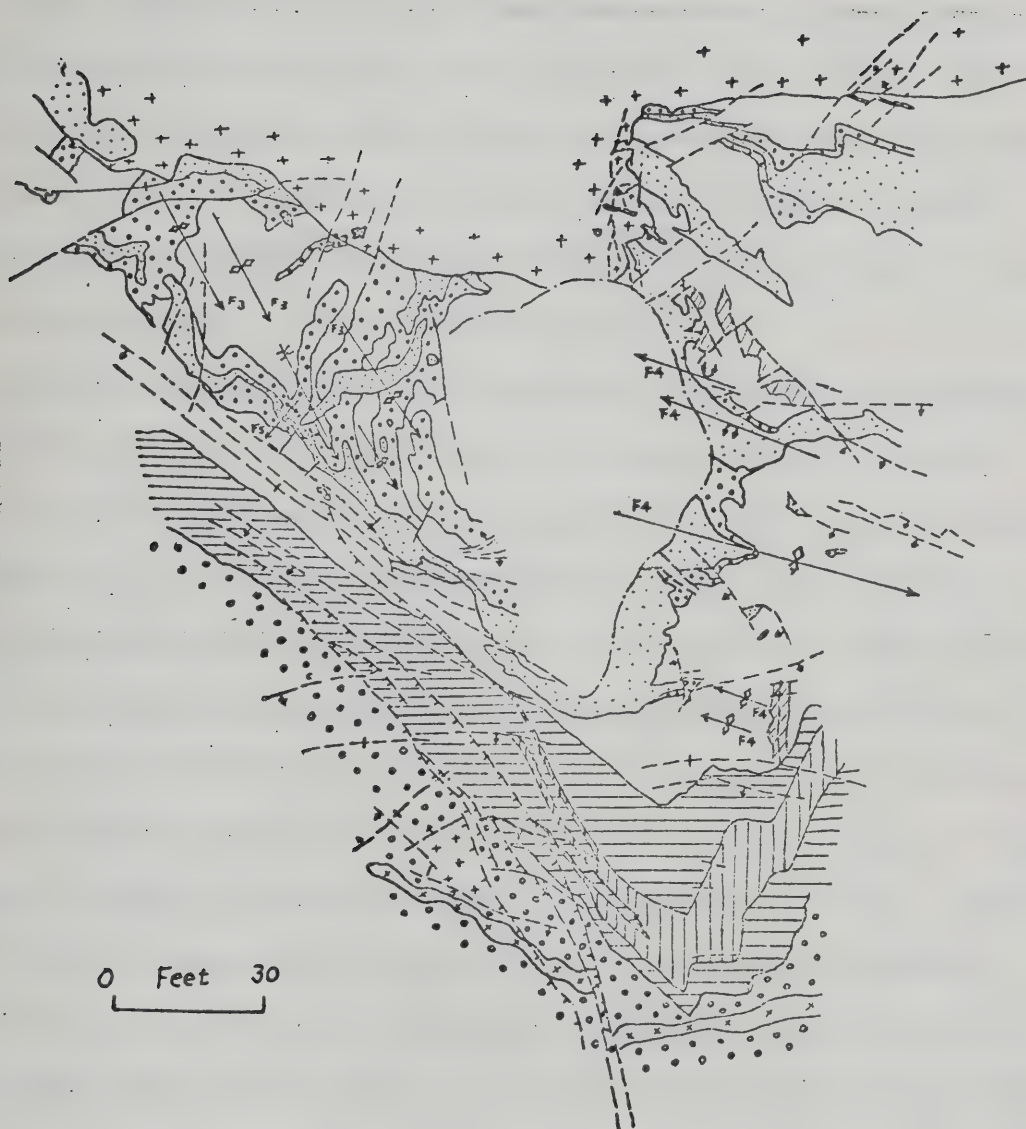


Fig. III-5. Geological map of the Faro No. 1 open-pit (modified after Jennings, personal communication, 1974).

cite. A zone of breccia about 300 feet thick occurs above the orebody at its southeastern part (Faro No. 3); the breccia contains angular fragments of schistose rocks of highly variable size (several feet to 1/10 inch) randomly scattered in a very fine-grained matrix of chlorite, and no mineralization was seen in the fragments or the matrix. The breccia zone grades laterally and vertically into undisturbed phyllite and schist. A number of flat-lying intrusive sills or dikes of quartz-monzonite, quartz-diorite, and hornblende diorite porphyry occur in the breccia zone as well as in the schistose rocks.

The structural styles in the host rocks of the orebody are essentially the same as those in the previously described Lower Paleozoic rocks. A well-developed foliation F_2 outlined by closely-spaced zones of muscovite is seen in most of the schistose rocks. Small rootless folds developed between F_2 planes and defined a preferred orientation F_1 . The banded texture or layering commonly observed in massive sulfide ores coincide with F_2 foliation in the host rocks. This banding or layering generally dips SW at gentle to moderate angles in much of the orebody, as does F_2 in the host rocks (Tempelman-Kluit, 1972). Small-scale folds or lamination corresponding to F_1 , are only occasionally observed in the orebody or ore specimen. Generally speaking, the orebody plunges gently SE at 12-20°, and is conformable with the F_2 foliation of enclosing schistose rocks that trend WNW (284°-295°) and dip SW at variable angles, and with the fold axis of NW-trending isoclinal folds. Another set of secondary folds trends EW with a gentle plunge of 5-10°W, and, superimposed on F_2 foliation, produce gentle warping of the orebody in conformity with secondary foliation (see Fig. III-4). The position of the orebody seems to be mainly controlled by F_2 foliation and associated isoclinal folding.

(ii) Ore and Gangue Minerals. The orebody consists of 50% by volume of massive to disseminated sulfide minerals of which pyrite constitutes a quarter or more. The remaining major ore minerals, in order of decreasing abundance, include sphalerite, pyrrhotite, galena, chalcopyrite and marcasite. Magnetite, arsenopyrite, bournonite, tetrahedrite (Tempelman-Kluit, 1972) and covellite (Gondi, 1972) are present as minor or trace constituents, although only magnetite and arsenopyrite have been observed in one of the specimens used in this study. Gangue minerals commonly observed are, in order of decreasing abundance, quartz, barite, ferromanganese carbonates (siderite, manganosiderite), minor calcite and dolomite, and trace amounts of sericite and chlorite. Undetermined phosphate minerals have been observed.

Ore Minerals

Pyrite forms large- to medium-grained, euhedral to subhedral crystals and displays a variety of crystal form as subrounded, cubic, porphyroblastic, fragmented or brecciated, partly corroded, and cryptoclastic aggregates. Pyrrhotite is abundant in the northwestern part of the orebody (Faro No. 1) and near intrusive contact in which it forms granular aggregates interfoliated with other sulfides and gangue; the zonal distribution of pyrrhotite in Faro No. 1 orebody has been outlined by Campbell and Ethier (1974). It is generally very rare or absent in the central and southeastern part of the main orebody (Faro No. 3), in which it forms either as very tiny exsolution blebs in sphalerite or as rimming and/or filling streaks around and in other sulfide and gangue minerals.

Sphalerite is commonly associated with pyrite and galena and forms massive polycrystalline aggregates or foliations. Wherever it occurs with galena, they are mutually intergrown or "interstitially" fill the matrix.

Chalcopyrite occurs as exsolution blebs in sphalerite, veins or rims in pyrite and quartz, and veins (with galena) in host rocks near the lower contact of the orebody; exsolution of chalcopyrite in sphalerite ranges from small oriented spherules to larger angular grains and streaks.

Marcasite generally forms "alteration rim" or pseudomorphs after pyrite and pyrrhotite, commonly occurring as aggregates or fine mottled blondish grains or large clear yellowish white crystals.

Magnetite is very rare in most of the drill core ore specimens from the central and southeastern part of the orebody, and only one occurrence has been observed; it is pinkish to creamy grey and occurs closely with siderite. Magnetite is essentially restricted to the northwestern contact with the intrusive (Gondi, 1972).

Gangue Minerals

Of all the gangue minerals observed in ore specimens, quartz is by far the most common, and occurs in different proportions and shapes commonly as subhedral to anhedral grains intergrown or interlocked in sulfides (mainly pyrite) and sometimes barite, and occasionally as veins or fracture-fills in other primary sulfides. Under the microscope quartz shows uniform extinction.

Barite is the next abundant gangue mineral, predominantly occurring in the central and southeastern part (Faro No. 3) of the orebody. No

barite has been reported from the zone near the intrusive contact. Generally, barite occurs as intergrown nearly white grains with the sulfides, and very rarely as remobilized veinlets (with quartz) cutting the sulfides-barite-quartz matrix. It is especially common in banded and sandy ores (see below). Under microscope barite is medium brownish grey, smooth to mottled-surface, subhedral and equigranular, and generally show pearly white to brown internal reflection; it commonly forms intergrowths with sphalerite, galena and quartz in the "interstitials" of pyrite, and less common with pyrite.

Widespread occurrence of carbonate minerals of a wide range of solid solution has been detected in this study. However, carbonate occurrence appears to be more pronounced near the northwestern part of the orebody (Campbell and Ethier, 1974) as compared to the sporadic occurrence in the central to southeastern part. The carbonate minerals are mainly siderite, but contain a wide range of solid solutions of Mn, Ca, Mg (in the order of decreasing abundance) and inclusions of sphalerite, pyrite, quartz and possibly ilmenite (?). They generally occur intimately with pyrite and sphalerite. Under the microscope, the carbonates are mottled medium to dark purplish grey, subhedral to anhedral patches and streaks, commonly showing reddish to pearly brown internal reflection and occasionally twinning lamellae. Coexistence of carbonates and barite in the same ore specimen is rare, and only two such specimens from the northwestern part (DDH 66-2) of the orebody are known.

A few occurrences of sericite and possibly chlorite in or adjacent to quartz, siderite and pyrite are observed in two ore specimens from the southeastern part of the orebody (DDH 66E9 436 and DDH 67-10 632).

The latter specimen contains a few rare phosphate minerals occurring together with mica minerals. These have been identified to belong to the plumbogummite group, probably a combined occurrence of plumbogummite and deltaite. Under the microscope, they are medium to dark grey, generally isotropic, oval to subrounded and frequently veined and surrounded by sulfides and quartz.

Photomicrographs of ore and gangue minerals in some ore specimens are shown in Plate III-4.

(iii) Ore Texture. The mesoscopic and microscopic textures in ore specimens display typical deformed and metamorphic features; only very rarely are some poorly preserved primary features observed. Typical textures of the ore are described below.

(a) Massive and porphyroblastic ore (Plate III-5): this texture is characterized by medium- to large-grained (0.5 to 3 mm) porphyroblasts of massive, densely packed sulfides with small amounts of gangue minerals. Internal small-scale structures such as foliation and banding are generally lacking or indistinctive. Under the microscope, the ore is composed of porphyroblastic, euhedral to anhedral, partly fragmented pyrite and "interstitial" aggregates of intergrown sphalerite, galena, quartz and/or minor barite. Sometimes chalcopyrite is seen associated with sphalerite or formed veins in or cemented around pyrite. Patches of siderite are seen partly replacing pyrite. Minor marcasite occurs as small patches rimming or partially pseudomorphous after pyrite.

(b) Foliated (or banded) and porphyroblastic ore (Plate III-5): the texture is commonly observed in the ore and is characterized by

faintly to distinctly foliated aggregates or bands of sulfides outlined by segregation of porphyroblastic pyrite, sphalerite, galena, quartz and/or barite; the banding is emphasized locally by streaking and form orientation of some of these minerals. In the central and southeastern part of the orebody, the foliation or banding of sulfides and gangue is generally not pronounced but rather the ore is massive-looking, and barite often forms equigranular aggregates with the sulfides. At the northwestern margin near the intrusive contact, banding or layering is sometimes very pronounced and closely-spaced quartz-siderite layers separate the sulfide aggregates enriched in pyrrhotite and occasionally, magnetite. The foliation or banding appears to coincide with F_2 foliation in the enclosing host rocks.

(c) Fragmented (or brecciated) and clastic ore (Plate III-6): some ore specimens display a very complex texture of random intermixing of sulfides and gangues in various proportions and grain size. Typical features observed are as follows:

1. Densely crystallized pyrite fragments set in a disseminated to massive quartz and sulfide matrix; sometimes the pyrite fragments form a separate aggregate which is bordered or bounded by quartz-sulfide matrix.

2. Deformed massive to disseminated sulfides contain randomly distributed clasts or breccias of gangue minerals, most commonly quartz, and sometimes quartz, carbonate and mica (host rocks ?). The sulfides are commonly veined by the same gangue minerals. This feature is common near the base of the orebody.

3. Clasts or veins of sulfides or sulfide-bearing quartz veins

occur in quartz-chlorite-muscovite or quartz-muscovite schists near the lower contact of orebody and host rocks; some of these schistose rocks are strongly sheared. The sulfides are mainly chalcopyrite and galena with minor pyrite and sphalerite.

(d) "Sandy" ore (Plate III-6): a few ore specimens in the southeastern part of the orebody are quartz or barite-cemented, pyritic "sandy" ore, containing interstitial or disseminated sphalerite and galena. The ore is loosely packed, massive and lacks bandings or foliation. Under the microscope, the ore contains subrounded pyrite intergrown with barite, quartz, and "interstitial" sphalerite and galena; minor chalcopyrite occurs as cement or vein in and around pyrite.

(b) Grum Deposit. The deposit is located at the southwestern flank of Mount Mye, immediately at the southwestern side of a small lake, Doal Lake. It is approximately 5 miles NE of Faro town (Fig. III-2).

Originally owned by Kerr Addison Mines Ltd., the deposit was located by AEX Minerals Corporation Ltd. of Vancouver (now Canadian Natural Resources Co. Ltd.) in 1974 and is currently jointly owned and being developed by the two companies. The writer with R.E. Folinsbee had the opportunity of collecting drill core specimens and also access to some of the drill hole sections (through courtesy of Dr. Stanley Reamsbottom, geologist on the property) in June, 1974.

The deposit contains a discovery zone of about a maximum of 8,000 feet in length, 1,000 to 1,400 feet in width, and several ore horizons at depth (Aho, Northern Miner, Oct. 17, 1974). Tonnage estimate has not been disclosed, but is likely to exceed 30 million tons. Published ore grades so far indicate an average of 4.19% Pb, 6.81% Zn, 0.25% Cu, and 2.09 oz/ton Ag.

(1) Immediate Mine Geology. Outcrops in the vicinity of Doal Lake are scarce except about one mile to the N, W and SW where Cambro-Ordovician greenstone and phyllitic rocks are exposed. Further to the N and NE, intrusive rocks of Anvil Batholith are exposed. Some rubble of phyllitic rocks do occur on the ground in the vicinity.

The major rock types observed in the drill cores which represent significant ore horizons are mainly quartz-sericite phyllite, quartz chlorite phyllite and graphite phyllite. To the SE at the small Champ claims and Vangorda deposit, the host rock appears to be biotite muscovite plagioclase phyllite with graphitic phyllite in the upper part, and overlain by a basic volcanic pile (Jennings, personal communication, 1974). A drill hole plan in the area and a cross section are shown in Fig. III-6 and Fig. III-7, respectively. The cross section is constructed on the basis of drill hole information provided to the writer by Kerr Addison Mines Ltd.. From a preliminary investigation of ore intersections in drill holes, the orebody appears to occur as separate layers and dip gently to moderately to the SW, and plunge gently NW-NNW along major axis. Several fractured and sheared zones were encountered in the drill holes, in which sulfide-bearing fault breccias were observed. Some altered schistose rocks composed entirely of light blue mariposite and quartz with minor carbonate occur near these sheared zones. Two thin layers of interbedded massive sulfides occur in the upper part and closely associated with chloritic and graphitic phyllites. Thicker layers of massive to disseminated and partly brecciated ores occur in quartz-sericite phyllite in close association with graphite phyllite.

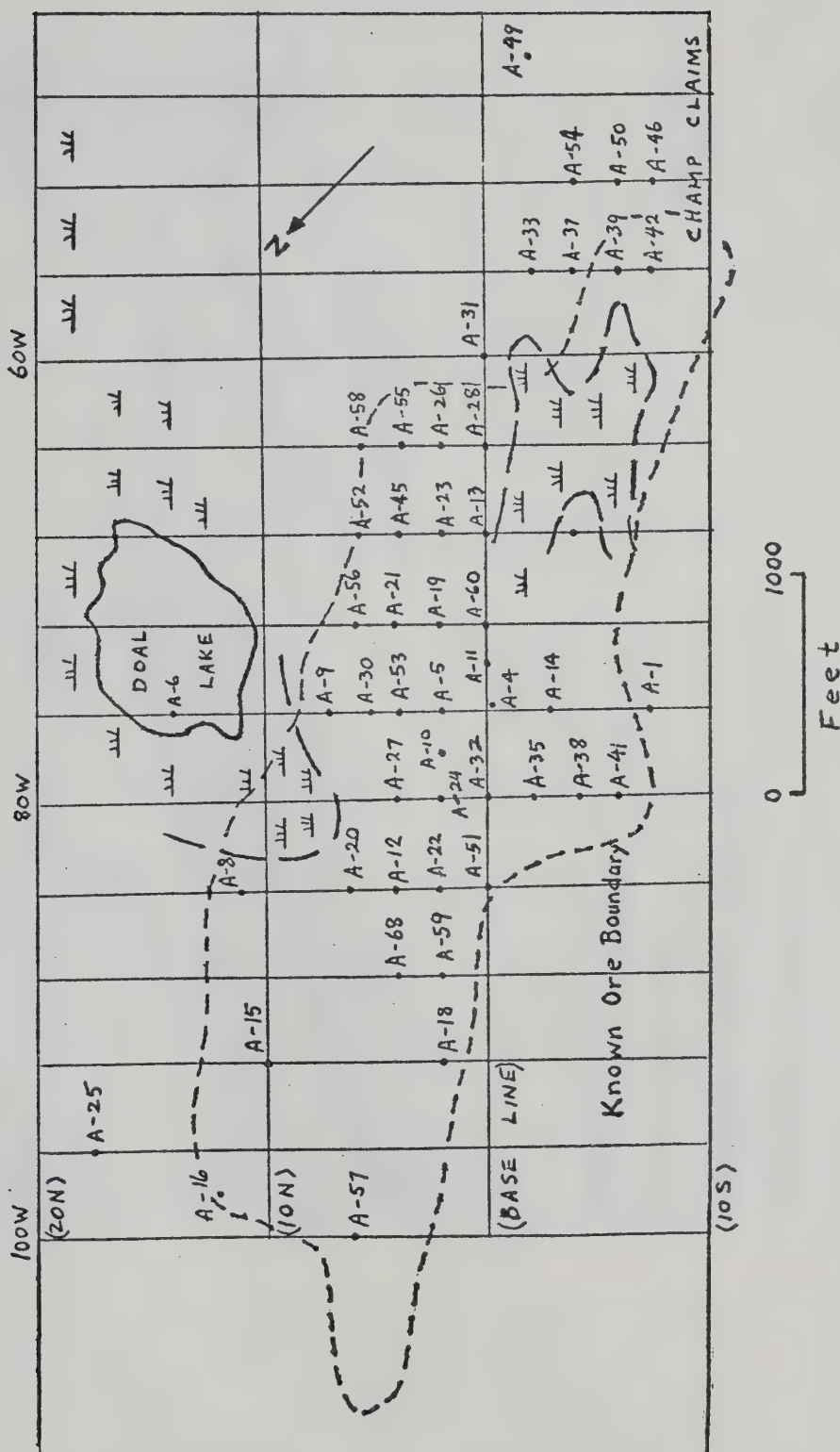


Fig. III-6. Drill hole plan of the Grum deposit (Kerr claims) (period ending 1974; courtesy of Kerr Addison Mines Ltd.); the known boundary of the orebody is also shown.

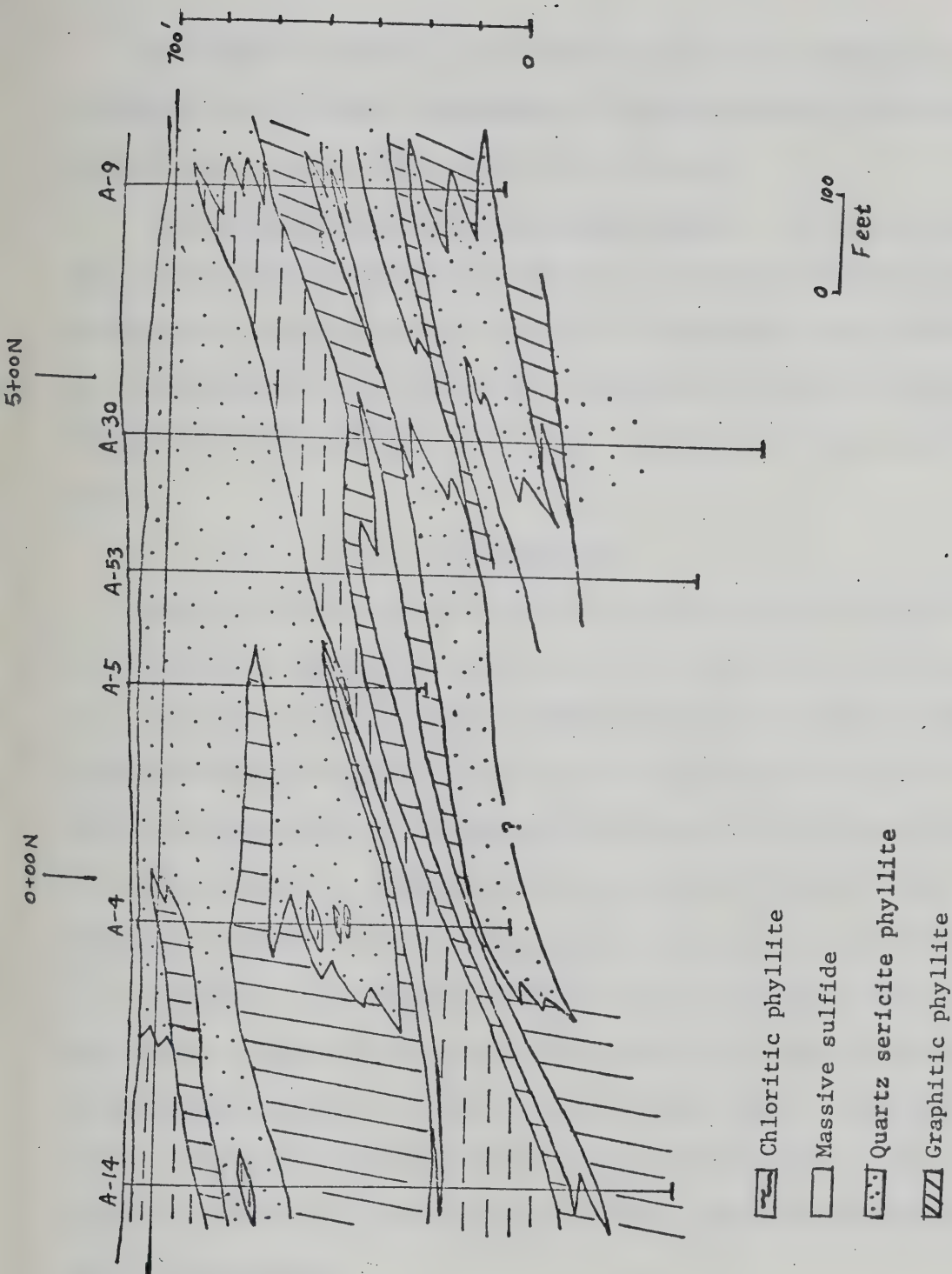


Fig. III-7. Cross section of the Grum deposit.

The orebody appears to be conformable with the schistosity in the enclosing rocks; limited measurements indicate that the schistosity which defines F_2 foliation trends NW and dips SW.

(ii) Ore and Gangue Minerals (Plate III-7). The opaque minerals are, in the order of decreasing abundance, pyrite, sphalerite, galena, pyrrhotite, marcasite and chalcopyrite. In some specimens sphalerite is about equal in amount to pyrite. Magnetite is a trace constituent. Gangue minerals observed so far include quartz, carbonates, barite and mica.

Ore Minerals

Pyrite is medium- to fine-grained (0.5 mm or less) commonly occurs as equigranular aggregates interbanded with sphalerite and galena, and less commonly as disseminated to brecciated grains in deformed host rocks and occasionally as fine-grained aggregates in fragmented ore. Under the microscope, the banded pyrite layers show distinct spherulitic to subrounded grains intergrown with sphalerite and galena; other types display subhedral, cubic to equigranular grains and are partly corroded.

Sphalerite is invariably fine-grained and intergrown with galena, and occurs commonly as interbands with pyrite, and also as disseminated to brecciated grains in deformed ores and host rocks. Under the microscope, sphalerite and galena commonly form "interstitial-fill" or poorly developed myrmekitic intergrowths; sometimes galena forms exsolution blebs in sphalerite.

Pyrrhotite and marcasite are mostly altered from or pseudomorphous after pyrite, but some pyrrhotite grains also form exsolutions or veins in sphalerite. Under the microscope, the two minerals are distinctly anisotropic, and pyrrhotite displays distinct twinning lamellae.

Chalcopyrite is a minor constituent and occurs mainly as blebs, patches and veinlets in sphalerite and galena.

Only one occurrence of magnetite has been observed in a folded disseminated bedded specimen in which abundant siderite and some marcasite and pyrrhotite occurred. Under the microscope, it is a creamy grey mineral with a pinkish brown tint and occurs adjacent to siderite.

Photomicrographs of ore and gangue minerals in some representative ore specimens are shown in Plate III-7.

Gangue Minerals

Quartz is the dominant gangue mineral and occurs as fine-grained aggregates interlocked with the sulfides and also as clasts or veins in the deformed ores.

Carbonates are minor gangue minerals and consist mainly of siderite with solid solutions of Mn, Ca, Mg. Under the microscope, they are medium grey, mottled to cloudy, and display twinned lamellae.

Barite occurs in a few ore specimens, including interbanded or "interbedded" and massive "sandy" types. It forms fine-grained crystals in the sulfide matrix, and also occurs as remobilized veinlets.

Very occasionally mica minerals are observed in the ore specimens.

(iii) Ore Texture. The ores can be classified into two types, massive and disseminated. Massive ores can be subdivided into interbanded, sandy and fragmented ores. Disseminated ores are largely seen in folded and sheared sulfides.

(a) Massive interbanded ore (Plate III-8): the ore is composed almost entirely of fine-grained sulfides and subordinate amounts of quartz and other gangue minerals. It is well-banded or thinly "bedded",

generally ranges from 1 mm to 5 mm in thickness, but some pyritic bands are up to 1 cm in thickness. From a limited number of coexisting occurrences of schistose rocks and banded ores, it appears that the banding in ores is essentially conformable to the foliation in the enclosing rocks. However, it is not certain whether this banding represents entirely crenulation foliation F_2 or inherent compositional layering F_1 .

(b) "Sandy" ore: a few ores exhibit a massive, poorly consolidated, vaguely banded texture and are characterized by equigranular pyrite, sphalerite, galena, quartz and rare barite. Minor chalcopyrite and marcasite are seen interspersed in the ores.

(c) Massive fragmented ore (Plate III-9): It is composed of "clastic" fragments of fine-grained pyrite and quartz set in a matrix of disseminated fine- to medium-grained sulfides (pyrite, pyrrhotite and minor sphalerite), siderite and quartz mixture. The ore is generally massive and resembles tuff breccia in texture.

(d) Deformed and disseminated ore (Plate III-9): there are actually two types of ores - one is a folded recrystallized disseminated ore containing or in contact with fragments and clasts of rocks and quartz veins. Grain size of sulfides is generally larger than those in massive ore. The other type is a sparsely disseminated pyritic aggregate containing minor sphalerite and galena in deformed sericitic and partly graphitic phyllite, in which quartz and mica clasts and streaks (sometimes defining "window" of fold hinges) are common.

(c) Vangorda Deposit. The deposit is the oldest discovery (1953) in the district and has been inactive for many years; however, the discovery of Grum deposit in 1974 has put the Vangorda deposit and the Swim Lakes deposit into an entirely new economic light.

The deposit is located at Vangorda Creek on the SSW flank of Mount Mye about 5 1/2 miles ENE of Faro town. Published figures indicate an average grade of 3.18% Pb, 4.96% Zn, 0.27% Cu, 1.76 oz/ton Ag and 0.02 oz/ton Au with an estimated reserve of 9.4 million tons; 12.6 million tons of essentially barren sulfides are reported in addition to the ore zone.

The deposit is partly exposed in Vangorda Creek. The core shack on the property was visited in 1974 and some outcrops downstream from the deposit were examined in 1973. Large sections of the cores are missing and many cores are shambled. The writer has managed, however, to collect certain sections of sulfide core specimens for the study. Some drill plan and ore intersection figures were kindly provided by Kerr Addison Mines Ltd..

(i) Immediate Mine Geology. The outline and cross sections of the deposit are shown in Fig. III-8 (after Tempelman-Kluit, 1972). The deposit is an irregular tabular mass partly enveloped (above and below) by a narrow zone of buff white quartz-chlorite sericite phyllite which is in turn enclosed in a sequence of phyllitic rocks of Cambro-Ordovician age, mainly quartz-chlorite-muscovite-biotite phyllite or schist and in part graphitic phyllite. Greenstone volcanic flows and tuffs are exposed together with the phyllitic rocks at and near Vangorda Creek. Crenulation foliation F_2 is generally well-developed in the enclosing rocks and small folds defining compositional layering F_1 occurs between F_2 foliation surfaces.

The major axis of the orebody trends and plunges very gently NW, and is about 2,500 feet long; the width is about 500 feet and the average

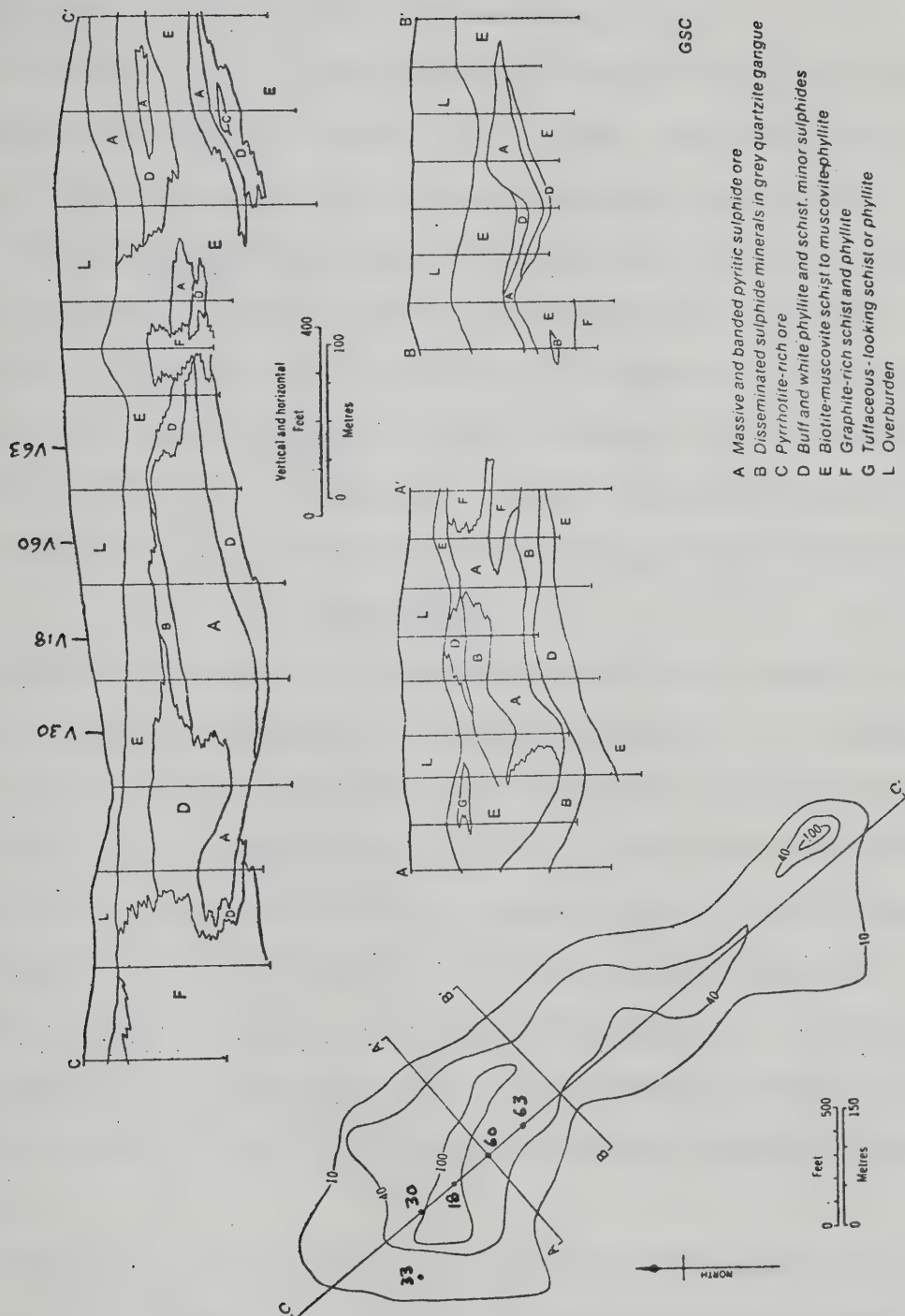


Fig. III-8. Isopach map and cross sections of the Vangorda deposit (after Tempelman-Kluit, 1972).

thickness is 70 feet with a maximum thickness of 200 feet. The orebody dips very gently to the SW. Therefore the orebody appears to be conformable with the schistosity of the enclosing rocks.

A "bleached" zone of rocks forming an irregular halo around the orebody has been noted by Tempelman-Kluit (1972). The nature and origin of this zone is unknown and has not been examined by the writer.

(ii) Ore and Gangue Minerals. The major ore minerals include pyrite, sphalerite, pyrrhotite, galena and chalcopyrite. Magnetite, marcasite and arsenopyrite occur in minor to trace amounts. Tennantite has also been reported among the sulfides (Chisholm, 1957). Gangue minerals include quartz, carbonates and barite (Tempelman-Kluit, 1972); even though barite has not been observed in the specimens available.

Ore Minerals

Pyrite forms fine- to medium-grained (up to 2 mm) subhedral to anhedral crystals, occasionally also as porphyroblasts. In the specimens examined, pyrite often occurs with pyrrhotite, carbonates and sphalerite. In fact, pyrrhotite and carbonates are quite widespread and abundant in the specimens; this is probably due to sampling bias and limitation (good representative lead-zinc-rich cores were not available). Pyrrhotite occurs as fine-grained aggregates replacing pyrite and possibly sphalerite; under the microscope, in addition to patches adjacent to these sulfides, pyrrhotite forms exsolution streaks or veins.

Sphalerite occurs as fine-grained aggregates interbanded with or interstitial to pyritic aggregates, and commonly forms intergrowths with galena wherever seen. Galena is a minor constituent in the spec-

imens examined. Chalcopyrite occurs commonly with pyrite and sphalerite as exsolution blebs, veins and interstitial-fills.

Magnetite is a fairly common mineral observed in the specimens examined, and occurs closely associated with carbonates and pyrrhotite. Marcasite occurs as small mottled patches pseudomorphous after pyrite and pyrrhotite; it appears to be more common in some deformed banded ores. Arsenopyrite is observed as irregular patches or streaks in two specimens of deformed banded ores, and appears to have replaced other minerals, notably quartz, carbonates, and pyrrhotite.

Gangue Minerals

Quartz and carbonates are the only gangue minerals observed in the specimens examined. They are both widespread and relatively abundant, forming fine-grained aggregates as large clasts, veins, interstitial-fills. Under the microscope, quartz shows uniform extinction, whereas carbonates display excellent twin lamellae. A wide range of solid solutions have been determined for the carbonates, which are largely ferromanganese, with varying amounts of Ca, Mg and minute trace inclusions possibly of sphalerite and mica.

Photomicrographs of ore and gangue minerals in some ore specimens are shown in Plate III-10.

(iii) Ore Texture (Plate III-11). The predominant texture observed in the ore specimens examined is a rough but well-defined banding of recrystallized and aggregated pyrite and sphalerite plus carbonates in a grey quartz or "quartzite" gangue rich in pyrrhotite and magnetite. Some porphyroblastic pyritic bands are also observed. The bands are alternately pyrite-quartz and sphalerite-pyrrhotite-carbonates outlined

by streaking and form orientation of the sulfides and gangue. The banding has the same orientation as the F_2 foliation in the enclosing rocks; a folded compositional layering at angles to the banding and apparently corresponding to F_1 in the host rocks is seen locally (Tempelman-Kluit, 1972).

(d) Swim Lakes Deposit. The deposit is located on the hill edge WNW of Swim Lakes, about 10 miles SE of Faro town. It was discovered in 1964 and drilled in subsequent years with a cumulative footage of about 15,000 feet. Published figures indicate the presence of 5 million tons of ore containing 3.75% Pb, 4.8% Zn, 1.5 oz/ton Ag and minor Cu and Au. The ore zone has a major axis about 1,500 feet long and nearly 50 feet wide that trends NW and dips NE at 25° . The average thickness of the orebody is about 70 feet with a maximum of 280 feet in one drill intersection.

The writer has not visited the property or the core shack, and most of the core specimens used in the present study were kindly provided by various geologists, including Tempelman-Kluit, Jennings, Reamsbottom and Cathro. The account of the outline and cross sections of the orebody and some of the mineralogical aspects is from Tempelman-Kluit (1972). The area north of Swim Lakes was visited and examined by the writer in 1973. Some drill hole plan and intersection assay figures were made available to the writer by Kerr Addison Mines Ltd..

(i) Immediate Mine Geology. Outcrop is scarce near the deposit and the orebody itself is not exposed. Small outcrops of grey phyllite of Cambro-Ordovician are found nearby. The outline and cross sections of the deposit (Tempelman-Kluit, 1972) are shown in Fig. III-9. The

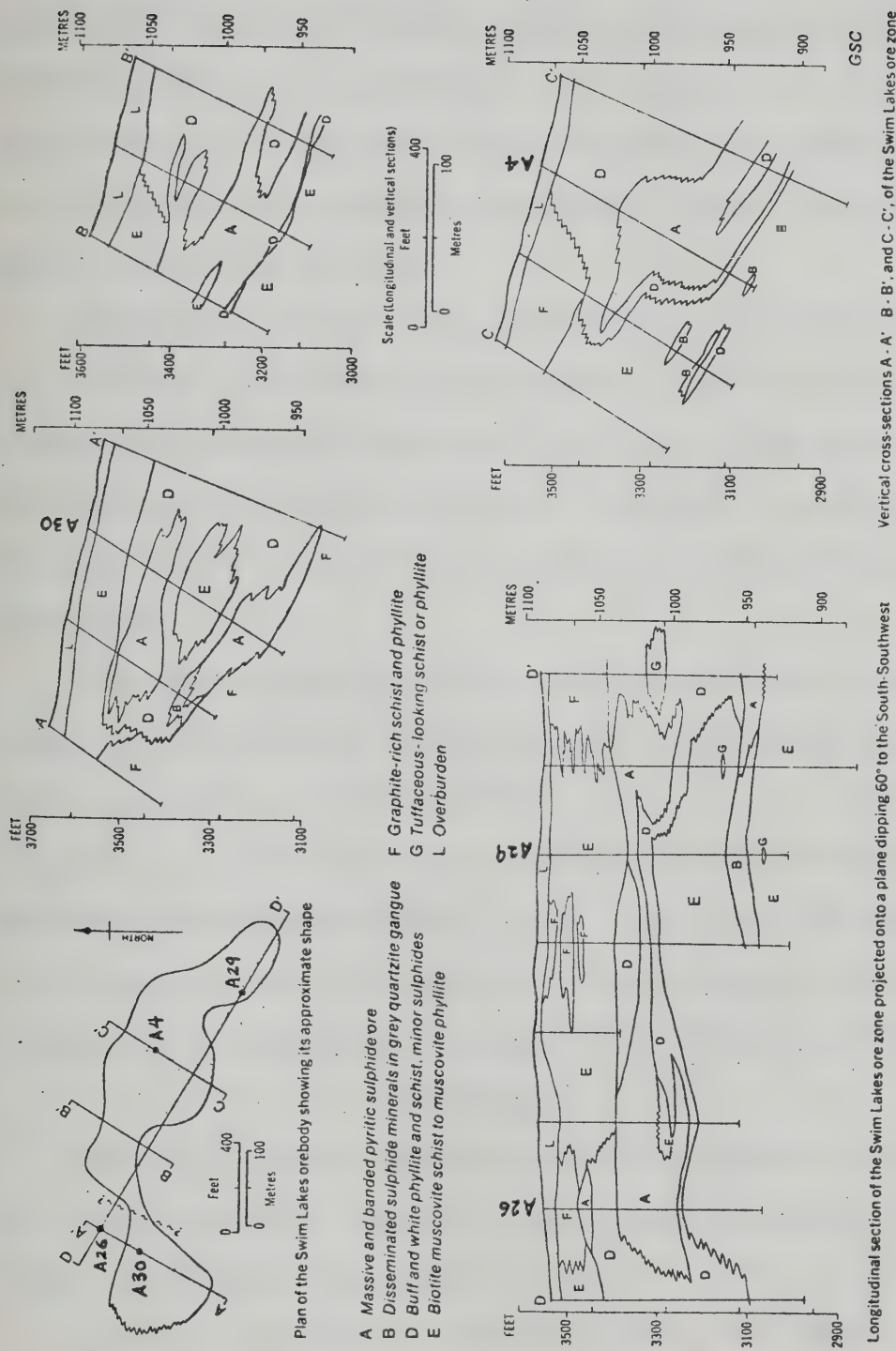


Fig. III-9. Cross sections and map of the Swim Lakes deposit (after Templeman-Kluit, 1972).

orebody is an irregular, tabular, finger-like zone of sulfides partly enveloped by a sequence of buff white quartz-rich sericite phyllite, quartz-chlorite-biotite-muscovite phyllite and graphite phyllite. Tuffaceous laminae in the phyllitic rocks are generally rare, and greenstone volcanic was intersected in only one hole. The tuffaceous rocks are dull green rocks containing fine-grained calcite, chlorite and minor quartz, albite, and muscovite.

Crenulation foliation F_2 is well defined by muscovite in the phyllitic rocks in which small folds defining F_1 between F_2 are also observed. Most rocks near the deposit and north of Swim Lakes display a NW-trending and NE-dipping schistosity presumably corresponding to F_2 . The trend and dip of the orebody appear to be conformable with this schistosity.

(ii) Ore and Gangue Minerals. Ore minerals make up about half the volume of the orebody and include, in order of decreasing abundance, pyrite, sphalerite, galena, pyrrhotite, marcasite and chalcopyrite. Magnetite is a minor constituent. Arsenopyrite and tetrahedrite have also been noted (Tempelman-Kluit, 1972). Gangue minerals noted are quartz, barite, carbonates, and mica. Gypsum occurs as fine prismatic crystals and is commonly found along fractures (Tempelman-Kluit, 1972).

Ore Minerals

Pyrite is the major sulfide and occurs as fine-grained (0.1 to 0.5 mm) cubic to subhedral crystals. Under the microscope some pyritic grains are fragmented and partly corroded.

Sphalerite and galena are the most abundant ore minerals near the central part of the orebody but decrease gradually towards the margin

(Tempelman-Kluit, 1972). Under the microscope, the minerals are mutually intergrown as equigranular aggregates and interstitial-fills around pyrite. In one specimen examined, colloform outline of sphalerite has been observed.

Pyrrhotite is relatively minor and occurs as isolated streaks adjacent to pyrite and sphalerite. Generally it follows foliation in a specimen.

Minor chalcopyrite occurs in sphalerite as tiny exsolution blebs or replacing pyrite. It has been noted that chalcopyrite tends to be more abundant where pyrrhotite is plentiful. Thin, steeply-dipping, regular veinlets of chalcopyrite and pyrrhotite cut banded sulfides locally and transgress their foliation. Marcasite is rare and secondary after pyrite wherever observed.

Magnetite, where observed, occurs closely with carbonates and pyrite and is creamy grey with a pinkish brown tint under the microscope.

Gangue Minerals

Quartz is the major gangue mineral and occurs commonly as disseminated grains or aggregates with the sulfides and only locally as porphyroblastic clasts. Barite is quite common in ore specimens and occurs as fine-grained dissemination, aggregates outlining bands or boudinages, and locally clasts or lenses. About 1% in volume of barite has been estimated for the Swim Lakes deposit. Under the microscope quartz and barite commonly occur as equigranular aggregates intergrown with sulfides in various proportions and occasionally as cementing or interstitial filling. Remobilized and folded barite bands are locally seen.

Carbonate minerals are quite commonly observed in the gangue and closely associated with pyrite and magnetite. Solid solutions including Ca, Mg were detected in the carbonates which are mainly ferromanganese. These carbonates commonly show twinned lamellae under the microscope.

Photomicrographs of ore and gangue minerals in some ore specimens are shown in Plate III-10.

(iii) Ore Texture (Plate III-12). The most common texture in the ore is alternate banding of pyrite and minor quartz, barite with thinner layers of sphalerite, galena, barite and quartz. The banding is considered to correspond with the foliation F_2 of the phyllitic host rocks. Small rootless folds outlining compositional layering F_1 between the F_2 planes were noted (Tempelman-Kluit, 1972). Banding outlined by barite and quartz lenses or streaks in sulfides is locally quite common.

Occasionally the ore shows a rather massive or disseminated texture in which banding is only vaguely recognizable.

PLATE III-1

PHOTOMICROGRAPHS OF ROCK SPECIMENS (TRANSMITTED LIGHT)

Anvil Range District, Yukon

A. Sample KWA13-1: Eclogite, 7 miles SE of Rose Mountain

Euhedral chlorite-rimmed garnet (Gt), fine-grained omphacite (Om), hornblende (Hb), and clinozoisite (Cz) replaces pyroxene. Plane light, X25.

B. Sample KSLK31-1A: Eclogite, western tributary of Vangorda Creek

Chlorite-rimmed garnet (Gt), fine-grained omphacite (Om), hornblende (Hb), and minor quartz. Plane light, X25.

C. Sample KSLA13-4: Eclogite, 7 miles SE of Rose Mountain

Partly chlorite-rimmed garnet (Gt), large hornblende (Hb), fine-grained omphacite (Om), muscovite (Mu), clinozoisite partly replacing garnet, minor quartz (Q). Open nicol, X25.

D. Sample 66-3-172: Greenstone, Faro core sample

Fine- to medium-grained plagioclase (Pl), hornblende (Hb), and pyroxene (Px). Plagioclase and quartz in groundmass. Crossed nicol, X25.

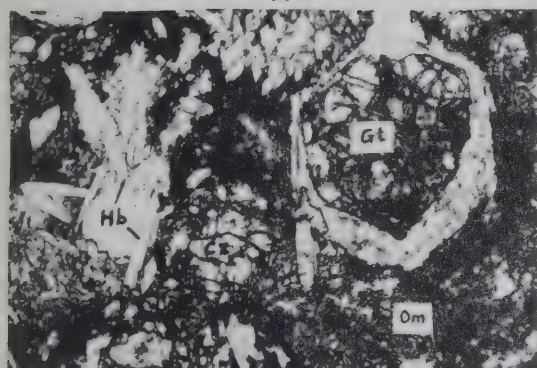
E. Sample KSLK25-4: Foliated greenstone, 8 miles NNE of Mount Mye

Relict grains of partly chloritized pyroxene (Px) and plagioclase (Pl). Foliation is recognizable by form orientation of grains. Groundmass is fine-grained plagioclase, pyroxene and chlorite. Open nicol, X25.

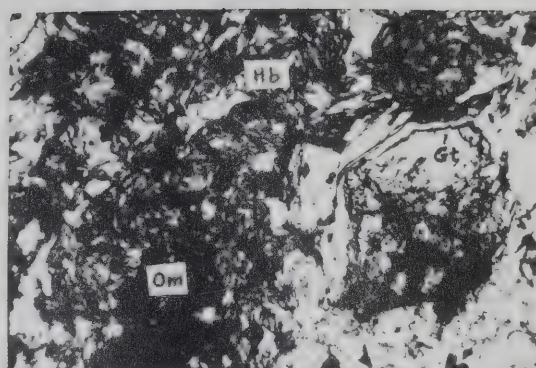
F. Sample KSLK25-4: Foliated greenstone, 8 miles NNE of Mount Mye

Same as E. Crossed nicol, X25.

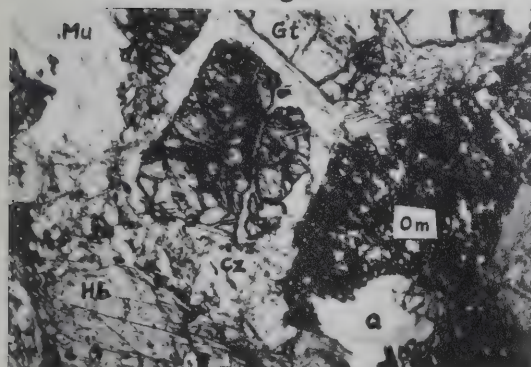
A



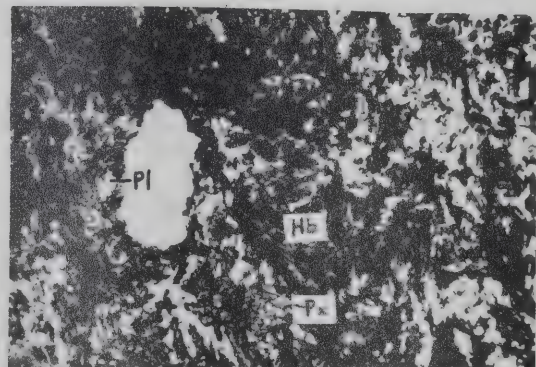
B



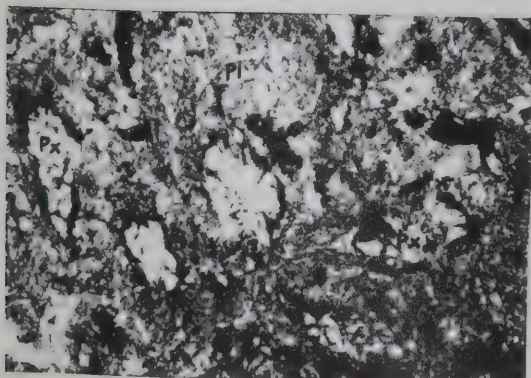
C



D



E



F

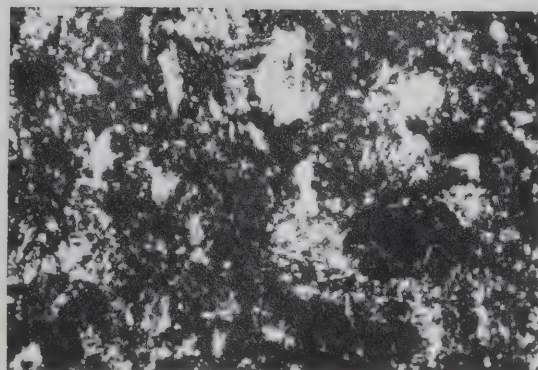


PLATE III-2

PHOTOMICROGRAPHS OF ROCK SPECIMENS
(TRANSMITTED LIGHT, OPEN NICOL, X25)

Anvil Range District, Yukon

A. Sample 67-3: Banded tuff, Faro core specimen

Relict grains of hornblende (Hb), partly altered to epidote and sericite, minor pyroxene (Px) and quartz. X96.

B. Sample KSLK25-4-1: Laminated green chert, 8 miles NNE of Mount Mye

Thin needles of glass (plagioclase? obsidian?) aligned subparallel to bedding (left-right) containing layers of epidote-quartz mix (dark, cloudy) and microcrystalline quartz (white). X96

C. Sample KSLK20-1A: Quartz mica phyllite, 2 miles N of Swim Lakes

Kink cleavages define L₃ (horizontal lineations) in folded F₂. Brighter and medium-grained calcite and sericite (center) interfolded with darker fine-grained chlorite and quartz (right, and near left edge).

D. Sample 66-8-868: Quartz-chlorite-mica schist, Faro core specimen

Biotite (Bt) and muscovite (Mu) forming bird-eye structures at left. Relict grains of pyroxene (Px) and biotitized hornblende (Hb) in quartz. A layer of chlorite (Ch) in central left.

E. Sample 66-10-485: Quartz-chlorite-mica schist "breccia", Faro core specimen

"Breccias" or fragments of schistose rock composed of quartz, chlorite, muscovite and minor hornblende set in a groundmass of "tuff breccia" composed of quartz, chlorite, mica, and opaque iron oxides.

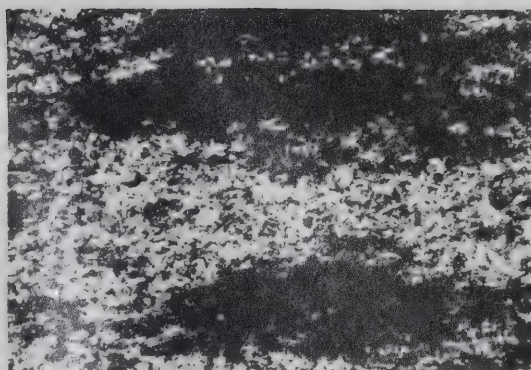
F. Sample KSLA12-2B: Serpentinized peridotite, Pelly River bank S of Orchay Lakes

Relict grains of olivine (Ol) veined by and serpentinized to antigorite (At), enstatite (En) partly serpentinized to bastite. Opaque minerals are identified as magnetite, ilmenite and perovskite.

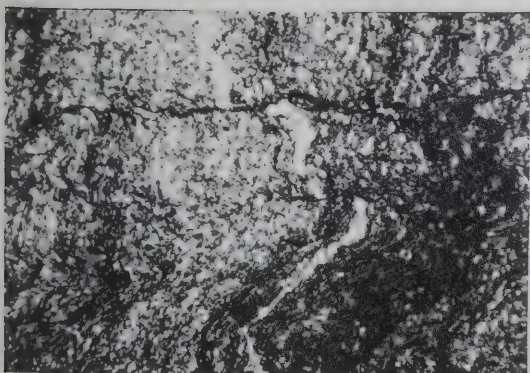
A



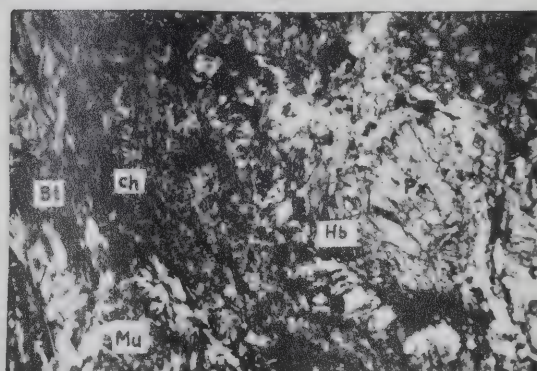
B



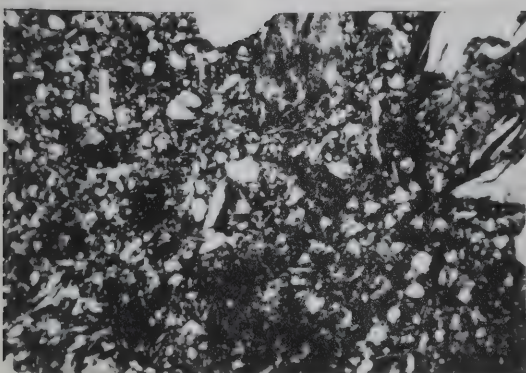
C



D



E



F

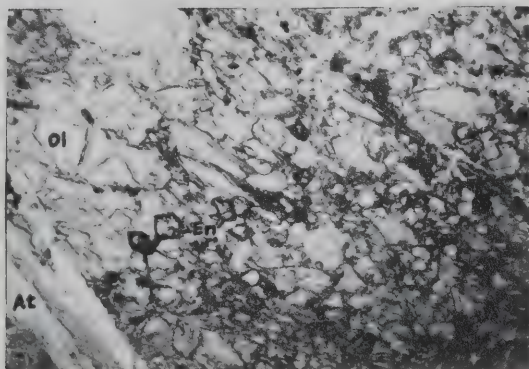


PLATE III-3

PHOTOMICROGRAPHS OF ROCK SPECIMENS (TRANSMITTED LIGHT)

Anvil Range District, Yukon

A. Sample KSLK25-2: Basalt flow, 8 miles NNE of Mount Mye

Medium-grained laths of plagioclase (Pl), uralitized hornblende (Hb), and pyroxene epidotized to prehnite (Pn). Plane light, X25.

B. Sample KSLK25-2: Basalt flow, 8 miles NNE of Mount Mye

Same as A. Crossed nicol, X25.

C. Sample KSLA12-1: Massive basalt flow, Pelly River bank S of Orchay Lakes

Saussuritized plagioclase (Pl), strongly uralitized and epidotized hornblende (Hb), and small grains of pyroxene (Px), mostly augite. Minor fine-grained chlorite (mostly penninite ?) streaks in the groundmass. X25.

D. Sample KSLA12-1: Massive basalt flow, Pelly River bank S of Orchay Lakes

Same as C. Crossed nicol, X25.

Frances Lake District, Yukon

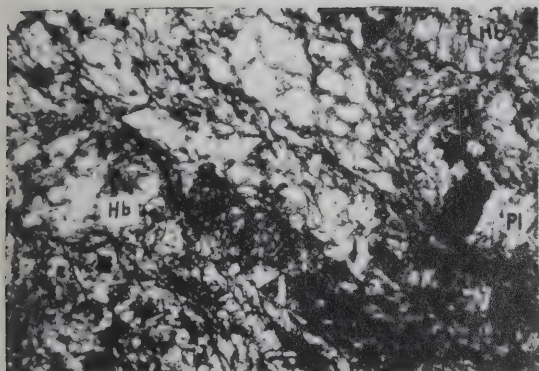
E. Sample 139-1: Calcareous phyllite, west of East Arm

Relict grains of calcite (Cc) and microcrystalline quartz (Q) set in a groundmass of fine-grained epidote, chlorite, calcite and quartz. X25.

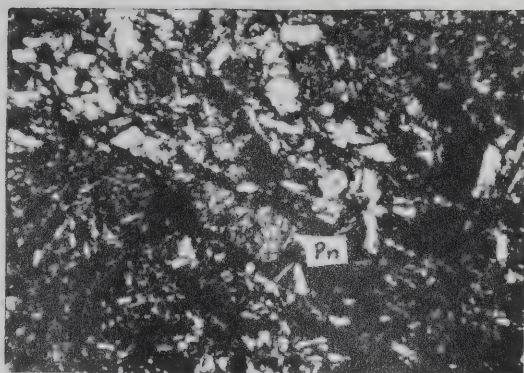
F. Sample 139-1: Calcareous phyllite, west of East Arm

Same as E. Crossed nicol, X25.

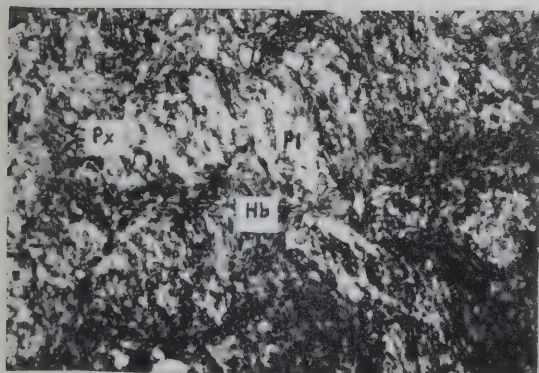
A



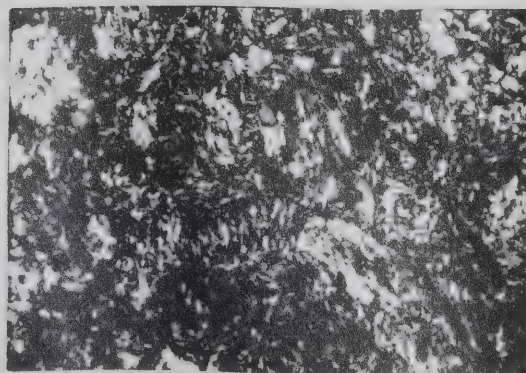
B



C



D



E



F

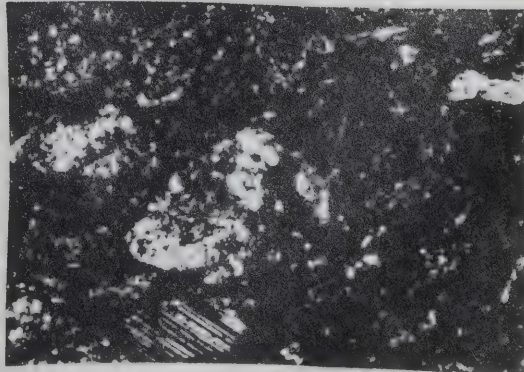


PLATE III-4

PHOTOMICROGRAPHS OF ORE SPECIMENS
(REFLECTED PLANE LIGHT, X38)

Faro Deposit

A. Sample DDH67-4-460: Massive ore

Porphyroblastic pyrite (Py) with intergrown sphalerite (Sp) and galena (Gn). Siderite (Sd) replaces sulfides.

B. Sample DDH67-6-602: Massive foliated ore

Intergrown sphalerite (Sp), galena (Gn), barite (dark grey) and pyrite (Py). Minor quartz (black). Note colloform outline at sphalerite-galena boundary.

C. Sample DDH67-6-762: Banded ore

Fine-grained intergrown sphalerite (Sp) and galena (Gn) and some fractured pyrite (Py). Quartz veins cut the specimen.

D. Sample DDH67-10-549: Porphyroblastic ore

Brecciated and fractured pyrite (Py) porphyroblasts veined or partly replaced by quartz (Q), siderite (black), sphalerite (Sp), chalcopryite (Cpy), and marcasite (Mc). Note cubic form of recrystallized pyrite in vein.

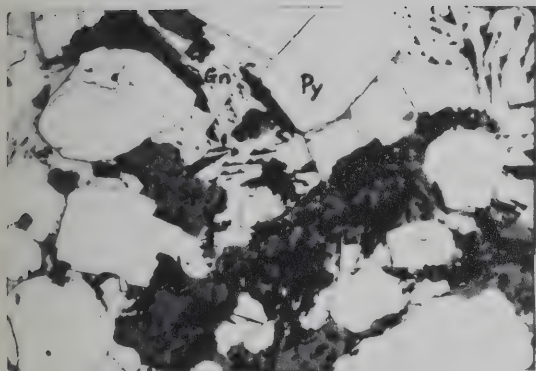
E. Sample DDH66-22-305: Foliated baritic ore

Partly corroded, porphyroblastic pyrite (Py) and intergrown sphalerite (Sp), galena (Gn), and barite (black). Note colloform outline of sphalerite. Minor quartz (Q).

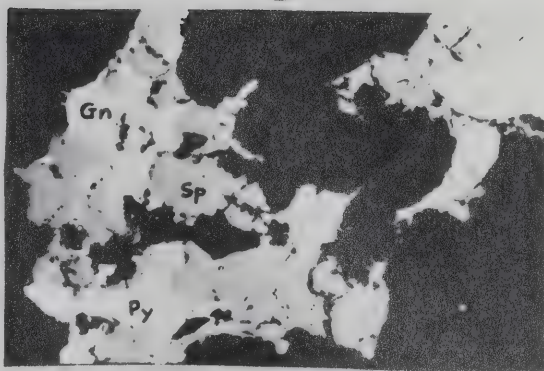
F. Sample from Faro open-pit: Strongly foliated ore

Foliation or schlieren outlined by form orientation of grains of pyrite (Py), pyrrhotite (Po), sphalerite (medium grey), galena (light grey streaks), chalcopryite (Cp) and quartz (Q).

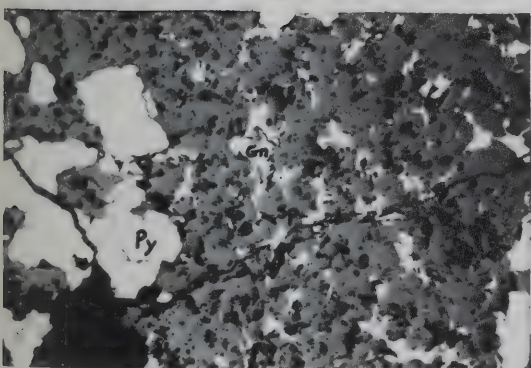
A



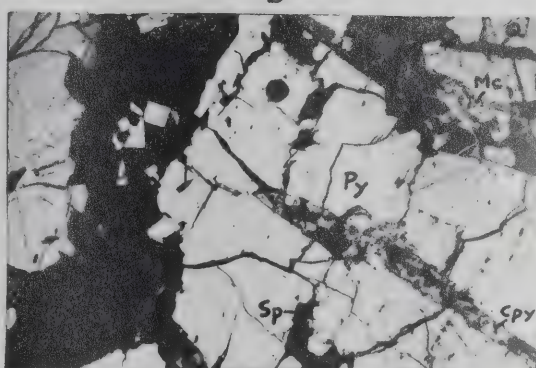
B



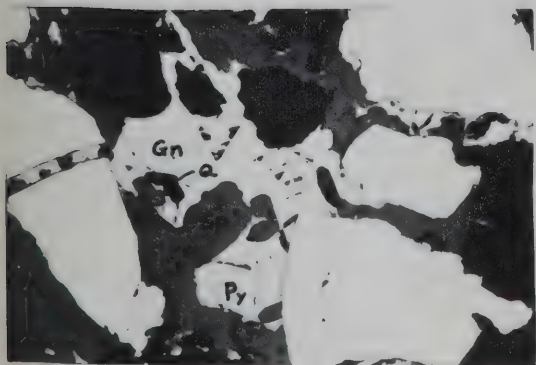
C



D



E



F

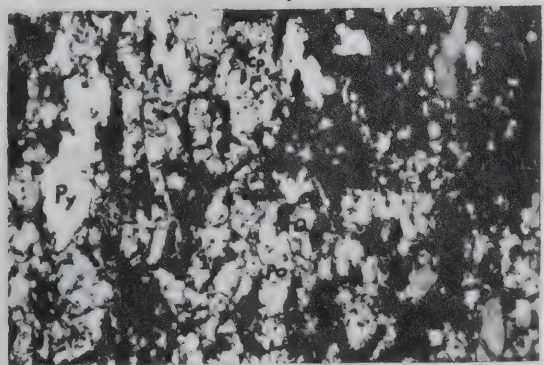


PLATE III-5

PHOTOGRAPHS OF ORE SPECIMENS
(REFLECTED PLANE LIGHT)

Faro Deposit

A. Sample DDH66-22-305: Massive foliated ore

Pyrite (light grey), sphalerite-galena (dark grey), barite (pearl white); typical baritic ore.

B. Sample DDH66-2-283: Massive banded ore

Form orientation of pyrite (light grey), sphalerite-galena (dark grey), barite (pearl white to light greyish white); minor quartz (white).

D. Sample DDH66E9-299: Massive ore

Weak foliation of barite, sphalerite, galena, pyrite and quartz; typical baritic ore.

D. Sample DDH67-6-762: Massive porphyroblastic ore

Foliation or banding is visible.

E. Sample DDH67-6-602: Massive foliated ore

Form orientation of barite (light grey to pearly white), sphalerite-galena (medium to dark grey); typical baritic ore.

F. Sample DDH67-10-632: Massive porphyroblastic ore

Contains pyrite (light grey), sphalerite and galena (medium grey), and fragments or clasts of siliceous and phyllitic rock at left.

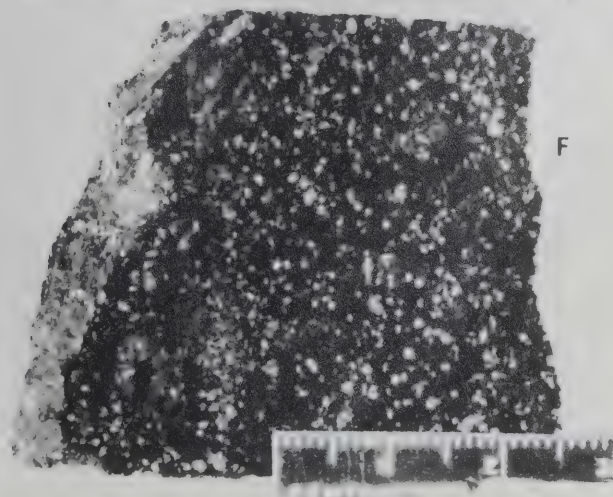
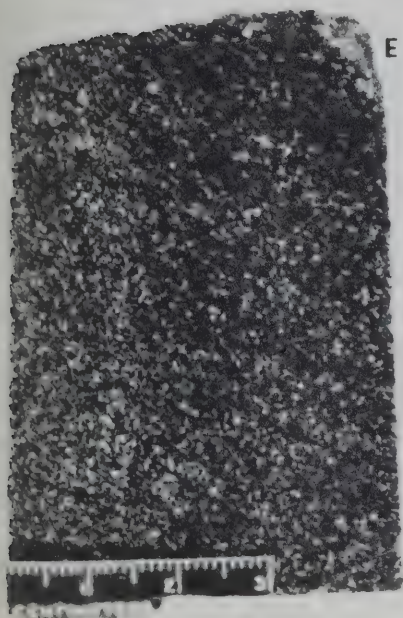
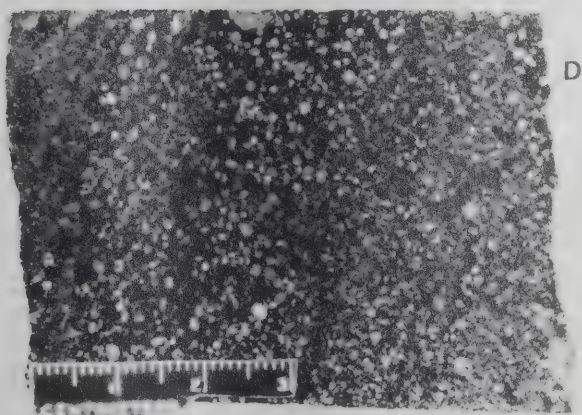
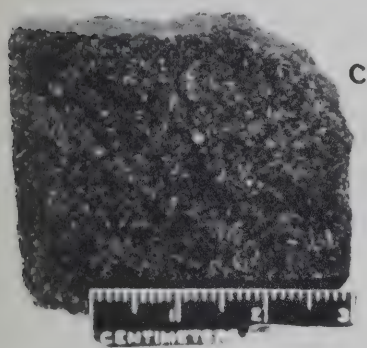
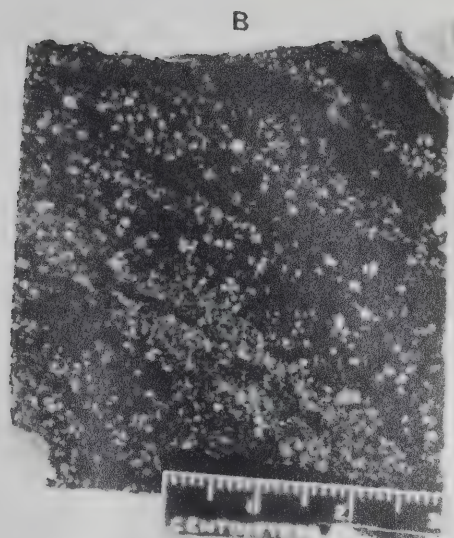
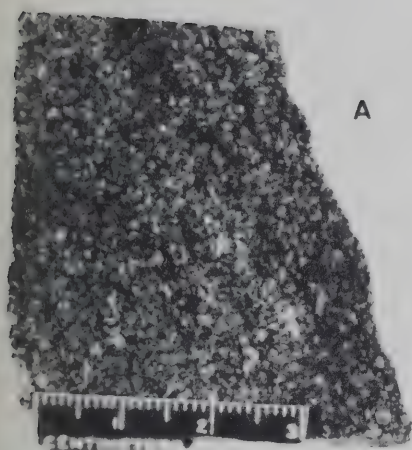


PLATE III-6

PHOTOGRAPHS OF ORE SPECIMENS
(REFLECTED PLANE LIGHT)

Faro Deposit

A. Sample DDH-66E9-436: Deformed fragmented ore

Massive sulfide fragments (central) set in and veined by quartz-mica phyllite and quartz. Note sharp termination of massive sulfides at upper contact.

B. Sample DDH66-10-573: Deformed brecciated ore

Fragments of pyrite (light grey), pyrrhotite (medium grey), sphalerite-galena (dark grey) at top and strongly altered clasts or breccias of quartz and barite below.

C. Sample DDH67-6-754: Folded ore

Porphyroblastic sulfides and siliceous clasts or fragments.

D. Upper DDH67-6-710: "Sandy" ore

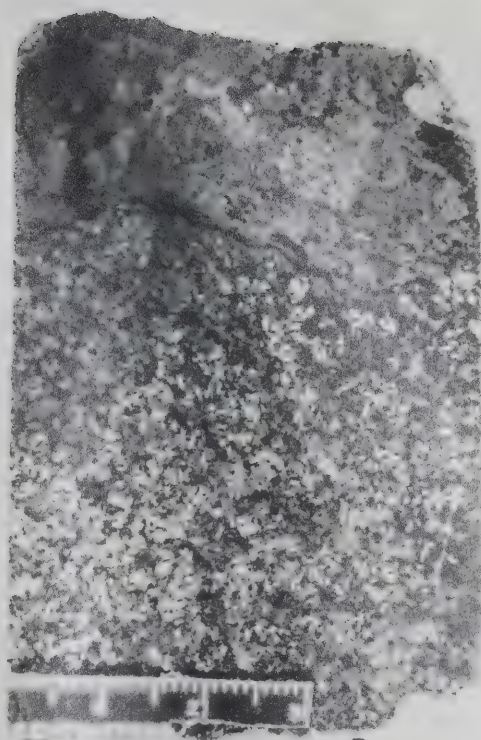
Loosely cemented equigranular pyrite (light medium grey), barite (white to light grey), and sphalerite-galena (dark grey to black).

Lower DDH66-10-634: Pyritic "sandy" ore

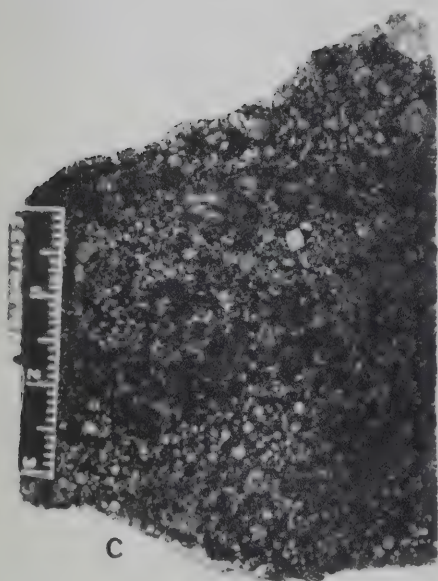
Same texture as above, except coarser-grained and with more sphalerite and galena. Note abundant barite grains near top.



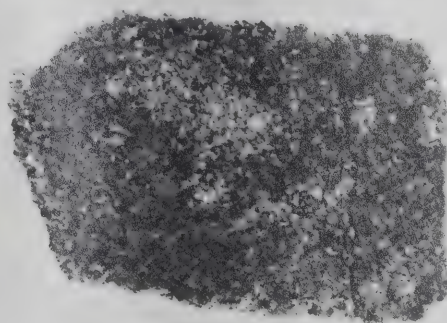
A



B



C



D

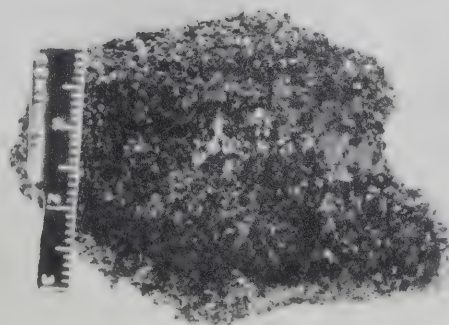


PLATE III-7

PHOTOMICROGRAPHS OF ORE SPECIMENS
(REFLECTED PLANE LIGHT, X38)

Grum Deposit

A. Sample DDH-A5-422: Banded ore

Subrounded to pellet-like pyrite (Py) with finely intergrown sphalerite (Sp), galena (Gn) and quartz (Q).

B. Sample DDH-A10-529: Banded ore

Subrounded to pellet-like pyrite (Py) scattered in very finely intergrown sphalerite (Sp), galena (Gn) and quartz (Q). Larger patches of siderite (Sd) partly replace the sulfides at upper right.

C. Sample DDH-A10-744: Massive folded ore

Partly corroded subhedral pyrite (Py) with intergrown sphalerite (Sp), galena (Gn) and chalcopyrite (Cpy). Larger patches of siderite (Sd) and magnetite (Mgt) replace other sulfides. Some grains of magnetite and pyrrhotite (Po) are also seen replacing other sulfides.

D. Sample DDH-A10-774: Banded ore

Granular subhedral pyrite (Py) with intergrown sphalerite (Sp), galena (Gn), barite (Brt) and quartz (Q).

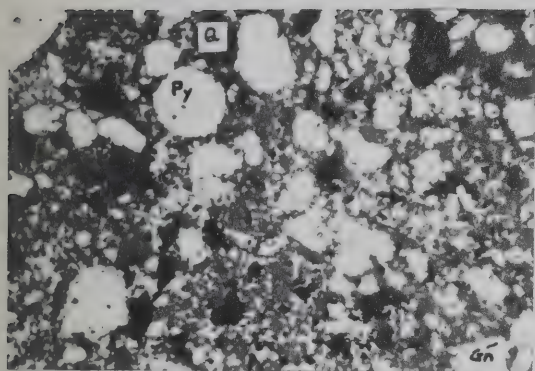
E. Sample DDH-A10-802A: Banded ore

Cubic and angular euhedral pyrite (Py) and intergrown sphalerite (Sp), galena (Gn). Siderite (Sd) and minor quartz (Q) replace sulfides.

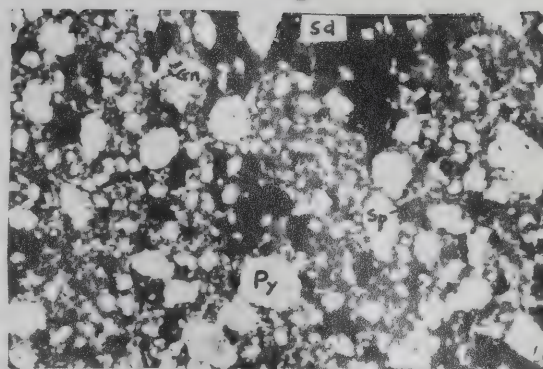
F. Sample DDH-A12-538: Banded ore

Contact between pyrite (Py) rich band and sphalerite (Sp) and galena (Gn) rich band. Note coarser grain size of pyrite at left in contrast to very fine-grained intergrown sphalerite, galena and quartz.

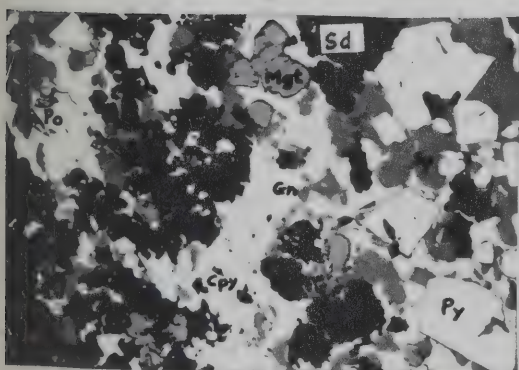
A



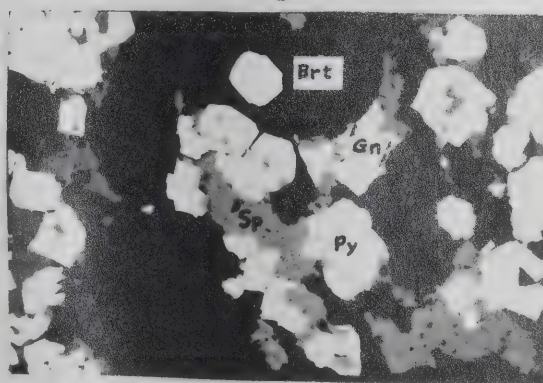
B



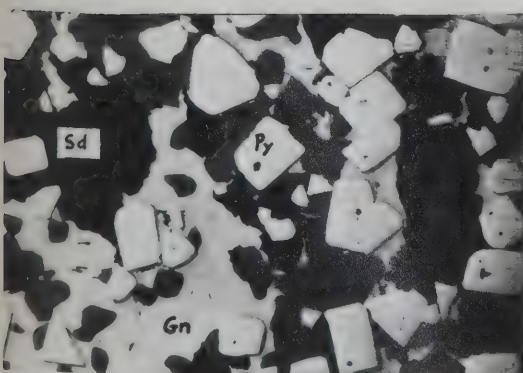
C



D



E



F

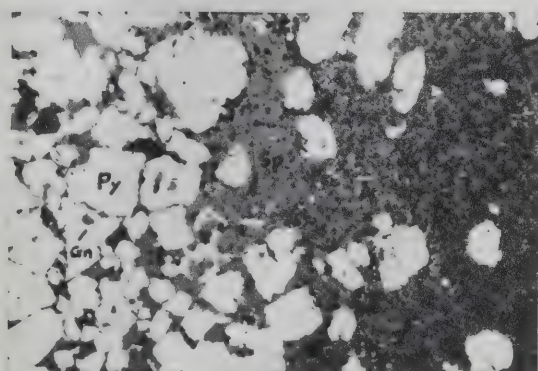




PLATE III-8

PHOTOGRAPHS OF ORE SPECIMENS
(REFLECTED PLANE LIGHT)

Grum Deposit

A. Sample DDH-A5-425: Banded ore

Fine-grained pyritic bands (grey) and sphalerite and galena-rich bands (dark) with disseminated pyrite.

B. Sample DDH-A10-529: Banded ore

Some quartz clasts disseminated in sulfide bands.

C. Sample DDH-A11-497: Banded ore

Sphalerite-galena-rich bands (dark) delicately banded with fine-grained pyrite-rich bands. Some quartz clasts disseminated in the former.

D. Sample DDH-A10-774: Massive interbanded ore

Sphalerite, galena, pyrite and barite veined by quartz and barite. Note coarser pyrite at lower part and finer sphalerite-galena near upper part of each alternation resembling "graded bedding".

E. Sample DDH-A12-538: Massive interbanded ore

Delicate banding of pyrite, sphalerite, galena and quartz.

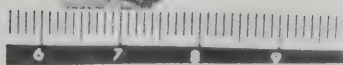
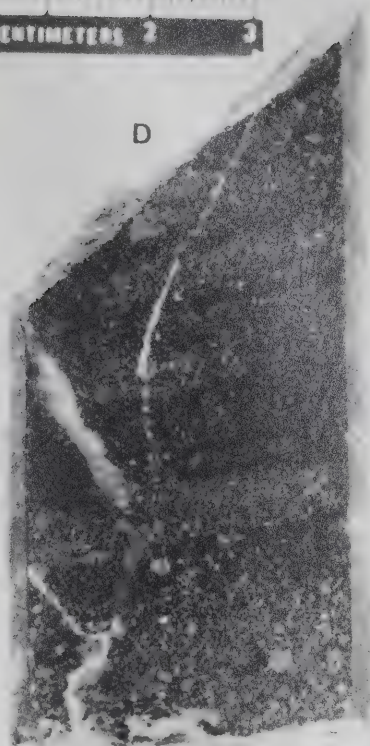
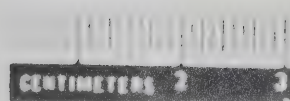
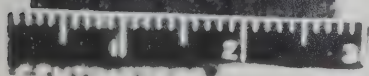
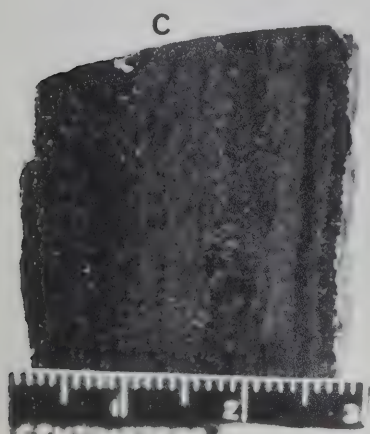
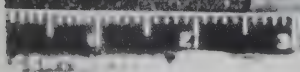
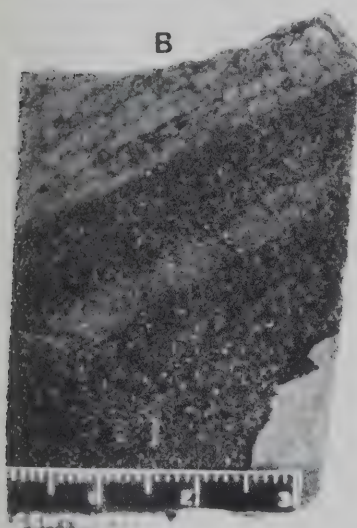
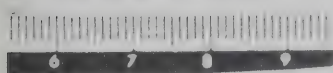
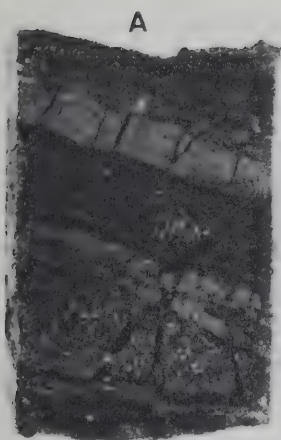


PLATE III-9

PHOTOGRAPHS OF ORE SPECIMENS
(REFLECTED PLANE LIGHT)

Grum Deposit

A. Sample DDH-A10-575.5: Deformed massive ore

Fragments of deformed quartzose phyllite (dark grey) and clastic quartz (medium grey).

B. Sample DDH-A10-744: Massive folded ore

Contains deformed bands of sulfides, clastic fragments of quartz-siderite (medium grey) and quartz veins.

C. Sample DDH-A11-503: Brecciated ore

Pyrite breccia fragments (grey) and small quartz clasts (white) set in a matrix of disseminated fine- to medium-grained sulfides, siderite and quartz.

D. Sample DDH-A10-616:

Disseminated sulfides (mainly pyrite, minor sphalerite, galena) in sheared quartz-mica phyllite (dark grey). Sulfides show apparent replacement relationship to rock.

E. Sample DDH-A10-802

Clastic pyrite aggregates (medium grey) containing minor sphalerite and galena in quartz-mica graphitic phyllite. Note fragments and streaks of rock (dark grey) and quartz (white) in central part and F₂ foliation of phyllite at top. Some thin quartz veins cut the specimen.

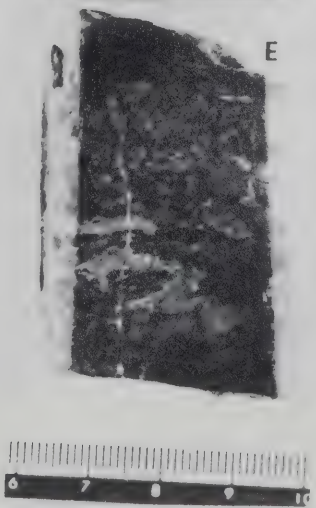
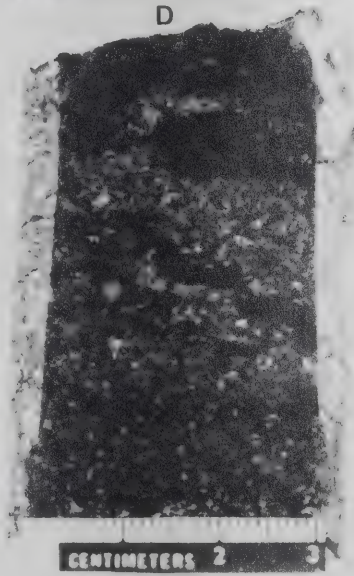
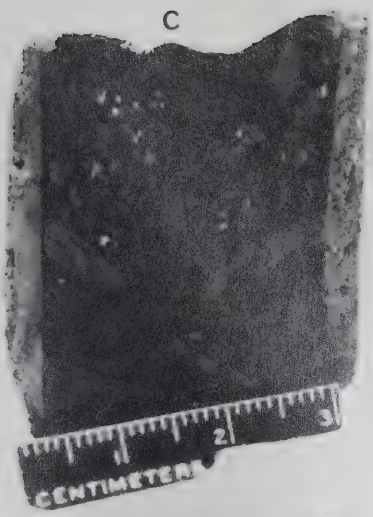


PLATE III-10

PHOTOMICROGRAPHS OF ORE SPECIMENS
(REFLECTED PLANE LIGHT, X38)

Swim Lakes Deposit

A. Sample DDH-A4-281: Banded ore

Angular to cubic pyrite (Py) set in sphalerite (Sp) and minor galena (Gn). Siderite (Sd) occurs as patches in sphalerite and pyrite. Note contact between recrystallized angular pyrite and fine-grained "primary" pyrite.

B. Sample DDH-A4-426: Massive ore

Intergrown sphalerite (Sp), galena (Gn) replaced by siderite (Sd), pyrite and magnetite (Mgt). Note colloform outline of sphalerite.

C. Sample DDH, location unknown: Massive ore

Slightly corroded pyrite (Py) and intergrown sphalerite (Sp) and galena (Gn). Siderite (Sd) and magnetite (Mgt) replace sulfides.

Vangorda Deposit

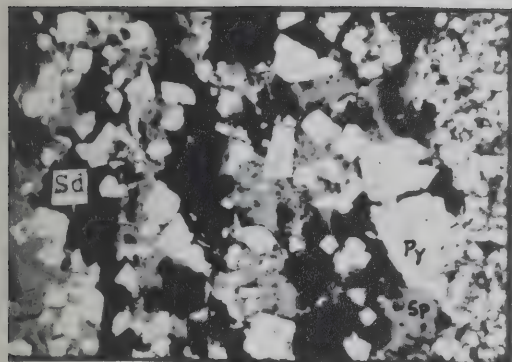
D. Sample DDH-18-120: Deformed banded ore

Deformed band containing arsenopyrite (Asp), pyrrhotite (Po), sphalerite (Sp), galena, magnetite (Mgt), siderite (Sd), and quartz (Q). Note contact with a pyritic band at extreme left.

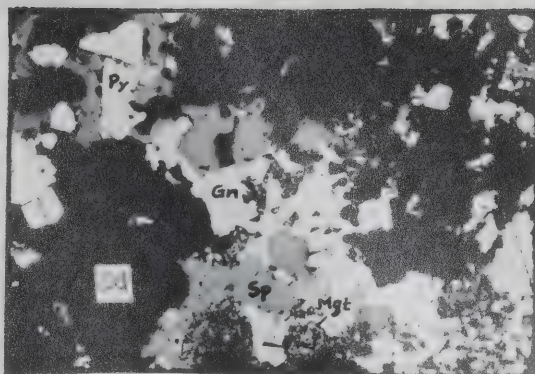
E. Sample DDH-33-279: Deformed banded ore

Angular, partly corroded pyrite (Py) and intergrown sphalerite (Sp) and galena (Gn). Siderite (Sd), magnetite (Mgt) and pyrrhotite (Po) replace sulfides.

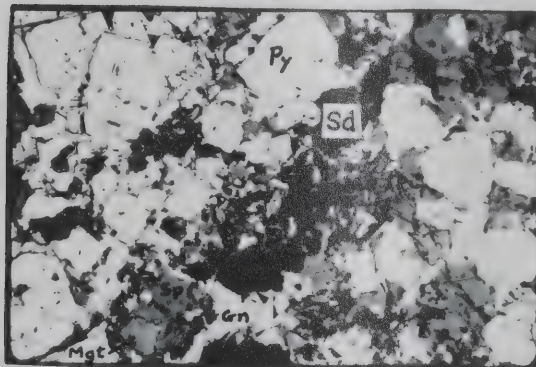
A



B



C



D



E

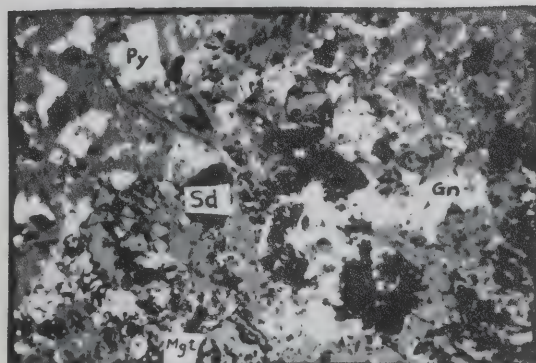




PLATE III-11

PHOTOGRAPHS OF ORE SPECIMENS
(REFLECTED PLANE LIGHT)

Vangorda Deposit

A. Sample DDH18-120: Banded ore

Bands of recrystallized pyrite and minor quartz (light grey) interfoliated with darker bands of siderite, magnetite, pyrrhotite and minor sphalerite.

B. Sample DDH63-135: Foliated massive-ore

Contains medium-grained pyrite (medium grey), pyrrhotite, magnetite, siderite and sphalerite bands (dark grey) and quartz clasts (light grey).

C. Sample DDH18-205: Massive folded ore

Fine-grained sulfides (grey) mostly pyrite and minor sphalerite, pyrrhotite, and siderite and magnetite bands (dark grey).

D. Sample DDH18-189: Partly banded and recrystallized massive ore

Fine-grained foliated sulfides in quartz-carbonate matrix (light grey and dark grey areas at bottom and top). Some recrystallized and porphyroblastic pyrite formed in sideritic carbonate zone at upper part.

E. Sample DDH63-223: Recrystallized "porphyritic" massive ore

Contains angular pyrite and medium-grained quartz fragments (light grey) in a quartz-siderite-magnetite matrix.

F. Sample DDH33-279: Deformed disseminated ore

Sulfides (light grey) are mainly pyrite, sphalerite, galena and pyrrhotite in siliceous matrix rich in quartz and carbonates.

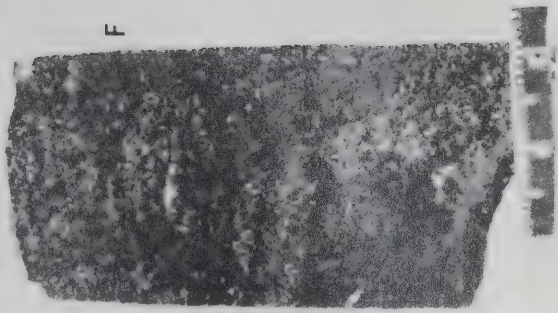
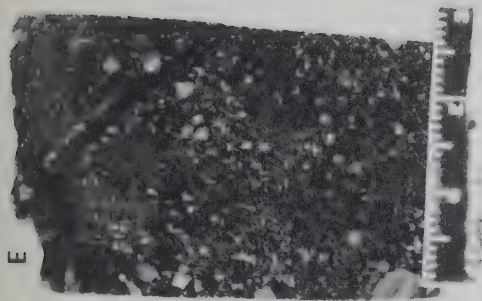
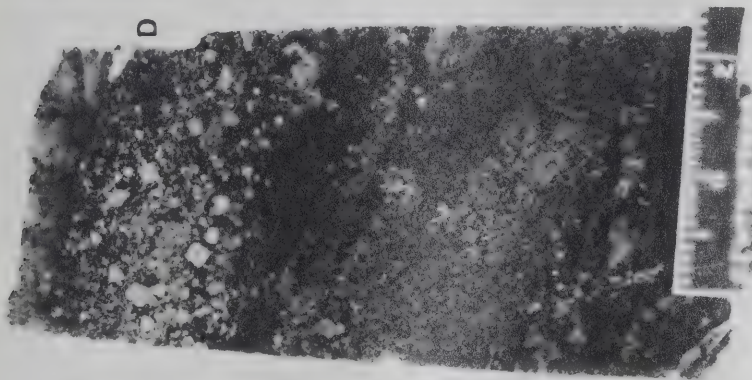
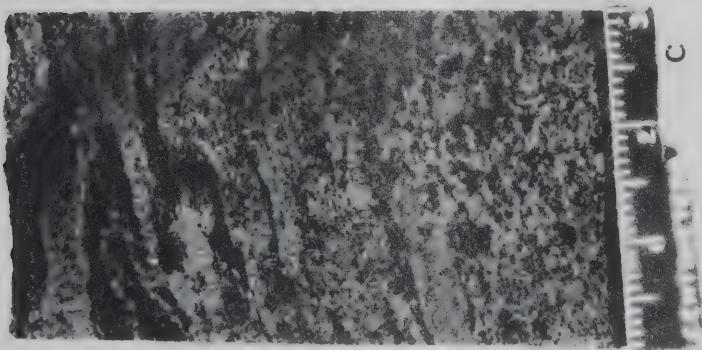
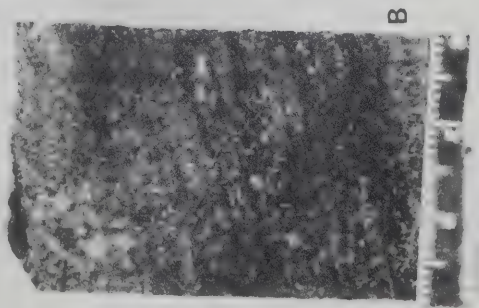
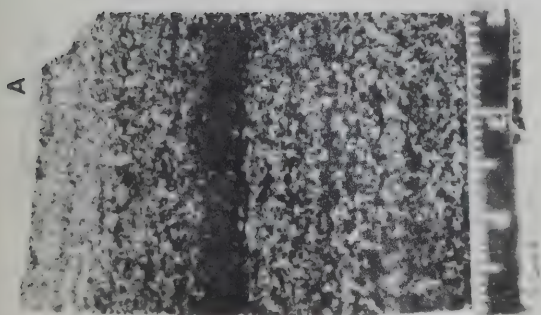


PLATE III-12

PHOTOGRAPHS OF ORE SPECIMENS
(REFLECTED PLANE LIGHT)

Swim Lakes Deposit

A. Sample DDH-A4-281: Banded ore

Delicate banding of fine-grained pyrite (light grey), sphalerite-galena (medium grey), and siderite and quartz (dark grey). Note some tiny disseminated quartz and barite grains (white).

B. Sample DDH-A4-258: Massive foliated ore

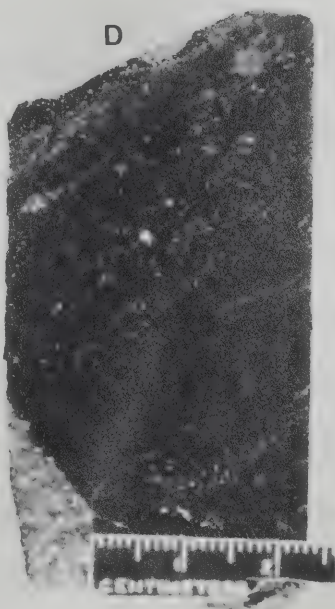
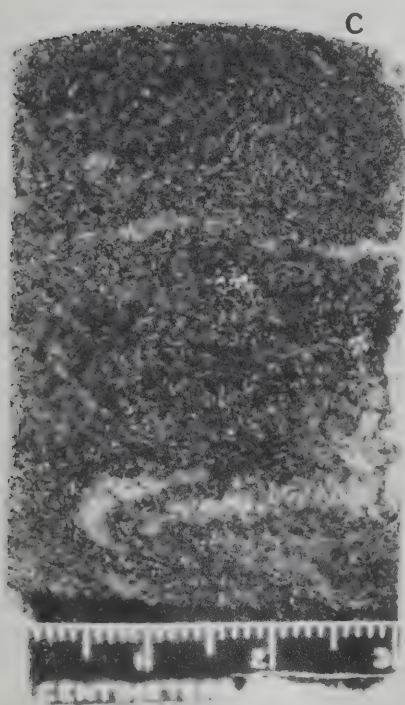
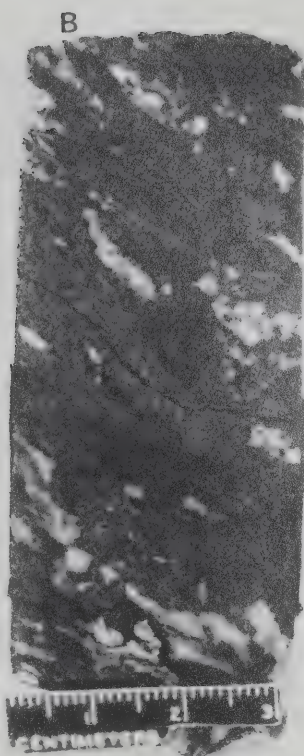
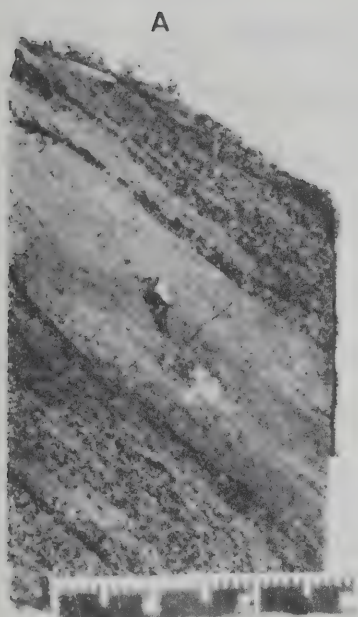
Very fine-grained sulfides showing "patches" of pyritic (light grey) and sphalerite-galena-rich (medium grey) roughly coincide with foliation outlined by form orientation of lenses of barite and quartz. Note small sideritic carbonate veins (black).

C. Sample DDH-A4-296: Massive folded ore

Interfolded sulfides and quartz-barite (white) layers. Pyrite (light grey), sphalerite (medium grey) and minor galena (bright white) set in a matrix mostly occupied by siderite and minor quartz.

D. Sample DDH-A4-457: Massive foliated ore

Disseminated to thinly foliated pyrite (light grey) in dense sphalerite, galena and carbonate-rich matrix. Some siliceous clasts or patches at top.



C. FRANCES LAKE DISTRICT

1. Location and Access

The district under study covers an area on both sides of the northern and central part of the East Arm of Frances Lake (Fig. III-10). There are several base metal sulfide occurrences in the district, including one lead-zinc-silver deposit on Thompson Creek situated on the eastern shore of the East Arm. The district is about 95 miles NNW of Watson Lake and about 100 miles ESE of Ross River and located between latitudes $61^{\circ}24'N$ to $61^{\circ}36'N$ and longitudes $129^{\circ}15'W$ to $129^{\circ}35'W$.

The district can be reached by float aircraft or helicopter from Watson Lake or by the Watson Lake road to the west shore of the West Arm of Frances Lake and then by boat in the summer or by bombardier in the winter to the camp site.

2. Physiography

The district is located physiographically at the western edge of the NS-trending Frances Lake belt which outlines a mountain range composed mostly of Cretaceous batholiths. In the eastern part of the district, the batholith forms the core of Mount Hunt which includes a series of steep ridges as high as 7,000 feet. To the southwest Simpson Tower, also cored by intrusive rocks, reaches a height of 5,500 feet. Areas to the west, southeast and along Anderson Creek are mainly low rounded hills and open valleys which were probably formed by the last Pleistocene glaciers. In places fault scarp topography is pronounced.

The drainage system in the eastern part is controlled by Mount Hunt and numerous creeks have carved out steep gulleys which flow radially

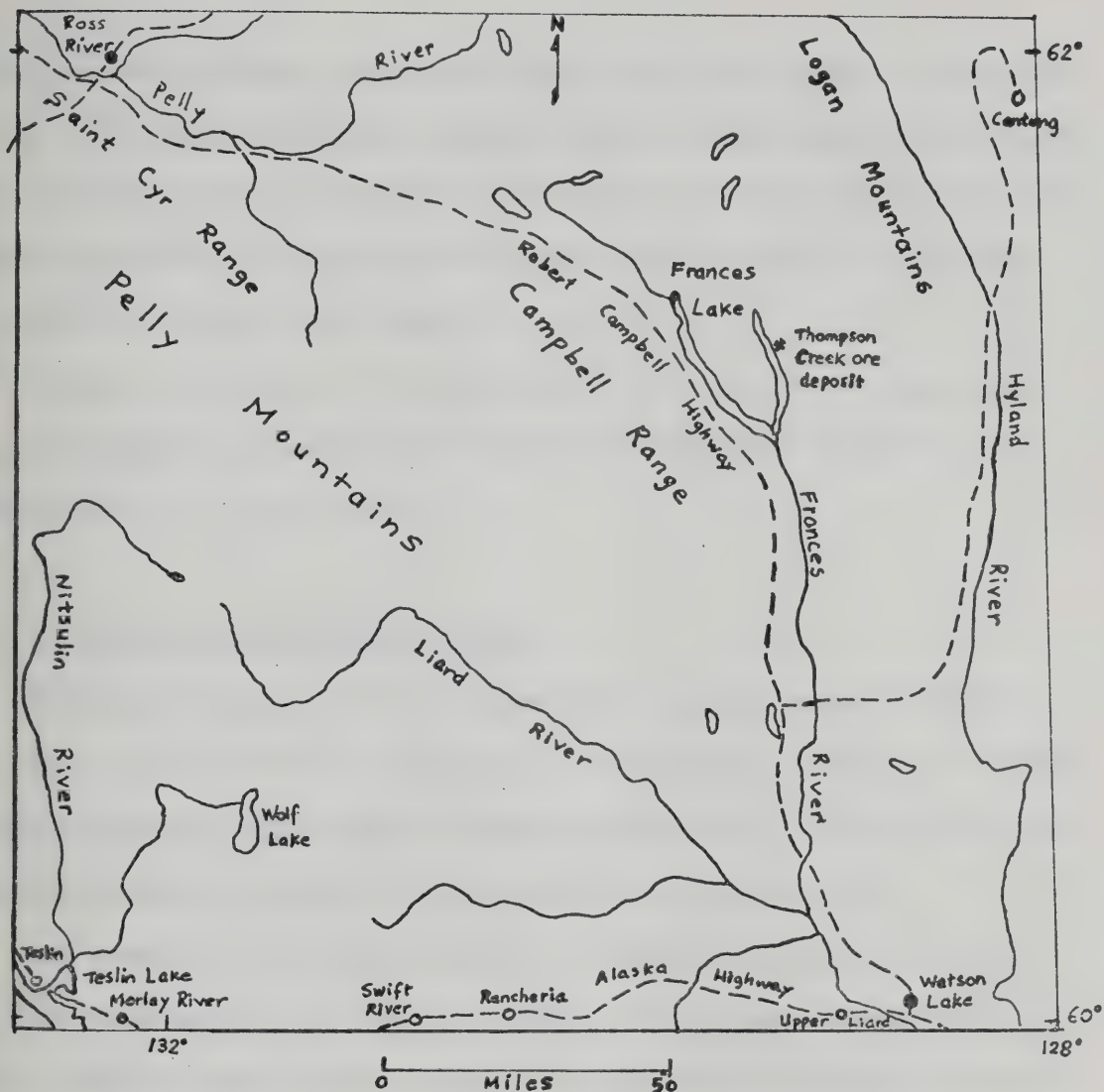


Fig. III-10. Location of Thompson Creek ore deposit, Frances Lake district, Yukon.

from the mountain range. Anderson Creek, which flows WSW into East Arm, is one of the major drainages from the high mountain ranges to the east. The drainage system of the western part is controlled by moderately high ranges running NS and parallel to Frances Lake; creeks flow into East Arm and West Arm from this range.

Cirques are common at the headwaters of creeks in the Mount Hunt ranges, whereas rock-basin ponds are abundant near the summit of the moderate to low rounded hills.

3. Fieldwork and Exploration History

Geological mapping of the Frances Lake map-area began in 1953 by E.F. Roots of the G.S.C.. Geologists of the survey carried out numerous mapping programs in the map-area subsequently, these include L.H. Green and J.A. Roddick in 1960, and S.L. Blusson in 1962 and 1965.

The Thompson Creek deposit and the related claims were acquired by Matt Berry Mines Ltd. of Toronto in 1965. The deposit was drilled in 1966, 1968 and 1969. Further claims were staked or acquired in the surrounding areas in 1971. In 1970, a joint venture project was embarked to carry out systematic detailed geological mapping, a geophysical survey of the district and further drilling. Companies participating in the project included Canadian Nickel Co. Ltd., Metallgesellschaft Canada Ltd. and Matt Berry Mines Ltd.

Detailed geological mapping of the district was accomplished in 1971 by the writer and H. Thalenhorst for the Joint Venture project.

The drilling program was resumed in 1973 but no significant results were obtained.

4. General Geology

A general geological map of the district showing major rock units and related structures is shown in Fig. III-11. Correlation of some geological boundaries is uncertain due to overburden.

Table III-2 gives ages, estimated thickness and features of major rock units of the district.

Flanking the western and northern sides of Mount Hunt and at the western side of the East Arm, a series of metasediments and minor volcanic tuffs and flows of Cambrian age is exposed. At the western and southeastern parts, a younger sequence of metasediments (Ordovician to Mississippian) overlies the Cambrian strata in apparent unconformity.

Rocks surrounding the batholiths are generally converted to hornfelses which include banded and massive calc-silicate rocks, spotted flinty rocks and massive biotite hornfelses.

Intrusive rocks forming batholiths are mainly Middle Cretaceous biotite quartz monzonites.

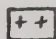
More detailed descriptions on rock units of Cambrian to Devonian strata, hornfelses and intrusive rocks are given in Appendix III-4.

5. Structural Geology and Regional Metamorphism

(a) Internal Structures. Internal structures observed in rock units of the district probably represent at least two major phases of deformation. The older deformation is most pronounced and can be represented by an earliest folding, a later development of foliation and refolding. The earliest folding has a regional axis (in both sides of the East Arm) trending NNW and plunging gently in that direc-

LEGEND FOR FIG. III-11

Middle Cretaceous

 Biotite quartz monzonite

(Intrusive Contact)


Hornfelses and skarns

C Carbonate-rich calc-silicate hornfels

S Silicate-rich calc-silicate hornfels


B Biotite hornfels

Devonian-Mississippian

 Micaceous slate and shale with intercalated greywacke


(Unconformity ?)

Silurian-Devonian

 Intercalated quartzite, dolomite, dolomitic slate, and minor limestone

(Conformity)

Middle Ordovician-Silurian


 Black slate and shale, locally dark impure limestone


(Unconformity)

Middle and Upper Cambrian

 Black siliceous phyllites and slates, locally graphitic and chloritic

 Quartz-sericite-chlorite schist

 Metavolcanics

 Intercalated calcareous phyllites, silty phyllites, and phyllitic limestone

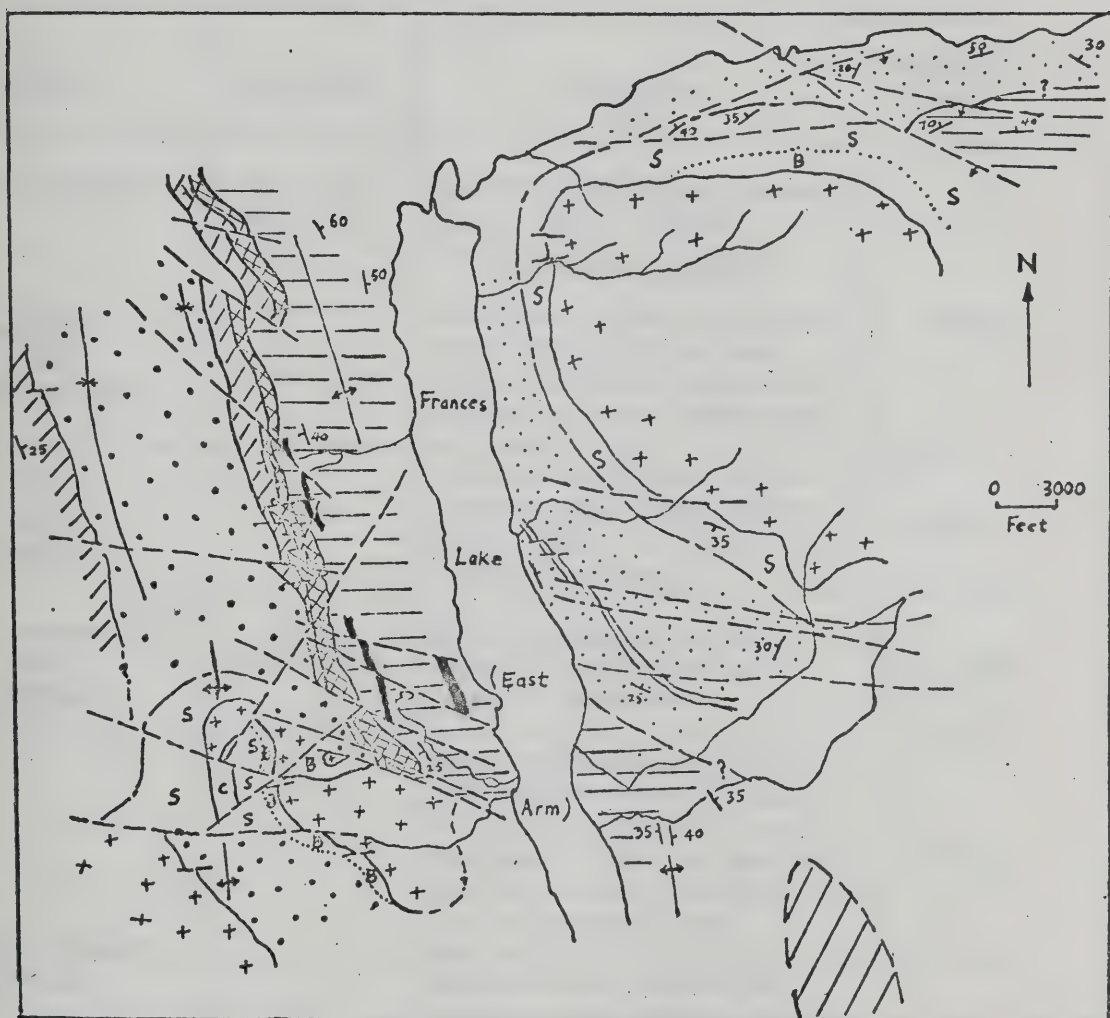


Fig. III-11. Geological map of the Frances Lake district, Yukon.

TABLE III-2

Stratigraphic Section of the Frances Lake District, Yukon

PERIOD	FORMATION	LITHOLOGY	THICKNESS (feet)
Middle Cretaceous	Mt. Hunt Batholith	Biotite quartz monzonite, minor aplite dikes (Intrusive Contact)	4,000 ?
Devonian and Mississippian		Micaceous slate and shale with intercalated grey- wacke, locally dolomitic limestone near upper part	
Silurian and Devonian		Interfingered and inter- calated quartzite, dolo- mitic slate, dolomite and minor limestone	~1,000
Middle Ordovician and Silurian	Road River	Black shale and slate locally grade into dark impure limestone	1500-2000
Middle & Upper Cambrian		Black siliceous phyllites and slates locally graph- itic and chloritic, con- taining a layer of quartz- sericite-chlorite schist in the central part	4,500
		Intercalated banded cal- careous to silty phyllites, shales and phyllitic lime- stone; minor volcanic layers in central and upper part	1,500
		(Base not seen)	

tion (defined by Lower Hemisphere Schmidt Net projection of over 150 fold axis measurement in the district). Development of a closely-spaced foliation F_2 took place at a later time and generally has not been much affected by a later refolding; F_2 may or may not be parallel to sedimentary banding F_1 , and sometimes tends to obscure or even obliterate F_1 . Usually only one foliation is found, but rarely two conjugate planes may be observed; this older foliation is usually not recognizable in the field. In Cambrian rocks especially in the lower member, F_2 trends NW and dips 20° NE; whereas in the other rock units, F_2 trends N and dips 20° W. This is due to the fact that F_2 in the former rocks parallels the axial planes of strongly recumbent folds in which all actual F_1 planes dip NE, whereas the overall dip is SW. In some places, F_2 planes are slightly folded indicating either an outlasted folding beyond formation of F_2 or a later refolding; this feature is more commonly observed in rock units younger than the Cambrian strata.

A second phase of deformation is characterized by the development of more widely-spaced foliation planes (F_3) usually angular to F_1 or sedimentary bedding planes, and a folding which refolded the F_1 and F_2 with a fold axis trending NE and plunging $20-25^\circ$ in that direction. F_3 can be considered as an axial plane foliation which probably developed by a stronger deformation (higher temperature ?) than the older one as evidenced by the unique occurrence of biotite confined to F_3 planes. F_3 foliation occurs as the most conspicuous partings in the Cambrian rocks. Intersection of F_3 with F_2 (or F_1) commonly outlines a lineation on the surface of these rocks. The youngest folding observed in various rock units commonly displays rather open, sometimes flexure-like folds with amplitude and wavelength of a few to a few

tens of feet; locally drag-folding develops in more competent rocks. In the black quartz sericite phyllite south of Anderson Creek, open and recumbent slip folding and minor smaller-scale drag-folding are very common. Also, in the Silurian-Devonian dolomite sequence, open flexure-like folding with wavelengths of a few tens of feet but without development of foliation is common. Drag-folding and minor subisoclinal slip folding are common in calc-silicate hornfels, especially in the calcareous unit.

The two deformations appear to have occurred in two widely separated intervals; an older deformation of pre-Devonian and probably post-Ordovician, and a younger deformation related to Middle Cretaceous granitic intrusion. In the eastern part of Frances Lake map-area, post-Late Ordovician regional folds were observed to have been modified by the granitic intrusion (Blusson, 1966).

(b) Faults. Major fault systems in the district can be divided into two types: major EW and NW-SE directions and minor NE-SW directions. The former faults appear to have the most severe effects with apparent right lateral movements of a few thousand feet (up to 1 mile). The NE-SW directed faults are the least abundant and appear to have only minor offsets and dip to the SE.

All faults appear to dip at steep angles to near vertical. The age of movements cannot be determined at present, but most of them seem to post-date granitic intrusions or be related to them.

(c) Regional Metamorphism. The grade of regional metamorphism observed in rock units is within the greenschist facies; more precisely, the highest phase of metamorphism probably took place under the conditions of the quartz-andalusite-plagioclase-chlorite subfacies of the greenschist facies of the Abukuma type (Winkler, 1967). This is in

contrast to Monger and Hutchison (1971) who show this district to be underlain by rocks displaying the "prehnite-pumpellyite-metagreywacke facies and/or zeolite facies". The grade of metamorphism seems to decrease in a westerly direction in the district. In fact, the strata of Ordovician or younger ages are essentially unmetamorphosed except for a weak slaty cleavage developed in pelitic rocks. Fossils in Silurian-Devonian rocks and impure limestone in Ordovician strata also suggest that those rocks were not subjected to any significant regional metamorphism. In contrast, the Cambrian rocks are generally strongly schistose and generally metamorphosed. Therefore the age of the regional metamorphism is most probably Cambro-Ordovician, and certainly pre-dates the Silurian rocks. Blusson (1966) suggested that the regional metamorphism in the general Frances Lake map-area probably pre-dates the Devono-Mississippian strata.

The critical, coexisting minerals for the above subfacies classification are biotite, chlorite, and andalusite in the metapelites, and hornblende and plagioclase in the metavolcanics, even though the latter two minerals have not been determined with certainty.

6. Ore Deposits

There are several mineralization occurrences in the district, but only one potential orebody has been drilled and developed over a number of years. The deposit therefore constitutes the topic of this study in the Frances Lake district.

(a) Immediate Mine Geology. The deposit is located near the mouth of Thompson Creek where it flows into the East Arm along the eastern shore. A total known strike length of about 2,000 feet of ore zone has been outlined. Drill results indicate an average grade of 7.99% Pb,

7.65% Zn, 0.43% Sb, 0.14% Cu, and 3.1 oz/ton Ag. It is believed that the ore zone is still open both along strike and down dip.

A geological map of the immediate area of the Thompson Creek deposit is shown in Fig. III-12, and two cross sections are shown in Fig. III-13. The upper member of Cambrian strata in the vicinity of the deposit has been subdivided in detail into several lithological subunits. The lowermost subunit is an undivided sequence, at least 150 feet thick, of light grey to dark grey pyritic phyllites which only in rare cases show sedimentary banding; they are, however, almost always characterized by abundant thin, dark pseudo-beds due to the presence of black, organic material which is clearly aligned parallel to the foliation. Some drill holes intersected narrow sections of non-banded black phyllites in the grey phyllite sequence.

A layer of quartz-sericite-chlorite schist is locally present within the grey phyllite and is believed to represent a tuffaceous rock deposited contemporaneously with the surrounding phyllites. The maximum thickness is about 150 feet. Two varieties were encountered and include a coarse-grained rock with abundant quartz eyes or clasts and a fine-grained type lacking quartz eyes. This quartz-sericite-chlorite schist in the drill holes can be correlated with a similar sericite schist exposed on surface SE of the Thompson Creek deposit.

Rocks in which ore horizon occurs overlie the grey phyllite and are characterized by very dark grey to black phyllite, always containing about 1 to 5% sedimentary layers or bands of white and green color in about equal amounts. The green layers or lenses are mainly composed of chlorite, epidote, and minor carbonate and sericite; white layers are mainly quartz and minor carbonate. Above the base of the black phyllite, there occur three horizons of black phyllite with greater

LEGEND FOR FIG. III-12



Upper Grey Phyllite - black and white layers



Black Phyllite - white and green layers (10%)



Black Phyllite - white and green layers (5%)



Ore Zone



Quartz-sericite-chlorite schist (metatuff)



Lower Grey Phyllite - mostly without sedimentary layers

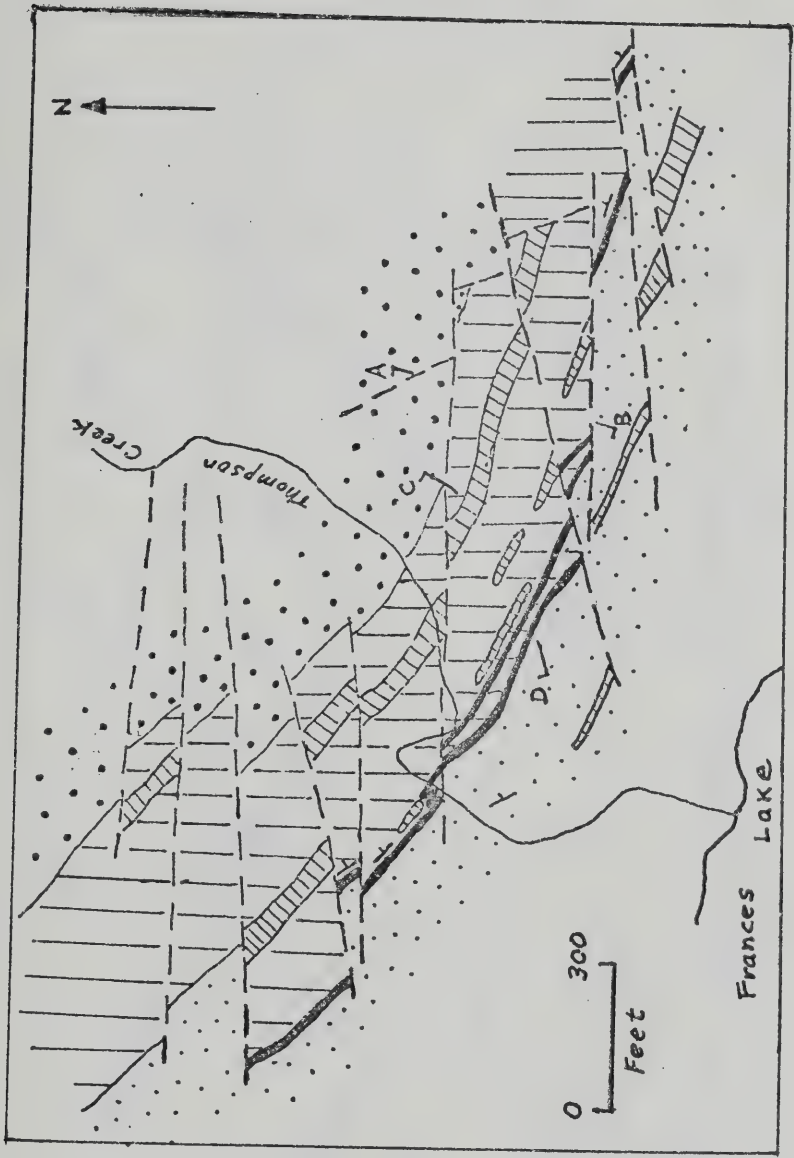


Fig. III-12. Geological map of the Thompson Creek deposit,
Frances Lake district, Yukon.

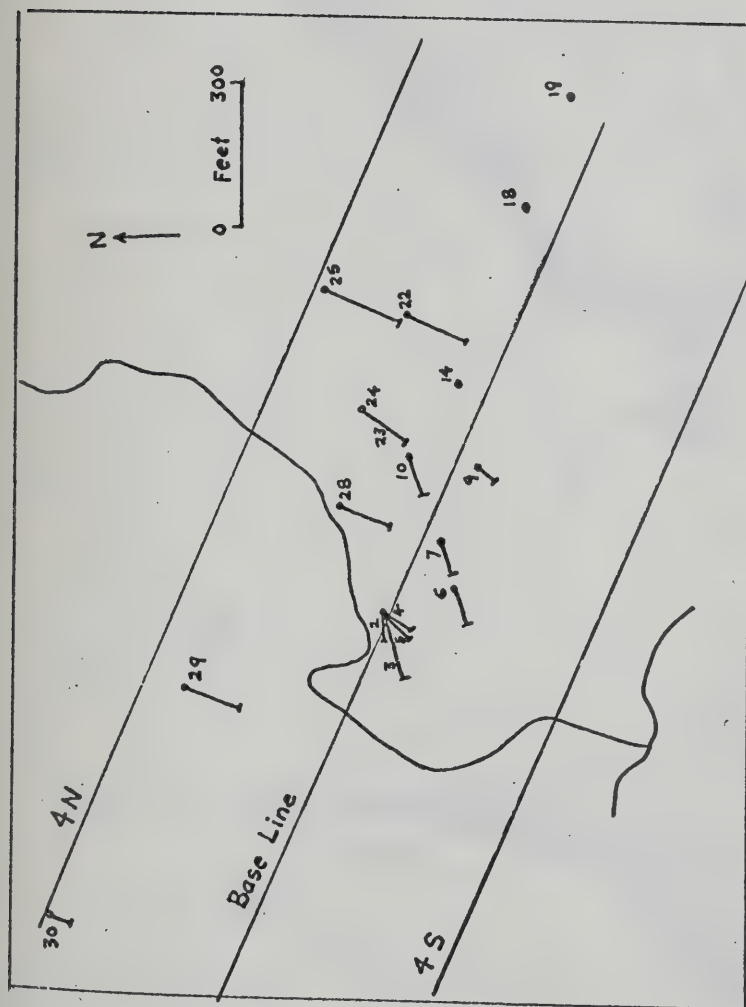


Fig. III-12a. Locations of drill holes from which samples are analyzed and studied in this thesis.

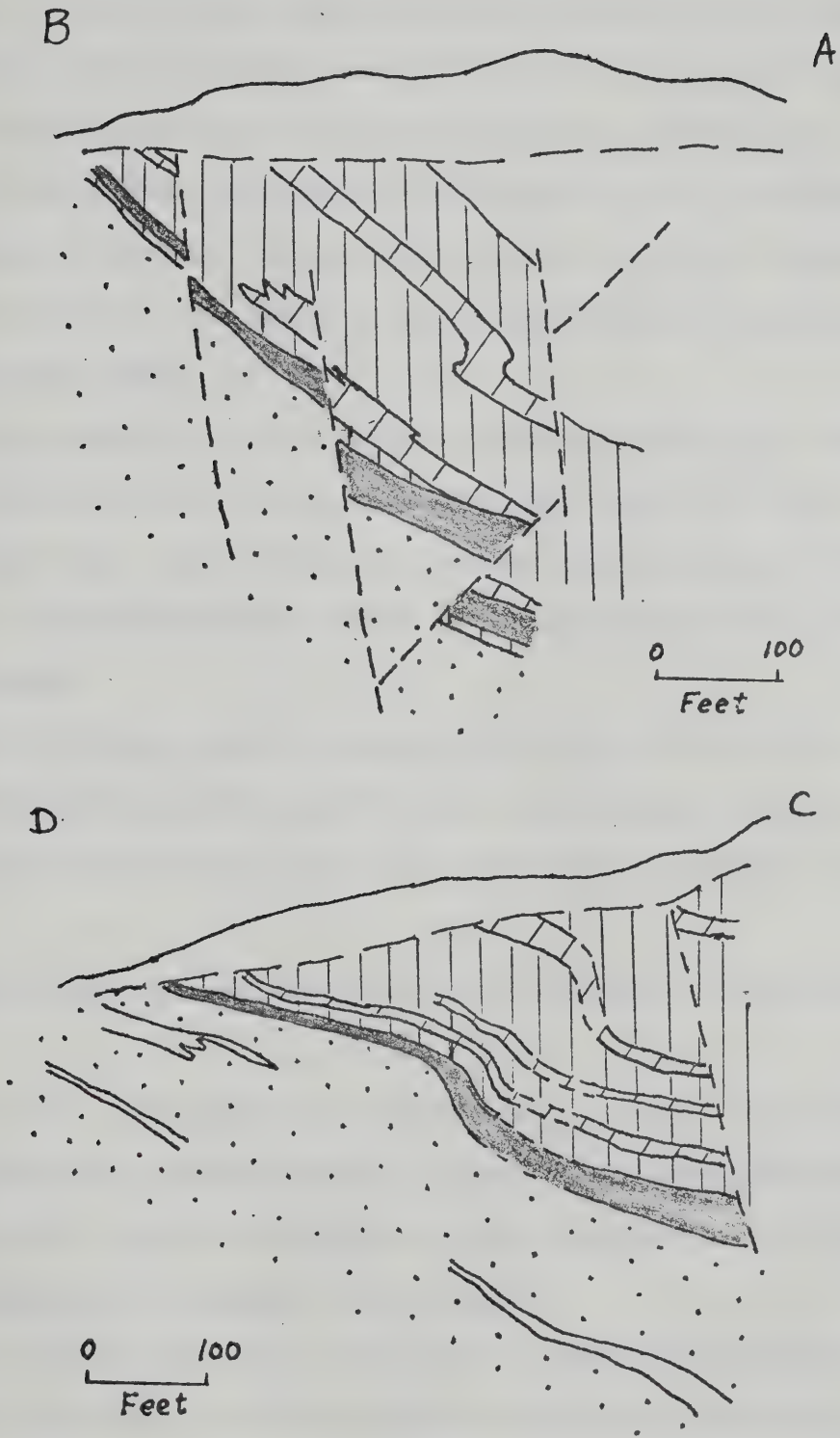


Fig. III-13. Cross sections of the Thompson Creek deposit, Frances Lake district.

amounts (10-20%, sometimes 20%) of green and white layers. These horizons appear 30 feet, 50 feet, and 120 feet above the base of the black phyllites and are 20 feet, 10 feet and 15-35 feet thick, respectively.

Very rarely grey phyllite occurs within the black phyllite sequence but it is of minor importance in the central part of the deposit, but appears to increase towards the SE where it evidently replaces large sections of the black phyllites perhaps indicating a major facies change in that direction.

The upper sequence is a grey phyllite displaying sedimentary banding which in the lower 100 feet is made up of white and black bands, and above this slight color differences between adjacent bands of different grain size outline white (quartz) bands interfoliated with black (graphitic) bands.

A black to dark grey phyllite sequence with up to 10% white and green bands was intersected in one drill hole and probably belongs to a somewhat higher stratigraphic level than the upper grey phyllite sequence.

Photomicrographs of some major host rocks are shown in Plate III-13.

In all of the above-mentioned subunits massive portions of quartz-carbonate (ankerite or siderite) occur at least in part conformable to the bedding and/or have been remobilized during metamorphism and folding as can be demonstrated in at least two instances.

The main ore zone occurs as a thin band or layer a few feet immediately above the base of the black phyllite subunit and is generally about 20 to 30 feet thick; the ore zone follows this stratigraphic position for at least 2,000 feet northwestward along strike and dips to the NE at about 30°. One or two much less extensive and continuous

lenticular layers above the main ore zone can be seen in some drill intersections. Drill results at the southeastern part of the deposit indicate a decreasing degree of ore mineralization in the same stratigraphic position; this, together with the indicated facies change in the phyllites (see above), gives the impression of a primary limit to mineralization in this direction.

In most intersections, transgressive foliation (F_3) is observed to be discordant to bedding and generally shows dip of less than 20° ; only in rare cases, especially in rocks with great amount of banding, transgressive foliation has not developed and a foliation commonly follows bedding planes. Most folds observed in the host rock sequence have a wavelength of a few inches up to a few feet, and folds with wavelengths of several tens of feet to 100 feet seems to be less frequent. It has been found that bedding dips relatively uniformly towards the NE in most intersections; significant folding occurs only in the northwestern part of the deposit. A series of E-W striking faults dipping steeply (75° - 85°) N transect the area of the deposit and slice up the ore horizon considerably. Most of these faults have a left-lateral movement of 50 to 200 feet and only two of the faults have an apparent right-handed movement. The faults are accompanied by a zone of shattering and minor faulting in adjacent rocks and partly by intensive leaching and/or alteration (mica minerals \rightarrow clay minerals, in part without distortion of the older phyllite structures); the fault zone is generally much wider than the main fault breccia zone of mud formed on the actual slip plane. Quartz-carbonate-chlorite has been deposited in parts of these faults, often associated with pyrite and/or pyrrhotite, and in one case (DDH26A) with coarse-grained sphalerite and galena. In the southeastern part of the deposit a NNW-SSE trending thrust fault was recognized, dipping 60°

to 65° SW. It has apparently been offset by the EW faults and has duplicated the ore horizon in DDH25. A similar but smaller fault was found in DDH31 in the northwestern part.

(b) Ore and Gangue Minerals. Ore minerals observed in the Thompson Creek deposit are, in decreasing order of abundance, sphalerite, galena, pyrite, pyrrhotite, chalcopryite, Sb-Pb sulfosalts, marcasite, chalcocite, and arsenopyrite. The latter three minerals are trace constituents. Pb-Sb-Cu sulfosalt minerals are mostly meneghinite and minor boulangerite, with a trace of bournonite (?). Gangue minerals are predominantly quartz and carbonates, with very minor sericite, chlorite and graphite which probably were derived from the host rocks.

(i) Ore Minerals. Sphalerite and galena constitute the major portion of the sulfide ores, and they are usually intergrown with each other. Sphalerite generally forms fine- to medium-grained aggregates or bands and exhibits massive to disseminated texture on hand specimens. It is medium grey to light brown in color and sometimes contains exsolution or inclusions of chalcopryite, pyrrhotite and rarely pyrite. On hand specimens, galena is generally recrystallized and coarse- to medium-grained, and occasionally shows deformation features such as galena tails (steely galena), flow banding, and fragmented clasts. Under the microscope, development of intersecting cleavages outlined by triangular pits is sometimes observed, and could very well be glide-twin-lamellae resulting from the action of stress (Ramdohr, 1969). HCl etching did not succeed in revealing the lamellae, however.

Pyrite commonly occurs as disseminated grains, veinlets and deformed aggregates in ore and gangue minerals, only rarely as intergrown "emulsions" in galena and sphalerite. Pyrrhotite occurs closely with pyrite, chalcopryite, sphalerite, and carbonates as bordering fine-

grained aggregates and irregularly-shaped patches, and occasionally as inclusions in or veinlets cutting galena and sphalerite. Chalcopyrite forms exsolutions in sphalerite and also as veinlets with pyrrhotite in other ore minerals.

Sulfosalt minerals generally occur as intergrowths and as veinlets in carbonates. In the former occurrence the main sulfosalt minerals are meneghinite, boulangerite and rare bournonite or jamesonite; they form medium to large unoriented grains with irregular boundaries with galena; twinning lamellae are observed in a few of these sulfosalts and these could possibly be bournonite or jamesonite. In the latter occurrence meneghinite occurs either exclusively as veinlets and streaks (striae) or with galena in veinlets of galena-sphalerite. Under the microscope, the sulfosalt minerals are very similar to galena in most optical features except they generally show a faint greenish grey tint, lack triangular pits and some show anisotropism and very weak internal reflection.

Very small amounts of marcasite, chalcocite and arsenopyrite are seen as small, idiomorphic grains either associated with pyrite or as veinlets in gangue minerals.

(ii) Gangue Minerals. Quartz and carbonates are the predominant gangue minerals and they occur mostly as brecciated to granulated, medium- to coarse-grained aggregates or clasts disseminated in and intermixed with ore minerals. Carbonate minerals are mainly Fe-Mn carbonates, but also contain solid solutions of Ca and Mg. They are light brown to medium grey, commonly display twinning lamellae both in hand specimens and under the microscope. Quartz and carbonates usually contain inclusions or veinlets of other minerals such as chalcopyrite, pyrrhotite,

marcasite, and sulfosalt minerals. Sphalerite is usually seen in contact with carbonate minerals.

Other gangue minerals observed include very minor amounts of sericite, chlorite and graphite; most of these were probably mobilized from host rocks near fault zones.

Photomicrographs of ore and gangue minerals of some typical ore specimens are shown in Plate III-14.

(c) Ore Texture. The ores are typically deformed and brecciated, displaying a rather massive but strongly remobilized texture in which ore and gangue minerals are mixed in a random pattern: granulation, contortion and flow banding are the common features observed, which probably were due largely to metamorphic mobilization, faulting and brecciation. Late veining of sulfosalts and sulfides in quartz and carbonate matrix is also observed on a few occasions.

Typical textures of ores in hand specimens and drill cores are shown in Plate III-15.

PLATE III-13

PHOTOMICROGRAPHS OF ROCK SPECIMENS (TRANSMITTED LIGHT)

Frances Lake District

A. Sample 139-3: Calcareous phyllite, west of East Arm

Patches and grains of calcite (Cc), quartz (Q) with foliations of biotite and sericite at left. Plain light, X25.

B. Sample DDH8-114': Quartz-sericite-chlorite phyllite, Thompson Creek

Folded F₁ separated by complexly folded F₂ (top-bottom of photo); transposition of F₁ to F₂ is apparent. Quartz (white), sericite (faint grey, mainly between foliations of quartz), and chlorite (Ch), (medium grey, mainly along F₂). X25

C. Sample DDH19-257': Quartz-sericite-chlorite schist, Thompson Creek

Sericite (Sc) probably originally hornblende, quartz (Q), and relicts of plagioclase (Pl), and epidote (Ep). Foliation is outlined by form orientation of grains (top-bottom of photo). Crossed nicol, X25.

D. Sample DDH28-66.5': Quartz-chlorite-sericite phyllite, Thompson Creek

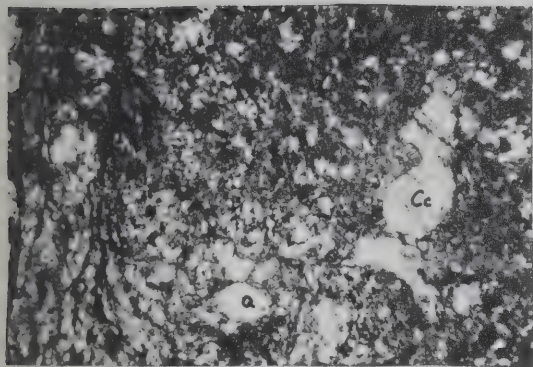
Foliations (F₂) of quartz (white), chlorite (Ch), and epidote (Ep), most probably prehnite (?). Minor calcite (Cc). Foliation is horizontal in photo. X25

E. Sample DDH3-28.5': Quartz-sericite phyllite, Thompson Creek

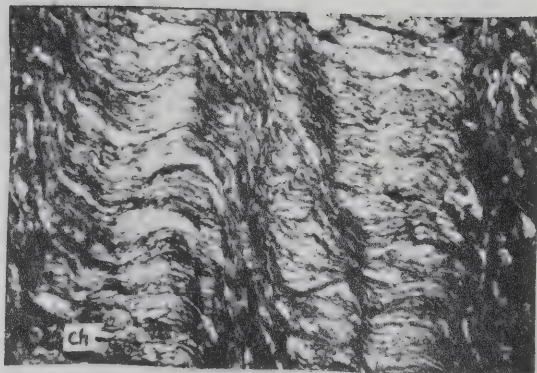
Lineation (probably intersection of F₂ and F₃) is seen cross cutting F₂ foliations (top-bottom of photo) composed of quartz (dark) and sericite (light grey). Crossed nicol, X25.

F. Sample DDH22-365': Deformed and banded sulfide, Thompson Creek

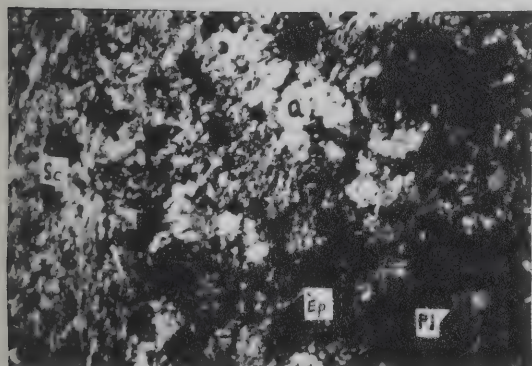
Contact of banded sulfides (left) and phyllite (right); phyllite composed of clastic quartz (white), chlorite (dark grey to black) and sericite (grey). X96



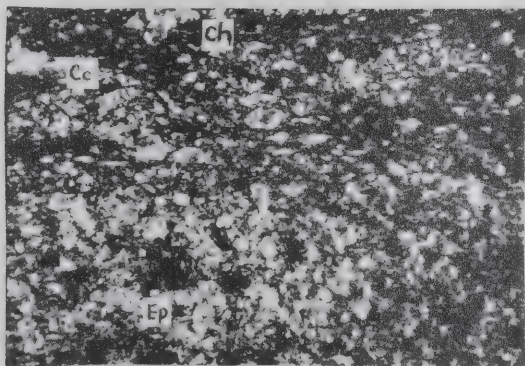
A



B



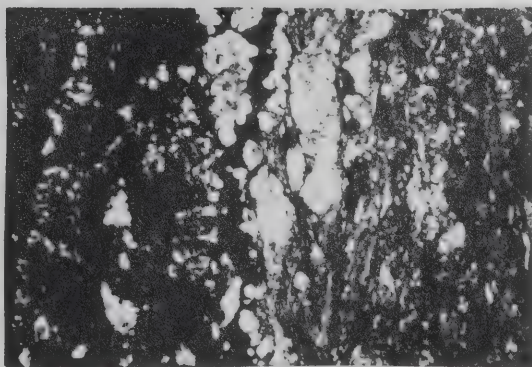
C



D



E



F

PLATE III-14

PHOTOMICROGRAPHS OF ORE SPECIMENS (REFLECTED LIGHT)

Thompson Creek Deposit

A. Trench Sample KSL572-6

Meneghinite (medium grey) in galena (light grey) and sphalerite (dark grey), black patches at left are siderite. Minor small pyrite and pyrrhotite grains (white). Plain light, X38

B. Sample DDH4-43.5'

Veins of galena (white), sphalerite (medium grey) carrying meneghinite (light grey) in sideritic carbonate (dark grey to black, twinned at left). Minor quartz grains in sulfides and carbonates. X38

C. Sample DDH6-34.5': Deformed and banded ore

Contact of bands of sphalerite (grey) and galena (white). Note mutual myrmekitic intergrowth of both sulfides. Sulfides are replaced and veined by quartz (black). Minor pyrrhotite (Po) grains in sulfides. X38

D. Sample DDH6-34.5'A

Meneghinite (white) veins in siderite (medium grey) and quartz (dark grey and black). X38

E. Sample DDH24-308: Deformed and banded ore

Intergrown galena (light grey) and sphalerite (medium grey), and chalcopryrite (Cp) replaced by pyrrhotite (Po), pyrite (Py) and quartz (black). X38

F. Sample DDH25-474A: Deformed and banded ore

Sphalerite (medium grey) band in contact with galena (white) rich band. Pyrrhotite (Po) and quartz (black) replace sulfides. X38

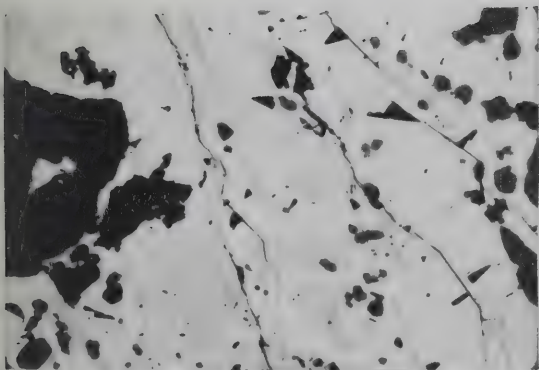
G. Sample DDH28-158: Deformed ore

Intergrown galena (greyish white), sphalerite (medium grey), boulangerite (light grey) and chalcopryrite (tiny dots in sphalerite at left) replaced by pyrrhotite (Po), pyrite (Py), quartz (black) and marcasite (Mc). Note myrmekitic intergrowth of marcasite with pyrrhotite. X38

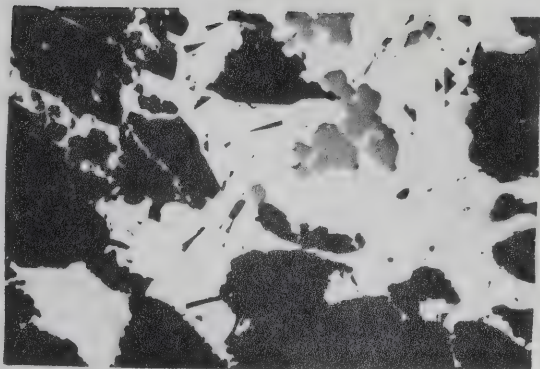
H. Sample DDH28-158

Same as G. Crossed nicol, X38. Note twinned lamellae of boulangerite and pyrrhotite.

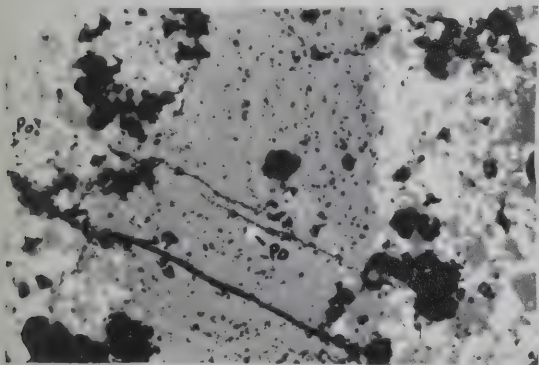
A



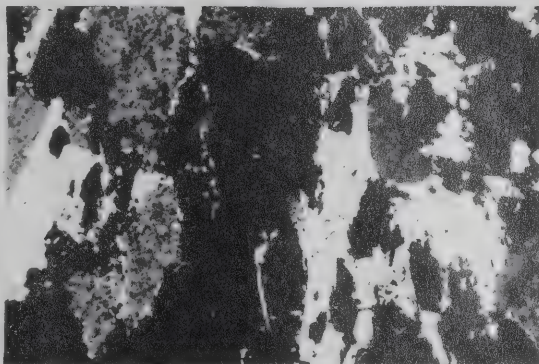
B



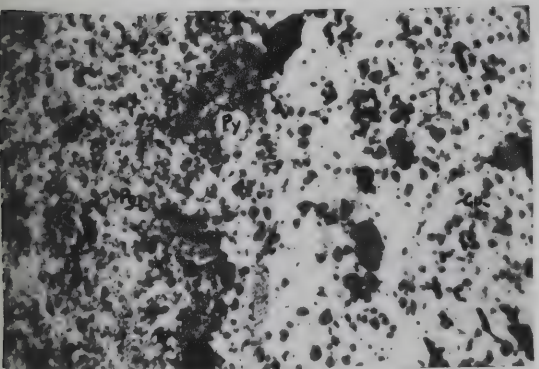
C



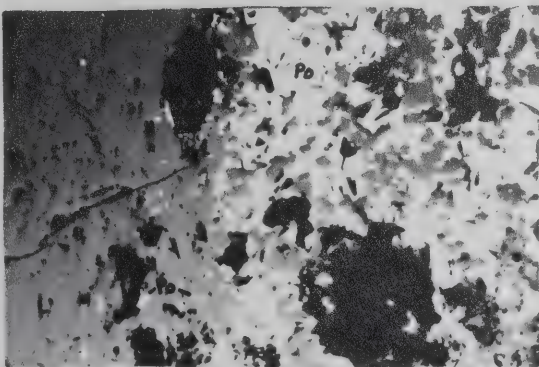
D



E



F



G



H

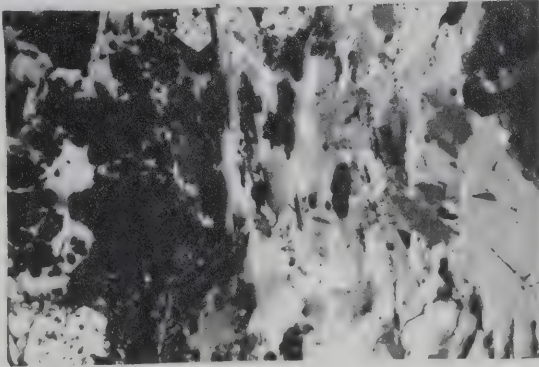


PLATE III-15

PHOTOGRAPHS OF ORE SPECIMENS (REFLECTED LIGHT)

Thompson Creek Deposit

A. Sample DDH22-340.5': Deformed and banded ore

Sphalerite (dark grey) and galena (medium grey) and "granulated" quartz porphyroblasts (white). X38

B. Sample DDH25-462'

"Granulated" aggregates of sphalerite (dark grey) and quartz (white) minor galena is associated with sphalerite. X38

C. Trench Sample KSL572: Deformed massive ore

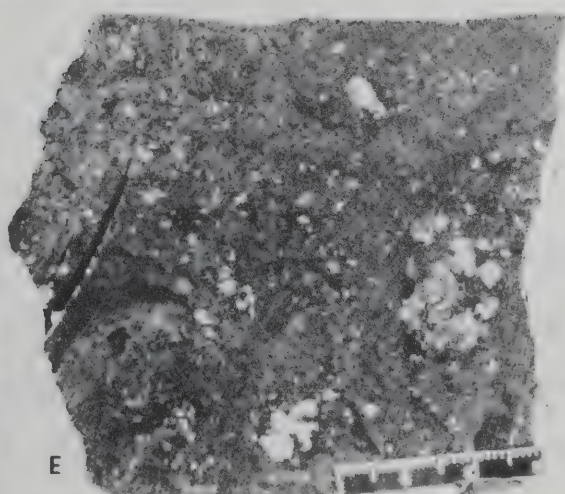
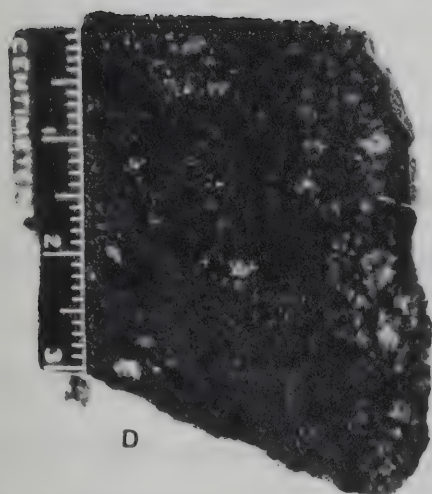
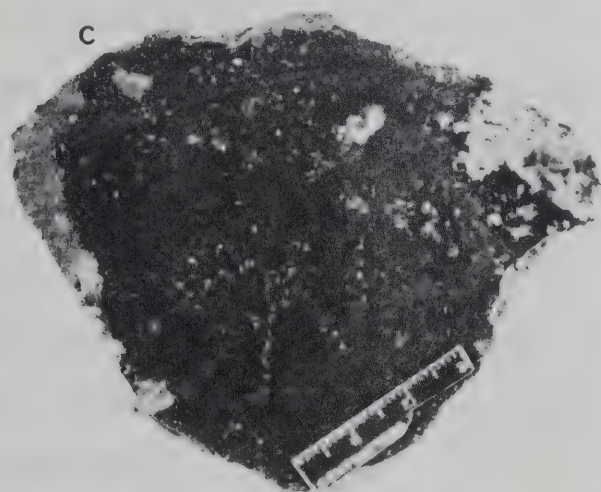
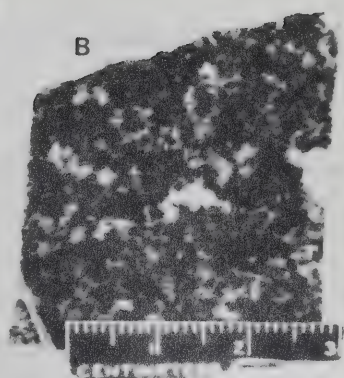
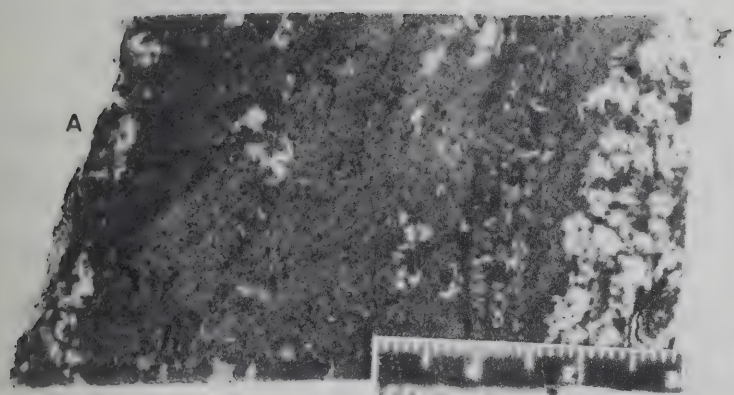
Sphalerite (dark grey) and galena (medium and light grey) with disseminated quartz and pyrite. Some quartz and siderite porphyroblasts.

D. Sample DDH28-158: Deformed massive ore

Aggregates or patches of carbonates and quartz porphyroblasts replace sulfides. X38

E. Trench Sample KSL572-1: Deformed massive - brecciated ore

Large porphyroblasts of quartz (white) and patches of carbonates (dark grey) forming vague flow banding and granulation.



D. HOWARD'S PASS DISTRICT

1. Location and Access

The district in which the newly discovered stratiform zinc-lead deposits of Canex Placer Ltd. of Vancouver is situated covers a large area along the border of Yukon and District of Mackenzie, N.W.T., from approximately latitude $62^{\circ}26'N$ to $62^{\circ}37.5'N$ and longitude $129^{\circ}04'W$ to $129^{\circ}45'W$. Mineral claims surrounding the Canex Placer's property cover from latitude $62^{\circ}24'N$ to $62^{\circ}41.5'N$ and longitude $129^{\circ}02'W$ to $129^{\circ}55'W$. The district is located at the southwestern side of the NW-trending Selwyn Mountains, about 8 to 10 miles SW of the South Nahanni River, and covers the headwaters of the Pelly River one branch of which originates at Summit Lake, about 10 miles SW of the Canex Placer's main deposit (see Fig. III-14).

The district can be reached by float planes to Summit Lake from the towns of Ross River or Watson Lake and then by a helicopter service stationed at Summit Lake.

2. Physiography

The district belongs to the Selwyn Mountains physiographic province of Bostock (1970) and is characterized by high mountain ranges and steep but broad river valleys. Meandering and slow flowing marsh-land type streams and small rivers form W to SW flowing headwaters of the Pelly River in most of the district. A few NE to SE flowing streams and small rivers drain the northern and eastern edges of the district and flow into South Nahanni River to the NE.

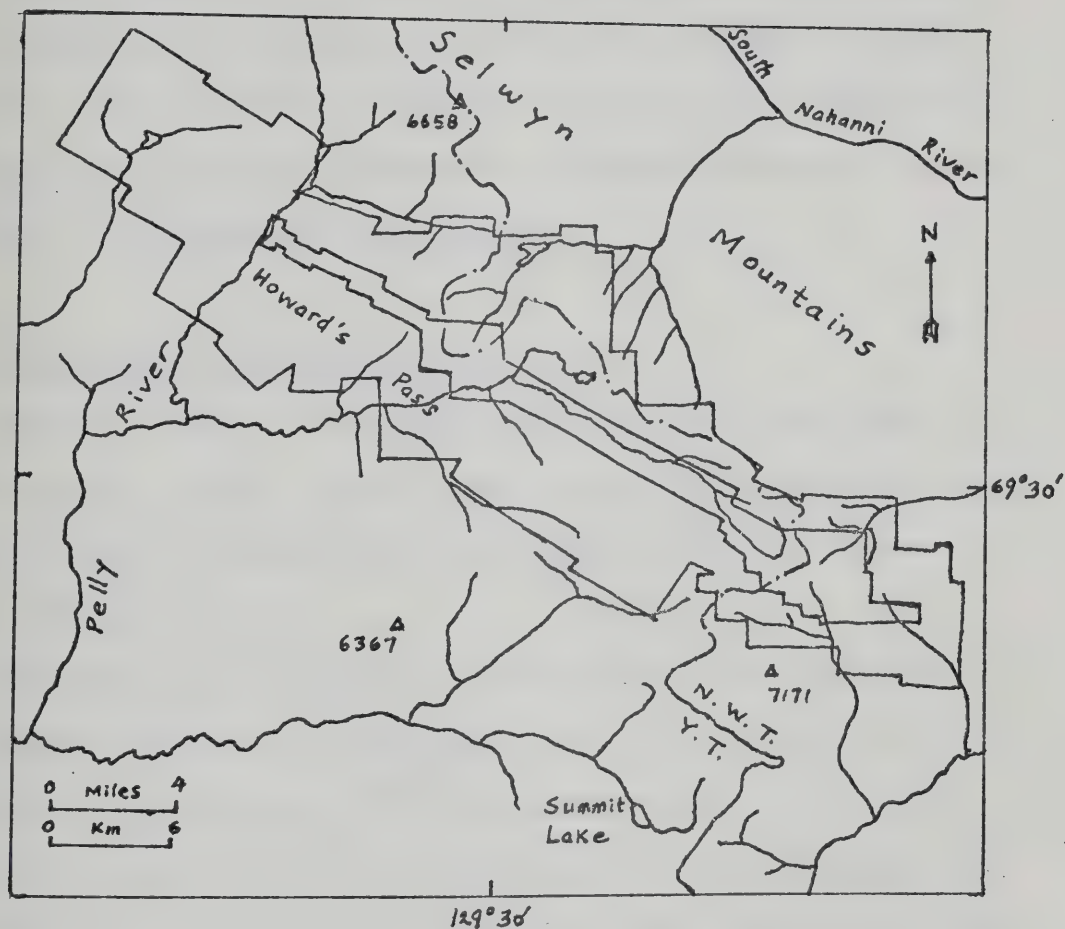


Fig. III-14. Location map of the Howard's Pass district and the Summit Lake region. The inner outline shows Canex Placer's claim groups, the outer outline shows claim groups of other companies.

The district has been extensively glaciated to at least 6,500 feet elevation. The ice movement at higher elevations was mainly NNE to NW; at lower elevations ice movement followed the present drainage system.

Generally speaking, in the eastern and southeastern part of the district high mountain ranges with steeper river valleys are common, whereas in the western and northwestern part low rounded ridges with broad river valleys are the conspicuous topographic features. Cirques are common at the summit of many ridges.

3. Fieldwork and Exploration History

Geological mapping of the Nahanni map-area (the western part of which coincides with the Howard's Pass district) was carried out on a scale of 1 inch = 4 miles by Green and Roddick (1961) and Blusson (1963, 1967) of the G.S.C..

Exploration in the district was essentially non-existent until the geological information published by Blusson in 1972 which led to a staking rush in the winter of 1972 and spring of 1973. Canex Placer Ltd. of Vancouver was the first company to stake in the district and apparently covered the best potential ground; many companies and individuals followed suit and staked around Placer's property; these include Dynasty Explorations Ltd., Vestor Explorations Ltd., Cominco Ltd., Noranda Explorations Ltd., Al Kulan of Ross River, and others.

Drilling and trenching in the Placer's main zone (XY claims) were started in 1973 and drilling continued in 1974 and 1975. Trenching in other parts of the claim group was also carried out in 1973. In 1974 Dynasty Explorations Ltd. of Vancouver and Shield Resources Co. Ltd.

of Edmonton jointly drilled part of their Pas claims just NW of the Placer's main zone. Noranda Explorations Ltd. drilled its barite property W of Placer's main zone in 1973-1974.

At the time of writing, development and production plans of Canex Placer Ltd. have not been disclosed.

4. General Geology

The information on general geology of the district comes from various sources; these include:


1. Field mapping by the writer for Vestor Explorations Ltd. in 1973.
2. Geological data provided by G. House and J. Morganti who worked for Canex Placer Ltd. in 1973 and 1973-1975, respectively.
3. Crude stratigraphic information in the district and adjacent areas given by Blusson (1967).

The generalized geological map of the Summit Lake region SW of South Nahanni River (including the Howard's Pass district) is shown in Fig. III-15. Stratigraphic section of the region is presented in Table III-3.


In the southern and southeastern part of the region S and E of Summit Lake, Lower Cambrian and older strata of conglomerate, sandstone, gritty quartzite and shale occupy most of the mountain ranges. Sinuous belts of Cambro-Ordovician carbonates with minor siltstone occurs in the main part of the district as well as SW of the Summit Lake region. Narrow belts of Ordovician-Silurian siltstones and shales occur in the district. A thick sequence of Devonian or younger strata

LEGEND FOR FIG. III-15

Devonian and Younger

 Conglomerates, sandstones, shales

Ordovician-Silurian

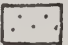
 Siltstones, turbidite near upper part

Cambro-Ordovician

 Limestone, dolomite, minor siltstone

 Red bed: Sandstone, sandy dolomite and orthoquartzite

Lower Cambrian and Older

 Conglomerate, sandstone, gritty quartzite, and shale

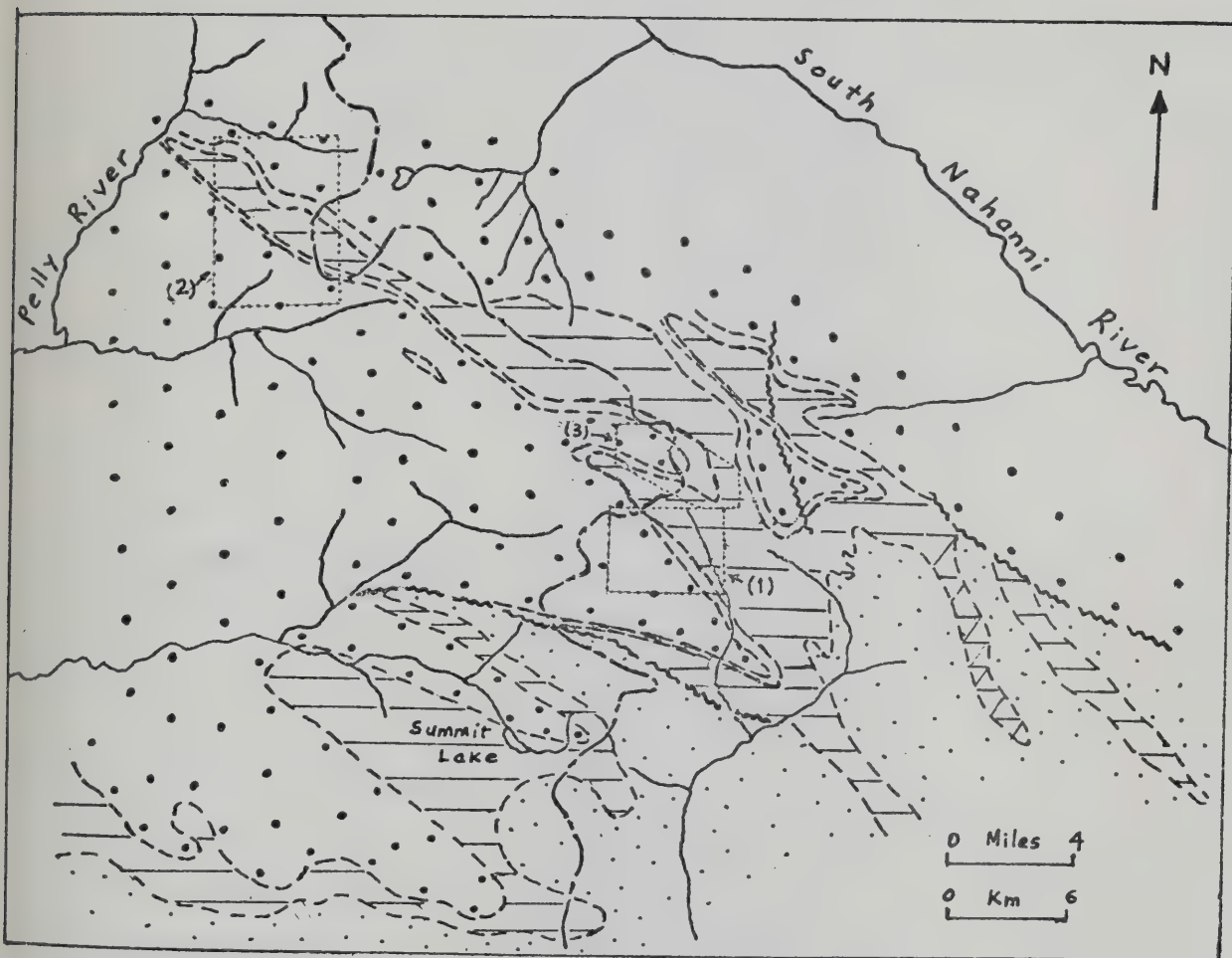


Fig. III-15. Geological map of the Summit Lake region, Yukon Territory - Northwest Territories.

Block (1): Outline of Fig. III-16.

Block (2): Outline of Fig. III-17.

Block (3): Outline of Fig. III-18.

Stratigraphic Section of the Summit Lake Region, Y.T.-N.W.T.

PERIOD	FORMATION	LITHOLOGY	THICKNESS (feet)
Devonian and Mississippian	Yara Peak Group	Chert and shale pebble conglomerate, interbedded sandstone, shale and siltstone, minor red iron oxide bands or rings in the upper part sandstone and siltstone	>3,000
Siluran	Road River	Black siliceous siltstone, sandstone interbeds in the uppermost part containing layers and clasts of black chert, limestone and barite Grey dolomitic siltstone: pyritic and graphitic near base, more siliceous near top. Bears clay flakes and is commonly flaggy	~ 600
Ordovician		Siliceous and shaly siltstone, containing black chert beds and limestones clasts, partly pyritic Cherty siltstone, abundant siliceous shale partings near top. Lead-zinc mineralization.	500-600
		Cherty limestone and siltstone, abundant clasts and lenses of limestone Black graphitic and graptolitic siltstone, calcareous near base and pyritic, graphitic or siliceous near upper part	(≤1,000)
Upper Cambrian and Lower Ordovician	Rabbitkettle	Transition zone limestone and dolomite laterally grade into massive calcareous siltstone Wavy banded interbedded limestone and dolomite locally containing thin shaly partings Silty and sandy limestone and dolomite, massive siltstone locally calcareous near base (Red bed; sandstone, sandy dolomite and orthoquartzite in SE part)	>1,000
Lower Cambrian and Older	Grit unit	Varicolored slates, siltstones and phyllites, ne minor quartzite	8,000
		Maroon and green shale	3,000
		Calcareous, gritty feldspathic sandstone and quartzite, quartz and feldspar pebble conglomerate with interbedded silty shale and slate; locally containing thin bedded impure limestone	>9,000

composed of grits, sandstones and shales occupy a large area in the central, northern and western parts of the Summit Lake region.

Two detailed geological maps of parts of the district (see Fig. III-14 for location of these maps) are presented in Fig. III-16 and Fig. III-17, respectively.

Detailed descriptions on rock units from Lower Cambrian to Mississippian are given in Appendix III-5.

5. Structural Geology

(a) Folding. Regional folding in the district is generally tight and vertical to slightly overturned. Major fold (F_1) trends WNW (300° - 320°) and plunges at 10 - 20° to the NW; two types of secondary or parasitic folds were observed occurring with the major fold, their axial planes and plunges are similar to those of the major fold but the dips of axial planes are variable. A regional penetrative cleavage S_1 was commonly observed in pelitic rocks and appears to be axial planar to F_1 . The development of different fold patterns is mainly dependent on lithology and non-penetrative structural style. Generally speaking, both major and secondary meso-to-minor folds usually are more abundant and better developed in incompetent rocks. In the conglomerates, F_1 folding is broad and open; meso-folds affect the interbedded sandstone and shale member but not the conglomerates themselves; folding in limestone is not intense but development of meso- or micro-folds was observed and they are generally subisoclinal folds; the siltstone units are more tightly folded and small isoclinal concentric folds were observed; bedding in these units is generally obscure but is recognizable where the cleavage is less intense. S_1 cleavage, where observed, generally "fans" across F_1 with a fan width or angle of about 20° ; some of

LEGEND FOR FIG. III-16 AND FIG. III-17

Devonian-Mississippian



Chert and shale pebble conglomerate



Interbedded sandstones and siltstones

Silurian



Siliceous and dolomitic siltstone, generally pyritic and laminated

Ordovician



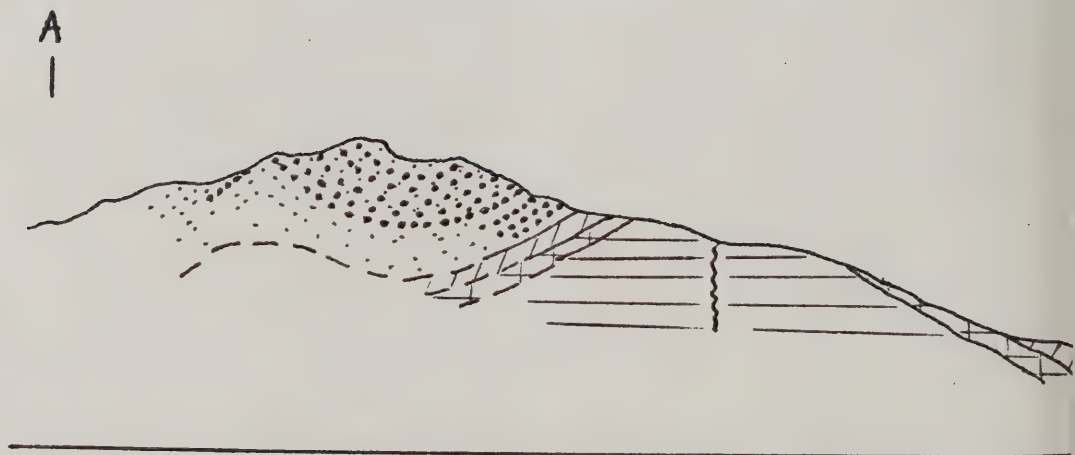
Black graphitic siltstone with cherty, calcareous and siliceous layers

Upper Cambrian



Wavy banded limestone and silty limestone

Cross section A - A', Fig. III-17



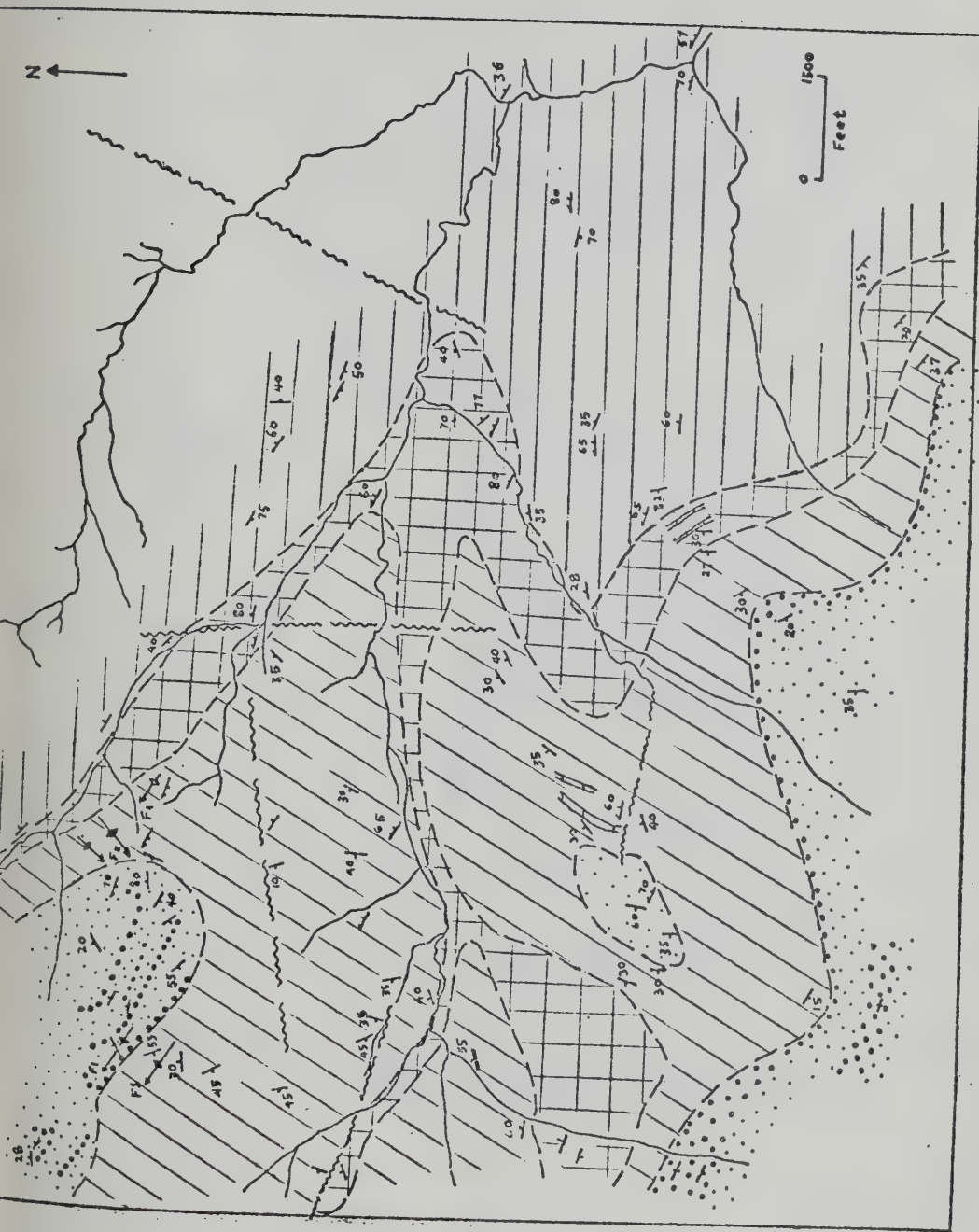


Fig. III-16. Geological map of an area in the southeastern part of the Howard's Pass district.

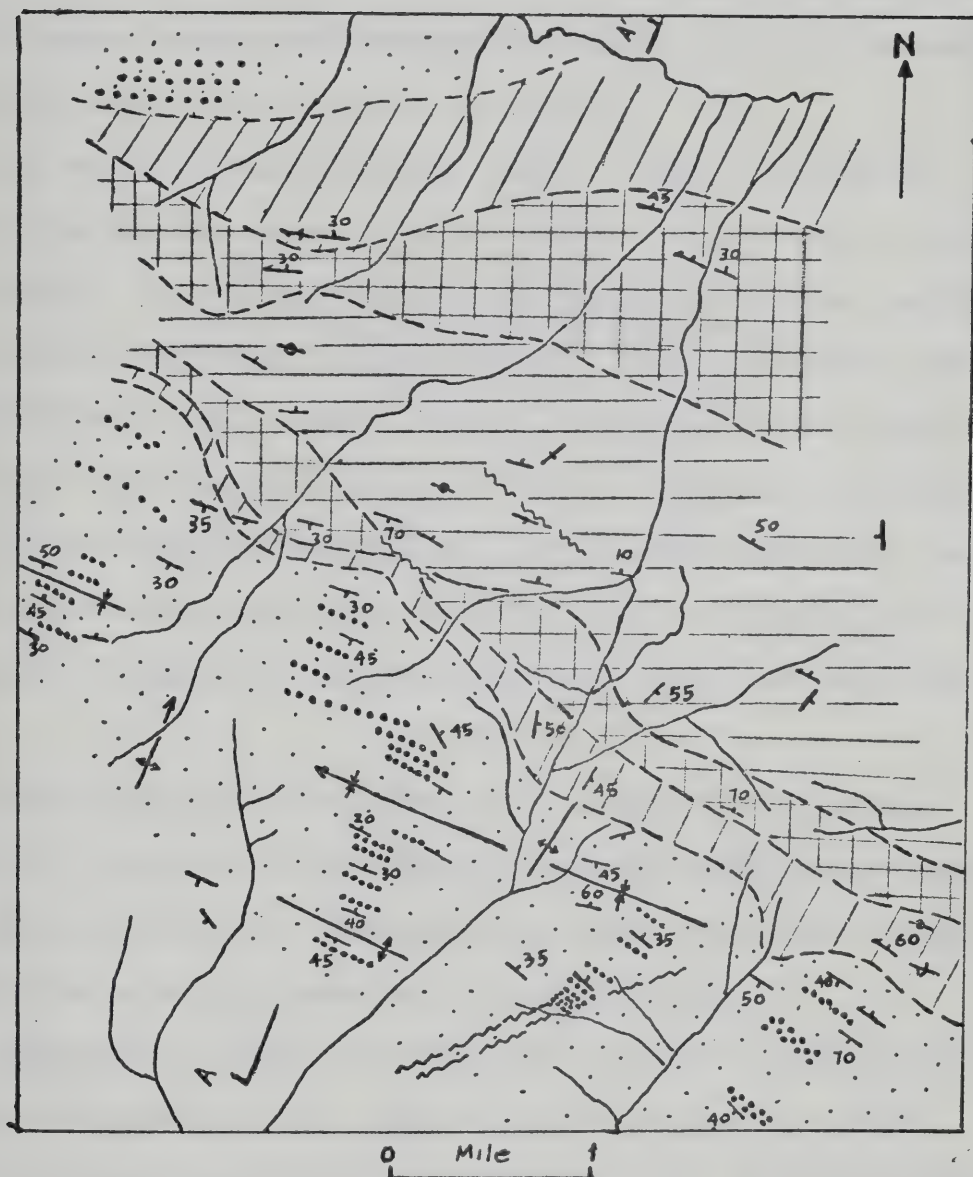


Fig. III-17. Geological map of an area in the northwestern part of the Howard's Pass district.

the cleavages are commonly filled with remobilized quartz or carbonate, and in the case of mineralized beds are filled with sulfides, cleavage-slip appears to be the main type of deformation.

In the areas investigated by the writer, a second period of regional folding (F_2) was observed in the Silurian and the Devono-Mississippian strata. It is a gentle and open fold with a fold axis trending NNE to NE and plunging quite steeply (60° - 80°) to the SW (in area just S of Placer's main zone, see Fig. III-16) and to the NE in the northwestern part of the district (see Fig. III-17). A joint set S_2 trending 20° - 30° and dipping vertically is the axial planar cleavage of the F_2 folds. Quartz calcite veins occur in S_2 joints and tension gaps and appear to be the result of remobilization during the second period of folding.

Near the headwater of Flat River, about 40 miles SE of the district, the S_1 cleavage associated with F_1 regional folding was observed to clearly pre-date granitic intrusion suggesting a post Devono-Mississippian and pre-Middle Cretaceous age for the deformation.

(b) Faulting. Faulting presumably occurs during the same period as the major regional folding. Scale of faulting varies from minor fractures to larger scale local to regional faulting. The small-scale fractures or faults generally have a parallel trend to the regional axial plane cleavage, the displacement on these shears appear small and a strike-slip movement occurs in a local scale. Larger scale local to regional faulting generally truncates the major folds and appears to be normal faulting with minor lateral displacement. The development of this faulting probably occurred slightly later than the F_1 folding.

The regional axial plane cleavage is thought to play an important part in the deformation history of the area, the cleavage planes have

formed strike-slip cleavage, or fracture cleavage, and there is a small displacement along each cleavage plane - taken together the displacement would be quite large.

6. Ore Deposits

The main ore zone in the XY claims of Canex Placer Ltd. is by far the largest deposit in the district (Fig. III-14); there are also several mineralization occurrences in the ANNIV claims of Placer as well as in other companies' claim groups. Placer's main zone constitutes the topics of this study in the Howard's Pass district.

(a) Immediate Mine Geology. A geological map of the Canex Placer's main zone is shown in Fig. III-18; two cross sections of the main zone are shown in Fig. III-19. Lead-zinc mineralization occurs in the cherty siltstone and partly in the cherty limestone members of Middle Ordovician strata. Ore grade of drill core specimens is variable due to the fine-grain and disseminated or laminated nature of the mineralization, but typical thin laminated ores have an average grade of 6% Zn, 1 to 2% Pb; ore reserve tonnage has not been published, but an estimate of about 100 million tons appears conservative.

Stratigraphy of the rock units in the main zone is similar to that described above for the general district (Table III-3). The rock units are generally affected by the NW-trending major folds and truncated or offset by numerous normal faults, mainly trending NE. Generally speaking, the main zone is characterized by a synclinorium developed in the Yara Peak area with slight overturning to the NE. Rocks S of Yara Peak on the southern limb of the synclinorium generally outcrop in small tight isoclinal folds with well developed axial plane cleavage. To the N of Yara Peak, beyond the northern limb of the synclinorium the wavy

LEGEND FOR FIG. III-18

Devonian and Mississippian



Chert and shale pebble conglomerate, interbedded sandstone and siltstone

(Unconformity)

Silurian



Siliceous siltstone, minor chert and barite



Fetid silty limestone



Clay-flakes bearing dolomitic siltstone

(Conformity)

Ordovician



Siliceous siltstone, minor black chert and limestone



Cherty siltstone, major Pb-Zn mineralization



Cherty limestone or calcareous siltstone, minor Pb-Zn mineralization



Graphitic, graptolitic siltstone

(Sedimentation break ?)

Upper Cambrian and Lower Ordovician



"Transition Zone" limestone and dolomite, grade laterally into calcareous siltstone



Wavy banded limestone and dolomite



Massive silty and sandy limestone and dolomite

(Base not seen)

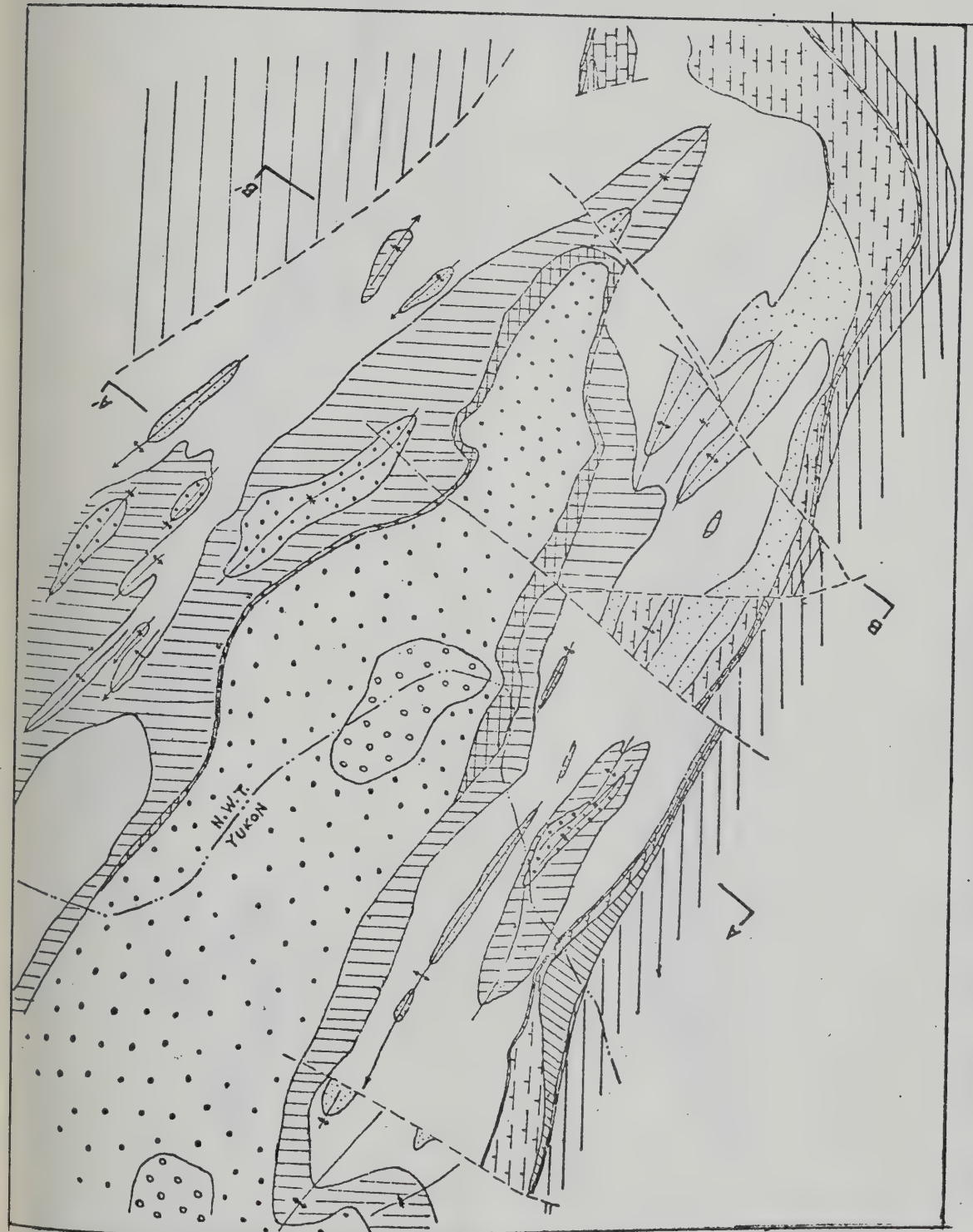
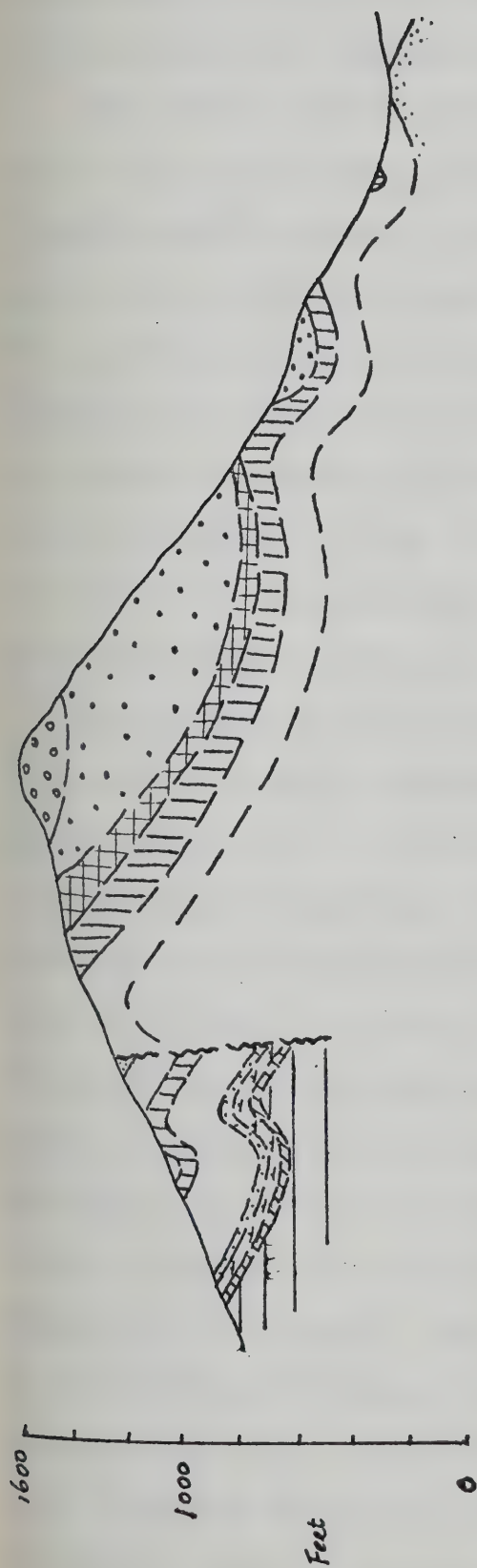
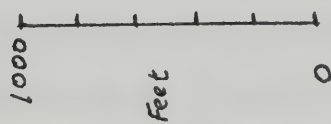


Fig. III-18. Geological map of the Canex Placer's main ore zone (XY claims), Howard's Pass district (modified after Morganti, 1975, personal communication).



B



B'

Fig. III-19. Cross sections of the Canex Placer's main ore zone, Howard's Pass district.

banded limestone unit is exposed in the core of an anticline, and at a large outcrop an anticline with amplitude of about 100 feet and plunge of 12°W was observed; small-scale isoclinal folds were not seen.

Rock types in which mineralization occurs are mainly light to dark grey, cherty to calcareous, very fine-grained and laminated siltstone; remobilized sulfide layers or pods together with sheared calcite and/or quartz are occasionally observed along S_1 cleavages in these rocks. This remobilization occurred in both hand specimen and outcrop scales. High-grade galena-rich pods or "cross faults" aligned parallel to S_1 are observed in trenches in the main zone. Sphalerite and galena layers intersecting primary bedding at low angles in cherty siltstone specimens are also commonly encountered and believed to result primarily from de-watering compaction cleavage (see Plate III-17C).

The thickness of the mineralized cherty siltstone is estimated to be about 50 feet, and if the mineralization that extended to part of the cherty limestone unit is included, the total thickness of stratiform mineralization bed could be as much as 100 feet. The aerial extent of mineralization in the main zone is about 2 miles long and 1.5 miles wide. No definite correlation of the aerial extent of mineralization in the district has ever been made. However, cherty siltstone and calcareous siltstone of a similar age and lithology, containing smaller and lower grade stratiform zinc-lead mineralization, occurs in ANNIV claims of Placer and Pas claims of Dynasty, about 14 miles and 3 miles, respectively NW of the main zone. If these occurrences are considered as the extension of the mineralization, then the aerial extent could indeed be very large. Alternatively, all these occurrences could possibly be separate mineralization centers with zinc-lead grade decreasing laterally outwards and vertically until it reaches the background levels of sediments.

The main zone deposit appears to contain several mineralized silt-stone horizons separated by sulfides - poor cherty to calcareous, pyritic sediments. The enclosing sediments are essentially composed of quartz, calcite, dolomite, illite and carbonaceous matter.

(b) Ore and Gangue Minerals. The ore minerals are mainly very fine-grained (often only a few microns in diameter) and occur as thin laminations conformable to bedding and disseminated grains; coarse-grained patches or aggregates are very rare except in remobilized pods or streaks. The main sulfide minerals, in decreasing order of abundance, are pyrite, sphalerite, galena, chalcopryite, marcasite, and possibly bornite or chalcocite. The latter three minerals occur only in very minor to trace amounts and are not seen in many specimens. There are two types of pyrite - framboidal pyrite generally a few microns in size occurs as disseminations or laminations along bedding or dispersed in the matrix of a specimen; and coarser-grained subhedral to angular crystals of pyrite form massive aggregates which appear to be recrystallized after and segregated from framboidal pyrite, and are probably diagenetic in origin. The second type of pyrite appears to be abundant in folded and remobilized beds as well as associated with the concentration of sphalerite and galena, whereas framboidal pyrite is rarely seen associated with zinc-lead mineralization, except occasionally where the mineralization is weak and of a disseminated nature. Sphalerite is present as fine-grained disseminations and monomineralic layers or laminations (up to 1 mm thick) and less commonly as remobilized bands or pods; its color is usually pale greyish white but some appears to be light brown. Galena commonly occurs with sphalerite as discontinuous "threads" that can be monomineralic or

grade into the adjacent sphalerite as fine-grained disseminations; it also forms small unmixing intergrowth blebs and streaks in sphalerite. Some coarse-grained galena occupies remobilized pods or cross-faults in association with pyrite. Disseminated to thinly bedded sphalerite, galena and pyrite are sometimes strongly replaced by remobilized layers or aggregates of the same sulfides with patches of sheared calcite.

Chalcopyrite occurs as small isolated grains or patchy aggregates in sphalerite. On one occasion, some tiny bluish copper sulfide minerals identified as bornite, occur as rims around pyrite. Marcasite is present as small mottled, blondish minerals forming aggregates interstitially in the groundmass, and appears to be primary in origin.

Non-sulfide minerals made up the rest of the groundmass and they include, in order of decreasing abundance, carbonates, clay mica (mostly illite and some vanadium-mica), carbonaceous matter, and quartz. Carbonate minerals are mostly calcite and dolomite; they occur in the groundmass as small patches or grains along bedding as well as randomly distributed thin laths or streaks; some remobilized specimens contain secondary sheared and/or crushed fibrous calcite in contorted bands or veins, often containing some fine-grained quartz aggregates. Quartz also occurs in the groundmass as interlocking minute streaks or finely dispersed grains in small amounts. Clay mica minerals probably make up most of the silt fraction of the rock, and illite is by far the most abundant component, with minor amounts of vanadium-bearing mica (roescolite ?) and chlorite (Plate III-16E). Roescolite (?) occurs as thin laths or needles aligned parallel to the bedding together with carbonaceous matters; it sometimes shows straight extinction and is generally

white creamy grey in polished section. Carbonaceous matter (Plate III-16E and G) is omnipresent in most of the specimens investigated; it occurs as smooth, purplish to brownish creamy aggregates, partly broken or fractured, in the groundmass with other carbonates, quartz and micas; in remobilized sulfide layers replacing sulfides; as minute streaks aligned parallel to laminations; and in quartz veins cutting sulfide beds. The carbonaceous matter has a low reflectivity ($\sim 5\%$) and some is characterized by wavy extinction and weak anisotropism. Chemical impurities were detected in most of the carbonaceous matter and include V, Zn, Ca, K, Ti and S.

Photomicrographs of some typical ore and gangue minerals are shown in Plate III-16.

(c) Ore Texture. There are basically three types of prominent textures in the mineralized specimens: finely laminated ore with minor dissemination and framboidal pyrite, folded beds with some minor recrystallization and mobilization, and highly contorted beds with prominent recrystallization, mobilization, and brecciation.

The laminated and disseminated ore is by far the major mineralization type, and is characterized by very fine-grained sulfides faintly laminated and/or disseminated throughout the host rocks which usually are enriched in sedimentary pyrite beds or disseminations. In detail this type of ore is sometimes slightly disturbed and small amounts of mobilization can be observed; some of this mobilization may be due to pre-consolidational sedimentary loading or compaction and some may be due to post-depositional tectonic disturbance.

As tectonic deformation increases in intensity and scale, folding, recrystallization, mobilization of sulfides into S_1 cleavages and

brecciation also increase in intensity and frequency. Micro scale slip folding, thickening of sulfide beds, contorted bands or streaks of sulfides, increase in grain size with recrystallization, and brecciation and veining are among the common features observed. Some high-grade coarse-grained galena and pyrite with sheared fibrous calcite and quartz "veins" probably reflect the ultimate tectonic deformation on the sulfide ores.

Some typical textures observed in hand specimens of ores are shown in Plate III-17.

PLATE III-16

PHOTOMICROGRAPHS OF ORE SPECIMENS
(REFLECTED LIGHT, OPEN NICOL, X38)

Canex Placer's Main Zone

A. Sample DDH6-234

Interbedded framboidal pyrite (central) and diagenetic (recrystallized) subangular pyrite aggregates at both sides. Note carbonaceous matter (medium grey) closely associated with diagenetic pyrite. Groundmass is very fine-grained clay mica (dark grey) and carbonaceous matter.

B. Sample DDH6-274

Disseminations of fine-grained sulfides (mainly sphalerite; very minor galena) in siltstone groundmass and remobilized and folded, thinly bedded sulfide layers of sphalerite (light grey) and galena (white); very minor pyrite grains. Note tectonic thickening of sulfide layers at right.

D. Sample DDH29-418.5

Laminated (bedding: top-bottom of photo) framboidal pyrite in siltstone groundmass (with very small carbonaceous matter). Disseminated sphalerite grains (central left, white) form "replacement" or "overgrowth" of pyrite. Minor quartz (medium grey) is associated with sphalerite.

D. Sample DDH29-579.3

Disseminated to poorly laminated sulfides (mainly sphalerite and minor galena) replaced or "overgrew" on tiny disseminated-bedded framboidal pyrite (obvious at right). Groundmass is mainly quartz (medium grey), calcite (dark grey thin needles or laths) and disseminated grains of clay mica (dark grey - black dots). Bedding is top-bottom of photo.

E. Sample DDH32-168

Thinly bedded roescolite (?) (white) and carbonaceous matter (light grey) in groundmass of very fine-grained clay mica, carbonaceous matter and disseminated tiny framboidal pyrite.

F. Sample DDH34-267

Disseminated to poorly bedded sulfides (mainly sphalerite and minor galena) in siliceous (cherty) siltstone groundmass (quartz and minor clay mica). Thin laths of reoriented calcite (dark grey) replace sulfides. Bedding is left-right of photo.

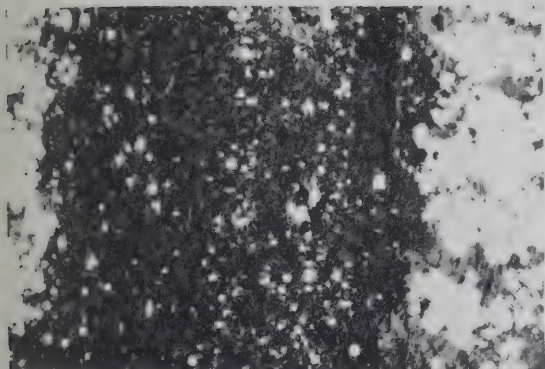
G. Sample DDH34-330A

Disseminated to poorly bedded galena (white) and sphalerite (Sp) (at right of photo) in a groundmass of quartz (light grey), calcite and clay mica (both dark grey to black). Sulfides with partly fractured and faceted carbonaceous matters (light medium grey) were remobilized into a cleavage (at left of photo). Bedding is top-bottom of photo.

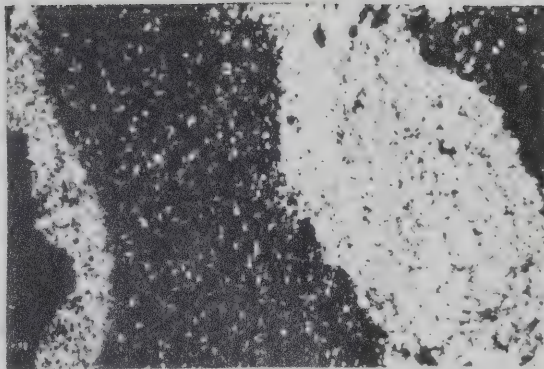
H. Trench Sample T-19-1

Laminated sphalerite (light grey), minor galena (white) and pyrite (Py, and in a sphalerite layer at extreme right of photo). Groundmass is mainly quartz (dark grey) and clay mica (black).

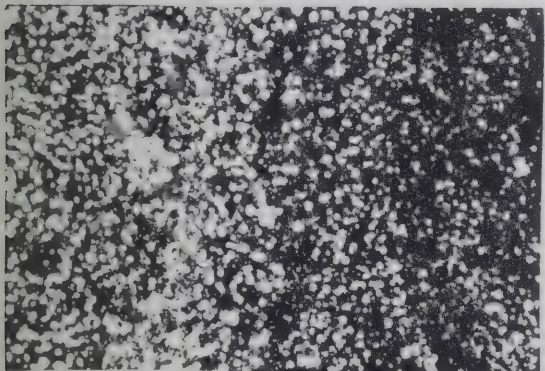
A



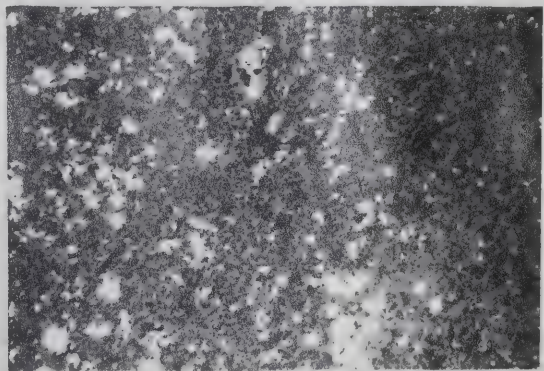
B



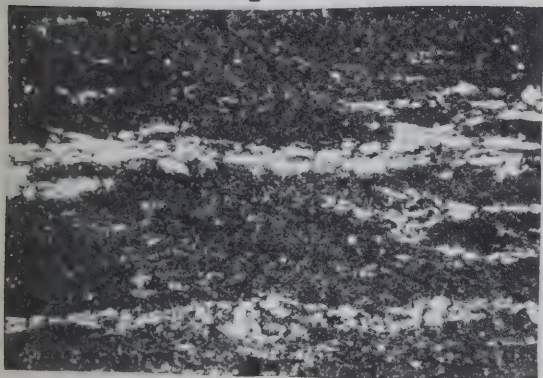
C



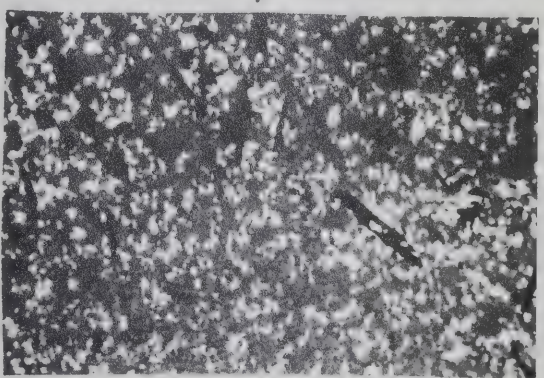
D



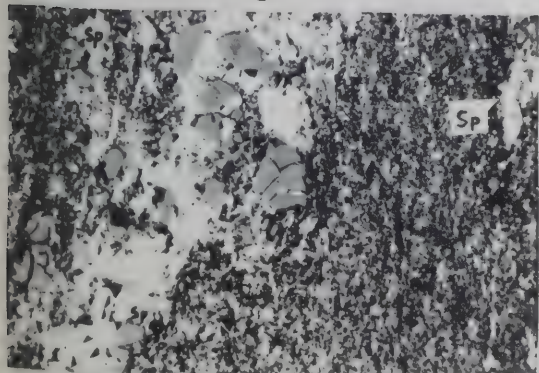
E



F



G



H

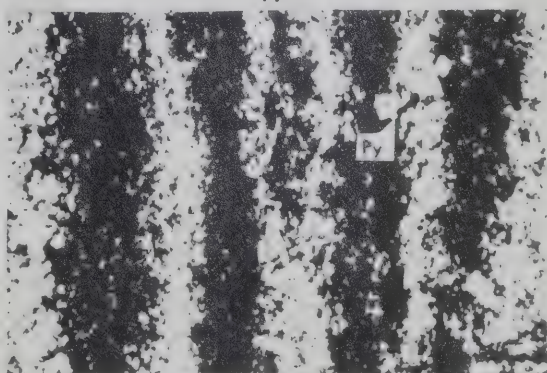


PLATE III-17

PHOTOGRAPHS OF ORE SPECIMENS
(REFLECTED LIGHT)

Howard's Pass District

A. Sample DDH74-P-2-225': (Pas claims, Dynasty Explorations Ltd.)

Slightly folded, finely laminated cherty siltstone containing remobilized streaks of sulfides (mainly sphalerite, minor pyrite, galena; pale grey at right and central top of photo) and coarse galena "lens" (white, upper left). Note angular intersection of sulfide streaks to laminations. X38

B. Sample DDH74-P-1-144': (Pas claims, Dynasty Explorations Ltd.)

Laminated cherty-siliceous siltstone containing tiny disseminated pyrite (white dots). A small folded calcite vein at upper right of specimen. X38.

C. Trench No. 18: Placer's main zone, "north band"

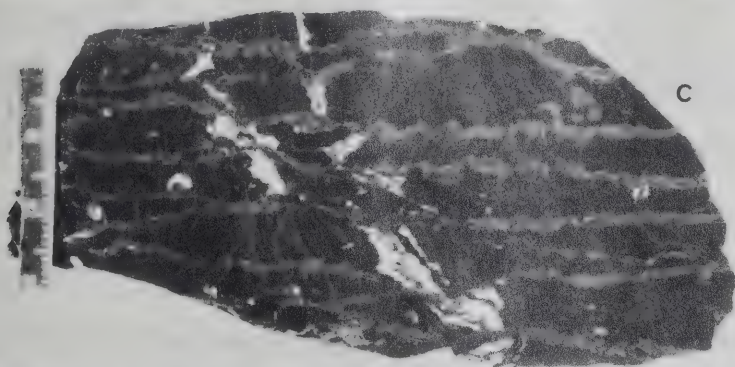
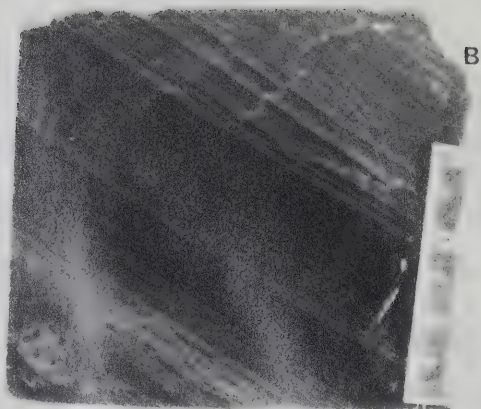
Thinly bedded cherty siltstone (faint laminations) and mobilization of sulfides (mainly sphalerite, minor galena and pyrite) along S_1 cleavages (dewatering compaction cleavages?). Some remobilized and sheared calcite (white) streaks. X38

D. Trench No. 19: Placer's main zone, "north band"

Thinly bedded cherty siltstone and remobilized streaks of sulfides (light grey in upper part of specimen) and calcite (white), X38.

E. Trench No. 18: Placer's main zone, "south band"

Tightly folded, laminated cherty siltstone and remobilized veinlets and streaks of sulfides (light grey) and calcite (white). Note a thicker "layer" of remobilized sulfides (mainly sphalerite) at right edge of specimen. X38



Chapter IV
CHEMICAL PETROLOGY

A. INTRODUCTION

Chemical analyses of major and trace elements in basalts, eclogites and their minerals from the Anvil and Frances Lake districts are presented in this Chapter. Petrogenetic interpretations and classifications are made following demonstration of characteristics of rocks and/or minerals in various correlation diagrams and the principles and validity of these diagrams are briefly discussed.

Analyses and interpretation of many conformable volcanic rocks close in time and space to the ore deposits are useful in elucidating the nature of volcanism and its geological setting in the Anvil Range and Frances Lake districts.

Eclogites from the Anvil Range district were analyzed in order to estimate metamorphic conditions and enable correlations to be made with other eclogite terrains. The analytical results of whole rock eclogites and their minerals, and discussion on the original rock types and tectonic implication of the eclogites are presented in Appendix IV-1.

Different methods were employed and therefore intercomparisons using mutual specimens were made during various stages of the thesis work. The methods included Atomic Absorption Spectrometry (AA), Multiple radio frequency argon plasma emission spectrometry (MRFAPE), X-ray fluorescence spectrometry (XRF), Induced Neutron Activation Analysis (INNA), and Electron Microprobe Analyser (EMPA). AA and MRFAPE analyses were made by Barringer Research Ltd. of Toronto in the fall of 1975, XRF analyses were made by J. Holland of Oxford in 1974 through the kind arrangement of R. St.J. Lambert; EMPA analyses were made by the writer at the University

of Alberta in the summer and fall of 1975; and INNA analyses of U and Th were made at McMaster University. Specific methods used will be mentioned in conjunction with the presentation of the analytical results.

B. ANVIL RANGE DISTRICT

1. Lower Paleozoic Volcanic Rocks

Submarine volcanic greenstones occurring in the upper part of the Cambro-Ordovician strata appear to be conformable with the sediments and thus provide a key to the nature of volcanism and hence geological setting of this period.

Chemical analyses of major and trace elements in 12 "fresh" volcanic rocks were made; analyses of major elements in 4 rocks were already published by Tempelman-Kluit (1972). These analyses are presented in Table IV-1. Locations of the specimens analyzed are shown in Fig. IV-1. As can be seen from the intercomparison of specimen 67-28b, the methods employed seem to yield major element results agreeable within analytical error, and therefore reported results from the two different laboratories are acceptable. The overall precision of the MRFAPE results is $\pm 3\%$ for the trace elements (i.e. at $\leq 0.1\%$ concentration level) and $\pm 2\%$ for major elements at above 95% confidence level.

Various criteria have been used to classify and distinguish volcanic rocks. The chemical procedures commonly used are various empirical chemical correlation and discrimination diagrams or normative mineral compositions of the rocks (particularly useful for fresh fine-grained rocks when petrographic criteria are unsuitable). The former are useful in characterizing the affinity of the analyzed rocks in various boundaries or fields defined by large numbers of chemical data, although one must

TABLE IV-1

Chemical Analyses of Cambro-Ordovician Volcanic Rocks,
Anvil Range District, Yukon

	K20-1A	K20-3A	K20-3B	K25-4	67-28	67-319	67-340C
SiO ₂	46.37	48.58	46.48	49.63	45.41	49.67	47.87
Al ₂ O ₃	14.97	15.68	15.01	16.47	15.69	16.81	15.59
ΣFeO	10.26	9.35	10.84	10.08	10.08	8.45	10.18
MgO	8.52	8.82	8.83	6.77	8.38	6.32	6.86
CaO	10.42	8.64	8.45	7.57	9.63	8.39	9.32
Na ₂ O	2.30	2.63	3.71	2.75	4.78	3.15	2.68
K ₂ O	0.87	0.93	0.21	0.68	0.35	0.72	0.57
TiO ₂	1.73	1.08	1.92	1.72	1.30	1.61	2.45
P ₂ O ₅	0.16	0.12	0.18	0.16	0.15	0.16	0.21
MnO*	0.20	0.20	0.20	0.20	0.20	0.20	0.20
CO ₂ *	0.10	0.10	0.10	0.10	0.10	0.10	0.10
H ₂ O*	4.00	4.00	4.00	4.00	4.00	4.00	4.00
Co	126	110	121	93	139	113	132
Cr	875	575	625	203	2035	192	416
Ni	449	176	239	58	630	120	161
V	275	208	333	289	269	296	397
Zn	208	160	200	167	205	278	191
Ag	10	6	10	6	10	6	1
Pb	65	60	20	<5	60	225	15
Cu	32	32	164	1	248	114	125
Sr	169	695	464	164	371	246	760
Be	-	1	2	1	1	-	1
Zr	89	89	111	103	59	119	148
Nb	-	-	-	-	-	18	7
U**	0.5	-	-	0.6	-	-	-
Th**	2.8	-	-	2.3	-	-	-

Analytical Method: MRFAPE and AA

Analyst: R. Cruetz, Toronto

* Assumed contents (H₂O and CO₂: based on minimum values reported - in Tempelman-Kluit (1972); MnO: based on average of XRF results and Templeman-Kluit's average).

** Induced neutron activation analysis (INNA, McMaster University).

TABLE IV-1 (cont'd)

	67-19b	67-37	67-403a	67-442b	67-28b	67-28b**
SiO ₂	46.35	45.70	46.99	47.23	47.63	47.52
Al ₂ O ₃	15.16	15.78	14.36	14.60	12.06	12.41
ΣFeO	10.21	10.30	10.58	11.48	11.04	10.80
MgO	8.31	7.93	8.21	8.20	9.08	8.95
CaO	11.26	10.98	11.53	9.44	9.49	9.06
Na ₂ O	2.34	2.69	2.56	2.01	4.43	4.06
K ₂ O	0.76	0.20	0.30	0.10	0.10	0.20
TiO ₂	1.09	1.20	1.28	2.10	1.72	1.55
P ₂ O ₅	0.23	0.24	0.29	0.39	0.32	0.20
MnO	0.19	0.17	0.20	0.18	0.16	-
CO ₂ *	0.10	0.10	0.10	0.10	0.10	-
H ₂ O*	4.00	4.00	4.00	4.00	4.00	4.00
Ni	701	729	348	109	246	
Zn	116	111	115	114	93	
Cu	256	137	142	48	96	
Ba	141	6	48	30	384	
Sr	384	211	331	470	241	
Rb	43	1	1	1	3	
Zr	86	132	127	193	141	
Nb	16	23	21	34	20	
Y	11	16	15	18	20	
U***	0.3	0.4	0.4	0.8	1.4	
Th***	1.8	3.0	2.4	3.7	2.0	

Analytical Method: XRF

Analyst: J. Holland, Oxford

* Assumed contents (based on minimum values reported in Tempelman-Kluit, 1972).

** MRFAPe analysis; water content assumed.

***Induced neutron activation analysis (INNA, McMaster University).

TABLE IV-1 (cont'd)

	TK-A	TK-B	TK-C	TK-D
SiO ₂	46.80	46.20	48.50	46.70
Al ₂ O ₃	14.90	15.40	15.90	16.50
Fe ₂ O ₃	2.20	2.20	3.50	2.10
FeO	8.80	8.60	6.20	10.30
MgO	7.60	6.80	5.50	5.60
CaO	6.50	8.60	11.80	4.40
Na ₂ O	4.70	3.90	2.30	2.40
K ₂ O	0.20	0.20	0.40	1.70
TiO ₂	1.68	1.60	1.38	3.12
P ₂ O ₅	0.14	0.14	0.13	0.59
MnO	0.26	0.43	0.16	0.07
CO ₂	0.10	0.10	0.20	2.30
H ₂ O	4.20	4.10	4.90	5.80

Analyses reported in Templeman-Kluit (1972); analytical method: wet chemical analysis.

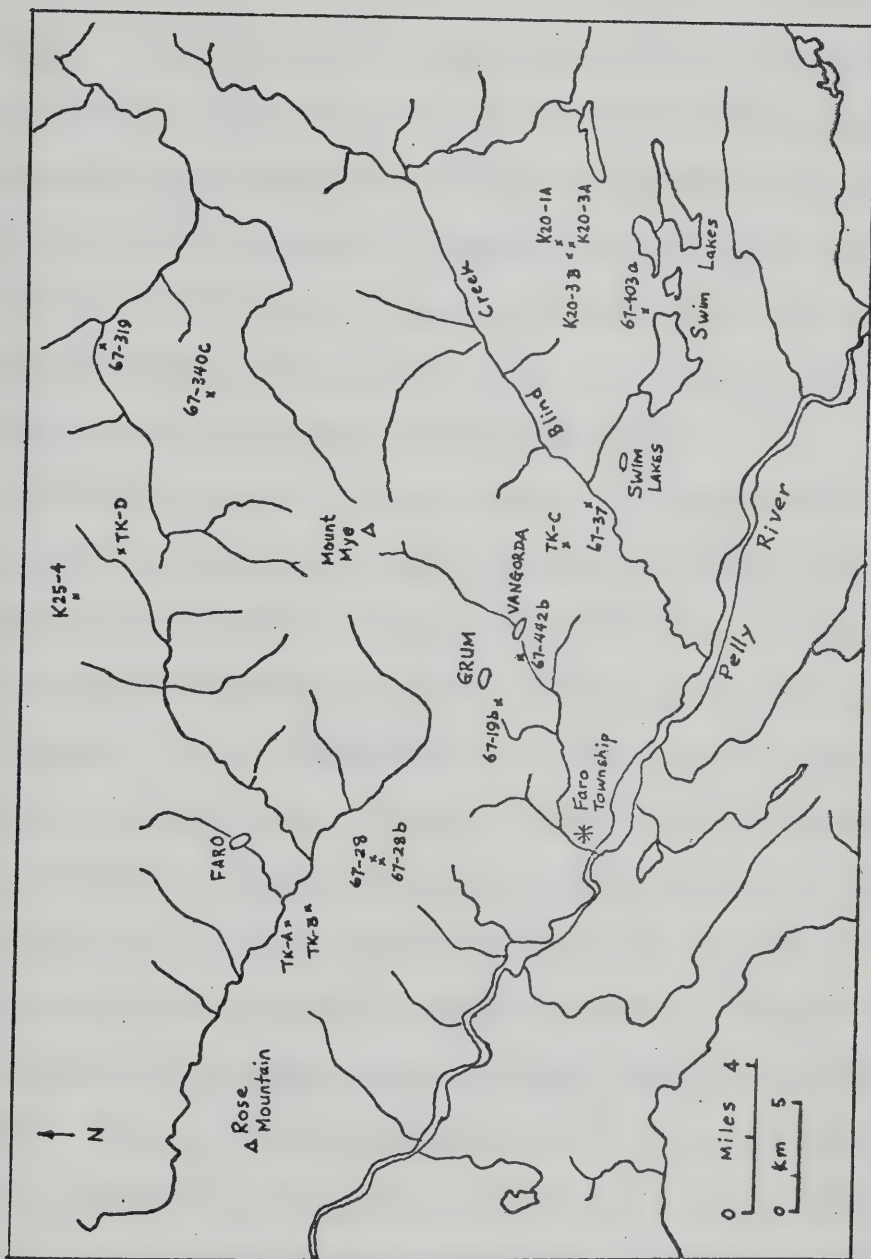


Figure IV-1. Locations of Lower Paleozoic volcanic rock specimens, Anvil Range district, Yukon.

keep in mind that this type of classification is inherently limited in that it represents a synthesis of an existing body of data and there is no assurance that it can be applied universally. The normative composition, especially the degree of silica saturation can be applied to any basaltic liquid, if the ambiguities that arise from the late stage or post-crystallization oxidation of iron can be resolved (Kay et al., 1970).

(a) Chemical Correlations. Rock specimens analyzed were collected from widely separated locations and therefore are representative of Cambro-Ordovician basic volcanic rocks in the Anvil Range districts. The analyses vary little among all the rocks and are considered to represent an overall chemical variation for these rocks.

Chemical characterization of major series of volcanic rocks has recently been convincingly demonstrated by Miyashiro (1974, 1975). The total FeO/MgO ratio of residual magma increases at least in the early and middle stages of fractional crystallization in practically all igneous rock series; it may not increase in the late stage of some series. Hence, this ratio or parameters related to it may be used to represent the degree of fractional crystallization. Miyashiro has shown that in a typical tholeiitic series of volcanic rocks, ΣFeO , TiO_2 (or Ti), and V content increases first and then, passing a maximum, begins to decrease with advancing fractional crystallization (that is, with increasing $\Sigma\text{FeO/MgO}$). In a typical calc-alkalic series, these elements decrease monotonically and rapidly with advancing fractional crystallization. Cr, Ni contents of both rock series were found to decrease rapidly with advancing fractional crystallization. Using S.I. (solidification index of Kuno) as a degree of fractional crystallization, Kawabe (1974) shows that Ni, Cr, and Co contents in oceanic tholeiites and island arc basalts

behave in a distinctly different manner and thus can be used as an indicator in differentiating the two rock types.

Other correlations are based on a similar principle, and use Ti as a common parameter. Pearce (1975) and Pearce and Cann (1973) suggest Ti-Zr, Ti-Zr-Sr, Ti-Zr-Y and Ti-Cr correlations to discriminate among ocean floor basalts, "within-plate basalts", and island arc basalts (low K tholeiites, calc-alkalic basalts); Rhodes (1973) uses a P_2O_5 - TiO_2 plot to separate fields of oceanic ridge basalts, oceanic island tholeiites, and alkalic basalts; based on the generally low concentrations of TiO_2 , K_2O and P_2O_5 , Pearce et al. (1975) suggest the use of this ternary plot to distinguish oceanic and continental (non-oceanic) basalts.

In Fig. IV-2, FeO , TiO_2 , Ni and V contents are plotted against $\Sigma FeO/MgO$. Most of the analyses fall in or close to a field from which most of volcanic rock series originate and it is defined by a large number of abyssal tholeiites from the mid-oceanic ridges (Engel et al., 1965; Melson and Thompson, 1971; Thompson et al., 1973, etc.). It is only fair to point out that there exists a large number of analyses of tholeiite rock series from island arcs, ocean islands, and even stable continents which are scattered in these diagrams and overlap this "abyssal tholeiite" field. Therefore, in order to elucidate the real setting of the present rocks, we need to reduce and narrow down the variables of different geological settings. A general discussion and interpretation of petrogenesis for the rocks will be presented following the next section. In this section, stepwise chemical discriminations are made and their implications are proposed.

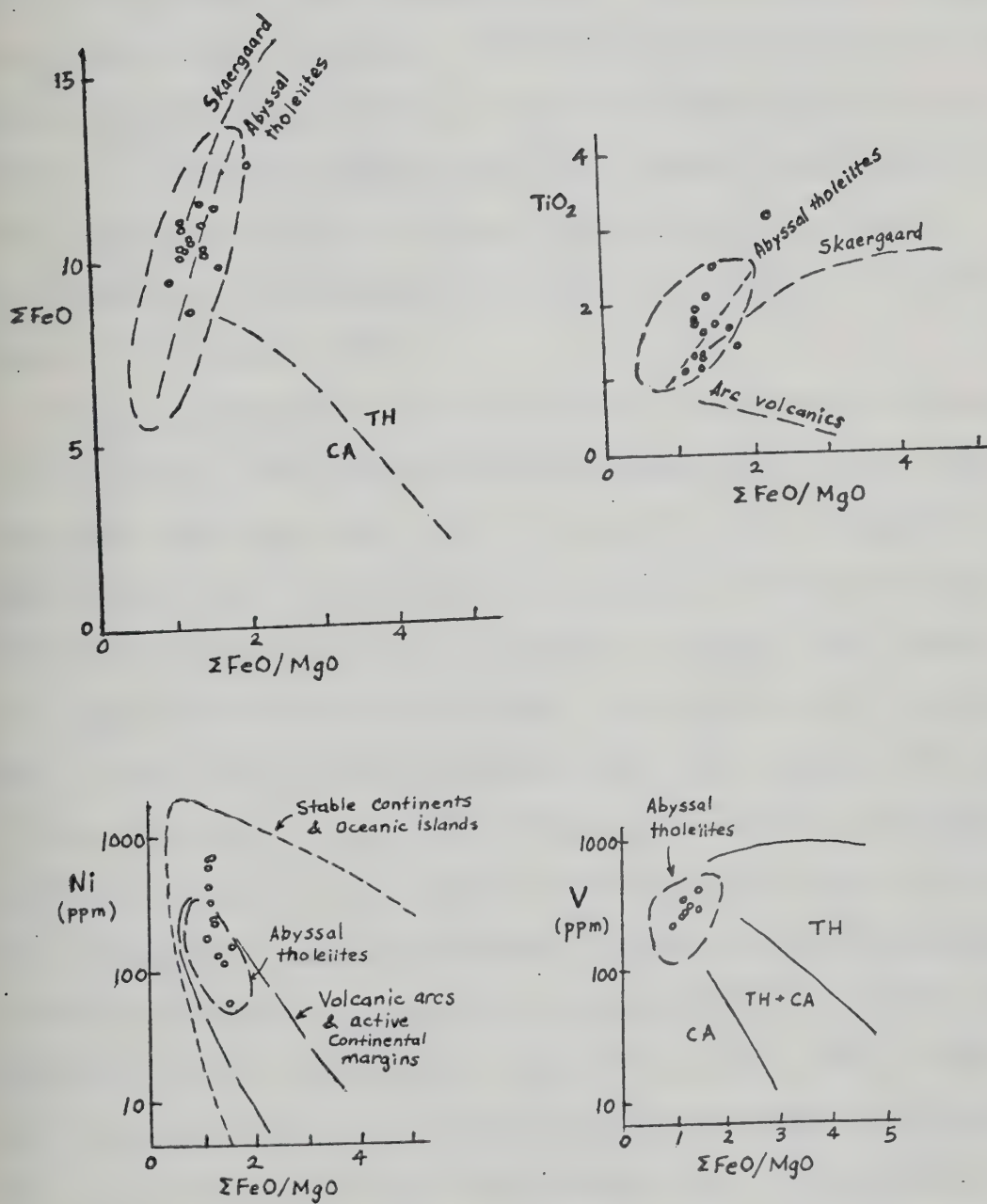


Fig. IV-2. Discrimination diagrams of ΣFeO , TiO_2 , Ni and V vs. $\Sigma\text{FeO}/\text{MgO}$. TH: tholeiitic; CA: Calc-alkalic.

Fig. IV-3 shows correlation of Ni, Cr versus solidification index S.I. [where $S.I. = MgO \times 100 / (MgO + \text{total FeO} + Na_2O + K_2O)$] of the analyses; fields of large numbers of abyssal tholeiites and island-arc basalts are indicated (after Kawabe, 1974). Fig. IV-4 shows a distinction between 2 major rock series: tholeiitic and calc-alkalic; all the analyses plot within the boundary of tholeiitic rocks. From these two diagrams, it appears that most or all of the analyses have a strong affinity with abyssal tholeiites and are distinctly not calc-alkalic. This impression is strengthened from a plot of the analyses in a A-F-M diagram as shown in Fig. IV-5.

Plots of analyses using Ti-Zr-Y, Ti-Zr-Sr, Ti-Zr and Ti-Cr diagrams are shown in Fig. IV-6; different fields of magma types are also indicated (after Pearce and Cann, 1973). In Ti-Zr-Cr plot, a magma type of "within-plate basalt" (ocean island or continental flood basalts) is implied; whereas in Ti-Zr-Sr plot, 8 out of 12 analyses plot in ocean floor basalt and low K_2O tholeiite fields, and 4 plot in the calc-alkalic field. In the Ti-Zr and Ti-Cr diagrams, most of the analyses fall within or close to the field of ocean floor basalts. It should be noted here that Sr (also Rb and K) can be highly affected by the process of alteration or greenschist facies metamorphism. Yttrium is generally enriched in minerals of late stage fractional crystallization (e.g. apatite), and sometimes in ilmenite and magnetite (Cornwall and Rose, 1957); furthermore, the regional variation of Y in basaltic rocks appear to be greater than interlaboratory variation, fractionation stage, or petrographic type (Prinz, 1967). Therefore, the first two discriminants in Fig. IV-6 are subject to many complicated factors and uncertainties (see for example, plotting of Troodos volcanic rocks by Pearce, 1975). Ti and Zr are

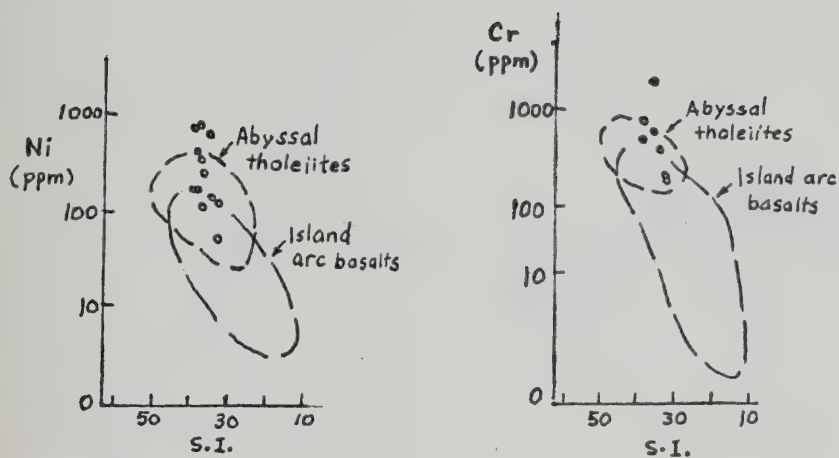


Figure IV-3. Correlations of Ni and Cr versus solidification index (S.I.).

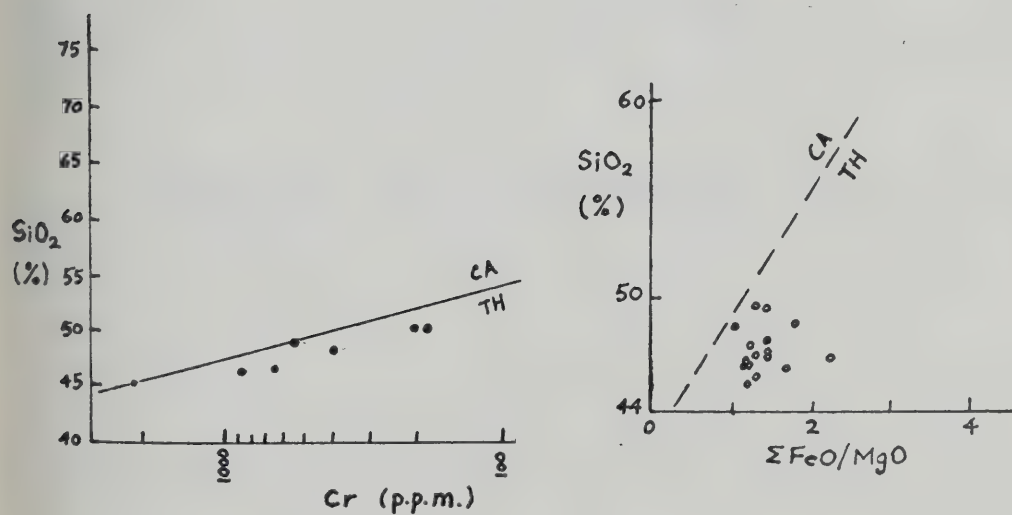


Fig. IV-4. Correlations of SiO₂ versus Cr and ΣFeO/MgO.

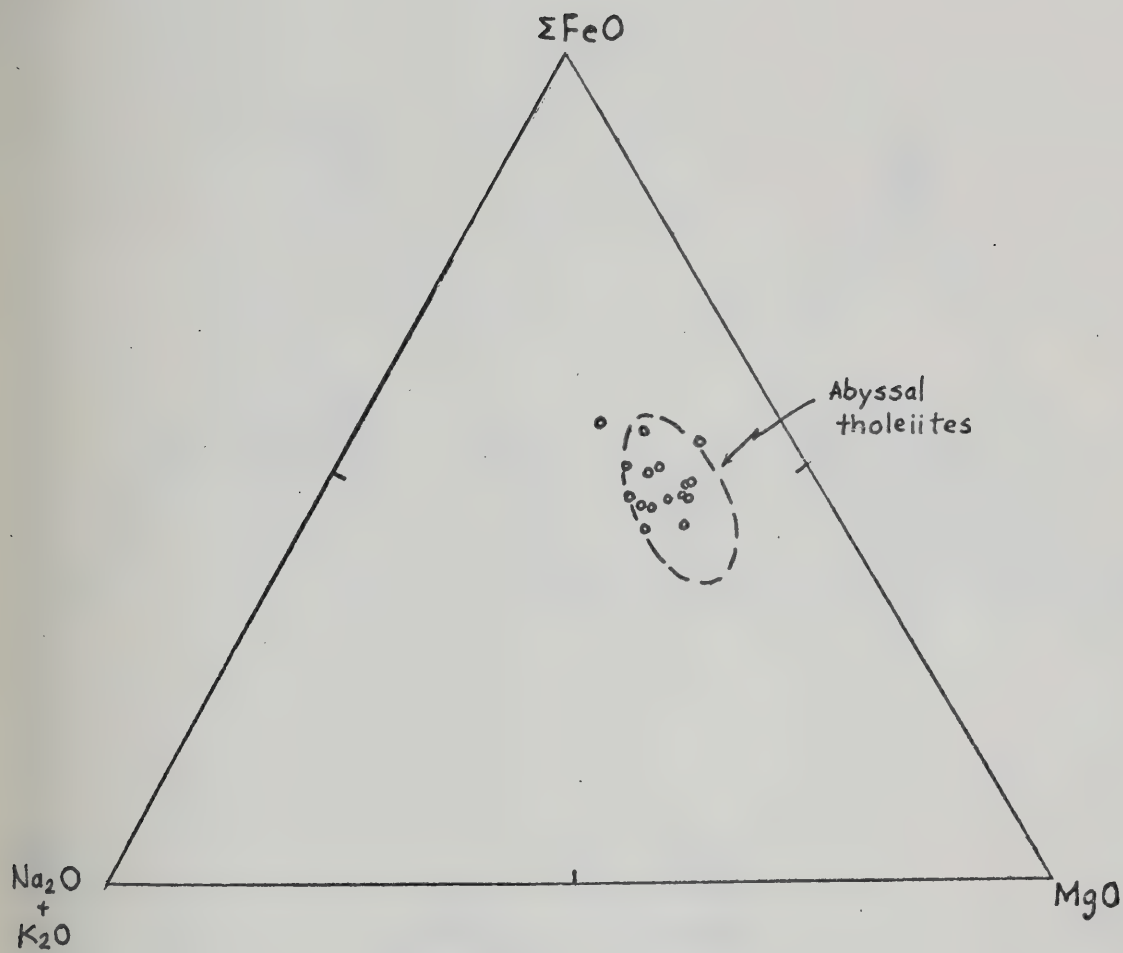


Figure IV-5. Plots of Anvil volcanics in an A-F-M diagram.

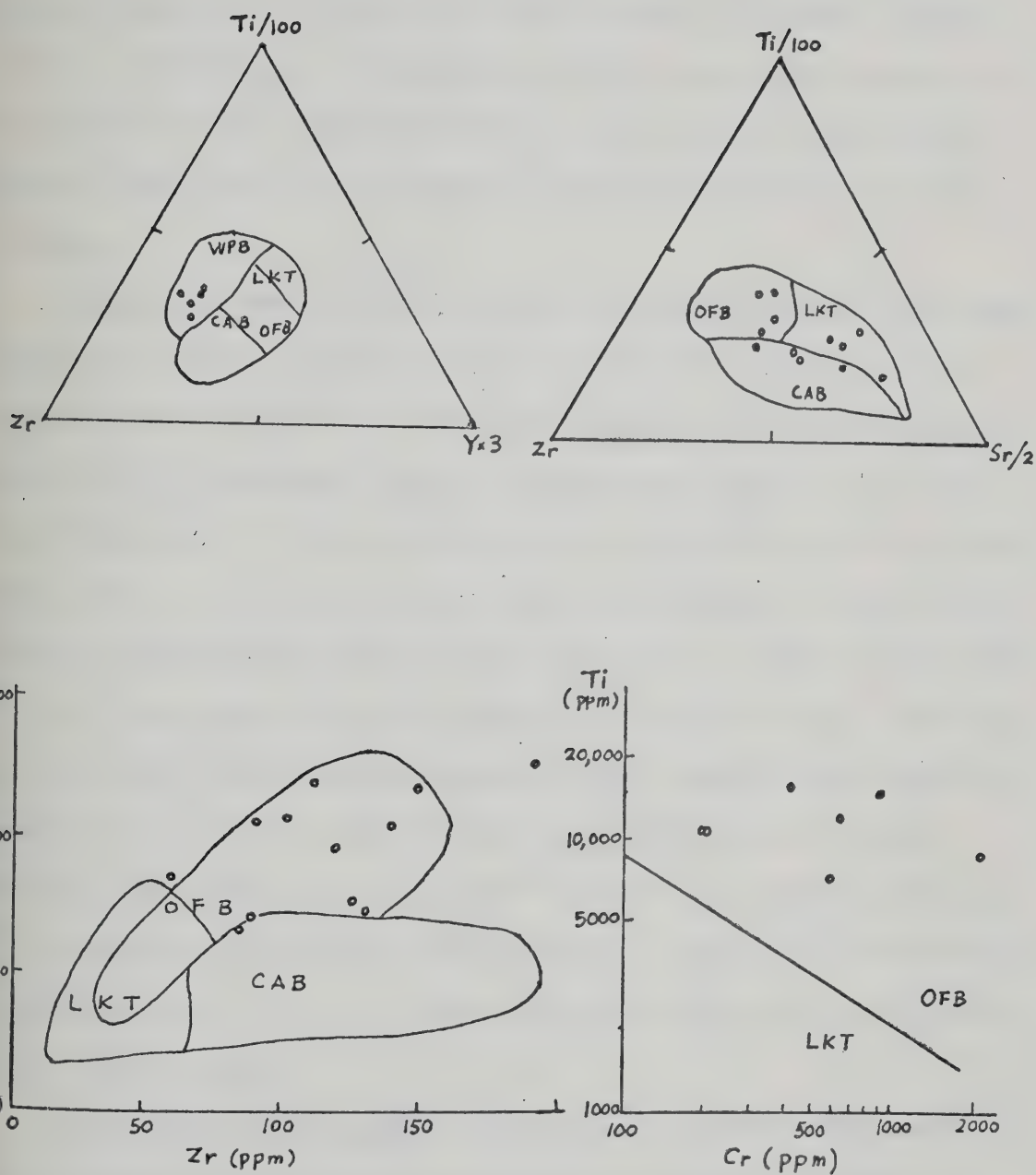


Fig. IV-6. Discrimination diagrams of Ti-Zr-Y, Ti-Zr-Sr, Ti-Zr and Ti-Cr. WPB: within plate basalts; LKT: low-K tholeiites; CAB: calc-alkalic basalts; OFB: ocean floor basalts.

both insensitive to alteration process (Cann, 1970; Pearce and Cann, 1973) and enriched in the early and middle stage of fractional crystallization. Furthermore, a relatively consistent implication deduced from this correlation has been demonstrated by Pearce and Cann for Troodos volcanic rocks which were interpreted by Miyashiro (1973) to be island arc types.

Distinction between oceanic and non-oceanic (continental) and among ocean ridge, oceanic island and alkalic basalts is attempted by using diagrams shown in Fig. IV-7. Most of the analyses fall in the oceanic basalt field in the ternary plot of $\text{TiO}_2\text{-K}_2\text{O-P}_2\text{O}_5$, whereas in the $\text{P}_2\text{O}_5\text{-TiO}_2$ diagram, most of the analyses again are distinctly related to ocean-ridge basalts. A study of deep-sea weathering of basalts by Hart (1970) indicates that the above three elements are lost to seawater in the order $\text{Ti} > \text{K} > \text{P}$, and weathered basalts tend to be enriched in K_2O . Pearce et al. (1975) also show that metamorphosed oceanic basalts tend towards K_2O enrichment and leave the oceanic field in the $\text{TiO}_2\text{-K}_2\text{O-P}_2\text{O}_5$ diagram. The four points that plot outside the "oceanic field" probably reflect a more pronounced effect of this complex change. But since the majority of the analyses fall within the oceanic field, the rocks are very likely of oceanic basalt origin.

(b) Normative Compositions. The CIPW and molecular (Niggli and Barth) normative compositions of the rocks are presented in Table IV-2. Since all of the rocks analyzed are metamorphosed greenstones, the total water contents are preserved in the normative compositions and the sums are recalculated to 100% (Melson and Van Andel, 1966). The relative proportions of normative minerals are, however, relatively constant even without this recalculation. Partial reduction of Fe_2O_3 to 1.50 wt % has

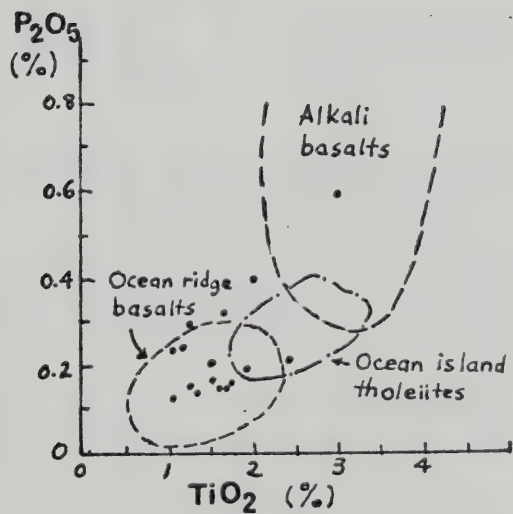
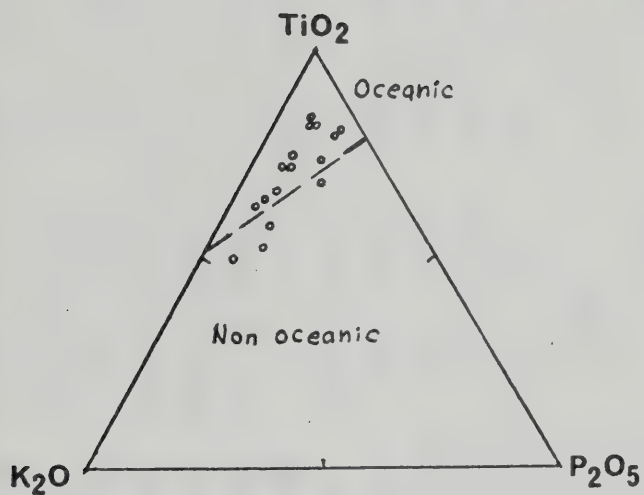


Figure IV-7. Discrimination diagrams of TiO_2 - K_2O - P_2O_5 and P_2O_5 - TiO_2 .

Normative Compositions of Cambro-Ordovician Volcanic Rocks, Anvil Range District, Yukon

	K20-1A		K20-3A		K20-3B		K25-4		67-28		67-319		67-340C	
Q	0	0	0	0	0	0	2.17	2.02	0	0	1.03	0.95	0.15	0.14
Ne	0	0	0	0	1.11	1.29	0	0	11.38	13.05	0	0	0	0
Or	5.16	5.15	5.50	5.44	1.24	1.23	4.02	4.03	2.07	2.02	4.28	4.26	3.37	3.39
Ab	19.50	20.67	22.24	23.37	29.18	31.31	23.26	24.72	19.44	20.13	26.80	28.30	22.69	24.18
An	28.01	27.98	28.22	27.95	23.44	23.15	30.58	30.62	20.33	19.84	29.76	29.63	28.85	28.97
Di	18.37	18.17	11.15	10.97	14.02	13.70	4.80	4.74	21.42	20.67	8.89	8.79	12.99	12.89
Hy	6.06	6.21	15.79	16.11	0	0	23.90	24.26	0	0	18.15	18.62	19.18	19.67
O1	11.60	12.32	7.14	7.58	18.60	19.47	0	0	14.91	15.41	0	0	0	0
Mt	3.63	2.62	3.62	2.59	3.63	2.58	3.62	2.62	3.63	2.55	3.64	2.62	3.63	2.63
Il	3.29	2.41	2.05	1.49	3.65	2.64	3.27	2.40	2.47	1.77	3.07	2.24	4.66	3.43
Ap	0.37	0.34	0.28	0.25	0.42	0.37	0.37	0.33	0.35	0.31	0.37	0.34	0.49	0.44
H ₂ O	4.0	4.0	4.0	4.0	4.0	4.0	4.0	4.0	4.0	4.0	4.0	4.0	4.0	4.0
$\left(\frac{\text{Mg}}{\text{Mg}+\text{Fe}^{2+}}\right)$.6618		.6964		.6536		.6142		.6633		.6543		.6141	
$\frac{\text{Ab}}{\text{An}+\text{Ab}}$.4248		.4554		.5749		.4466		.5036		.4885		.3843	
$\frac{\text{Px}}{\text{Px}+\text{Pl}+\text{O1}}$.2924		.3187		.1826		.3477		.2815		.3234		.6157	
$\frac{\text{Pl}}{\text{Px}+\text{Pl}+\text{O1}}$.5687		.5969		.6946		.6523		.5226		.6766			

Note: first column - CIPW norms; second column - molecular norms.

	TK-A		TK-B		TK-C		TK-D		67-19b
Q	0	0	0	0	2.37	2.21	4.62	4.22	0 0
Ne	2.30	2.66	1.31	1.53	0	0	0	0	0
Or	1.21	1.19	1.20	1.19	2.35	2.37	10.13	9.99	4.50 4.48
Ab	36.37	37.97	31.04	32.74	19.33	20.67	20.46	21.40	19.82 20.95
An	19.38	19.07	24.26	24.13	31.68	31.92	18.10	17.85	28.65 28.54
Di	10.29	9.94	14.78	14.38	20.86	20.67	0	0	20.88 20.53
Hy	0	0	0	0	11.45	11.66	26.30	25.54	1.86 1.89
Ol	19.40	19.75	15.93	16.28	0	0	0	0	14.06 14.75
Mt	3.26	2.31	3.97	2.85	4.15	3.01	3.07	2.18	3.63 2.60
Il	3.26	2.35	3.08	2.25	2.60	1.93	5.97	4.31	2.07 1.51
Ap	0.33	0.29	0.33	0.30	0.30	0.27	1.38	1.22	0.53 0.48
H ₂ O	4.20	4.20	4.10	4.10	4.90	4.90	5.80	5.80	4.00 4.00
C							4.16	4.47	
Mg/Mg+Fe ²⁺ (Atomic)	.6061		.5849		.5919		.4921		.6576
Ab/(An+Ab)	.6656		.5758		.393		.5453		.4233
<u>Px</u>									
Px+Pl+Ol	.1024		.1718		.3878		.4055		.2667
<u>Pl</u>									
Px+Pl+Ol	.6525		.6429		.6122		.5945		.5684

TABLE IV-2 (cont'd)

	67-37		67-403a		67-442b		67-28b	
Q	0	0	0	0	1.64	1.53	0	0
Ne	0	0	0	0	0	0	4.44	5.14
Or	1.19	1.19	1.77	1.76	0.59	0.60	0.59	0.58
Ab	22.95	24.24	21.59	22.81	17.05	18.24	29.28	30.60
An	30.65	30.51	26.72	26.61	30.61	30.86	12.73	12.54
Di	18.42	18.07	23.05	22.63	11.20	11.13	26.09	25.41
Hy	2.01	2.03	5.49	5.55	26.36	26.95	0	0
Ol	14.26	14.90	10.67	11.15	0	0	15.24	15.88
Mt	3.72	2.62	3.61	2.59	3.63	2.64	3.62	2.57
Il	2.30	1.68	2.42	1.77	4.00	2.96	3.27	2.36
Ap	0.56	0.50	0.67	0.60	0.91	0.83	0.74	0.66
H ₂ O	4.00	4.00	4.00	4.00	4.00	4.00	4.00	4.00
Mg/Mg+Fe ²⁺ (Atomic)	.6443		.6442		.6194		.6545	
Ab/(An+Ab)	.4427		.4616		.3715		.7094	
$\frac{Px}{Px+Pl+Ol}$.2314		.3261		.4407		.3131	
$\frac{Pl}{Px+Pl+Ol}$.6071		.5520		.5593		.5041	

been adopted in calculating the norms so as to approximate "original" fresh abyssal tholeiites (Miyashiro et al., 1970; Kay et al., 1970).

The relative proportions of normative diopside, hypersthene, and olivine of all the analyses are shown in Fig. IV-8a. Five analyses plot within the olivine tholeiite field, four at the transitional fields of olivine tholeiite-alkalic olivine basalt (Di-Ol join) and olivine tholeiite-quartz tholeiite (Di-Hy join), five plot in the field of alkalic olivine basalt and two in quartz tholeiite. The basalts having a trace percent normative quartz would have contained no quartz when the oxidized iron (Fe^{+3}) is adjusted for metamorphism or alteration, and an undersaturation of silica for most rocks is inferred. Thus a complete transition from tholeiite to alkali basalts is indicated for most of the analyzed rocks using the normative Di-Ol-Hy plot. A similar transition has been demonstrated for mid-Atlantic ridge basalts at 45°N (Kay et al., 1970) and for the Indian Ocean (Cann, 1969; Kempe, 1973). The relative proportions of Di-Ol-Hy are evidently not sufficient to resolve these rocks from some other basalt occurrences - e.g. ocean island basalts also show a complete transition (Kay et al., 1970).

Miyashiro et al. (1970) and Shido et al. (1971) have proposed the use of a Pl(Ab+An) - Ol(Fo+Fa) - Px(Di+Hy) plot in characterizing magma types of the abyssal tholeiites. Depending on the first mineral to crystallize, the rocks are called olivine- and plagioclase-tholeiites, respectively; continued crystallization drives the residual liquids to the "cotective curve" between the olivine and plagioclase fields. Subsequent cotective crystallization results in an increase of pyroxene and crystallization of clinopyroxene. The analyses are plotted in this normative Pl-Ol-Px diagram as shown in Fig. IV-8b. Most of the analyses (right of

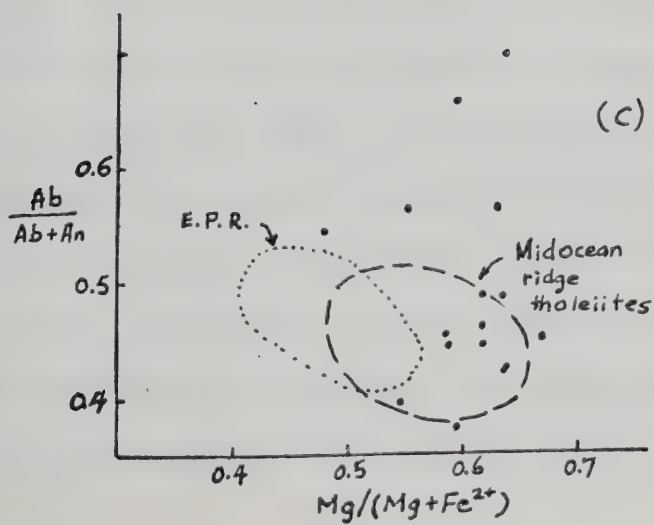
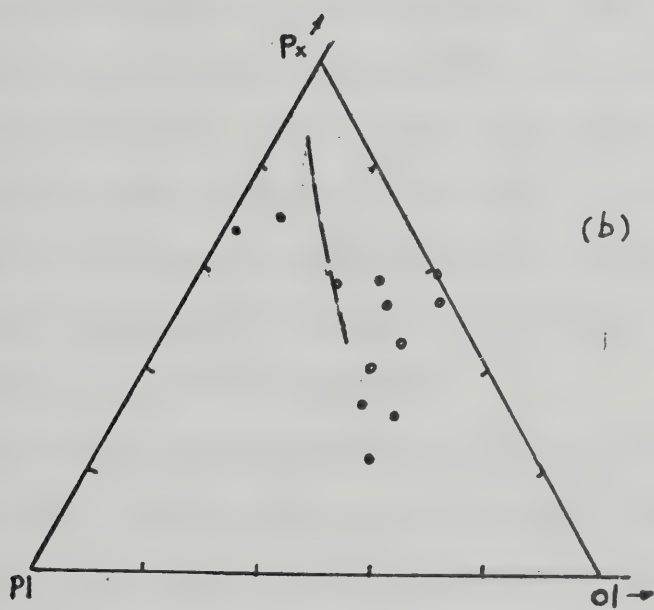
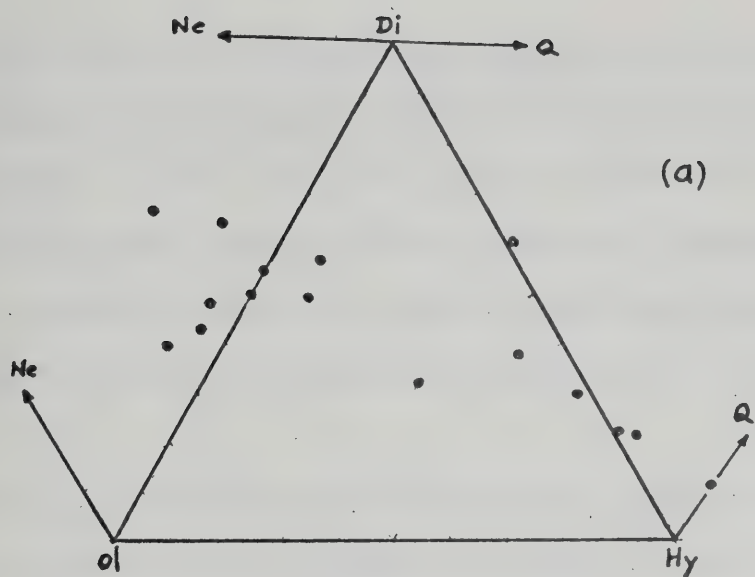


Fig. IV-8. Normative compositions of Anvil volcanics.

cotective curve) plot in or close to the field of olivine tholeiites, only two analyses in the plagioclase tholeiites (left of cotective curve). If this indication is valid, then the magmatic liquids of the tholeiitic rocks analyzed may have some diversities in chemical composition, which in turn are probably related to the depth of magma generation, extent of partial melting, liquid-solid separation mechanism, etc. (Shido et al., 1971).

Another way of comparing the relation between normative composition and degree of fractional crystallization is shown in Fig. IV-8c in which normative ratio of $Ab/(Ab+An)$ is plotted against atomic ratio of $Mg/(Mg+Fe^{2+})$. Four analysis points plot significantly above the abyssal tholeiite field for mid-ocean ridges of the world, whereas most of the other analyses plot within or close to the field. No distinct relation between degree of fractional crystallization and normative plagioclase can be detected, indicating that the magmatic liquids were mainly of another composition (i.e. olivine tholeiite).

One of the most distinctive features of abyssal tholeiites is the range of $Mg/(Mg+Fe^{2+})$ atomic ratios: most mid-ocean ridge basalts have a range of 0.55 to 0.65, East Pacific rise basalts: 0.47 to 0.60, South Atlantic basalts: 0.68 to 0.71, and Caribbean Sea basalts: 0.52 to 0.65. The $Mg/(Mg+Fe^{2+})$ ratios of the Anvil greenstones range from 0.48 to 0.66 (Table IV-2), well within the range of all mid-ocean ridge basalts.

(c) Petrogenetic Discussion. Average composition of the Anvil greenstones is compared in Table IV-3 with that of fresh, altered and metamorphosed basalts from the mid-oceanic ridges, geosynclinal basalts in Japan and Ethiopian Rift basalts. Most abyssal tholeiites from the mid-oceanic ridges of the world typically contain very low K_2O , TiO_2 and other large

TABLE IV-3

Comparison of Cambro-Ordovician Basalts in
Anvil Range District with Basalts from other Regions

	(1)	(2)	(3)	(4)	(5)	(6)	(7)
SiO ₂	47.26	47.92	50.11	49.28	46.9	47.84	47.3
Al ₂ O ₃	15.30	15.95	15.35	15.31	15.5	13.41	14.1
Fe ₂ O ₃	2.50	4.58	2.93	2.39	3.1	10.96	6.7
FeO	7.92	6.05	5.55	7.85	8.6		7.3
MgO	7.61	6.38	8.24	8.27	6.9	9.95	6.0
CaO	9.15	10.73	8.94	10.87	10.4	11.65	10.8
Na ₂ O	3.09	2.91	3.55	2.62	3.0	2.23	2.5
K ₂ O	0.52	0.53	0.07	0.24	1.3	0.22	1.3
TiO ₂	1.69	1.84	1.13	1.72	3.0	1.19	2.0
P ₂ O ₅	0.22	0.25	0.13	0.20	0.39	0.08	0.4
MnO	0.20	0.19	0.14	0.17	0.16	0.10	0.2
CO ₂	0.10	-	-	-	-	-	-
H ₂ O	4.00	2.19	3.56	1.00	0.8	3.24	1.45
	99.56	99.52	99.70	99.92	100.05	100.87	100.05

- (1) Average of 16 analyses, Cambro-Ordovician greenstones, Anvil Range District, Yukon.
- (2) Average of 24 seafloor-weathered ridge basalts; Hart, 1970.
- (3) Average of 5 greenstones, Mid-Atlantic Ridge, 22°N latitude; Melson, 1966.
- (4) Average of 209 mid-oceanic ridge basalts; source - Hyndman, 1972; Cann, 1969; Melson and Thompson, 1971; Kempe, 1973.
- (5) Average of 178 alkali olivine basalts; Mason, 1967.
- (6) Average of 52 spilitized greenstones ("Geosynclinal basalts", Axial Mikabu Zone, Japan); Hattori *et al.*, 1972.
- (7) Average of 25 basalts, Aden series, Ethiopian Rift Valley; Mohr, 1963.

ion lithophile (LIL) elements (Rb, Cs, Sr, Ba, Y, Zr, light rare-earths, Hf and U), low total iron, P_2O_5 and Fe_2O_3/FeO ratio (<0.4), high Ni, Cr, Co, CaO, $Na/K \geq 10$, olivine and plagioclase being common phenocryst phases whereas pyroxene phenocrysts are rare, and are usually olivine normative (i.e. plot within Di-Ol-Hy ternary). They are considered to have been derived from shallow mantle (low velocity zone) and experienced considerable olivine and plagioclase fractionation (Kay et al., 1970; Schilling, 1973). On the other hand, tholeiitic and alkali olivine basalts from ocean islands and aseismic ridges (e.g. ninety East Ridge, Indian Ocean) have higher LIL elements and some have higher FeO ($>13\%$), TiO_2 ($>2.2\%$), K_2O ($>0.4\%$) and P_2O_5 ($>0.25\%$). Intermediate to "acidic" rocks ("oceanic andesite", SiO_2 : 55-60%) are frequently encountered, and have higher Sr^{87}/Sr^{86} than mid-oceanic ridge basalts. Schilling (1973) has suggested that a rising deep-mantle plume as a magma source for the LIL element enriched, more differentiated tholeiitic rocks from the oceanic island and aseismic ridge (collectively termed island tholeiites), whereas O'Hara (1973) proposed two fractional crystallization processes for causing large LIL element abundance changes without large changes in major element composition of the residual magma: (1) low-pressure fractionation of olivine, plagioclase and clinopyroxene for abyssal tholeiites and (2) high-pressure fractionation of garnet and clinopyroxene for island tholeiites. Another model involving different degrees of melting at different P and T to derive two basalt types from the same source has also been suggested, but it is inconsistent with major element abundances (Green, 1970) and would require isotopic fractionation during partial melting (Peterman and Hedge, 1971). The two models are not mutually exclusive, since garnet fractionation could be an important process for magmas originating from

a deep-mantle plume. However, any model appealing to fractional crystallization (or partial melting) of a homogenous source to derive basalts with similar major element abundances but very different LIL element abundances must involve a special set of conditions; it seems unlikely that the required multiphase fractional crystallization could consistently develop two distinct basalt types (Frey et al., 1974).

Major and trace element data for the Anvil greenstones, in conjunction with the normative composition, indicate a strong affinity to abyssal tholeiites of mid-ocean ridge systems. Uncertainty in assigning some analyses to alkali olivine basalt may be due to the fact that even low temperature alteration (seafloor weathering and halmyrolysis) can convert a LIL element depleted abyssal tholeiite to alkali olivine basalts by marked increases in alkali metals, Sr, Ba, and light rare-earth elements (Hart, 1970; Thompson, 1973). In addition high-T alteration was probably operative after the consolidation of the Anvil basalts. Recent studies on the effect of low temperature alteration also show that loss of Ca, Mg, Si and gain of Fe^{+3} , K, H_2O , Pb, Cu, U with essentially no change in Sc, V, Cr, Co, Ni, Y, Ti, Zr, Hf, and heavy rare-earth elements take place (Hart, 1970; Aumento, 1971; Thompson, 1973; Frey et al., 1974). A study of 5 greenstones dredged from the mid-Atlantic ridge at 22°N latitude by Melson indicate a similar trend of chemical exchange during low-grade regional metamorphism, even though a more complex process of elemental exchange may have been superimposed. The chemical effects of high temperature seawater interaction (hydrothermal alteration), late magmatic deuteric alteration and metasomatism, and low-grade burial metamorphism on abyssal tholeiites are not clear at the present level of knowledge although the formation of albite, epidote, chlorite,

calcite, and actinolite in greenstones or spilites thought to be of abyssal tholeiite origin was widely cited as being a result of low-grade regional metamorphism (Coombs, 1974; Battey, 1974; Melson, 1966; Yoder, 1967).

The striking similarity in major chemistry of the Anvil greenstones with seafloor-weathered mid-ocean ridge basalts reported by Hart (1970) is very interesting, and also to a lesser extent, is the similarity with the greenstones from mid-Atlantic Ridge. In this connection, the depletion in K_2O , TiO_2 , Fe_2O_3 and enrichment in MgO of the Anvil greenstones relative to alkali olivine basalts are just the opposite of the alteration trend and are difficult to explain if most of the Anvil greenstones were originally of alkali olivine basalt composition. High Ti, Na, K abundances in addition to normative nepheline are characteristics of alkali olivine basalts from ocean islands and adjacent regions (Frey, 1970).

Basalts with high Al_2O_3 have been considered to be derived from less differentiated magmas by fractional crystallization of olivine (Green and Ringwood, 1967; O'Hara, 1968; Kushiro, 1973). This mechanism requires decreasing $Mg/(Mg+Fe^{+2})$ as Al_2O_3 increases. This correlation is not observed in such a plot as shown in Fig. IV-9a. Possible fractionation paths with percentages involved are indicated in the figure, and it can be readily observed that removal (crystallization) of approximately equal amounts of olivine and plagioclase from a less differentiated, "primary" magma (Frey et al., 1974) can produce most of the Anvil basalt compositions. Most mid-ocean ridge basalts are now considered to have been derived from a relatively undifferentiated, "primary" basaltic magma that has undergone only limited olivine fractionation through fractional crys-

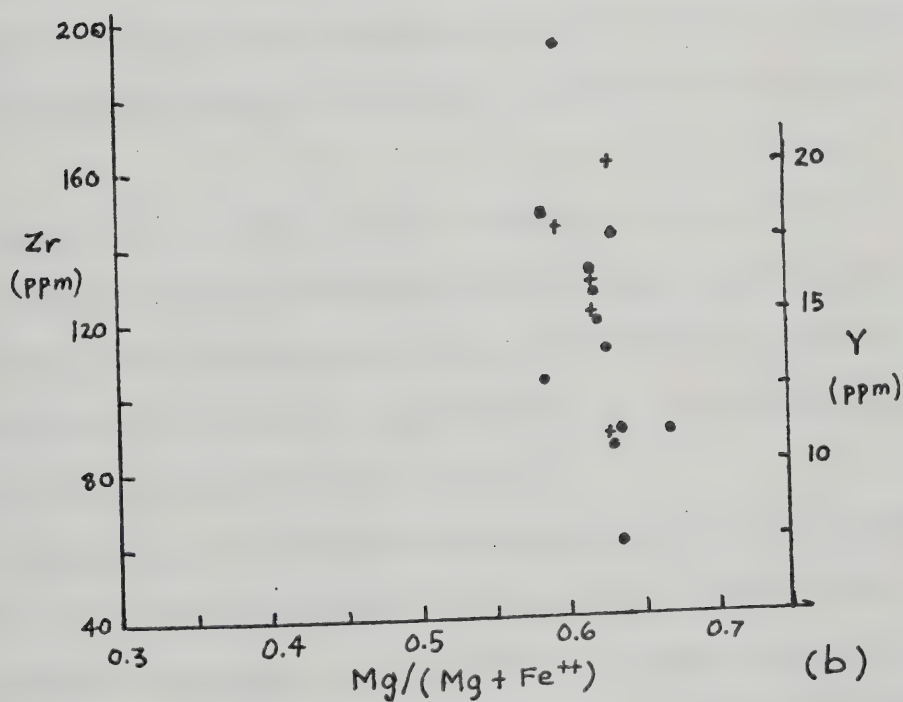
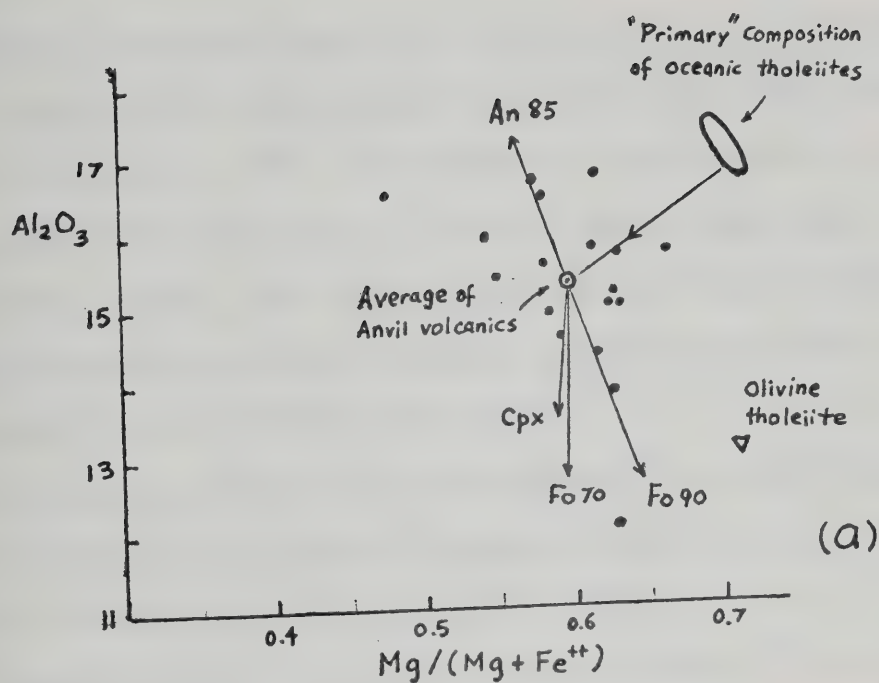


Figure IV-9. Al_2O_3 , Zr, and Y versus atomic ratio $\text{Mg}/(\text{Mg} + \text{Fe}^{++})$; in (b), solid circle: Zr vs $\text{Mg}/(\text{Mg} + \text{Fe}^{++})$; cross: Y vs. $\text{Mg}/(\text{Mg} + \text{Fe}^{++})$.

tallization of olivine and plagioclase, and occasionally, clinopyroxene (Miyashiro et al., 1970; Shido et al., 1971; Kay et al., 1970; Frey et al., 1974; Bance et al., 1975). The implication deduced from Fig. IV-9a confirms this view and points to a similar type of magma source and crystallization process. The limited extent of fractional crystallization of olivine and plagioclase in magmatic liquids of the Anvil rocks can be deduced from the following observations:

(i) Relatively constant ratio of $\text{Mg}/(\text{Mg}+\text{Fe}^{+2})$ or total FeO/MgO which is an index of the degree of fractional crystallization (Miyashiro et al., 1970; Shido et al., 1971; Miyashiro, 1973).

(ii) Lack of positive correlation between $\text{Mg}/(\text{Mg}+\text{Fe}^{+2})$ and Zr or Y which is an element most readily accommodated in the crystalline phases of olivine, plagioclase or chromitite and is enriched in residual liquid in direct proportion to decreasing liquid fraction (Fig. IV-9b).

(iii) Relatively constant to slight increase in TiO_2 and total FeO values over a narrow range of total FeO/MgO ratios suggesting no significant Fe-Ti oxide fractionation in a primary magma and a low oxidation condition of fractional crystallization as is characteristic of most abyssal tholeiites (Shido et al., 1971).

It is concluded that the Cambro-Ordovician greenstones in the Anvil Range district most likely extruded on an ocean floor either as mid-ocean ridge abyssal tholeiites or transitional tholeiites typical of the regions close to ocean islands or aseismic ridges. The rocks were probably associated with a continental rifting or separation which took place during late Proterozoic and Cambrian. Transitional tholeiites and some alkali olivine basalts probably were emplaced in an off-ridge

axis volcanism or as chains of elevated volcanoes formed by a central eruption volcanism away from the ridge axis. The similarity between modern alkali olivine basalts and Ethiopian Rifts basalts may be noted in this connection (see Table IV-3, columns 6 and 7). Basalts from the axial trough and volcanic islands of the Red Sea have a composition range between typical mid-ocean ridge abyssal tholeiites and alkali olivine basalts or "island tholeiites" (Chase, 1969; Coleman *et al.*, 1973) whereas those in the Ethiopian and African Rift Valleys or along Saudi Arabia Coastal Plain away from the Red Sea axial trough are dominantly alkali olivine basalts (Coleman, 1973; Saggerson and Williams, 1964; Mohr, 1963).

C. FRANCES LAKE DISTRICT

1. Lower Paleozoic Volcanic Rocks.

Foliated massive greenstones form two or three layers in the middle part of a thick metasedimentary sequence of Middle to Upper Cambrian age (Chapter III). Three samples from the upper layers were collected from separated localities in the northern and southern Simpson Tower area west of the East Arm Frances Lake (Fig. IV-15).

Chemical analyses together with normative compositions are presented in Table IV-7. Precision and reliability of the analyses have been mentioned previously (see Table IV-1).

The distinctive features of the Frances Lake greenstones are high Na_2O , K_2O , Ba, Rb, U, Th, low Al_2O_3 and total FeO, nepheline normative and silica-undersaturated. Minerals observed are sodic plagioclase (oligoclase and/or albite), common hornblende, chlorite, minor quartz, sphene, ilmenite and rare biotite and volcanic glass (?).

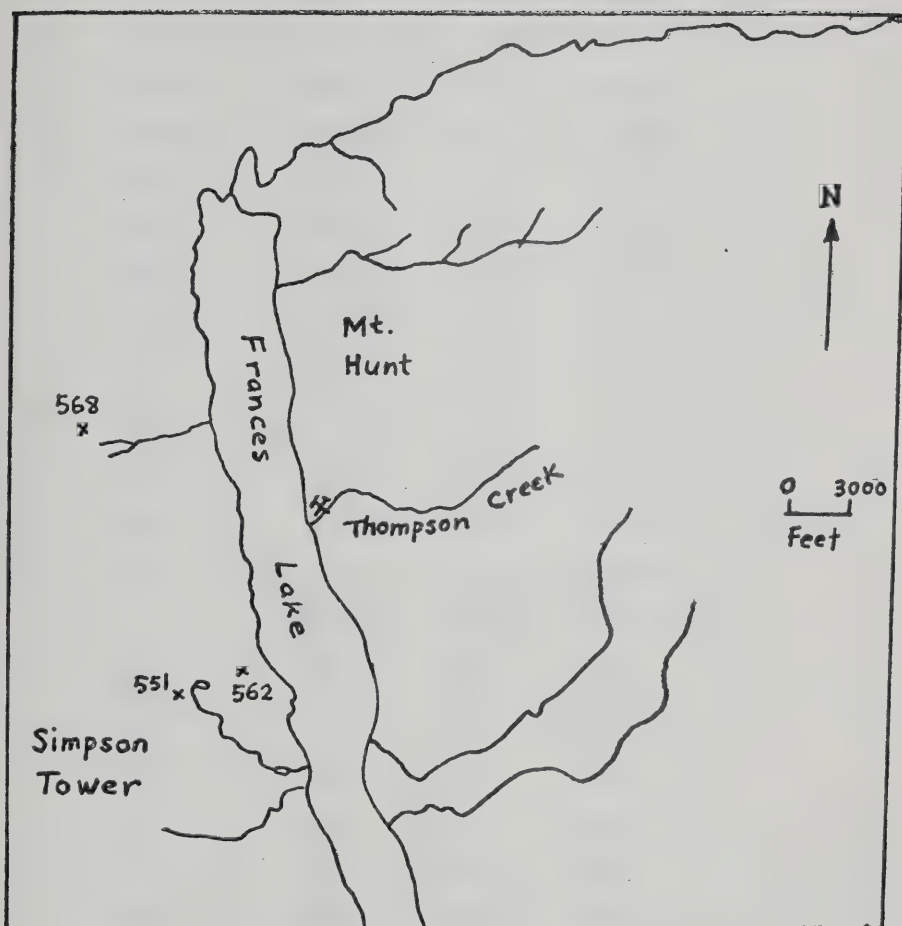


Figure IV-15. Locations of volcanic rock samples, Frances Lake district.

TABLE IV-7

Chemical and Normative Compositions of Greenstones of the
Frances Lake District

	FL-551	FL-562	FL-568
SiO ₂	49.93	52.23	51.74
Al ₂ O ₃	10.20	15.02	12.92
ΣFeO	9.19	9.60	9.71
CaO	10.85	6.62	8.24
MgO	9.56	5.89	8.38
Na ₂ O	7.76	6.30	6.54
K ₂ O	0.26	2.09	1.04
TiO ₂	1.72	1.87	1.25
P ₂ O ₅	0.29	0.16	0.19
MnO	0.24	0.18	0.17
S	-	-	0.04
	100.00	99.96	100.22
Ba	678	723	549
Nb	9	X	X
Zr	120	89	96
Y	14	X	X
Sr	179	398	342
Rb	38	74	51
Zn	286	191	191
Cu	117	36	9
Ni	276	312	117
Cr	X	580	232
Co	X	134	94
V	X	296	322
Pb	X	360	60
Ag	X	8	6
Be	-	1	-
U	X	1.4	6.8
Th	X	5.1	7.6

TABLE IV-7 (cont'd)

	FL-551		FL-562		FL-568	
	(1)	(2)	(1)	(2)	(1)	(2)
Or	1.54	1.48	12.36	12.10	6.15	5.96
Ab	15.83	16.12	30.93	32.12	27.93	28.69
An	0	0	6.53	6.39	2.60	2.52
Ne	19.06	21.50	12.12	13.94	15.08	17.16
Ac	4.34	4.01	0	0	0	0
Di	42.03	39.88	20.70	19.78	30.14	28.69
Ol	11.00	11.16	11.26	11.25	13.51	13.62
Mt	0	0	2.18	1.54	2.18	1.52
Il	3.27	2.30	3.55	2.55	1.86	1.32
Ap	0.67	0.58	0.37	0.33	0.44	0.39
Po	0	0	0	0	0.11	0.13
Ns	2.26	2.97	0	0	0	0

(1) C.I.P.W. Norms.

(2) Molecular Norms.

Norms and $\text{Mg}/(\text{Mg}+\text{Fe}^{2+})$ calculated assuming $\text{Fe}_2\text{O}_3 = 1.50 \text{ wt.}\%$.

X: not analyzed; -: not detected.

Chemical correlations using similar discrimination diagrams as for the Anvil greenstones reveal the following:

1. When $\text{Na}_2\text{O} + \text{K}_2\text{O}$ are plotted against SiO_2 (Fig. IV-16), the analyses appear to lie in between two undersaturated differentiation trends, close to mugearite and hawaiite compositions. The two trends are alkali basalt \rightarrow trachyte and trachybasalt \rightarrow phonolitic trachyte. The Frances Lake greenstones are only moderately differentiated as indicated by the positions of the analyses along the trends.

2. When Zr, Cr and Sr are plotted against Ti (Fig. IV-17) the analyses have an affinity to oceanic basalt, but also plot in the low potassium tholeiite field (Fig. IV-17b).

3. When total FeO, TiO_2 , Ni and V contents are plotted against total FeO/MgO (Fig. IV-18), and P_2O_5 against TiO_2 (Fig. IV-19), the analyses invariably fall in the field of abyssal tholeiites. This again emphasizes the relatively undifferentiated nature of the greenstones, presumably subjected to limited olivine and titanomagnetite crystal fractionation.

The Frances Lake greenstones are thus a group of volcanic rocks that are silica-undersaturated, nepheline normative, alkali basalts to tholeiites with a strong oceanic affinity. The relatively high concentrations of Ba, Rb, Na and high (Or+Ab)/An ratios, on the other hand, indicate a moderately differentiated nature.

Parental magmas of the ocean islands and related regions are widely believed to have diversified compositions - nepheline-normative alkali basalts, olivine tholeiites, undersaturated peralkaline basalts (basanites, nephelinites) and potassic alkali basalts, in decreasing order of abundance (Carmichael *et al.*, 1974). Similarly Pb and Sr isotopic variations among ocean island basalts have also been widely recognized

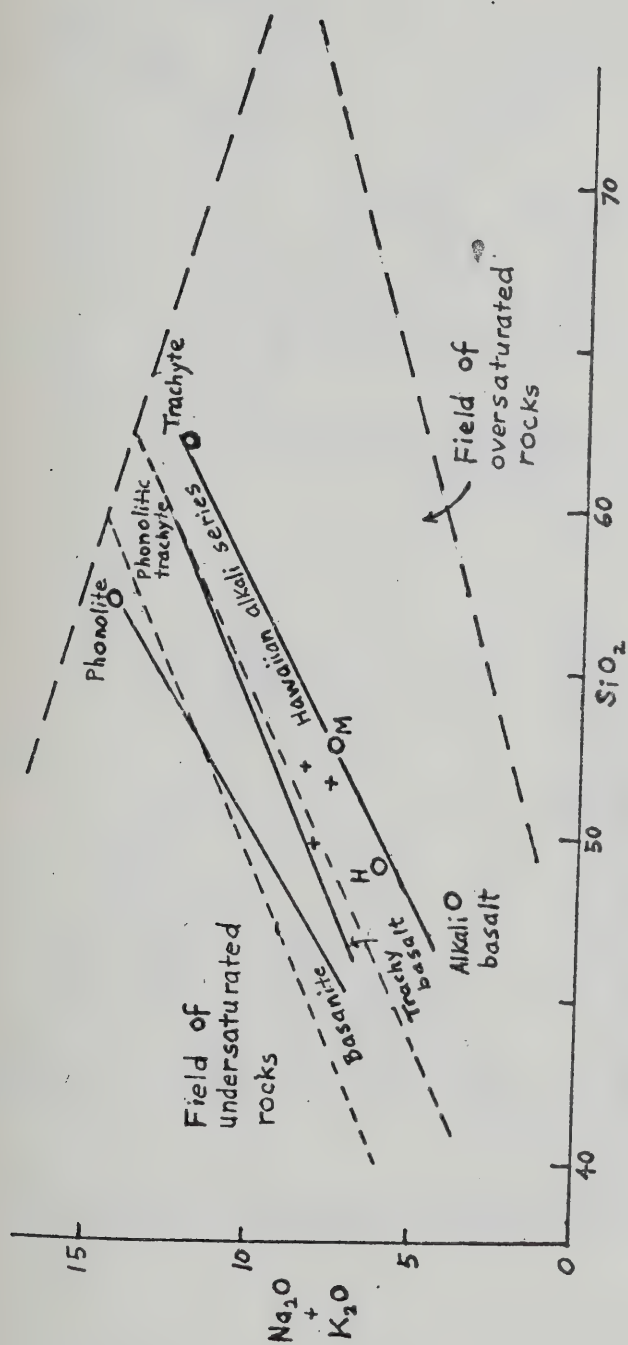


Figure IV-16. $\text{Na}_2\text{O} + \text{K}_2\text{O}$ versus SiO_2 plot showing various undersaturated differentiation trends and Frances Lake volcanic data.
H: Hawaiite; M: Mugearite.

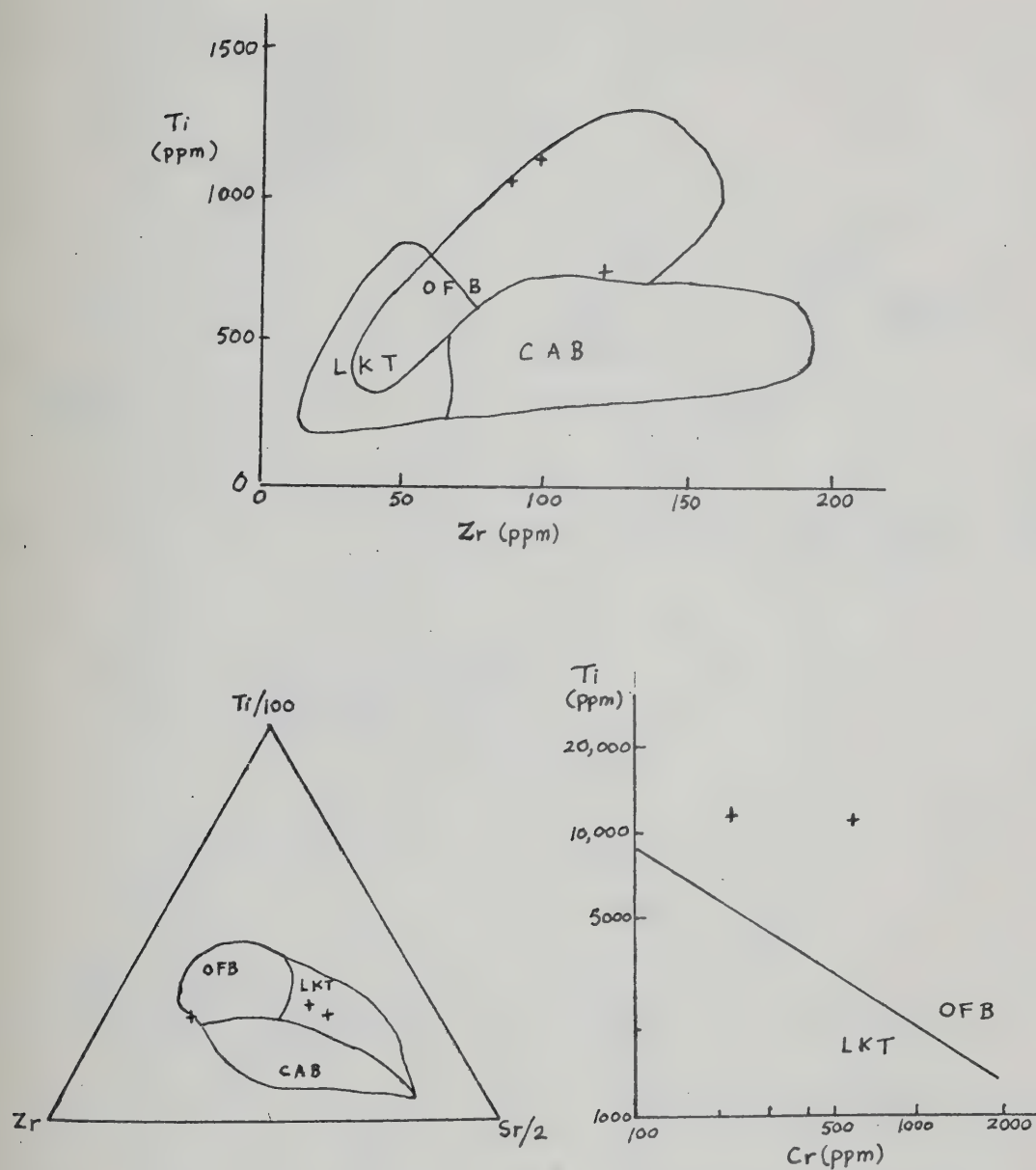


Fig. IV-17. Discrimination diagrams of Ti-Zr, Ti-Zr-Sr and Ti-Cr.

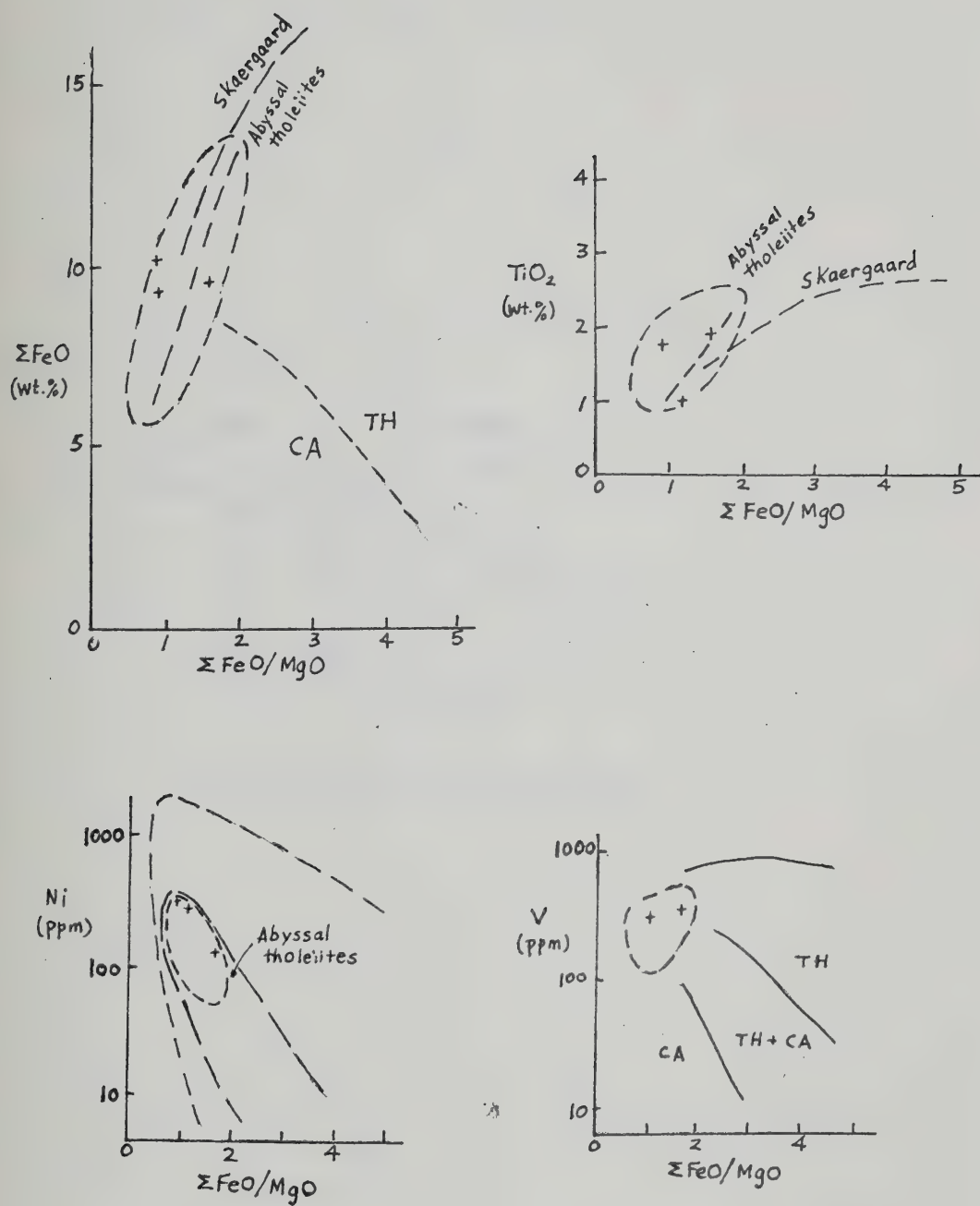


Fig. IV-18. Discrimination diagrams of ΣFeO , TiO_2 , Ni and V vs. $\Sigma\text{FeO}/\text{MgO}$.

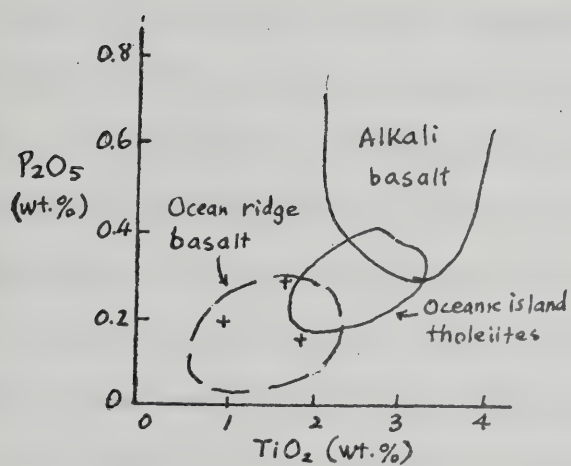


Figure IV-19. P_2O_5 versus TiO_2 .

(see Hedge, 1966; Hedge and Peterman, 1970; Tatsumoto, 1966a, b; Gast et al., 1964; McDougall and Compston, 1965; Moorbath and Walker, 1965). Likewise, there is a high concentration of large ion lithophile (LIL) elements ($K_2O = 3-5\%$; $Rb = 30-100$ ppm, $Ba = 300-800$ ppm, $Sr = 500-1000$ ppm, $Rb/K = .002$, $Ba/Sr = 0.5$ to 0.9) in alkali basalts of ocean islands (Engel et al., 1965).

Chemical and mineralogical data thus suggest that the greenstones from Frances Lake district strongly resemble alkali basalts in regions on or close to oceanic islands, and represent a group of rocks that were subjected to mild differentiation by fractional crystallization of olivine, plagioclase and clinopyroxene which gave rise to enrichment in Na_2O , K_2O and depletion in Mg relative to Fe. Differentiation by fractional crystallization and possibly other processes in shallow reservoirs at the base of or immediately below the crust has been suggested as possible mechanism of oceanic island basalts (Carmichael et al., Chapter 8, 1974).

Comparison of the lower Paleozoic Anvil and Frances Lake greenstones reveal that the former are mainly olivine normative with slight silica-saturation, abyssal tholeiites whereas the latter are nepheline-normative, strongly undersaturated, sodic alkali basalts with high concentrations of Ba, Rb, U, Th. Engel et al. (1965) and McBirney and Gass (1967) noted a decreasing degree of silica saturation with increasing distances from the mid-ocean ridge axis, i.e. silica-saturated tholeiitic basalts are mainly developed over deep ocean floor and ridges whereas alkali basalts are largely confined to the upper parts of the higher submarine volcanoes and oceanic islands. Likewise Aumento (1967, 1968) has observed that abyssal tholeiites with normative olivine occur mainly in median rift valleys, high Al olivine tholeiites on crest walls,

and a region transitional to alkali basalts on crests away from the rift valleys. If an analogy can be made, then the volcanic rocks of Cambro-Ordovician age in the Anvil-Frances Lake districts were probably erupted in a mid-ocean ridge to ocean island environment as continental separation occurred over an extended period from late Proterozoic to lower Paleozoic time. The situation is comparable to the Red Sea rift zone, associated volcanic islands and adjacent continental rift valleys where abyssal tholeiites transitional to alkali olivine basalts occur.

The cause of this regional variation in compositions away from mid-oceanic ridge probably lies in the different levels of partial melting at Low Velocity Zone. Melting below the oceanic ridge generally occurs at shallower level due to the elevation or "doming" of Low Velocity Zone, whereas away from ridges melting occurs in deeper level of the zone. Higher geothermal gradient and higher degree of melting at shallow depths (20-60 km) are required to produce parental magmas of oceanic tholeiites; on the other hand, oceanic island volcanism is generated by undersaturated magmas or their derivatives with a source region in the Low Velocity Zone (Green, 1972, Fig. 7).

Chapter V

CHEMICAL COMPOSITIONS OF ORES AND GANGUES

A. INTRODUCTION

Chemical compositions of sphalerites, pyrrhotites, barites, carbonates, sulfosalts and bulk ore samples from Anvil, Frances Lake and Howard's Pass ore deposits are presented in this Chapter. The mineral and bulk ore analyses are used not only to characterize each deposit, but also to estimate certain pertinent features of either depositional or metamorphic/deformational conditions and to provide basic data for later considerations of solubilities and related problems (see Chapter VIII).

Analytical methods, corrections and computational procedures for these analyses are indicated in conjunction with the presentation of chemical data, and readers are referred to appendices for detailed accounts.

B. ANVIL RANGE DISTRICT

1. Pyrrhotite

Selected samples of pyrrhotite texturally associated with sphalerite, pyrite and/or carbonates were analyzed for Fe, S, Ni, Co, Cu and Mn by electron microprobe using an energy dispersive detector. The results represent 10 to 15 spot counts of an average of 5 grains per sample with a total counting period of 500 seconds or more. Operating conditions, standards used, standard-sample analytical sequence and computer programs used for correction are given in Appendix V-1.

Chemical compositions of pyrrhotite samples from Faro, Grum, Vangorda and Swim Lakes ore deposits are listed in Table V-1. Calculation of molecular percents of all solid solutions and stoichiometry was done using an APL computer program MOL (Appendix V-2).

TABLE V-1

Chemical Composition of Pyrrhotites from the Anvil Ore Deposits

Sample No.	(Weight Percent)					S	FeS	(Mole Percent)				(Atomic Percent)	
	Fe	Ni	Co	Cu	Mn			NiS	CoS	CuS	MnS	Fe	Fe/S
(Farø)													
67-4 593	59.44	.15	.09	-	-	40.33	99.62	.24	.14	-	-	45.75	.85
67-6 754	60.10	.09	.06	-	-	39.75	99.76	.14	.09	-	-	46.42	.87
"Anvil"	59.41	.13	-	-	-	40.46	99.79	.21	-	-	-	45.70	.84
(Grum)													
A10-507	59.87	.08	-	-	-	40.04	99.87	.13	-	-	-	46.17	.86
A10-744	60.23	.08	-	-	-	39.70	99.87	.12	-	-	-	46.53	.87
A12-819	59.94	.11	.06	-	-	39.90	99.73	.17	.09	-	-	46.25	.86
(Swim Lakes)													
Swim-X	60.02	.13	-	-	-	39.85	99.79	.21	-	-	-	46.33	.87
(Vangorda)													
V18-120	60.81	.07	-	-	-	39.11	99.89	.11	-	-	-	47.14	.89
V33-279	60.67	.04	.05	-	-	39.24	99.86	.06	.08	-	-	46.99	.89
V35-153	61.13	.13	.04	-	-	38.70	99.74	.20	.06	-	-	47.50	.91
V60-180(2)	60.27	.064	-	-	-	39.66	99.90	.10	-	-	-	46.57	.87
V63-135	59.36	.31	.17	.61	.48	39.07	97.57	.48	.26	.88	.80	46.06	.87
V63-143	60.25	.09	-	-	-	39.66	99.86	.14	-	-	-	46.56	.87

-: not detected

As emphasized by Scott (1974), the Fe-S system is a cornerstone for the understanding of phase relations and thermochemistry of many other important systems including Zn-Fe-S, Cu-Fe-S, Fe-Ni-S and Fe-As-S. Pyrrhotite is in fact a complex phase in which the Fe/S ratio varies by omission of Fe from a NiAs type structure. Between its maximum melting temperature of 1190°C and 308°C, the full width of the pyrrhotite phase field is occupied by a single solid solution, Fe_{1-x}S (Hexagonal pyrrhotite), in which iron vacancies are randomly distributed in the cation sites of the NiAs (1C) structure (Arnold, 1971; Kullerud, 1967). At lower temperatures, the work of Nakazawa and Morimoto (1971), Scott and Kissin (1973), Kissin (1974) has shown that iron vacancies become increasingly ordered with decreasing temperature and various superstructures occupy the pyrrhotite phase field (Fig. V-1). This figure indicates that for most naturally occurring pyrrhotites at lower temperatures, monoclinic pyrrhotites (Fe_7S_8) occupy most of the pyrrhotite phase field and grade into ordered "hexagonal" pyrrhotite at slightly higher temperatures or Fe atomic percents.

The Anvil ore deposits were subjected to low grade greenschist facies regional metamorphism and some thermal metamorphism. The metamorphic effect is believed to be strongest at Faro, and it decreases as one goes southeast to Grum, Vangorda, and Swim Lakes deposits (Tempelman-Kluit, 1970b). Occurrence of pyrrhotite (and marcasite) in these deposits is probably related to regional metamorphism through the reduction of pyrite, and is especially enhanced by thermal metamorphism near intrusive contacts (see Chapter III). As will be shown later, however, formation temperatures of these deposits as deduced from the studies of fluid inclusions and sulfur isotopes are generally between 170 and 250°C. It is not known whether the lower temperature limit of greenschist facies metamorphism can extend below 250°C at reasonable

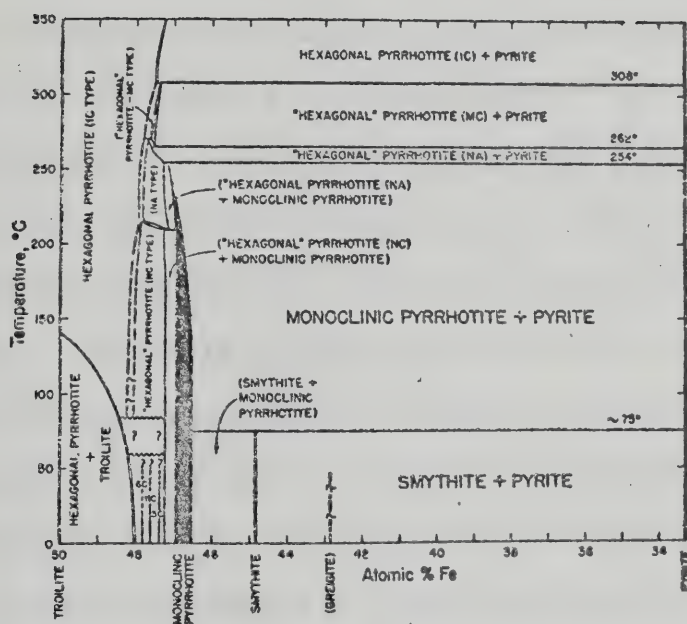


Fig. V-1. Temperature vs. atomic % Fe showing phase relationships in the central portion of Fe-S system below 350°C (after Kissin, 1974).

crustal pressures and geothermal gradients. Hyndman (1972) suggests that common regional metamorphism ranges from about 300-400°C to 700-800°C, and from about 2 or 3 Kb to 8 Kb. At 2 Kb, the corresponding temperature of the low-medium pressure metamorphism is about 300°C (Miyashiro, 1972). If 250°C is taken to be the temperature at which most pyrrhotite last equilibrated with other mineral phases, it is evident from the range of Fe atomic percents (Table V-1) and Fig. V-1 that Anvil district pyrrhotite except for samples V35-153 and V18-120 are monoclinic, while the exceptions appear to be ordered "hexagonal" pyrrhotite or a mixture of ordered "hexagonal" pyrrhotite with monoclinic pyrrhotite. On the other hand, if 300°C is taken as the metamorphic temperature at which pyrrhotite last equilibrated, then all the pyrrhotite would be classified as ordered "hexagonal" pyrrhotite. Arnold (1967, 1969) and Yund and Hall (1969) reported 47.3-47.5 atomic % Fe for the lower (sulfur-rich) limit of hexagonal pyrrhotite and metastability of monoclinic pyrrhotite at 290-308°C. The compositional variation (Fe/S ratio) in the Anvil pyrrhotite probably reflects either metastability or a slow rate of breakdown at lower temperatures (Yund and Hall, 1969).

The main value of the Fe-S system is in understanding the thermochemistry, particularly the relationships among pyrrhotite composition, temperature, pressure and activities of FeS and S₂. For the reaction representing the sulfidization of pyrrhotite to pyrite or reduction of pyrite to pyrrhotite— $2\text{FeS}_2 \rightleftharpoons 2\text{FeS} + \text{S}_2$, the pyrite-pyrrhotite solvus and the variation in activity of FeS (a_{FeS} , related to stoichiometric FeS at the same temperature) can be expressed as functions of temperature and fugacity of sulfur (f_{S_2}). Increasing pressure on the pyrite-pyrrhotite solvus causes only a small increase in a_{FeS} , f_{S_2} , and the position of the solvus (Toulmin and Barton, 1964; Barton and Skinner, 1967; Scott, 1974). Since most published figures

on the above-mentioned phase relationships are calculated at one atmosphere, yet most ore-forming processes take place at pressures greater than one atmosphere, it is interesting to investigate the effect of higher confining pressure on the location of the pyrite-pyrrhotite solvus. For Anvil pyrrhotite, lower limit of confining pressures (see next section on sphalerite geobarometry) is in the range of 2-2.5 Kb; a diagram depicting the variations in a_{FeS} , location of the solvus, and boundary of monoclinic and hexagonal pyrrhotite as functions of temperature and f_{S_2} at 2.5 Kb is shown in Fig. V-2.

The fugacities of sulfur at which the Anvil pyrrhotite last equilibrated can be estimated from the locales of the pyrite-pyrrhotite solvus and the monoclinic-hexagonal pyrrhotite phase boundary at specific temperatures (Fig. V-2). At 250°C, $\log f_{\text{S}_2}$ ranges between -12.5 ~ -13.5, whereas at 300°C, $\log f_{\text{S}_2}$ ranges between -10.3 ~ -10.7. The py-po solvus is consistent with an a_{FeS} isopleth of about 0.3 at these temperatures.

The relatively high concentrations of Co (average 780 ppm) and Ni (average 1130 ppm) and low average Co:Ni ratio (<1) in the Anvil pyrrhotite contrast with pyrrhotites from Precambrian massive sulfide ores which have high Co, low Ni and Co:Ni ratios well over 1 (Roscoe, 1965; Hawley and Nicol, 1961; Farkas, 1973).

2. Sphalerite

Forty-one samples of sphalerite texturally associated with pyrite, pyrrhotite and/or carbonate minerals were analyzed for Zn, Fe, Cd, Mn, Co and S. Cu is not detected. Analyses were made by electron microprobe using an energy dispersive detector and wavelength dispersive detector (for Cd, Mn). Similar counting rate and period as for pyrrhotite was employed, and details

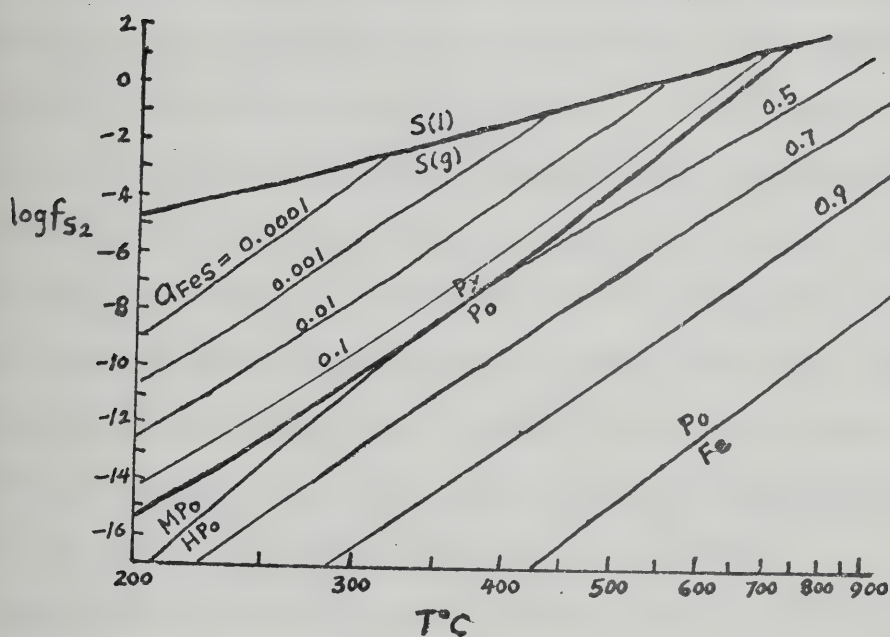


Fig. V-2. Sulfur fugacity vs. temperature diagram showing variations of the activity of FeS in pyrrhotite and pyrite at 2.5 Kb. Positions of solvuses and the monoclinic-hexagonal pyrrhotite phase boundary are estimated from the data of Toulmin and Barton (1964) and Miyazaki et al. (1974), respectively.

on operating conditions and standards are given in Appendix V-1.

Chemical compositions of sphalerite samples from Faro, Grum, Vangorda and Swim Lakes ore deposits together with calculated mole percents of all solid solutions and stoichiometry are given in Table V-2. APL computer program MOL was used for the calculation. Fe, Zn and Mn contents in a total of 39 sphalerite grains were scanned and 7 X-ray photographs were taken by microprobe; our examples of these scanning traces and photographs are shown in Fig. V-3 and Plate V-1, respectively. No evidence of zoning or discrete FeS-rich patches were detected. The Fe, Zn and Mn contents change over very small distances and reflect small irregular inhomogeneities. An overall compositional uniformity is, however, obvious on a small grain sample scale. FeS contents of sphalerites in both sp-py-po and sp-py assemblages appear to have a minima near the central part of the sulfide layer in Faro (cf. DDH 66-2, DDH 66E9, and DDH 67-6) and a decrease with depth but with a repetition near the central part in the Grum deposit (cf. DDH A-10). No regular variations with depth can be detected.

Sphalerite is one of the most refractory sulfides (Barton, 1970) and displays a wide range of Fe contents as a function of conditions of formation (Kullerud, 1953; Barton and Toulmin, 1964; Toulmin and Barton, 1966; Scott and Barnes, 1971; Scott, 1974); it therefore may be useful in indicating environments of sulfide deposition or deformation. Kullerud (1953) proposed the use of Fe content in sphalerite coexisting with pyrrhotite as a geothermometer but he based this on an incorrect assumption that FeS activity of pyrrhotite did not depart appreciably from unity. The original concept of sphalerite geothermometry is probably invalid. However, the recent advances in the knowledge of phase relations in Fe-Zn-S system both above and below 300°C (Barton and Toulmin, 1966; Scott and Barnes, 1971;

TABLE V-2

Chemical Composition of Sphalerites from the Anvil Ore Deposits

Sample No.	Sulfide Assemblage*	(Weight Percent)**						(Mole Percent)					(Atomic Ratio) Σ Cations: S
		Zn	Fe	Cd	Mn	S	Co	ZnS	FeS	CdS	MnS	CoS	
(Faro)													
66-2 283	(1)	52.80	10.49	0.15	2.49	34.08	-	77.49	18.04	0.13	4.35		0.98
342	(2)	52.29	11.08	X	2.17	34.46	-	77.05	19.13		3.82		0.97
400	(2)	55.34	8.10	0.21	1.56	34.20		81.97	15.10	0.18	2.75		0.97
474	(1)	60.02	5.86	X	0.09	34.03	-	89.59	10.25		0.16		0.97
486	(1)	54.98	10.59	0.13	0.12	34.19	-	81.33	18.35	0.11	0.22		0.97
66E9 299	(2)	53.08	11.30	0.18	1.09	34.35		78.39	19.55	0.15	1.91		0.97
337	(7)	59.54	6.43	X	0.07	34.34	-	88.65	11.23		0.12		0.96
376	(1)	57.87	8.08	X	0.10	33.94	-	85.79	14.03		0.18		0.98
401	(1)	56.08	9.94	0.05	0.09	33.85	-	82.65	17.16	0.04	0.16		0.98
436	(1)	55.72	10.16	X	0.05	34.08	-	82.32	17.59		0.09		0.97
66-10 634	(7)	56.98	8.82	0.11	0.20	33.90	-	84.28	15.28	0.09	0.35		0.98
67-4 460	(1)	53.19	11.20	0.11	1.42	34.08	-	78.14	19.27	0.10	2.49		0.98
593	(5)	55.61	10.11	X	0.16	34.16	-	82.21	17.52		0.27		0.97
67-6 602	(4)	56.12	9.68	0.18	0.26	33.76	-	82.68	16.71	0.15	0.46		0.99
710	(1)	57.02	8.73	X	0.14	34.11	0.04	84.52	15.16		0.25	0.07	0.97
754	(6)	54.92	10.67	0.10	0.10	34.21	-	81.24	18.49	0.09	0.18		0.97
762	(1)	54.77	10.60	0.13	0.32	34.17	-	80.95	18.37	0.11	0.57		0.97
67-10 549	(8)	55.20	10.45	0.11	0.14	34.11	-	81.57	18.09	0.10	0.25		0.97
632	(7)	55.44	10.37	0.16	0.03	33.99	-	81.86	17.94	0.14	0.06		0.98

TABLE V-2 (cont'd)

Sample No.	Sulfide Assemblage*	(Weight Percent)**					S	Co	(Mole Percent)				CoS	(Atomic Ratio) Σ Cations: S	
		Zn	Fe	Cd	Mn	Fe			ZnS	FeS	CdS	MnS			
(Faro)															
66-22 305	(1)	59.95	5.95	0.11	0.09	33.90	-		89.36	10.39	0.10	0.16			0.97
Anvil pit #1	(4)	56.08	9.76	X	0.21	33.91	0.05		82.69	16.86		0.37	0.08		0.98
(Grum)															
A5-422	(1)	59.21	6.57	X	0.08	34.12	0.03		88.32	11.49		0.14	0.05		0.96
A10-507	(4)	56.67	9.56	X	0.05	34.16	-		83.43	16.48		0.09			0.98
529	(5)	56.14	8.48	0.14	0.04	35.21	-		84.78	15.03	0.12	0.07			0.92
575.5	(2)	60.21	5.64	X	0.05	34.08	0.06		89.94	9.87		0.09	0.10		0.96
616	(5)	56.49	9.42	0.14	0.17	33.78	-		83.31	16.27	0.12	0.30			0.99
693	(1)	57.66	8.45	X	0.12	33.77	0.03		85.13	14.61		0.21	0.05		0.98
744	(6)	58.69	7.40	0.09	0.10	33.73	-		86.92	12.84	0.08	0.17			0.98
774	(1)	61.28	4.99	0.16	0.04	33.54	-		91.11	8.68	0.13	0.08			0.98
802A	(1)	61.45	4.89	X	0.04	33.62	0.05		91.33	8.51		0.07	0.08		0.98
A11-594	(8)	59.33	6.59	0.07	0.04	33.97	-		88.38	11.50	0.06	0.07			0.97
A12-538	(1)	61.22	4.98	X	0.04	33.69	0.05		91.16	8.69		0.07	0.08		0.98
819	(3)	56.51	9.46	X	0.16	33.78	-		83.37	16.34		0.29			0.98
A13-150	(7)	62.03	4.48	0.14	0.02	33.34	-		92.06	7.79	0.12	0.03			0.99

TABLE V-2 (cont'd)

Sample No.	Sulfide Assemblage*	Zn	Fe	Cd	Mn	S	Co	ZnS	FeS	CdS	MnS	CoS	(Atomic Ratio) Σ Cations: S
(Swim Lakes)													
Swim-X	(3)	55.11	10.47	0.10	0.27	34.05	-	81.34	18.10	0.09	0.48		0.98
(Vangorda)													
V18-120	(9)	55.99	9.90	0.17	0.19	33.74	-	82.44	17.07	0.15	0.34		0.99
V33-279	(4)	56.68	9.43	0.08	0.12	33.69	-	83.45	16.26	0.07	0.22		0.99
V35-153	(10)	56.16	10.02	0.03	0.06	33.73	-	82.61	17.26	0.03	0.11		0.99
V60-180(2)	(4)	57.33	9.11	0.11	0.10	33.35	-	84.09	15.64	0.09	0.18		1.00
V63-135	(3)	55.61	10.58	0.10	0.31	33.40	-	81.28	18.10	0.09	0.53		1.00
143	(3)	56.30	9.61	0.11	0.05]	33.94	-	83.19	16.63	0.09	0.09		0.98

*Sulfide Assemblage: (1) Py + Gn, (2) Py + Gn + Mc, (3) Py + Po, (4) Py + Po + Gn, (5) Py + Po + Gn + Mc, (6) Py + Po + Gn + Cp, (7) Py + Gn + Cp, (8) Py + Gn + Cp + Mc, (9) Py + Po + Gn + Aspy, (10) Py + Po + Cp.

**Electron microprobe analyses. Cd and Mn, where both are present, were analyzed by a wavelength dispersive detector, the rest by an energy dispersive detector.

X: not analyzed; -: not detected.

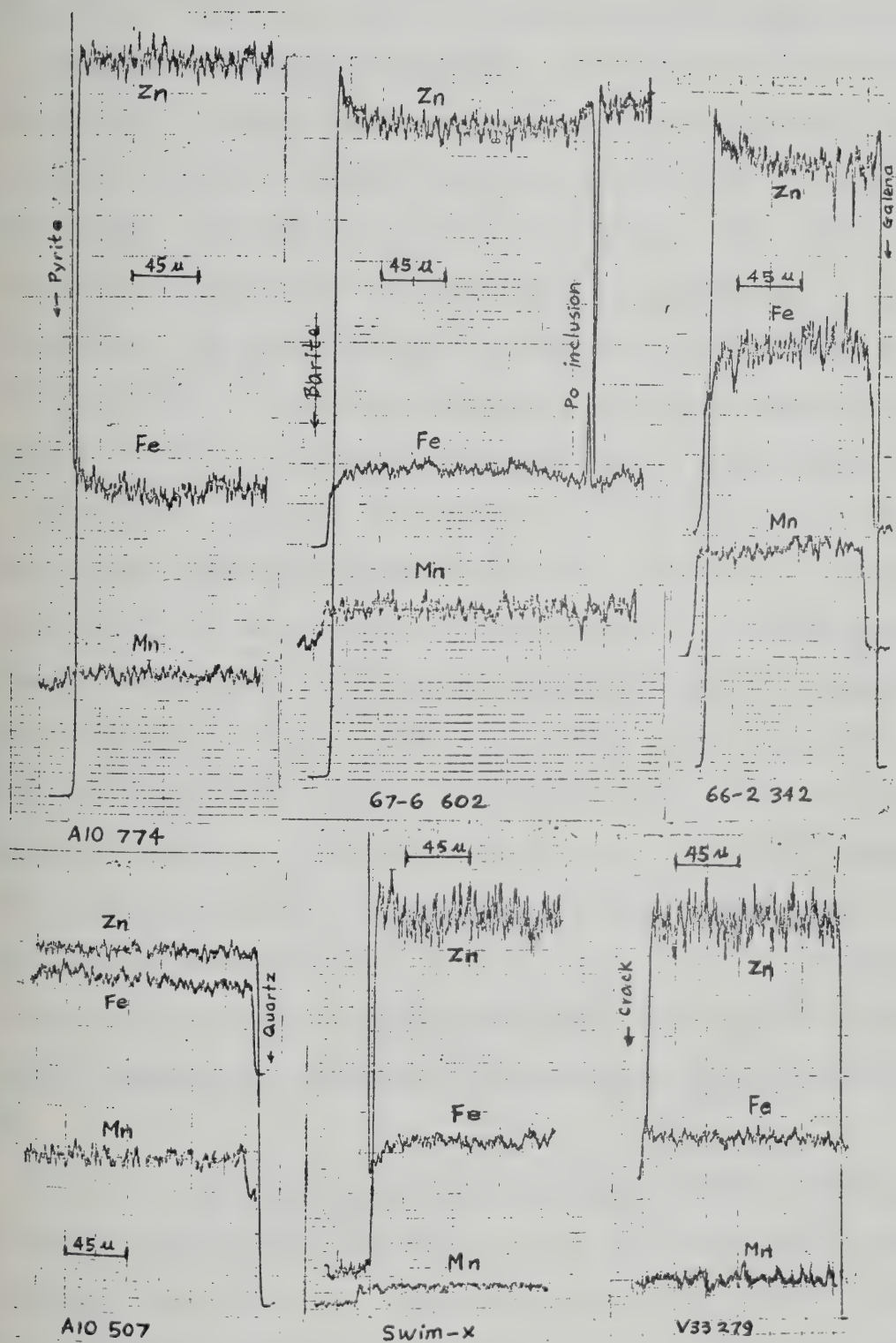


Fig. V-3. Electron microprobe X-ray scanning traces of sphalerite grains, Anvil Range district.

Kissin, 1974) make it possible to estimate pertinent thermochemical information, such as fugacity of sulfur, pressure and equilibrium temperature.

(a) Pressure and Fugacity Estimate. In a system in which activity of FeS is buffered by pyrite and pyrrhotite, sphalerite becomes less FeS-rich with increasing pressure because the partial molar volume of FeS in sphalerite is larger than that of ZnS (Barton and Toulmin, 1966). This change of sphalerite composition on the pyrite-pyrrhotite solvus over a wide range of temperatures and pressures has been estimated by Scott (1973), and Scott and Barnes (1971). A temperature-sphalerite composition diagram with pyrite-pyrrhotite solvus isobars derived from their work is shown in Fig. V-4.

Inspection of Table V-2 reveals that sphalerite compositions are variable when only pyrite is present but show much less spread in FeS mole percent when pyrite and pyrrhotite are both present. The three phases are generally assumed to be in equilibrium during deposition or metamorphism under the influence of a_{FeS} buffer (Scott, 1974). Other components such as Co, Ni, Cd, Mn and Cu are unlikely to have much of an effect on the phase relations in Fig. V-4. The slope of the 2.5 and 5.0 Kb isobars probably remains vertical below 300°C until they encounter the slope reversal of the py-po solvus or the stability field of monoclinic pyrrhotite at about 250°C. The 7.5 Kb isobar may show curvature below 600°C, but may also be vertical if more measurements are conducted; its slope is not fully resolved at present.

Pressure estimates of the sphalerite-pyrite-pyrrhotite assemblage of the Anvil ore deposits are made from Fig. V-4 using data for mole % FeS in sphalerite from Table V-2. The results are shown in Table V-3. The range of pressure estimates is consistent with the low-medium greenschist facies metamorphism and deformation history discussed before. Generally

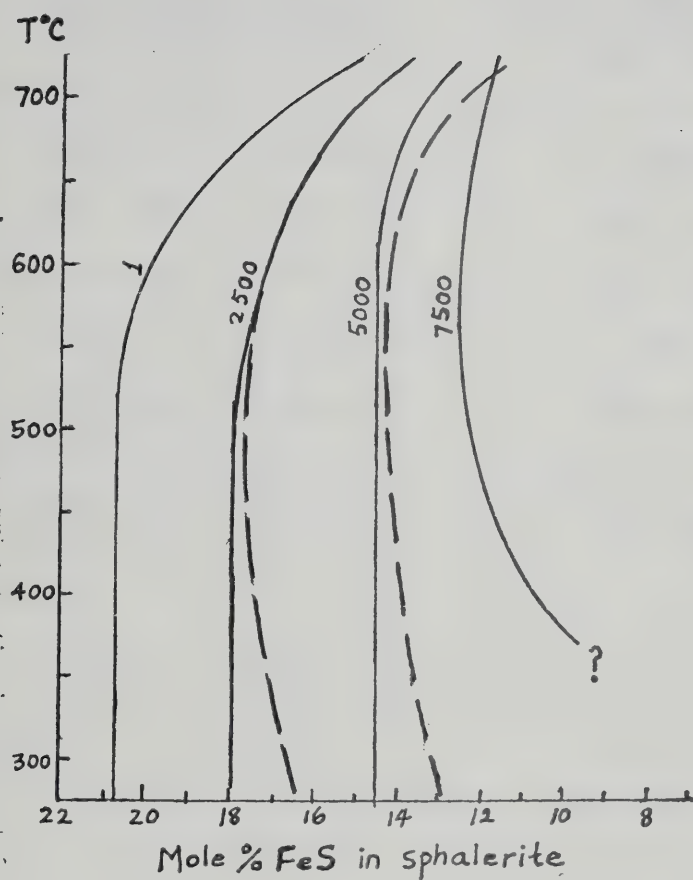


Fig. V-4. Sphalerite-pyrite-pyrrhotite solvus isobars as functions of temperatures and mole % FeS in sphalerite. Solid lines: experimental curves, dashed lines: calculated curves (in bar unit) (after Scott, 1973; Scott and Barnes, 1971; and extrapolations).

TABLE V-3

Pressure Estimates of Anvil Ore Deposits by Sphalerite
Geobarometry

Ore Deposits	Pressure (Kb) Estimated from Calculated Isobars (Scott, 1973)		Pressure (Kb) Estimated from Experimental Isobars (Scott, 1973)
	(300°C)	(250°C)	(300°C)
Faro	2.5 - 1.5	2.0 - 1.0	3.65 - 2.0
Grum	5.2 - 2.7	4.7 - 2.2	5.70 - 3.6
Swim Lakes	1.6	1.3	2.3
Vangorda	3.4 - 1.6	2.8 - 1.3	3.70 - 2.3
Average	3.7 - 1.9	3.2 - 1.4	4.40 - 2.6

speaking, maximum pressures of 4-5 Kb are considered to be representative of metamorphic pressures asserted on the Anvil ore deposits if temperature reached 300°C.

Composition of sphalerite in equilibrium with pyrrhotite, pyrite + pyrrhotite, and pyrite can be expressed as a function of fugacity of sulfur and temperature at elevated pressures if the pressure effect on the sphalerite-pyrite-pyrrhotite solvus is taken into consideration. Higher pressure generally shifts the solvus to lower FeS contents and slightly higher sulfur fugacity at constant temperature (Barton and Toulmin, 1966; Scott, 1974). A sulfur fugacity-temperature diagram showing sphalerite compositions at 2.5 Kb has been constructed and shown in Fig. V-5. The sphalerite-pyrite-pyrrhotite solvus lies in the 10-20 mole percent FeS range below 700°C and is almost parallel to the 10 mole percent FeS isopleth between 300 and 200°C. Over the range of mole percent FeS in the Anvil sphalerite, the corresponding $\log f_{S_2}$ range estimated from Fig. V-5 lies between -10 to -11.5 at 300°C, and -12.5 to -14 at 250°C. These sulfur fugacity values agree very well with those estimated from the pyrrhotite-pyrite solvus in Fe-S system, indicating that a_{FeS} was indeed buffered by pyrite and pyrrhotite and the sp-py-po assemblage, where occurring, was by and large in equilibrium during the last metamorphism.

(b) Equilibrium Temperature. Sphalerite-pyrite-pyrrhotite equilibrium is difficult to attain at low temperatures (below 300°C) in the laboratory; but Scott and Kissin (1973) and Kissin (1974) have postulated the phase relations for the Fe-Zn-S system below 300°C at 1 bar on the basis of a few experimental points, analyses of natural sphalerites from low temperature assemblages and knowledge of the Fe-S system. The pressure effect on these phase relations below 300°C can be estimated by assuming a pressure coef-

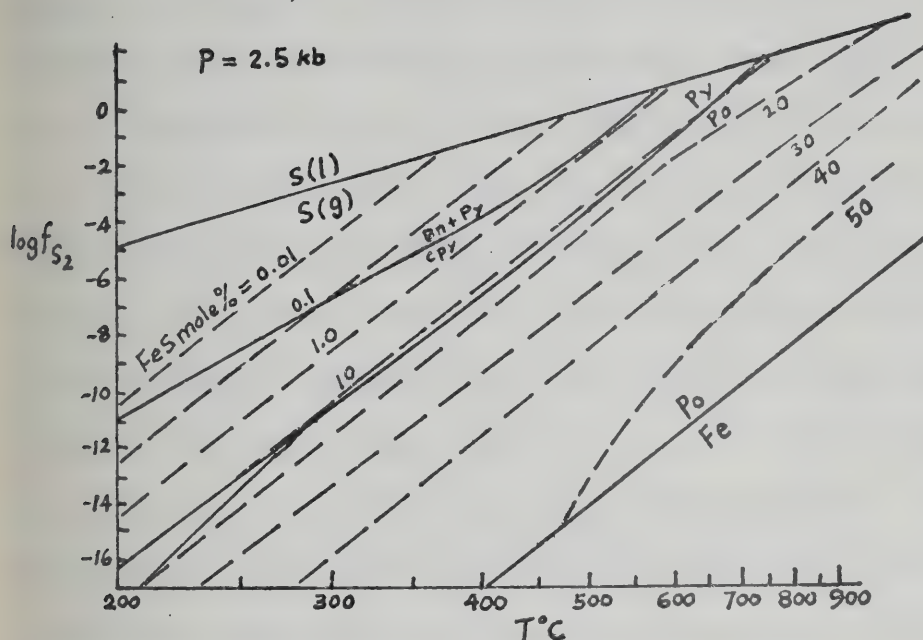


Fig. V-5. Sulfur fugacity-temperature diagram showing mole % FeS in sphalerite at 2.5 Kb. Positions of solvuses and monoclinic-hexagonal pyrrhotite boundary are estimated from data of Barton and Toulmin (1966) and Miyazaki *et al.* (1974), respectively.

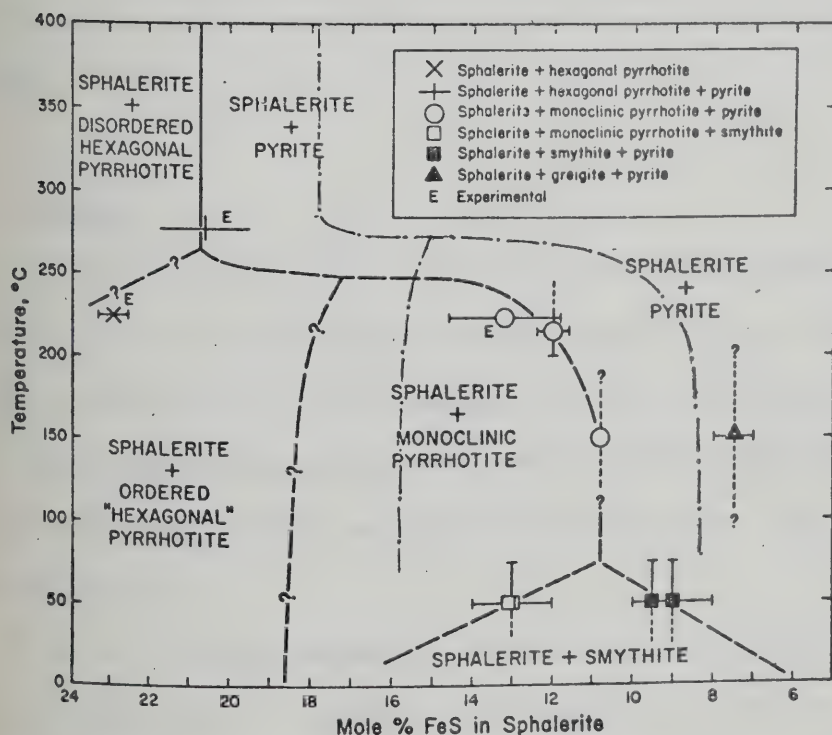


Fig. V-6. Phase assemblages of Fe-Zn-S system below 300°C as functions of temperature and mole % FeS in sphalerite. Pressure effect of 2.5 Kb is indicated by the dash-dot-curves shifting to the right (after Scott and Kissin, 1973).

ficient of 7°C per Kb on the $sp+py+po$ (monoclinic) phase boundary and that pressure effect on $sp+py+monoclinic\ po$ solvus below 300°C is of similar order of magnitude to that on $sp+py+hexagonal\ po$ solvus above 300°C (Scott, 1975, oral communication). Phase assemblages of the Fe-Zn-S system below 300°C and at 2.5 Kb as functions of temperature and mole percent FeS in sphalerite are shown in Fig. V-6. The phase boundary between $sp+monoclinic\ po$ and $sp+ordered\ "hexagonal"\ po$ at this pressure is not clear, presumably it might shift to the right (lower FeS content) but the magnitude involved is unknown due to lack of experimental evidence even at 1 bar. It is evident from Fig. V-6 and Table V-2 that over the range of the Anvil sphalerite compositions, both $sp+py$ and $sp+py+po$ assemblages were equilibrated at a temperature of about 280°C at 2.5 Kb confining pressure during the last metamorphism or thermal event. At higher confining pressure (e.g. at about 4-5 Kb), the assemblages probably existed at a metamorphic temperature of 300°C.

3. Barite

Barite coexisting with sphalerite, galena and pyrite occurs extensively in Faro, Grum, Swim Lakes and possibly Vangorda ore deposits (see Chapter III), especially in areas least affected by thermal metamorphism. Analyses of barite were made by means of a combination of analytical methods - electron microprobe, MRFAP, and dithiozone-extraction. The results are reported in Table V-4.

Pb, Sr, Ca and presumably Zn can substitute for Ba in barite structure to a limited extent, and form solid solutions as $PbSO_4$, $SrSO_4$, $CaSO_4$ and $ZnSO_4$. Other elements Fe, Mn, Ni, Co, Mg, and K were also reported in

TABLE V-4

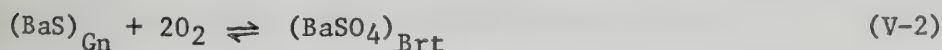
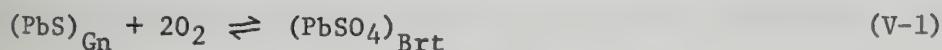
Chemical Composition of Barites from Faro and Grum Ore Deposits,
Anvil Range District

	66-2 283	66E9 299	66-10 634	66-22 305	67-6 602	67-6 710	A10-774
Ba	58.71	58.07	58.33	58.50	58.94	n.a.	n.a.
S	13.61	13.57	13.63	13.67	13.83	"	"
O	26.36	27.05	26.45	26.30	26.34	"	"
Sr	n.a.	n.a.	0.12**	0.138**	n.a.	0.189**	0.148**
Ca	"	"	0.079**	n.d.**	"	0.008**	n.d.**
Pb	"	0.054*	0.020*	0.1315*	"	0.020*	0.0406*
Zn	0.27	0.039	0.030	0.200	0.16	n.a.	0.0350
Fe	0.49	0.30	0.47	0.35	0.24	"	n.a.
Mn	0.16	0.19	0.14	0.14	0.16	"	"
Ni	0.11	0.15	0.15	0.18	0.08	"	0.003**
Co	0.26	0.23	0.28	0.27	0.18	"	n.a.
Na	n.a.	n.a.	n.d.**	0.04**	n.a.	0.01**	"
Total	99.97	99.65	99.97	99.92	99.93	-	-
PbSO4							
(mole fraction)	-	6.1	2.3	0.15	-	2.3	4.6
x 10 ⁻⁴							

* Dithiozone extraction

** Multiple radio frequency argon plasma emission (MRFAPe) spectrometry.

natural or synthetic barium sulfate but solely as oxides (Palache *et al.*, 1951; Sakai, 1971). Among the solid solutions, BaSO_4 is isostructural or of similar ionic radius to SrSO_4 and PbSO_4 , but not with CaSO_4 or ZnSO_4 , which have a different structure due to the smaller sizes of Ca^{++} and Zn^{++} . It is likely that the distribution of Pb and Sr between coexisting minerals (sulfate-sulfide) may occur under equilibrium conditions in a hydrothermal environment. However, no stable strontium sulfide was ever reported in nature and the thermochemical parameters for strontium sulfide-barite reaction are virtually unknown. On the other hand, barite and galena are stable coexisting minerals and thermochemical data exist for the reactions



It is therefore possible to use barite-galena pairs as an indicator of oxygen fugacity (f_{O_2}) during ore deposition if the activity of PbSO_4 in barite or BaS in galena or both are known (Kajiwarra and Honma, 1972). The equilibrium constants K for the above reactions are:

$$K_{\text{V-1}} = \frac{a_{\text{PbSO}_4(\text{Brt})}}{a_{\text{PbS}(\text{Gn})} \times (f_{\text{O}_2})^2} \quad (\text{V-3})$$

$$K_{\text{V-2}} = \frac{a_{\text{BaSO}_4(\text{Brt})}}{a_{\text{BaS}(\text{Gn})} \times (f_{\text{O}_2})^2} \quad (\text{V-4})$$

where $a_{i(j)}$ is activity of i component in solid solution j . Since barite and galena contain essentially BaSO_4 and PbS , the values of $a_{\text{PbS}(\text{Gn})}$ and $a_{\text{BaSO}_4(\text{Brt})}$ should be equal to unity in nearly pure galena and barite; rearranging equations V-3 and V-4,

$$K_{\text{V-1}} = \frac{a_{\text{PbSO}_4(\text{Brt})}}{(f_{\text{O}_2})^2} \quad (\text{V-5})$$

$$K_{\text{V-2}} = \frac{1}{a_{\text{BaS}(\text{Gn})} \times (f_{\text{O}_2})^2} \quad (\text{V-6})$$

Activity isopleths of $\text{PbSO}_4(\text{Brt})$ and $\text{BaS}(\text{Gn})$ as functions of f_{O_2} and temperatures have been constructed (Fig. V-7) from equations V-5 and V-6 using the free energy (ΔG) data for reactions V-1 and V-2 (Holland, 1965) and the relation $\Delta G = -RT \ln K = 4.576061 T \log K$; T is temperature in ° Kelvin, K the equilibrium constant, and R the gas constant ($=1.9872$ cal per mole per degree). Stability boundaries of $\text{ZnSO}_4 - \text{ZnS}$ and $\text{CaSO}_4 - \text{CaS}$ are also shown in Fig. V-7. The calculation was made by an APL computer program ACT as shown in Appendix V-2.

The activity of a component representing the solute end member in a given solid solution series is proportional to its mole fraction, and the recent experimental studies on BaSO_4 - PbSO_4 system (Takiyama, 1967; Bostrom et al., 1967; Sugitani et al., 1969; Takano et al., 1969) suggest that the BaSO_4 - PbSO_4 solid solution series does not deviate drastically from ideality. Thus as a first approximation, we can assume that a_{PbSO_4} in barite solid solution is nearly equal to its mole fraction.

The PbSO_4 mole fractions estimated from Pb contents in Anvil barite samples (Table V-4) range between 10^{-3} and 10^{-5} , with an average of about 10^{-4} . Thus the estimated a_{PbSO_4} in barite from Anvil ores is about 10^{-4} . From Fig. V-7 it is evident that the f_{O_2} during ore deposition must have been 10^{-37} to 10^{-38} at 200°C and $10^{-32.5}$ to $10^{-33.5}$ at 250°C . The full range of filling temperatures determined from primary fluid inclusions in Anvil barite, as will be shown later, is between $170^\circ \sim 240^\circ\text{C}$; the corresponding f_{O_2} range is between $10^{-40.5} \sim 10^{-41}$ and $10^{-34} \sim 10^{-34.5}$. If the temperature range is representative of ore formation, then f_{O_2} must have been around 10^{-35} at 240° - 250°C , and around 10^{-40} at 170° - 200°C . It appears probable that the higher the formation temperature, the higher was the oxygen fugacity involved in the formation of barite-bearing ores.

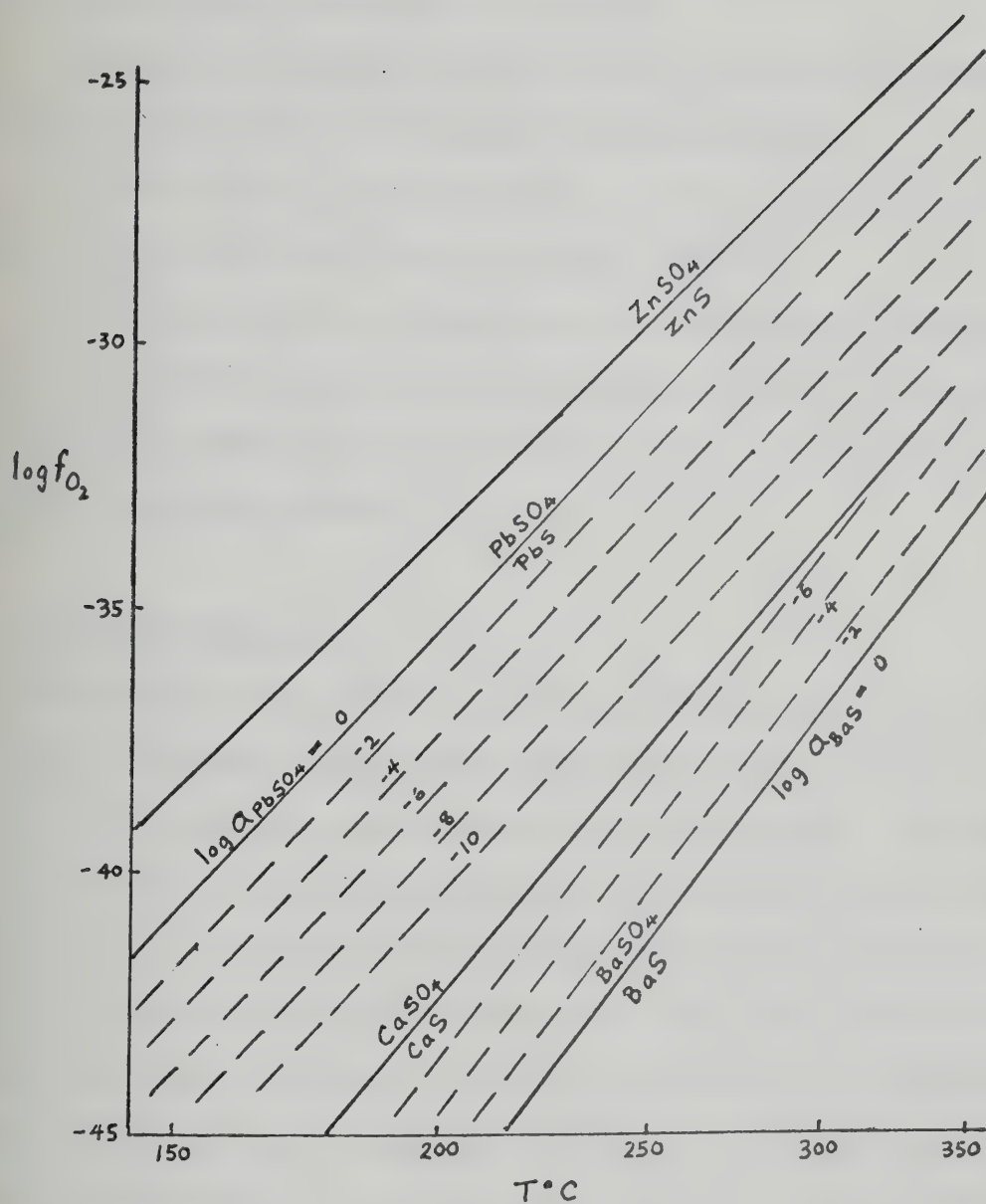


Fig. V-7. Activity isopleths of $(PbSO_4)_{\text{Barite}}$ and $(BaS)_{\text{Galena}}$ as functions of oxygen fugacity and temperature. $P = 1 \text{ atm}$. Numbers on isopleths indicate activities in logarithmic unit. Stability fields of $ZnSO_4$ - ZnS and $CaSO_4$ - CaS are also shown.

Average chemical compositions of Anvil barite and those of Kuroko barite, hotspring barite and modern marine barite are compared in Table V-5. The following observations can be made:

(i) Sr and Ca contents in Anvil barites are lower than Kuroko barites but comparable to those in hotspring or marine barites;

(ii) Pb content is slightly higher in Anvil barites than Kuroko and marine barites but lower than for hotspring barites;

(iii) Fe, Mn, Zn, Ni, Co contents in Anvil barites are generally higher than those in marine barite, indicating either formation in an area of high ferromanganese deposition or a higher amount of impurity detected by electron microprobe analysis.

4. Carbonate Minerals

Nineteen carbonate minerals in ore specimens from the Faro, Vangordø, Grum and Swim Lakes orebodies were analyzed for Fe, Mn, Ca, Mg, Zn and Ba by electron microprobe using an energy dispersive detector. CO₃ contents were calculated by assuming stoichiometric distribution of major cations in the carbonate structure. The analytical results and estimated mole % of solid solutions are listed in Table V-6. Structural formula of these carbonate minerals are given in Table V-7. Description of analytical method and related details can be found in Appendix V-1. Calculations of mole percents of solid solutions were made by the APL computer program MOL which is listed in Appendix V-2.

Data in Tables V-6 and V-7 indicate that the carbonates in Faro are siderites variously substituted by Mg, Mn and Ca. ZnCO₃ and BaCO₃ solid solutions were detected only in 2 samples from DDH66-2. Carbonates from Vangorda show a wider range of composition, including siderite, rhodochro-

TABLE V-5

Comparison of Chemical Composition of Barites from Anvil Ores, Kuroko, Hotsprings and Marine Basins (in wt. %)

	Anvil	Kuroko ^{1,2} (7)*	Hotsprings ² (13)*	Marine Basins		
				Japan Sea ² (5)*	Lau Basin ³ (2)*	Baja ⁴
Sr	0.15 (0.12~0.19)	0.58 (0.23~1.25)	0.30 (0.12~0.73)	0.23 (0.13~0.47)	1.4, 2.0	1.0 (0.2~3.4)
Ca	0.008	0.044 (0.034~0.053)	0.047 (0.036~0.064)	0.09 (0.044~0.20)		
Pb	0.053 (0.02~0.13)	0.015 (0.002~0.042)	2.0 (0.53~3.14)	0.016 (0.007~0.237)		
Fe	0.37				.046~.071	.026
Mn	0.16 (0.14~0.19)					
Zn	0.122 (0.035~0.270)				.011	.020
Ni	0.11 (0.003~0.15)				.009	
Co	0.24 (0.18~0.28)				.013	
Mg			0.036			
Cu						.012
Na	(0.03~0.12)					

1. Kajiwara and Honma (1972); 2. Takano and Watanuki (1974);

3. Bertine and Keene (1974); 4. Church (1970).

* number of analyses

Chemical Composition of Carbonate Minerals from Anvil Ore Deposits

Sample No.	(Weight %)			Ca	Mg	Zn	Ba	CO ₃ *	(Mole %)				MgCO ₃	ZnCO ₃	BaCO ₃
	Fe	Mn							FeCO ₃	MnCO ₃	CaCO ₃				
66-2 342	42.49	1.20		0.96	1.80	0.36	0.16	53.13	83.39	2.31	2.93		10.76	0.54	0.08
400	32.44	9.83		1.56	1.88	0.48	0.55	53.25	65.45	20.16	4.39		8.71	0.83	0.45
474	39.45	1.19		0.85	3.22	1.24	-	54.05	78.42	2.40	2.37		14.71	2.10	-
66E9 401	35.50	3.54		0.61	4.87	0.28	-	55.20	69.11	7.00	1.65		21.78	0.46	-
67-4 460	43.26	1.12		0.33	1.74	0.56	-	53.00	87.70	2.31	0.93		8.09	0.96	-
593	37.61	0.56		1.19	4.84	0.53	-	55.26	73.14	1.11	3.23		21.63	0.88	-
67-10 549	38.04	5.40		1.02	2.03	0.10	-	53.41	76.54	11.05	2.87		9.37	0.17	-
632	40.75	1.39		0.80	2.74	0.56	-	53.77	81.43	2.82	2.24		12.56	0.95	-
Anvil pit #1	45.78	0.10		0.48	0.78	0.49	-	52.38	93.92	0.20	1.37		3.66	0.86	-
V18 120	9.10	6.35		17.68	5.85	1.77	-	59.25	16.50	11.70	44.67		24.38	2.74	-
V33 279	13.82	23.72		1.63	4.77	0.56	-	55.50	26.75	46.68	4.41		21.24	0.92	-
V35 153 #1	29.64	10.97		0.72	3.78	0.34	-	54.55	58.39	21.96	1.98		17.10	0.57	-
#2	20.83	15.10		0.90	6.30	0.55	-	56.31	39.76	29.29	2.40		27.64	0.90	-
V60 180 #2	7.48	5.52		18.27	7.36	0.93	-	60.44	13.30	9.98	45.26		30.05	1.42	-
V63 135	9.22	4.73		18.90	6.80	0.10	-	60.25	16.44	8.57	46.97		27.87	0.16	-
143	14.69	21.33		1.52	4.06	3.65	-	54.74	28.84	42.57	4.15		18.31	6.12	-
Swim-X	22.44	17.89		2.09	2.79	0.58	-	54.21	44.49	36.04	5.76		12.72	0.99	-
A10-503	11.17	2.50		18.82	6.99	0.19	-	60.33	19.89	4.52	46.72		28.58	0.29	-
744	35.62	7.20		0.46	2.66	0.35	-	53.72	71.25	14.63	1.28		12.24	0.60	-

* Calculated value

Structural Formula and Stoichiometry of Carbonates from Anvil Ore Deposits

Sample No.	Structural Formula	Total cations CO ₃	Mineral Name
(Farø)			
66-2 342	Fe _{0.83} ^{Mg} 0.11 ^{Ca} 0.03 ^{Mn} 0.02 ^{Zn} 0.005 ^{Ba} 0.0008 ^{CO₃}	0.996	Mg-siderite
400	Fe _{0.66} ^{Mn} 0.20 ^{Mg} 0.09 ^{Ca} 0.04 ^{Zn} 0.008 ^{Ba} 0.005 ^{CO₃}	1.003	Mn-siderite
474	Fe _{0.78} ^{Mg} 0.15 ^{Mn} 0.02 ^{Ca} 0.02 ^{Zn} 0.02 ^{CO₃}	0.990	Mg-siderite
66E9 401	Fe _{0.69} ^{Mg} 0.22 ^{Mn} 0.07 ^{Ca} 0.02 ^{Zn} 0.005 ^{CO₃}	1.005	Mg-siderite
67-4 460	Fe _{0.88} ^{Mg} 0.08 ^{Mn} 0.02 ^{Ca} 0.01 ^{Zn} 0.01 ^{CO₃}	1.000	siderite
593	Fe _{0.73} ^{Mg} 0.22 ^{Ca} 0.03 ^{Mn} 0.01 ^{Zn} 0.01 ^{CO₃}	1.000	Mg-siderite
67-10 549	Fe _{0.77} ^{Mn} 0.11 ^{Mg} 0.09 ^{Ca} 0.03 ^{Zn} 0.002 ^{CO₃}	1.002	Mn-siderite
632	Fe _{0.81} ^{Mg} 0.13 ^{Mn} 0.03 ^{Ca} 0.02 ^{Zn} 0.01 ^{CO₃}	1.000	Mg-siderite
Anvil pit #1	Fe _{0.94} ^{Mg} 0.04 ^{Ca} 0.01 ^{Mn} 0.002 ^{Zn} 0.01 ^{CO₃}	1.002	Mg-siderite
(Vangørda)			
V18-120	Ca _{0.85} ^{Mg} 0.49 ^{Fe} 0.33 ^{Mn} 0.23 ^{Zn} 0.05 ^{(CO₃)₂}	0.975	Fe-dolomite
V33-279	Mn _{0.47} ^{Fe} 0.27 ^{Mg} 0.21 ^{Ca} 0.04 ^{Zn} 0.01 ^{CO₃}	1.000	Fe-Mg-rhodochrosite
V35-153 #1	Fe _{0.58} ^{Mn} 0.22 ^{Mg} 0.17 ^{Ca} 0.02 ^{Zn} 0.006 ^{CO₃}	0.996	Mn-Mg-siderite
153 #2	Fe _{0.40} ^{Mn} 0.29 ^{Mg} 0.28 ^{Ca} 0.02 ^{Zn} 0.01 ^{CO₃}	1.000	Mn-Mg-siderite

TABLE V-7 (cont'd)

Sample No.	Structural Formula	Total cations CO ₃	Mineral Name
(Vangorda)			
V60-180	Ca _{0.90} Mg _{0.60} Fe _{0.26} Mn _{0.20} Zn _{0.03} (CO ₃) ₂	0.995	Fe-dolomite
V63-135	Ca _{0.94} Mg _{0.56} Fe _{0.33} Mn _{0.17} Zn _{0.003} (CO ₃) ₂	1.002	Fe-dolomite
143	Mn _{0.43} Fe _{0.29} Mg _{0.18} Zn _{0.06} Ca _{0.04} CO ₃	1.000	Fe-Mg-rhodochrosite
(Swim Lakes)			
Swim - X	Fe _{0.44} Mn _{0.36} Mg _{0.13} Ca _{0.06} Zn _{0.01} CO ₃	1.000	Mn-Mg-siderite
(Grum)			
A10-503	Ca _{0.93} Mg _{0.57} Fe _{0.40} Mn _{0.09} Zn _{0.006} (CO ₃) ₂	0.998	Fe-dolomite
744	Fe _{0.71} Mn _{0.15} Mg _{0.12} Ca _{0.01} CO ₃	0.990	Mn-Mg-siderite

site and ankeritic dolomite. Carbonates from Grum and Swim Lakes are siderite and/or ankeritic dolomite. Generally speaking, about 70% of the analyzed carbonates belong to the siderite group, 20% are ankeritic dolomites and 10% rhodochrosites.

Partition of major elements in the carbonates is shown in Fig. V-8. The following observations can be made:

- (i) Negative correlation of Fe and Mn in all the carbonates; the four ankeritic dolomites (V18-120, V60-180, V63-135 and A10-503) show lower Fe and Mn contents (Fig. V-8b);
- (ii) Ca and Mn appear to be positively correlated in most carbonates except the four ankeritic dolomites which show a negative correlation (Fig. V-8a);
- (iii) Ca-Fe and Fe-Mg are weakly negatively correlated in most carbonates except the dolomites which show low Fe, high Ca (Fig. V-8b and c).
- (iv) The distribution of Mg-Mn, and Ca-Mg appear to be random in all carbonates.

The observations indicate that in most carbonates, Fe or Mn strongly substitute for each other, and to a lesser extent, Ca-Fe and Fe-Mg also substitute for each other. Ca and Mn probably behave in a similar manner in substituting other elements in most carbonates except in the dolomites.

Siderite and dolomite with less than 10 mole % MnCO_3 are plotted in a $\text{FeCO}_3\text{-CaCO}_3\text{-MgCO}_3$ diagram (Fig. V-9) with subsolidus relations at $350^\circ - 550^\circ\text{C}$ and $2\frac{1}{2}$ Kb from the work of Rosenberg (1967). Rosenberg found that the ordered solid-solution series $\text{CaMg}(\text{CO}_3)_2\text{-CaFe}(\text{CO}_3)_2$ in which ankerite lies, terminates at a three-phase ankerite-calcite-siderite field (Fig. V-9a), and that the upper limit of Fe solubility in ankerite increases with temperature. The ankerite compositions which are stable with siderite and calcite at experimentally determined temperatures are also shown in Fig.

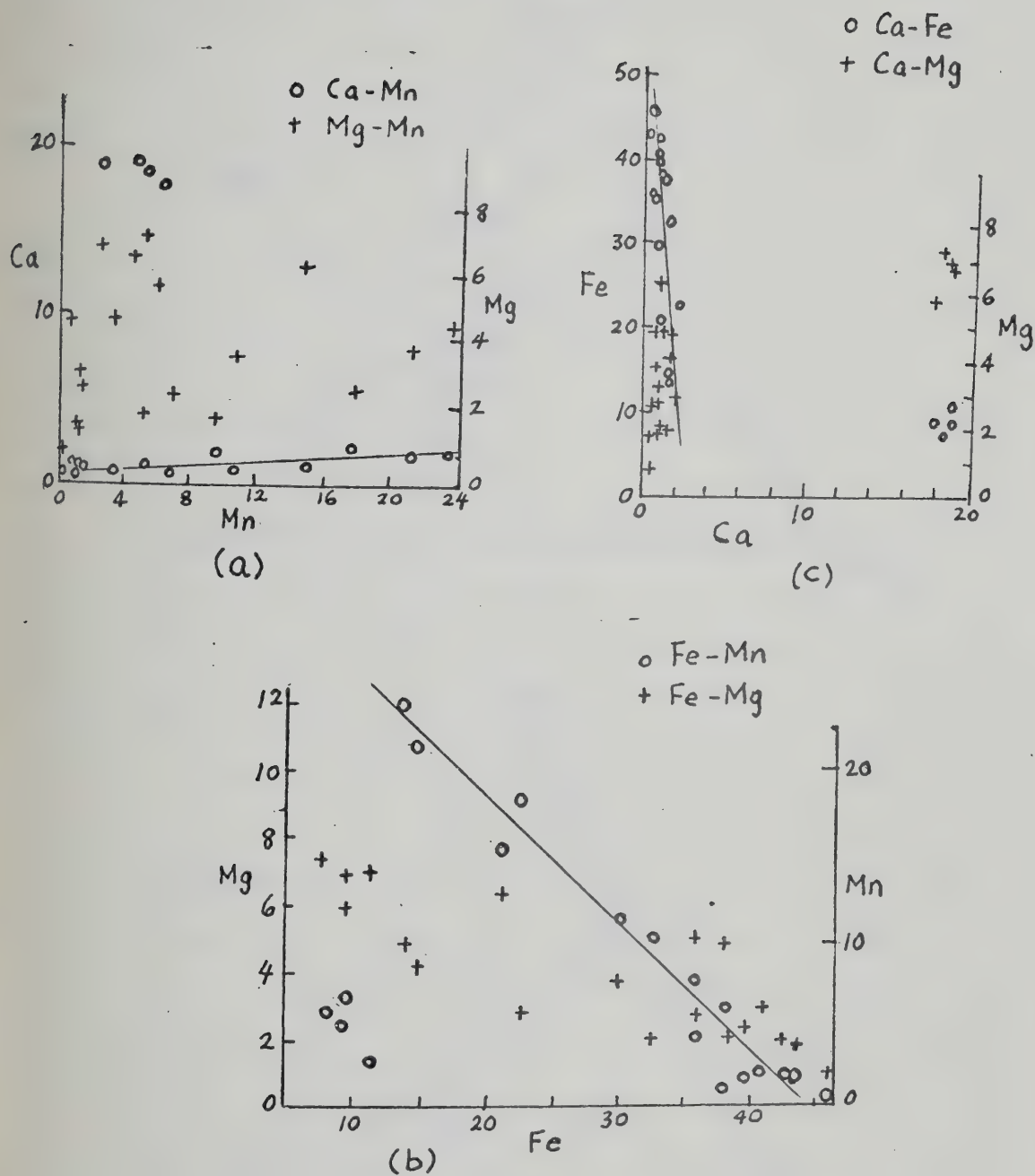


Fig. V-8. Partition of major elements in the Anvil carbonates.
Unit is in weight percent.

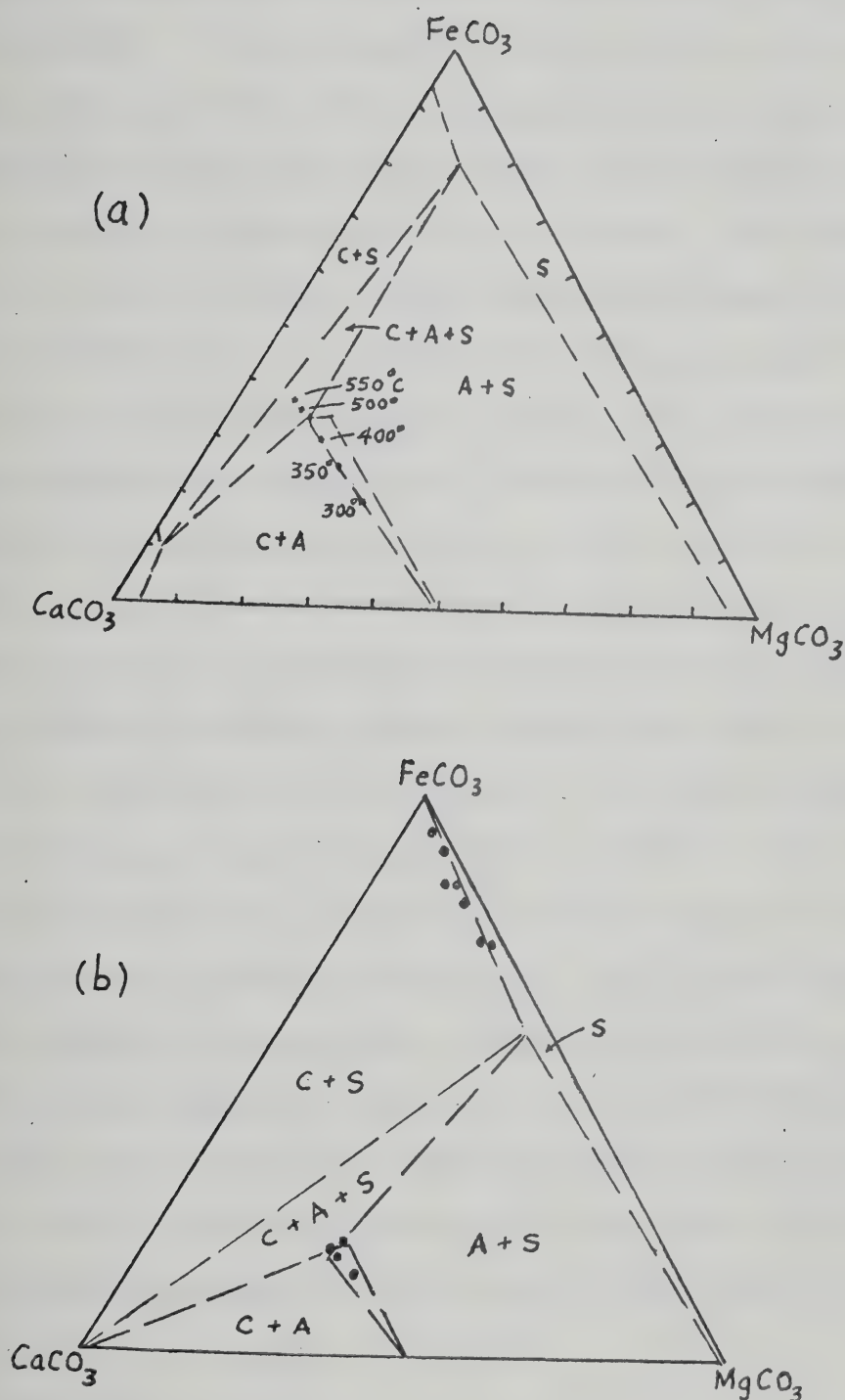
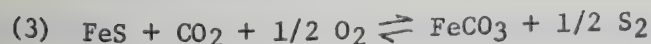
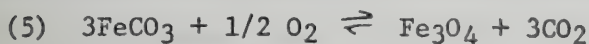


Fig. V-9. (a) Compositions of carbonates with subsolidus relations at 450°C; the limiting ankerite composition at temperatures ranging from 550°C to 350°C (after Rosenberg, 1967). (b) Extrapolated subsolidus relations at 300°C for the Anvil carbonates. C: calcite solid solution; S: siderite solid solution; A: ankerite solid solution; solid dots: data points.

V-9a. A diagram depicting these solid solution relations at 300°C has been constructed by extrapolation of Rosenberg's experimental results and is shown in Fig. V-9b. It can be observed that most ankeritic dolomites lie at or below the experimental ankerite composition (X) indicating that the Anvil ankerites were formed at or below 300°C. Sample A10-503 from Grum lies in the boundary of ankerite-siderite and calcite. All siderites plot in siderite or siderite-calcite boundary near the FeCO_3 apex. The shifting of position of siderites to the calcite-siderite boundary results from ignoring the presence of small amounts of MnCO_3 in the carbonates.

Mineral assemblages associated with the carbonates as revealed by petrography of ore specimens are generally: pyrite, pyrrhotite, marcasite, magnetite, and trace carbonaceous matter (graphite?). Graphite is present in most host rocks intimately associated with the Anvil ore deposits as lenses of graphitic schist, graphitic mica schist, etc. (see Chapter III). No hematite has been observed. The amount of magnetite as compared to that of sideritic carbonates is generally small. The stability relations in Fe-C-O-S system as functions of other physico-chemical parameters such as temperature, pressure, f_{O_2} , f_{S_2} , f_{CO_2} and $f_{\text{H}_2\text{O}}$ have been experimentally or theoretically considered by many authors, among them Holland (1959, 1965a), Yui (1966a,b), French and Rosenberg (1965), Seguin (1965, 1971) and Shikazono (1973). Mineralogical and textural features of the iron sulfide-carbonate-oxide assemblages in Anvil ores suggest the following chemical reactions during regional and/or thermal metamorphism (if we may assume equilibrium):





Phase relations of py-po for reaction (1) have been discussed previously. Reaction (6) and similar reactions such as py-magnetite are for practical reasons insignificant due to the very rare occurrence of py-po-mgt (without siderite). Therefore, we will consider only reactions (2) to (5), under two separate categories, sulfide-carbonate and carbonate-oxide systems, the latter, being the lower limiting assemblage for the metamorphism, will be discussed first.

(a) Carbonate-oxide System. Yui (1966b) has demonstrated that siderite is decomposed to magnetite at lower oxygen fugacities according to reaction (4) because of the decomposition of CO_2 to graphite (C) and oxygen. Consequently the assemblage of siderite and magnetite without graphite will be formed by reaction (5) and is stable within a rather narrow temperature interval. If the assemblage siderite-magnetite-graphite is taken as a stable end-product of metamorphism on Anvil ores, then reaction (4) can be used as first approximation to determine fugacities of oxygen and CO_2 during metamorphism. Based on free energy data for reactions such as $\text{CO}_2 = \text{C} + \text{O}_2$, $\text{CO}_2 = \text{CO} + 1/2 \text{O}_2$, Yui gives the relations of absolute temperature and fugacities of oxygen and CO_2 in equilibrium with the siderite-magnetite-graphite assemblage as follows:

$$\log f_{\text{O}_2} = 8.63 - 24700/T$$

$$\log f_{\text{CO}_2} = 8.67 - 4110/T$$

Thus at 300°C , $\log f_{\text{O}_2} = -34.5$, and $\log f_{\text{CO}_2} = 1.5$; and at 250°C , $\log f_{\text{O}_2} = -38.6$, $\log f_{\text{CO}_2} = 0.81$. These values probably represent maximum and minimum fugacities attained during metamorphism. The stability fields of iron oxides, siderite and graphite as functions of f_{O_2} and temperature are

shown in Fig. V-10 (modified after Yui, 1966b). If water is present in the stage of metamorphism as pore fluids, small amounts of graphite might become hydrocarbons, i.e. methane, etc., and dissociation of H_2O and CO_2 might occur in the pore fluids. Yui has shown that for the temperature range $100^\circ\text{--}500^\circ\text{C}$, $\log f_{H_2}/f_{H_2O}$ ratios in equilibrium with the siderite-magnetite-graphite assemblage are greater than -3, and at 300°C , the ratio is -2.38. A dissociation curve of water ($2H_2O = 2H_2 + O_2$ at $\log f_{H_2}/f_{H_2O} = -2.38$) is found to be almost identical to and superimposed on curve A in Fig. V-10. If the amount of the pore fluids is sufficiently large to keep the f_{H_2}/f_{H_2O} ratio constant, the f_{O_2} of the fluid varies with temperature along curve A, and at the intersection of curves A and B ($f_{CO_2} = 10^{+1.5}$ atm), $T=300^\circ\text{C}$, $f_{O_2}=10^{-35}$, siderite is decomposed to magnetite according to reaction (5). If the amount of pore fluids is not sufficient to prevent composition variation in the fluids by the decomposition of siderite to magnetite, the variation of oxygen fugacity with temperature is not simple; presumably f_{H_2}/f_{H_2O} ratios and f_{CO_2} will increase as a result of CO_2 production accompanying siderite decomposition. If the pore fluid is mainly CO_2 , at 300°C , $\log f_{O_2} = -35$, $\log f_{CO_2} = 1.5$, then $\log (f_{CO}/f_{CO_2}) = -3.7$, and $\log f_{CO} = -2.2$.

As pointed out by Yui, siderite is capable of self-oxidation at lower oxygen fugacities according to the reaction,



Thus, addition of oxygen is not necessary for the formation of magnetite by siderite, and additional CO_2 only favors the formation of siderite rather than magnetite. This might explain the scarcity of magnetite as compared to relatively abundant siderite in the Anvil ores. The scarcity of graphite within massive ores of Anvil ore deposits suggests that siderite was decomposed to magnetite according to reaction (5) with a rise in f_{O_2} to f_{CO_2}

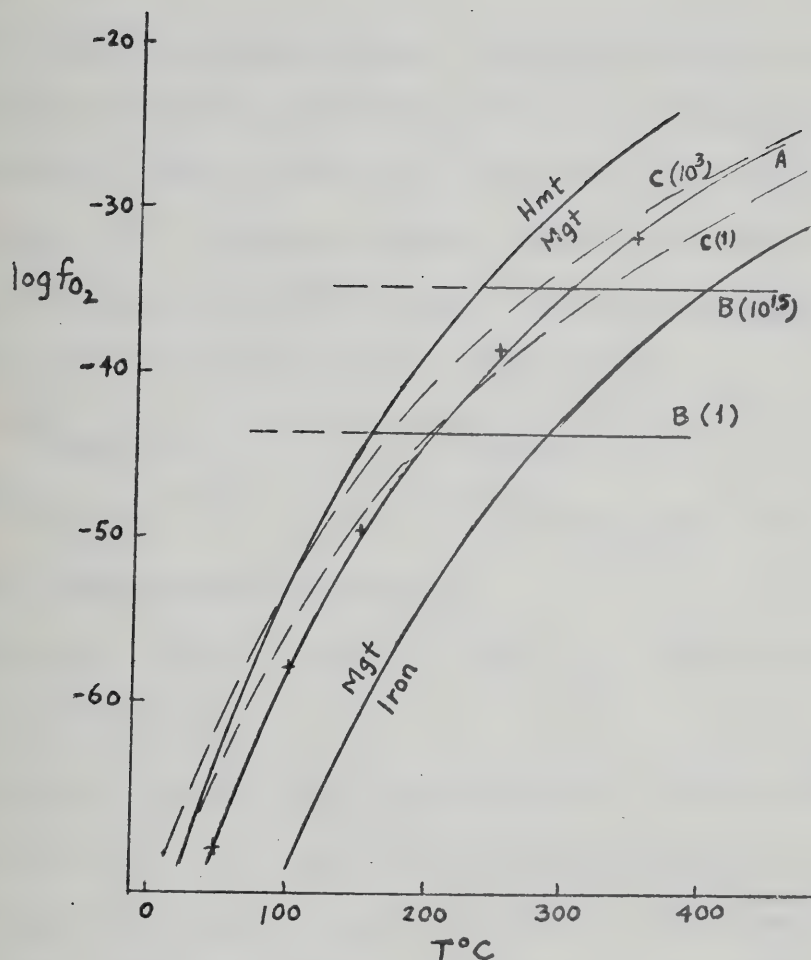


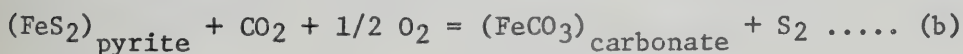
Fig. V-10. Stability fields of magnetite, hematite, siderite and graphite as functions of oxygen fugacity and temperature. Values in parentheses are CO_2 fugacities in bar unit. Also shown are equilibrium curves for the following reactions:



Crosses indicate the position of a dissociation curve of water ($f_{H_2}/f_{H_2O} = 10^{-2.38}$, see text) which is almost identical to curve A (modified after Yui, 1966b).

ratio caused by escape of CO_2 or dissociation of H_2O and/or CO_2 in pore fluids.

(b) Sulfide-carbonate System. Sideritic carbonates are found texturally coexisting with pyrite, sphalerite and occasionally pyrrhotite. Formation of siderite or FeCO_3 in carbonates is apparently the result of reactions (2) and possibly (3). Therefore chemical relations between FeS contents in sphalerite $(m_{\text{FeS}})_{\text{sp}}$ and FeCO_3 contents in carbonate $(m_{\text{FeCO}_3})_{\text{cb}}$ both coexisting with pyrite can be described by reactions as:



and the combined expression becomes:

$$\log a_{\text{FeS}} = 1/2 \log a_{\text{FeCO}_3} - 1/2 \log f_{\text{CO}_2} - 1/4 \log f_{\text{O}_2} + 1/2 \log K_a^2 \cdot K_b \quad (V-7)$$

where K_a and K_b refer to equilibrium constants for the reactions (a) and (b), respectively. The activities of FeS and FeCO_3 can be approximated by molalities of FeS and FeCO_3 since the activity coefficients of FeS and FeCO_3 do not deviate significantly from unity in the temperature range $250^\circ\text{--}300^\circ\text{C}$ (Barton and Toulmin, 1966; Shikazono, 1973); mole fractions of FeS in sphalerite and FeCO_3 in carbonate can thus be used as a close approximation of molalities. These are plotted on a $\log m_{\text{FeS}} - \log m_{\text{FeCO}_3}$ diagram as shown in Fig. V-11. It can be observed that variation in m_{FeCO_3} is large in comparison with a relatively constant m_{FeS} ; four groups (A, B, C, D in Fig. V-11) can be distinguished and the average m_{FeCO_3} and m_{FeS} values of each group are used to estimate the magnitude of increase in f_{CO_2} and f_{O_2} from A to D. If f_{CO_2} is held constant, then f_{O_2} of the sulfide-carbonate system would increase very slightly from group A to group D (i.e. from Vangorda - Swim Lakes - Faro and Grum). On the other hand, if f_{O_2} is held

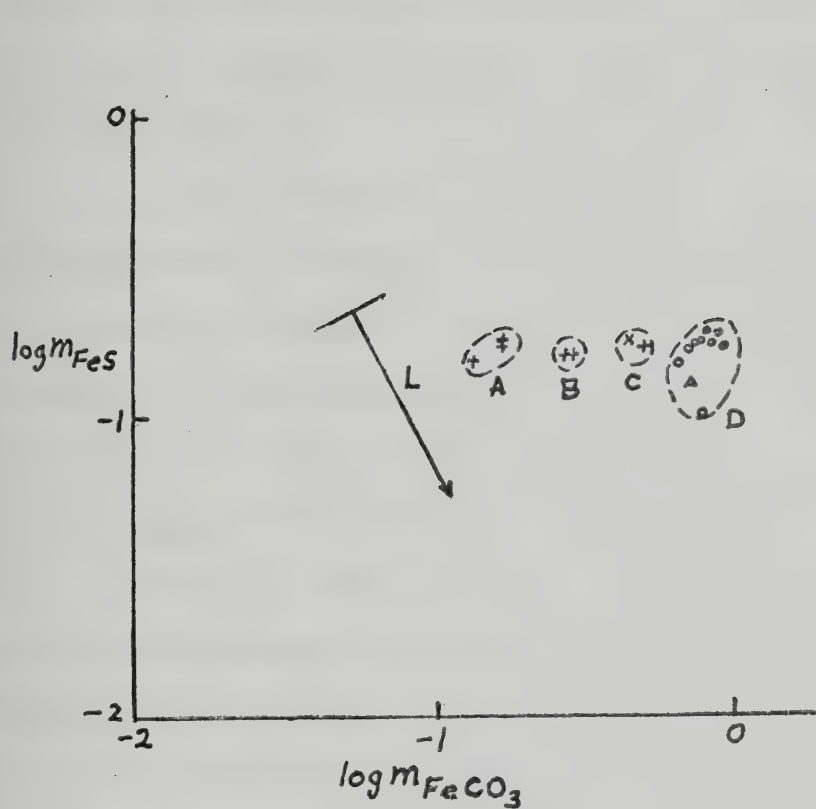


Fig. V-11. FeS contents of sphalerites versus $FeCO_3$ contents of carbonates from Anvil ore deposits. A line L shows increasing order of $2\log f_{CO_2} + \log f_{O_2}$ (equation V-7).

- o: Faro
- +: Vangorda
- x: Swim Lakes
- Δ : Grum

constant, then f_{CO_2} would also increase. The magnitude of f_{CO_2} increment is much larger than that of f_{O_2} increment. This observation is therefore consistent with the fact that a higher proportion of f_{CO_2} over f_{O_2} would favor formation of siderite rather than magnetite (siderite is more abundant in Vangorda than in Faro).

In order to estimate oxygen fugacities during the stage of sulfide-carbonate equilibration, activities (= molalities) of FeS in sphalerite and FeCO_3 in carbonate are compared as functions of f_{O_2} and f_{S_2} in Fig. V-12. FeS mole percents in sphalerite are generally between 10 and 20, whereas FeCO_3 mole percents in carbonates are between 13% and 94%, averaging 55% (correspond to a_{FeCO_3} of $10^{-0.9}$ and $10^{-0.03}$, averaging $10^{-0.3}$), and f_{CO_2} is about $10^{1.5}$. Fixing f_{CO_2} , temperature, FeS contents in sphalerites and FeCO_3 contents in carbonates, we can understand the relation between a_{FeS} and a_{FeCO_3} and mineral stability fields as functions of oxygen and sulfur fugacities. The wedge-shaped areas outlined by the intersections of four lines (A, A', B, B' or A, A', C, C') define the possible range of oxygen fugacities at given temperature. The position of the pyrite-pyrrhotite-magnetite triple point lies very close to the intersection points of A'-B' and A'-C' in both 250°C and 300°C diagrams (Fig. V-12a and b), indicating that the assemblage pyrite-pyrrhotite-sphalerite-siderite-magnetite was probably equilibrated at conditions of $T=250^\circ\text{--}300^\circ\text{C}$, $f_{\text{CO}_2} \leq 100$ bars, and f_{O_2} range between 10^{-33} and 10^{-40} bars with sphalerite containing up to 20 mole % FeS buffered by pyrite and pyrrhotite at $f_{\text{S}_2} = 10^{-11.5} - 10^{-14}$. Specifically, if $f_{\text{CO}_2} = 10^{1.5}$, then the most probable range of f_{O_2} is about 10^{-36} to 10^{-40} at 250°C, and about 10^{-30} to 10^{-34} at 300°C; the range may be indicative of the maximum and minimum conditions during the metamorphic event in which the sulfide-carbonate-oxide assemblage was equilibrated.

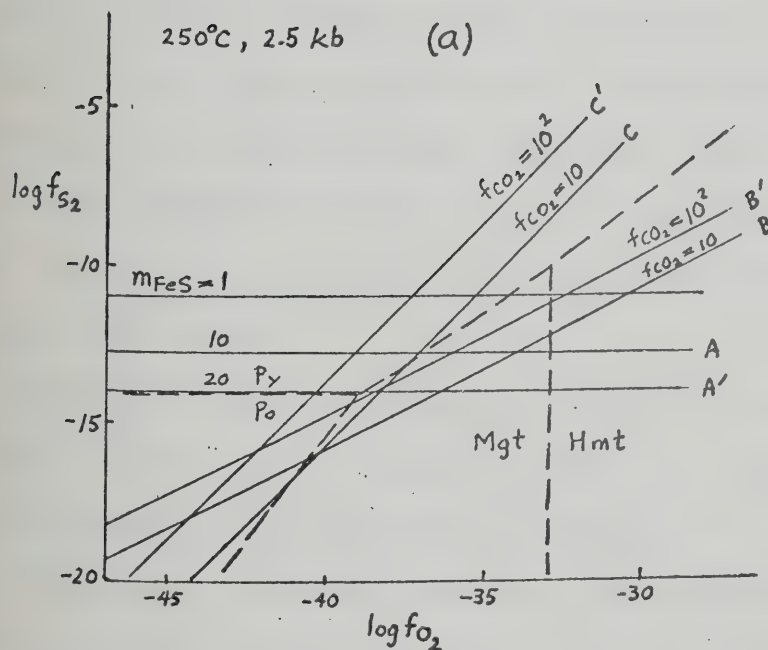
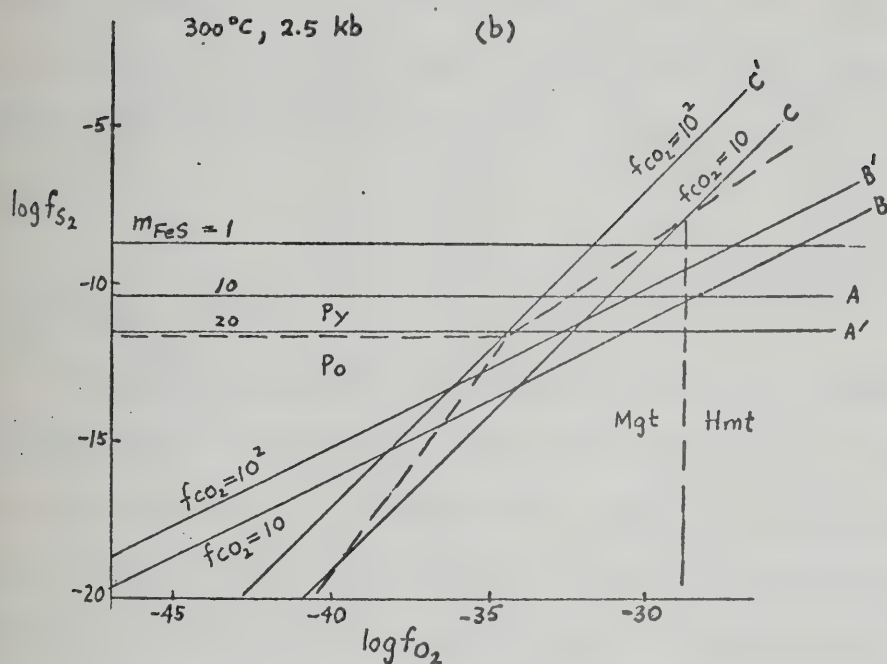


Fig. V-12. Activity isopleths of FeS and FeCO_3 as functions of fugacities of oxygen and sulfur. Stability fields of pyrite, pyrrhotite, magnetite and hematite are superimposed for comparison (dashed lines). Solid lines are activity isopleths of:

A) mol % FeS in sphalerite (A: 10 mol %; A': 20 mol %).

B) a_{FeCO_3} in carbonate = 10^{-1} (B: $f_{\text{CO}_2} = 10$; B': $f_{\text{CO}_2} = 10^2$) for $\text{FeS}_2 + \text{CO}_2 + 1/2 \text{O}_2 = \text{FeCO}_3 + \text{S}_2$ (pyrite-siderite).

C) a_{FeCO_3} in carbonate = 10^{-1} (C: $f_{\text{CO}_2} = 10$; C': $f_{\text{CO}_2} = 10^2$) for $\text{FeS} + \text{CO}_2 + 1/2 \text{O}_2 = \text{FeCO}_3 + 1/2 \text{S}_2$ (pyrrhotite-siderite).

The estimates of f_{O_2} in Fe-C-O-S system are again consistent with those derived from Fe-S, Fe-Zn-S, Fe-C-O systems. Table V-8 summarizes all the derived fugacities of gaseous phases in the above systems for the Anvil ore deposits.

5. Bulk Ores

In this section, extensive data on ore grades from chemical analyses of drill hole sulfide sections in Faro, Vangorda, Grum and Swim Lakes ore deposits are summarized. The drill hole assay data used were provided to the writer through the courtesy of Cyprus Anvil Mining Corporation Ltd. (for Faro), and Kerr Addison Mines Co. Ltd. (for Vangorda and Swim Lakes). Data on the Grum deposit are those published by the AEX Minerals Corporation Ltd. in 1974 (now Canadian Natural Resources Co. Ltd). A total of 16 bulk ore samples from Faro drill holes also has been selected for chemical analyses of 18 major and minor elements by means of MRFAPE spectrometry. These analyses were made in order to characterize certain other metals (e.g. Fe, Mn, Ba, Co, Ni, etc.) which are usually not analyzed in drill hole bulk samples.

The summary on average grades of drill hole bulk ores from Faro, Grum, Vangorda and Swim Lakes is presented in Table V-9. The chemical analyses of 16 bulk ores from Faro are listed in Table V-10.

The analysis of bulk ore samples for minor elements has severe limitations in interpretation and elucidation of the ore-forming process. Generally only empirical partition relationship (such as conditions of dilute solution, equilibrium or random scatter) and some sort of chemical variations in relation to depths, ore types, etc. can be deduced from bulk ore analysis. It is not the purpose of the writer to pursue a detailed study of minor element partitions or zoning in the Anvil ore deposits but rather

TABLE V-8

Estimated Fugacities of Gaseous Phases (in log units)
During Metamorphism of the Anvil Ore Deposits

System	T°C	f_{S_2}	f_{O_2}	f_{CO_2}	f_{CO}	$\frac{f_{CO}}{f_{CO_2}}$	$\frac{f_{H_2}}{f_{H_2O}}$
Fe-S	300	-10.3~-10.7					
	250	-12.5~-13.5					
Fe-Zn-S	300	-10.0~-11.5					
	250	-12.5~-14.0					
Fe-C-O	300		-34.5	1.50	-2.20	-3.7	-2.4
	250		-38.6	0.81	-3.56	-4.4	-2.5
Fe-C-O-S	300	-10.4~-11.7	-30~-34				
	250	-12.8~-14.0	-36~-40				

TABLE V-9

Average Grades of Faro, Vangorda, Grum and
Swim Lakes Ore Deposits

Deposit	(weight percent)			(ppm)		References
	Pb	Zn	Cu	Ag	Au	
Faro	3.40	5.72	0.16	37	-	(1), (2)
Vangorda	3.16	4.96	0.27	55	0.63	(3)
Grum	4.19	6.81	0.25	65	-	(4)
Swim Lakes	3.14	4.97	0.15	45	0.55	(5)

(1) Tempelman-Kluit (1972); (2) Gondi (1972);
(3) Chisholm (1959); (4) Northern Miner (June 27,
August 22, Oct. 3, 1974), average of 23 drill holes
totalling 2035 feet; (5) Kerr Addison Mines Ltd.
assay records, average of 5 drill holes totalling
460 feet.

Chemical Analyses of Drill Hole Ore Specimens, Faro Deposit

Sample No.	(Wt. %)		(ppm)													
	Fe	Mn	Cu	Ag	Cd	Co	Cr	Ni	V	Sr	Be	Ti	As			
66-2 283	31.84	0.46	713	59	13	101	127	30	8	12	0.3	3	180			
474	54.11	0.02	67	10	12	287	187	43	6	1	0.2	3	350			
486	58.45	0.07	993	8	8	402	213	40	21	2	0.3	38	350			
66E9 299	15.15	0.20	347	57	14	41	67	19	6	21	0.3	4	65			
337	46.61	0.03	363	34	17	102	162	30	6	n.d.	0.2	5	240			
376	35.32	0.04	96	44	22	72	137	32	8	1	0.2	18	180			
436	37.01	0.05	886	7	9	117	147	36	30	3	0.4	93	420			
66-10 634	46.00	0.02	1455	19	8	120	186	31	6	4	0.1	13	270			
66-22 305	25.16	0.02	130	25	11	30	115	26	5	3	n.d.	12	120			
67-4 460	44.53	0.12	97	46	10	276	158	51	12	1	0.3	30	220			
593	37.73	0.09	533	18	21	160	164	34	19	9	0.5	88	230			
67-6 602	15.38	0.06	503	60	17	33	63	20	5	25	0.2	10	75			
710	41.13	0.02	1121	27	7	35	147	28	6	8	0.2	5	220			
762	36.53	0.10	371	23	23	207	149	31	7	1	0.1	26	390			
67-10 549	55.59	0.49	2921	17	8	257	221	66	11	2	0.6	6	200			
632	18.43	0.03	223	29	31	35	91	26	20	2	0.2	63	n.a.			

to estimate the overall metallic compositions of these ore deposits as a basis for the study of initial metal abundances and solubilities in ore solution to be made in a later chapter.

The metallic compositions of a massive sulfide deposit can best be estimated by extensive chemical analysis of large drill hole specimens; the routine and complete chemical assays of drill cores for Pb, Zn, Ag, Cu and occasionally Au by the companies provide a good average estimate for these elements. Since Fe, Ba and Mn were never analyzed in normal routine chemical assays of drill cores, their estimation can only be made by either selective bulk ore analysis or indirectly by mineralogical compositions of representative bulk ore specimens. The former has been made only for Faro deposit (Table V-10). Volume percentages of total sulfide mass and each component sulfide phase in Faro have been estimated by Gondi (1972) and Campbell and Ethier (1973) and in Vangorda by Chisholm (1959). The writer has made additional assessments of volume percentages of iron sulfides, barite and siderite by means of point counting on typical massive ores from Grum, Vangorda and Faro; the volume percents of pyrite and pyrrhotite in Grum agree well with those in Faro estimated by Campbell and Ethier (1973). The volume proportions of total sulfides and each sulfide phase in Faro, Vangorda and Grum and Swim Lakes are summarized in Table V-11. No data on the proportions of iron sulfides in the Swim Lakes deposit are available.

Fe in the deposits mainly occurs in pyrite, pyrrhotite, sphalerite and in minor amount in magnetite, siderite, chalcopyrite, marcasite and arsenopyrite. Fe content of pyrrhotite and sphalerite were given previously. Fe contents estimated from the former three sulfides account for more than 95% of total Fe in the deposits. Pb, Zn, Cu weight percents deduced from their volume data are greater than observed grades given in Table V-9,

Mineral Compositions of Anvil Ore Deposits (volume percents)

Deposit	Py	Sp	Gn	Po	Cpy	Mc	Mgt	Sdt	Aspy	Brt	Total Sulfide Mass	Ref.
Faro	51	21	7	4	0.5	-	-	0.5 ⁽⁴⁾	-	1 ⁽⁴⁾	85	(1), (2)
Vangorda	21	15	9	6	3.6	0.6	0.6 ⁽⁴⁾	1.2 ⁽⁴⁾	3	-	60	(3)
Grum	50	11*	3*	5	-	-	-	-	-	0.5	70	(4)
Swim Lakes	-	7.5*	2*	-	0.15*	-	-	-	-	1	50	(5)

(1) Campbell and Ethier (1973)

(2) Gondi (1972)

(3) Chisholm (1959)

(4) Present Writer

(5) Tempelman-Kluit (1972)

*Estimated values from average grades in Table V-9.

indicating than an over-estimation of galena, sphalerite and chalcopryrite by Campbell and Ethier (1973) and Chisholm (1959). The excess volume percents are assigned to iron sulfides (pyrite and pyrrhotite) since they are the predominant phases in the deposits. A best estimate of metallic compositions of the Anvil ore deposits is presented in Table V-12.

Relative abundance of ore metals in the Anvil ore deposits can be expressed as their atomic ratios as shown in Table V-13; copper in Faro is taken to be 1. These ratios will be used in a later chapter to estimate relative abundance of metals in initial ore solution if certain reasonable assumptions are made and pertinent physico-chemical factors applied.

There are certain interesting aspects of element variations observable from the drill hole assay data and analytical results in Faro deposit. First of all, Ag content appears to be greater near the upper part of sulfide layer in drill holes 66-2, 66E9, 66-22 and 67-6 (Fig. V-13a). Copper appears to have a crude negative correlation with Pb and Zn content (this is especially apparent in drill holes 66E9, 66-22 and 67-4) (Fig. V-13b). On the other hand, Mn/Fe ratios tend to increase whereas Co/Ni ratios and As, V, Ni, Co, Cu contents decrease towards the upper part of the orebody (Table V-10). Even though structural complexity in Faro still does not allow positive establishment of stratigraphic top and bottom, the general consensus is that the position in which the orebody now lies has not changed significantly since ore deposition. Tatsumi and Oshima (1966) and Lambert and Sato (1974) have shown that in Kuroko deposits of Japan, Cu decreases as Pb and Zn increase stratigraphically upwards, and As, Sb, V, Ag, Au increase and Ni and Co decrease. The trend of As and V is obviously opposite in Faro as compared to Kuroko, but other trends are similar. Also, Lambert and Sato (1974) have shown that Co/Ni ratios are higher in yellow

TABLE V-12

Metallic Compositions of the Anvil Ore
Deposits (Weight %)

	Faro	Vangorda	Grum	Swim Lakes
Fe	36.92	29.31	31.01	25.20*
Zn	5.72	4.96	6.81	4.97
Pb	3.40	3.16	4.19	3.14
Ba	0.49	-	0.30	0.68
Cu	0.15	0.27	0.25	0.15
Ag (ppm)	37	55	65	45
Au (ppm)	-	0.63	-	0.55
As	0.02	1.84	-	-
Mn	0.11	-	-	-

* Minimum estimate based on 40 vol. % Py,
7.5 vol. % Sp, and 0.15 vol. % Cpy.

TABLE V-13

Atomic Ratios of Metals in Anvil Ore Deposits
Copper in Faro is taken to be 1

	Fe	Zn	Pb	Ba	Cu	Ag	Au($\times 10^{-4}$)	As	Mn
Faro	280	37	7.0	1.5	1	0.01	-	0.11	0.85
Vangorda	222	32	6.5	-	1.8	0.02	1.35	10.4	-
Grum	235	44	8.5	0.9	1.7	0.03	-	-	-
Swim Lakes	191	32	6.4	2.1	1	0.02	1.18	-	-

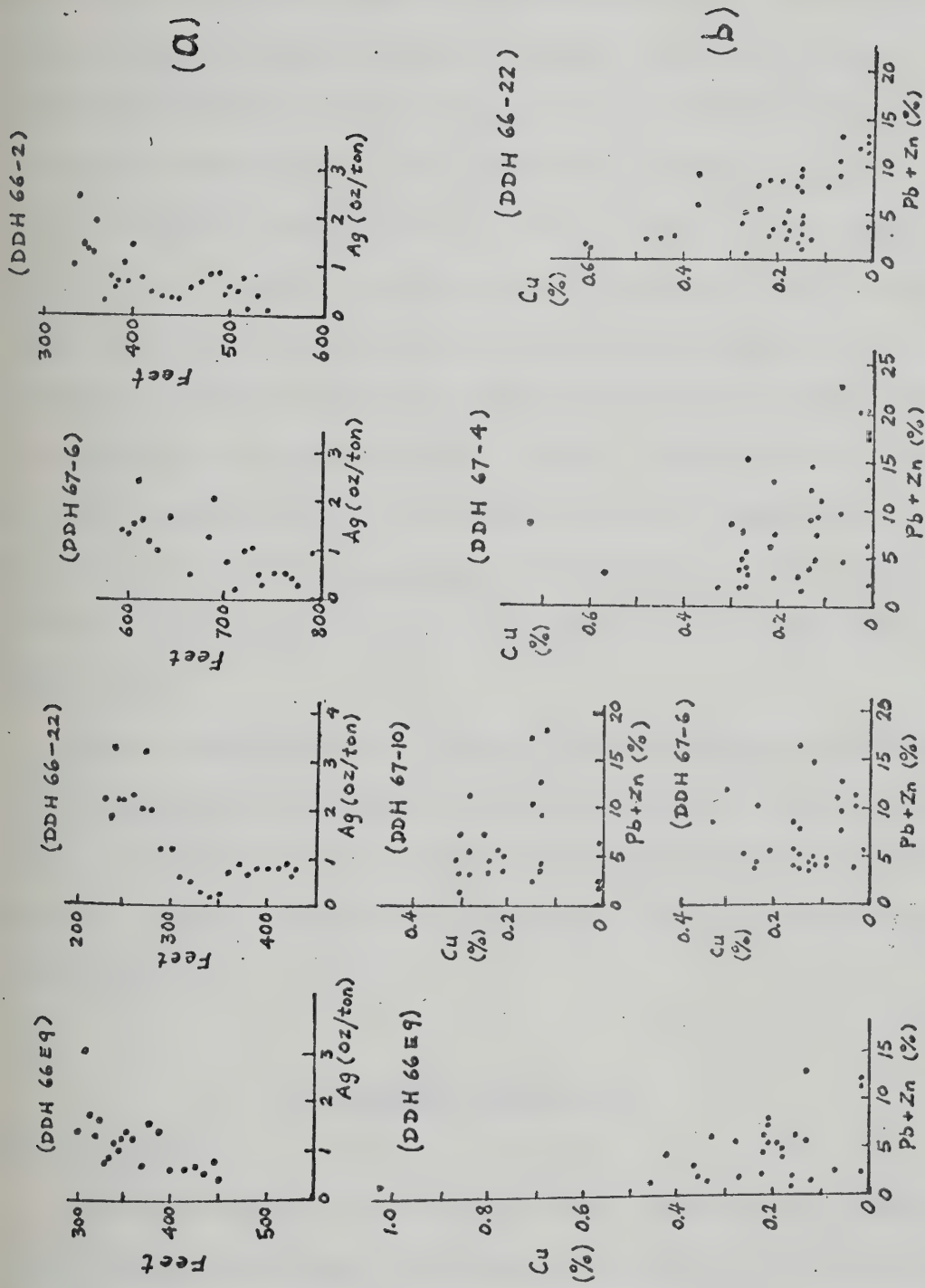


Fig. V-13. (a) Variation of Ag contents with depths, Faro deposit. (b) Correlation of Cu with Pb+Zn in drill holes, Faro deposit.

ore (Oko) and siliceous ore (Keiko) but lower in black ore (Kuroko); again showing a decreasing trend upwards. Average Co/Ni ratio of Faro ores is about 4.2, considerably higher than the cupriferous ores of Cyprus (Troodos massif) and Beshi (Japan) of basic volcanics association (Co/Ni \sim 2), but lower than the Ergani deposit in Turkey (Co/Ni \sim 7.4). In a study of Mn/Fe ratio in the Heath Steel massive sulfide deposit, Whitehead (1973) suggested that the ratio is higher before and after the main stage of massive sulfide deposition in a volcanic-sedimentary environment, and that it increases with a decreasing thickness of massive sulfide (e.g. peripherally to a sulfide depositional basin). Mn/Fe ratios in Faro show a crude <shaped trend, with very high ratios in the upper part. Whether the minima near the central part really represents the "main stage" of sulfide deposition or was caused by some other processes is not known. We may correlate the minima with a pyrrhotite-rich "core" outlined in the Faro No. 1 orebody (Campbell and Ethier, 1973).

Average molecular ratios of Pb, Zn and Cu in Faro, Vangorda and Swim Lakes deposits show similarity to other 'conformable' lead-zinc deposits of the world in both a Pb-Zn binary plot and Pb-Zn-Cu ternary plot (Tempelman-Kluit, 1972). The ratios in Grum deposit also show good similarity to world deposits.

C. FRANCES LAKE DISTRICT

1. Pyrrhotite

Pyrrhotite texturally related to pyrite, chalcopyrite, sphalerite and/or sideritic carbonates was analyzed for Fe, S, Ni, Co, Cu, Mn by electron microprobe using an energy dispersive detector. Similar counting rates, operating conditions and standards as those for Anvil pyrrhotite analysis were employed.

The chemical composition of pyrrhotite samples from Thompson Creek deposit, Frances Lake district is shown in Table V-14.

The deposit has been subjected to lower greenschist facies metamorphism and two periods of structural deformation, the younger of which is related to mid-Cretaceous granitic intrusion. Formation of late stage pyrrhotite, siderite, sulfosalts and some pyrite was probably related to metamorphism. The temperature range of metamorphism can be estimated from homogenization temperature measurements on secondary CO₂-rich gas-liquid inclusions in quartz and by sulfur isotope fractionation temperatures of sphalerite-galena pairs which are associated with pyrrhotite, siderite, and pyrite. A range of 280° to 350°C and an average of 300°C probably characterizes the metamorphism. Furthermore, an average metamorphic pressure of about 4 Kb (range 3 to 6 Kb) can be estimated from sphalerite-pyrrhotite-pyrite assemblage using sphalerite geobarometry (see later section).

If the Thompson Creek pyrrhotites were last equilibrated with other mineral phases during metamorphism at about 300°C, it is evident from the range of Fe atomic percents (Table V-14) and Fig. V-1 that the pyrrhotites are all hexagonal. The fugacities of sulfur at which the pyrrhotites last equilibrated can be estimated from the position of the pyrite-pyrrhotite solvus from a temperature- f_{S_2} diagram at 4 Kb as shown in Fig. V-14; at 300°C, f_{S_2} is $10^{-9.8}$, and at 350°C f_{S_2} is 10^{-7} ; a_{FeS} is 0.1 at these temperatures. a_{FeS} is considerably lower than that in the Anvil Fe-S system and probably reflects a deficiency of Fe either in metamorphic fluids or in original sulfide assemblages which were reequilibrated during metamorphism.

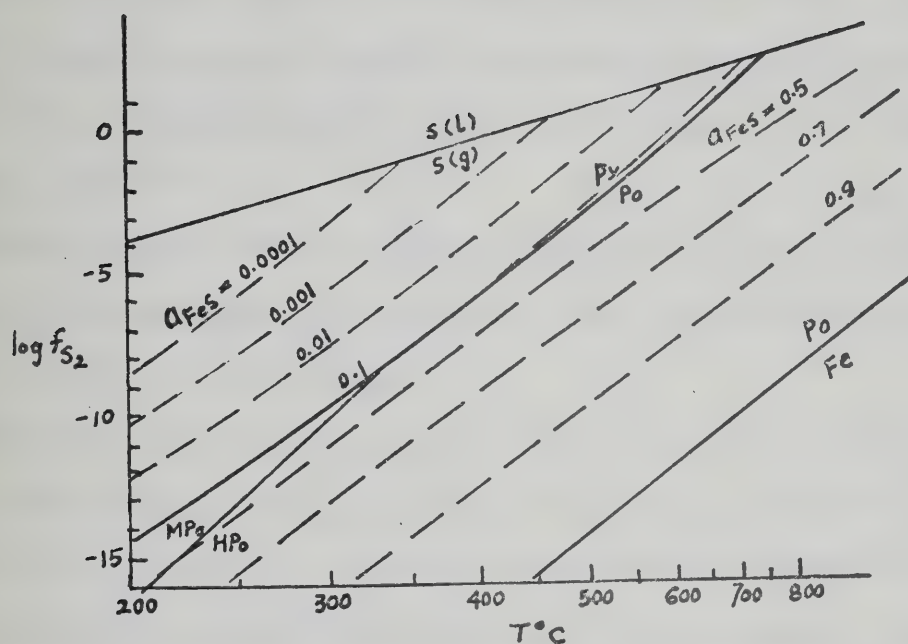


Fig. V-14. Sulfur fugacity vs. temperature diagram showing variation of activity of FeS in pyrrhotite and pyrite at 4 Kb. Positions of solvuses and monoclinic-hexagonal pyrrhotite phase boundary are estimated from data of Toulmin and Barton (1964) and Miyazaki *et al.* (1974), respectively.

2. Sphalerite

Selected samples of sphalerite associated texturally with either pyrite or pyrrhotite and/or siderite were analyzed by electron microprobe using an energy dispersive detector and wavelength dispersive detector (for Cd, Mn). Counting rate and operating conditions are the same as those for Anvil sphalerite.

Chemical compositions of sphalerite samples are listed in Table V-15 together with calculated mole percents of solid solutions and stoichiometry between sulfur and metal cations.

Microprobe X-ray scanning traces of Zn, Fe and Mn and photomicrographs across individual sphalerite grains do not reveal any systematic zoning or discrete FeS-rich patches, and overall compositional uniformity is indicated even though small irregular variations exist in a few samples. Examples of these scanning traces and photomicrographs are shown in Fig. V-15 and Plate V-2 respectively. FeS weight percents in sphalerite do not show any regular variation with depth or laterally within the ore horizon.

Table V-15 shows that FeS mole percents in sphalerite are more variable and generally have a lower range ($7.37 \sim 15.70$) when pyrite and pyrrhotite are not coexistent with sphalerite, whereas the FeS mole percents are about $11.51 \sim 17.22$ with an average of 14.77 when three phases coexist.

Estimation of pressure during metamorphism when sp-py-po assemblage was equilibrated can be made by using Fig. V-5 and FeS mole percent data from Table V-15. Pressures so estimated are as follows:

A) Pressures estimated from experimental isobars:

$3.0 \sim 6.3$ Kb (average: 4.7 Kb)

B) Pressures estimated from calculated isobars:

(at 300°C) $2.2 \sim 5.7$ Kb (average: 3.8 Kb).

(at 350°C) $2.5 \sim 6.2$ Kb (average: 4.3 Kb).

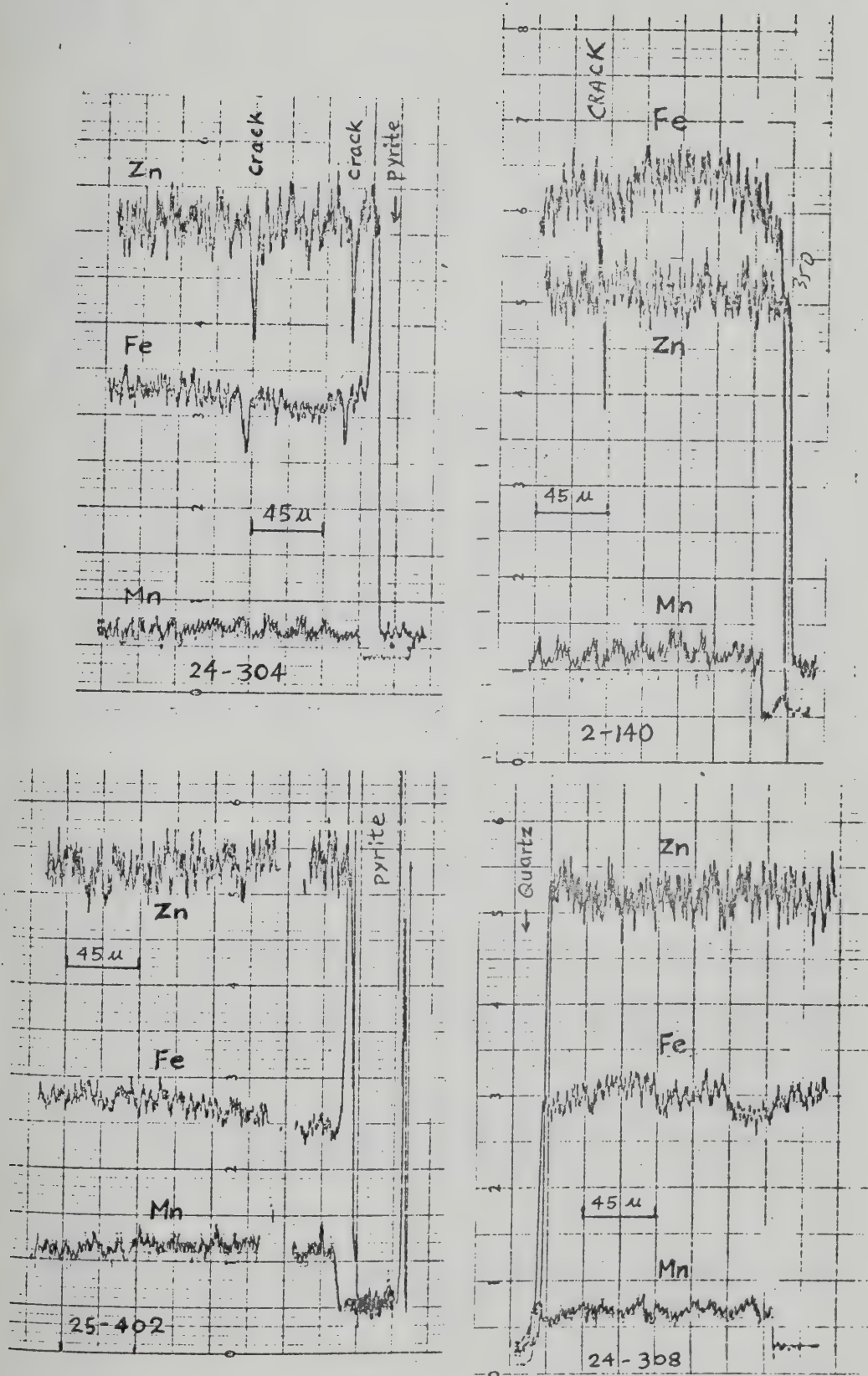


Fig. V-15. Electron microprobe X-ray scanning traces of sphalerite grains, Thompson Creek deposit.

TABLE V-15

Chemical Compositions of Sphalerites from Thompson Creek Ore Deposit

DDH Sample No.	Mineral Assemblage	(Weight Percent)						(Mole Percent)						Atomic Ratio Σ Cation: S	
		Zn	Fe	Cd	Mn	Co	Cu	S	ZnS	FeS	CdS	MnS	CoS		CuS
2-140	(5)	59.73	6.70	X	X	-	-	33.57	88.38	11.62					0.99
3-65 #1	(1)	55.98	10.06	X	X	-	-	33.96	82.62	17.38					0.98
#2	(1)	58.77	7.37	X	X	-	-	33.87	87.19	12.81					0.98
3-41.8	(1)	57.87	8.26	X	X	.049	.44	33.38	85.05	14.21		.08	.67		1.00
4-37	(3)	61.28	4.58	X	X	.053	-	34.08	91.86	8.05		.09			0.96
4-43.5	(8)	60.14	6.42	X	X	-	-	33.44	88.89	11.11					0.99
6-34.5	(3)	61.28	4.78	X	X	-	-	33.93	91.62	8.38					0.97
7-95	(5)	58.05	7.33	X	X	.033	-	34.59	87.06	12.89		.055			0.95
10-174.5	(7)	58.06	8.44	X	X	-	-	33.50	85.45	14.55					0.99
10-176	(2))	55.90	9.95	.157	.026	-	-	33.98	82.60	17.22	.126	.046			0.98
11-79	(1)	52.49	6.56	X	X	-	.615	34.34	87.54	11.51			.947		0.95
14-250 #1	(3)	60.10	6.22	X	X	.054	-	33.63	89.11	10.80		.09			0.98
#2	(4)	62.54	4.25	X	X	-	-	33.21	92.63	7.37					1.00
22-365	(1)	58.33	6.78	.24	.086	-	-	34.56	87.68	11.96	.209	.154			0.94
23-288.5	(4)	61.73	4.92	X	X	-	-	33.45	91.46	8.54					0.99
24-286.5	(2)	56.32	9.55	X	X	.04	.644	33.45	82.57	16.39		.065	.97		1.00
24-304 #1	(1)	57.59	8.64	X	X	-	-	33.77	85.06	14.94					0.98
#2	(1)	56.58	9.70	X	X	-	-	33.72	83.28	16.72					0.99

DDH Sample No.	Mineral Assemblage	(Weight Percent)						(Mole Percent)						Atomic Ratio Σ Cation: S		
		Zn	Fe	Cd	Mn	Co	Cu	S	ZnS	FeS	CdS	MnS	CoS		CuS	
24-308	(1)	56.80	8.91	.211	.052	-	-	34.03	84.24	15.48	.181	.092				0.97
25-402	(2)	57.99	7.88	.292	.202	-	-	33.63	85.75	13.65	.251	.356				0.99
25-464	(2)	57.48	8.09	.259	.596	-	-	33.58	84.76	13.97	.222	1.046				0.99
25-474c	(1)	57.21	8.36	.292	.15	-	-	33.98	84.93	14.55	.251	.265				0.97
28-158	(1)	56.52	9.19	.323	.035	-	-	33.94	83.72	15.94	.278	.062				0.98
30-89	(3)	59.34	6.63	X	X	-	-	34.04	88.42	11.58						0.97
30-94 #1	(9)	60.95	5.37	X	X	.041	-	33.65	90.59	9.34			.068			0.98
#2	(9)	57.14	9.12	X	.113	-	-	33.45	84.10	15.70						1.00

Mineral assemblages: (1) Py + Po (2) Py + Po + Sd (3) Py (4) Py + Sd (5) Po + Cpy (7) Po + Sd
 (8) Sd (9) Cpy + Sd

* Electron microprobe analyses: Cd and Mn, where both are presented, were analyzed by wavelength dispersive detector, the rest by an energy dispersive detector.

X: not analyzed; -: not detected.

Thus a range of 2 to 6 kilobars and an average of about 4 Kb are the probable metamorphic pressures for the Thompson Creek deposit.

A sulfur fugacity-temperature diagram showing FeS mole percents in sphalerite at 4 Kb has been constructed and shown in Fig. V-16. The sp-py-po solvus lies near the 10 mole percent isopleth below about 500°C. Over the range of FeS mole percents in the Thompson Creek sphalerites, the corresponding sulfur fugacities from Fig. V-16 are $10^{-9.6}$ to 10^{-10} at 300°C, and $10^{-7.3}$ to $10^{-7.7}$ at 350°C. These sulfur fugacities agree well with those estimated from the py-po solvus in Fe-S system.

3. Carbonate Minerals

Seven carbonate minerals in ore specimens from drill holes were analyzed for Fe, Mg, Mn, Ca, Zn by electron microprobe using an energy dispersive detector. Procedures of analysis and calculation of CO_3 , solid solution mole percents, etc. are the same as for the Anvil carbonates. Chemical compositions of analyzed carbonates are given in Table V-16 together with calculated mole percents of solid solutions and structural formulae. From this table, it is evident that all the carbonates are siderite with Mg-siderite predominant, followed by Mn-Mg siderite as a minor variety.

Correlation of major elements in the carbonates is shown in Fig. V-17.

The following observations can be made:

- (i) Negative correlation of Fe and Mn, Ca and Mg, and Mn-Mg in all carbonates, the latter two correlations are curvilinear.
- (ii) Fe and Ca, Fe and Mg, and Ca-Mn appear to have a weakly positive correlation in the carbonates.

Therefore Fe-Mn, Ca-Mg and Mn-Mg substitute for each other in the carbonates.

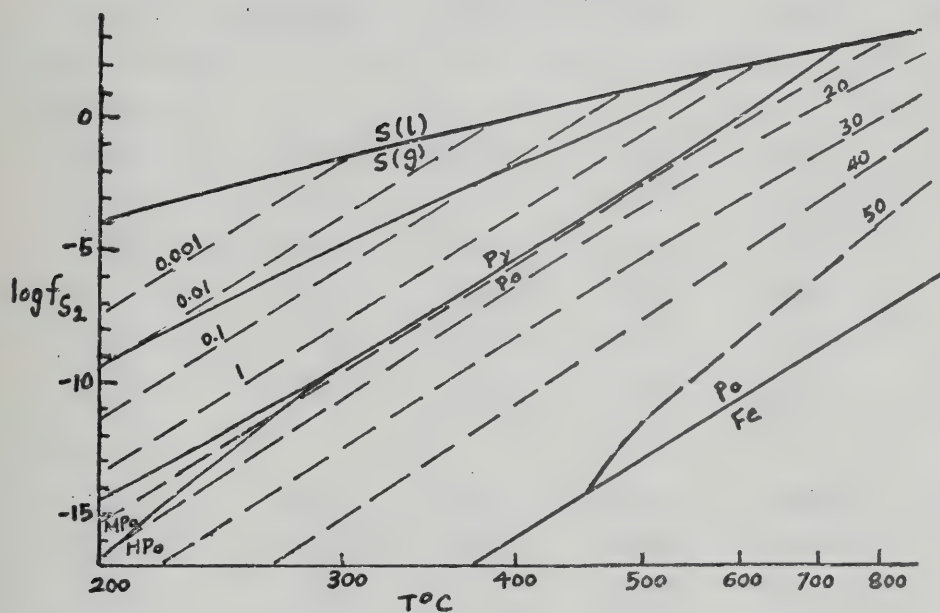


Fig. V-16. Sulfur fugacity vs. temperature diagram showing mole % FeS in sphalerite at 4 Kb, Thompson Creek deposit.

TABLE V-16

Chemical Composition of Carbonate Minerals from the
Thompson Creek Deposit

	(Sample No.)					
	4-43.5	6-34.5(A)	14-250	23-288.5	24.286.5	25.402.5
(weight %)						
Fe	36.75	37.66	39.21	37.17	34.53	24.92
Mn	2.50	4.12	3.77	4.52	8.55	17.49
Ca	0.16	0.30	0.44	0.21	0.15	0.85
Mg	4.78	3.57	2.45	3.54	2.86	2.57
Zn	0.81	0.07	0.66	0.32	0.10	0.35
CO ₃ *	55.00	54.29	53.47	54.24	53.81	53.82
(mole %)						
FeCO ₃	71.79	74.54	78.67	73.65	68.96	49.76
MnCO ₃	4.96	8.29	7.70	9.10	17.35	35.50
CaCO ₃	0.44	0.82	1.22	0.58	0.41	2.37
MgCO ₃	21.46	16.23	11.28	16.13	13.10	11.78
ZnCO ₃	1.34	0.12	1.13	0.54	0.17	0.59

Structural Formula:

4-43.5	Fe _{0.72} Mg _{0.21} Mn _{0.05} Zn _{0.01} Ca _{0.004} CO ₃	(Magnesian siderite)
6-34.5(A)	Fe _{0.75} Mg _{0.16} Mn _{0.08} Ca _{0.008} Zn _{0.001} CO ₃	"
14-250	Fe _{0.74} Mg _{0.11} Mn _{0.08} Ca _{0.01} Zn _{0.01} CO ₃	"
23-288.5	Fe _{0.74} Mg _{0.16} Mn _{0.09} Ca _{0.006} Zn _{0.005} CO ₃	"
24-286.5	Fe _{0.69} Mn _{0.17} Mg _{0.13} Ca _{0.004} Zn _{0.002} CO ₃	(Mangano-magnesian siderite)
25-402.5	Fe _{0.50} Mn _{0.36} Mg _{0.12} Ca _{0.02} Zn _{0.006} CO ₃	"

*Calculated values

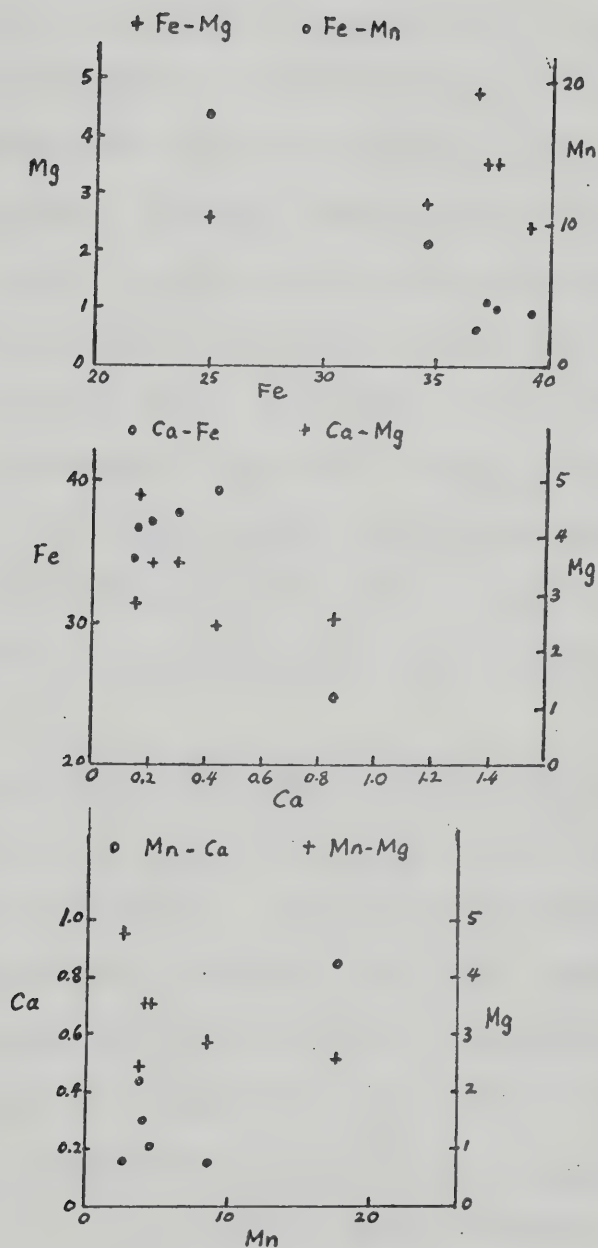


Fig. V-17. Correlation of major elements in the Thompson Creek carbonates. Unit is in weight %.

Mineral assemblages associated with carbonates are: pyrite, pyrrhotite, chalcopyrite and sphalerite in most ore specimens. Late stage Pb-Sb sulfosalt minerals generally occur as streaks and veinlets in carbonates. No magnetite or hematite has been observed in ore specimens. Therefore, the assemblage suggests the reactions of sulfide-carbonate during metamorphism (late stage "mineralization" sequence) as discussed in the previous section for the Anvil carbonates. Chemical relations between FeS contents in sphalerite and FeCO_3 contents in carbonate both coexisting with pyrite can be treated as for the Anvil sulfide-carbonate system. Mole percents of FeS and FeCO_3 are compared in Fig. V-18. Variations of m_{FeS} and m_{FeCO_3} appear to be quite large and follow the slope of $2 \log f_{\text{CO}_2} + \log f_{\text{O}_2}$, changing from A, B, C to D. If carbon dioxide fugacity was constant, then oxygen fugacity of the sulfide-carbonate system would have increased from A to D; if oxygen fugacity was constant, then carbon dioxide fugacity would have also increased.

Oxygen fugacity range of the sulfide-carbonate system can be estimated from a f_{O_2} - f_{S_2} diagram (Fig. V-19) showing phase relations of activities of FeS in sphalerite and FeCO_3 in carbonates. As a first approximation, mole percents of FeS and FeCO_3 are equivalent to the activities. FeS mole percents in sphalerites coexisting with pyrite and pyrrhotite are generally between 11.5 and 17, averaging 15; whereas FeCO_3 mole percents in carbonates are between 49.8 and 78.7, averaging 69.6 (corresponding to a_{FeCO_3} of $10^{-0.3}$ and $10^{-0.1}$, averaging $10^{-0.16}$). f_{CO_2} estimated from measurements on CO_2 -rich inclusions in quartz (see Chapter VI) has an average of $10^{2.0}$. Fixing FeS mole percents in sphalerite, FeCO_3 mole percents in carbonates, temperature and f_{CO_2} , we can estimate f_{O_2} from Fig. V-19; the wedge-shaped area outlined

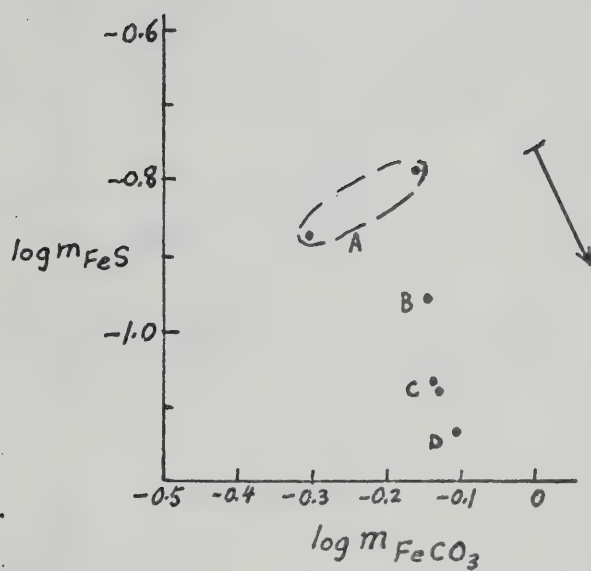


Fig. V-18. FeS contents of sphalerites vs. FeCO_3 contents of carbonates from Thompson Creek deposit. A line L shows increasing order of $2\log f\text{CO}_2 + \log f\text{O}_2$ (equation V-7).

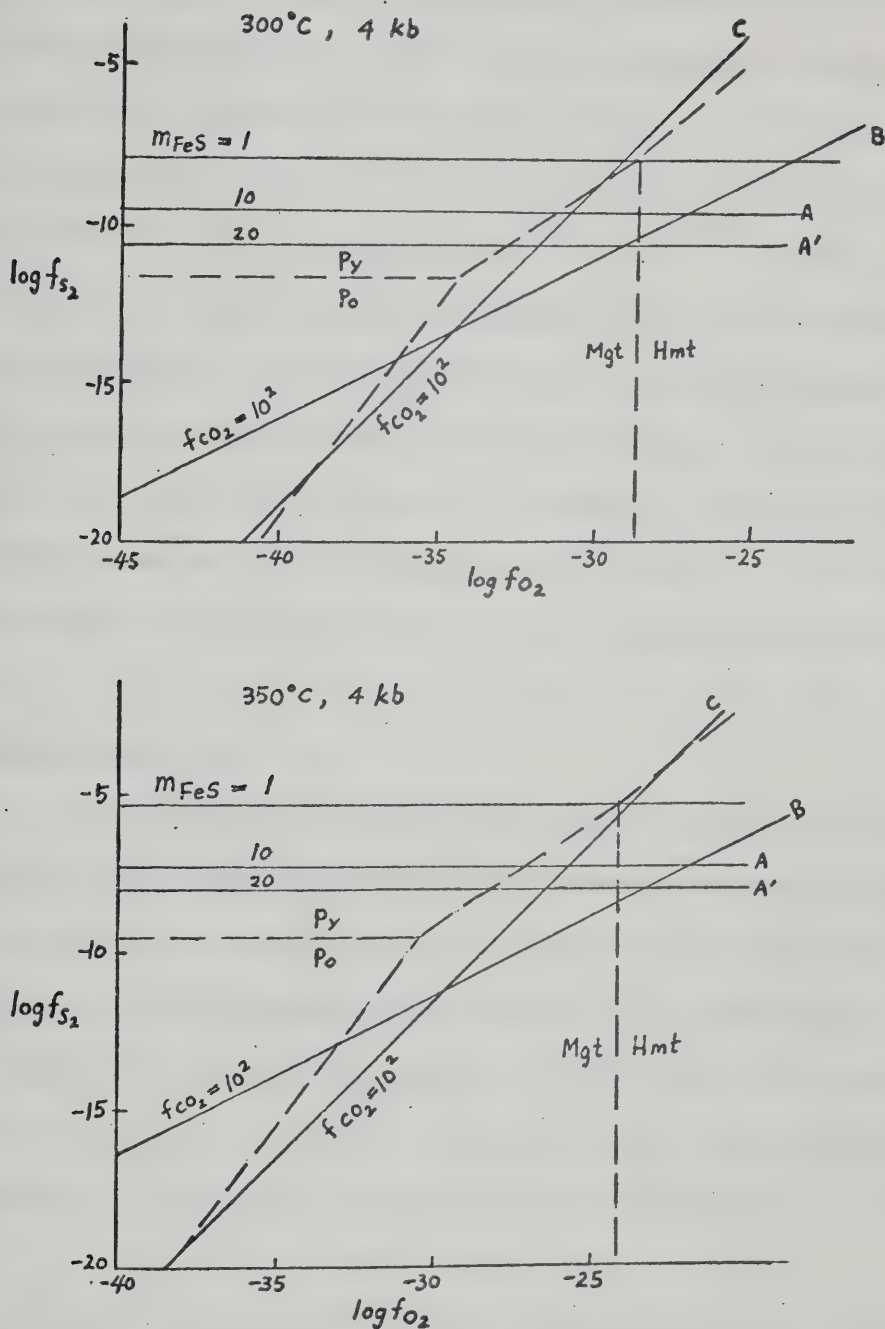


Fig. V-19. Activity isopleths of FeS and $FeCO_3$ as functions of fugacities of oxygen and sulfur. A: FeS mole % in sphalerite (A: 10 mole %, A': 20 mole %). B: a_{FeCO_3} in carbonate = $10^{-0.2}$ at $f_{CO_2} = 10^2$ for $FeS_2 + CO_2 + 1/2 O_2 = FeCO_3 + S_2$ (pyrite-siderite). C: a_{FeCO_3} in carbonate = $10^{-0.2}$ at $f_{CO_2} = 10^2$ for $FeS + CO_2 + 1/2 O_2 = FeCO_3 + 1/2 S_2$ (pyrrhotite-siderite).

by the intersections of four lines A, A', B, and C defines the possible range of oxygen fugacities at a given temperature. Py-po-mgt triple point lies outside the wedge-shaped area, indicating that magnetite was never equilibrated with iron sulfides or carbonates. If $f_{S_2} = 10^{-10}$ (corresponding to 15 mole % FeS), and $f_{CO_2} = 10^{-2}$, the most probable range of f_{O_2} is about 10^{-28} to $10^{-31.2}$ at 300°C, and about $10^{-22.4}$ to 10^{-27} at 350°C.

This range of f_{O_2} may be representative of maximum and minimum conditions during metamorphism in which sulfide-carbonate system was equilibrated.

A high f_{CO_2} and a relatively large proportion of f_{CO_2} to f_{O_2} in the Thompson Creek deposit would favor formation of siderite rather than magnetite; decomposition of siderite to magnetite or oxidation of iron sulfides to magnetite obviously did not take place in a high f_{CO_2} environment.

4. Sb-Pb Sulfosalt Minerals

Sulfosalt minerals closely associated with galena and as streaks and veinlets in siderite were described previously. Chemical analyses by electron microprobe using a wavelength dispersive detector were made for Pb, Sb and Cu. Bi, As and Fe are present in trace quantity in some samples; they were not analyzed. The results represent 10 to 15 counts (50 seconds per count) on 5 to 10 grains per sample. Operating conditions, standards, analytical sequence and correction procedure used are described in Appendix V-1.

X-ray scanning photomicrographs by electron probe on sulfosalt minerals were taken to investigate element distribution and sample homogeneity. Some examples are shown in Plate V-3 (a) and (b). Overall homogeneity is indicated.

Chemical compositions of sulfosalt minerals (Table V-17) indicate that the sulfosalts are mainly meneghinite approaching the composition of $\text{CuPb}_{13}\text{Sb}_7\text{S}_{24}$, and a few are boulangerite approaching the composition $\text{Pb}_5\text{Sb}_4\text{S}_{11}$. Meneghinite in sample 14-250B has a composition of $\text{Pb}_{13}\text{Sb}_7\text{S}_{24}$ with only trace copper. S content was calculated from anionic stoichiometry but not analyzed directly.

Meneghinite and boulangerite occur mainly as late stage replacement or "intergrowths" in galena and sometimes as post-ore remobilized veinlets in siderite or sulfides. Therefore they represent an assemblage formed during the late stage of ore deposition or post-ore thermal events. Occurrence of Pb-Sb and other sulfosalt minerals with lead-zinc sulfides in hydrothermal-sedimentary ore deposits has been noted in many places; notably: meneghinite, boulangerite, bournonite, etc. in the upper part of the black ore zone of Kuroko deposits, Japan (Matsukuma *et al.*, 1974); jamesonite, polybasite, pyragyrite, etc. in Mount Isa (Blanchard and Hall, 1942), boulangerite, meneghinite, bournonite, etc. in Broken Hill (Stillwell, 1926; Ramdohr, 1950; and Woodward, 1965); boulangerite and jamesonite in Sullivan Mine, B.C. (Irvine, 1972), and boulangerite, bournonite and freieslebenite ($\text{Pb}_3\text{Ag}_5\text{Sb}_5\text{S}_{12}$) in Rosebery, Tasmania (Brathwaite, 1969).

In a study of phase relations in the Pb-Sb-S system, Garvin (1973) found that stable phases in the assemblage boulangerite-robinsonite-zinckenite-"phase IV" decreases from 4 phases at 500°C through 3 phases (without "phase IV") at 400°C to 2 phases (boulangerite and zinckenite) at 300°C. Furthermore, boulangerite forms in stable assemblages containing from near 100 mole percent to about 54 mole percent PbS, and zinckenite is stable in compositions ranging from zero mole percent to 46 mole percent PbS.

TABLE V-17

Chemical Composition of Sulfosalt Minerals from Thompson Creek Deposit.

	Pb	Sb	Cu	S	Structural Formula
4-43.5	61.657 (29.73)	20.846 (17.10)	0.947 (1.49)	16.551 (51.67)	$\text{Cu}_{0.7}^{\text{Pb}}\text{Sb}_{13.8}\text{S}_{7.9}\text{S}_{24}$
6-34.5	62.158 (30.18)	20.39 (16.85)	1.22 (1.93)	16.232 (51.04)	$\text{Cu}_{0.9}^{\text{Pb}}\text{Sb}_{14.2}\text{S}_{7.9}\text{S}_{24}$
9-94	61.745 (29.59)	20.246 (16.51)	1.289 (2.02)	16.72 (51.88)	$\text{Cu}_{0.9}^{\text{Pb}}\text{Sb}_{13.7}\text{S}_{7.6}\text{S}_{24}$
14-250A	56.096 (26.20)	26.525 (21.09)	0.096 (0.15)	17.38 (52.57)	$\text{Pb}_{5.5}\text{Sb}_{4.4}\text{S}_{11}$
14-250B	62.112 (29.64)	20.436 (16.60)	0.102 (0.16)	17.35 (53.60)	$\text{Cu}_{0.07}^{\text{Pb}}\text{Sb}_{13.3}\text{S}_{7.4}\text{S}_{24}$
23-288.5	61.315 (29.25)	20.698 (16.81)	1.065 (1.66)	16.923 (52.28)	$\text{Cu}_{0.8}^{\text{Pb}}\text{Sb}_{13.4}\text{S}_{7.7}\text{S}_{24}$

TABLE V-17 (cont'd)

	Pb	Sb	Cu	S	Structural Formula
25-402.5	56.084 (26.09)	26.279 (20.80)	0.007 (0.01)	17.63 (53.09)	Pb _{5.4} Sb _{4.3} S ₁₁
572-6	61.696 (29.86)	20.965 (17.27)	0.946 (1.49)	16.393 (51.37)	Cu _{0.7} Pb _{14.0} Sb _{8.1} S ₂₄
Meneghinite (CuPb ₁₃ Sb ₇ S ₂₄)	(28.9)	(15.5)	(2.2)	(53.3)	
Boulangerite (Pb ₅ Sb ₄ S ₁₁)	(25)	(20)		(55)	

First row: weight percent
(): atomic percent

The absence of zinckenite in the Thompson Creek deposit suggests that boulangerite was probably formed in an assemblage containing at least 54 mole percent PbS and below 300°C during the late stage mineralization. In the temperature range of 300° ~ 400°C, addition of 2 mole percent of Sb₂S₃ solution to galena results in the appearance of a substantial amount of boulangerite (Garvin, 1973).

Hoda and Chang (1975) have shown that meneghinite solid solutions in PbS-Cu₂S-Sb₂S₃ ternary systems covers a region starting from the composition CuPb₁₃Sb₇S₂₄ and extending toward the PbS-poor and Sb₂S₃-rich compositions. The field of meneghinite solid solution shrinks significantly from 500° down to 300°C (Fig. V-20). Composition field of the Thompson Creek meneghinites is very restricted and plots at the PbS-rich side of the meneghinite field, indicating that they probably formed below 300°C.

Fluid pressure during main stage sulfide mineralization in the Thompson Creek deposit is about 0.1 to 0.17 kilobar, as deduced from salinity and density data on primary fluid inclusions in quartz (see Chapter VI); similar pressure probably acted during late stage sulfosalt mineralization. Sulfur fugacity during late stage mineralization can be estimated from a sulfur fugacity-temperature diagram (Fig. V-21) constructed at one kilobar and from free energy data for sulfidation reactions of meneghinite and boulangerite (Craig and Barton, 1973). If sulfosalt mineralization occurred at about 250°C, sulfur fugacity was about 10^{-14} for sulfidation of boulangerite and 10^{-15} for sulfidation of meneghinite. If some sulfosalts were remobilized (recrystallized) during regional or thermal metamorphism, then at a temperature of 300°C and pressure of 4 Kb, sulfur fugacity would have been about 10^{-11} for sulfidation of boulangerite and about 10^{-12} for sulfidation of meneghinite.

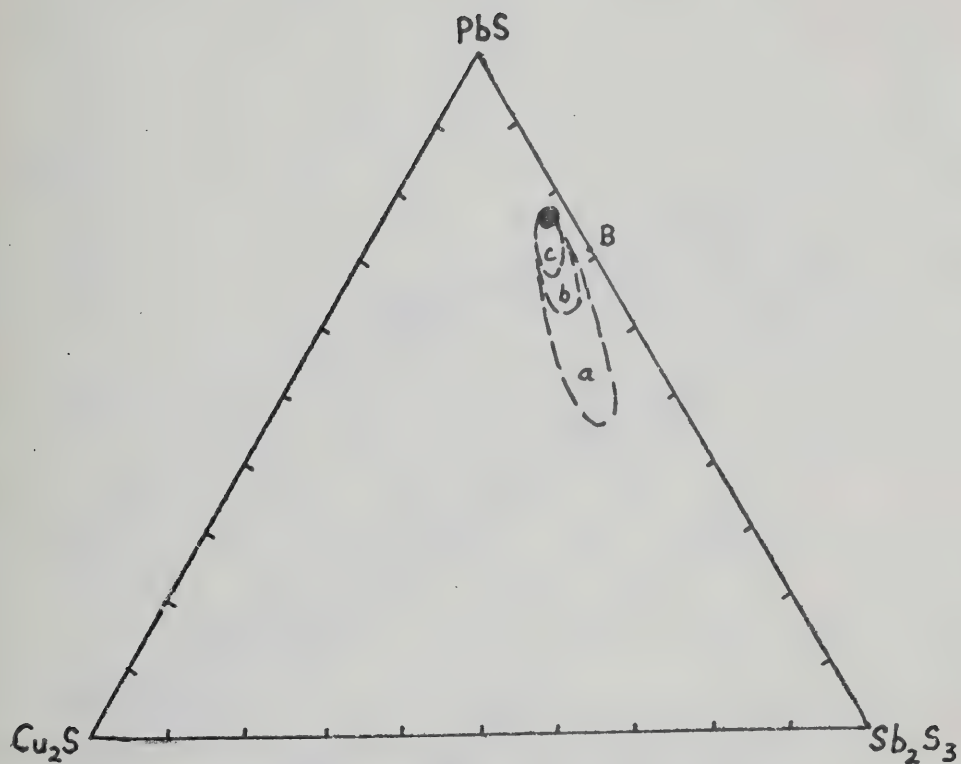


Fig. V-20. Phase relations in the system $\text{PbS-Cu}_2\text{S-Sb}_2\text{S}_3$. Meneghinite solid solution field: (a) 500°C , (b) 400°C , (c) 300°C . Solid circle: 6 data points of Thompson Creek meneghinites. B: boulangerite.

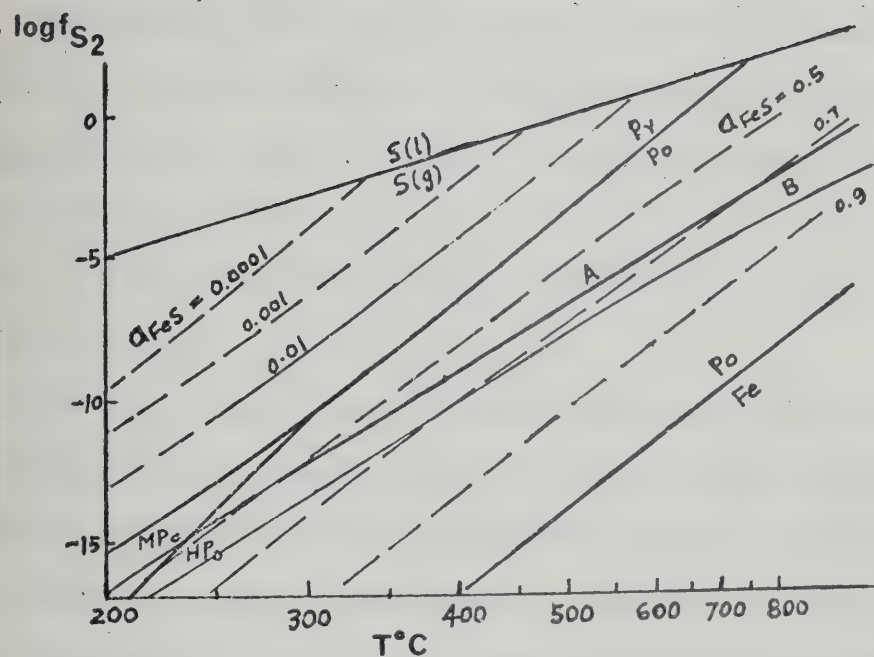


Fig. V-21. Sulfur fugacity vs. temperature diagram showing sulfidation curves of meneghinite and boulangerite at 1 Kb. Other solvuses are also shown. Curve A: $\frac{5}{3} \text{PbS} + \frac{4}{3} \text{Sb} + \text{S}_2 = \frac{1}{3} \text{Pb}_5\text{Sb}_4\text{S}_{11}$; Curve B: $\frac{2}{21} \text{Cu}_2 + \frac{51}{21} \text{PbS} + \frac{4}{3} \text{Sb} + \text{S}_2 = \text{CuPb}_{13}\text{Sb}_7\text{S}_{24}$.

5. Bulk Ores

Chemical assay data of Pb, Zn, Ag and Sb from drill hole ore sections in Thompson Creek ore deposit are summarized below. The data used are taken from an unpublished company report of the Joint Venture (Caninco-Metallgesellschaft Canada - Matt Berry Mines Ltd.) by L. LaPrairie in 1970. In addition, selected drill hole ore samples were analyzed for other elements such as Cu, Fe, Mn, etc. Ore grade reported below represents the average of assay data from a total of 147 feet of sulfide drill hole inter-sections (83 feet for Sb):

Pb: 7.99 wt.%; Zn: 7.65 wt.%; Ag: 3.102 oz/ton or 97 ppm; and

Sb: 0.43 wt.%.

Chemical analysis of 9 selected ore samples was made by MRFAPE spectrometry; the results are given in Table V-18. The averages of Fe, Cu and Mn are used to represent, as first approximations, the average concentration of these elements in Thompson Creek deposit. Sporadic ore assays of Cu are generally between 0.1 to 0.2 wt.%. Error in estimation of overall composition of Fe in the whole deposit is probably small.

The relative atomic ratios of Pb, Zn, Sb, Cu, Ag, Fe and Mn are calculated and shown in Table V-19; Sb is taken to be 1. These ratios will be used in a later chapter to estimate initial metal abundances in the ore solution responsible for the formation of Thompson Creek ore deposit.

Ag is enriched in the Thompson Creek deposit; plotting of molecular ratios of Ag with those of Pb and Sb (using drill hole assay data) shows a strong positive correlation of Ag with Pb (Fig. V-22a) and to a lesser extent, that of Ag with Sb (Fig. V-22b). Ag probably occurs as argentite solid solutions in sulfosalt minerals or galena, even though electron microprobe failed to detect any significant Ag content in these minerals.

TABLE V-18

Chemical Analyses of Bulk Sulfide Ores From
Thompson Creek Deposit (ppm)

Sample No. (DDH)	(Weight %)		Mn	As	Cd	Ag	Ni	Co	Cr
	Fe	Cu							
9-87	12.11	2963	4818	400	57	58	39	17	62
22-340.5	4.01	1286	679	65	61	62	28	22	49
23-288.5	4.01	257	1849	10	56	16	59	11	36
24-304	5.39	788	1201	150	59	59	52	17	36
25-462.5	5.62	1696	2465	150	54	61	56	12	46
29-293.5	2.29	993	893	70	55	63	32	7	26
30-89	3.44	1928	459	500	56	62	18	8	28
28-158	4.47	2371	1057	2600	43	59	32	8	33
Trench Sample 572-1	15.15	555	7862	560	30	58	28	16	75
Average	6.277	1426	2365	500	52	55	38	13	43

TABLE V-19

Relative Atomic Ratios of Metals in
Thompson Creek Deposit
Antimony is taken to be 1

Pb	Zn	Sb	Fe	Mn	Cu	Ag($\times 10^{-4}$)
10.9	33	1	31.8	1.2	0.6	2.5

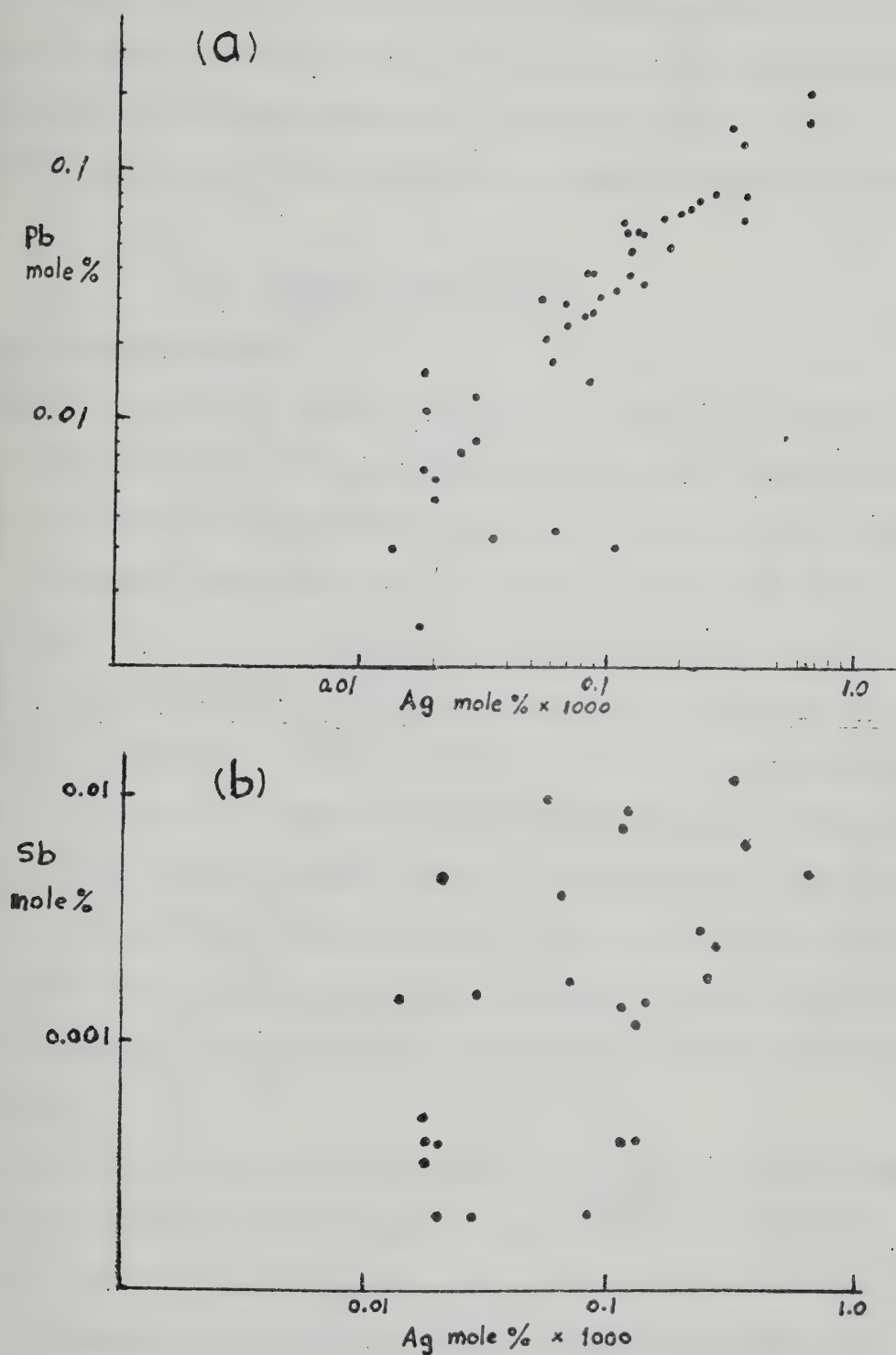


Fig. V-22. Molecular ratios of Pb, Ag, Sb in Thompson Creek ore deposit, Frances Lake district. (a) Pb vs. Ag, (b) Sb vs. Ag.

Plotting of average molecular ratios of Pb, Zn and Cu in a Pb-Zn binary plot and Pb-Zn-Cu ternary plot (Fig. V-23 a and b) shows that the Thompson Creek deposit plots slightly above the Pb-Zn trend line of major conformable ore deposits, whereas it shows similarity to these deposits in Pb-Zn-Cu plot.

D. HOWARD'S PASS DISTRICT

1. Ore-bearing Sediments

Chemical analyses of drill hole samples of cherty to calcareous siltstone containing lead-zinc mineralization were made for Placer's main zone and the Pas claims of Dynasty-Shield Resources by means of MRFAP spectrometry. The results are given in Table V-20. Pb, Zn grade of 33 representative samples from drill hole ore-bearing siltstones in Placer's main zone and data on average element content of 300 samples of sediments in the Ordovician strata (which includes the ore-bearing unit in the district) are given in Table V-21 and Table V-22, respectively (Morganti, personal communication, 1975). Data in Tables V-20 and V-21 characterize the concentrations of major and minor elements in the ore-bearing siltstone unit whereas data in Table V-22 summarize the overall background concentration of major and minor elements in the Ordovician Road River Formation in the Howard's Pass district.

Geochemistry of metal-rich black shale and related rocks has been the topic of many studies in the literature (e.g. Krauskopf, 1955, 1967; Vine, 1966, 1969; Vine and Tourtelot, 1969, 1970; Davidson and Lakin, 1961, 1962). Geochemistry of stratiform lead-zinc deposits in argillaceous rocks has also been extensively discussed in the literature, notably, McArthur River deposit (Croxford and Jephcott, 1972; Lambert and Scott, 1973), Mount Isa deposit (Stanton, 1962), Kupferschiefer deposit (Wedepohl, 1964, 1971;

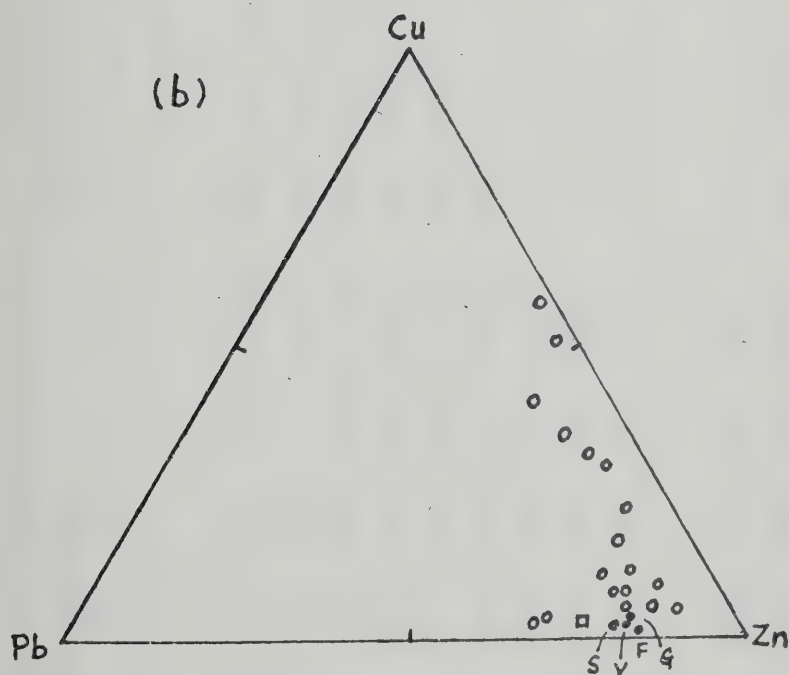
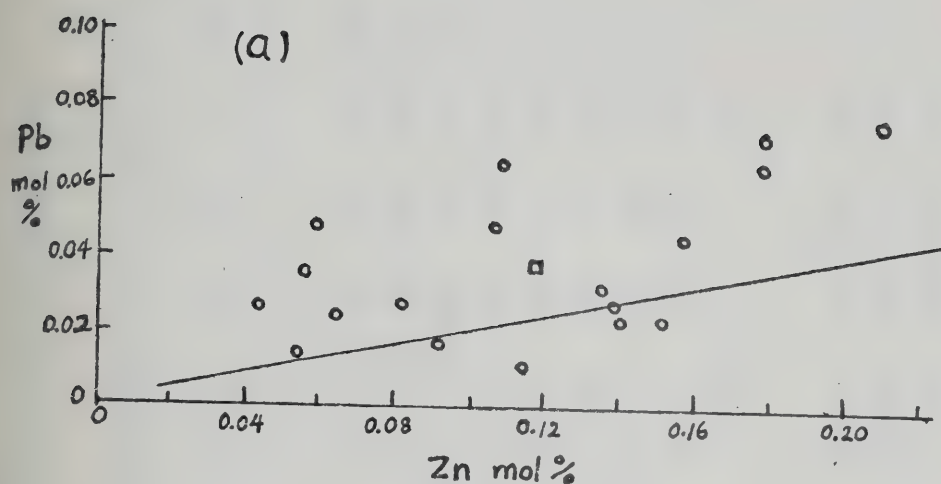


Fig. V-23. Molecular ratios of Pb, Zn, Cu in Thompson Creek ore deposit, Frances Lake district. (a) Pb vs. Zn; trend line of conformable Pb-Zn deposits is after Stanton (1958). Circles: average ratio of a single drill hole ore horizon; square: average ratio of all drill holes. (b) Pb-Zn-Cu. Circles are conformable Pb-Zn deposits in Australia, Ireland and New Brunswick (after Stanton, 1958). Square: average ratio for Thompson Creek deposit. Also shown are F: Faro, V: Vangorda, G: Grum, S: Swim Lakes.

TABLE V-20

Chemical Analyses of Cherty and Calcareous Siltstones with Lead-Zinc Mineralization,
Howard's Pass District

DDH Sample No.	(weight percent)			K	Al	(p.p.m.)		Mn	Cd	Ag	Co	Ni	Cr	Sr	V	Be	Th	Ba
	Fe	Ca	Na			Ti	Cu											
(Canex Placer)																		
6-234	13.04	0.43	0.31	0.83	1.04	625	96	75	10	3	65	106	98	4.1	639	5.0	X	4
15-233	4.24	4.37	2.67	1.59	0.62	330	152	572	36	4	72	94	71	26.7	332	2.4	X	16
18-444	9.67	0.17	0.97	0.83	1.50	826	110	189	24	3	51	112	107	3.6	717	5.3	X	4
29-362	7.93	1.87	4.40	2.23	2.00	1237	107	195	55	6	55	150	93	1.6	672	6.4	X	10
29-418.5	13.63	0.43	1.27	1.13	1.29	768	137	208	31	5	69	115	127	4.2	559	4.1	X	4
30-346	31.72	0.19	0.33	1.19	0.96	575	120	164	9	4	28	104	170	4.2	515	4.0	X	4
36-279	1.72	0.09	4.00	0.05	0.21	93	57	164	60	4	122	35	61	1.0	78	1.0	X	4
Trench #4-3	n.d.	9.80	4.36	1.92	0.08	43	30	176	60	3	57	23	33	26.7	68	1.1	X	32
Trench #10*	0.1	5.0	X	X	X	-	200	200	-	10	-	20	-	-	200	-	100	-
(Pas Claim)																		
74 P-1 144	0.91	9.31	2.79	2.03	0.25	117	57	182	33	3	70	34	75	33.9	81	1.0	X	32
74 P-2 225**	2.40	14.12	0.19	2.53	0.33	159	90	157	6	1	61	34	58	55.5	133	1.4	X	140
74 P-2 215	5.05	35.05	0.06	8.00	0.85	515	30	384	2	3	72	64	56	113.0	333	4.0	X	100

* Data provided by G. House, Univ. of Alaska (personal communication, 1975).

** Black cherty siltstone with laminated pyrite, no lead-zinc mineralization observable.
n.d.: not detected; X: not analyzed.

TABLE V-21

Ore Grade of Siltstones from Drill Holes and Trench,
Howard's Pass District

DDH	Footage	Pb	Zn	DDH	Footage	Pb	Zn
6	234	0.31	0.50	30	345	1.25	6.22
	274	0.02	0.10		346	1.25	6.23
	288	7.20	9.68		353	1.17	6.32
	466.5	14.20	13.40		355	1.17	6.30
12	231	17.60	16.10	32	168	3.00	5.72
15	233	1.56	9.76		177.5	2.40	11.70
18	444	1.76	2.19		178.5	2.40	11.70
	502.5	2.34	2.61		189	2.29	0.80
29	167	0.24	0.61	34	267	2.28	8.24
	314	4.75	13.80		330	14.70	15.00
	328.5	6.17	8.05		330A	14.70	15.00
	362	2.34	8.64	36	279	5.25	14.00
	381	8.08	10.00	37	270	1.07	5.68
	418.5	2.96	11.50	Trench #4-3		3.85	23.57
	426.5	3.78	10.40	(Pas claims)			
	434.5	0.96	3.84	P-1	144	1.60	17.25
	437.5	1.23	8.32	P-2	215	0.14	0.90
	562.7	2.42	3.56		225	0.23	3.28
	563	2.42	3.56				
	579.3	2.30	7.25	Average		3.833	7.695

TABLE V-22

Average Element Content of Rocks in Ordovician Strata,
Howard's Pass District

Element	(ppm)	Element	(wt. %)
Mo	22	Fe	1.7
Cu	59	Ca	4.5
Zn	200	Mg	1.0
Pb	65	SiO ₂ *	76.0 (46.0~96.0)
Cd	4	Al ₂ O ₃ *	3.0
Mn	171		
Ni	84		
Co	14		
Ag	1		
Ba	900 ?	(Bias due to the inclusion of analyses of Silurian baritic siltstones ?)	
Na	200		

* Average of 170 samples, by X-ray fluorescence analysis.

All others are averages of 300 samples by atomic absorption analysis.

Haranczyk, 1970). Common features of element enrichment exist in those deposits and shales, but as would be expected from the various possible processes of enrichment, some characteristics observable in some deposits are not readily seen in others. The mechanisms for enrichment of trace metals in shales include principally ionic substitution in clay minerals, adsorption on clay minerals, adsorption on metallic hydroxides, precipitation of insoluble compounds (e.g. sulfides), and adsorption on or reaction with organic matter. A more realistic approach to the geochemistry of metal-rich black shales has been made by the study of Vine and Tourtelot (1970). From a statistical analysis of chemical data of 779 samples from North American sedimentary provinces, they concluded that characteristic metal enrichment can be best correlated with and explained by element occurrence in different component fractions of an argillaceous rock —

(i) detrital mineral fraction: Al, Ti, Ga, Zr, Sc; also may include Be, B, Ba, Na, K, Mg, Fe.

(ii) carbonate fraction: Ca, Mg, Mn, Sr.

(iii) organic fraction: locally Ag, Mo, Zn, Ni, Co, Cr, V; less commonly, Co, Pb, La, Y, Se, U, Tl.

In a large number of cases, enrichment is correlated with organic fraction. Geochemical studies of McArthur River and Kupferschiefer deposits also support the definite enrichment of V, Mo, Ni, Cr, U, S, etc. in organic or bituminous components.

Comparison of the mole percents of Pb and Zn (Fig. V-24) shows a crude positive relationship with an average lying very close to the trend line for the conformable ore deposits in the world. Another characteristic feature is that Pb and Zn appear to decrease in concentration upward in a drill hole and to have a repetition of or "cyclic" enrichment starting

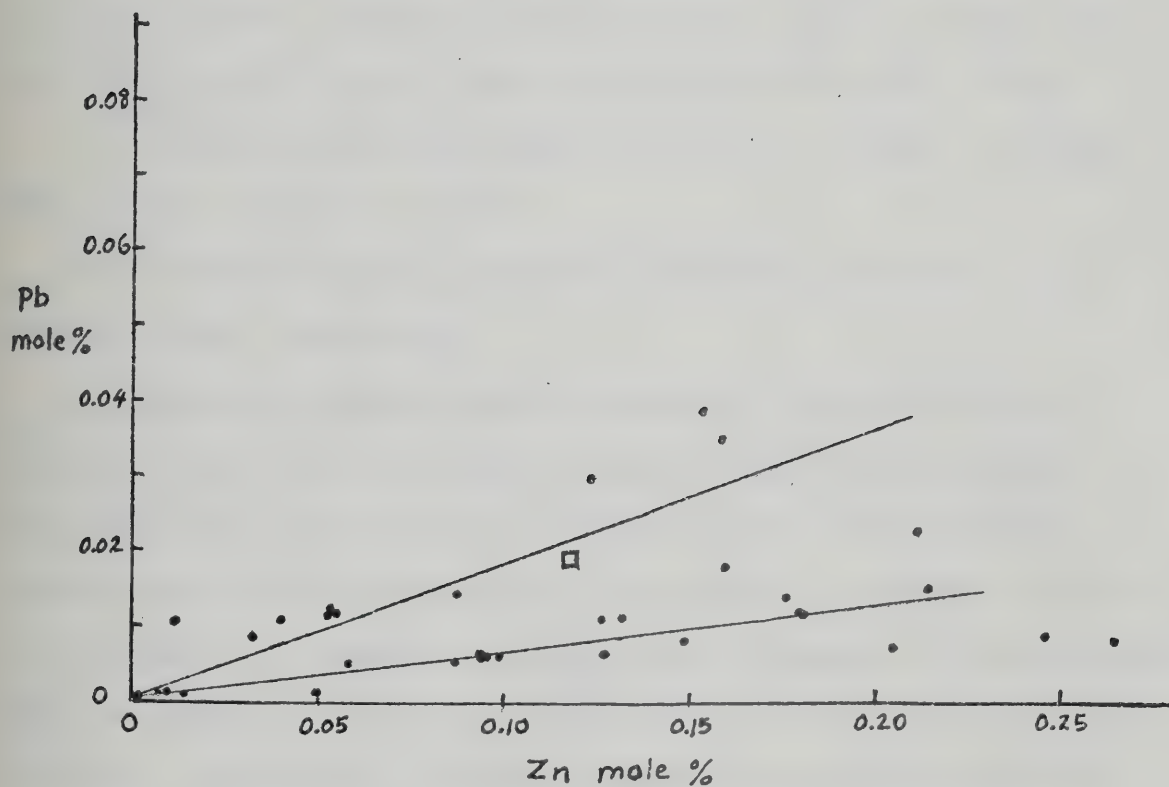


Fig. V-24. Molecular ratios of Pb and Zn in ore-bearing siltstones, Howard's Pass district. Square: mean ratio.

every 100 ~ 150 feet towards stratigraphic top (DDH29, Table V-21). The overall variation of Pb and Zn is quite large due to the very fine-grained and delicately laminated nature of most of the ore-bearing siltstones.

Comparison of elements in Tables V-20 and V-21 reveals the following characteristic features (Figs. V-25 and V-26):

(i) Positive intercorrelation in four groups of elements - V, Ni, Cr, Cu, Fe, Ag (Fig. V-25a, b, c, and Fig. V-26c), Ti, Al, V (Fig. V-25d and e), Ca, Sr, Ba, K (Fig. V-26g, h, and i) and Cd, Zn (Fig. V-26e).

(ii) Negative correlation among Pb, Zn and Cu, Fe, Ag, V, Ba (Fig. V-25c and Fig. V-26a, b, c, d, f).

(iii) Slightly negative to constant correlation between Pb, Zn and K, Na or Al (Fig. V-25f and g).

Carbonaceous or organic matter is omnipresent in ore-bearing siltstones; enrichment of V and Ni may be related to this organic matter. The positive correlation of Cr, Cu, Fe and Ag with V and Ni indicates a possible genetic relationship between these elements and organic fraction. Al, Ti and part of V probably occurs in either authigenic or detrital grains such as roscoelite or other mica or clay minerals. Ca and Sr and partly Ba probably are enriched in carbonate fraction, while some Ba and K are probably enriched in detrital feldspar fraction. Cd is positively correlated with Zn indicating its enrichment in sulfide fraction.

On the other hand, Pb and Zn are enriched in specimens in which Cu, Fe, Ag, V and Ba are low, suggesting that Pb and Zn may have a different source and probably are not associated with organic fraction.

The nearly constant correlation between Pb, Zn and Na, K and a slightly negative correlation between Pb, Zn and Al indicate that Pb, Zn were added to or substitute (overwhelmed) the authigenic or detrital mineral accumulation during syngenetic or diagenetic processes.

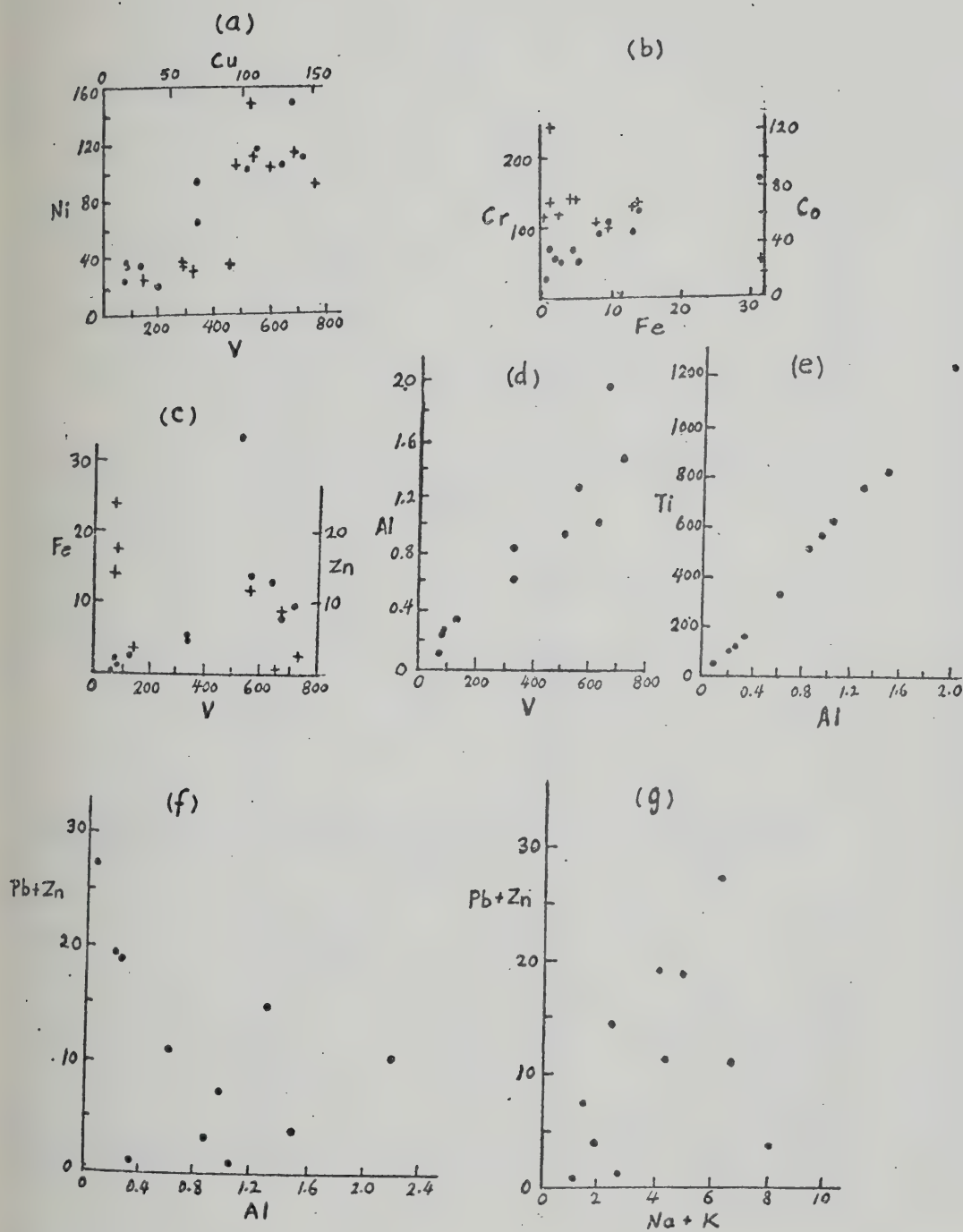


Fig. V-25. Comparison of elements in ore-bearing siltstones, Howard's Pass district. (a) o: Ni vs. V; +: Ni vs. Cu; (b) o: Cr vs. Fe; +: Fe vs. Co; (c) o: Fe vs. V; +: V vs. Zn.

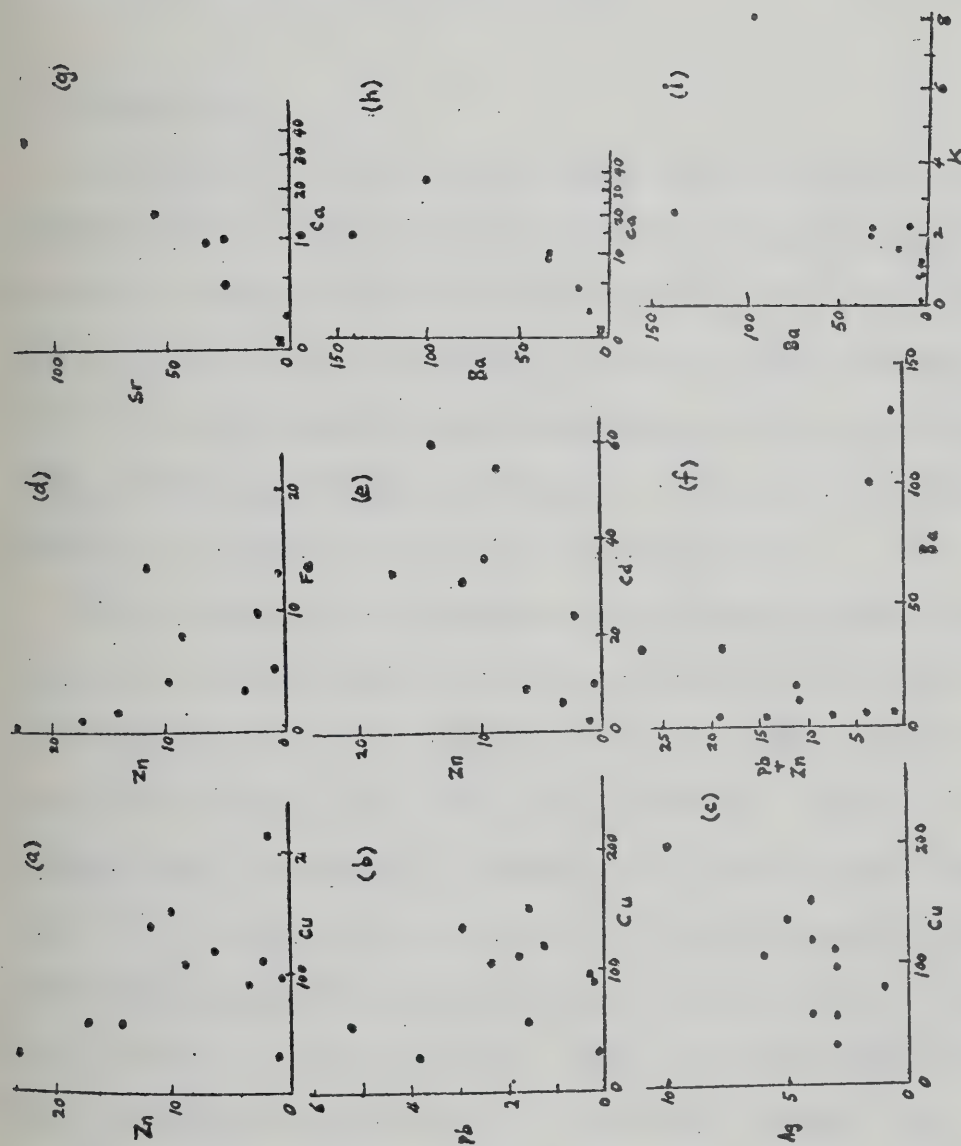


Fig. V-26. Comparison of elements in ore-bearing siltstones, Howard's Pass district.

Fig. V-27 summarizes the distribution of elements in ore-bearing siltstones as compared to their background concentrations in all other rock units in the district. Slight enrichment of concentration levels of Ag, Co, Cd, Fe, and Na and almost unchanged concentration of Cu, Ni, Mn, Al and Ca in ore-bearing siltstones can be observed.

2. Sphalerite

Sphalerite in ore-bearing siltstones usually occurs as fine-grained disseminations or laminations with coexisting diagenetic pyrite and galena. Analyses of sphalerite from drill hole ore-bearing siltstone samples were made by means of electron microprobe using an energy dispersive detector. Similar operating conditions and correction procedure to the Anvil and Thompson Creek sphalerites were employed. The results and calculated mole percents and stoichiometry are given in Table V-23.

FeS mole percents in sphalerite do not show any direct relation either to depth or lateral extent. The overall concentration of FeS is low (0.63 to 4.94 mole %, average 2.27 mole %). X-ray scanning traces (Fig. V-28) and photomicrographs (Plate V-4) across individual sphalerite grains reveal no significant inhomogeneity or zoning. The concentration level and the range of FeS are comparable to those from low temperature hydrothermal-sedimentary ore deposits, such as Kuroko deposits (range: 0.1 ~ 5.2 FeS mole %, average: FeS mole %; Urabe, 1974), and sphalerites in drill cores from the Waiotapu geothermal field, New Zealand (range: 0.4 ~ 3.5, average: 2.0 FeS mole %; Browne and Lovering, 1973).

If sphalerite crystallized at low temperature in equilibrium with pyrite and if the relation between activities and molalities of FeS do not change in the sphalerite-pyrite field at low temperature, then it is possible to

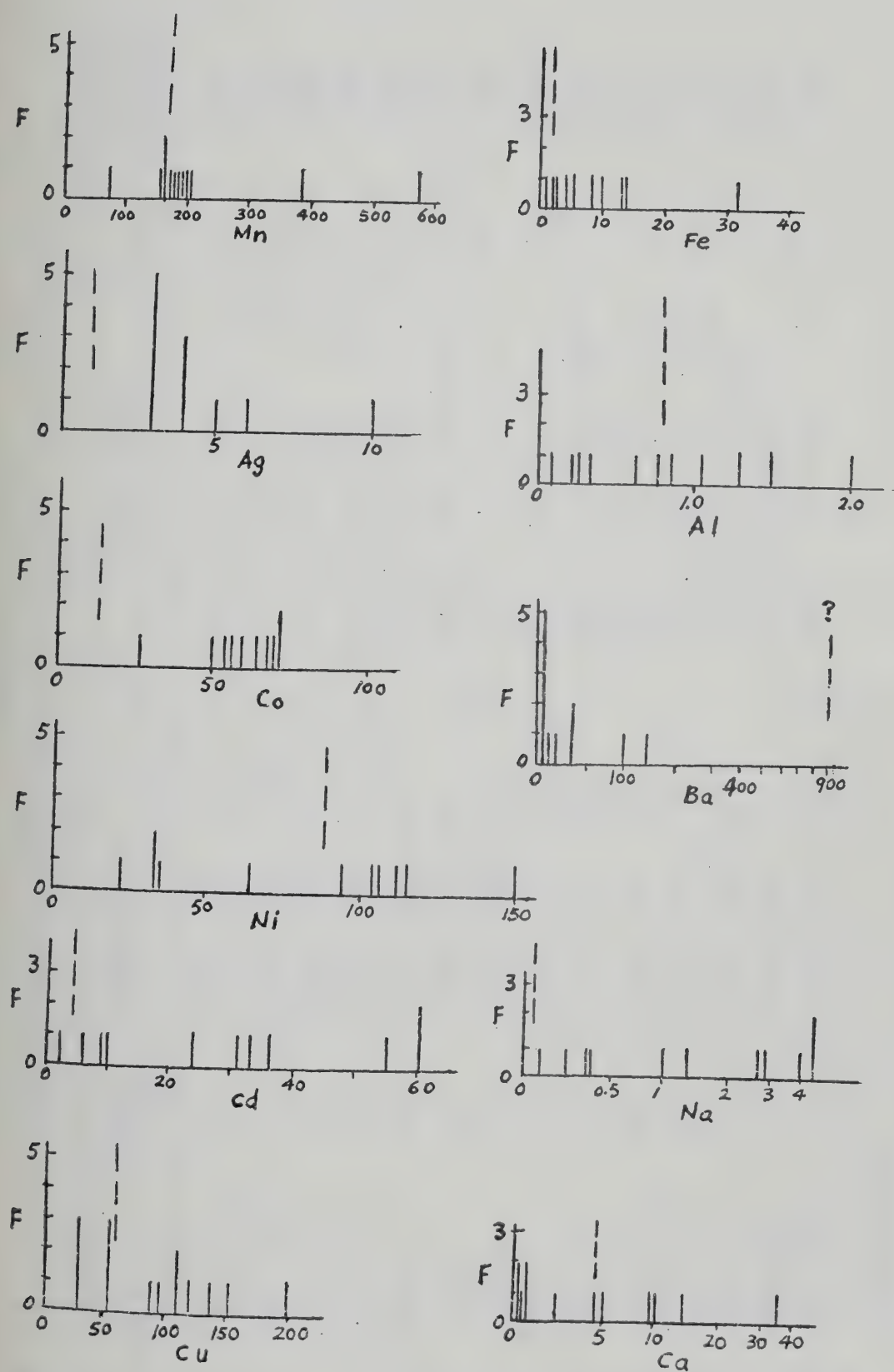


Fig. V-27. Distribution of elements in ore-bearing siltstones as compared with that in the background (dash line), Howard's Pass district. F: frequency.

TABLE V-23

Chemical Compositions of Sphalerites from Placer's Main Zone, Howard's Pass District

DDH Sample No.	Sulfide Assemblage	(weight percent)			Co	Ni	S	(mole percent)			CoS	NiS	(Atomic Ratio) Cations/Sulfur
		Zn	Fe	Mn				ZnS	FeS	MnS			
6-234 #1	(1)*	66.200	1.524	-	-	-	33.344	97.38	2.62	-	-	-	1.00
#2	(1)*	65.976	0.841	-	-	-	33.092	98.53	1.47	-	-	-	0.99
6-274	(1)	65.537	0.701	-	.033	-	33.729	98.71	1.24	-	0.06	-	0.97
15-233	(1)*	65.389	1.315	-	-	-	33.295	97.70	2.30	-	-	-	0.99
18-502.5	(2)	64.870	1.191	-	-	-	33.927	97.89	2.11	-	-	-	0.96
24-358	(4)*	65.05	1.479	-	-	-	33.532	97.41	2.59	-	-	-	0.98
29-328.5	(3)*	64.578	1.458	.041	-	-	33.924	97.35	2.58	0.07	-	-	0.96
381	(1)*	64.886	1.372	.057	-	-	33.685	97.48	2.42	0.10	-	-	0.97
426.5	(1)	65.675	0.828	-	-	.392	33.106	97.90	1.45	-	-	0.65	0.99
579.3	(1)*	63.484	2.818	-	-	-	33.698	95.06	4.94	-	-	-	0.97
30-355	(1)	65.879	0.819	-	-	-	33.302	98.56	1.44	-	-	-	0.98
32-168	(1)*	64.881	1.741	.031	.033	-	33.314	96.85	3.04	0.06	0.05	-	0.99
177.5	(1)*	64.478	1.958	-	-	-	33.522	96.56	3.44	-	-	-	0.98
34-267	(1)	65.617	1.008	-	-	-	33.355	98.23	1.77	-	-	-	0.98
330A	(1)	65.272	1.084	-	-	-	33.634	98.09	1.91	-	-	-	0.97
36-279	(1)	64.932	1.355	-	.049	-	33.665	97.53	2.38	-	0.08	-	0.97
37-270	(2)	65.296	1.135	.06	-	-	33.548	97.90	1.99	0.11	-	-	0.98
Trench #11A	(1)	65.978	0.355	-	-	-	33.668	99.37	0.63	-	-	-	0.97
Trench #19-1	(1)	64.805	1.646	-	-	-	33.549	97.11	2.89	-	-	-	0.98

Sulfide Assemblage:

(1) Py + Gn; (2) Py + Gn + Cpy; (3) Py + Gn + Mc;
 (4) Py + Gn + Mc + Cpy; *: occurrence of framboidal pyrite.

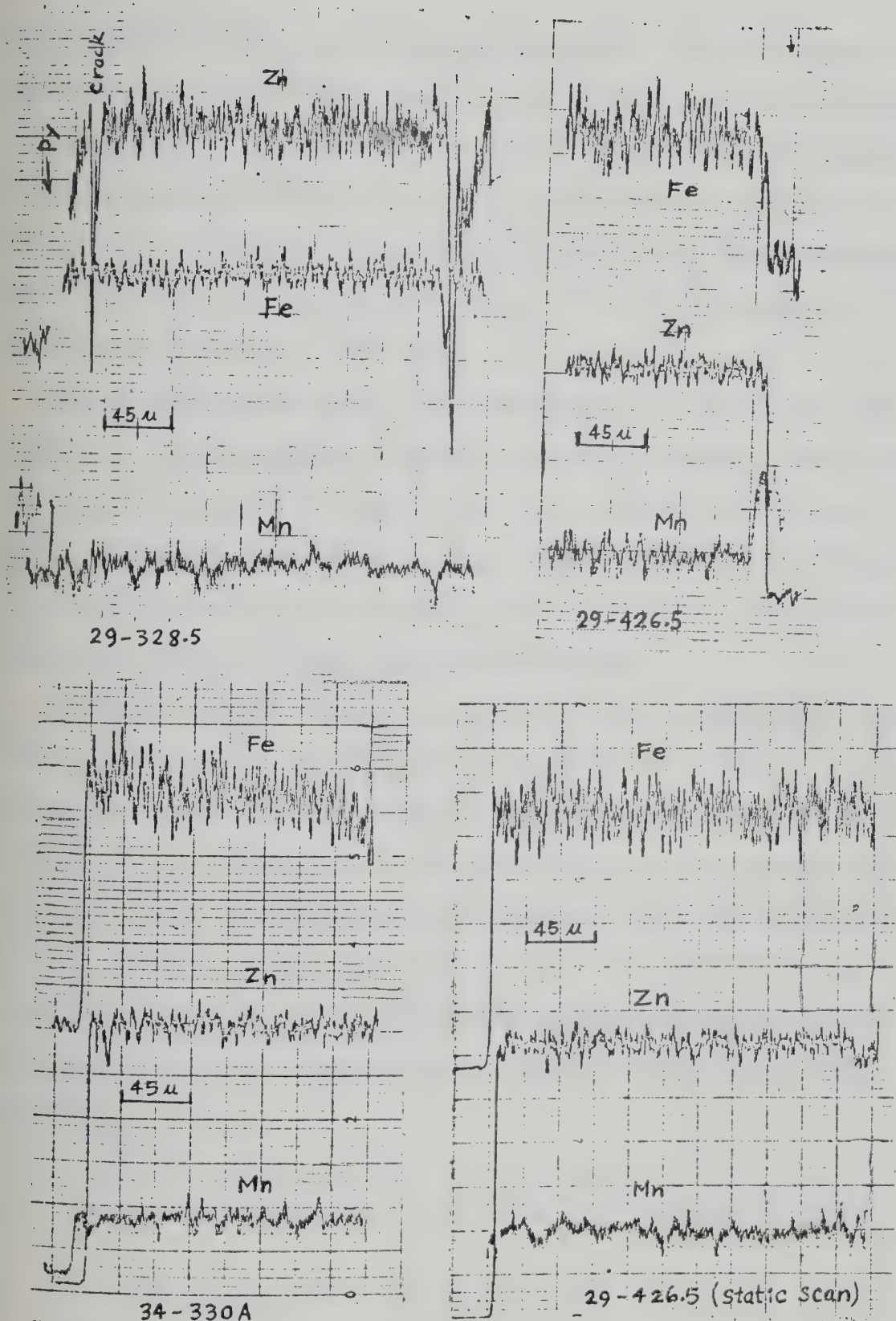


Fig. V-28. Electron microprobe X-ray scanning traces of sphalerite grains, Howard's Pass district.

estimate sulfur fugacity during sphalerite formation. Fluid inclusion and sulfur isotope studies indicate that the ores formed at around 150°C and at a fluid pressure of about 50 bars (see Chapters VI and VII); extrapolating the data of Barton and Toulmin (1966) and Scott and Barnes (1971) down to 150°C without correcting for pressure effect (Fig. V-29), the corresponding sulfur fugacities range between 10^{-16} to $10^{-17.5}$, with an average of 10^{-17} (for FeS mole % between 0.6 and 5.0).

Low FeS contents are found to be characteristic of sphalerites crystallizing at low temperatures in equilibrium with sulfur-rich iron sulfide such as pyrite, greigite or smythite (Scott and Kissin, 1973; Williams, 1974). Sphalerites in the Howard's Pass district usually coexist with pyrite which recrystallized or grew diagenetically from framboidal iron sulfides derived from greigite or other incipient pyrite gels.

Total load pressure estimate cannot be made for the sphalerites because of the lack of validity in extrapolating the sphalerite geobarometer proposed by Scott and Barnes (1971) and Scott (1973) below about 250°C. Due to slope reversal of sp-py-hexagonal po to sp-py-monoclinic po phase boundary and sharp shift of the sp-py-monoclinic po boundary to lower FeS content (cf. Fig. V-7), extrapolation is difficult. A study on the sphalerite composition in Broadlands geothermal field, New Zealand by Browne and Lovering (1973) also confirms the lack of validity of the sphalerite geobarometry below about 300°C.

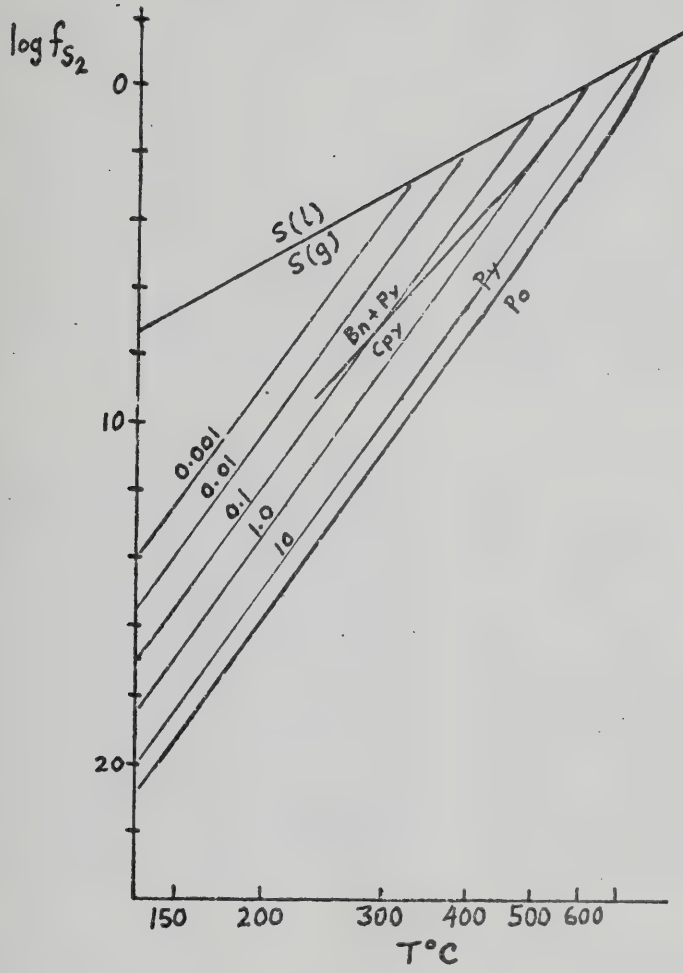


Fig. V-29. Sulfur fugacity vs. temperature diagram showing mole % FeS in sphalerite at 1 bar.

—

<p>1. The first part of the paper discusses the importance of the study of the history of the English language. It is argued that the study of the history of the English language is essential for a full understanding of the language and its development.</p>	<p>2. The second part of the paper discusses the importance of the study of the history of the English language. It is argued that the study of the history of the English language is essential for a full understanding of the language and its development.</p>
<p>3. The third part of the paper discusses the importance of the study of the history of the English language. It is argued that the study of the history of the English language is essential for a full understanding of the language and its development.</p>	<p>4. The fourth part of the paper discusses the importance of the study of the history of the English language. It is argued that the study of the history of the English language is essential for a full understanding of the language and its development.</p>
<p>5. The fifth part of the paper discusses the importance of the study of the history of the English language. It is argued that the study of the history of the English language is essential for a full understanding of the language and its development.</p>	<p>6. The sixth part of the paper discusses the importance of the study of the history of the English language. It is argued that the study of the history of the English language is essential for a full understanding of the language and its development.</p>
<p>7. The seventh part of the paper discusses the importance of the study of the history of the English language. It is argued that the study of the history of the English language is essential for a full understanding of the language and its development.</p>	<p>8. The eighth part of the paper discusses the importance of the study of the history of the English language. It is argued that the study of the history of the English language is essential for a full understanding of the language and its development.</p>

PLATE V-1

ELECTRON MICROPROBE X-RAY PHOTOMICROGRAPHS OF ORE SPECIMENS

Anvil Range, Yukon

- A. DDH66-2 400: Average atomic number composition figure.
Sp: sphalerite, Gn: galena, Sd: siderite.
- B. DDH66-2 400: FeK α distribution; black areas are quartz or barite.
- C. DDH66-2 400: MnK α distribution; bright areas are Mn-siderite.
- D. DDHA10-616: FeK α distribution; Mc: marcasite.
- E. Swim-X: FeK α distribution; Mgt: magnetite.
- F. Swim-X: MnK α distribution; bright areas are Mn-Mg-siderite.

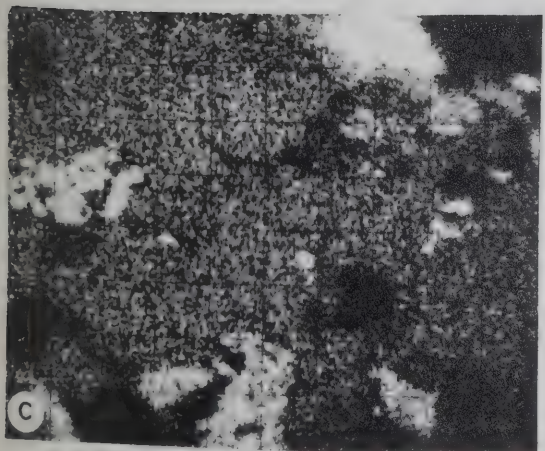
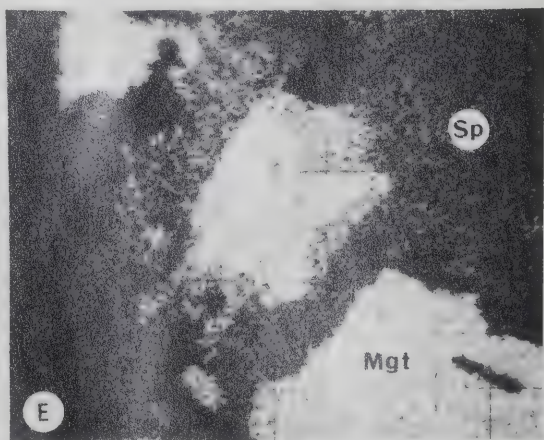
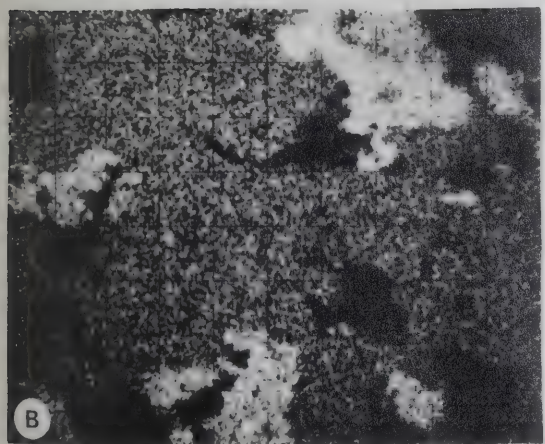
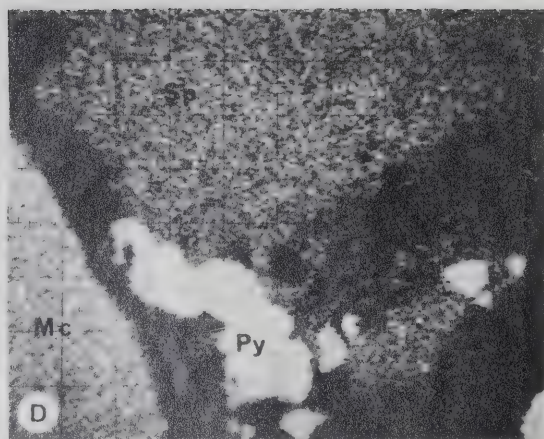
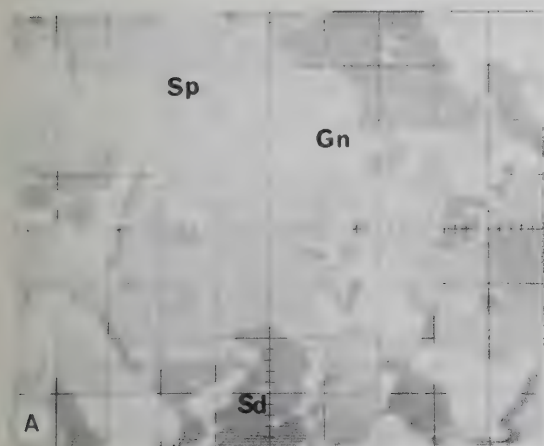


PLATE V-2

ELECTRON MICROPROBE X-RAY PHOTOMICROGRAPHS OF SPHALERITES

Thompson Creek Deposit, Yukon

- A. DDH25-402.5: Average atomic number composition figure.
Sp: sphalerite, Bl: boulangerite.
- B. DDH25-402.5: FeK α distribution; bright areas are pyrite.
- C. DDH25-464: FeK α distribution.
- D. DDH25-464: MnK α distribution; bright dots are Mn siderite.
- E. DDH24-286.5: Average atomic number composition figure.
Sd: siderite.
- F. DDH24-286.5: FeK α distribution.

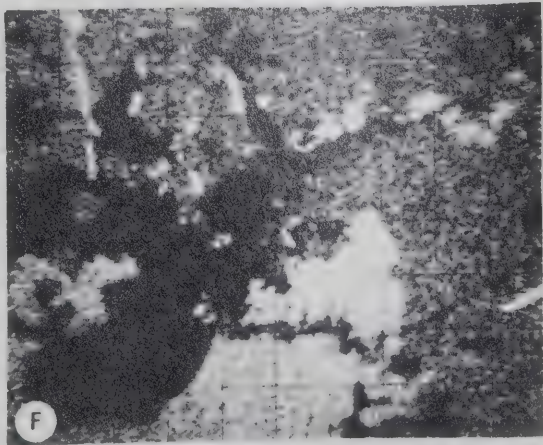
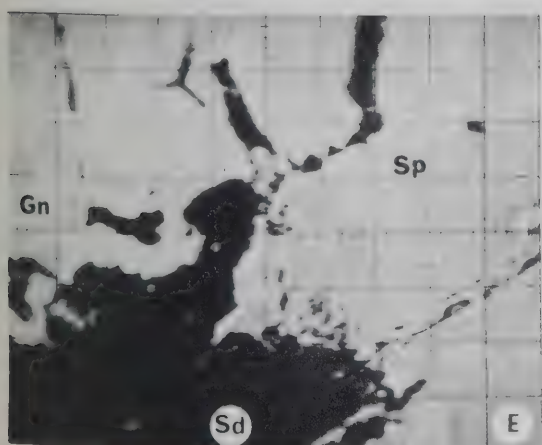
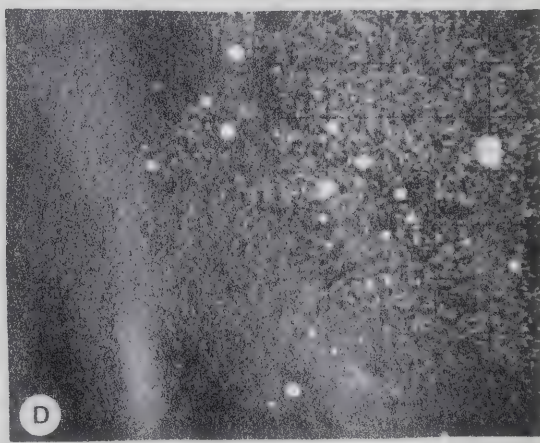
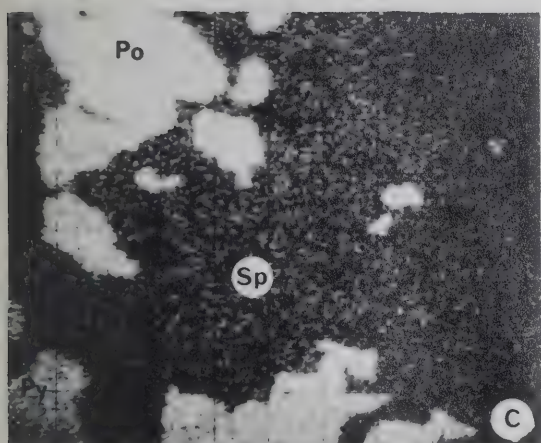
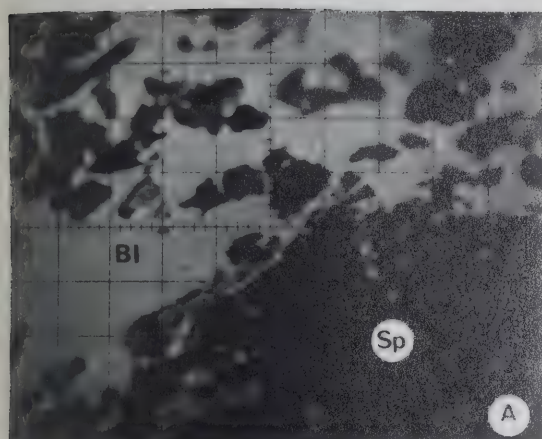


PLATE V-3

ELECTRON MICROPROBE X-RAY PHOTOMICROGRAPHS OF SULFOSALT MINERALS

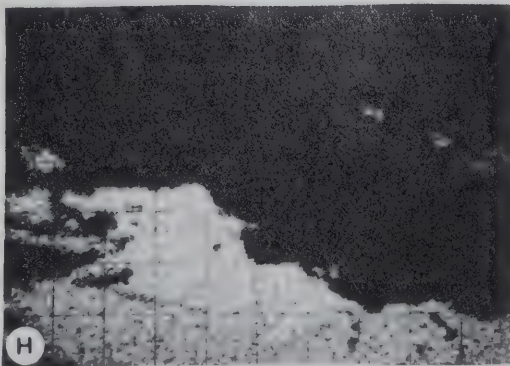
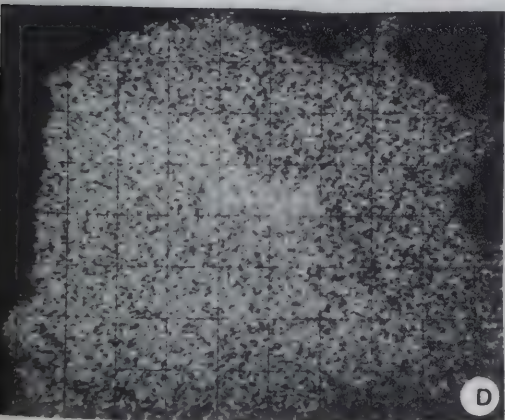
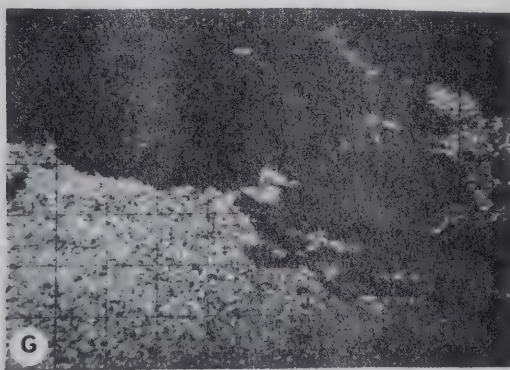
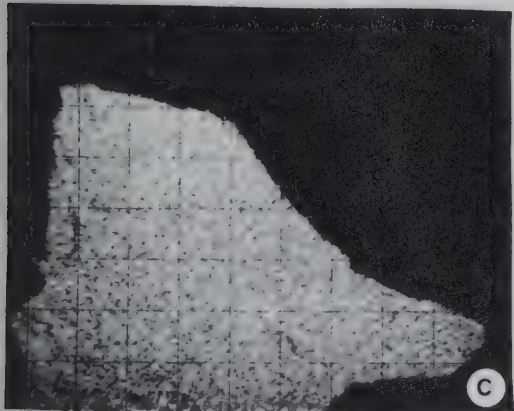
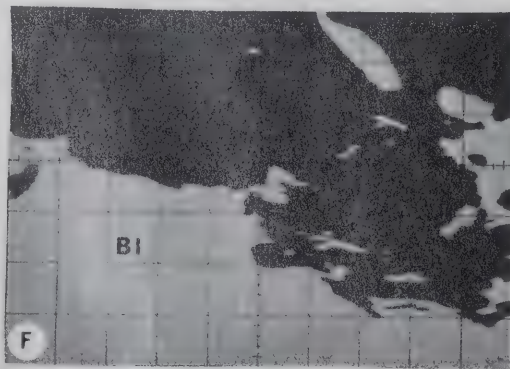
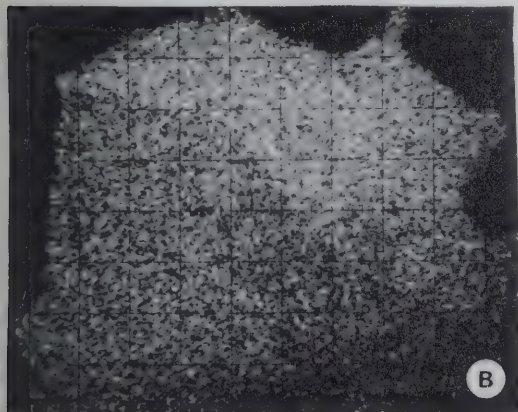
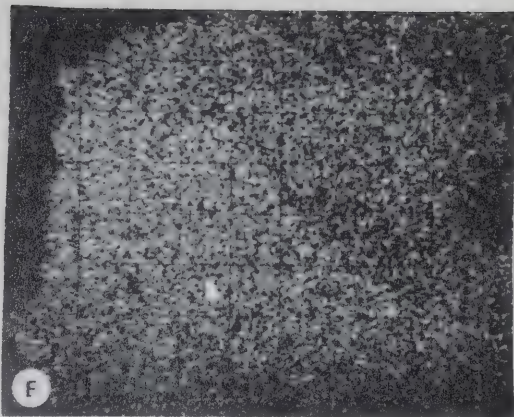
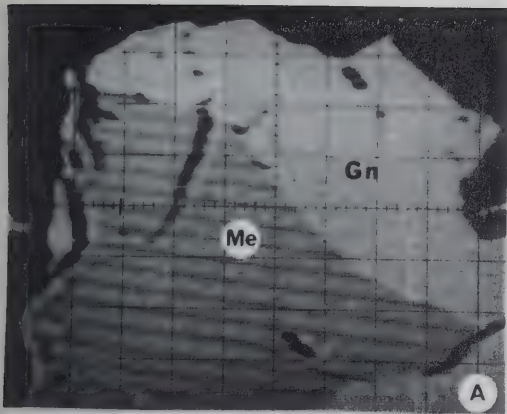
Thompson Creek Deposit, Yukon

Plate V-3a

- A. DDH4-43.5: Average atomic number composition figure.
- B. DDH4-43.5: PbMa. Me: meneghinite.
- C. DDH4-43.5: SbLa.
- D. DDH4-43.5: CuKα.
- E. DDH4-43.5: AsLa.
- F. DDH14-250: Average atomic number composition figure. B1: boulangerite.
- G. DDH14-250: PbMa.
- H. DDH14-250: SbLa.

Plate V-3b

- A. DDH6-34.5: Average atomic number composition figure.
- B. DDH6-34.5: PbMa.
- C. DDH6-34.5: SbLa.
- D. DDH6-34.5: CuKα.
- E. Trench 572-6: Average atomic number composition figure.
- F. Trench 572-6: PbMa.
- G. Trench 572-6: SbLa.
- H. Trench 572-6: CuKα.



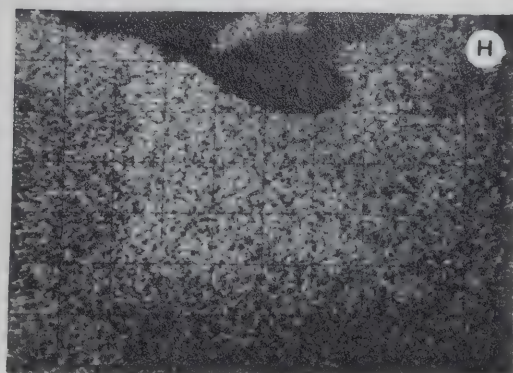
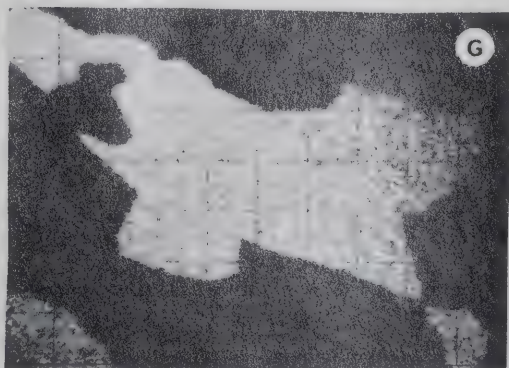
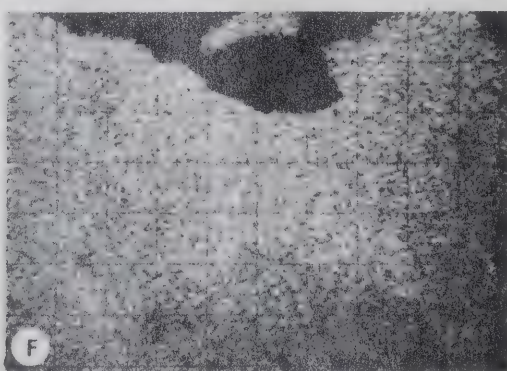
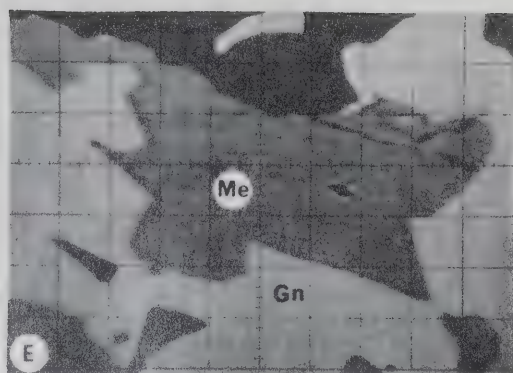
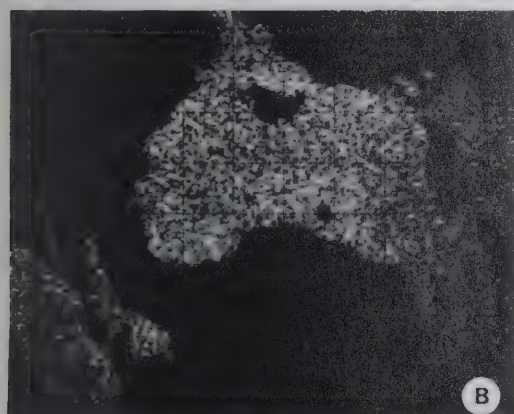
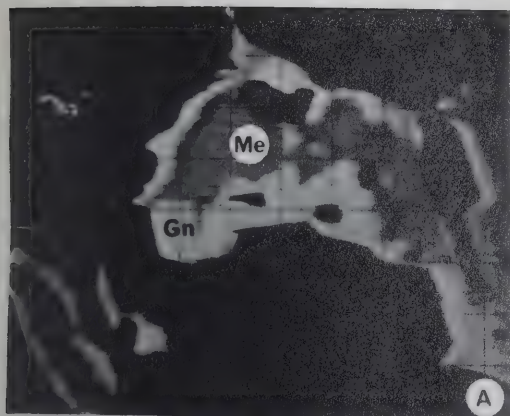
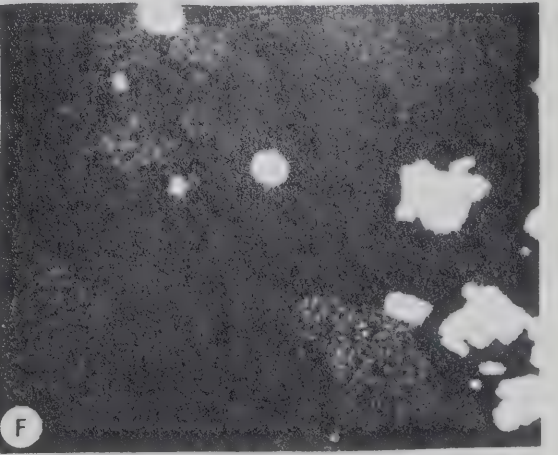
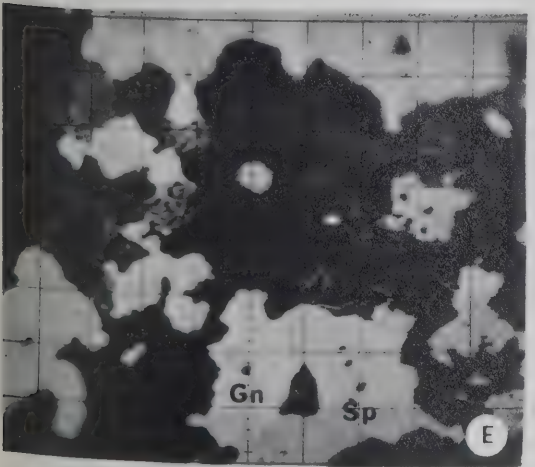
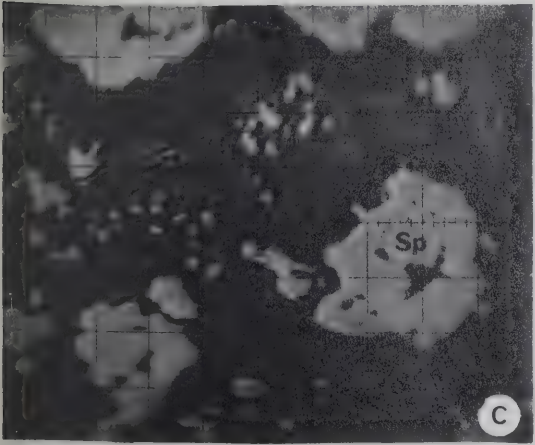
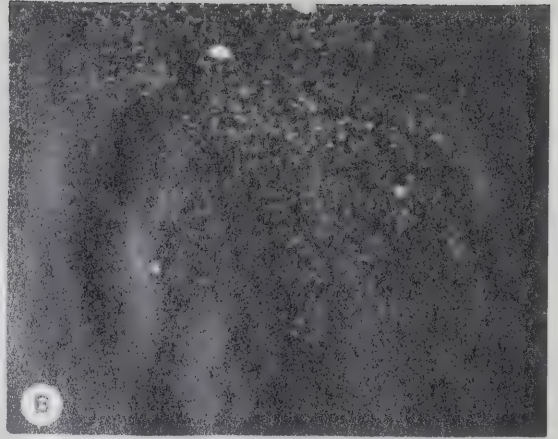
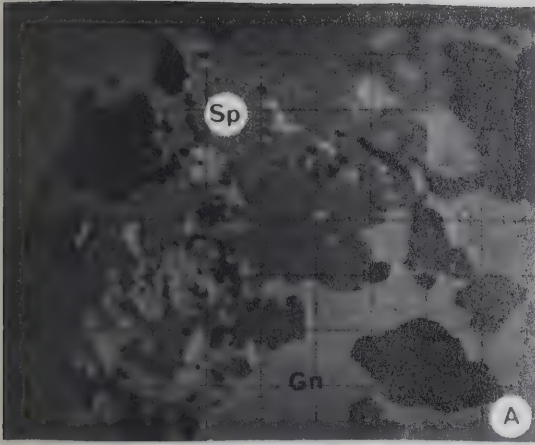


PLATE V-4

ELECTRON MICROPROBE X-RAY PHOTOMICROGRAPHS OF ORE SPECIMENS

Howard's Pass District

- A. DDH6-274: Average atomic number composition figure.
- B. DDH6-274: FeK α .
- C. DDH29-579.3: Average atomic number composition figure.
- D. DDH29-579.3: FeK α (bright dots are framboidal pyrite).
- E. DDH32-177.5: Average atomic number composition figure.
- F. DDH32-177.5: FeK α (bright rounded dots are framboidal pyrite, bright aggregates at right are single-crystal, "ore stage" pyrites).



Chapter VI

FLUID INCLUSION STUDIES

A. INTRODUCTION

Tiny inclusions of fluids such as aqueous solution, carbon dioxide, oil, etc. are trapped during crystal growth or recrystallization in various geological processes. New phases such as gas bubble, immiscible liquids, daughter minerals formed in these trapped inclusions upon cooling. These fluid inclusions provide us with a direct record of the fluid media in which occurred many geological processes, including ore deposition. A study of fluid inclusions in ore or closely associated gangue minerals provides certain important physico-chemical data for the fluid media from which these minerals were formed.

A reliable distinction between primary, pseudosecondary and secondary fluid inclusions is essential to a meaningful inclusion study: Care must also be taken to avoid using inclusions which may have subjected to changes after the initial fluid entrapment; processes such as leakage (natural or artificial), necking down, etc. could greatly modify the true fluid compositions. Most of the criteria of inclusion origin applied in the present study have been reviewed by Roedder (1967, 1972). In brief, fluid inclusions can be classified into three types: inclusions that were trapped by sealing off crystal growth irregularities or fluid inhomogeneities during the formation of the enclosing mineral (primary inclusions), inclusions trapped by healing fractures formed in the crystal during its growth (pseudosecondary inclusions), and inclusions that were trapped by healing of fractures formed at some subsequent time (secondary inclusions).

Primary inclusions are identified mainly by the following criteria:

- (i) restriction to growth layers which sometimes are defined by color banding, growth lines with minute mineral "debris", etc.,
- (ii) attachment to inclusions of foreign minerals caught up by the host crystal during its growth,
- (iii) sharp truncation at twin contacts or extension into both sides of a twin,
- (iv) large, scattered "isolated" inclusions that were not associated with fractures or other secondary features,
- (v) inclusion distribution which outlines "ghost" crystal forms or growth layers as tear-like, bullet-like, and needle-like forms.

Pseudosecondary inclusions are identified by the following criteria:

- (i) inclusions occurring in short, limited healed fractures within individual growth layers or on crystal growth surfaces,
- (ii) inclusions that align in a plane and grade downward in size toward the center of a host crystal, indicating that the crack was widest at the surface of the crystal and tapered inward.

In addition to these criteria, freezing and filling temperatures of some of these pseudosecondary inclusions were used to distinguish them from secondary inclusions which presumably formed under greatly different temperatures to those of the primary inclusions. However, the distinction between pseudosecondary and secondary inclusions often proved difficult; most pseudosecondary inclusions were tentatively identified on the basis of their occurrence on healed fractures of short extent occurring deep in the host crystal. Secondary inclusions were easily identified as those occurring along healed fractures that completely crosscut the host crystal or at least reached one exterior face. In aggregate samples of a given

mineral and in intergrowths of minerals, inclusions in any plane crossing the grain or mineral contacts were regarded as secondary.

B. EXPERIMENTS

Extensive observation and description of physical properties of fluid inclusions (such as size, shape, distribution, type, fluid and solid phases, refractive indices, and filling degrees of fluid phases) were made by means of an optical microscope. The fluid inclusions were studied in thin, flat plates, polished on both surfaces; plate thicknesses were generally kept to 1 mm or less for good optics and to reduce thermal lag in subsequent heating or freezing experiments. Small chips of specimens containing fluid inclusions were observed under microscope while being crushed in solvents with a specially designed crushing stage (Roedder, 1970). Qualitative identification of gases in the inclusions vapor bubbles can be made on the basis of the solubility and reaction of various gases (water vapor, CO_2 , CH_4 , etc.) in different solvents (glycerine, BaCl_2 , Ba(OH)_2 , kerosene, etc.).

Freezing and heating experiments on fluid inclusions were performed on a freezing-and-heating stage attached to elements of Chaixmeca microthermometer in the Fluid Inclusion Laboratory, Department of Geology, under the supervision of Dr. Roger Morton. Extensive calibration of the microthermometer against the freezing and melting points of synthetic standards over a wide range of temperatures (-120°C to $+500^\circ\text{C}$) were carried out before, in between and after the experimental studies of the inclusions. The instrument yields temperatures with a standard deviation of $\pm 0.5^\circ\text{C}$ over the temperature range calibrated. To reduce thermal lag and obtain thermal equilibria, all freezing and heating experiments were made with a heating rate of $1^\circ\text{C}/\text{minute}$ or slower.

C. ANVIL RANGE DISTRICT

Fifty polished plates were prepared from ore and gangue minerals (sphalerite, quartz, barite) in aggregate massive sulfide samples from Faro, Grum and Swim Lakes ore deposits. After extensive observation and identification, only thirteen specimens were found to contain fluid inclusions optically good enough for freezing and heating experiments. A total of 26 freezing experiments on 29 fluid inclusions and 32 heating experiments on 26 fluid inclusions were made.

1. Types of Inclusions (cf. Plate VI-1 and Plate VI-2)

Several distinct types of fluid inclusions were distinguished in the Anvil minerals on the basis of their degree of filling and manner of homogenization. Each of these is characteristic of a distinct type of original fluid or special conditions of entrapment. In many cases, only a small percentage of the inclusions present in a given sample could be classified with certainty and some samples containing many otherwise satisfactory inclusions had to be rejected because they could not be classified confidently. The following types were identified:

(i) Type I - liquid-rich inclusions: this type of inclusion is the most common and occurs in all the minerals examined. It is characterized by high degrees of liquid filling with the vapor content ranging from a few percent to as high as 30%. All of these inclusions in minerals except vein barite homogenize in the liquid phase at temperatures ranging from 168° to 252°C. Their salinity is generally low and quite uniform, ranging from 2.3 to 9.2 wt. % NaCl. Type I inclusions were probably produced by the entrapment of original liquids at hydrothermal temperatures. The liquids were probably homogeneous dilute aqueous brines during massive sulfide deposition.

(ii) Type II - gas-rich inclusions: these inclusions are characterized by very large vapor bubbles that occupy at least 60~70% of the inclusion volume. The vapor phases contain certain amounts of compressed CO₂ gas in addition to water vapor (steam) but not enough to form visible liquid CO₂ on cooling of the inclusions. Type II inclusions are very rare in the Anvil minerals, and are seen only in one specimen (67-4 460 quartz) in which they occur besides type I inclusions. They probably represent entrapment of a dilute gas-like fluid of low density containing water vapor and small amount of compressed supercritical CO₂.

(iii) Type III - 3-phase liquid inclusions: these inclusions are characterized by the presence of a vapor phase and two liquid phases: an aqueous phase and a liquid CO₂ phase. These inclusions homogenize in the liquid phase at temperatures higher than type I inclusions, ranging from 250° to 270°C. Minor occurrence of type III and type I inclusions in close proximity suggest immiscibility of a H₂O-rich fraction and CO₂-rich fraction in some of the inclusion fluids. Most of the type III and coexisting type I inclusions appear to be pseudosecondary in origin, and they constitute only a minor portion of the inclusions examined. Type III inclusions are somewhat more common in minerals from Swim Lakes deposit, but the total number of specimens studied is small and probably does not fully represent the real situation.

(iv) Type IV - multiphase daughter mineral-bearing inclusions: these inclusions contain, besides a vapor and an aqueous liquid phase, at least one daughter mineral, and some as many as three daughter minerals. Halite is by far the most common daughter mineral; it was identified by its cubic form, isotropism, low relief against quartz, and its formation of NaCl·2H₂O upon freezing. A second mineral with simple cubic form is suspected to be

sylvite on the basis of its rapid solution on heating and its failure to form hydrate upon cooling. Some opaque minerals, mostly unidentified but suspected to be hematite, occur as specks or flakes in a few inclusions. Roedder and Skinner (1968) suggest a mechanism of auto-oxidation of the inclusion fluids caused by leakage of hydrogen as being responsible for the formation of iron oxide. These opaque specks remain undissolved even at temperatures much higher than the filling temperatures of the inclusion fluids. Daughter mineral-bearing inclusions are generally very rare and constitute less than 5% of the primary and pseudosecondary inclusions examined.

2. Results

Data and information directly obtained from the freezing and heating experiments and other physico-chemical data derived from the experimental results are summarized in this section.

(a) Freezing Reactions and Products. In most specimens examined, the freezing behavior of the inclusion fluids is normal for NaCl-bearing brines. Ice forms in the majority of the undersaturated inclusions with less than 23.3 wt. % NaCl (Roedder, 1963). The ice is distinctly seen as rounded grains of high negative relief and low birefringence in inclusions as it melts. Vapor bubble becomes strongly deformed when the inclusion fluid is frozen, generally down to -80°C or lower. For a few daughter salt-bearing inclusions, those inclusions containing visible halite crystals are very reluctant to freeze, even down to -90°C , and the products are commonly very difficult to see in the supercooled inclusions; presumably the halite reacts with the enclosing brine to form $\text{NaCl} \cdot 2\text{H}_2\text{O}$ (Roedder, 1963) and does not reappear until temperatures rise to its melting point of around 0°C .

Daughter salt mineral suspected to be sylvite does not react to form any hydrate during freezing, nor do the suspected opaque flakes of hematite. Liquid CO₂-bearing type III inclusions can be identified below the critical point of CO₂ (+31°C), and in some cases, apparent type I inclusions develop an annular ring of liquid CO₂ just below 10°C, thus confirming their type III character.

A few inclusions with large bubbles of compressed gas yield vague, jagged but visible masses of unknown isotropic material at temperatures up to about 5° to 6°C; this material is probably CO₂ hydrate (CO₂·5 $\frac{3}{4}$ H₂O) and not liquid CO₂. As the inclusions warm up, this jagged material gradually smooths out and dissociates into a small liquid phase and the main gas phase. The significance of the dissociation temperatures of CO₂ hydrate will be discussed later.

Since liquid CO₂ phase at room temperature (25°C) has a pressure of 63.8 bars, the appearance of liquid CO₂ phase just below room temperature indicates that type III inclusions in the Anvil minerals must have formed at a pressure below 63 bars.

(b) Salinity. Freezing methods developed by Roedder (1962, 1963) offer the best way of estimating salinities of inclusions that lack daughter crystals of halite. Salinities are estimated from the freezing point depression of the inclusion fluids as measured on a microscopic freezing stage. It is assumed that the amount of NaCl that would be required to produce the measured freezing point depression (equivalent NaCl content) is roughly the amount of the total salt actually present.

Most of the primary and pseudosecondary inclusions in the Anvil mineral belong to type I liquid-rich inclusions, therefore estimation of salinity was made by means of freezing temperatures. Dissolution temper-

atures of daughter salt crystals do provide another means of estimating salt content (Keevil, 1942), however, it is not a universally valid method since salt crystal-bearing inclusions are very minor in the total population of fluid inclusions.

Equivalent NaCl weight percents in all the inclusions tested are given in Table VI-1. The freezing temperatures reported represent averages of at least duplicate runs of final dissolution of ice upon warming from freezing down to -60°C or lower. First melting points of ice were generally well above -21.1°C (first melting point of pure NaCl brines), ranging from -3° to -15°C . This suggests that most of the fluids present during ore deposition were indeed aqueous NaCl brines, and other dissolved salts such as KCl or CaCl_2 were present in negligible amounts.

One striking feature of the salinities of the Anvil ore fluids is their low and uniform salt concentrations in the primary inclusions. The average NaCl contents of ore fluids in the three deposits are: Faro, 8.33 wt. %; Grum, 5.93 wt. %; and Swim Lakes, 5.15%.

The equivalent NaCl weight percents of type III CO_2 -rich inclusion, as determined from Swim Lakes barites, are generally low and around 7 wt. %. Type I inclusions in barite vein in massive sulfides from Faro and Grum contain a similar concentration of NaCl, ranging from 6.5 to 7.7 wt. %.

(c) Filling Temperatures. Filling or homogenization temperatures were measured on the same fluid inclusions after each freezing experiment. In all runs, the heating rate was greatly reduced as the filling temperature was approached so that inclusions would have time to equilibrate. Repeated runs of the same inclusion usually checked to within 3° to 5°C . These uncertainties are considered negligible experimental errors.

Filling temperatures of all inclusions examined are given in Table VI-1. The temperatures recorded were those at the exact moment when the fluid phases homogenized by expansion of the liquid phase. Minimum temperature in one specimen (A4-457 barite) is also listed since a clear image of the disappearing phase was lost above the quoted temperature. Pressure correction was not applied to the temperatures reported. Pressure correction is the amount of temperature which must be added to the filling temperature of an inclusion to obtain the true trapping temperature. If the fluid that is trapped in an inclusion is on the liquid-vapor curve of a P-T diagram (i.e. it is boiling or nearly boiling), there is no pressure correction needed for the filling temperature; both steam and liquid inclusions will then homogenize at the temperature of trapping. A pressure correction becomes necessary only when the pressure at the time of trapping was greater than this vapor pressure. As will be shown later, Anvil ores were formed on shallow seafloor at a fluid pressure of 45 to 140 bars; therefore we can estimate the amount of pressure correction for NaCl-H₂O system from the data of Klevtsov and Lemmlein (1959) and Lemmlein and Klevtsov (1961). The estimated pressure correction is an addition of about 10°C.

Average temperatures (uncorrected for pressure) of primary and pseudo-secondary inclusions for the three deposits are: Faro, 215°C; Grum, 200°C; Swim Lakes, 195°C. Therefore the most probable trapping temperatures of ore fluids for the Anvil deposits range from 205°C to 225°C.

It is interesting to note that fluid inclusions in barite veins from Faro and Grum homogenize at a much lower and narrow range of temperatures (130°~133°C) than the massive sulfide ores. The nature of the occurrence of these veins is not clear. If they were formed by fissure filling during

TABLE VI-1

Salinity and Filling Temperature Data of Fluid Inclusions in Barite, Quartz and Sphalerite, Anvil Ore Deposits

Sample	Mineral	Inclusion Type	No. of Freezing Runs*	Freezing T°C	NaCl Wt. % equiv.	No. of Filling Runs*	Filling T°C	Dissociation T° of CO ₂ Hydrate	Remarks
(Farø)									
66E9 401	Q	P-I	2 (1)	-5.0	7.90	2 (1)	200		
66-22 305	Brt	PS-I	1 (2)	-4.8	7.70	2 (2)	207		
							242		
67-4 460	Q	P-I	1 (1)	-5.5	8.50	2 (2)	178		
							200		
67-6 602	Brt	P-I	1 (3)	-6.0	9.20	2 (3)	242~252		
		PS-III				2 (1)	270		
70-6 249	Brt (vein)	P-I	3 (1)	-4.5	7.20	2 (1)	132		
(Grum)									
A10 774	Brt (vein)	P-I	1 (2)	-4.4	7.10	2 (2)	130~133		
	Sp	P-I	1 (2)	-4.7	7.50				
A10 802A	Brt	P-I	1 (1)	-2.1	3.60	2 (1)	168~170		
A12 819	Q	P-I	1 (1)	-4.1	6.70	2 (1)	231		

TABLE VI-1 (cont'd)

Sample	Mineral	Inclusion Type	No. of Freezing Runs*	Freezing T°C	NaCl Wt. % equiv.	No. of Filling Runs*	Filling T°C	Dissociation T° of CO ₂ Hydrate	Remarks
(Swim Lakes)									
A4 457	Br _t	P-I	5 (3)	-1.3	2.30	2 (2)	> 140		
		PS-I	2 (2)	-4.6	7.40	2 (1)	211~213		
A4 296	Br _t	P-I	1 (2)	-3.0	4.98	2 (3)	183~192		At growth zone of host crystal
A30 397	Q	P-I	1 (1)	-2.5	4.20	2 (1)	168		
		PS-III						5 ~ 6	
Swim X	Br _t	P-I	1 (1)	-4.9	7.80	2 (2)	204		
							220		
		PS-III	2 (2)	-4.4	7.50	2 (1)	255~258		
Swim 9	Br _t	PS-I	1 (1)	-2.5	4.20	2 (2)	173.5		
							220		
		PS-III	1 (3)	-4.0	6.50			6.2	

P: Primary ; PS: Pseudosecondary

*Number in parentheses = number of inclusions tested.

the late stage of ore deposition near the upper part of the orebody, then this temperature range probably set a lower limit for the sulfide deposition.

Pseudosecondary type III CO₂-rich inclusions in barites from Swim Lakes and Faro homogenize at 257° to 270°C. According to Roedder (1967) and Smith and Little (1959), the filling temperatures would be true depositional temperatures for inclusions that trapped only one of the two immiscible phases, but maximum temperatures for inclusions that captured a mixture. Most of the filling temperatures from type III inclusions in Anvil minerals are between 257° to 270°C and are probably maximum temperatures since they contain a mixture of CO₂ and aqueous brine.

(d) CO₂ Contents. Fluid inclusions that contain 7~8 wt. % CO₂ generally show only apparent two phases at room temperature and do not show any visible liquid CO₂ phase (Takeuchi, 1971). Upon cooling, small amounts of liquid CO₂ or CO₂ hydrate form around vapor bubbles. For inclusions containing even less CO₂, only trace CO₂ hydrate but no liquid CO₂ phase would form upon cooling. Therefore, the phase proportions (volume) of liquid CO₂ or CO₂ hydrate vary according to the concentration of CO₂ in the inclusions. Takeuchi (1971) has shown that by using the volume proportions of liquid CO₂ and vapor phase to those of the inclusions at low temperature (15°C), rough estimate of CO₂ weight percent can be made.

Measurements of the volumes of liquid CO₂, vapor bubble and the inclusions have been made in 6 pseudosecondary type III inclusions at around 15°C by means of a micrometer ocular on a freezing stage. Using the diagram (Fig. VI-1) as suggested by Takeuchi, weight percents of CO₂ are estimated from these volume measurements. The results are given in Table VI-2. Also shown are the estimated wt. % of immiscible CO₂ in the pseudo-

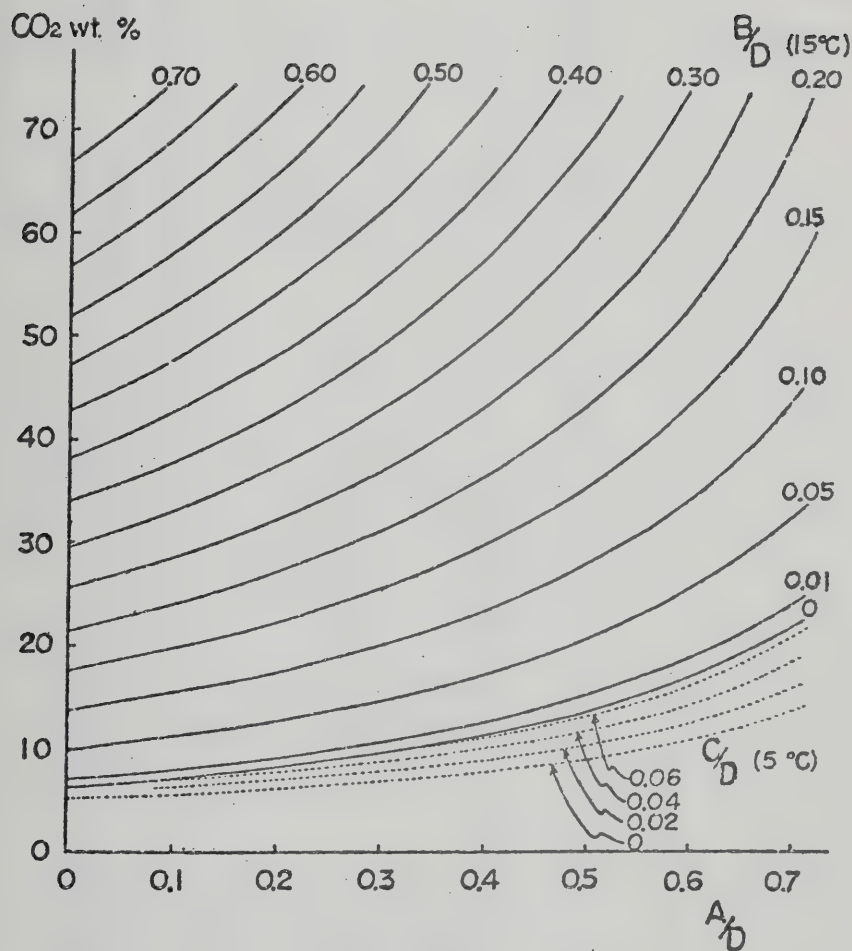


Fig. VI-1. A diagram for estimating CO₂ wt. % by volume ratios of phases in fluid inclusions. A: vapor bubble volume; B: liquid CO₂ volume; C: CO₂ hydrate volume; D: inclusion volume (after Takeuchi, 1971).

TABLE VI-2

Volumes and Concentrations of CO₂ in Fluid Inclusions from
Swim Lakes Barites

Type III Inclusions	Volume % of Liquid CO ₂	Volume % of Vapor Bubble	Weight % CO ₂ in Inclusions	% of Type III Inclusions	Weight % of Immiscible CO ₂
Swim-X #1	7.6	0.3	12.0	50	6.0
#2	12.0	0.8	7.3	50	3.7
Swim-9 #1	23.8	6.5	25.0	25	6.3
#2	26.0	6.6	27.0	25	6.8
A4-426 #1	40.6	1.6	38.0	10	3.8
#2	27.3	1.9	28.0	10	2.8
Mean					4.9

secondary inclusion fluids. The overall estimate of the concentration of immiscible CO₂ in the fluids averages about 5 wt. %, or about 2 mole %.

The uncertainty in estimating thicknesses of inclusions contributes the largest errors to the volume estimates; although care was taken to measure those inclusions with symmetric dimensions, such as spheres, ellipsoids, cubes or rectangular cubes. However, it is felt that these estimates of CO₂ concentrations are adequate and valuable for the purpose of semiquantitative evaluation of immiscible CO₂ concentration level in the inclusion fluids.

(e) Fluid Densities. Knowing the salinities and filling temperatures, it is possible to estimate the densities of the ore fluids from the experimental or theoretical data for H₂O-NaCl system given in the literature (Lemmlein and Klevtsov, 1961; Ellis and Golding, 1963; and Haas, 1971). Strictly speaking, densities derived from these data are actually critical densities at the vapor-liquid 2-phase fields for aqueous salt solutions, and because fluid pressures on the system at the time of trapping are usually higher than vapor pressures assumed, these densities must be considered as maximum estimates.

Density estimates are made for type I inclusions in all the minerals, and the results are given in Table VI-3. It is evident that estimates by the experimental data of Ellis and Golding (1963) agree well with those by the theoretical data of Haas (1971); estimates of densities by the experimental data of Lemmlein and Klevtsov (1961) are lower by as much as 0.05 gm/cc. These densities are in reasonable agreement with estimates of Roedder (1967) who infers that most hydrothermal ore deposits have formed from fluids with densities normally in the range of 0.5 to slightly over 1.0 gm/cc.

TABLE VI-3

Density Estimates of Type I Inclusion Fluids
In Barite and Quartz, Anvil Ore Deposits

Sample	Mineral	Density (gm/cc)		
		(1)	(2)	(3)
(Faro)				
66E9 401	Q	0.90	0.91	0.85
66-22 305	Brt	0.87	0.87	0.82
67-4 460	Q	0.92	0.93	0.88
67-6 602	Brt	0.87	0.88	0.82
70-6 249	Brt (vein)	0.97	0.98	0.93
(Grum)				
A10 774	Brt (vein)	0.97	0.98	0.93
A10 802A	Brt	0.91	0.91	0.88
A12 819	Q	0.86	0.87	0.83
(Swim Lakes)				
A4 296	Brt	0.90	0.90	0.87
A4 457	Brt	0.90	0.90	0.85
A30 397	Q	0.91	0.92	0.88
Swim X	Brt	0.90	0.91	0.85
Swim 9	Brt	0.88	0.87	0.86

(1) Ellis and Golding (1963)

(2) Haas (1971)

(3) Lemmlein and Klevtsov (1961)

At the time of massive sulfide ore deposition, the ore fluids were dilute aqueous brines of moderately low densities (0.8 to 0.9 gm/cc) while the temperatures were moderately high (200°C or more); at the time of vein emplacement, densities of the ore fluids rose to about 0.97 gm/cc with a decline in temperatures (130°~140°C) and a maintenance of similar fluid salinity.

For the sake of a complete record, densities of liquid CO₂ and gaseous CO₂ in type III inclusions have also been estimated from the empirical data given by Amagat (1892). Liquid CO₂ in the inclusions generally homogenize in the temperature range of 10° to 20°C, corresponding to densities of liquid CO₂ of 0.86 to 0.77 gm/cc and to those of gaseous CO₂ of 0.13 to 0.19 gm/cc. Corresponding CO₂ pressures (P_{CO₂}) are between 44 to 56 bars.

3. Discussion

From the above data, it is possible to present some pertinent interpretations concerning the possible variation of density, salinity and temperature in the ore fluids, estimates of depositional pressure, water depth and the possible role of boiling during ore deposition, and the nature of immiscible CO₂-rich fluids.

(a) Density-Salinity-Temperature Variation. The aqueous brines as now preserved in the fluid inclusions in the Anvil hydrothermal minerals are possibly the mixture of an ascending hydrothermal solution and seawater, as the Anvil deposits were believed to have formed in a marine sedimentary and volcanic sequence. The mixing mechanism is also indicated by the following evidence.

Firstly, a positive correlation exists between salinities and temperatures of the aqueous brines (Fig. VI-2a). Mixing of an ascending hot and relatively saline brine with cold seawater* (containing 2.9 wt. % or 0.5 m NaCl at 20°C) will give rise to small temperature and salinity variations in the finally mixed aqueous brine from which ore deposition occurred. Hotter brine, presumably least subjected to mixing and cooling process, will maintain a higher salinity approaching that of the ascending solution; whereas the cooler brine will be less saline due to a larger degree of mixing with seawater.

Secondly, a negative correlation exists between densities and temperatures (and thus a negative correlation between densities and salinities) of the aqueous brines (Fig. VI-2b). Density of seawater at 20°C is about 1.023. Higher density and lower temperature are to be expected in the brine with increasing fraction of seawater in the mixture. If the original aqueous brines had a density lighter than seawater, it would float up in the surrounding seawater and mix rapidly with each other; as mixing proceeds, the density of the mixed brine approaches that of seawater (as evidenced by a density of 0.97 of the late stage fissure filling of barite ?) and may further exceed it. The result is that the brine will begin to sink and flow downward along depressions, forming brine pools similar to those of the Red Sea.

Other independent evidence supporting a mixing mechanism comes from a slight negative correlation of salinity with sulfur isotope compositions of sulfides (Fig. VI-2c). The correlation is not distinct and probably reflects a limited number of samples or a complex fractionation process other than

*For the present purpose, the temperature and NaCl concentration of seawater may be considered constant throughout geologic time (see Holland, 1965b).

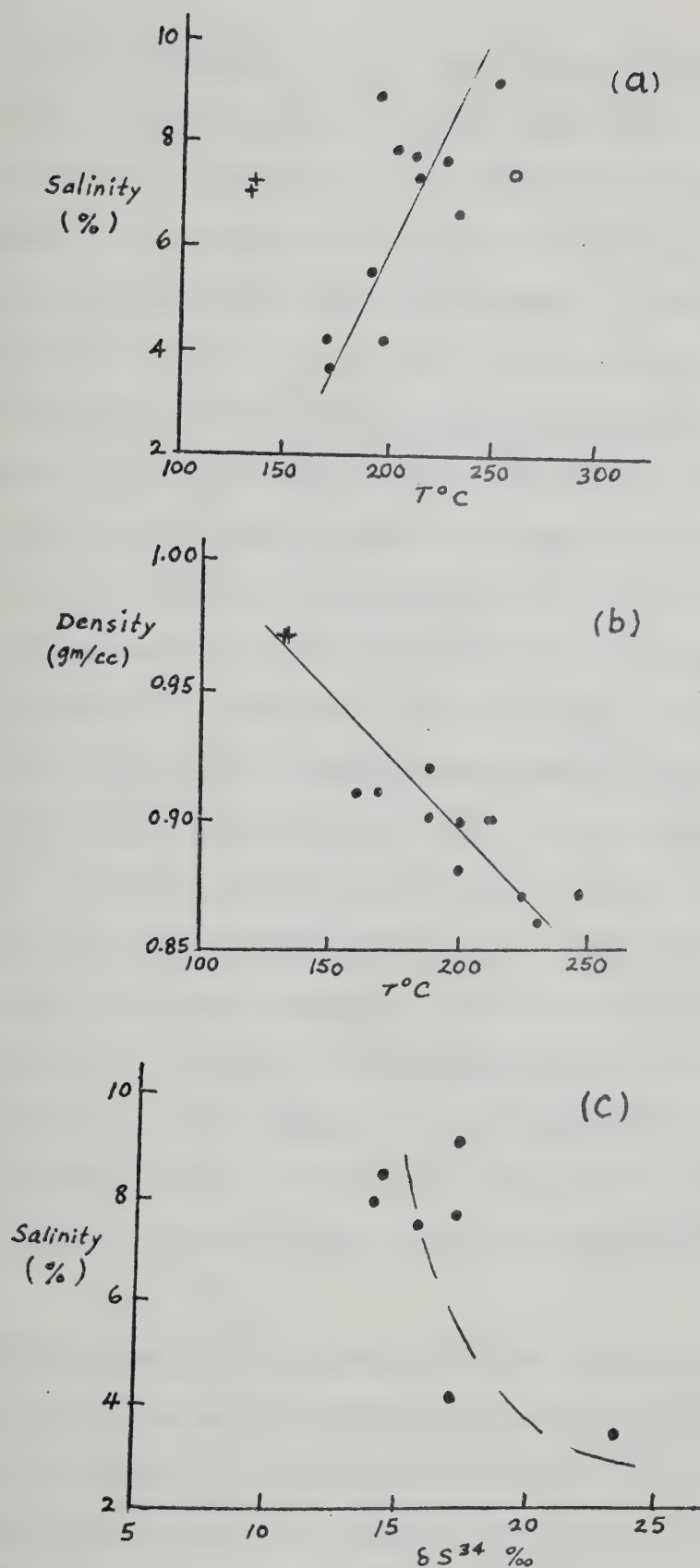


Fig. VI-2. Correlation of salinity, density, and temperature data of fluid inclusions in Anvil minerals. Solid circles: type I; open circle: type III; crosses: type I in barite veins.

simple mixing with seawater in the final fixing of isotope compositions of the brine. Cambrian seawater probably had a δS^{34} of 31‰. Heavier δS^{34} sulfides were precipitated from brines with an increasing admixture of seawater. The indistinct correlation is also due to the complex partition of dissolved sulfur species in response to minor fluctuating conditions, some of which probably arose through mixing by seawater.

(b) Pressure and Water Depth During Ore Deposition. When the original aqueous brines were discharged on the seafloor and mixing with seawater occurred, they must have been in a liquid state in order to form massive sulfide deposits on seawater-rock interface; boiling of these brines before reaching the seafloor would result in precipitation of all the constituents (including NaCl) in place, filling any open space available (Ridge, 1973). The existence of stratabound massive sulfide deposits in marine sediments and/or volcanic rocks in many regions itself suggests that most of the "ore fluids" do not boil before they reach the seafloor. The chance of boiling depends largely on the vapor pressures and temperatures of the ore fluids, salinity, confining pressures and depth of the overlying body of seawater. If the confining pressure on the ore fluid is larger than the vapor pressure at given temperature and salinity, then no boiling would occur. In this sense the confining pressure and water depth required to prohibit boiling below seafloor provide a minimum magnitude.

Confining hydrostatic (seawater, without an overlying layer of rocks) pressure on the discharged "ore fluid" of the Anvil deposits can be estimated from a fluid pressure-temperature diagram (Fig. VI-3) as a function of salinity and density; this diagram is modified after Lemmlein and Klevtsov (1961) and Ohmoto and Rye (1970). Average values of filling temperatures

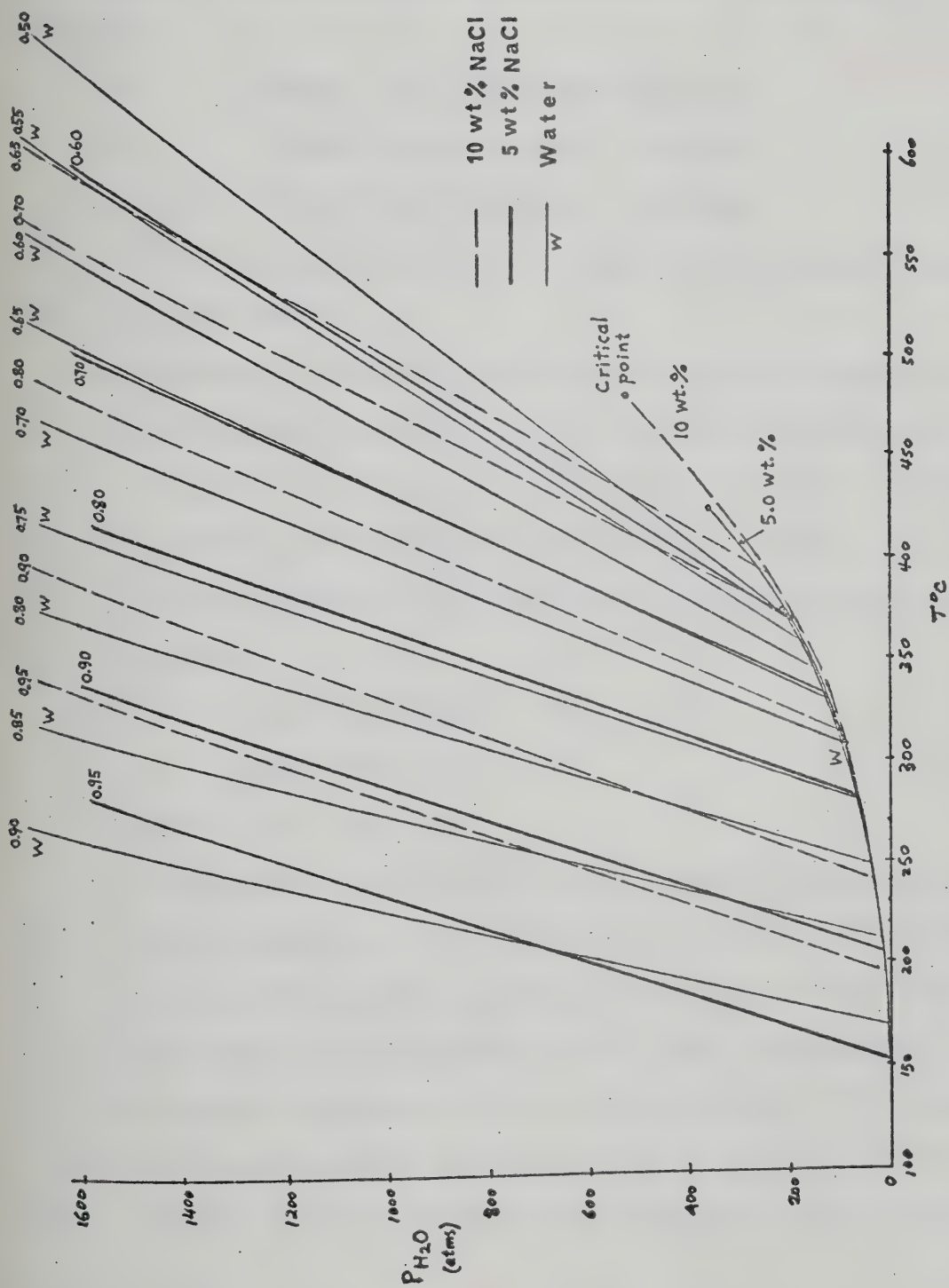


Fig. VI-3. Fluid pressure vs. temperature diagram as a function of salinity and density.

(pressure-corrected), salinities and densities obtained from primary type I fluid inclusions are used in estimating the hydrostatic pressures. The estimated confining pressures on the ore fluid of each deposit are as follows:

Faro:	140 bars	(max. estimate*: 300 bars)
Grum:	45 bars	(max. estimate: 120 bars)
Swim Lakes:	105 bars	(max. estimate: 230 bars)

The error in these pressure estimates is about 10% due to minor variation in filling temperatures.

Vapor pressures of NaCl-H₂O solutions as a function of temperature and salinity under hydrostatic head or in a compositionally-thermally layered system have been calculated by Haas (1971). Allowing the minor temperature variation of the Anvil ore fluids (200° to 250°C), the range of vapor pressures at known salinities of the ore fluids is estimated to be (cf. Table VI-4):

Faro:	15.1 ~ 38.6 bars
Grum:	15.0 ~ 38.3 bars
Swim Lakes:	14.7 ~ 37.7 bars

It is evident from the comparison of the estimated hydrostatic pressures and vapor pressures of the ore fluids that most of the fluids must have reached the seafloor without boiling. Some cooling of the mixed brines may have taken place upon discharge and before precipitation of sulfides. The original ascending fluids may have been added to the seawater at temperatures somewhat higher than those given by filling of fluid inclusions. If 260°C is taken arbitrarily as the initial temperature of the

*Estimate obtained by using maximum filling temperature and salinity data.

TABLE VI-4

Vapor Pressures and Minimum Depths of Seawater
To Permit a Solution to Reach Seafloor
Without Boiling

T°C	NaCl Wt. %				
	5	10	15	20	
150	3.25	3.07	2.88	2.70	bars
	29.00	27.60	26.00	24.70	meters
200	15.10	14.47	13.83	13.20	bars
	131.00	123.00	115.00	107.00	meters
250	38.60	36.97	35.53	33.70	bars
	335.00	320.00	305.00	290.00	meters
300	83.20	79.67	76.13	72.60	bars
	725.00	694.00	663.00	632.00	meters
330	124.50	119.10	113.80	108.40	bars
	1080.00	1035.00	990.00	945.00	meters
350	150.00	143.80	137.50	131.30	bars
	1301.00	1246.70	1192.00	1138.00	meters

original fluid, the corresponding vapor pressure will be around 44~46 bars over the salinity range of 5 to 8 wt. % NaCl. This pressure is equal to the minimum confining pressure of the seawater (45 bars). If the initial temperature of the original fluid was about 300°C, corresponding vapor pressure will be about 80 to 83 bars. Since boiling evidence is generally lacking in fluid inclusions in Anvil minerals, the initial temperature would have to be lower than 300°C, possibly 250°C.

The depth of the overlying seawater at the time of ore deposition can be estimated from the above confining hydrostatic pressure using a pressure gradient of 0.1145 bar/meter for seawater. Thus we obtain the depths as:

Faro: 1230 meters (max. estimate: 2620 meters)

Grum: 400 meters (max. estimate: 1048 meters)

Swim Lakes: 920 meters (max. estimate: 2009 meters)

The minimum depth to permit aqueous brines to reach seafloor without boiling is, at 250°C, 326~335 meters over the salinity range of 5 to 8 wt. % NaCl (Table VI-4). Therefore the ore fluids must have been discharged onto a seafloor at depths of more than 400 meters, and as deep as 1230 meters. Spooner and Fyfe (1973) estimate the hydrostatic pressures of overlying seawater at most mid-ocean ridges (+2 to +4 km deep) to be 200~400 bars; likewise, Ridge (1973) estimates a pressure of more than 209 bars over the Red Sea deep brines (Atlantis II) at a depth of about 2000 m.

The above pressure and depth estimates are only of minimum magnitude; the actual pressures and depths during ore deposition could have been greater.

(c) Nature of Immiscible CO₂-rich Fluids. Immiscible CO₂-H₂O fluids as represented by coexistence of type I and type III pseudosecondary inclusions probably represent a unique case of fluid immiscibility in a CO₂-rich system under moderately high CO₂ pressure.

It is not known whether the immiscible fluids occurred as a result of sporadic introduction of "deep-seated" juvenile solutions into the aqueous ore solutions or as metamorphic fluids introduced during recrystallization and metamorphism.

Experimental data on the dissociation pressures of CO₂ hydrate by Larson (1956) and Takeuchi and Kennedy (1965a) provide a means of estimating internal CO₂ pressures in the inclusions. In some type III inclusions in 2 minerals from Swim Lakes deposit (A30-397 Quartz and Swim-9 Barite), CO₂ hydrates dissociate to CO₂ gas plus aqueous brine at temperatures of about 5° to 6.2°C (Table VI-1), indicating internal CO₂ pressures in the range of about 30 to 42 bars (Fig. VI-4). Since liquid CO₂ phases are also common below room temperature (10° to 20°C) in a lot of these inclusions, the internal CO₂ pressures must be at least as high as 45 bars. These liquid CO₂ phases are generally not visible at above 20°C, indicating that the internal CO₂ pressures are less than 56.3 bars (Amagat, 1892). The most probable range of CO₂ pressures for the immiscible fluids is about 30~56 bars. The presence of NaCl and other dissolved salts in the inclusion fluid would tend to lower this maximum limit of CO₂ pressures.

Since CO₂ concentration in the overall immiscible fluids is estimated to be only about 5 wt. %, the most reasonable CO₂ pressure appears to be the lower limit of 30 bars. Over the temperature range of 257° to 270°C and salinity of 7 wt. % NaCl (I=1.2), the corresponding CO₂ fugacity (f_{CO_2})

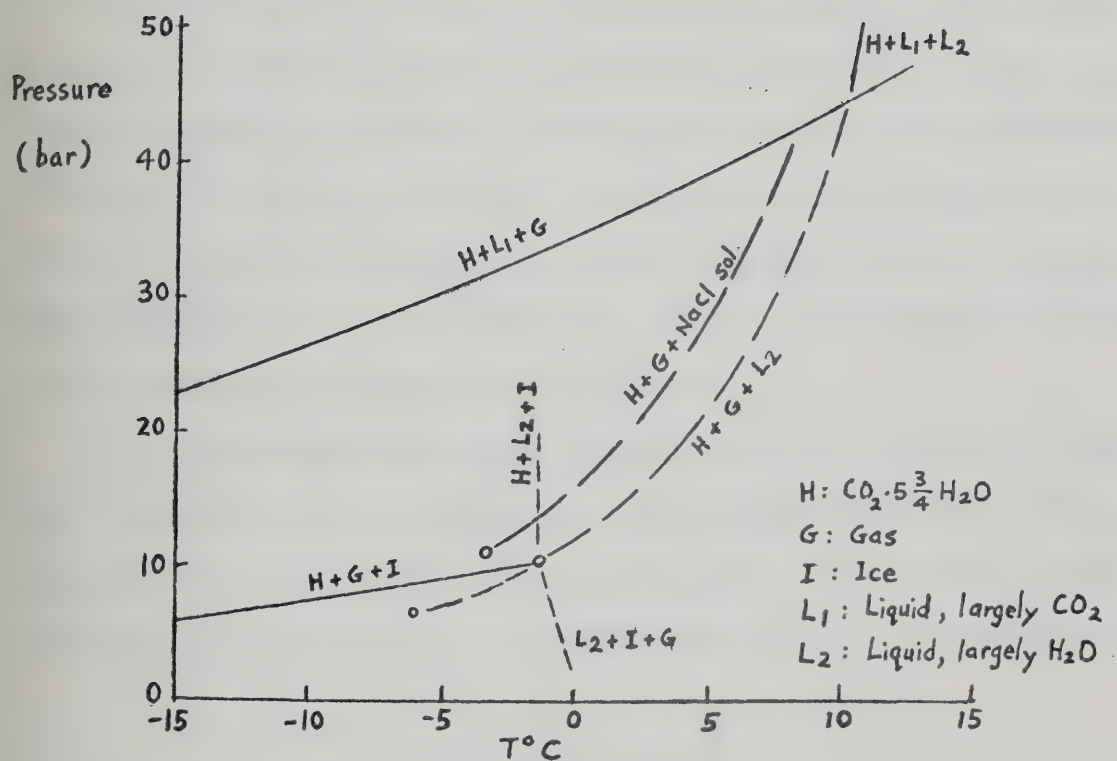


Fig. VI-4. Dissociation curves of CO_2 hydrate at low pressures (after Larson, 1956; and Takeuchi and Kennedy, 1965a).

in the immiscible fluids is about 43 bars ($10^{1.6}$ bars). It is noteworthy that this estimate from fluid inclusions agrees well with a f_{CO_2} of $10^{1.5}$ at 300°C estimated from siderite-sulfide assemblages (Fe-C-O-S system) (Chapter V).

It is likely that the immiscible CO₂-rich and H₂O-rich fluids were introduced during "late stage" sub-seafloor metamorphism by either mixing of "juvenile" CO₂-rich fluid with "interstitial" aqueous brines present in the still permeable deposits or increasing concentration of CO₂ in late stage hydrothermal fluids. Takeuchi (1971) and Takeuchi and Kennedy (1965b) have shown that a decline in pressure or salinity would tend to concentrate CO₂ in hydrothermal solutions. The significance of sub-sea-floor metamorphism due to circulation of hot brines in geothermal systems has been emphasized by Spooner and Fyfe (1973).

It is also possible that minor boiling of the late stage ore fluids might bring about immiscibility of CO₂-rich and H₂O-rich phases. It is not clear, however, why Swim Lakes minerals show a larger number of type III pseudosecondary inclusions, presumably this is due to sampling bias.

D. FRANCES LAKE DISTRICT

Ten polished plates were prepared from quartz and sphalerite from Thompson Creek deposit, Frances Lake district. All sphalerite specimens are too dim for optical observations of fluid inclusions or heating and freezing experiments. Only six aggregate quartz specimens were found to be suitable for fluid inclusion study. In addition, three quartz and six siderite chip samples were observed in crushing stage under the microscope.

1. Types of Inclusions (cf. Plate VI-3)

Inclusion types identified in the quartz plates are essentially similar to those observed in the Anvil minerals, namely, type I liquid-rich inclusions, type II gas-rich inclusions, type III CO₂-rich inclusions, and type IV daughter mineral-bearing inclusions. Type I inclusions make up about 50% of the total primary and pseudosecondary inclusions observed, while type II and type III inclusions are about 30%, with type IV inclusions about 10%. Secondary inclusions are mostly type I with minor type III.

Type I inclusions commonly have a degree of filling of 70 to 90%, but a few of them have a critical degree of filling as low as 50~60 percent. The latter inclusions fall in the gap between low filling degree inclusions and type II gas-rich inclusions which usually have filling degree below 35 to 20%. Type II inclusions are found in some specimens to co-exist with other types of inclusions. They are generally minor and constitute less than 10% of the inclusions. Type III inclusions are quite common and make up about 20% of the inclusion population; they can be further classified into three varieties according to their freezing and homogenization behaviors: the first variety has an annular ring of liquid CO₂ formed around vapor phase upon freezing or expansion of inner vapor phase upon warming, the second variety has an inner vapor phase developed in the liquid CO₂ upon freezing or homogenization in the liquid phase upon warming, the third variety does not show any liquid CO₂ phase or freezing but develops CO₂ hydrates in the inclusions on warming back to room temperature. These different behaviors reflect a gradation in CO₂:H₂O ratios in the inclusion fluids. The occasional occurrence of type III and type I inclusions indicate immiscibility in some ore fluids.

Type IV inclusions, where seen, usually contain one daughter halite crystal, but some contain halite and possibly sylvite. No other daughter minerals have been observed.

2. Results

(a) Reactions and Products Formed During Freezing or Crushing. Reactions and products observed in type I, type III, and type IV inclusions upon freezing are essentially the same as for Anvil. Characteristic variations in behavior upon freezing or warming in type III inclusions have been noted above.

Reactions and products formed during crushing of quartz and siderite chips in glycerine, kerosene, $\text{Al}\cdot\text{BaCl}_2$ and $\text{Ba}(\text{OH})_2\cdot 8(\text{H}_2\text{O})$ solutions generally confirm the presence of compressed gases such as CO_2 . In glycerine and kerosene, significant numbers of gas bubbles were generated or evolved; and in $\text{Al}\cdot\text{BaCl}_2$ and $\text{Ba}(\text{OH})_2\cdot 8(\text{H}_2\text{O})$ solutions, gases expanded and left traces of visible brownish to white films of precipitation (BaCO_3). All these reactions and products confirm the presence of highly compressed gases such as CO_2 .

(b) Salinity. Estimation of salinity (equivalent NaCl wt. %) was made in type I and type III inclusions which represent the bulk of the ore fluids. The results are shown in Table VI-5. First melting temperatures of ice as high as -21°C were recorded, but most range between -5° to -14°C , indicating that most of the saline solutions are aqueous NaCl brines, and salt content varied in these solutions. Other dissolved salts such as KCl or CaCl_2 appear in minor to negligible amounts.

The salinity range of the type I inclusions is between 5 to 15 wt. % NaCl , and that of type III between 12.2 to 20.2 wt. %. Type III inclusions

TABLE VI-5

Salinity and Filling Temperature Data of Fluid Inclusions in Quartz,
Thompson Creek Deposit

Sample	Mineral	Inclusion Type	No. of Freezing Runs*	Freezing T°C	NaCl Wt. % equiv.	No. of Filling Runs*	Filling T°C
7-95	Q	P-I	1 (1)	- 9.00	12.8	1 (1)	230
		P-III	1 (2)	- 9.90	13.8	1 (2)	252
24-304	Q	P-I	1 (2)	- 6.75	10.3	2 (1)	201
		P-III	1 (5)	- 8.40	12.3	1 (2)	299
							305
25-462.5	Q	P-I	1 (3)	- 3.30	5.4	2 (1)	201~206
		P-III	2 (1)	- 8.40	12.2	1 (3)	296
							323
							345
572-2	Q	P-I	2 (2)	- 7.80	11.4	2 (3)	198
		PS-III	2 (3)	-16.60	20.2		201.5~206
572-3	Q	P-I	1 (2)	- 8.30	12.2	2 (1)	210
572-4	Q	P-I	2 (1)	- 7.00	14.9	1 (1)	230
		P-III	2 (1)	-13.40	17.2	1 (2)	286

* Number in parentheses: number of inclusions tested.

have high salinity than type I inclusions in the same mineral.

(c) Filling Temperatures. Filling temperatures were measured on the same inclusions after each freezing experiment. Repeated runs on the same inclusions indicate an experimental error of 3° to 5°C. The results are given in Table VI-5. Pressure correction to be applied to the filling temperatures is about 10°C based on a pressure of 100 to 170 bars estimated for immiscible CO₂-H₂O type III fluids (see later section).

Since type I inclusions probably represent fluids that trapped only one of the two immiscible phases, their filling temperatures are probably true depositional temperatures subjected to pressure correction; on the other hand, type III inclusions represent fluids that trapped both liquid and gas and therefore would give maximum depositional temperatures (Smith and Litter, 1959; Roedder, 1967; Kelly and Turneaure, 1970). The most probable range of temperatures for type I inclusions are 210° to 240°C, and that for type III inclusions about 230° to 320°C.

(d) CO₂ Contents. Measurements of volumes of liquid CO₂, vapor bubble and the inclusions have been made in type III inclusions at around 15°C and weight percents of CO₂ are estimated from these volume measurements by using Fig. VI-1. The results are given in Table VI-6. The crude estimate of overall CO₂ concentration in the original fluids would be about 4.4 wt. % or 1.9 mole percent.

(e) Fluid Densities. Density estimates were made for type I inclusions and the results are shown in Table VI-7. Estimates by the data of Ellis and Golding (1963) and of Haas (1971) agree well, while those by the data of Lemmlein and Klevtsov (1961) are lower.

The ore fluids were evidently moderately dense aqueous brines of densities between 0.89 to 0.94 gm/cc at temperatures around 210° to 240°C.

TABLE VI-6

Volumes and Concentrations of CO₂ in Fluid Inclusions from Thompson Creek Quartz

Type III Inclusions	Volume % of Liquid CO ₂	Volume % of Vapor Bubble	Weight % of CO ₂ in Inclusions	% of Type III Inclusion	Overall Weight % of Immiscible CO ₂
572-4	15.2	7.1	19.0	20	3.8
24-304	13.6	1.9	16.4	20	3.3
25-462.5 #1	32.8	0.2	32.0	20	6.2
#2	28.7	5.2	30.0		
Mean					4.4

TABLE VI-7

Fluid Densities of Type I Inclusions in
Quartz, Thompson Creek Deposit

Sample	Density			Corrected Temperatures (°C)
	(1)	(2)	(3)	
7-95	0.91	0.92	0.83	240
24-304	0.93	0.94	0.86	210
25-462.5	0.89	0.89	0.86	214
572-2	0.93	0.94	0.86	210
572-3	0.93	0.94	0.85	220
572-4	0.92	0.94	0.83	240
Mean	0.92	0.93	0.85	222

(1) Ellis and Golding (1963)

(2) Haas (1971)

(3) Lemmlein and Klevtsov (1961)

Liquid CO₂ in the inclusions generally homogenize in the temperature range of 7° to 18°C, corresponding to densities of liquid CO₂ of 0.88 gm/cc and to those of gaseous CO₂ of 0.15 to 0.17 gm/cc. Corresponding CO₂ pressures are then between 41 to 53.8 bars (Fig. VI-4).

3. Discussion

Apparent immiscibility, as indicated by the occurrence of type I with type III and sometimes type II inclusions, can be caused by one of the following three critical phenomena:

- (i) cooling of supercritical fluids of varied density,
- (ii) entrapment of a dense CO₂-rich fluid and a dense water-rich fluid coexisting in a heterogeneous system of immiscible fluids,
- (iii) entrapment of aqueous brine and coexisting steam in a "boiling" system with some CO₂ content.

The first case, cooling or condensation of supercritical fluids, can be ruled out on the ground of moderately high salinity in the inclusion fluids; according to data of Sourirajan and Kennedy (1962), critical temperatures of the inclusion fluids with 5 to 20 wt. % NaCl would be 425° to 600°C; these are far above critical for even pure water in the pressure range 100~170 bars and above the filling temperatures of fluid inclusions in the Thompson Creek quartz.

As a consequence of cooling of supercritical fluids, there should be inclusions with filling degrees of all intergradations; the very rare occurrence of type I inclusions with critical filling degree (i.e. about 55 vol. %) cannot be logically explained by supercritical entrapment when other type I, type II and type III inclusions are quite common.

Roedder and Coombs (1967) suggest that boiling of a pure NaCl brine would cause fluid immiscibility and would grade imperceptibly into immiscibility in a CO₂-rich system with increasing CO₂ pressures. If CO₂ pressures as estimated from fluid inclusions are low, entrapment of immiscible CO₂-H₂O fluids in a heterogeneous system can generally be dismissed as a potential cause of fluid immiscibility (Kelly and Turneaure, 1970).

The CO₂ pressures estimated from homogenization temperatures of liquid CO₂ in type III inclusions are about 41 to 53.8 bars using data given by Amagat (1892). The relatively high CO₂ pressures in these inclusions could be the reason for immiscibility in a heterogeneous CO₂-H₂O system. It is possible that boiling of aqueous brines under moderately high CO₂ pressures is the main cause of the inclusion fluid immiscibility observed.

Evidence of boiling also comes from a comparison of confining pressures and vapor pressures estimated for type I and type III inclusions. The approximate confining pressure for NaCl-H₂O system is estimated to be 105 bars (corresponding to a water depth of 917 meters) from Fig. VI-3 using an average density of 0.93 and average salinity of about 10 wt. % NaCl. For NaCl-CO₂-H₂O system, confining pressures can be estimated by the intersection of isochores of salinity and gaseous CO₂ density (Fig. VI-5) at an average temperature of 290°C for type III inclusions. Pressures range between 150 and 170 bars (corresponding to 1310 and 1485 meters of water depth). Thus the most probable range of confining pressures is between 100 and 170 bars. On the other hand, vapor pressures in NaCl-CO₂-H₂O system can be estimated from type III inclusions using experimental data of Takeuchi and Kennedy (1965b). At 12.7 wt.% NaCl, T° = 290~300°C, and 4.4 wt. % CO₂ vapor pressure in NaCl-CO₂-H₂O system is estimated

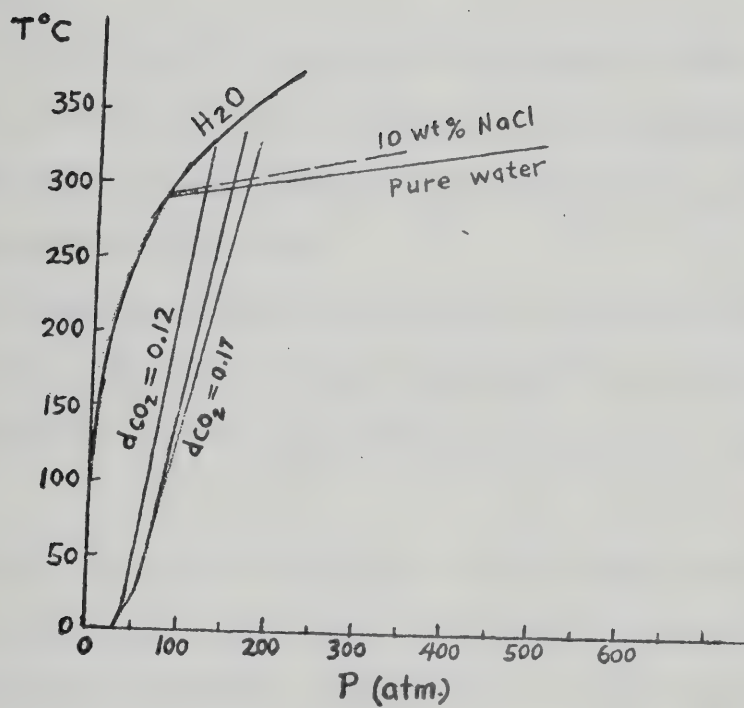


Fig. VI-5. P-T diagram for H₂O-CO₂-NaCl (modified after Kolfun, 1965; Groves and Solomon, 1969).

to be about 320 bars. Thus vapor pressure in the original fluids was evidently higher than confining pressure, and the fluids would have boiled before reaching the seafloor. It follows that the ore deposit was probably formed by open space-filling or replacement in the buried sediments below the seafloor.

Changes in conditions or properties of ore fluids during boiling and ore deposition can be seen from a comparison of fluid salinity, density and temperature data in type I and type III inclusions (Fig. VI-6). The following observations can be made:

(i) At higher temperatures ($\sim 300^{\circ}\text{C}$), ore fluids were moderately high saline brines of varied densities (moderately low to moderately high, from 0.81 to 0.92 gm/cc), the vapor phase separated at this stage was of low density.

(ii) The ore fluids were boiled in a system under relatively high CO_2 pressures; salinity declines to 10 wt. % NaCl or less as temperature declines to just above 200°C as a consequence of cooling caused most probably by active boiling and heat conduction to wall rocks, the ore fluids at this stage were considerably denser (0.89 to 0.94 gm/cc).

(iii) In inclusions that trapped both immiscible fluids, fluid densities vary sharply with temperature and salinity, indicating possibly greater fluctuation in conditions and properties of ore fluids during active boiling.

The Thompson Creek ore zone occurs as two to three thin bands or layers following sedimentary bedding; later deformation (folding and faulting) affected both the ore bands and surrounding sediments. If the ores were formed as epigenetic or diagenetic replacement of the sediments as a consequence of boiling, they must have been transported as chloride

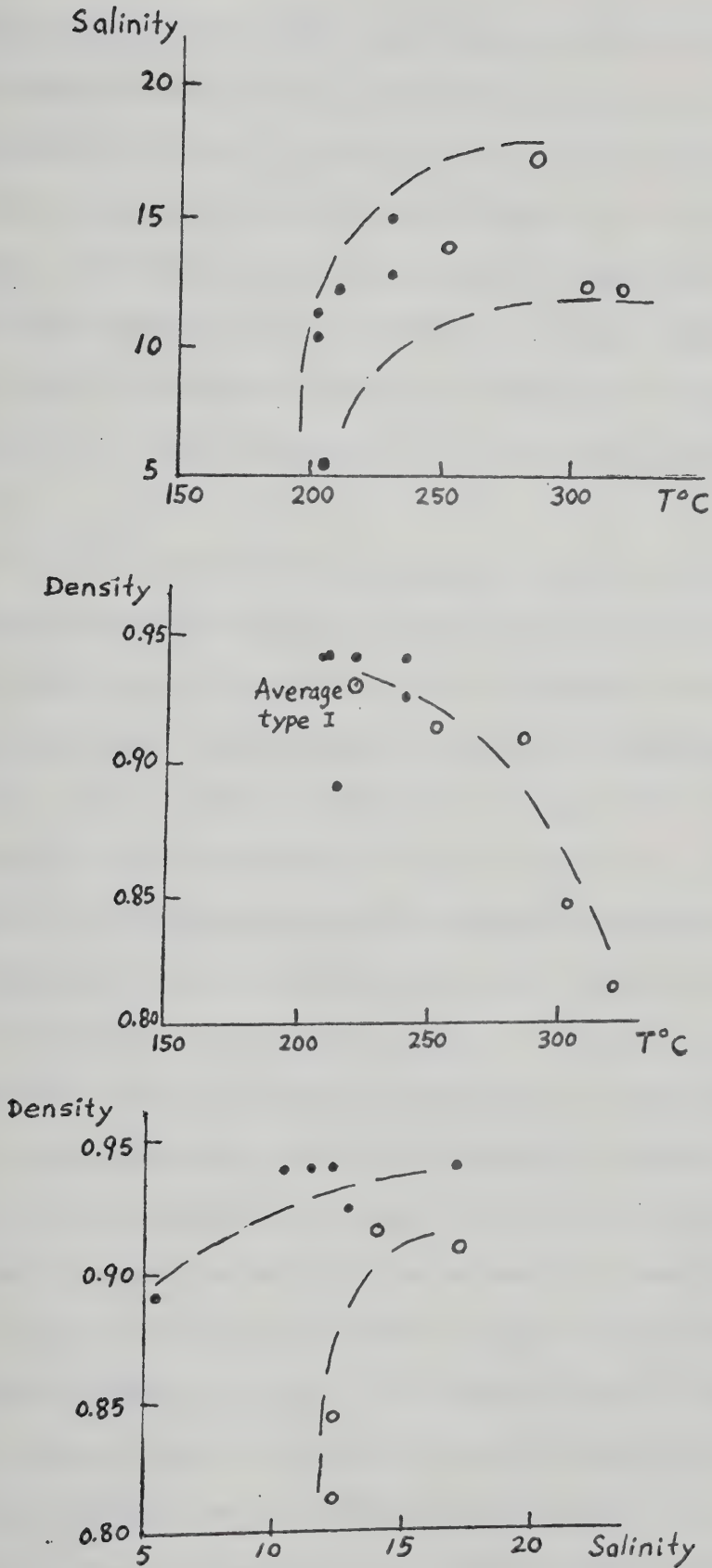


Fig. VI-6. Correlation of salinity, density and temperature data of fluid inclusions in Thompson Creek minerals. Solid circles: type I; open circles: type III.

ion complexes and reached the semi-consolidated sediments or open space in rocks in which sulfur was being generated in place or was being brought in from a different source. The small size of the ore deposit implies either an immature cessation of boiling or a termination in sulfur generation or supply. If the amount of open space was filled before boiling had ceased, the vapor pressure would rise and the remaining liquid would cease to boil until and if the vapor pressure was sufficient to rerupture the overlying rocks or to allow connection to be made with other open fracture systems.

The ore fluids were probably deep-seated in origin, heated or "metamorphic" formation waters derived from leaching of and circulation through sedimentary rocks (volcanic sediments, shale, limestone, sandstone) during late stage (epigenetic ?) hydrothermal activity in a deep basin. As will be shown later, sulfur isotope compositions of iron sulfides in country rocks and oxygen isotope compositions of quartz in the ores suggest that sulfur was mainly acquired at the site of deposition whereas the fluid (water) was probably heated formation or pore water derived from the meta-sediments or volcanics in the adjacent region. The site at which ore fluids boiled (i.e. ore deposition) was probably at a shallow depth below the seafloor, since asymptotic decline of diagenetic sulfide dissolved in pore fluids of marine sediments with depths of burial is generally sharp and the sulfur originally buried with the sediments is insignificant in quantity as compared with dissolved sulfide in pore fluids (Goldhaber, 1974). At greater depths, it is most difficult to acquire enough in situ sulfur for ore deposition unless a simultaneous or coincidental flux of sulfur-bearing solutions from a different source is available. If this reasoning holds, then the time-space relationship of the ore deposition and country rocks in the Thompson Creek deposit must have been very close

and in the strict sense it was formed as a diagenetic ~ epigenetic, strata-bound replacement orebody in deep sea environment.

E. HOWARD'S PASS DISTRICT

An attempt was made to examine and study fluid inclusions in ore or gangue minerals from the district. However, due to the extremely fine-grain size of most of the minerals, only a few fibrous calcite patches were found to contain inclusions suitable for optical examination. These calcite patches generally occur as remobilized to contorted bands in the ore-forming siltstones.

Three polished plates of calcite were found to be suitable for fluid inclusion study. In addition, chips of calcite from the other 3 specimens were examined in a crushing stage under the microscope.

1. Types of Inclusions (cf. Plate VI-4)

Inclusion type found in the calcite plates consists almost entirely of type I liquid-rich inclusions. Filling degree of these inclusion is high, generally around 90~95 vol. %, and only rarely 70 vol. %. A lot of inclusions can be readily identified as primary or pseudosecondary on the basis of their occurrence within growth layers or twins of calcite host. Secondary inclusions are also abundant but they generally occur along cleavages or in crosscutting healed fractures.

Crushing of some calcite chips reveals inconclusively small amount of compressed gases (?) contained in the fluid inclusions; and in only a few inclusions, a phase other than ice was suspected to form upon warming up from freezing; and it is tentatively believed to be a CO₂ hydrate. A few inclusions also show a very faint brownish tint (?) around vapor

bubbles indicating some sort of hydrocarbon such as methane (?). All the above observations are not conclusive because of the cloudiness of the calcite and the very small size of the inclusions.

Freezing behavior of most of the inclusions is normal for NaCl-bearing solutions, with ice being the only phase formed above about -21°C . Other dissolved salts are therefore insignificant.

2. Results

(a) Salinity and Filling Temperatures. Estimation of equivalent NaCl wt. % and filling temperatures was made on type I inclusions. The results are reported in Table VI-8. First melting temperatures are between -6.5 to -12.5°C , but temperatures as low as -14.5°C have been observed.

Two distinct features of salinity in calcite of different occurrences can be observed. Samples 34-330 and A-T-11 are fibrous calcite patches associated with finely laminated to disseminated ore-bearing calcareous siltstone, whereas sample SL-14 is a highly sheared calcite occurring in a cross-fault containing remobilized pods of coarsely crystallized galena and pyrite. Salinity of the former two samples ranges between 9.8 to 13.8 wt. % NaCl (average: 11.5 wt. %), whereas that of the latter is only 4.2 wt. % NaCl. It is believed that the sheared calcite with associated re-crystallized galena and pyrite reflects the ultimate tectonic deformation of the ore-bearing sequence (see Chapter IV).

Filling of inclusion fluids takes place in the liquid phase, and the filling temperatures recorded have a uniform range of 155° to 181°C , with an average of 166°C . A few inclusions appear to have homogenized at temperature as low as 145°C , but the final disappearance of vapor phases could not be ascertained due to overall obscurity of these inclusions.

TABLE VI-8

Salinity, Filling Temperature and Density Data of Fluid Inclusions in Calcite,
Howard's Pass District

Sample	Inclusion Type	No. of Freezing Runs*	Freezing T°C	NaCl Wt. % equiv.	No. of Filling Runs*	Filling T°C
34-330	P-I	2 (2)	-6.50	9.8	2 (1)	163
	PS-I	1 (1)	-9.30	13.1	1 (1)	177
		2 (3)	-9.95	13.8	2 (5)	155
						155
Trench A-T-11	P-I	3 (7)	-7.88	11.5	2 (4)	155
						164
						172
						172
SL-14	P-I	2 (2)	-2.50	4.2	1 (3)	155
	-					155
						174
Mean						165

* Number in parentheses: number of inclusions tested.

These temperatures are probably the true depositional temperatures during the formation of calcite and presumably associated ore minerals. No pressure correction was made since it is negligibly small (see later section on pressure estimate).

(b) Fluid Densities. The densities of inclusion fluids were estimated for NaCl-H₂O system using the data of Ellis and Golding (1963), Haas (1971) and Lemmlein and Klevtsov (1961). The estimates are given in Table VI-9.

It is evident that fluid densities in calcite associated with thin bedded ore-bearing siltstones are generally higher (0.97 to 1.0) than the density in sheared calcite associated with remobilized-recrystallized sulfides (0.93). The original fluids during calcite and ore formation were probably dense, saline brines in the pore waters of marine sediments or formation waters migrated from other sites.

3. Discussion

No evidence of boiling has been detected in the inclusions. Confining hydrostatic pressure, neglecting lithostatic pressure, on the original solutions in marine sediments can be estimated from Fig. VI-3 using the experimental results of salinity, temperature and density, and a maximum estimate of 53 bars is thus obtained at density = 0.98 gm/cc, $T^{\circ}=170^{\circ}\text{C}$, and salinity ≥ 10 wt. % NaCl. This pressure corresponds to a depth of 464 m of overlying seawater. Vapor pressure of the fluids is estimated to be about 4.4~7.3 bars in a temperature range of $150^{\circ}\sim 170^{\circ}\text{C}$ and a salinity of 11.5 wt. % NaCl. Evidently no boiling occurred.

Rough estimate of water depth during ore-bearing siltstone sedimentation is about 200~400 meters (Morganti, 1975, personal communication).

TABLE VI-9

Density Estimate of Inclusions Fluids in
Calcite, Howard's Pass District

Sample	Inclusion Type	Densities (gm/cc)		
		(1)	(2)	(3)
34-330	P-I	0.96	0.97	0.91
	PS-I	0.98	1.00	0.91
A-T-11	P-I	0.98	0.98	0.91
		0.97	0.98	0.91
SL-14	P-I	0.93	0.93	0.91

(1) Ellis and Golding (1963)

(2) Haas (1971)

(3) Lemmlein and Klevtsov (1961)

Therefore the estimate of 464 meters must represent the maximum depth of seawater when ore formation in siltstone occurred.

It is of vital importance to understand the stage of calcite formation in relation to "ore brine" introduction in the sediments. Judging from the abundance of carbonates as detrital fractions in sediments and their apparent association with "dewatering" compaction cleavages in which abundant ore minerals are concentrated, the calcite minerals possibly represent detrital fractions incorporated or remobilized in the sediments under similar conditions and through similar fluid media as the ore minerals. Temperature estimates from sulfur isotope fractionation among sulfide minerals generally agree with the filling temperature range, indicating at least similar thermal condition under which calcites and sulfides were formed.

No distinct phase of hydrocarbon or organic matter was detected in the inclusions studied, even though carbonaceous matter was observed in most of the ore-bearing specimens investigated.

F. SUMMARY

Fluid inclusion studies of the hydrothermal minerals in ore deposits from Anvil Range, Frances Lake and Howard's Pass districts reveal important physico-chemical data for the fluid media in which ore deposition occurred.

The studies show that during massive ore deposition, Anvil ore fluid inclusions had a filling temperature range of 170-250°C, a salinity range of 2.3-9.2 wt. % NaCl, an immiscible CO₂ content of about 5 wt. %, and a density range of 0.8-0.9 gm/cc. Variation of density, salinity and temperature in the ore fluids responsible for Anvil deposits can be best interpreted in terms of mixing of discharging heated connate brines with seawater on the sea-floor before ore deposition occurred. Depositional or confining

hydrostatic pressure on the discharged ore fluids is estimated to have a minimum range of 45-140 bars and a maximum range of 120-300 bars, corresponding to a water depth of minimum 400-1230 meters or maximum 1048-2620 meters. Consideration of confining and vapor pressures at given temperatures and salinities indicates that boiling did not occur when the ascending hot brines were discharged and mixed with seawater and brine pool was formed on the sea-floor. Immiscible CO₂-rich and H₂O-rich fluids were likely to have been introduced during "late stage" sub-sea-floor metamorphism by either mixing of "juvenile" CO₂-rich fluid with "interstitial" aqueous brines or increasing concentration of CO₂ in late stage hydrothermal fluids.

Fluid inclusions in quartz from the Thompson Creek deposit display a filling temperature range of 198-345°C, a salinity range of 5-20 wt. % NaCl, a CO₂ concentration of 4.4 wt. %, and a density range of 0.81-0.94 gm/cc. The ascending ore fluids were moderately rich saline brines of varied densities at high temperatures (~300°C). These were boiled in a system under relatively high CO₂ pressures (41 to 53.8 bars) as salinity declined to 10 wt. % or less and temperature declined to just above 200°C due to cooling, and the density of the ore fluids rose to 0.89 ~ 0.94 gm/cc. Confining pressure was estimated to be between 100~170 bars, corresponding to 874~1485 meters of water depth. The deposit is interpreted to have formed by diagenetic-epigenetic stratabound replacement of the deep sea sediments as a consequence of boiling of the ore fluids.

Fluid inclusions in calcite from ore-bearing siltstone in the Howard's Pass district show that filling temperatures ranged between 155~181°C, averaging 165°C, salinities ranged from 4.2~13.8 wt. % NaCl, and fluid densities were between 0.93~1.0 gm/cc. Confining hydrostatic pressure

was probably around 50 bars and water depth during ore formation in siltstone was less than 464 meters.

PLATE VI-1

PHOTOMICROGRAPHS OF FLUID INCLUSIONS IN QUARTZ AND BARITE
(TRANSMITTED LIGHT)

Anvil Ore Deposits

Faro

A. 66E9-401 Quartz

Primary type I inclusions with small degree of filling.

B. 66E9-401 Quartz

Primary inclusions: a large type IV inclusion containing at least two birefringent unidentified daughter minerals (X) and type I inclusions; one inclusion contains an opaque flake of daughter mineral (hm: possibly hematite).

C. 66-22 305 Barite

Pseudosecondary (?) inclusions of type I and one type III inclusion containing a vapor phase (V), liquid CO₂ (L₁) and aqueous solution (L₂).

D. 67-4 460 Barite

Primary inclusion of type I with near critical degree of filling, some small type II gaseous inclusions (g) are in view but slightly out of focus.

E. 67-4 460 Barite

Primary inclusions of type I and type II gaseous inclusion (g).

F. 67-6 602 Barite

PII inclusions of abundant type I and an immiscible type III containing a vapor phase (V), liquid CO₂ (L₁) and aqueous solution (L₂). Filling temperatures of type III inclusions average around 270°C.

G. 67-6 602 Barite

Subrounded and faceted type I pseudosecondary inclusions; a dark rim in a faceted inclusion near center is an optical effect, not multiple fluid phases.

H. 70-6 249 Barite Vein

Primary type I inclusions with one type III inclusion near lower center. A large type IV multiphase inclusion near top contains a vapor phase (V), liquid phase and at least 3 daughter minerals (h: halite, s: sylvite ?, and hm: hematite).

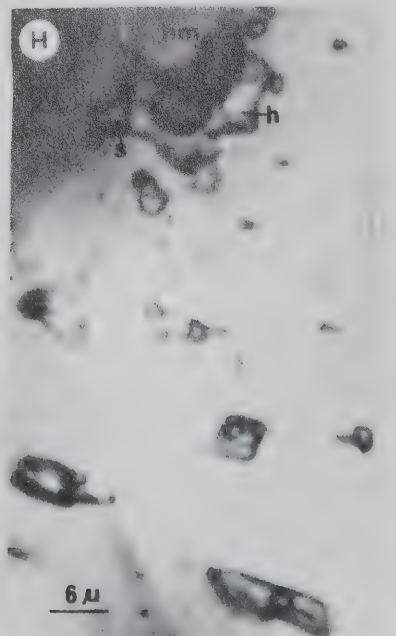
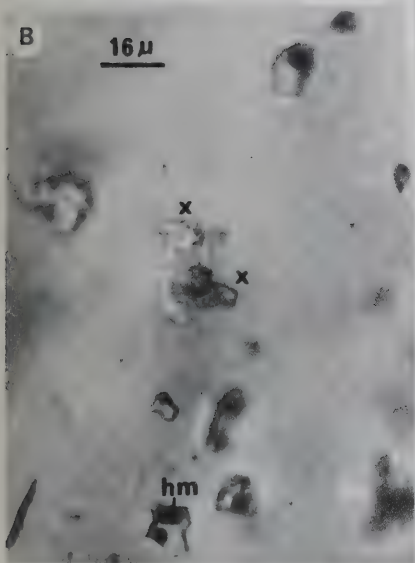
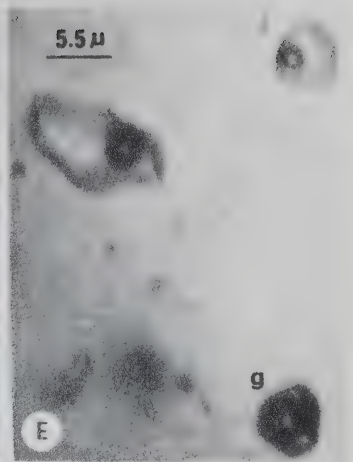
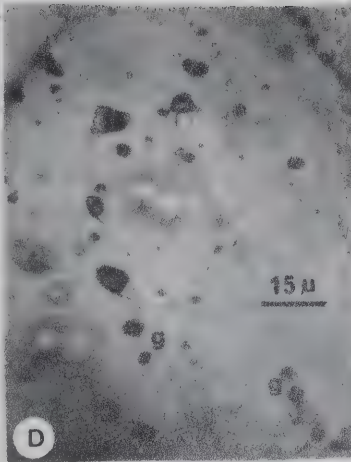
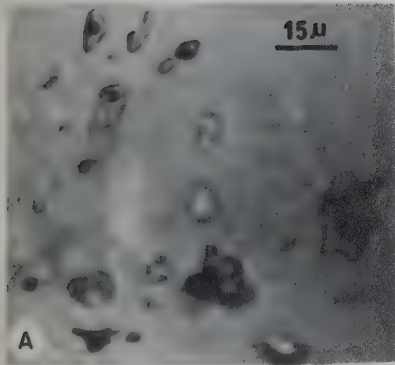


PLATE VI-2

PHOTOMICROGRAPHS OF FLUID INCLUSIONS IN BARITE AND QUARTZ
(TRANSMITTED LIGHT)

Anvil Ore Deposits

Swim Lakes

A. A4-296 Barite

Primary type I inclusion.

B. A4-296 Barite

PII type I inclusions and a type III inclusion (III) containing a vapor and two liquid phases (Liquid CO₂ and aqueous solution).

C. Swim 9 Barite

Coexistence of pseudosecondary type I and type III inclusions.

D. Swim 9 Barite

Type III CO₂-rich inclusions; in another area of the same specimen.

E. A4-457 Barite

Pseudosecondary type III inclusions.

F. A30-397 Quartz

Primary (?) type I (blurred, out of focus) and a type III inclusion with distinct annular ring.

Grum

G. A10-774 Barite Vein

Abundant primary type I inclusions; a solid inclusion of sphalerite near upper right. All inclusions homogenize at about 130°C.

H. A12-819 Quartz

Pseudosecondary type I inclusions; note smaller inclusions just below the plane of focus are aligned in an inclined plane and tapered out.

I. A12-819 Quartz

Primary type I inclusions.

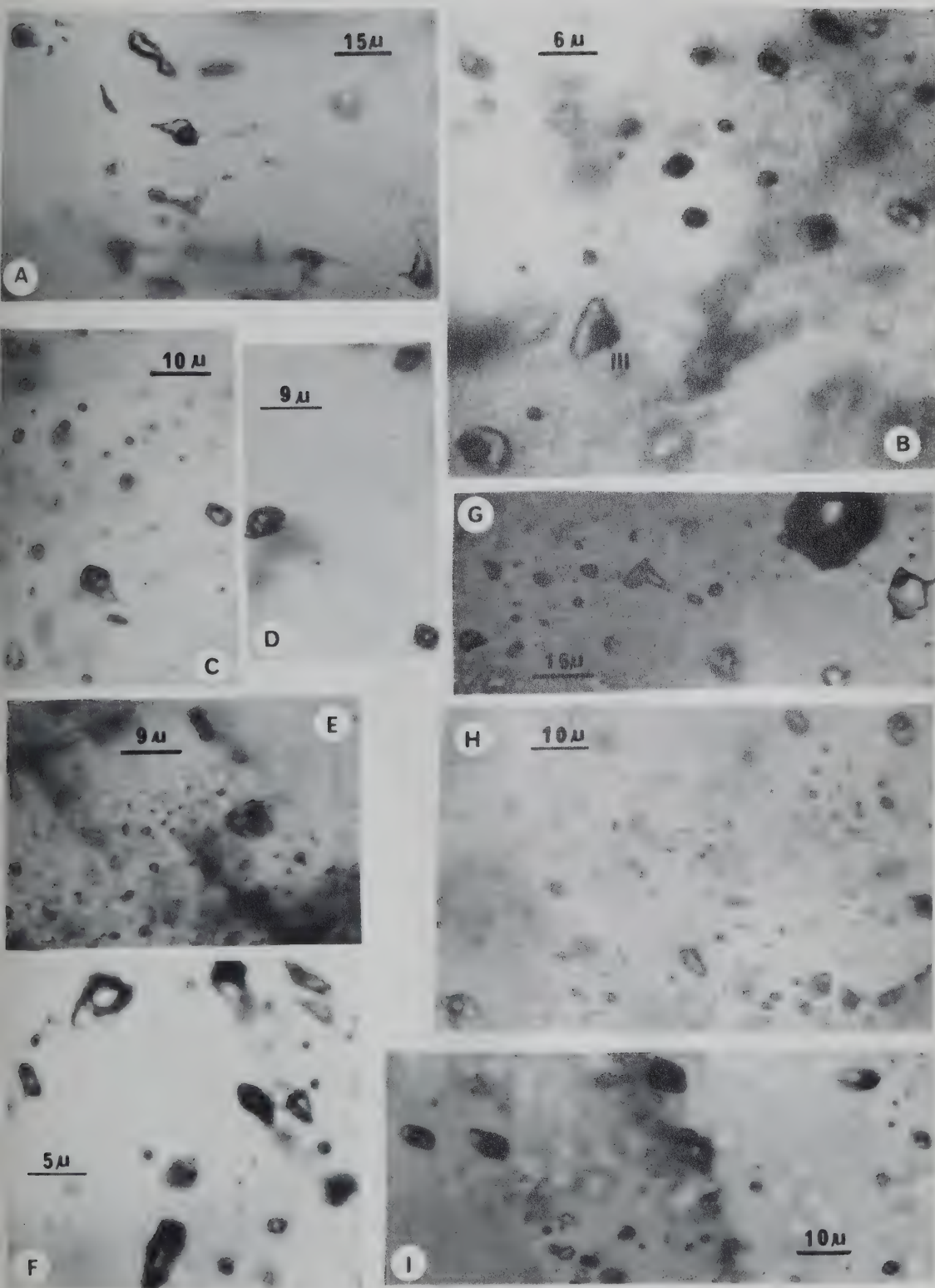


PLATE VI-3

PHOTOMICROGRAPHS OF FLUID INCLUSIONS IN QUARTZ
(TRANSMITTED LIGHT)

Thompson Creek Deposit

A. 7-95 Quartz

Primary inclusions of type I with near critical degree of filling and type IV containing a vapor and a daughter mineral, probably halite (h).

B. 7-95 Quartz

Primary type I inclusions and a type IV inclusion containing a vapor, liquid and a daughter mineral (h: halite).

C. 7-95 Quartz

Coexistence of primary type I (I), type III (III), and type II gas-rich (g) inclusions.

D. 24-304 Quartz

Occurrence of different types of primary inclusions: smaller type I inclusions; larger type II gas-rich inclusions (g); and larger type IV inclusions (IV) containing vapor, liquid and 2 daughter minerals (possibly halite and sylvite).

E. 24-304 Quartz

Primary type I inclusions.

F. 25-462.5 Quartz

A large apparent 2-phase liquid inclusion; on freezing, this inclusion shows an annular ring of liquid CO₂ and the inner vapor bubble expands on warming up.

G. 572-4 Quartz

Pseudosecondary type I inclusions.

H. 572-4 Quartz

Occurrence of primary type I and type III inclusions.

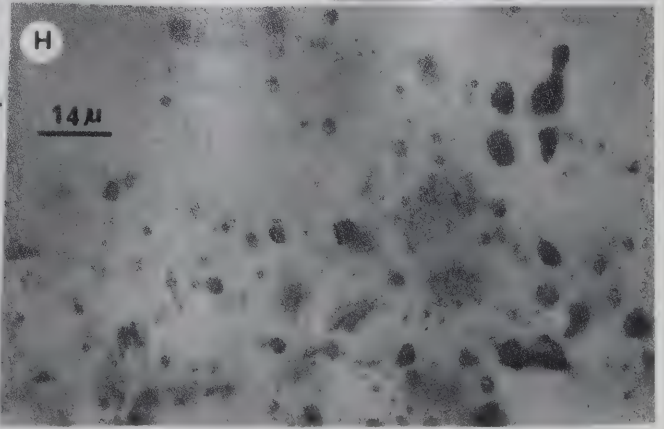
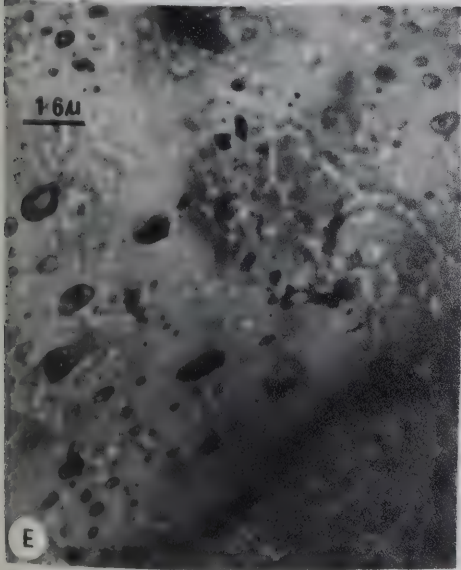
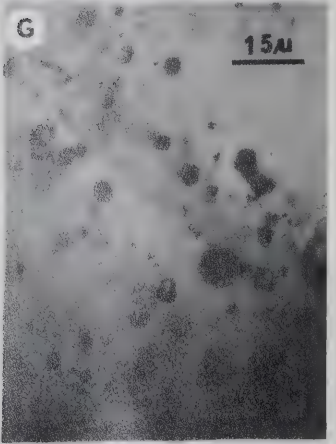
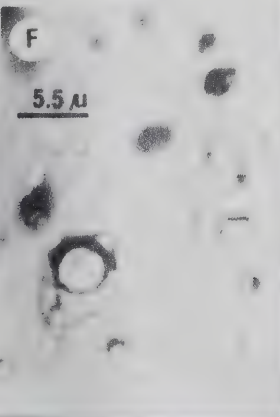
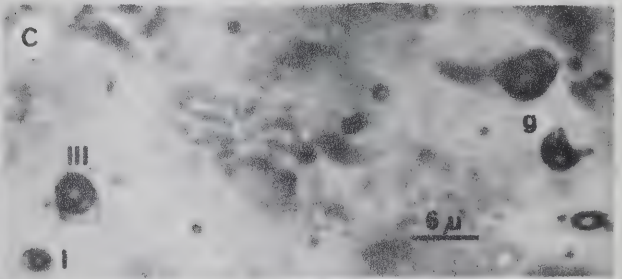
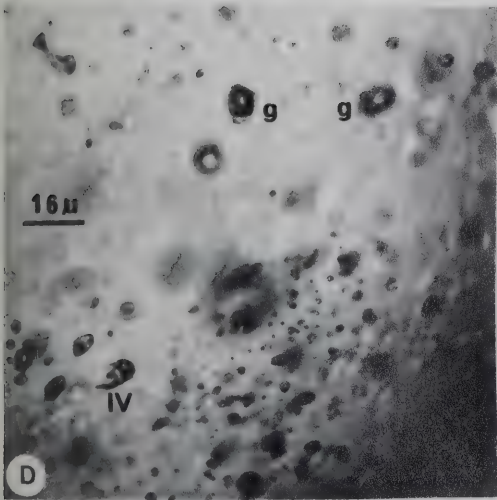
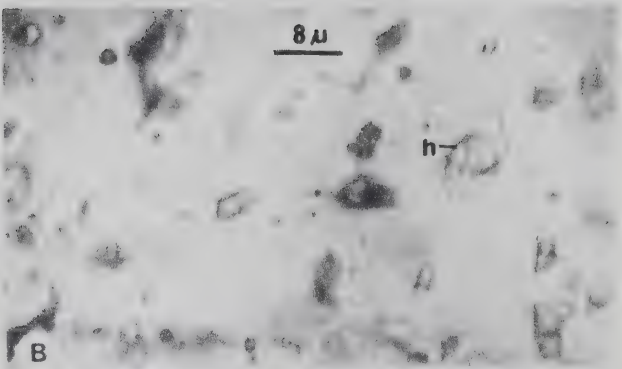
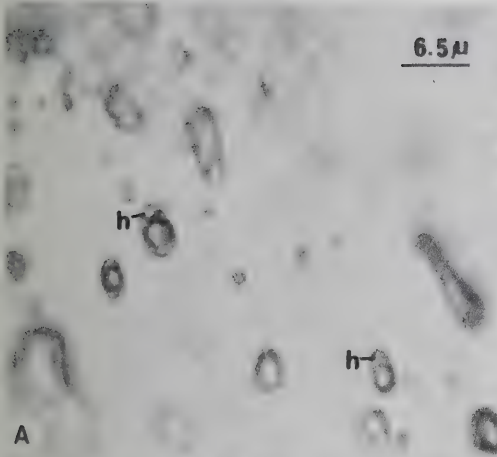
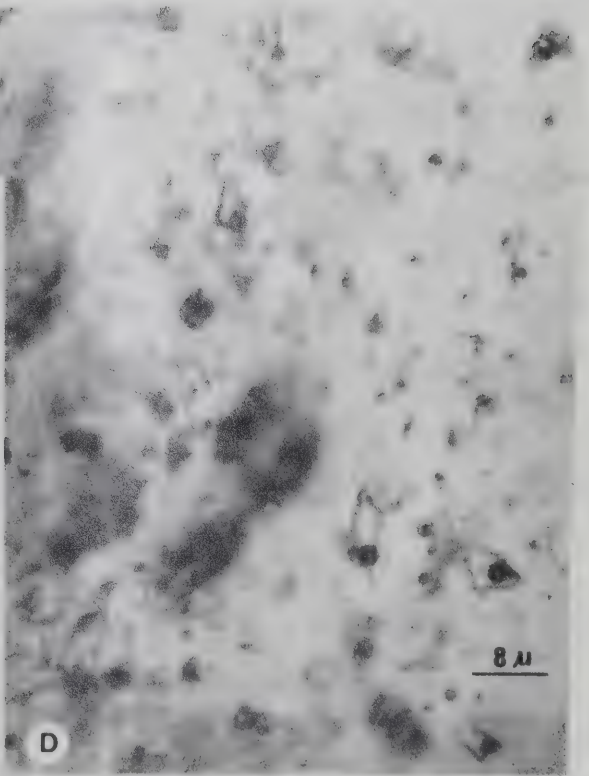
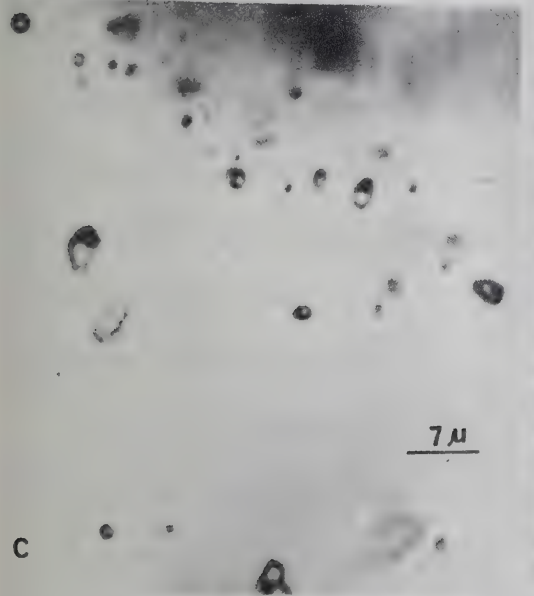
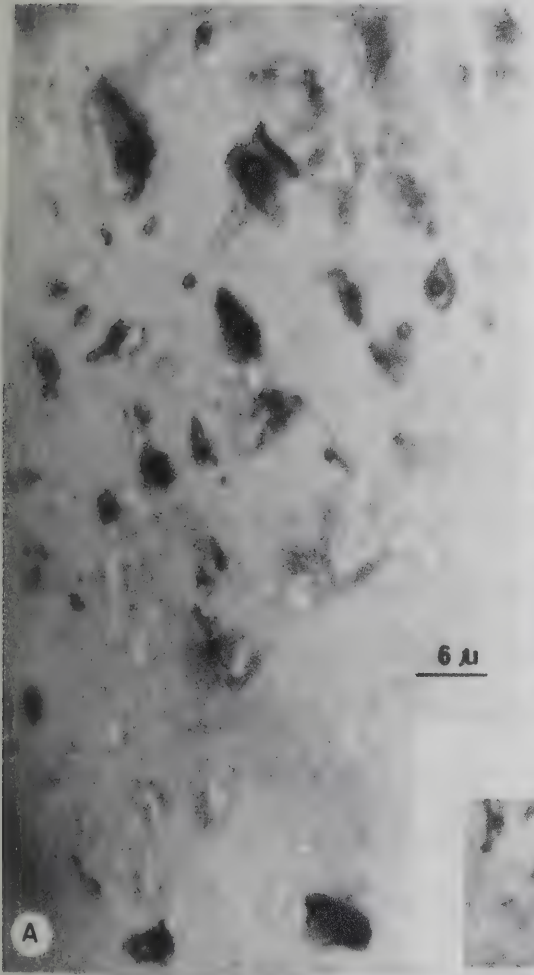


PLATE VI-4

PHOTOMICROGRAPHS OF FLUID INCLUSIONS IN CALCITE
(TRANSMITTED LIGHT)

Howard's Pass District

- A. 34-330 calcite. Primary type I inclusions, all within a single twin of calcite.
- B. 34-330 calcite. Primary type I inclusions occurring within growth layers (at left and right of photo).
- C. A-T-11 calcite. Abundant pseudosecondary type I inclusions within calcite grain.
- D. 34-330 calcite. Primary type I inclusions.



Chapter VII

ISOTOPE GEOCHEMISTRY OF ORE DEPOSITS

A. INTRODUCTION

In this chapter, isotope data of sulfur, oxygen and lead are presented for the deposits under study. It is hoped that through the study of isotope compositions of sulfide, sulfate and silicate minerals, some important aspects of the physico-chemical conditions and characteristics of ore formation may be better defined and understood. From the study of stable isotopes, one can obtain certain information concerning the geochemistry of ore solutions (temperature of ore formation, isotope compositions of ore solutions, concentration and types of dissolved sulfur species in ore solutions, pH and f_{O_2} variation during ore deposition, and possible source of sulfur, etc.). From the study of lead isotopes, one hopes to achieve a better understanding of the source material for the lead in the ores and/or rocks, age of ore mineralization, and if anomalous lead patterns are distinct, cause and process of mixing of lead isotopes.

Sulfur and lead isotope compositions in ore sulfides and/or sulfates and rock sulfides have been determined for Anvil Range district, Frances Lake district and Howard's Pass district. In addition, oxygen isotope compositions in quartz from Thompson Creek deposit, Frances Lake district, have also been determined.

Due to the extensive nature of this study, only a brief review of the background information on principles, experiments and systematics of pertinent isotope studies is presented. The readers are referred to the relevant literature for detailed accounts of these matters.

B. STUDY OF STABLE ISOTOPES

1. General Statement

(a) Sulfur Isotopes. Four stable isotopes of sulfur vary in their natural abundance as follows: $S^{32} = 95.1\%$, $S^{33} = 0.74\%$, $S^{34} = 4.2\%$, and $S^{36} = 0.02\%$. However, the ratio S^{34}/S^{32} in nature has been found to vary as much as $\pm 15\%$. Since in the troilite phase of meteorites the S^{34}/S^{32} variation is very small and varies only $\pm 0.015\%$ from a ratio of 0.0450045 (McNamara and Thode, 1950; Ault and Jensen, 1963), the variation is conveniently expressed by δS^{34} units as:

$$\delta S^{34}_{\text{sample}} (\%) = \frac{(S^{34}/S^{32})_{\text{sample}} - (S^{34}/S^{32})_{\text{Troilite standard}}}{(S^{34}/S^{32})_{\text{Troilite standard}}} \times 1000$$

i.e., all calculations in S^{34} composition are made with respect to the standard troilite, commonly taken as that from the Cañon Diablo meteorite, and expressed in parts per thousand (‰).

The literature on the application of sulfur isotopes to problems of ore genesis is very extensive; among the earliest works we can cite Kulp et al. (1956), Vinogradov et al. (1956), Jensen (1957, 1959), Tupper (1960) and Stanton (1960). Before the work by Sakai (1968) and subsequent advances by Ohmoto (1970, 1972), Kajiwarra (1971) and Rye and Ohmoto (1974), the "traditional" system of interpreting and understanding the sulfur isotope data has been based largely on empirical discrimination of the range of the data and comparison with the pre-existing body of data, although the significance of source of ore solutions and fractionation processes on the isotopic variations had been noted (Nakai and Jensen, 1964; Tatsumi, 1965; Puchelt, 1967; Jensen, 1967). Since Sakai's work, understanding of sulfur isotope fractionations among sulfides, sulfates and aqueous sulfur ions under equilibrium conditions has been greatly

enhanced by both theoretical and experimental works of many workers, including Bachinski (1969), Grootenboer and Schwartz (1969), Kajiwar et al. (1969), Kajiwar and Krouse (1971), Rye and Czamanske (1969), Czamanske and Rye (1974), Puchelt and Kullerud (1969), Schiller et al. (1970) and Kiyosu (1973). The agreement among the various experimental data are, however, not satisfactory, and experimental data for the isotope fractionation factors between sulfide minerals and aqueous sulfur ions are few, although Ohmoto (1972) has summarized the isotope fractionation factors between aqueous H_2S and other sulfide minerals and aqueous sulfur species (HS^- , $S^{=}$, $SO_4^{=}$) as functions of temperatures. The new advances made by Sakai, Ohmoto, Kajiwar and Rye are the vigorous application of thermochemistry of aqueous solutions such as temperature, pH, f_{O_2} , ionic strength, total dissolved sulfur to the interpretation of isotope data and to the quantitative estimate of sulfur isotope composition of total dissolved sulfur in ore solutions ($\delta S_{\Sigma S}^{34}$). The basis of their contributions is the recognition of large isotope fractionations among various aqueous sulfur species, particularly between oxidized and reduced forms of sulfur, in hydrothermal solutions under chemical and isotopic equilibrium conditions.

Parallel to these advances, works of Sasaki (1970), Sasaki and Kajiwar (1971), Sangster (1968, 1971), Sakai et al. (1970) have contributed to a better understanding of the role of seawater sulfates in many hydrothermal-sedimentary ore deposits and pointed to possible isotope exchange equilibrium conditions of sulfate-sulfide in some deposits.

(b) Oxygen Isotopes. Oxygen is the most abundant element of the earth's crust; it is composed of three stable isotopes: O^{16} , O^{17} and O^{18} . The relative abundance of these isotopes in air oxygen is 99.759:0.0374:0.2039, respectively (Nier, 1950). O^{18}/O^{16} ratio in nature may

vary by as much as 10%, or from 1:475 to 1:525. The isotope ratio in an oxygen-bearing sample is reported by δO^{18} units as:

$$\delta O^{18}_{\text{sample}} (\%) = \frac{(O^{18}/O^{16})_{\text{sample}} - (O^{18}/O^{16})_{\text{standard-SMOW}}}{(O^{18}/O^{16})_{\text{stand.-SMOW}}} \times 1000$$

Thus, the oxygen isotope data are reported with respect to the most convenient standard - ocean water. A particular set of ocean water values, designated Standard Mean Ocean Water (SMOW) by Craig (1961) is the most common standard in present-day use.

Since H_2O is the dominant constituent of ore fluids, a knowledge of its origin is fundamental to any theory of ore formation. The ultimate source of the H_2O can only be revealed by studying some geochemical parameter based on the water molecules themselves. Oxygen isotope analyses provide such a parameter because natural waters of various origins exhibit systematic differences in their O^{18} (as well as deuterium) contents. The oxygen isotope compositions of natural fluids can be approximated by either direct measurement of the fluid itself in a geothermal area or of fluid inclusions in the minerals of an ore deposit, or by isotope analysis of minerals and calculation of O^{18}/O^{16} ratios of waters in equilibrium with the minerals at their temperature of formation.

The application of oxygen isotope data to problems of ore deposits and natural hydrothermal fluids is extensive in the literature. Early works in this field include Clayton and Epstein (1958), Craig et al. (1956), Craig (1963) and James and Clayton (1962).

2. Experiments and Calibrations

(a) Mineral Separation and Purification. Separation of pure mineral phases of galena, sphalerite, pyrite, barite and quartz was made by means

of conventional procedures using heavy liquid gravitational separation (methylene tetrabromide and methylene iodide), and a Franz magnetic separator. The purity of all mineral separates was checked under a binocular microscope; impure separates were further purified by means of preferential chemical dissolution procedure developed by the writer (see Appendix VII-1). For all fine-grained mineral separates such as those of Howard's Pass district, this procedure was generally applied prior to any extraction or collection of gasses.

The purity of all mineral separates after these procedures was generally greater than 95%, some approaching 100% purity.

(b) Conversion to Ag₂S. Barite samples were reduced in a boiling reducing mixture (HI-HNO₃-H₃PO₄) under an N₂ atmosphere. The generated H₂S gas was allowed to bubble through distilled water and react with Cd-acetate solution to form a CdS precipitate. The bubbling rate was carefully controlled to 2 bubbles/second. Each reduction took 30 minutes to one hour. The CdS precipitate was collected, converted to Ag₂S by adding 0.1 m Ag(NO₃)₂ solution, and boiled for at least 10 minutes. The Ag₂S was then recovered in a teflon-filter cup by rinsing with concentrated NH₄OH and distilled water. The cup was dried in an electric oven at about 100°C for 12 hours and Ag₂S was carefully collected for SO₂ combustion.

Some fine-grained separates with impurity were boiled in different concentrations of HCl solution with SiC or metallic Sn chips as a reducing agent (see Appendix VII-1). The generated H₂S was converted to CdS and Ag₂S in a manner similar to the procedure described above.

Isotope analyses of SO₂ gasses derived from direct combustion and combustion subsequent to Ag₂S conversion of some commercial grade sulfides

agree very well (see later section on Howard's Pass district) and thus the procedure of acid decomposition and H_2S generation did not produce any detectable isotope fractionation.

(c) Collection of SO_2 Gasses. Combustion and collection of SO_2 gas from pure sulfides were made in a quartz-pyrex extraction line in the Stable Isotope Laboratory, Dept. of Geology. The line consists essentially of a quartz tube combustion chamber, pyrex tube vacuum line with three cold traps, two thermocouples, diffusion pump, mechanical pump and breakseals. Cu_2O (Fisher reagent grade), pre-heated to 300°C in vacuum to remove traces of CO_2 and other impure gasses, was used in the combustion as an oxygen donor. The pure sulfide and Cu_2O were ground, weighed and mixed (in a fixed O/S ratio*) in an agate mortar and the mixture was packed between quartz wool in a small (OD: 0.8 cm), open-ended quartz tube. The sample was put into the quartz chamber which was then evacuated and heated to more than 1000°C and as high as 1100°C . Upon combustion (generally 10 minutes, some required up to 20 minutes), the evolved SO_2 and other trace gasses such as CO_2 were trapped with liquid nitrogen in the second cold trap while H_2O was trapped separately with a cryogenic mixture of carbon tetrachloride-chloroform-dry ice in the first cold trap. Any excess oxygen was pumped off. CO_2 was allowed to expand and pumped off when the SO_2 was frozen back in the second cold trap by a mixture of n-pentane (ethanol) and liquid nitrogen held at approximately -120°C . The SO_2 was then allowed to expand and be trapped in a graduated column again; upon isolation and expansion of SO_2 gas, the yield measurement was recorded. The SO_2 was then transferred into a standard breakseal and collected.

*A molar ratio of O/S of 4:1 (or in excess) was used in combustion of ZnS , PbS , FeS_2 and Ag_2S .

(d) Calibration of Standards. Calibration of isotope composition of working line standard (Fisher reagent grade SO₂ gas) against the compositions of other SO₂ artificial standards with well-known or well-calibrated δS^{34} values with respect to Cañon Diablo troilite was made prior to, in between, and after each period of isotope analyses on the mass spectrometer. Using this procedure, all the other corrections such as oxygen factor correction (from Cu₂O), machine factor, etc. can be internally eliminated.

Three calibration runs were made during the course of mass spectrometer measurements: Oct. - Dec. 1974, May 1975 and June 1975. The results of these calibrations are listed in Table VII-1 together with the derived correction formulae. The results indicate that the calibrated sulfur isotope compositions of all standards analyzed agree very well to within experimental errors.

(e) Mass Spectrometer Measurement. The isotope analyses were performed on a 12" radius of curvature, 90° sector magnetic-analyzer (Nier, 1947; McKinney et al., 1950) gas source mass spectrometer in the Dept. of Physics, University of Alberta. The mass spectrometer is equipped for alternate introduction of SO₂ gas and simultaneous collection of mass 64 ($S^{32}O_2^{16}$) and mass 66 ($S^{34}O_2^{16}$) through ionization by a tungsten filament. The ratio was measured by a voltmeter and a frequency converter and processed and printed by a built-in computer. Normally 4 sets of mass 66/mass 64 ratio (or mass 46/mass 44 in the case of CO₂ gas) were recorded for each alternate SO₂ gas (line standard, sample or other artificial standard). The computer printed out the average mass 66/mass 64 ratio of the sample versus that of the line standard after 9 recordings of alternate gas introductions were made.

Breakseals containing SO₂ gasses can be connected to the vacuum line of the gas inlet system of the mass spectrometer through Cajon vacuum-tight fitting joints.

TABLE VII-1

Calibration of Mass Spectrometer SO₂ Line Standard Against Other Artificial SO₂ Standards,
1974 ~ 1975

Standards	Average δS^{34} (Versus Line Standard)			Calculated δS^{34} (Versus Cañon Diablo Troilite		
	Oct.-Dec. 1974*	May 1975**	June 1975**	Oct.-Dec. 1974	May 1975	June 1975
NBS #120 (native sulfur)	- 2.63 (11)*** ± .08	- 0.94 (6) ± .10	- 0.85 (6) ± .13	1.45	1.54	1.68
NBS #200 (Ivigtut Pbs)	- 3.29 (11) ± .06	- 1.58 (5) ± .06	- 1.43 (5) ± .07	0.68	0.80	1.03
Troilite (Mayerthorp, Peace River)	- 3.21 (4) ± .06	- 1.51 (2) ± .04	-	0.79	0.88	-
ZnS (Pine Point)	15.86 (1)	16.53 (2) ± .04	-	21.75	21.63	-
PbS (commercial grade)	- 8.88 (2) ± .05	- 7.74 (6) ± .12	- 7.67 (6) ± .08	- 5.73	- 6.28	- 5.90
BaSO ₄ "merck" (commercial grade)	- 1.46 (10) ± .13	0.00 (1)	-	2.81	2.62	-
Pine Creek NW (sour gas)	16.40 (1)	18.15 (2) ± .10	18.89 ± .05	23.49	23.49	23.68
W. Drumheller (sour gas)	5.20 (1)	7.05 (1)	6.90 (3) ± .14	10.52	10.73	10.32
Ag ₂ S (McMaster Standard)	- 8.50 (3)	- 6.87 (2) ± .14	-	- 5.34	- 5.27	-
V-18 189 ZnS (Vangorda)	7.74 (2) ± .05	-	9.71 (5) ± .06	13.46	-	13.44
10-174.5 Pbs (Frances Lake)	6.03 (2) ± .07	-	7.78 (1)	11.48	-	11.30

* Calibrated by S.W. Burnie, S.L. Kuo and R. Haverslew. $\delta S^{34}_{CDT} = 1.158 \delta S^{34}_{X-LS} + 4.5$

** Calibrated by S.L. Kuo. $\delta S^{34}_{CDT} = 1.1498 \delta S^{34}_{X-LS} + 2.62$ (for May, 1975); $\delta S^{34}_{CDT} = 1.1148 \delta S^{34}_{X-LS} + 2.622$ (for June, 1975).

*** Numbers in parentheses indicate numbers of standard measurements.

(f) Collection of CO₂ Gasses. Purified quartz samples were dried overnight in a "dry box" under N₂ atmosphere and placed in a stainless steel tubing attached to CO₂ extraction line. BrF₅ was introduced into the tubing after evacuation, and the decomposition of quartz was enhanced by heating to more than 500°C. The generated O₂ was then allowed to expand through a combusted pure graphite which produced CO₂ and was trapped with liquid nitrogen in a cold trap. Yield measurement was recorded and CO₂ was transferred to a breakseal and collected.

The mass spectrometric measurement was made on the same mass spectrometer as for SO₂ except for the using of a commercial CO₂ standard. The calibration of the CO₂ line standard against other artificial standards was made by P. Thompson and J. Gray of the Dept. of Physics. The results are listed in Table VII-2.

From a plot of $\delta_{\text{L.S.}}^{46}$ versus $\delta_{\text{SMOW}}^{46}$, $\delta_{\text{x-SMOW}}^{46}$ ($\delta_{\text{SMOW}}^{46}$ of samples) can be obtained. Since fractionation factor between CO₂ and H₂O for the reaction* $\text{H}_2\text{O} + \text{CO}_2 \rightarrow \text{H}_2\text{CO}_3 \rightarrow \text{HCO}_3^- + \text{H}^+$ at 25°C can be described as:
 $\alpha_{\text{W}} = (\text{O}^{18}/\text{O}^{16})_{\text{CO}_2} / (\text{O}^{18}/\text{O}^{16})_{\text{H}_2\text{O}} = 1.04075 \pm 0.00016$ (Bottinga and Craig, 1969), 40.75‰ should be added to $\delta_{\text{x-SMOW}}^{46}$ to obtain $\delta_{\text{x-SMOW}}^{18}$. For quartz-water system over temperature range of 200° to 500°C, the fractionation factor $1000 \ln \alpha_{\text{Q-W}} = 3.38 \times 10^6 \times T^{-2} - 3.40$ (Clayton et al., 1972) and $\alpha_{\text{Q-W}} = 1000 + \delta_{\text{Q}}^{18}/1000 + \delta_{\text{W}}^{18}$, where Q: quartz, W: water.

*Complete reactions are:

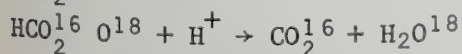
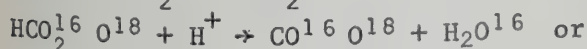
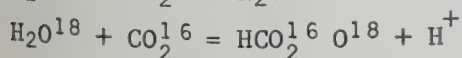
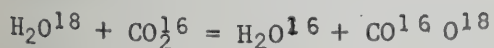


TABLE VII-2
Calibration of CO₂ Line Standard,
April 1975

Standard	$\delta^{46}_{\text{L.S.}} (\%)$	$\delta^{46}_{\text{SMOW}} (\%)$
SMOW	42.9	-
NBS1-A	17.9	-24
SLAP	-14.5	-55
Line Standard	-	- 1

$$\delta^{46} = \left[\frac{(C^{12}O^{18}O^{16}/C^{12}O^{16}O^{16})_x}{(C^{12}O^{18}O^{16}/C^{12}O^{16}O^{16})_s} - 1 \right] \times 1000$$

L.S. = line standard.

3. Anvil Range District

(a) Results. A total of 157 sulfur isotope analyses of sulfide, sulfate minerals and purified mill concentrates of PbS, ZnS and FeS₂ ("tail") was made. The samples analyzed represent a wide distribution in Faro and representative sections from Grum and Vangorda; samples from Swim Lakes represent sporadic sampling of three drill hole intersections. The data are believed to represent the full range and magnitude of sulfur isotope compositions of sulfide and sulfate minerals in the Anvil ore deposits.

The isotope data and calculated isotope fractionation temperatures are given in Table VII-3. The isotope fractionation factors used to calculate temperatures are based on the experimental data of Czamanske and Rye (1974) for sphalerite-galena pair, of Rye et al. (1974) for pyrite-galena pair, and of Sakai (1968) for barite-pyrite pair. The sulfur isotope fractionation between two sulfide or aqueous sulfur phases X and Y is presented as $\Delta\delta S_{X-Y}^{34}$ value, where

$$\Delta\delta S_{X-Y}^{34} = \delta S_X^{34} - \delta S_Y^{34} = 1000 \ln \alpha_{X-Y}$$

the fractionation factor α is defined as:

$$\alpha = \frac{(S^{34}/S^{32})_X}{(S^{34}/S^{32})_Y}$$

The isotope fractionation factors of sp-gn and py-gn pairs are:

$$1000 \ln \alpha_{sp-gn} = 7.0 \times 10^5 \times T(^{\circ}K)^{-2} \text{ (Czamanske and Rye, 1974)}$$

$$1000 \ln \alpha_{py-gn} = 9.3 \times 10^5 \times T(^{\circ}K)^{-2} \text{ (Rye et al., 1974)}$$

Isotope fractionation factor of barite-pyrite pair can be estimated from curves (Sakai, 1968) given in Fig. VII-2.

TABLE VII-3

Sulfur Isotope Compositions (δS^{34} in ‰) and Calculated Isotope Fractionation Temperatures of Minerals and Mill Concentrates from Anvil Ore Deposits, Yukon

Sample No.	Temperatures (°C)						
	Galena	Sphalerite	Pyrite	Barite	Δ_{Sp-Gn}	Δ_{Py-Gn}	Δ_{Brt-Py}
(Farø)							
66-2 283	14.5	17.4	16.9	30.6	236	349	470
342	-	14.2	14.5	27.5	-	-	-
400	12.6	15.3	15.0	28.2	236	349	490
474	7.9	10.4	11.1	-	256	266	-
486	9.3	12.0	11.6	-	246	363	-
66E9 299	-	19.5	19.9	31.1	-	-	-
337	9.4	12.1	12.4	-	236	284	-
376	11.7	14.0	13.8	-	279	392	-
401	11.6	14.1	14.4	-	256	303	-
436	13.0	15.0	15.1	-	319	392	-
66-10 573	16.2	-	-	-	-	-	-
634	8.6	11.1	11.6	24.9	256	284	480
66-22 305	14.6	17.1	18.2	29.9	256	235	530
67-4 460	11.6	14.3	15.0	-	236	250	-
593	12.0	14.9	15.1	-	218	275	-

TABLE VII-3 (cont'd)

Sample No.	Temperatures (°C)				
	Galena	Sphalerite	Pyrite	Barite	
					$\Delta_{\text{Sp-Gn}}$ $\Delta_{\text{Py-Gn}}$ $\Delta_{\text{Brt-Py}}$
67-6 602	14.9	17.2	17.9	31.6	279 284 470
667	8.6	11.0	11.5	-	267 293 -
710	10.8	13.5	14.1	27.7	236 258 470
754	14.3	16.9	17.7	-	246 250 -
790	13.0	15.2	13.2	-	291 - -
67-10 549	-	14.8	14.2	-	- - -
632	11.4	13.9	14.5	-	256 275 -
70-6 249	12.2	14.9	14.8	27.7	236 325 500
					254.8
(Mill concentrates)	(Pbs)	(Zns)	(FeS ₂)		
August, 1971	14.1	15.9	17.5		
July, 1972	14.0	15.1	-		
September, 1972	-	-	16.0		
April, 1973	13.7	15.0	15.9		
October, 1973	14.1	15.8	15.9		
May 1974	13.5	14.9	16.5		

Sample No.	Temperatures (°C)				
	Galena	Sphalerite	Pyrite	Barite	$\Delta_{\text{Sp-Gn}}$ $\Delta_{\text{Py-Gn}}$ $\Delta_{\text{Brt-Py}}$
(Vangorda)					
V18 114	-	14.6	15.3	-	
120	-	-	15.7	-	
189	-	13.5	13.6	-	
205	-	-	14.5	-	
V33 279	15.2	17.7	17.9	-	256 313
V35 153	-	-	14.3	-	
V60 180 #1	11.8	14.2	14.3	-	267 337
#2	-	14.0	14.1	-	
V63 135	-	14.2	14.8	-	
143	-	14.1	14.8	-	
223	-	-	13.5	-	
(Swim Lakes)					
A26 516	-	-	12.8	-	
A29 179	-	-	19.9	-	
A30 397	14.3	17.0	17.5	-	236 266
Swim #9	-	16.0	16.4	36.8	330

TABLE VII-3 (cont'd)

Sample No.	Galena	Sphalerite	Pyrite	Barite	Temperatures (°C)		
					$\Delta_{\text{Sp-Gn}}$	$\Delta_{\text{Py-Gn}}$	$\Delta_{\text{Brt-Py}}$
(Grum)							
A10 514	-	18.1	18.3	-			
529	-	13.8	14.4	-			
575.5	12.8	15.8	16.7	-	210	215	
616	12.2	14.6	15.6	-	267	250	
647	-	-	14.5	-			
693	10.8	14.2	15.4	-	181	177	
744	15.6	17.9	18.5	-	279	293	
774	-	15.8	15.1	32.4			370
802A	21.0	23.3	21.7	-	291	-	
802B	-	-	23.9	-			
813	-	23.7	24.7	-			
A11 497	13.0	15.7	16.5	-	236	243	
503	14.2	16.8	17.9	-	246	228	
594	15.0	17.0	17.9	-	319	293	
A12 538	14.0	16.6	16.1	-	246	387	
A13 150	12.5	15.1	15.6	-	246	275	

The δS^{34} values of sulfide ores typically range between 7.9 to 19.9‰ for Faro (13.7 to 17.5‰ for Faro mill concentrates), 10.8 to 24.7‰ for Grum, 11.8 to 17.9‰ for Vangorda, and 14.3 to 19.9‰ for Swim Lakes; δS^{34} values of barites from these deposits range between 24.9 to 36.8‰. This variation is plotted in histograms as shown in Fig. VII-1.

(b) Sulfur Isotope Fractionation. Under chemical and isotopic equilibrium conditions sulfur isotope fractionation between coexisting sulfide minerals or aqueous sulfur ions has been theoretically predicted (Sakai, 1968; Bachinski, 1969) and experimentally confirmed (Kajiwara *et al.*, 1969; Kajiwara and Krouse, 1971; Rye and Czamanske, 1969; Czamanske and Rye, 1974; Grootenboer and Schwartz, 1969; Schiller *et al.*, 1970; and Kiyosu, 1973). The general trend of the fractionation among coexisting phases is temperature-dependent, decreasing as the temperature increases. The fractionations among important aqueous sulfur ions and sulfide minerals are shown in Fig. VII-2. It is evident that the larger the separation of the curves for any two minerals or aqueous ions, the more sensitive will the pair be as an isotopic geothermometer. The order of sensitivity of fractionations to temperature among mineral pairs is: sulfate-sulfide > pyrite-galena > sphalerite (or pyrrhotite)-galena > pyrite-chalcopryrite > pyrite-sphalerite. Also it is evident that δS^{34} values of coexisting sulfides at a given temperature under equilibrium conditions should decrease in the following order: pyrite > sphalerite > chalcopryrite > galena.

The best criteria for achievement of equilibrium is that $\Delta\delta S^{34}$ values for different sulfide pairs (e.g. sphalerite-galena, pyrite-galena, or pyrite-sphalerite) give similar temperatures. If this ideal situation is not encountered, but any single pair gives consistent $\Delta\delta S^{34}$ values (and

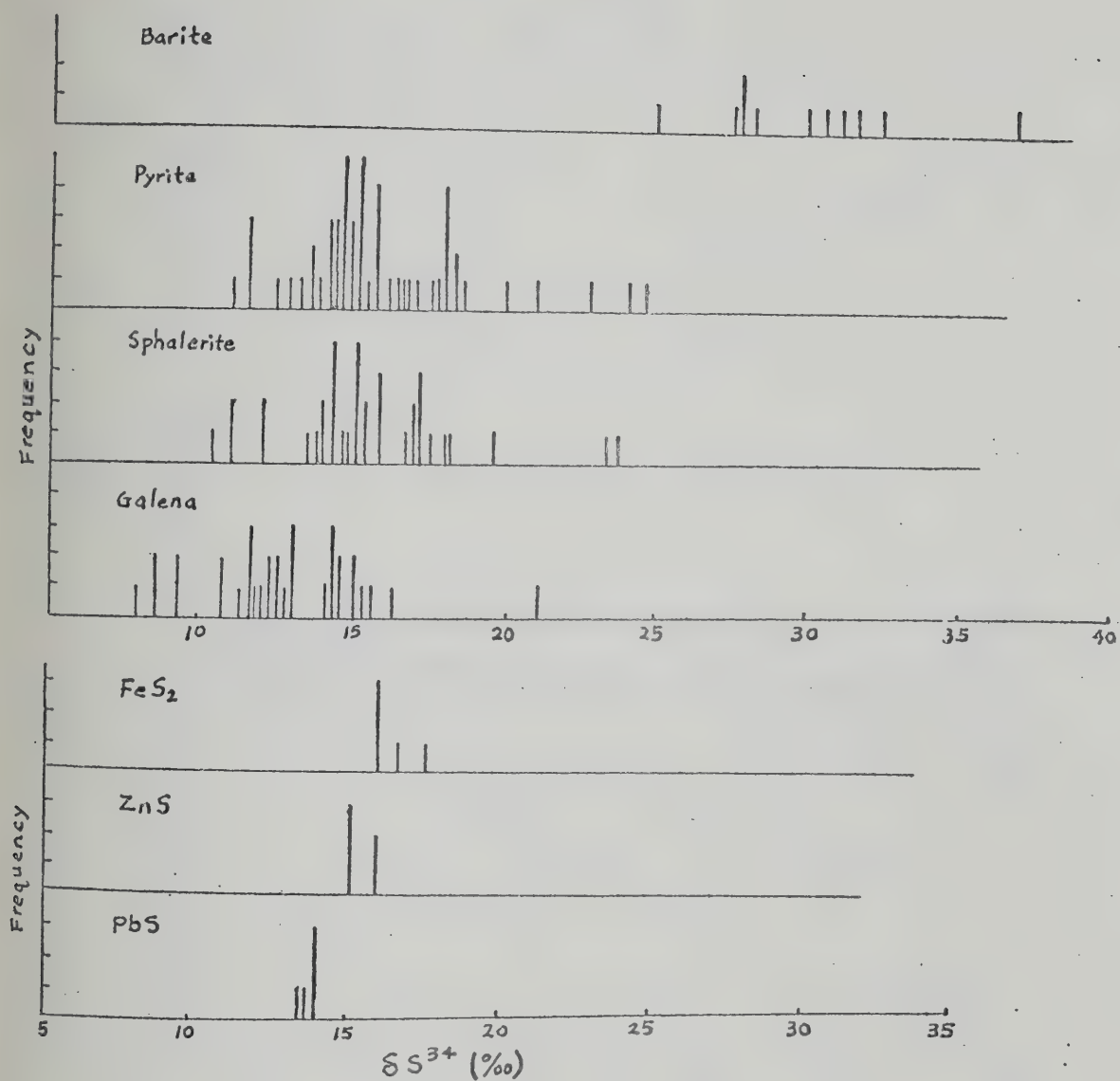


Fig. VII-1. Variation of sulfur isotope compositions in galena, sphalerite, pyrite, barite and mill concentrates from Anvil deposits.

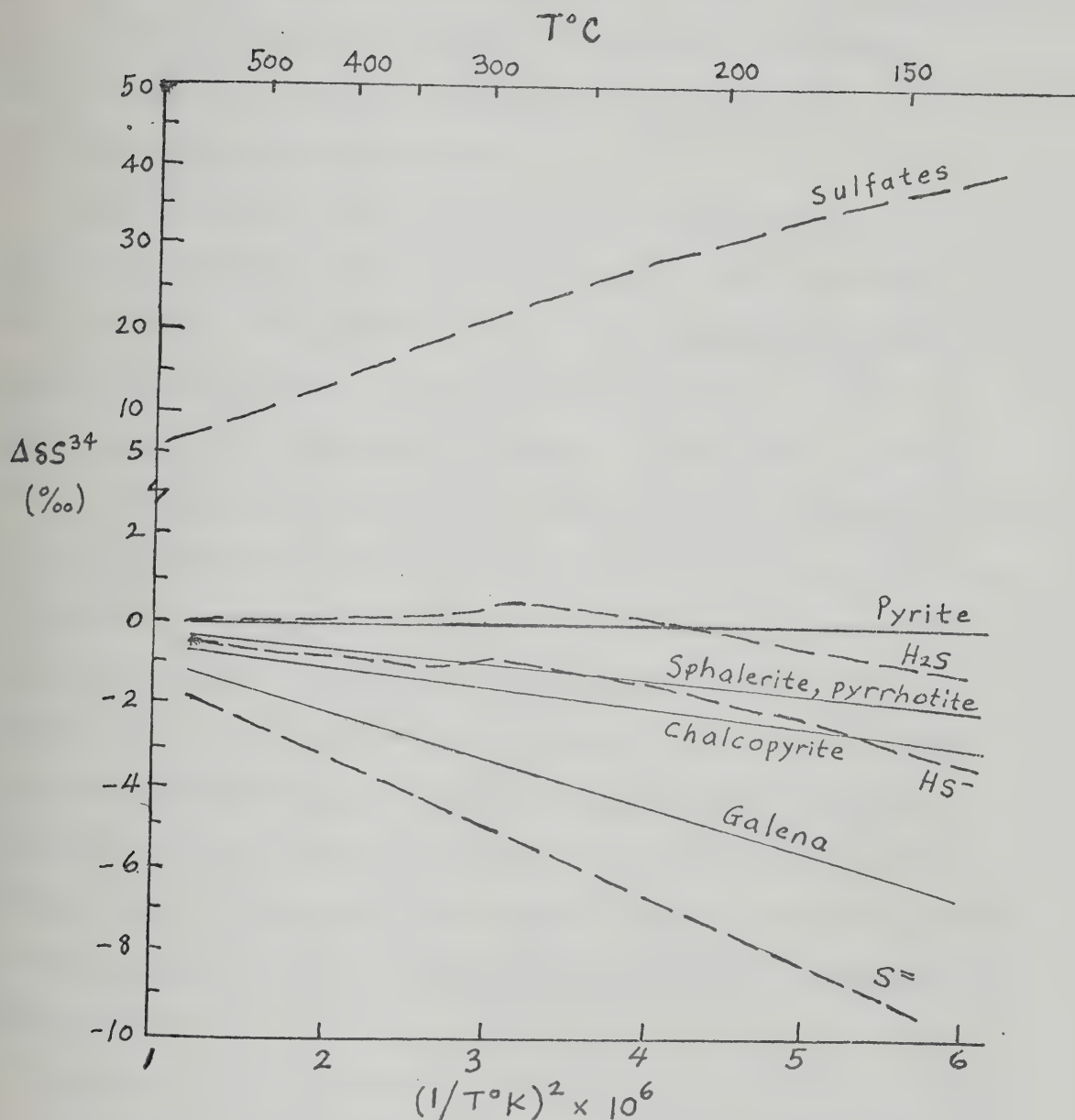


Fig. VII-2. Sulfur isotope fractionations among sulfur species and sulfide minerals plotted with respect to pyrite. Dashed lines indicate aqueous species, solid lines indicate minerals (after Rye and Ohmoto, 1974).

thus temperatures), then isotopic equilibrium may have been approached for this particular pair. Conversely, evidence for disequilibrium or other factors in the system can be predicted when δS^{34} values do not follow the above enrichment pattern.

The temperatures estimated from sulfur isotope fractionation between sphalerite and galena in the Anvil deposits fall in the range of 218° to 319°C for Faro, 181° to 319°C for Grum, 256~267°C for Vangorda, and 236°C for Swim Lakes. Temperatures estimated from the fractionation between pyrite and galena are, except for some pairs, consistent with sphalerite-galena temperatures. The exception is apparently due to the fact that pyrite tends to precipitate over a much larger part of the ore paragenesis than galena, and thus allows a greater chance of formation under different conditions or from different solutions (Rye and Ohmoto, 1974). However, the majority of the pyrites have δS^{34} values larger than coexisting sphalerite and galena and yield pyrite-galena temperatures in the range 177° to 313°C (average 264°C). The overall S^{34} enrichment in pyrite over sphalerite and galena can also be detected in mill concentrates of Faro Mine which represent a good average of the ore minerals.

Therefore, it is concluded that most pyrite was in isotopic equilibrium with sphalerite and galena and apparently with solutions which were uniform in temperature and chemical states (e.g. pH, f_{O_2} and $\delta S_{\Sigma S}^{34}$, etc.).

On the other hand, large isotope fractionation can also be seen between barite and sulfide minerals. Barite is quite common in the Anvil ore deposits and occupies 0.3 ~ 0.68 wt. % of the deposits (Chapter VI). The sulfur isotope fractionation between barite and pyrite is generally in the order of 11 ~ 17‰, but can be as high as 20‰ (Swim #9).

The isotope fractionation between sulfate and sulfide at elevated temperatures in nature has been the subject of controversy and uncertainty exists as to the cause and mechanism of fractionation (e.g. Sasaki, 1970; Sasaki and Kajiware, 1971). Fractionation between aqueous sulfate and other sulfide ions under complete isotope exchange equilibrium condition has been considered theoretically by Sakai (1957, 1968) from 25° to 500°C. However, estimated equilibrium temperatures of the Anvil sulfate-sulfide mineral pairs are unacceptably high (330° ~ 530°C), indicating either the difficulty of attaining isotope exchange equilibrium or other effects operative during ore deposition. Rapid attainment of isotope exchange equilibrium between native sulfur and sulfuric acid at 300° ~ 350°C (Oana and Ishikawa, 1965) and between pyrite and sulfuric acid at 280°C (Nakai, 1967) have been experimentally demonstrated; however, these experiments were conducted under the presence of excess native sulfur which is not generally expected under natural hydrothermal conditions of ore formation. It is possible that the observed isotope fractionation is not the result of direct exchange between sulfate and sulfide but represents the exchange equilibrium between SO_4^{2-} and some intermediate form of sulfur compounds from which sulfides might have formed with little isotopic fractionation (Sasaki, 1970). Grinenko et al. (1969) and Malinin and Khitarov (1969) have shown by experiments that chemical (inorganic) reduction of aqueous sulfate to H_2S , SO_3^{2-} and $\text{S}_2\text{O}_3^{2-}$ under hydrothermal conditions (100° to 450°C) takes place significantly above 200~250°C, and is most intense at 275°C or higher. Isotope fractionation factor in this reduction is estimated to be about 11% at 210°C and 17% at about 130°C. As pointed out by Grinenko et al. (1969), in the slow chemical reduction of sulfate under natural conditions at hydrothermal temperatures, isotope

fractionation depends not only on the reaction kinetic effect but also on the rate of isotope exchange between reaction products (H_2S , SO_2) striving for isotope equilibrium. In this case, isotope equilibrium may be partly established between sulfate and H_2S , either because the intermediate product of the reaction SO_2 exchanges its sulfur with H_2S and sulfate, or because the reaction between H_2S and sulfate is reversible. Sasaki and Kajiwara (1971) have also emphasized that the isotope exchange equilibrium between sulfate and sulfide may be partially attained in most instances; they also noted the possibility that the observed fractionation between sulfate and sulfide could be the relict of equilibrium at higher temperatures.

The mean δS^{34} value of the Cambrian seawater sulfate is 29~30‰, and those of the Ordovician, 25~29‰ (Thode and Monster, 1965; Davies and Krouse, 1975; Chukrov et al., 1975). The δS^{34} values of barite samples from Anvil ore deposits are either equal to or heavier than these Cambro-Ordovician seawater sulfates. Enrichment of S^{34} in sulfate remaining in solution can be produced as a result of precipitation of lighter isotope S^{32} in sulfides in sediments in basins with relatively restricted circulation to the open sea (Sangster, 1971). The resultant sulfates would have δS^{34} values slightly greater than their contemporaneous open seawater sulfate. The δS^{34} values of Anvil barites lie between the inferred value for Cambro-Ordovician seawater sulfate and the theoretical values for sulfate in isotope equilibrium with sulfides at 250°C (= δS^{34} values of pyrite + 25‰). Alternatively, it is possible that the aqueous sulfate which had been partially equilibrated with H_2S during initial mixing of ascending ore solutions and seawater might mechanically be diluted by diffusion or circulation of overlying seawater sulfate before and/or dur-

ing the barite deposition at somewhat later stage under slightly higher pH and/or f_{O_2} conditions.

(c) Chemical Environment of Ore Deposition. It seems certain that Cambro-Ordovician seawater sulfate has played a major role in determining sulfur isotope compositions of sulfide ores in the Anvil deposits. Mixing of seawater with ascending ore solutions seems to be the most likely mechanism for fixing final sulfur isotope compositions. The mixing can take place in the following three ways:

(i) seawater-rock interaction on the seafloor under geothermal conditions,

(ii) discharging of ascending "juvenile" ore solutions onto the seafloor,

(iii) recharging of deeply circulated and heated seawater onto the seafloor (Spooner and Fyfe, 1973; Kajiwarara, 1973a, b).

In any case, we are concerned with the chemical environment at which mixing and ore deposition took place.

The temperatures of ore deposition, from studies of fluid inclusions and sulfur isotope fractionation, are generally between 200° to 250°C. From the stability fields of mineral assemblages like pyrite, galena, barite and sericite (muscovite) associated in the ores, we can define the probable pH and f_{O_2} region at the above temperatures (Fig. VII-3a and b). In these figures, we can see that areas bounded by A, B, C and D define the probable pH and f_{O_2} region during ore deposition; the region lies in the transitional zone between H_2S and total oxidized sulfur species ($SO_4^{=}$, $HSO_4^{=}$, $KSO_4^{=}$, $NaSO_4^{=}$). It is also noted that total sulfur in the ore solution is probably between 0.1 to 0.001 mole/kg H_2O since the pyrite and barite fields with this range of total sulfur content are stable within

Figure VII-3

Comparison of the mole fractions of aqueous sulfur species with the stability fields of Fe-S-O minerals and barite. Dashed and solid lines: mineral stability boundaries; dotted lines: aqueous species boundaries.

----: Mineral stability fields at $\Sigma S = 0.001$ moles/kg H_2O .

-- : Mineral stability fields at $\Sigma S = 0.1$ moles/kg H_2O .

The barite solubility boundaries are given for an assumed barium concentration of 0.001 mole and $m_{Ba^{++}} m_{\Sigma S} = 10^{-4}$ (Ohmoto, 1972; Kajiwara, 1971).

The stability field of muscovite (sericite) is given for $I = 1.0$ and $K^+ = 0.1$ mole and calculated from the data of Hemley (1959).

The stability boundaries of aqueous sulfur species are given for mole fractions of 0.5.

Kl: Kaolinite; Ms: Muscovite; Kf: K-feldspar

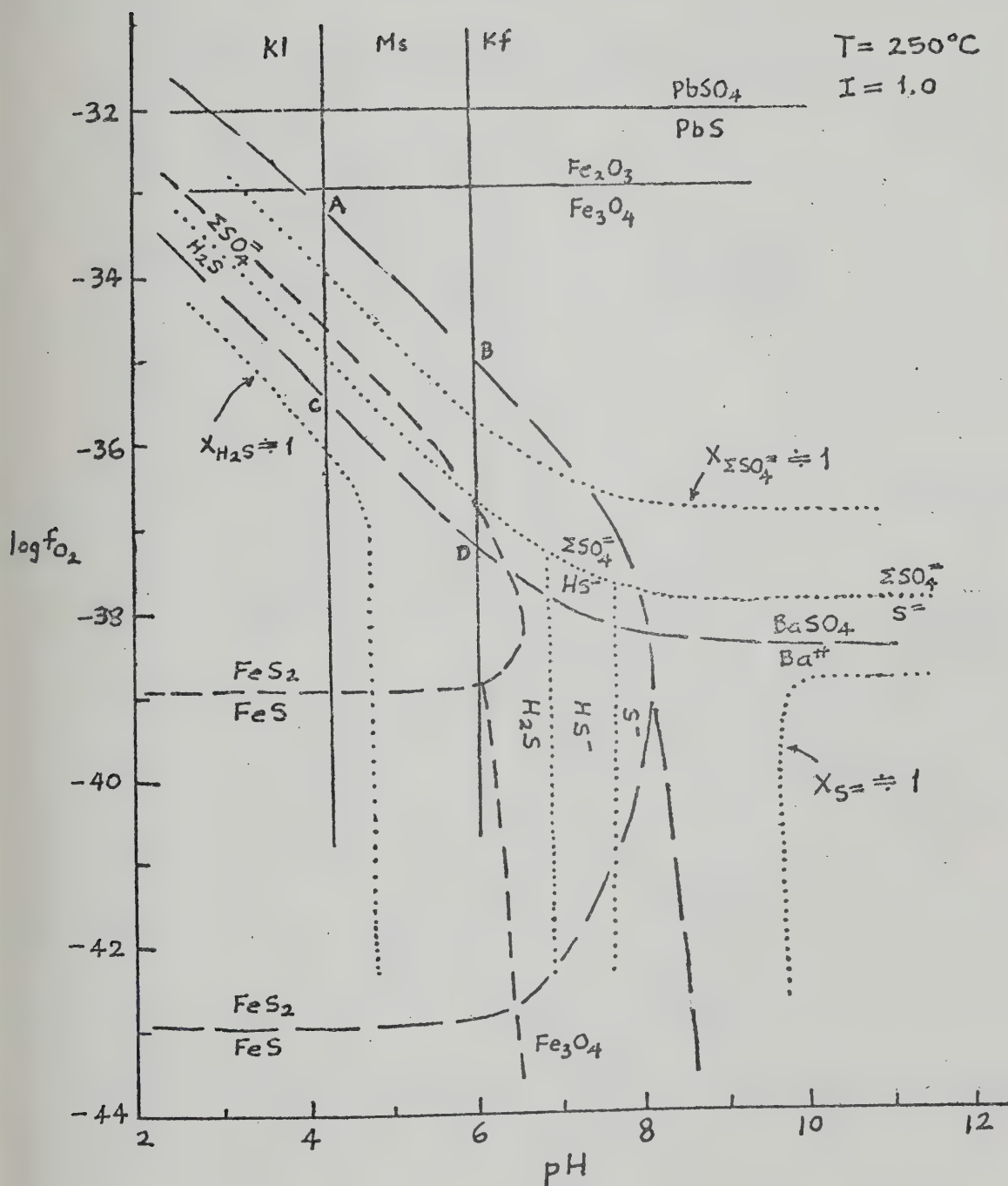


Fig. VII-3a.

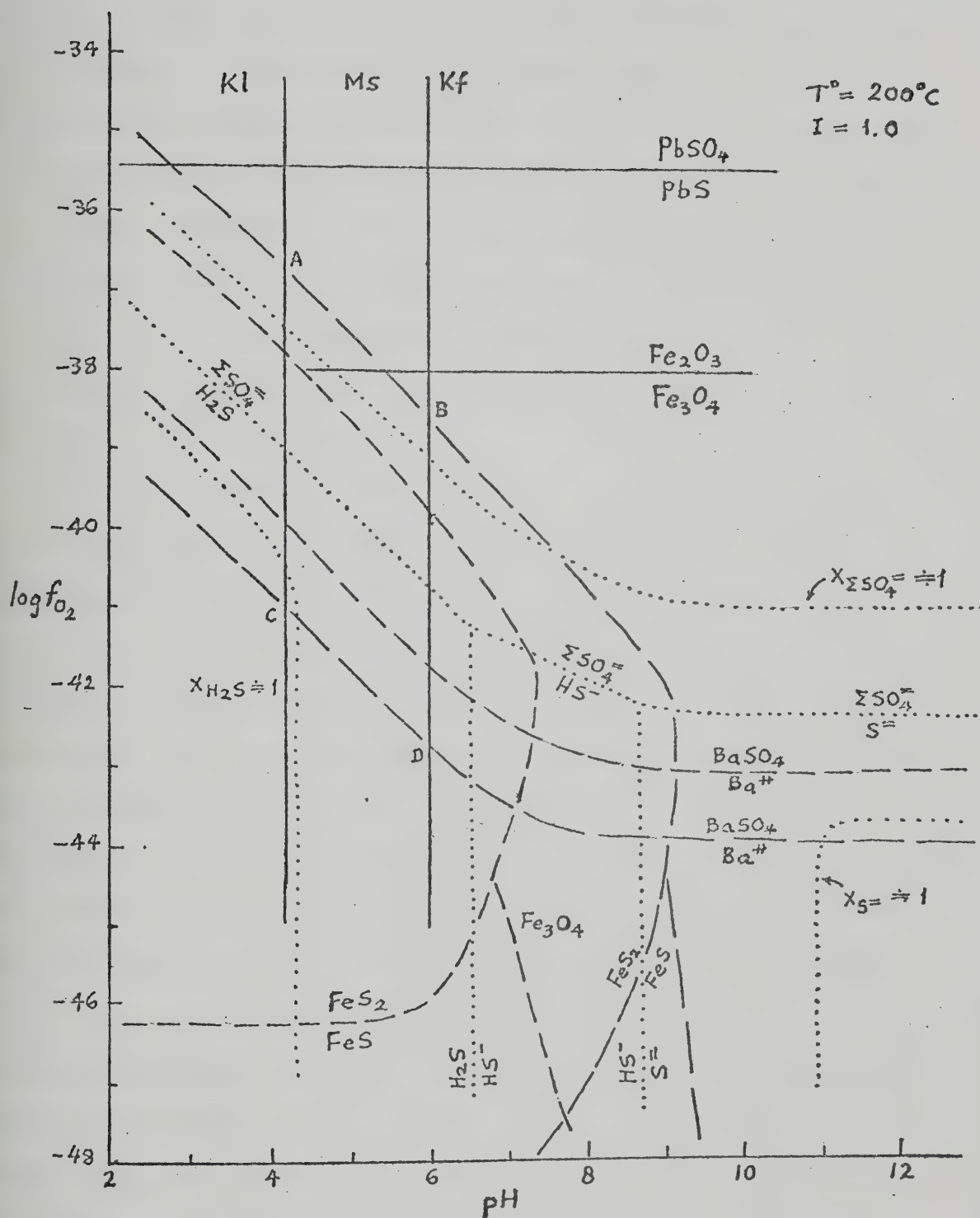


Fig. VII-3b.

the pH- f_{O_2} region. It will be shown later that a narrower range of total sulfur content in ore solution can be further defined by combining the diagrams with sulfur isotope compositions of sulfides and sulfates. The major factors which control the sulfur isotope compositions of minerals are, besides temperature, sulfur isotope composition of total dissolved sulfur species ($\delta S_{\Sigma S}^{34}$) in ore solutions, which is controlled by the source of sulfur, and the mole fractions of oxidized and reduced sulfur species in solution. Since the latter can be evaluated in terms of T, pH, ionic strength (I), and f_{O_2} of the ore solution, we can also evaluate the variation of δS^{34} of minerals in terms of T, pH, I and f_{O_2} . Under isotopic equilibrium conditions of aqueous sulfate and sulfide ions, $\delta S_{\Sigma S}^{34}$ can be approximated by $\delta S_{\Sigma S}^{34} = \sum \delta S_i^{34} \times X_i$, where i denotes the aqueous sulfur species H_2S , HS^- , $S^{=}$, $SO_4^{=}$ ($SO_4^{=}$, $HSO_4^{=}$, $KSO_4^{=}$ and $NaSO_4^{=}$) and X is the mole fraction (see Ohmoto, 1972). In the pH- f_{O_2} region defined by mineral assemblages at 200° and 250°C, the range of $\delta S_{\Sigma S}^{34}$ can be roughly estimated when the range of δS^{34} values of pyrite and barite in the deposits is approximated as that of H_2S and $SO_4^{=}$ in ore solution, respectively. Minimum estimate of f_{O_2} for ore deposition has been made from galena-barite pair (see Chapter V). The results of $\delta S_{\Sigma S}^{34}$ estimate are given in Table VII-4. Since seawater sulfate was probably dominant in the mixed solution during ore deposition, the range of $\delta S_{\Sigma S}^{34}$ for higher pH (6), $SO_4^{=}$ dominant field should therefore be more representative of the ore solution. The minimum $\delta S_{\Sigma S}^{34}$ value of about 25‰ is then taken as a first approximation. The overall mean value of the range is also around 25‰. It should be noted too that maximum $\delta S_{\Sigma S}^{34}$ in lower pH (4.2), H_2S dominant field and minimum $\delta S_{\Sigma S}^{34}$ in higher pH (6), $SO_4^{=}$ dominant field agree well and are around 25‰. Furthermore, pyrrhotites or minerals equilibrated with pyrrhotites

TABLE VII-4

ESTIMATES OF δS^{34} (ΣS) in Ore Solution,
Anvil Range District

Conditions	Range of δS^{34} (ΣS) (%)
1) $T = 200^{\circ}\text{C}$, $f_{O_2} = 10^{-40}$	
pH = 4.2, $X_{H_2S} = 0.9$, $X_{SO_4^{2-}} = 0.1$	17 ~ <u>30</u>
pH = 6.0, $X_{H_2S} = 0.1$, $X_{SO_4^{2-}} = 0.9$	<u>25</u> ~ 37
2) $T = 250^{\circ}\text{C}$, $f_{O_2} = 10^{-35}$	
pH = 4.2, $X_{H_2S} = 0.6$, $X_{SO_4^{2-}} = 0.4$	12 ~ <u>26</u>
pH = 6.0, $X_{H_2S} = 0.01$, $X_{SO_4^{2-}} = 0.99$	<u>24</u> ~ 36
	25 (mean)

are found to be close in sulfur isotope composition to total sulfur in ore solution and generally within a few permils (Ohmoto, 1972). Anvil pyrites examined by the writer have a maximum value of about 20‰ in Faro, 25‰ in Grum, 20‰ in Swim Lakes and 18‰ in Vangorda. Campbell and Ethier (1974) report δS^{34} values of pyrites in Faro No. 1 orebody in between 15.3 to 25.9‰ (average 21.7‰). Thus $\delta S_{\Sigma S}^{34}$ value is most probably around 20 to 25‰.

Based on the calculation of mole fractions of all aqueous sulfur species as functions of pH and f_{O_2} (see APL computer program XS, Appendix VII-2) at given temperature and ionic strength (derived from NaCl wt. % estimation in fluid inclusions), δS^{34} values of sulfide, sulfate minerals or aqueous sulfur species for a given $\delta S_{\Sigma S}^{34}$ can be expressed as functions of pH, f_{O_2} , T, I (see APL computer program DSI, Appendix VII-2), and the results for pyrite and barite are shown in Fig. VII-4a and b. It can be observed that over the range of δS^{34} values of pyrite (11~24‰) or barite (25~37‰) in between pH = 4.2 to 6.0 (sericite stability field), the most probable f_{O_2} range is 10^{-37} to 10^{-34} for pyrites and $10^{-35.5}$ to $10^{-33.3}$ for barites at 250°C (Fig. VII-4a), $10^{-41.5}$ to 10^{-39} for pyrites and $10^{-40.5}$ to 10^{-38} for barites at 200°C (Fig. VII-4b). It is worth recalling that estimates of minimum f_{O_2} from the galena-barite method give 10^{-35} at 250°C and 10^{-40} at 200°C (Chapter V). Conversely, by using these estimates of f_{O_2} , over the range of δS^{34} values of pyrite and barite, the most likely pH during ore deposition at 250°C is generally 4 to 5.5 for pyrite, and 5.5 to 6.0 for barites; and at 200°C, 4.3 to 5.5 for pyrites and 5.5 to 6.0 for barites. Therefore, it is apparent from the above observation that barite deposition probably took place in a slightly higher pH and f_{O_2} environment than the sulfide ores.

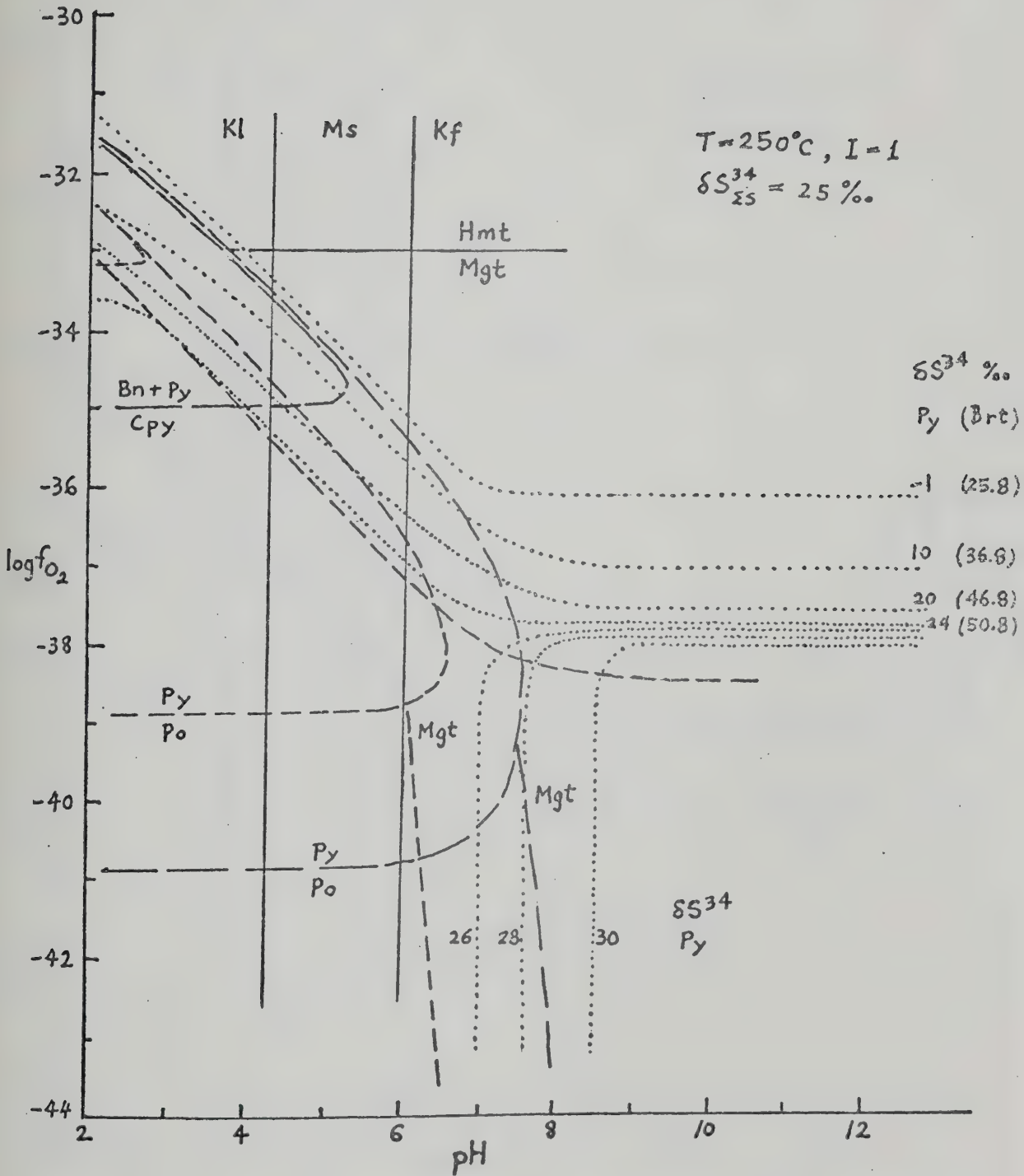


Fig. VII-4. (a) and (b), Comparison of the positions of δS^{34} contours of pyrite and barite with stability fields of minerals. Dashed and solid lines are mineral stability boundaries, dotted lines are δS^{34} contours.

- - - : Mineral stability fields at $\Sigma S = 0.01$ moles/kg H_2O .
 - - - - : Mineral stability fields at $\Sigma S = 0.001$ moles/kg H_2O .

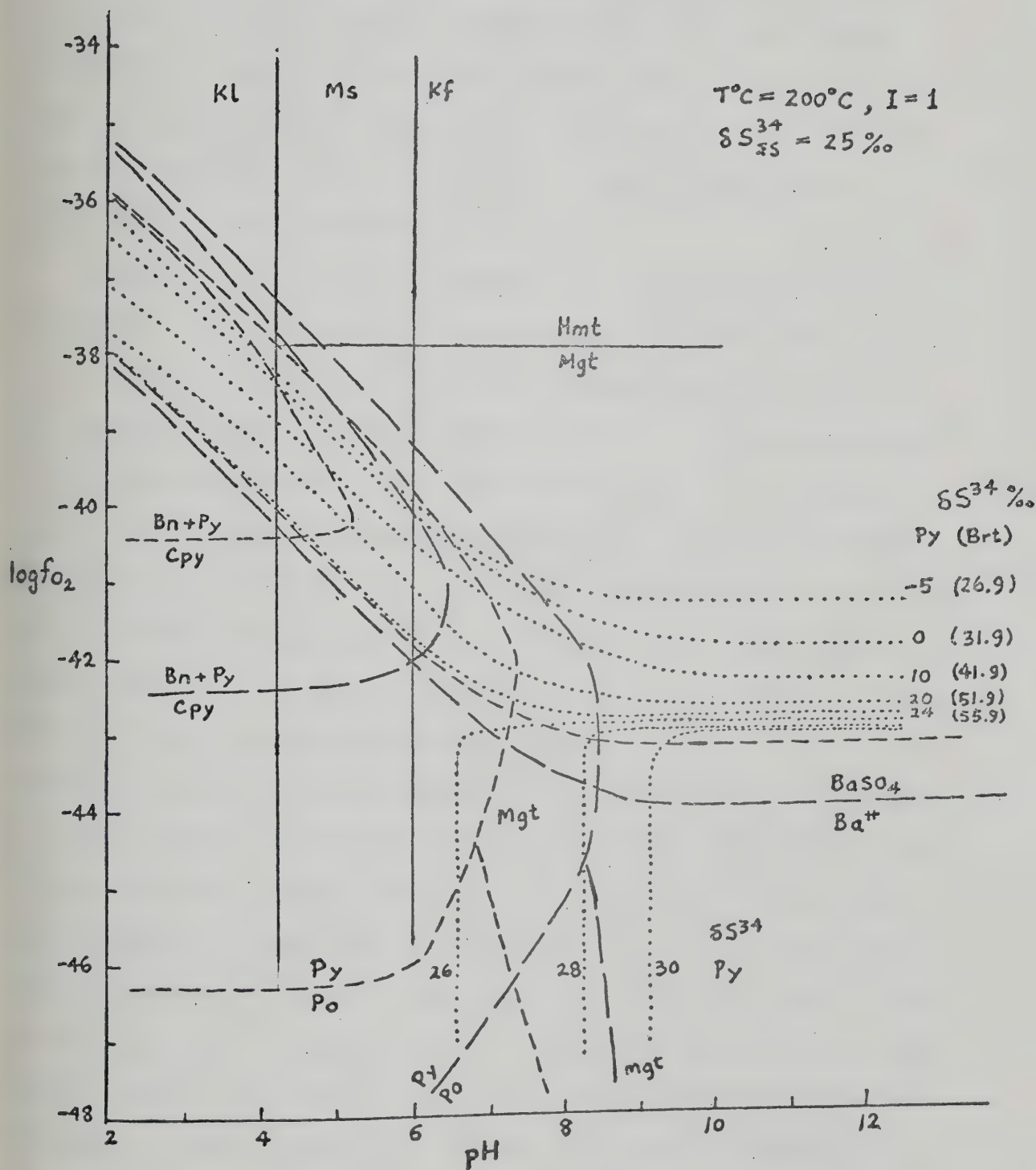


Fig. VII-4(b).

We can also estimate the approximate concentration of total dissolved sulfur (total sulfur content) in ore solutions from Fig. VII-4 by comparing mineral stability fields of chalcopyrite-pyrite+bornite, pyrite-pyrrhotite and barite constructed for various values of total sulfur content with sulfur isotope compositions of the minerals. It is indicated from this comparison that the total sulfur content of ore solutions was most probably around 0.01 to 0.001 mole/kg H_2O .

Finally, it is important to evaluate quantitatively the proportions of aqueous sulfur species in the mixing process. From the calculation of mole fractions of aqueous sulfur species in terms of pH, f_{O_2} , T and I, the important sulfur species and their proportions in ore solution during sulfide and barite formation are given in Table VII-5. It is evident that during sulfide deposition, H_2S and SO_4^{--} were in chemical equilibrium around pH of 4 to 5.0; SO_4^{--} increased in proportion as pH increased to 5.5; HS^- was a minor species and generally did not exceed 5 mole %. During barite deposition, the chemical environment was characterized by slightly higher pH and f_{O_2} , SO_4^{--} was the dominant species probably in partial equilibrium with H_2S which constituted less than 5 mole %; no HS^- was present.

Lusk (1972) has proposed a simple mixing model in which seawater sulfate is mixed with magmatic sulfur in a vent fluid system in which the redox condition is mainly SO_4^{--} , H_2S with negligible SO_2 . Assuming various mixing proportions of seawater sulfate and magmatic sulfur, the δS^{34} values of "final sulfate" in the mixed fluid in equilibrium with H_2S can be calculated. Taking a mean value of 30% as the isotopic composition of Cambro-Ordovician seawater sulfate, and δS^{34} values of pyrites as approximate compositions of vent fluid H_2S (range: 11 to 25%, mean: 15.6%), the δS^{34} values of the vent fluid mixture and "final sulfates" are calculated and

TABLE VII-5

Proportions of Aqueous Sulfur Species
During Ore Deposition,
Anvil Range District

T°C		Sulfide (pyrite) Deposition	Sulfate (barite) Deposition
200°C	X_{H_2S}	0.9 ~ 0.3	0.05 ~ 0.01
	$X_{SO_4^{2-}}$	0.1 ~ 0.65	0.95 ~ 0.99
	X_{HS^-}	< 0.05	-
250°C	X_{H_2S}	0.7 ~ 0.01	0.01
	$X_{SO_4^{2-}}$	0.3 ~ 0.99	0.99
	X_{HS^-}	0	0
pH		4.5 ~ 5.5	5.5 ~ 6.0

shown in Table VII-6. The following observations can be achieved from the calculation:

(i) At a redox condition of $\text{SO}_4^{=2} = \text{H}_2\text{S}$ (i.e. initial mixing), mixing proportion of seawater sulfate/magmatic sulfur is about 5:1 over the $\delta\text{S}_{\text{H}_2\text{S}}^{34}$ range of 11 to 25‰ at a vent fluid mixture isotope composition of 25‰ (= $\delta\text{S}_{\Sigma\text{S}}^{34}$ of the previous discussion) and "final sulfate" compositions of 25 to 39‰.

(ii) At a redox condition of $\text{SO}_4^{=2} = 1000 \times \text{H}_2\text{S}$ (i.e. $\text{SO}_4^{=2}$ dominant), mixing proportion of seawater sulfate/magmatic sulfur is at least 5:1 over the same range of H_2S isotope compositions at "final sulfate" and vent fluid mixture isotope compositions of 25‰.

(iii) A decline in temperature favors progressive S^{34} depletion in H_2S and S^{34} enrichment in coexisting sulfate when the composition of the latter is different from that of fresh seawater sulfate; whereas progressively more oxidizing conditions favor S^{34} depletion in the final sulfate compositions. Thus, sulfate can be either lighter or heavier than 30‰ under different redox conditions.

(iv)* A wide range of S^{34} enriched H_2S compositions (equivalent to compositions of precipitated sulfide minerals) could be produced by the physico-chemical conditions assumed provided that the mixing proportions of fresh seawater sulfate is more than 50% of total vent fluid sulfur (i.e. 1:1), redox conditions are not too reducing (i.e. not as reducing as in redox condition A: $\text{H}_2\text{S} \gg \text{SO}_4^{=2}$), and that temperatures are between 240-350°C.

*Ohmoto et al. (1976) reported that δS^{34} values of sulfide minerals formed in a basalt-seawater interaction experiment (conditions: $p=0.6\sim 1$ Kb, $T=300^\circ$, 400° , 500°C , water/rock weight ratio = 1, 2, and 3, and time = 170~270 days) have a range between +8.0 to +20.7‰. Thus the heaviest composition of sulfides approaches that of present-day seawater sulfate (~+20‰).

TABLE VII-6

Simple Mixing Model of Seawater Sulfate with Magmatic Sulfur in a Vent Fluid System

Vent Fluid Redox Conditions	Mixing Proportions Sulfate/Magmatic Sulfur	δS^{34} (%)			Final δS^{34} of Sulfate in Equilibrium with H_2S at $\delta SH_2S =$		
		Initial Sulfate	Initial Magmatic Sulfur	Vent Fluid Mixture	11%	15.6%	25%
a) $H_2S = 1000 \times SO_4^{2-} \gg SO_2$	100 : 1	30	0 (10)**	29.7 (29.8)**	-	-	-
	10 : 1	30	0 "	27.3 (28.1)**	-	-	-
	5 : 1	30	0 "	25.0 (26.7)**	-	-	25.0
	1 : 1	30	0 "	15.0 (20.0)**	-	-	-
	1 : 10	30	0 "	2.7 (11.8)**	-	-	-
b) $H_2S = SO_4^{2-} \gg SO_2^*$	100 : 1	30	0	29.7	48.4	43.8	34.4
	10 : 1	30	0	27.3	43.6	39.0	29.6
	5 : 1	30	0	25.0	39.0	34.4	25.0
	1 : 1	30	0	15.0	19.0	-	-
	1 : 10	30	0	2.7	-	-	-
c) $1000 \times H_2S = SO_4^{2-} \gg SO_2$	100 : 1	30	0	29.7	29.7	29.7	29.7
	10 : 1	30	0	27.3	27.3	27.3	27.3
	5 : 1	30	0	25.0	25.0	25.0	25.0
	1 : 1	30	0	15.0	15.0	-	-
	1 : 10	30	0	2.7	-	-	-

+ (Progressively more oxidizing) + +

+ + (Temperature) + +
decreases* Redox conditions analogous to those found in New Zealand geothermal bore effluents.
** Assuming mixing of sulfate with a fluid of $\delta S^{34} = 10\%$.

(v) Mixing of seawater sulfate with a hypothetical ore fluid having a δS^{34} value of +10‰ still produces vent fluid mixture with isotope compositions only slightly higher than that with magmatic sulfur (for mixing proportions of 5:1 up to 100:1, vent fluid mixture δS^{34} values are only higher by 1.7‰ or less).

Therefore, the "final" ore solution that was derived from mixing of ascending hydrothermal fluid with seawater probably had a proportion of $SO_4^{=}$ to H_2S of at least 5:1, or about 80 mole % $SO_4^{=}$, and 20 mole % H_2S .

The chemical environment in which original fluids discharged onto the seafloor and mixing and ore deposition took place was characterized by lower pH and f_{O_2} with considerable amounts of H_2S besides $SO_4^{=}$, temperature was probably slightly higher during sulfide ore deposition; as mixing and ore deposition proceeded, a rise in pH and f_{O_2} coupled with a slight decline in temperature and H_2S proportion witnessed the deposition of barite and the remaining sulfides.

4. Frances Lake District

(a) Results. Sixty-nine sulfur isotope analyses were made on galena, sphalerite and pyrite from the Thompson Creek ore deposit. The samples were taken from drill holes with significant ore intersections and are representative of the deposit. In addition, oxygen isotope analyses of quartz separates from five typical ore specimens were also made.

The sulfur isotope data and calculated isotope fractionation temperatures are given in Table VII-7. The isotope fractionation factor used to calculate temperatures for pyrite-galena pair is derived from a plot of $\Delta\delta S^{34}_{Py-Gn}$ versus $\Delta\delta S^{34}_{Sp-Gn}$ (Fig. VII-5) which gives an average of $1000 \ln \alpha_{Py-Gn} = 9.25 \times 10^5 \times T^{-2}$ with a range of $8.0 \sim 10.5 \times 10^5 \times T^{-2}$. This is in good agreement with that defined by Rye et al. (1974).

Sulfur Isotope Compositions (δS^{34} in ‰) and Calculated Temperatures of Galena, Sphalerite and Pyrite, Thompson Creek Deposit

Sample No.	Temperature (°C)				Remarks
	Galena	Sphalerite	Pyrite	Sp-Gn Py-Gn	
2-140	12.1	14.4	-	279	
3-41.8	11.9	14.2	-	279	
4-37	12.1	14.1	-	318	
43.5	9.9	12.0	-	304	
5-62.5	10.5	13.2	13.6	236 235*	
6-34.5	-	-	13.4		
7-95	10.9	13.5	-	246	
9-61.5	11.7	-	-		
94	9.8	12.1	-	278	
10-174.5	11.3	12.9	-	(388)	Trace mixture of sulfo-salt in sp separate
181	14.7	17.1	-	267	
14-252	-	-	14.5		Py in phyllite
18-187.5	11.2	13.3	-	304	Trace cpy mixture in galena separate
19-319	-	-	14.9		Py in quartz sericite schist
22-329.5	13.7	16.4	17.8	236 233**	
341.5	10.0	12.9	14.4	218 215**	
362	-	16.9	17.0		

TABLE VII-7 (cont'd)

Sample No.	Temperature (°C)				Remarks
	Galena	Sphalerite	Pyrite	Sp-Gn Py-Gn	
23-288.5	11.0	13.2	13.4	291 304*	Py in quartz sericite schist
413	-	-	14.4		
24-286.5	12.1	13.9	-	(350)	Trace cpy mixture in galena separate
308	12.4	14.3	-	(334)	
25-402.5	10.0	12.5	-	256	"
462.5	10.9	13.2	-	279	
463	10.1	12.3	-	291	246**
28-158	9.8	12.3	13.7	256	
163	12.2	14.6	-	267	205*
29-293.5	10.4	12.5	-	304	
30-89	9.6	12.7	13.1	202	262*
94	10.5	12.8	13.3	279	
105.75	12.1	14.3	15.1	291	319**
106	12.3	14.4	15.4	304	
Trench 572-3	13.0	-	-		194
4	13.4	-	-		
7	10.7	13.9	-		

* Calculated by $\Delta\delta\text{Spy-Gn} = 8.0 \times 10^5 \times T^{-2}$ (cf. Fig. VII-5).** Calculated by $\Delta\delta\text{Spy-Gn} = 10.5 \times 10 \times T^{-2}$ (cf. Fig. VII-5).

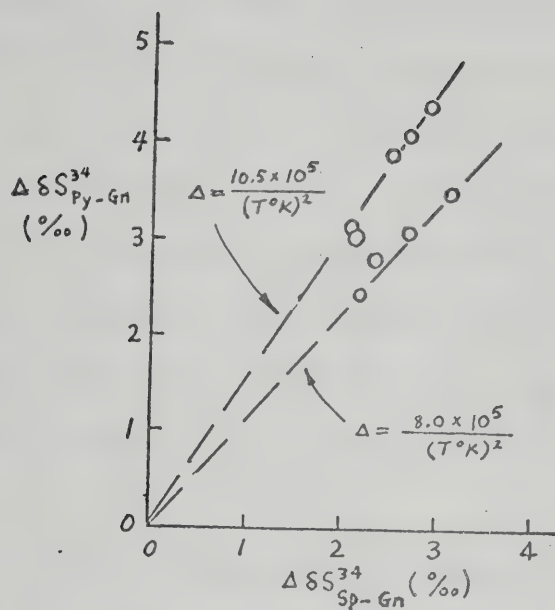


Fig. VII-5. Sulfur isotope fractionations between pyrite-galena and sphalerite-galena pairs, Thompson Creek deposit, Frances Lake district.

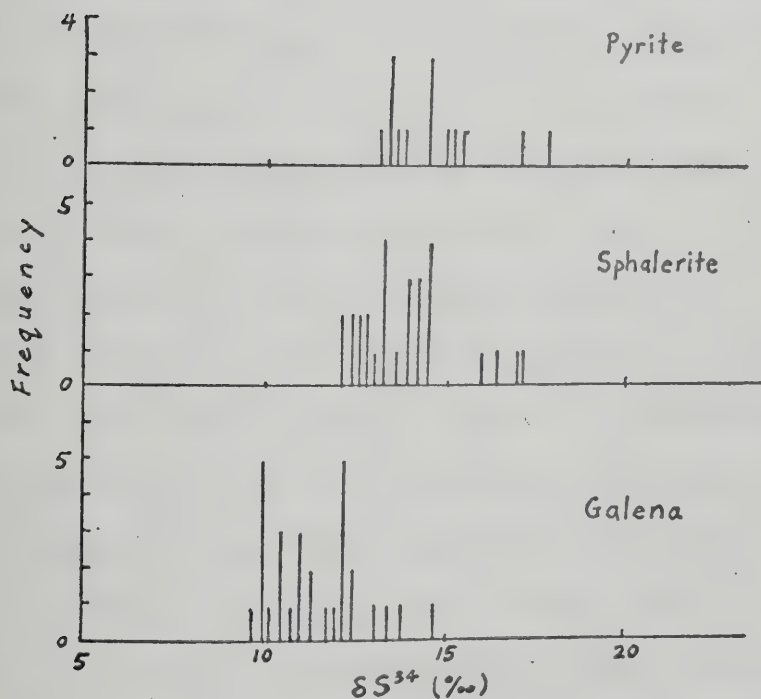


Fig. VII-6. Variation of sulfur isotope compositions in sulfide minerals, Thompson Creek deposit.

An attempt was made to analyze isotope composition of Sb-Pb sulfosalt minerals, but this was not successful due to too small quantity of separates and also the intimate mixture of galena in the separates. According to the results from Keno Hill - Galena Hill Pb-Zn-Ag-Cd deposits, Yukon (Boyle et al., 1970), sulfosalts generally overlap or are slightly lighter in sulfur isotope compositions than galena. Theoretical prediction based on bond strengths in minerals (Bachinski, 1969) also indicates that stibnite, an antimony sulfide, is lighter than galena in sulfur isotope composition.

The δS^{34} values of sulfide ores typically range between 9.6 and 17.8‰, the variation of the δS^{34} values of each mineral is shown in Fig. VII-6.

Disseminated pyrite in quartz-sericite eye schist (tuffaceous meta-sediments ?) and graphitic chlorite sericite schist in the drill hole intersection was also analyzed for sulfur isotope compositions. The results indicate a very narrow range of 14.4 to 14.9‰ and fall within the isotope composition range of pyrite from ores (13.1 to 17.8‰).

(b) Sulfur Isotope Fractionation and Chemical Environment. Comparison of the sulfur isotope compositions of galena, sphalerite and pyrite in ores reveals that isotope equilibrium has been attained among these sulfide minerals, as evidenced by the decreasing order of δS^{34} values pyrite > sphalerite > galena and the similar range of fractionation temperatures indicated by sphalerite-galena and pyrite-galena pairs. The higher temperatures indicated by the three sphalerite-galena pairs (10-174.5, 24-286.5, 24-308) are the consequence of contamination of chalcopyrite in galena and sulfosalt in sphalerite which tends to narrow the fractionation factor between the pair and thus yield apparently higher temperatures. Average temperature for sphalerite-galena isotope fractionation is 269°C and that for pyrite-galena is 259°C.

Fluid inclusion and sulfur isotope studies thus indicate a moderate range of formation temperatures for the deposit, ranging from 200 to slightly over 300°C. 250°C is chosen arbitrarily as an average formation temperature and will be used in the following thermochemical considerations.

Defining the stability fields of mineral assemblages pyrite, po, cpy, bn, hmt and mgt in terms of temperature, f_{O_2} and f_{S_2} (Fig. VII-7), we can estimate the range of f_{O_2} and f_{S_2} during ore deposition in which pyrite, chalcopyrite together with galena and sphalerite were stable assemblages. In the f_{O_2} -T diagram (Fig. VII-7a), pyrite-mgt curve defines the lower limit of f_{O_2} whereas pyrite-hematite curve defines the upper limit of f_{O_2} at given temperature; in the f_{S_2} -T diagram (Fig. VII-7b), pyrite-magnetite curve defines the lower limit of f_{S_2} whereas pyrite + bornite - cpy curve defines the upper limit of f_{S_2} at a given temperature. The estimates derived from these diagrams at 250°C are as follows:

$$f_{O_2}: 10^{-31} \text{ to } 10^{-38.5}$$

$$f_{S_2}: 10^{-8.5} \text{ to } 10^{-10.8}$$

Since fluid inclusion study indicates that the ore fluid boiled below the seafloor and ore deposition occurred as replacement in the sedimentary rocks, we can assume that the ores must have equilibrated with the mineral assemblage (quartz, sericite, and graphite) of the host rocks. Again, defining the stability fields of sericite (with excess quartz), graphite, pyrite, pyrrhotite, chalcopyrite, bornite in terms of f_{O_2} and pH at given temperature and specified ΣS , K^+ and C concentrations (Fig. VII-8), we can estimate the maximum possible range of f_{O_2} by py-po stability field at a maximum concentration of $\Sigma S = 0.1$ mole/kg H₂O (Ohmoto, 1972) and the most probable range of f_{O_2} by py+bn-cpy stability field also at the maximum

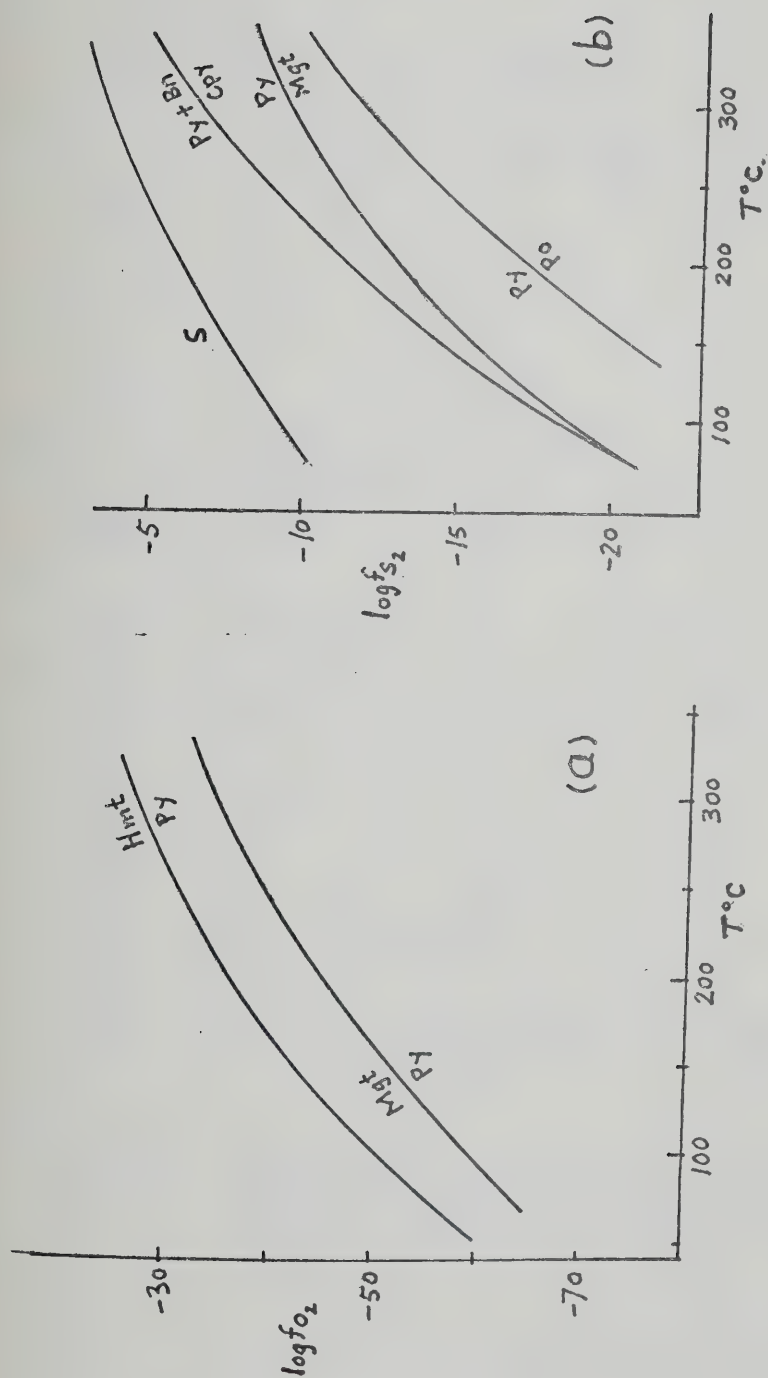


Fig. VII-7. Stability fields of mineral assemblages as functions of T , f_{O_2} and f_{S_2} .

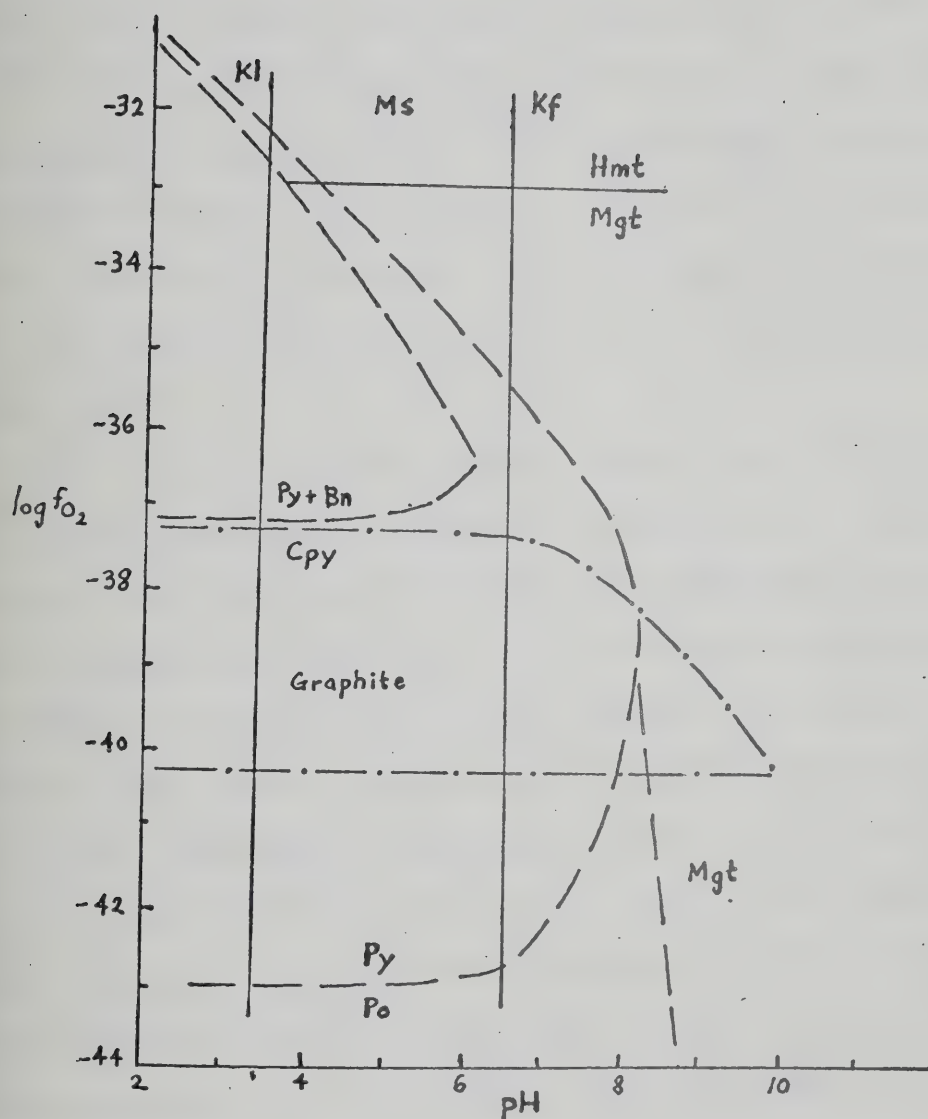


Fig. VII-8. Comparison of the positions of stability fields of Fe-S-O minerals, chalcopyrite, bornite, graphite and sericite (muscovite). $T=250^{\circ}\text{C}$, $I=2.0$.

- : Mineral boundaries at $\Sigma S=0.1$ moles/kg H_2O .
- .- : Graphite stability field at $\Sigma C=1$ mole/kg H_2O .
- : Sericite - K-feldspar (Kf) boundary at $\text{K}^+ = 0.001$ moles/kg H_2O , and kaolinite (Kl) - sericite boundary at $\text{K}^+ = 0.1$ moles/kg H_2O .

concentration of ΣS of 0.1 mole/kg H_2O . At $250^\circ C$, and within sericite stability field the maximum possible range of f_{O_2} during ore deposition is 10^{-33} to 10^{-43} and the most probable range of f_{O_2} is $10^{-32.6}$ to $10^{-37.2}$. The latter estimate agrees well with the f_{O_2} range estimated from independent method using Fig. VII-7a. Stability fields of sericite and graphite indicate a f_{O_2} range of $10^{-37.3}$ to $10^{-40.3}$. The field for sericite (muscovite) in Fig. VII-8 is the maximum stability field, since mK^+ in ore-forming fluids seldom lies outside of 0.001 to 1 m range (Ohmoto, 1972).

δS^{34} values of sedimentary pyrite average 14.6‰. The similarity of δS^{34} value in sedimentary pyrite and most pyrites in ores suggests that the latter might have been mainly derived from leaching or extraction from sedimentary sulfides. Pyrite as disseminations in quartz sericite eye schist and phyllitic rocks are very common in the region. On the other hand, the complete absence of any sulfate minerals or deposits in the adjacent areas suggest that aqueous sulfate species such as $SO_4^{=}$, $HSO_4^{=}$, $KSO_4^{=}$ and $NaSO_4^{=}$ could not have been present in any significant amount. The major possible aqueous species are then H_2S and its dissociation products HS^- and $S^{=}$. Sakai (1968) has shown that the apparent isotope composition of a H_2S solution, $\delta S_{\Sigma H_2S}$ is defined as:

$$\delta S_{\Sigma H_2S} = X_{H_2S} \cdot \delta S_{H_2S} + X_{HS^-} \cdot \delta S_{HS^-} + X_{S^{=}} \cdot \delta S_{S^{=}} \quad (VII-1)$$

where ΣH_2S is total aqueous sulfide ions (H_2S , HS^- and $S^{=}$) and X_i denotes mole fraction of each ion. He further showed that the isotope composition of a precipitated sulfide mineral δS_{sfd} is defined as:

$$\delta S_{sfd} = \delta S_{\Sigma H_2S}^{\circ} + \frac{\ln \alpha_{\Sigma H_2S}^{sfd} (T, pH)}{(1+R)} \quad (VII-2)$$

where $\ln \alpha_{\Sigma H_2S}^{sfd}$ is the fractionation factor between a sulfide mineral and aqueous sulfide ions as a function of T and pH, R is the atomic ratio of the precipitated sulfur (as sulfide minerals) to aqueous sulfide ions remaining in the solution, and $\delta S_{\Sigma H_2S}^o$ is the isotope composition of aqueous sulfide ions before the precipitation of the sulfide.

For finely porous wall rocks such as marine sediments or pyroclastic tuffs, it is reasonable to assume that mineralization results locally in total precipitation of aqueous sulfide ions (i.e. $R = \text{infinity}$); in this case, sulfur isotope composition of precipitated sulfide (such as pyrite) would approach $\delta S_{\Sigma H_2S}^o$ in solution as the second term in the right hand side of Equation VII-2 approaches zero. δS_{py}^{34} is usually larger than $\delta S_{\Sigma H_2S}^o$, but the difference would become very small as R approaches zero (Sakai, 1968). If δS^{34} values of sedimentary pyrite can be approximated to be $\delta S_{\Sigma H_2S}^o$ and pyrite in the main ore zone as δS_{sfd} , and if isotope equilibrium was maintained between the aqueous sulfide ions and precipitated sulfides, the maximum difference in isotope composition between sedimentary pyrite and the main ore pyrite would be taken as the minimum estimation of $\ln \alpha_{\Sigma H_2S}^{py}$ in the ore fluid. The maximum δS^{34} difference of the two pyrites is $17.8\text{‰} - 14.4\text{‰} = 3.4\text{‰}$. Defining $\ln \alpha_{\Sigma H_2S}^{py}$ ($= 3.4\text{‰}$) as a function of pH and T (Fig. VII-9a), we can estimate the probable pH range of the ore solution: at 250°C , pH is estimated to be about 7. pH of the ore solution can also be estimated by the following three independent methods:

(i) Defining $\delta S_{H_2S}^{34}$ as a function of pH, T, f_{O_2} and $\delta S_{\Sigma H_2S}^o$ (Fig. VII-9b, modified after the method proposed by Ohmoto, 1972), the most probable pH range is as follows:

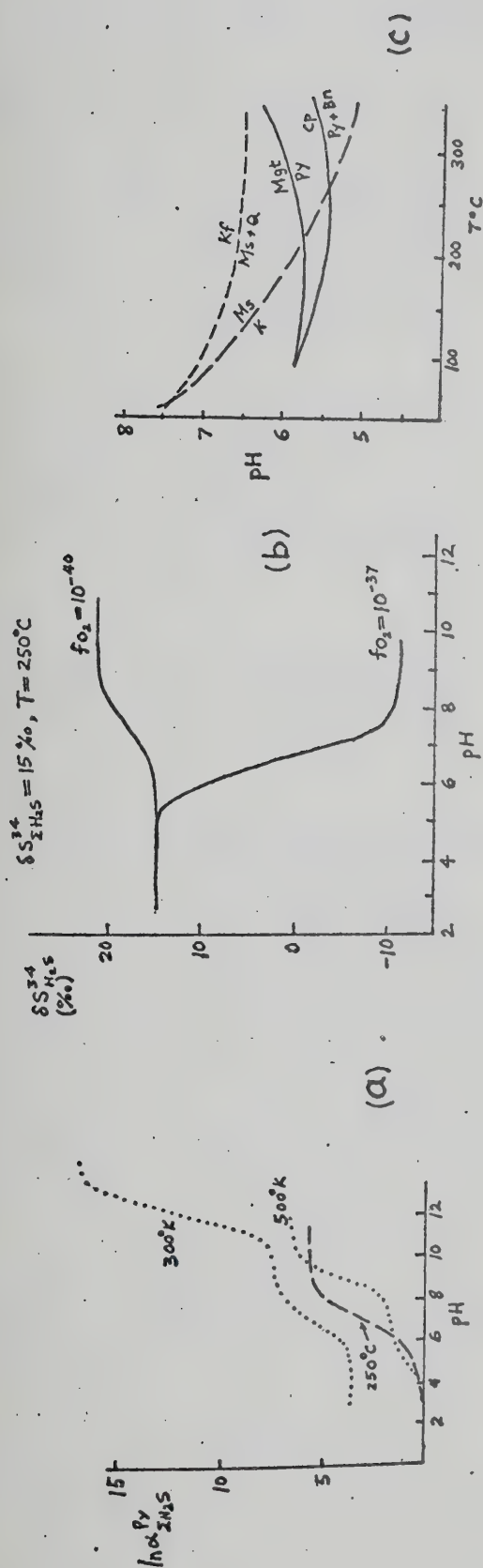


Fig. VII-9. (a) Comparison of the effect of change in pH on the $\ln \alpha_{\text{H}_2\text{S}}^{\text{py}}$ at different temperatures; the dotted curves are taken from Sakai (1968), the dashed curve is given for 250°C and calculated from the data of Sakai. (b) Comparison of the effect of change in pH on the $\delta S_{\text{H}_2\text{S}}^{34}$ values at different f_{O_2} values. $\delta S_{\text{H}_2\text{S}}^{34}$ values for H_2S (or pyrite) are where $\delta S_{\text{H}_2\text{S}}^{34} = 15\%$ at 250°C (modified after Ohmoto, 1972). (c) Stability fields of mineral assemblages as functions of pH and temperatures (modified after Kajiwara, 1973b).

at $\delta S_{py}^{34} = 13\%$, $f_{O_2} = 10^{-37}$, $T = 250^\circ\text{C}$, $\text{pH} = 5.5$ (minimum)

at $\delta S_{py}^{34} = 17.8\%$, $f_{O_2} = 10^{-40}$, $T = 250^\circ\text{C}$, $\text{pH} = 7.5$ (maximum)

(ii) Defining the stability fields of pyrite, magnetite, chalcopyrite and bornite as functions of pH and T (Fig. VII-9c), within the stability fields of pyrite and chalcopyrite, pH is estimated to be 5.5~5.9 at 250°C .

(iii) Defining the stability fields of sericite, quartz, kaolinite and K-feldspar in terms of pH, T (Fig. VII-9c), the probable pH range within the stability fields of sericite and quartz at 250°C would be around 5.5 to 6.6.

Therefore, the overall estimates of pH of ore solution in the Thompson Creek deposit indicate a possible range of 5.5 to 7.5, i.e. about neutral to slightly alkaline.

If isotope equilibrium was attained among the aqueous sulfide species and the precipitated sulfide minerals, it would be possible to further evaluate the relative amounts of the major sulfur species in the original ore solution. Taking 14.6% as the mean δS^{34} value for total aqueous sulfide species, we can define the isotope fractionation between each sulfide mineral and aqueous species (i.e. between galena- H_2S , sphalerite- H_2S , galena- HS^- , sphalerite- HS^- , galena- $\text{S}^{=}$, and sphalerite- $\text{S}^{=}$) in terms of T over the probable f_{O_2} range (10^{-37} to 10^{-40} , mean: $10^{-38.5}$). The data given by Sakai (1968), Kajiwara and Krouse (1971) and Czamanske and Rye (1974) for sulfide minerals and aqueous sulfur species are used to construct such a δS^{34} -T diagram as shown in Fig. VII-10. As stated before, minor uncertainties exist among these theoretical and experimental data. However, most of the isotope data of galena and sphalerite are best described by isotope fractionation with either H_2S dominant or HS^-

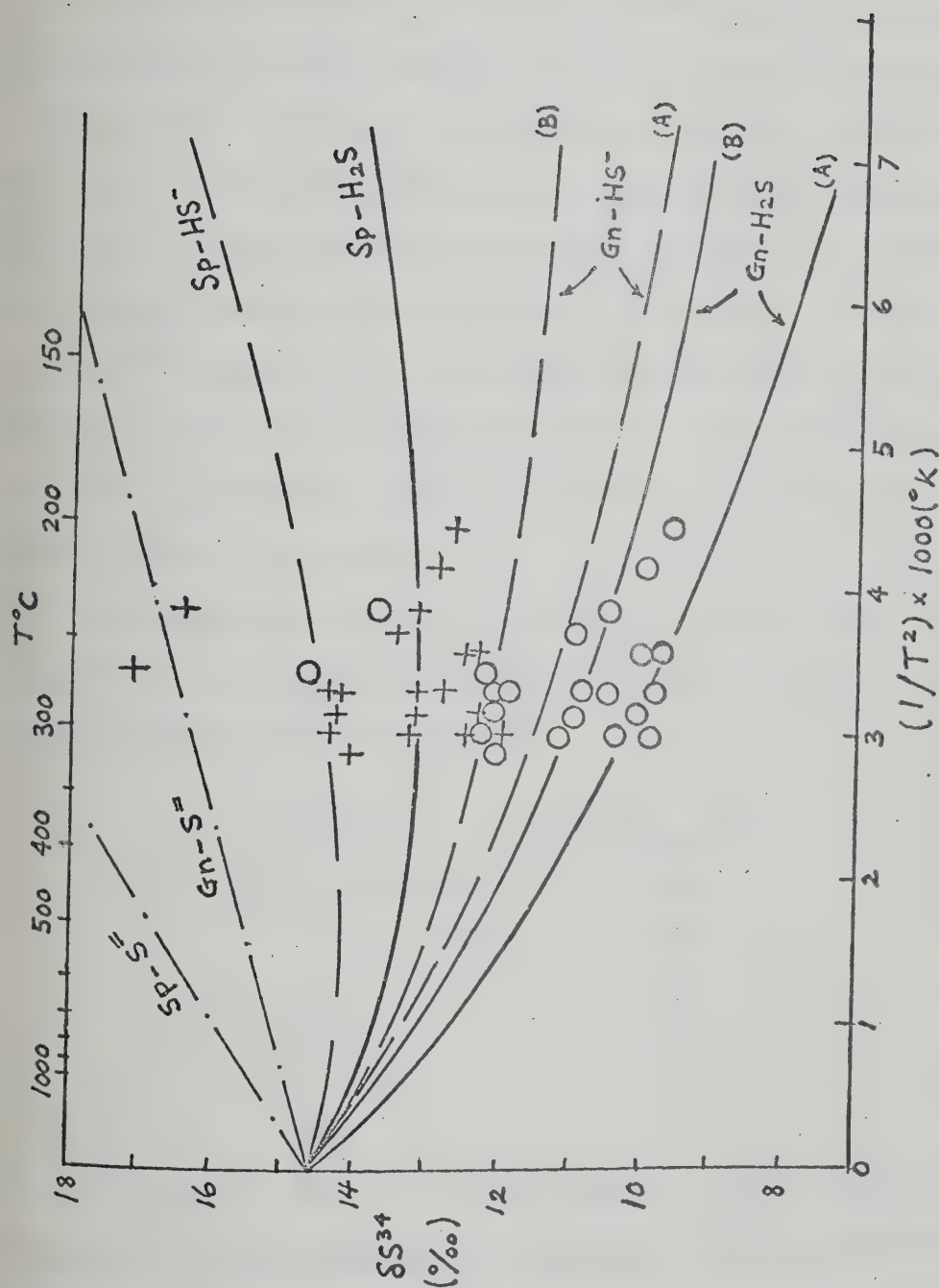


Fig. VII-10. δS^{34} vs. T diagram showing fractionation curves of sulfide minerals and aqueous sulfide species. The fractionation curves for galena-H₂S and galena-HS⁻ are constructed from the data of (A) Sakai (1968) and (B) Kajiwara and Krouse (1971), and Czamanske and Rye (1974). The remaining curves are constructed from the data of Sakai (1968). O: galena; +: sphalerite.

dominant solution as is apparent from the good fit of most data points to the fractionation curves. Fourteen out of 22 data points (63%) can be fitted to $\text{Gn-H}_2\text{S}$ and $\text{Sp-H}_2\text{S}$ curves; 6 out of 22 data points (27%) to Gn-HS^- and Sp-HS^- curves. The data points cannot be described by fractionation of sulfide minerals with $\text{S}^{=}$. Based on the extensive calculation of mole fractions of aqueous sulfur species in terms of f_{O_2} , pH, T, and I (using APL program XS, see Appendix VII-2; see also Ohmoto, 1972, Fig. 3), the relative amounts of H_2S and HS^- can be estimated at the selected thermochemical parameters. At 250°C , $I = 1.0$, at an average $f_{\text{O}_2} = 10^{-38.5}$ and $\text{pH} = 6.5$, the approximate mole fractions of H_2S and HS^- are 0.7 (70%) and 0.3 (30%), respectively. This estimate agrees well with the proportion indicated by the above fitting of data points to the fractionation curves.

(c) Oxygen Isotope Composition of Ore Solution. Oxygen isotope analyses were determined on five samples of quartz from the ores. Their isotope compositions are as follows:

Sample	δO^{18} (SMOW) (‰)
(Trench) 572 #1	13.9
" 572 #2	14.0
" 572 #4	13.3
DDH 2-140	13.7
DDH 7-95	13.4
(mean)	13.7

The data indicate a very uniform δO^{18} range. The δO^{18} values of quartz depend on δO^{18} of hydrothermal ore solutions, the temperature of crystallization and the extent of isotopic exchange. The isotope compositions of hydrothermal solutions may provide information pertaining to their origin. There are two approaches to determining δO^{18} values of hydro-

thermal solutions: (1) measurement of the isotope compositions of the fluid inclusions, (2) calculation of the isotope compositions of hydrothermal solutions in equilibrium with a hydrothermal mineral. The first approach is not preferred because firstly, fluid inclusions in silicate minerals may have undergone oxygen isotope exchange with the silicate oxygen at lower temperatures than that of the crystallization of the mineral (Rye, 1966), and secondly, mixing of fluid inclusions of different origins during extraction is unavoidable and might contribute to erroneous results. In the present work, δO^{18} of ore solution was calculated on the basis of the estimated temperature of crystallization of quartz, the quartz-water isotope fractionation factor, and the measured isotope composition of quartz samples. The calculation is based on the assumption that the quartz was in isotope equilibrium with the hydrothermal solution at the temperature of crystallization and that the amount of solution was negligible compared to the amount of silica. The oxygen isotope fractionation factor α for the quartz-water equilibrium in the temperature range of $200^\circ \sim 500^\circ\text{C}$ is given by Clayton et al. (1972) as:

$$1000 \ln \alpha_{Q-W} = 3.38 \times 10^6/T^{-2} - 3.40$$

Since

$$\alpha_{Q-W} = \frac{1000 + \delta O_Q^{18}}{1000 + \delta O_W^{18}}$$

Therefore,

$$\delta O_W^{18} = (1000 + \delta O_Q^{18} - 1000 \alpha_{Q-W}) \div \alpha_{Q-W}$$

If crystallization temperature of quartz is taken to be 250°C (cf. filling temperatures of fluid inclusions in quartz), and the mean $\delta O_Q^{18} = 13.7\text{‰}$, then the isotope composition of ore solution δO_W^{18} is estimated to be 4.6‰ .

Since no deuterium/hydrogen isotope ratio was available for the hydrothermal solution, we can only interpret the oxygen isotope data from

their affinity and range as compared to other natural waters. The δO^{18}_W value of 4.6‰ is too heavy for the solution to be pure seawater or meteoric water; on the other hand, oil field brines (essentially meteoric ground waters) are ruled out as a possible source on the ground that they generally display a large variation of δO^{18} (from highly negative to about 10‰), and that no evidence of hydrocarbons was ever found in fluid inclusions in quartz. Waters equilibrated with magmatic bodies or igneous rocks at high temperatures generally have δO^{18} values ranging from 5.5 to 10‰. Metamorphic pore waters, i.e. waters present during regional metamorphism of rocks, have a wide range of δO^{18} (5 to 25‰). Metamorphosed sedimentary rocks and their constituent minerals have a wide range in δO^{18} simply because they retain in large part their original sedimentary δO^{18} values during metamorphism: shales, limestones, and cherts all tend to be very rich in δO^{18} (15 to 35‰) whereas sandstones, graywackes, arkoses and volcanogenic sediments tend to be low in δO^{18} (8 to 13‰) (Taylor, 1974).

Devereux (1968) has found that δO^{18} values of quartz in greenschist facies rocks from Otago, New Zealand display a very uniform range from 13.8 to 16.9‰ (mean 14.5); likewise, Garlick and Epstein (1967) reported a uniform range of δO^{18} values (12 ~ 16‰) for quartz in metasedimentary schists from Vermont, U.S.A.. The metamorphic grade of these schists is similar to that of the phyllitic schists in the Frances Lake district, i.e. in the lower ~ medium greenschist facies. The δO^{18} of waters in equilibrium with the Otago schists as calculated from isotope fractionation of constituent minerals (quartz, albite, calcite, magnetite) is about 4‰ at 270°C (Devereux, 1968).

Waters present during metamorphism of sediments are mainly pore fluids in sediments and waters produced by dehydration of sedimentary minerals during metamorphism. Oxygen isotope - cation exchange through the medium of hydrothermal fluids can occur in rocks during regional metamorphism (Taylor et al., 1963). It follows that if the minerals in a rock are approaching isotope equilibrium any change in the δO^{18} of one mineral must be balanced by a change in the δO^{18} of another mineral or oxygen-bearing phase. However, the amount of change in δO^{18} for a particular mineral will depend on its relative abundance. An abundant mineral would act as an isotope "reservoir" and would change less than a rare mineral. If the quartz in the Thompson Creek ores was derived from waters present in rocks during metamorphism, and since quartz is abundant in the metasediments in Frances Lake district, the composition of quartz should vary only slightly for rocks equilibrating at various temperatures.

From extensive measurements of quartz in various types of hydrothermal ore deposits, Sugisaki and Jensen (1971) show that calculated δO^{18} of hydrothermal fluids start to decrease with decreasing temperatures just below 300°C, and they proposed that dilution and cooling of the fluids by mixing with O^{18} -poor meteoric ground water as a cause of lowering δO^{18} of the fluids. Dilution and cooling of the ore fluids below 300°C have been observed from the data of fluid inclusions in the Thompson Creek quartz (cf. Chapter VI). An interesting coincidence (?) is encountered when the δO^{18} and T data of Thompson Creek quartz are plotted on their δO_Q^{18} -T diagram (Fig. VII-11) as a function of δO_W^{18} . At 250°C and a δO_W^{18} of about 5‰, the corresponding δO^{18} of quartz is about 14‰!

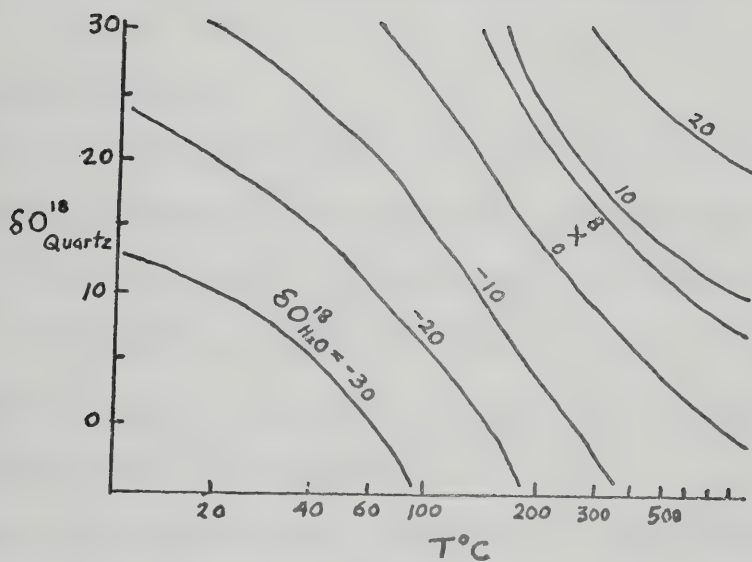


Fig. VII-11. Relationships between temperature and δ^{18} of quartz and δ^{18} of fluids from hydrothermal ore deposits (after Sugisaki and Jensen, 1971). Cross: Thompson Creek data point.

It is concluded that the ore solution responsible for the Thompson Creek ore deposit was probably derived from waters which were equilibrated with the sediments during burial and/or seafloor geothermal metamorphism (Spooner and Fyfe, 1973) immediately followed sedimentation and apparently was subjected to cooling and dilution caused by mixing with meteoric formation waters (?) and/or by boiling just below the seafloor.

5. Howard's Pass District

(a) Results. A total of 70 sulfur isotope analyses were made on pure galena, sphalerite and pyrite in the ore-bearing siltstone from the Canex Placer's main zone and Dynasty-Shield Resources' Pas claims in the Howard's Pass district. In addition, 3 isotope analyses of barite in siltstone from Ordovician and Silurian sequences in the adjacent areas were made to confirm the stratigraphy of the sequences.

The isotope data and calculated fractionation temperatures are given in Table VII-8. The temperatures deduced from sphalerite-galena isotope fractionation are generally in the range of 63° to 168°C (except 29-381), with a mean of 140°C. Fractionation temperatures for some pyrite-galena pairs in which pyrite is exclusively "single crystals", non-framboidal pyrite, are generally between 111 to 182°C, averaging about 142°C. Framboidal pyrite samples from ore-bearing siltstone show highly variable δS^{34} values and generally do not conform to the isotope enrichment trend of $Py > Sp > Gn$ which is taken to indicate an equilibrium isotope exchange condition. Excluding those samples which contain mixture of non-framboidal and framboidal pyrite, limited analyses of framboidal pyrite indicate a δS^{34} range of -3.2 to 23.9‰. Single crystal, non-framboidal pyrite, where positively identified and separated, show heavy δS^{34} values greater than 21%. Where pyrite separates contain a small mixture of framboidal pyrite,

TABLE VII-8

Sulfur Isotope Compositions and Estimated Temperatures of Sulfides, Howard's Pass District

Sample No.	δS^{34} (‰)			T°C		Remarks
	Gn	Sp	Py	Δ_{Sp-Gn}	Δ_{Py-Gn}	
(Placer's main zone)						
DDH6-274	17.9	21.9	23.5	145	135	(1)
288	17.7	21.6	-	151		
466.5	18.5	-	22.4			(3)
12-231	14.8	-	-			
18-502.5	17.6	21.2	22.7	168	154	(1)
19-539	22.3	26.2	-	151		
24-358	8.5	-	16.6			(3)
29-328.5	13.2	16.8	14.8	168		(3)
381	12.0	20.1	19.6	21?		(3)
426.5	12.6	16.6	-	145		
434.5	11.9	-	4.1			(2)
437.5	10.7	16.9	17.0	63	111	(1)
562.7	18.2	22.1	21.1	150		(3)
579.3	20.4	24.6	-	135		
30-345	11.8	15.8	-	145		
353A	11.3	15.3	1.4	145		(2)
32-177.5	13.3	19.4	-3.2	66		(2)
178.5	13.0	18.1	-	154		

Sample No.	δS^{34} (‰)			T°C			Remarks
	Gn	Sp	Py	Δ_{Sp-Gn}	Δ_{Py-Gn}		
32-189	13.6	-	21.0			(3)	
34-330A	11.1	15.0	-	151			
Trench 81-K	19.3	-	-				
A-T-3	19.3	-	-				
A-T-6	17.3	21.3	-	145			
T-18-N	16.9	20.8	-	154			
T-18-S	15.8	-	21.0		150	(1)	
T-19-1	17.7	21.6	23.2	145	138	(1)	
T-19-S	20.4	-	24.5			(3)	
CF #1	13.8	-	-				Remobilized pod in cross fault
CF #2	13.0	-	-				"
(Pas claims)							
DDH74P1-110	22.2	-	28.1		124	(1)	
134	23.5	-	28.0		182	(1)	
144	26.5	-	23.9			(2)	
74P2-225	24.0	-	20.1			(2)	

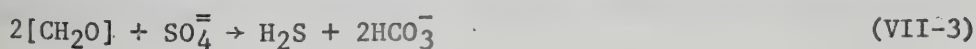
(1) Single crystal, non-framboidal pyrite ("ore-stage" pyrite).

(2) Framboidal pyrite.

(3) Non-framboidal with minor framboidal pyrite.

the δS^{34} values are more variable but still enriched in S^{34} (14.8~28.1%). Py-Gn fractionation temperatures were not calculated for these pyrites because the results might not reflect equilibrium isotope conditions.

(b) Sulfur Diagenesis in Sediments. During sedimentation and burial in a marine environment, reduction of trapped seawater sulfate in pore waters of sediments by bacteria is a major process in producing dissolved sulfur species (HS^- , H_2S) in pore waters. Since bacteria metabolize decomposable organic compounds for their growth requirements, and in the process initial sulfate is used to oxidize organic carbon in the absence of oxygen (valid for most bottom waters), high concentration of organic matter in the sediments should favor a more rapid disappearance or reduction of dissolved sulfate. If the reactive portion of organic matter in sediments can be considered to have the oxidation state of carbohydrate, bacterial reduction of sulfate will follow the stoichiometry of the following reactions (Manheim and Sayles, 1974; Goldhaber and Kaplan, 1974):



From the investigations of chemical compositions of pore waters of marine sediments from the present ocean (Manheim et al., 1970; Presley et al., 1970; Nissenbaum et al., 1972; Shiskina, 1958; Kaplan et al., 1963; Berner, 1964; Sweeney et al., 1973), the following general observations can be made:

(i) Dissolved sulfate in pore waters decrease to an asymptotic limit with increasing depths, while the residual sulfate becomes progressively enriched in S^{34} .

(ii) Dissolved sulfide in pore waters increases to a maximum and then decreases to a zone in which sulfate reduction becomes negligible or ceases; the dissolved sulfide generally shows a shift to an enrichment in S^{34} (Hartmann and Nielsen, 1969; Sweeney *et al.*, 1973).

(iii) The majority of pH values measured in pore waters are in the narrow range of 6.9 to 8.2, despite the fact that seawater initially buried is poorly buffered. If all sulfate is reduced from a given volume of pore waters (i.e. complete reduction) and the products remain in solution, the pH of such a solution is calculated to be about 7 (Nissenbaum *et al.*, 1972). Ben-Yaakov (1973) shows that the ultimate pH value in pore water with progressive depletion of dissolved sulfate (i.e. progressive enrichment of dissolved sulfide) is 6.9.

(iv) Alkalinity increases with increasing amount of dissolved sulfide in pore waters; alkalinity is believed to be a cumulative result of sulfate reduction, calcium carbonate precipitation, hydrolysis of basic nitrogen compounds, and authigenic silicate formation (Berner *et al.*, 1970).

(v) Absence of measurable dissolved sulfide in uppermost surface layers of sediments in which iron sulfide was rapidly formed by the reaction between iron oxide or hydroxide adsorbed on clay minerals and generated H_2S according to the reaction:



iron sulfide continues to react at a reduced rate at depth.

The formation of pyrite framboids in sediments has been suggested by Schneiderhohn (1923), Love (1965) and Rickard (1970) to have occurred through replacement of organic globules or cells with pyrite, i.e. the spheroidal texture of framboids is a pseudomorph requiring biogenic

involvement. On the other hand, Schouten (1946) suggested framboids are formed by multiple crystallization of pyrite from a "hydrous iron monosulfide precursor gel" of spherical form. Recent laboratory advances in synthesizing inorganically formed framboids (Berner, 1969; Farrand, 1970; Sunagawa et al., 1971; Sweeney and Kaplan, 1973) have eliminated the necessity of organic cells or globules to act as structures for framboid development. Sweeney and Kaplan (1973) synthesized pyrite framboids in both anhydrous and aqueous conditions. The mechanism for framboid formation can be summarized as follows:

(i) Spherical texture is developed when the initial iron sulfide precipitate (e.g. mackinawite, $\text{FeS}_{0.9}$) is transformed to greigite (Fe_3S_4) with elemental sulfur $3\text{FeS} + \text{S}^0 \rightarrow \text{Fe}_3\text{S}_4$.

(ii) As greigite further converts to pyrite through the reaction $\text{Fe}_3\text{S}_4 + 2\text{S}^0 \rightarrow 3\text{FeS}_2$, the spherical texture is either retained or changed by internal nucleation of pyrite crystals to form framboids.

Framboidal texture is therefore presumptive evidence for precursor, metastable iron sulfide phases such as mackinawite and greigite.

Downward ionic diffusion of sulfate into sediments and upward ionic diffusion of sulfide due to concentration gradients have been discussed by Goldhaber (1974) and Goldhaber and Kaplan (1974). However, it is possible that diffusion of sulfate and sulfide is only of minor importance in sulfur diagenesis.

During burial and compaction of sediments, upward displacement of pore waters must occur, and this is most pronounced near the sediment-water interface. In areas of slow sedimentation, the relative effect of water migration will be small, because the water content of sediments is relatively constant. In the rapidly depositing nearshore basins, deple-

tion of sulfate occurs quickly, but upward migration of water would not influence interaction between the solid and dissolved components (Goldhaber and Kaplan, 1974).

(c) Interpretation of Sulfur Isotope Data. Although moderately large variations in the δS^{34} values of sphalerite (15.0 to 26.2‰) and galena (8.5-26.5 ‰) occur, the relative constancy in $\Delta\delta S^{34}$ values (3.6 to 6.2‰) suggests that the two sulfides are isotopically related and probably formed in isotope equilibrium or under conditions approaching this, from a common sulfur source of variable composition. Single crystal, non-framboidal pyrite shows δS^{34} values greater than coexisting sphalerite and galena, indicating that this pyrite was in or approaching isotope equilibrium with sphalerite and galena. Negative values of $\Delta\delta S^{34}$ (pyrite-galena or pyrite-sphalerite) calculated for framboidal pyrite constitute good evidence that isotope equilibrium between this sedimentary pyrite and the Pb-Zn sulfides was not established. Therefore, on the basis of mineralogical and isotope evidence, two types of pyrite in the ore-bearing siltstone can be distinguished.

Isotope data of framboidal pyrite show a spread of about 27‰. The heaviest δS^{34} value is about 24‰, the minimum value of seawater sulfate of Ordovician age (Thode and Monster, 1965). Schwartz and Burnie (1973) show that a flat distribution ranging from δS^{34} of seawater sulfate to values about 25‰ lower in sedimentary sulfides typically indicates shallow marine or nearshore environments with bacterial reduction of seawater sulfate in a closed-system (closed "batches" of sulfate). The cyclic sedimentary sequences and widespread occurrence of carbonaceous matter and pyrite in the sequences in the Howard's Pass district tend to indicate quiet deposition of carbonaceous mud in a closed marine basin. The rela-

tively heavy δS^{34} values of these iron sulfides can be accounted for if the basin was closed or restricted by a subaerial barrier so that bacterial reduction of the limited supply of seawater sulfate periodically went almost to completion.

In shallow marine to nearshore environments, drastic lowering of sulfate concentration through dilution with freshwater will cause a minimum difference between δS^{34} values of dissolved sulfate and sulfide and a large amount of sulfide would form with δS^{34} equal or near to that of dissolved sulfate (Schwartz and Burnie, 1973).

Minimum limit of pH for the formation of acid-soluble metastable iron sulfides and elemental sulfur which subsequently react to form framboidal pyrite is 6.5 (Roberts et al., 1969; Rickard, 1969; Berner, 1964, 1970). If most pyrite formed in the uppermost sediment layers, then the pH would be between 7 and 8. Temperatures of most synthesis experiments and bottom sediments with pyrite formation are probably around $0 \sim 25^{\circ}\text{C}$. If the marine system of the Ordovician sedimentation in the Howard's Pass district can be approximated by a closed, anaerobic, iron oxide, CaCO_3 ($\pm\text{MgCO}_3$) and inert sediment-bearing system which lacks FeCO_3 (Gardner, 1973), the asymptotic $\text{SO}_4^{=}$ concentration in pore waters is estimated to have a minimum of 0.0045 mole/kg H_2O ; the $\text{SO}_4^{=}$ concentration in pore waters has been evaluated for modern marine sediments (among others, Kaplan, 1963; Clarke, 1942; Manheim and Sayles, 1971; Manheim et al., 1970; Sayles and Manheim, 1971; Sayles et al., 1971) and generally falls in the range of 0.005 to 0.01 mole/kg H_2O . Laboratory measurements on first and second dissociation constants of H_2S simulating sulfur diagenesis by Goldhaber (1974) indicate that dissolved sulfur in pore waters of marine sediments exists predominantly as HS^- (70 \sim 90% of the total), and H_2S (10 \sim 30%); $\text{S}^{=}$ comprises less than 1% of the total.

The isotope data of galena, sphalerite and "ore-stage" pyrite show a total spread of about 20% (8.5 to 28.0%), and require a different process of sulfur diagenesis than that for framboidal pyrite formation. Since the most probable temperature range of ore deposition is between 60 to 160°C with a mean of 140°C, bacterial reduction of sulfate in sediments does not seem to contribute the major dissolved sulfur for lead-zinc sulfide formation; besides, even allowing compaction as a major process for introducing metal ions towards the sediment surface or forming hot brine pools in the bottom sediment-water interface, the high temperatures require some other process to produce H_2S or HS^- for sulfide deposition. The ultimate cause for introducing hot brine with metal ions is difficult to resolve: thermal spring discharging into the closed basin would be a convenient process and readily account for the hot brine, although it is difficult to explain the fine-scale cyclic sequences involving mineralization: black calcareous siltstone (base) → bedded pyrite and minor lead-zinc sulfides in siltstone → grey, cherty or siliceous, Pb-Zn-rich calcareous siltstone (top) and repeat upward. A rather uniform periodical pulse of thermal spring discharge would be required to explain such cyclic sequences. If dewatering accompanying sediment compaction after burial is the major driving energy for introducing heated, metal ion-bearing brines migrating upward or laterally into the sediment surface on the closed basin, then cyclic sequences can be accounted for by a continuous and moderate sedimentation rate and accompanying compaction. Assuming a geothermal gradient of 30°C/km, the source area of major compaction and dewatering process would be at a depth of well over 2 km.

In any case, the isotope data and estimated temperatures require that a heat source be provided in the closed basin, sulfur can then be produced

by the following process as suggested by Toland (1960) and Orr (1974) as a precipitator of sulfides — chemical reduction of sulfate to H_2S and elemental sulfur without significant isotope fractionation through the reactions:

(i) sulfate-hydrogen sulfide reaction:



(ii) oxidation of hydrocarbon by S^0 :



(iii) net reaction:



These reactions are simply a more detailed mechanism for the chemical reduction of sulfate by organic matter in which H_2S is a catalyst as well as a reaction product. The net reaction is the same as for bacterial reduction of sulfate except that the ratio of H_2S to CO_2 will vary with the state of oxidation of the organic matter oxidized (Orr, 1974). The sulfate reduction process is therefore a kinetically controlled process that gives considerably less isotope fractionation than bacterial sulfate reduction because of some special circumstance. This circumstance is not understood but may involve the "closed-system effect" or complete reduction of sulfate supplied to the reduction site. Two possible circumstances can be offered for the marine system under consideration:

(i) If significant amounts of metal sulfides have formed by diffusion of seawater sulfate into the sediments without escape of sulfide produced, then δS^{34} of the sulfide will approach the δS^{34} value for seawater; as some sulfide forms near the sediment-water interface, the final δS^{34} of total sulfide in any particular stratigraphic layer will be less

than δS^{34} of seawater sulfate but may still be considerably larger than 0%. This will be found in places where organic content is high (thus a high content of reduced sulfur, including initial iron sulfide, elemental sulfur and dissolved sulfide), sedimentation rate is quite low, and the sulfate gradient is steep (i.e. rapid disappearance of dissolved sulfate with depths).

(ii) If the content of pyrite sulfur in the surface sediment is low, the influence of the reduced form of dissolved sulfate on δS^{34} is higher; and if some sulfide formation occurs from chemical reduction of trapped dissolved sulfate, δS^{34} of the sulfide can be relatively enriched in S^{34} and approaches the sulfate.

6. Summary

Sulfate isotope study of sulfide ores and barites from the Anvil deposits indicate that δS^{34} values of sulfide ores typically ranged between 7.9 to 24.7‰, and those of barites ranged between 24.9 to 36.8‰. Sulfur isotope fractionation temperatures estimated by sphalerite-galena pairs fall in the range of 181 to 319°C, and temperatures estimated from the fractionation between pyrite and galena are generally consistent with sphalerite-galena temperatures. Isotopic equilibrium between galena, sphalerite and pyrite was achieved in ore solutions, whereas only partial isotopic equilibrium was established between barite and sulfides. Thermochemical consideration indicates that δS^{34} of total dissolved sulfur in ore solutions was around 25‰, pH of the solutions was between 4~6 for the entire period of sulfide-sulfate deposition, oxygen fugacity during ore deposition typically ranged between $10^{-34} \sim 10^{-41.5}$ at 200 ~ 250°C. Important aqueous sulfur species in ore solutions during sulfide ore deposition were H_2S , $SO_4^{=}$ and HS^- ; and the total sulfur content of ore solutions

was around $0.01 \sim 0.001$ mole/kg H_2O . It is concluded that Cambro-Ordovician seawater sulfate played a major role in determining sulfur isotope compositions of sulfide ores in the Anvil deposits. Mixing of seawater with ascending hot brines seems to be the most likely mechanism for fixing final sulfur isotope compositions of the ore solutions.

δS^{34} values of sulfide ores in Thompson Creek deposit ranged between 9.6 to 17.8‰, and those of pyrite in country rocks ranged between 14.4 to 14.9‰. Temperatures estimated by sphalerite-galena isotope fractionation were between 194 and 318°C, averaging 269°C, and those by pyrite-galena pair were between 205 and 319°C, averaging 259°C. Isotope equilibrium was attained between the sulfide species. The range of f_{O_2} and f_{S_2} during ore deposition is estimated to be $10^{-37.3}$ to $10^{-40.3}$ and $10^{-8.5}$ to $10^{-10.8}$ bars, respectively. pH of the ore solution was neutral to slightly alkaline (5.5 to 7.5). Most of the isotope data of galena and sphalerite are best described by isotope fractionation with either H_2S or HS^- dominant solution.

δO^{18} values of quartz from Thompson Creek deposit range between 13.3 and 14.0‰, averaging 13.7‰; δO^{18} of ore solution was estimated to be 4.6‰. Waters equilibrated with sediments during burial and/or sub-sea-floor geothermal metamorphism seem a likely source for the ore solutions.

δS^{34} values of sphalerite, galena and "ore stage" pyrite in ore-bearing siltstone from Howard's Pass district have a range of 8.5 to 28.1‰, and those of sedimentary, framboidal pyrite typically display a large range of -3.2 to 23.9‰. Temperatures deduced from sphalerite-galena isotope fractionation are generally in the range of 63 to 168°C with a mean of 140°C, those for "ore stage" pyrite and galena fractionation are between 111 to 182°C, averaging 142°C. Sulfur isotope data of

sedimentary pyrite can be interpreted to indicate a shallow marine or nearshore environment with bacterial reduction of interstitial seawater sulfate in a closed system. Analogy with modern marine sediments shows that pH of pore waters was between 7 and 8, $\text{SO}_4^{=}$ concentration fell between 0.005 to 0.01 mole/kg H_2O , and dissolved sulfur existed predominantly as HS^- and H_2S . Isotope data and estimated temperatures of ore minerals require that a heat source be provided in a closed basin, and sulfur be produced by chemical reduction of sulfate to H_2S and elemental sulfur without significant isotope fractionation.

C. STUDY OF LEAD ISOTOPES

1. General Statement

The first lead isotope analysis was made in 1927 (Aston, 1927) and more detailed studies were undertaken before 1940 (Nier, 1938; Holmes, 1937). The general theory and mathematical models used in the interpretation of lead isotopes can be found in the literature (Russell and Farguhar, 1960; Kanasewich, 1962, 1968; Hamilton, 1965; Doe, 1970; Russell, 1972; Gale and Mussett, 1973; Richards, Page and Black, 1976; Richards, 1977 (in press)) and will not be reviewed here. However, pertinent equations for interpretation of isotope data will be presented.

The application of lead isotopes to the study of ore deposits has found new advances in recent years due to great improvement in analytical precision techniques (Catanzaro, 1967; Cameron et al., 1969; Tatsumoto et al., 1972; Barnes et al., 1973; Arden and Gale, 1974; Stacey et al., 1969; Cooper et al., 1969) and new and better determinations of lead isotope compositions of meteorites, U and Th decay constants and the age of the earth (Tatsumoto et al., 1973; Jaffey et al., 1971; LeRoux et al., 1963;

Tilton, 1973). Also, more realistic and dynamic approaches in interpreting the observed patterns of lead isotopes in ore deposits can be linked to many factors, among which long-term global tectonic interactions between crusts and mantle and large-scale sedimentary and orogenic processes play the major role.

Ore leads display either "primary" (or ordinary) or anomalous lead isotope patterns. Anomalous lead represents lead that has developed in more than one U-Th-Pb closed-system (i.e. multistage) and is generally believed to be derivative from a crustal source. On the contrary, controversy exists as to the source of the "primary" ore leads. Apparent uniformity of U/Pb and Th/U ratios calculated for the source of many stratiform deposits has been cited as evidence for the mantle as the source (Russell, 1956; Stanton and Russell, 1959; Ostic et al., 1967; Kanasevich, 1968); the same uniformity can be explained by concentration and thorough mixing of large volume of crustal rocks (e.g. sediments) which give rise to the "primary" ore leads (Chow and Patterson, 1962; Brown, 1965; Armstrong, 1968; Richards, 1971; Doe and Zartman, 1975). Th/U ratio calculated for the source region of primary leads is about 4 (Stacey et al., 1969; Cooper et al., 1969), which is similar to the average of measured Th/U ratios from shales (Rogers and Adams, 1969). Recent advances in the lead isotope measurement of Cenozoic oceanic basalts reveal that their lead isotope compositions are different from Cenozoic primary ore leads (Tatsumoto, 1966a and b; Gast et al., 1964; Gast, 1967; Patterson and Duffield, 1963; Oversby and Gast, 1970; Cooper and Richards, 1966; Oversby, 1971, 1972; Sun and Hanson, 1975; Sun and Jahn, 1975). The present-day values of U^{238}/Pb^{204} for the source region of basalt leads are significantly lower than those for stratiform ore leads (Gast, 1967). Isotopic and chemical heterogeneities in the

mantle have also been demonstrated (Gast et al., 1964; Tatsumoto, 1966a and b; Sun and Hanson, 1975; Zartman and Tera, 1973; Graeser, 1969). Therefore, the case for a more or less direct mantle source for the "primary" ore leads is now very weak. Furthermore, the writer will present data and reasoning to show that "primary" lead pattern is not necessarily characteristic of large stratiform ore deposits, that anomalous lead pattern should be more frequently observed in many deposits of the so-called conformable lead types in the future, and that the patterns observed are largely the consequence of generation, migration and mixing of ore solutions under varying conditions.

2. Experiments and Calibrations

(a) Lead Extraction. Lead in galena was separated by conventional methods involving acid decomposition, anion exchange and dithiozone extraction. Lead in pyrite, sphalerite and barite was also separated by the same method, except that some different procedures were employed. Detailed description of the method of lead separation and extraction is given in Appendix VII-3.

All glassware and teflon columns used in the separation and extraction of lead were washed in concentrated HNO_3 and rinsed with triple-distilled water before each operation. Only triple-distilled water was used in preparing dilute concentrations of reagents. All chemical reagents used were double-distilled. Although lead contamination after taking these precautionary measures was considered insignificant for common lead analysis, several duplicate analyses were made to provide a check on the contamination level. The level of contamination was found to be negligible and well within experimental error.

(b) Lead Mounting on Filaments. Purified lead acid solution was transferred to a previously outgassed rhenium filament using phosphoric acid and silica gel solution as a mounting medium. The lead phosphate-silica gel mixture presumably underwent chemical reaction on the filament when electric current was applied and finally formed a compound such as lead silica phosphate. A very small amount (~ 1 microgram or less) of lead is adequate for this type of emission source in the mass spectrometer to conduct more than one measurement. All analyses carried out in 1975 used the phosphate-silica gel mounting technique. Those carried out in 1973-1974 used lead sulfide mounted on a single tantalum filament and were performed with the $\text{Pb}^{207}\text{-Pb}^{204}$ double-spiked normalization procedure described by Compston and Oversby (1969). Supplementary analyses of standards and samples were made using $\text{Pb}(\text{OH})_2$ mounted on a rhenium triple-filament (Catanzaro, 1967). Some of the earlier results (Kuo and Folinsbee, 1974) are reported and used in the present study.

Detailed description of mounting procedures is given in Appendix VII-3.

(c) Mass Spectrometric Measurement. Lead isotope analyses were made on a 12" radius curvature, 90° sector, single focussing mass spectrometer (described by Cumming et al., 1971) in the Mass Spectrometry Laboratory, Dept. of Physics, University of Alberta. Digital techniques were used to control the magnetic current supply and to read the signal from the mass spectrometer. In the mass spectrometer source, the samples were ionized at 1.5 to over 2.0 amps. filament current in a vacuum of about 1×10^{-7} to 5×10^{-8} atm. and accelerated to 4.5 kV. The filament current varied from one analysis to another, depending on sample size, amount of volatile elements present, etc.. The mass spectrum was scanned by incremental

magnetic field sweeping, this scanning being synchronized with the data reading of the beam signal which is recorded in digital form on magnetic tape.

The data reduction techniques have been reported by Cumming et al. (1971). The lead isotope data recorded on magnetic tape were processed in the following series of operations: the data are filtered, peaks are located, peak heights adjusted for baseline are determined along with the respective times, ratios of peak heights are determined by a polynomial fitting. The data were processed by a FORTRAN computer program written by G.L. Cumming.

(d) Experimental Errors and Calibration of Standards. Analytical errors are attributed mostly to instrumental error derived from isotope fractionation in the mass spectrometer, inaccurate measurements of Pb^{204} mass spectra and non-linearity of the recording apparatus. The error caused by the latter varies in inverse proportion to peak height and results in a measured value lower than the true value, and is most pronounced for the Pb^{204} mass spectra. This error could be masked by other errors in the measurement of Pb^{204} spectra. Isotope fractionation in the mass spectrometer varies depending on the length of time of a measurement and the filament settings used. The most serious error occurs in measuring the small Pb^{204} mass spectrum because it is most susceptible to variations in background.

An indication of the expected Pb^{204} error and fractionation effect can be effected by the intercomparison of NBS standard #981 (Equal Atom Lead) as shown in Table VII-9. Earlier calibration of Broken Hill #1 Galena standard by double-spiked and triple-filament procedures is also given for reference. The calibrated and absolute values of the standards

TABLE VII-9

Calibration of Lead Isotope Standards NBS #981 Equal Atom Lead and
Broken Hill #1 Galena

Standard	No. of Analyses	Pb ²⁰⁶ Pb ²⁰⁴	Pb ²⁰⁷ Pb ²⁰⁴	Pb ²⁰⁸ Pb ²⁰⁴	Remarks
NBS #981	14	16.8839 ± .0237	15.4322 ± .0218	36.5076 ± .0521	Silica gel-phosphate method, Analysts: D. Kristic and S.L. Kuo
		16.9371	15.4913	36.7213	N.B.S. absolute values
(Normalization factor)		X1.00315	X1.00383	X1.00585	For silica gel-phosphate method in 1975
Broken Hill #1	15	15.989 ± .029	15.333 ± .024	35.470 ± .059	Double-spike method, Analysts: D. Kristic and S.L. Kuo
	5	15.991 ± .009	15.378 ± .011	35.575 ± .019	Triple-filament method, Analyst: S.L. Kuo
		16.004	15.394	35.668	Average of Cooper <u>et al.</u> (1969) and Stacey <u>et al.</u> (1969)
(Normalization factor)		X1.00094	X1.00398	X1.00558	For double-spike method in 1973
		X1.00081	X1.00104	X1.00262	For triple-filament method in 1973

are graphically shown in Fig. VII-12. It is evident that most errors can be attributed to Pb^{204} measurement uncertainty, even though some isotopic fractionation effect exists in the phosphate-silica gel emission procedure. The normalization factors, i.e. degree of deviation from absolute values, are also given in Table VII-9.

3. Results and Discussion

(a) Anvil Range District. Lead isotope analyses of galena, pyrite, sphalerite and barite from Faro, Grum and Swim Lakes deposits were made. The results given in Table VII-10 are presented as absolute ratios, having been normalized to the absolute ratios of the NBS or Broken Hill standards.

Lead isotope analyses of galena in massive ores and veins from the Anvil Range district have been previously reported by LeCouteur (1973). His results are used here for comparison.

The isotope data are presented graphically in Fig. VII-13a and b. It is obvious from the figures that the Anvil ore leads display a distinctly anomalous pattern. New and "better fit" growth curves have recently been proposed by many writers using new values of U and Th decay constants, precise measurement of troilite Pb and the age of the Earth (Sinha and Tilton, 1973; Oversby, 1973; Stacey and Kramers, 1975; Cumming and Richards, 1975; Doe and Zartman, 1975). Among these, the curves defined by Doe and Zartman and Cumming and Richards best approach the isotope data. Other curves (not shown) lie significantly below the data points. The curve given by Doe and Zartman (D + Z) represents "average orogene" throughout geologic time and average mixture of material from continental and upper mantle ("asthenosphere") sources. The curve by Cumming and Richards (C + R) allows for the known discrepancy in young

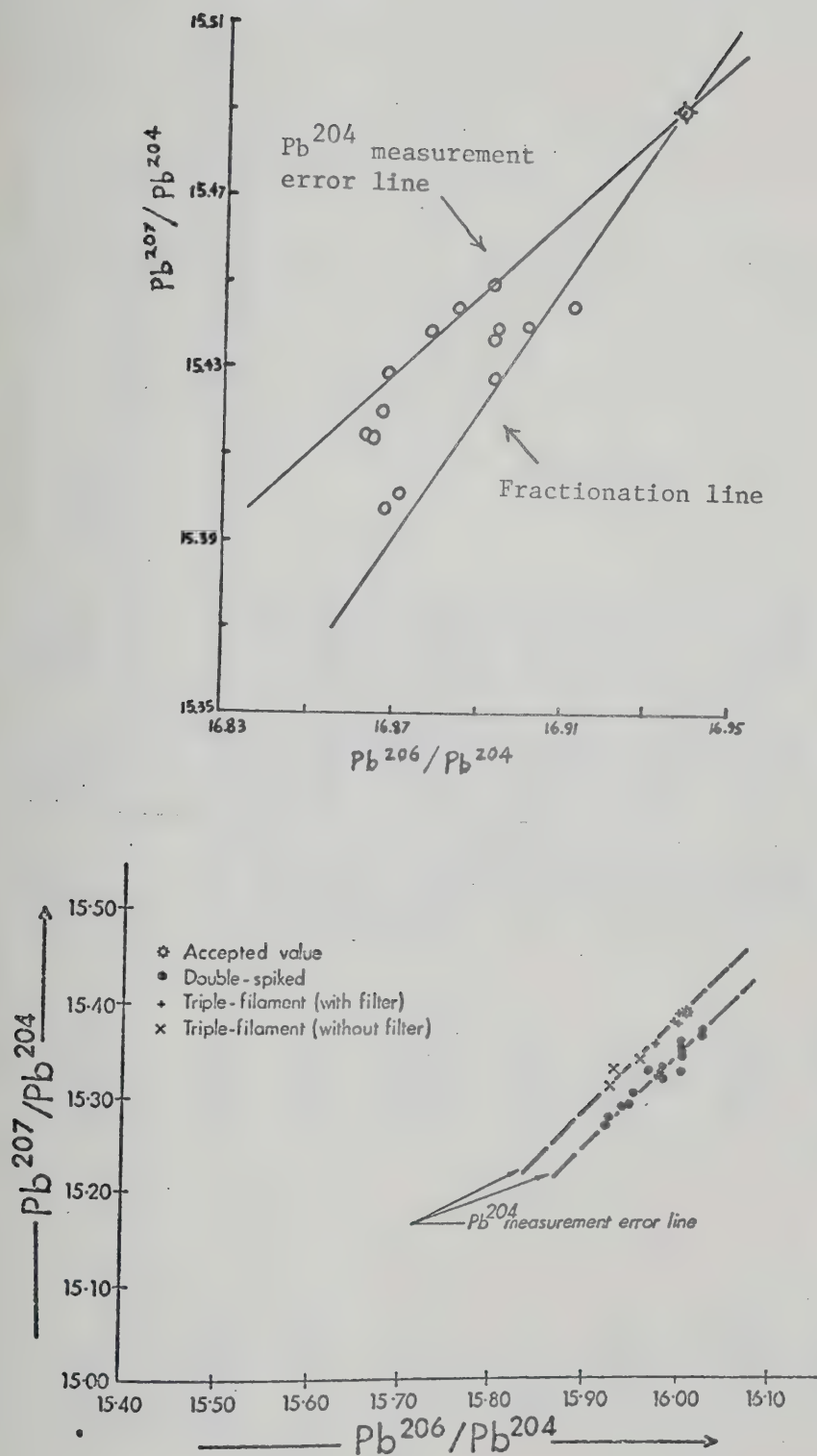


Fig. VII-12. Calibration of lead isotope standards.
 (a) N.B.C. #981 Equal Atom Lead Standard. Silica gel-phosphate method. Star: reported ratio by N.B.S. (1975 Analyses).
 (b) Broken Hill #1 Galena Standard (1973 Analyses).

TABLE VII-10

Normalized Lead Isotope Ratios of Ore Minerals, Anvil Ore Deposits, Yukon

Sample	Mineral	$\frac{\text{Pb}^{206}}{\text{Pb}^{204}}$	$\frac{\text{Pb}^{207}}{\text{Pb}^{204}}$	$\frac{\text{Pb}^{208}}{\text{Pb}^{204}}$	Remarks
(Faro)					
66E9-299	Barite	18.441 $\pm .015$	15.708 $\pm .013$	38.501 $\pm .031$	Silica gel-phosphate method
66-2 305	Barite	18.387 $\pm .014$	15.639 $\pm .012$	38.394 $\pm .030$	"
67-6 602	Sphalerite	18.632 $\pm .028$	15.682 $\pm .023$	38.690 $\pm .057$	"
67-6 790	Galena	18.413 $\pm .010$	15.664 $\pm .008$	38.424 $\pm .020$	"
67-6 790	Pyrite	18.403 $\pm .015$	15.645 $\pm .013$	38.356 $\pm .031$	"
67-10 632	Galena	18.475 $\pm .005$	15.714 $\pm .004$	38.557 $\pm .010$	"
67-10 632	Pyrite	18.507 $\pm .015$	15.705 $\pm .013$	38.602 $\pm .032$	"

TABLE VII-10 (cont'd)

Sample	Mineral	$\frac{\text{Pb}^{206}}{\text{Pb}^{204}}$	$\frac{\text{Pb}^{207}}{\text{Pb}^{204}}$	$\frac{\text{Pb}^{208}}{\text{Pb}^{204}}$	Remarks
Anvil Mine open pit sample #1	Galena	18.372	15.671	38.416	Double-spiked method
		$\pm .010$	$\pm .008$	$\pm .021$	
Anvil Mine open pit sample #2	Galena	18.412	15.709	38.456	"
		$\pm .004$	$\pm .004$	$\pm .008$	
(Grum)					
A10-744	Pyrite	16.447	15.578	36.425	Silica gel-phosphate method
		$\pm .025$	$\pm .024$	$\pm .055$	
		16.462	15.545	36.459	"
		$\pm .016$	$\pm .013$	$\pm .035$	
A10-774	Barite	18.449	15.655	38.379	"
		$\pm .014$	$\pm .012$	$\pm .028$	
A11-497	Galena	18.439	15.663	38.386	"
		$\pm .026$	$\pm .022$	$\pm .053$	
A11-497	Sphalerite	18.349	15.632	38.265	"
		$\pm .013$	$\pm .011$	$\pm .027$	

TABLE VII-10 (cont'd)

Sample	Mineral	$\frac{Pb^{206}}{Pb^{204}}$		$\frac{Pb^{207}}{Pb^{204}}$		$\frac{Pb^{208}}{Pb^{204}}$		Remarks
A12-538	Pyrite	18.472	$\pm .017$	15.667	$\pm .015$	38.415	$\pm .036$	Silica gel-phosphate method
A13-150	Galena	18.328	$\pm .014$	15.614	$\pm .012$	38.259	$\pm .029$	"
(Swim Lakes)								
Swim #9		18.346	$\pm .017$	15.663	$\pm .015$	38.401	$\pm .037$	"

"model ages" by providing for a steady linear change in U/Pb and Th/Pb throughout geological time.

In Fig. VII-13a most ore leads (except A10-744 pyrite and galena veins in Anvil batholith) form a short linear array slightly above the C + R curve, and a primary isochron calculated for their average values ($\text{Pb}^{206}/\text{Pb}^{204} = 18.388$; $\text{Pb}^{207}/\text{Pb}^{204} = 15.677$) gives a model age of 260 m.y., assuming "single-stage" evolution. This model age may be 150 m.y. too young for the true formation age (Doe and Stacey, 1975). Thus the average formation or mineralization age could be 410 m.y. Two analyses of galena in veins cutting Anvil batholith probably represent regenerated material from the pre-existing massive ores during intrusion or related deformation, and can be considered as further mixing of Anvil ore leads with a radiogenic lead (see also Fig. VII-13b). The galena vein data points are shown only for reference and are not used in calculating slope of anomalous lead lines. The least radiogenic lead shown by A10-744 pyrite in massive ore from Grum deposit is rather unexpected and surprising; duplicate analyses show that the values are real and not errors due to contamination or instrumental operation in the laboratory. The anomalous lead line fitted through all the massive ore leads (Fig. VII-13a) has a slope of 0.0593 ± 0.0097 and intersects the D + Z curve at about 500 ± 50 m.y. and 1400 ± 100 m.y. This secondary isochron implies that 1400 m.y. ago $\text{U}^{238}/\text{Pb}^{204}$ ratio was changed to a continuum of values which remained fixed between 1400 and 500 m.y. ago; in other words, there were "single-stage" leads at 1400 and 500 m.y. ago and second-stage leads at 500 m.y. ago whose $\text{U}^{238}/\text{Pb}^{204}$ ratios in the second-stage were either larger or smaller than those in the first stage. Only a "single-stage" lead at 1400 m.y. (A10-744 pyrite) and a series of second-stage

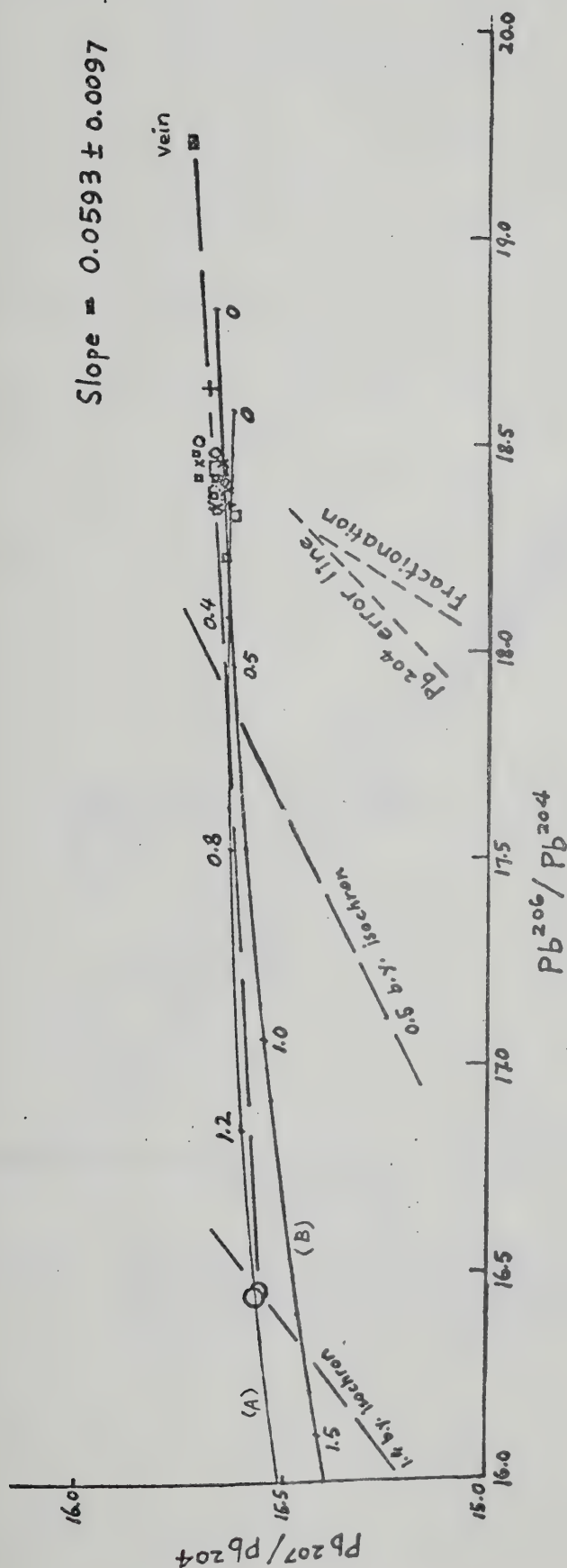


Fig. VII-13a. Lead isotope ratios for galena, sphalerite, pyrite and barite from massive ores and vein galena in Anvil area. Square: galena; cross: sphalerite; circle: pyrite; x: barite. Dotted field represents analyses by LeCouteur (1973). Curve (A): Doe and Zartman (1975); curve (B): Cumming and Richards (1975).

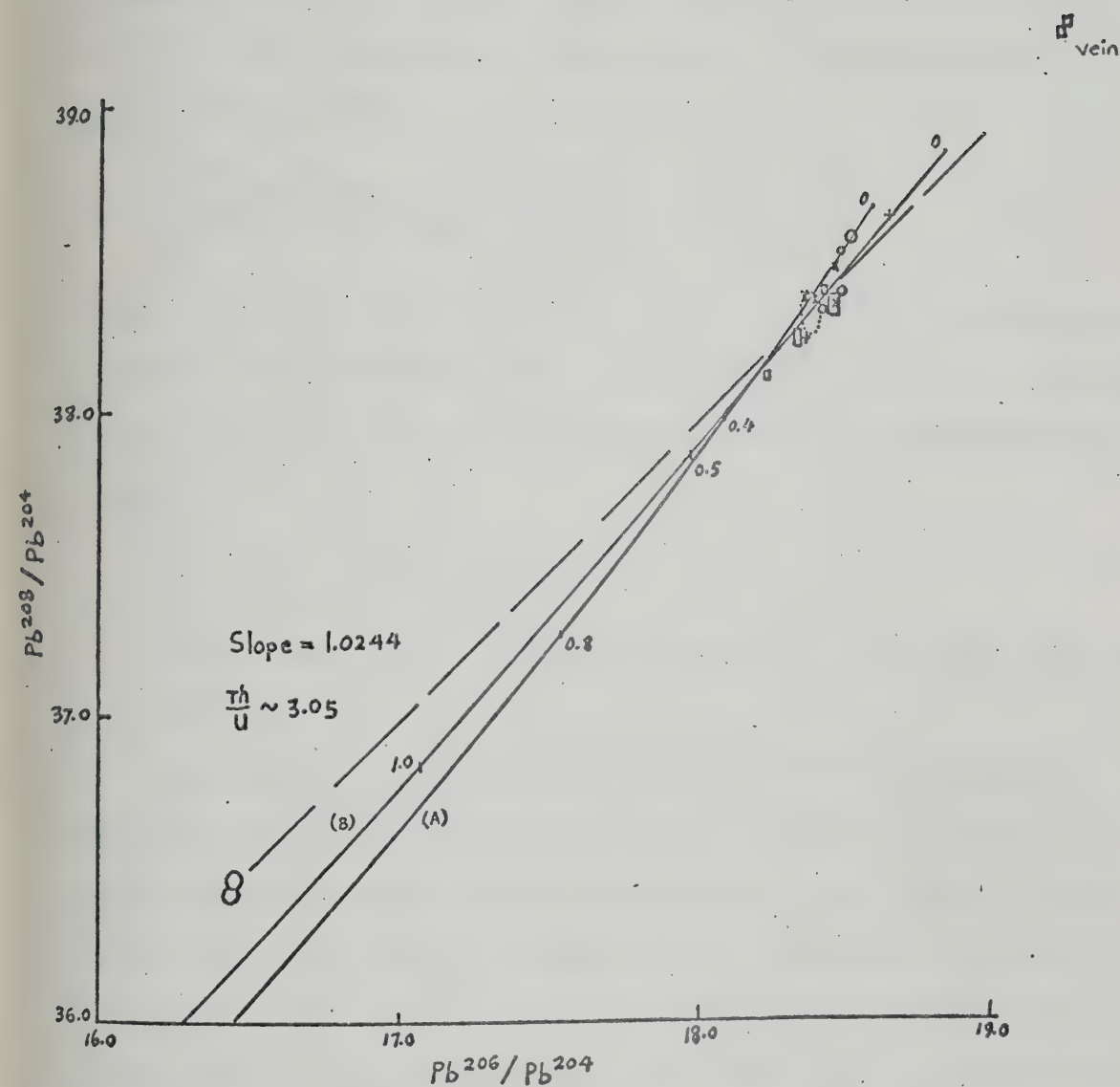


Fig. VII-13b. Lead isotope ratios for galena, sphalerite, pyrite and barite from massive ores and vein galena in Anvil area. Legend same as in Fig. VII-14a.

leads at 500 m.y. whose U^{238}/Pb^{204} ratios are larger than those in the first stage are observed. The anomalous lead line in Fig. VII-13a is tangential to the C + R curve. If the formation time of mineralization and of the source are similar, that is, if $t_m \rightarrow t_s$ in the equation (Doe and Stacey, 1974):

$$R = \frac{(Pb^{207}/Pb^{204})_{t_m} - (Pb^{207}/Pb^{204})_{t_s}}{(Pb^{206}/Pb^{204})_{t_m} - (Pb^{206}/Pb^{204})_{t_s}} = \frac{\lambda' e^{(\lambda' - \lambda)t_s^m}}{137.88 \lambda} \quad (VII-5)$$

where λ is decay constant of U^{238} ($= 0.155125 \times 10^{-9}$), λ' is decay constant of U^{235} ($= 0.98485 \times 10^{-9}$), and t_s^m is the "instantaneous evolution age", and R is the slope of an anomalous lead line. Rearranging Equation VII-5:

$$t_s^m = \ln(R \cdot \frac{137.88 \lambda}{\lambda'}) \div (\lambda' - \lambda)$$

The instantaneous evolution age of the Anvil ore leads is then calculated to be 306 m.y.

In Fig. VII-13b, the anomalous lead line defined by the massive ore data points has a slope of 1.0244 ± 0.0249 , and the corresponding value of Th/U ratio in the integrated source system is calculated to be about 3.05. The linear pattern also means that the ore lead in the region was incorporated in a crustal environment with a rather restricted or narrow range of Th/U ratios in the source rocks. Model age calculated for the average compositions of all massive ore leads ($Pb^{206}/Pb^{204} = 18.388$; $Pb^{208}/Pb^{204} = 38.370$) except A10-744 pyrite is about 250 m.y. on C + R curve, and about 170 m.y. on the D + Z curve.

As pointed out by Cumming and Richards (1975), many lead isotope ratios seem to exhibit a general age dependency, but the true geological ages applicable to these ratios are much less certain. This is not sur-

prising if we accept that effects caused by chemical heterogeneities among major source environments in the earth such as oceanic ridges, active continental margins, and various intraplate regions are superimposed on the isotope evolution of lead with time. Furthermore, as pointed out by Doe and Zartman (1975), extreme local isotopic variation can be produced by the igneous and mineralization processes in the crustal environment.

The anomalous and apparent multistage pattern of the Anvil ore leads can be explained by the following processes:

(i) Circulation and/or interaction of heated seawater through a large volume of rocks ultimately gave rise to pulses of discharging fluids on the seafloor; different pulses might have slightly different lead isotope compositions when precipitating mineral layers.

(ii) By and large the circulation and interaction probably took place in a rather "uniform" manner at shallower depths at which rocks were mostly sediments and volcanics with ages not too much different from the time of circulation-interaction-precipitation (i.e. we would expect closer relationship both in time and isotope composition between initial rock leads and ore leads).

(iii) Minor "deep" or "irregular" circulation through much older rock types such as the Helikian basement below the then sedimentary cover might extract less radiogenic "acid-volatile" leads in solution which, if not well-mixed with the bulk of the brine system, could possibly be preserved in the subsequently precipitated minerals or mineral layers. The only requirement for this process is that galena precipitated from the same solution should also have a less radiogenic composition since a solution containing iron, lead and zinc would become domi-

nated by galena lead. No data on A10-744 galena or sphalerite are available at present.

(iv) If a larger proportion of the extracted leads were derived from oceanic tholeiites and fine-grained sediments in the region (Chapter IV), isotope heterogeneity should be expected since modern oceanic tholeiites usually display distinct lead isotope heterogeneity (e.g. Cumming, 1976).

The above interpretation seems to be best substantiated by the observed isotope pattern and ages derived from intersections of the anomalous lead line with the "average orogenic evolution" curve of Doe and Zartman (1975) - mineralization (circulation-interaction-precipitation) probably took place around 500 ± 50 m.y. ago and minor older and less radiogenic lead of 1400 ± 100 m.y. probably represents material derived from Helikian basement rocks through deep or irregular circulation. If some small portions of the basement rocks were exposed through either block-faulting or uplifting as is common in the region of continental separation, even normal shallow circulation (e.g. $0.6 \sim 1.0$ km, cf. Muehlenbachs, 1976) would be enough to extract leads from these rocks.

The occurrence of variable and/or radiogenic leads derived by leaching of lead from country rocks with hot brines or volcanic fluids has been reported from a number of localities, e.g. the Salton Sea (Doe et al., 1966), the Red Sea (Cooper and Richards, 1969a), and New Zealand (Cooper and Richards, 1969b).

(b) Frances Lake District. Lead isotope analyses were made on galena and sphalerite from Thompson Creek deposit and pyrite from the host rocks. The normalized results are given in Table VII-11.

TABLE VII-11

Normalized Lead Isotope Ratios of Ore Minerals and Host Rock
Pyrites, Thompson Creek Deposit

Sample	Mineral	$\frac{Pb^{206}}{Pb^{204}}$	$\frac{Pb^{207}}{Pb^{204}}$	$\frac{Pb^{208}}{Pb^{204}}$	Remarks
(DDH)					
4-43.5	Galena	18.675 ± .011	15.701 ± .009	38.512 ± .022	(1)
9-61.5	Galena	18.669 ± .009	15.706 ± .008	38.610 ± .019	(1)
9-61.5A	Galena	18.688 ± .014	15.715 ± .012	38.650 ± .029	(2)
19-319	Pyrite	19.025 ± .010	15.748 ± .008	39.044 ± .020	(1) Pyrite from quartz sericite schist
23-413	Pyrite	18.900 ± .027	15.703 ± .022	38.630 ± .0555	(2) Pyrite from quartz sericite schist
30-89	Sphalerite	18.742 ± .025	15.716 ± .021	38.572 ± .053	(2)
30-94	Galena	18.717 ± .011	15.738 ± .009	38.647 ± .022	(1)
30-105.75	Galena	18.655 ± .008	15.672 ± .007	38.465 ± .016	(1)
(Trench)					
546-2	Galena	18.613 ± .013	15.684 ± .011	38.543 ± .027	(2)

(1) Analysis by double-spiked method

(2) Analysis by silica gel-phosphate method

The isotope data are plotted in Fig. VII-14a and b. The ore and sedimentary pyrite leads are isotopically related and they form an anomalous lead line with a slope of 0.1035 ± 0.0058 . The anomalous lead line intersects the D + Z curve at about 400 m.y. and the C + R curve at about 500 m.y. A two-stage calculation can be made for this secondary isochron using Equation VII-5: if mineralization age t_m is 400 m.y., the integrated age of the source material for the ore lead (t_s) is calculated to be 1450 m.y.; if the mineralization age t_m is taken to be 500 m.y., the integrated source age (t_s) is calculated to be 1380 m.y. The significance of this older age cannot be resolved with the available data at hand, except to postulate that the anomalous ore leads were probably the result of mixing an old lead with the rock leads in the region. Three metamorphosed stratabound deposits (Black Jack, Fir Tree, Ron of New Jersey Zinc Corp.) of lead-zinc-silver occur in the gneissic terrain about 30 miles east of the Frances Lake district; the age of mineralization is believed to be Proterozoic, even though precise stratigraphic control is difficult due to high grade metamorphism. If ore lead in the Thompson Creek deposit were derived from these or older deposits, then mixing with leads extracted from large volume of sediments could indeed produce the observed anomalous pattern. Alternatively, the ore lead could very well be the mixing product of underlying Helikian basement rocks and the Cambro-Ordovician sediments (reworked basement ?) if heated or metamorphic formation water traversed and leached lead and other metals from these rocks (see Chapter VI).

The scattered but crudely anomalous pattern of data points plotted in Fig. VII-14b probably indicate a variation in Th/U ratios in rocks from which the anomalous leads were derived; since a linear relationship

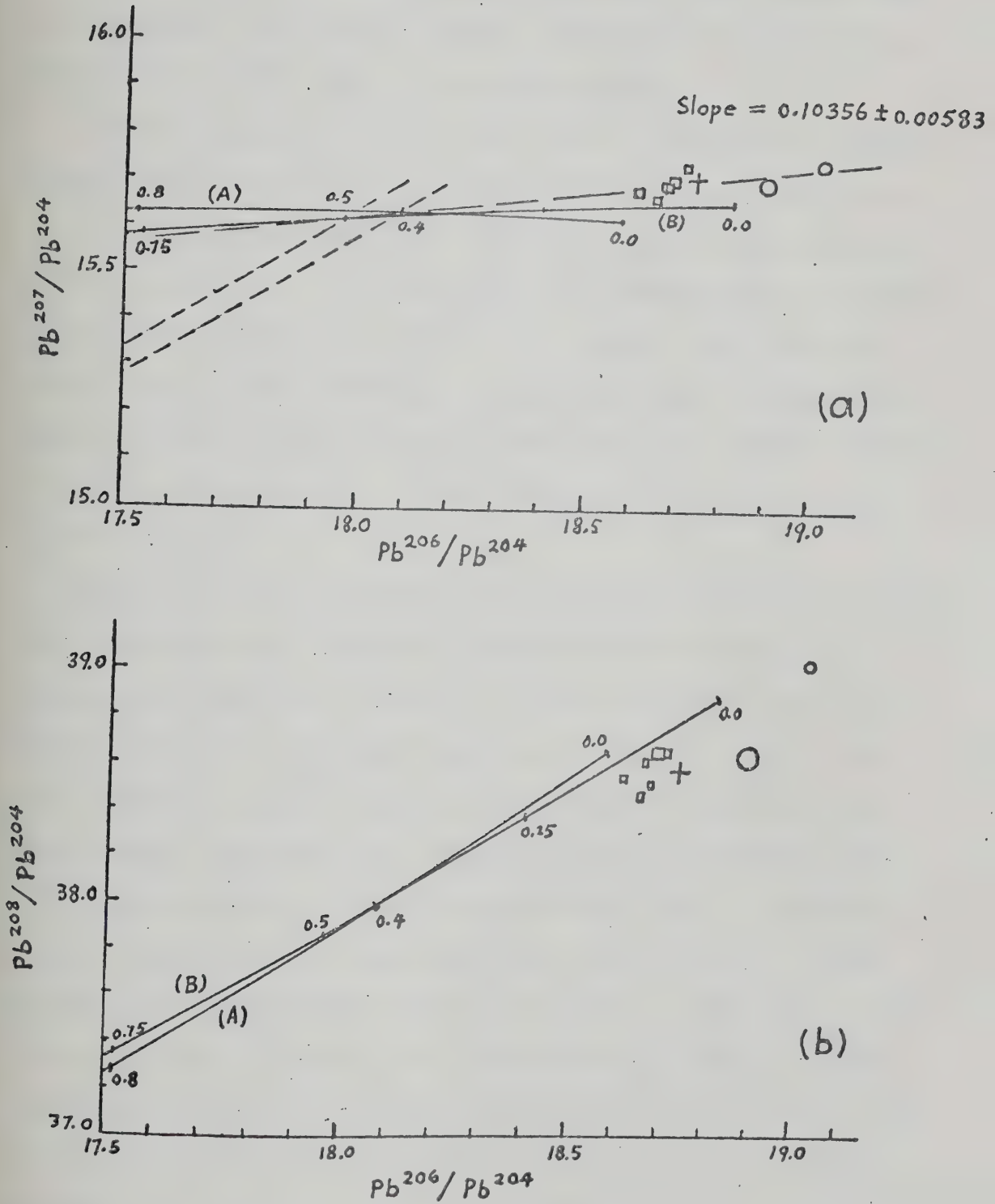


Fig. VII-14. Lead isotope ratios for ores and pyrite in host rocks, Thompson Creek deposit, Frances Lake district. Legend is the same as in Fig. VII-13.

should exist between "ordinary" and anomalous leads if the anomalous leads are mixtures of two uniform components, the scatter and non-linearity also suggest that mixing of several isotopically heterogeneous source materials was the main cause of ore lead formation.

The secondary isochron ages of 400 ~ 500 m.y. agree with the Middle to Upper Cambrian age of the host rocks in which mineralization occurs.

(c) Howard's Pass District. Lead isotope analyses were performed on galena, sphalerite, "ore-stage" pyrite and framboidal pyrite separates from ore-bearing siltstones, Howard's Pass district. Two sedimentary barites from siltstone of Silurian or younger age were also analyzed to compare with the ore and sedimentary pyrite leads. The results normalized to absolute ratios are given in Table VII-12 and presented graphically in Fig. VII-15a and b.

In Fig. VII-15a, ores and one sedimentary pyrite plot along a linear array displaying again a distinctly anomalous pattern. Barites from Silurian siltstones have a distinctly different slope from that of the ore and pyrite leads and appear unrelated to them. Thus the ores possibly originated prior to Silurian baritic siltstone deposition. Because a linear relationship with sedimentary pyrite in Ordovician siltstone is demonstrated, a sedimentary source seems likely. The best-fit anomalous line through the data points has a slope of 0.1367 ± 0.0087 and has an upper intersection with the D + Z curve at about 350 m.y. and with C + R curve at about 450 m.y. The uncertainty in age is probably about 50 m.y. The least radiogenic lead (DDH32-189 Galena) gives a model age of about 270 m.y. on the C + R curve. Assuming again a two-stage evolution, the integrated source age (t_s) can be calculated from Equation VII-5; if $t_m = 350$ m.y. t_s is estimated to be 2015 m.y.; if $t_m = 450$ m.y.,

TABLE VII-12

Normalized Lead Isotope Ratios of Ore Minerals, Sedimentary Pyrite and Barite from Siltstones, Howard's Pass District

Sample	Mineral	$\frac{Pb^{206}}{Pb^{204}}$	$\frac{Pb^{207}}{Pb^{204}}$	$\frac{Pb^{208}}{Pb^{204}}$	Remarks
(Placer's Main Zone)					
DDH6-274	Galena	18.693	15.737	38.864	
		$\pm .011$	$\pm .009$	$\pm .023$	
DDH6-274	Pyrite	18.672	15.690	38.840	"Ore-stage" pyrite
		$\pm .020$	$\pm .017$	$\pm .042$	
DDH29-434.5	Pyrite	18.588	15.684	38.654	Framboidal pyrite
		$\pm .018$	$\pm .014$	$\pm .034$	
DDH32-177.5	Galena	18.677	15.736	38.828	
		$\pm .021$	$\pm .017$	$\pm .043$	
DDH32-189	Galena	18.405	15.664	38.661	
		$\pm .028$	$\pm .023$	$\pm .058$	
DDH32-189	Pyrite	18.611	15.671	38.460	"Ore-stage" pyrite
		$\pm .021$	± 0.18	$\pm .043$	

TABLE VII-12 (cont'd)

Sample	Mineral	$\frac{\text{Pb}^{206}}{\text{Pb}^{204}}$			Remarks
		$\frac{\text{Pb}^{206}}{\text{Pb}^{204}}$	$\frac{\text{Pb}^{207}}{\text{Pb}^{204}}$	$\frac{\text{Pb}^{208}}{\text{Pb}^{204}}$	
Trench #19-1	Sphalerite	18.625	15.672	38.679	
		$\pm .012$	$\pm .010$	$\pm .024$	
(Pas claims, Dynasty-Shield Resources)					
DDH74P1-134	Galena	18.794	15.695	38.703	
		$\pm .028$	$\pm .024$	$\pm .058$	
DDH74P1-134	Pyrite	18.632	15.710	38.839	"Ore-stage" pyrite
		$\pm .017$	$\pm .014$	$\pm .035$	
(Gap claims, Vestor Explorations)					
NBAl-1		18.270	15.296	37.590	Disseminated barite in black
		$\pm .015$	$\pm .013$	$\pm .031$	siltstone, Silurian
(Trois claims, Vestor Explorations)					
SLKJ-10		19.085	15.685	38.505	Baritic siltstone, Silurian
		$\pm .011$	$\pm .009$	$\pm .021$	

Analyses were made by single filament, silica gel-phosphate method.

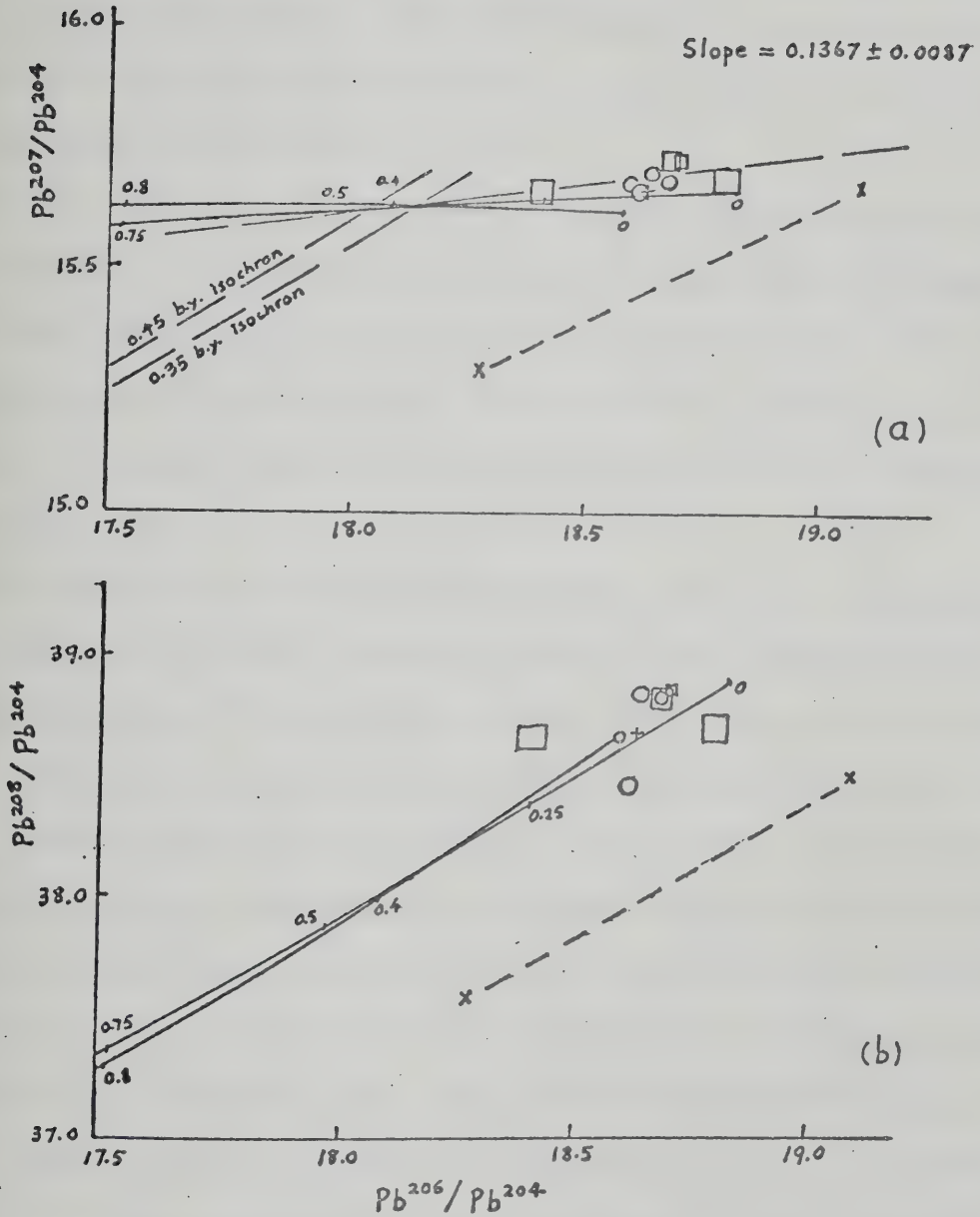


Fig. VII-15. Lead isotope ratios for ores, sedimentary pyrite and barites in siltstones, Howard's Pass district.

t_s will be 1960 m.y. The older age values are meaningless because no basement rocks of this age have ever been suspected to underlie the cratonic margin during lower Paleozoic time. It is also uncertain whether the lead component of this age represents material eroded or derived ultimately from the Bear craton further to the east.

In Fig. VII-15b, ore and pyrite leads are scattered around the thorogenic lead curves, indicating a variation in the Th/U ratios in source rocks and mixing of several isotopically heterogeneous source materials. The baritic siltstones plot significantly below the evolution curves. This behavior is characteristic of the upper crustal region which is enriched in U relative to Th.

The deposits in the Howard's Pass district have been interpreted to have formed in a closed or restricted basin with ore solution derived through squeezing of brines out of the adjacent basins or through dewatering of sediments by compaction. If the ore leads were derived from sources where sediment accumulation approximates a single cycle, closed-basin conditions in Precambrian terrains (modern analogues are the Baltic Sea, Hudson's Bay, Lake Superior, Great Slave Lake), then the resultant leads would be more radiogenic than those derived from sources such as multiply reworked sediments which approximate open ocean conditions (Doe and Zartman, 1975). Leads formed in enclosed basins or by lateral secretion (e.g. Mississippi Valley Pb-Zn ores) are generally highly radiogenic as compared to those formed in open ocean or from multiply reworked sediments (e.g. Pine Point deposit, N.W.T. and Bleiberg deposit, Austria).

(d) Discussion. Lead isotope data from stratiform deposits of Anvil Range and Howard's Pass districts and stratabound replacement deposit of Frances Lake district all without exception display distinctive isotope

heterogeneities and indicate multistage and anomalous lead isotope patterns. The data plot on or above the new evolution curves of Cumming and Richards (1975) and Doe and Zartman (1975) with present-day U^{238}/Pb^{204} values in the ore leads greater than about $9.1 \sim 9.2$. The relatively high U^{238}/Pb^{204} and Th/U values estimated for the environment in which mineralization took place indicate an exclusive or prominent upper crustal source for the ore and initial rock leads in the lower Paleozoic continental margin geosyncline.

The length of the anomalous lead line would depend upon the U/Pb ratio, the length of time available in the second stage (or higher stages), and the degree of homogenization in a geological system (Kanasewich, 1962). If the system remained closed and complete homogenization occurred, the final isotope ratios of ore leads could not be distinguished from a "single stage" ordinary lead. Such a situation is probably approximated in deposits of certain geological systems, e.g. island arc, active continental margin, orogenic belt, pelagic sediments. Logically speaking, however, the crust cannot be considered a perfect closed-system with respect to Pb, U, and Th and anomalous lead or isotope heterogeneity must result in more geological systems than was previously realized. Even in the relatively closed-systems mentioned above, irregularities in lead isotope compositions should be expected since the materials involved in homogenization (or mixing), degree of homogenization (or extent of recycling) and the residence time of ore fluids (from generation to precipitation) between individual systems or even within each system, are variable. Thus for example, Bathurst deposit (in Middle Ordovician rocks) is more radiogenic than Silurian deposits of Australia (e.g. Captain's Flat and Cobar, N.S.W.).

The anomalous leads observed in the Anvil Range, Frances Lake and Howard's Pass districts typically display a "short period" anomalous lead pattern as was defined by Kanasewich (1962). Short period anomalous leads have the following features:

(i) the duration of the second stage of lead evolution is short (generally less than a few tens or hundreds of million years) in comparison to the duration of the first stage.

(ii) experimental precision is essential to recognize some of the short period anomalous leads which display a short elongated field of data points.

(iii) the slope of most short period anomalous lead lines is very nearly tangential to a "single-stage" growth curve, presenting difficulty in estimating intersection ages.

The short linear arrays shown by most Anvil ore leads excluding A10-744 Pyrite and by the Thompson Creek and Howard's Pass ore leads have slopes either nearly tangent to or intersect the "single-stage" growth curve at very shallow angles, and the duration of the last stage (assuming simple two-stage evolution, but really should be multistage, see discussion above) is generally in the order of $100 \sim 200$ m.y.

However, the magnitude of this duration should not be considered absolute or accepted uncritically because the extent of isotope variation observed might be due to other factors discussed before rather than simple age dependency. All that can be said is that for these deposits, leads extracted from source rocks developed for a short period of time in the processes of transportation and mixing prior to final ore precipitation.

The significance of the common existence of short period anomalous lead patterns or isotope heterogeneity within large stratiform (conform-

able) ore deposits is hereby emphasized. Anvil deposits and Howard's Pass ores each probably amount to well over 100 million tons of lead and zinc ore. The modern examples (Fig. VII-16a) of short period anomalous leads can be found in the Red Sea (Chow, 1968; Cooper and Richards, 1969a; Delevaux et al., 1967; Delevaux and Doe, 1974), the Salton Sea (Doe et al., 1966) brines which precipitate heavy metal sulfides and oxides at present.

Ancient stratiform ore deposits that show distinctly anomalous leads (Fig. VII-16b and c) occur in all geological ages; these include:

(i) Miocene: Um Gheig, and related deposits, East-central Egypt along Red Sea coast (Doe and Zartman, 1975).

(ii) Miocene: Kuroko deposits, Japan (Doe and Zartman, 1975; Sato and Sasaki, 1973; Sato et al., 1973).

(iii) Middle Proterozoic: Mount Isa, and McArthur River (H.Y.C. deposit), Australia (Gulson, 1975; Richards, 1975).

(iv) Middle Proterozoic: Sullivan and related deposits in the Aldridge Formation, Kimberley district, B.C. (Leech and Wanless, 1962; Zartman and Stacey, 1971; LeCouteur, 1973).

(v) Hudsonian to Helikian (1900 ~ 1140 m.y.?): Ruttan Lake deposit, Manitoba (Haverslew, 1975).

(vi) Archean (2000 m.y.): Flin Flon and related deposits, Manitoba (Russell and Farquhar, 1960; Doe, 1967; unpublished data by Isotopes Inc. for Hudson Bay Metal Mining Co. Ltd., 1967; Stacey et al., 1969; Sinha, 1970; Sangster, 1972; Slawson and Russell, 1973).

(vii) Archean (2700 m.y.): Manitouwadge deposits, Ontario (Ostic, 1963; Ostic et al., 1967; Stacey et al., 1969).

(viii) Archean (3350 m.y.): Massive pyritic deposits in the Barber-ton Mountain Land and Murchison Range, Archean Greenstone Belt, South Africa (Saager and Koppel, 1976).

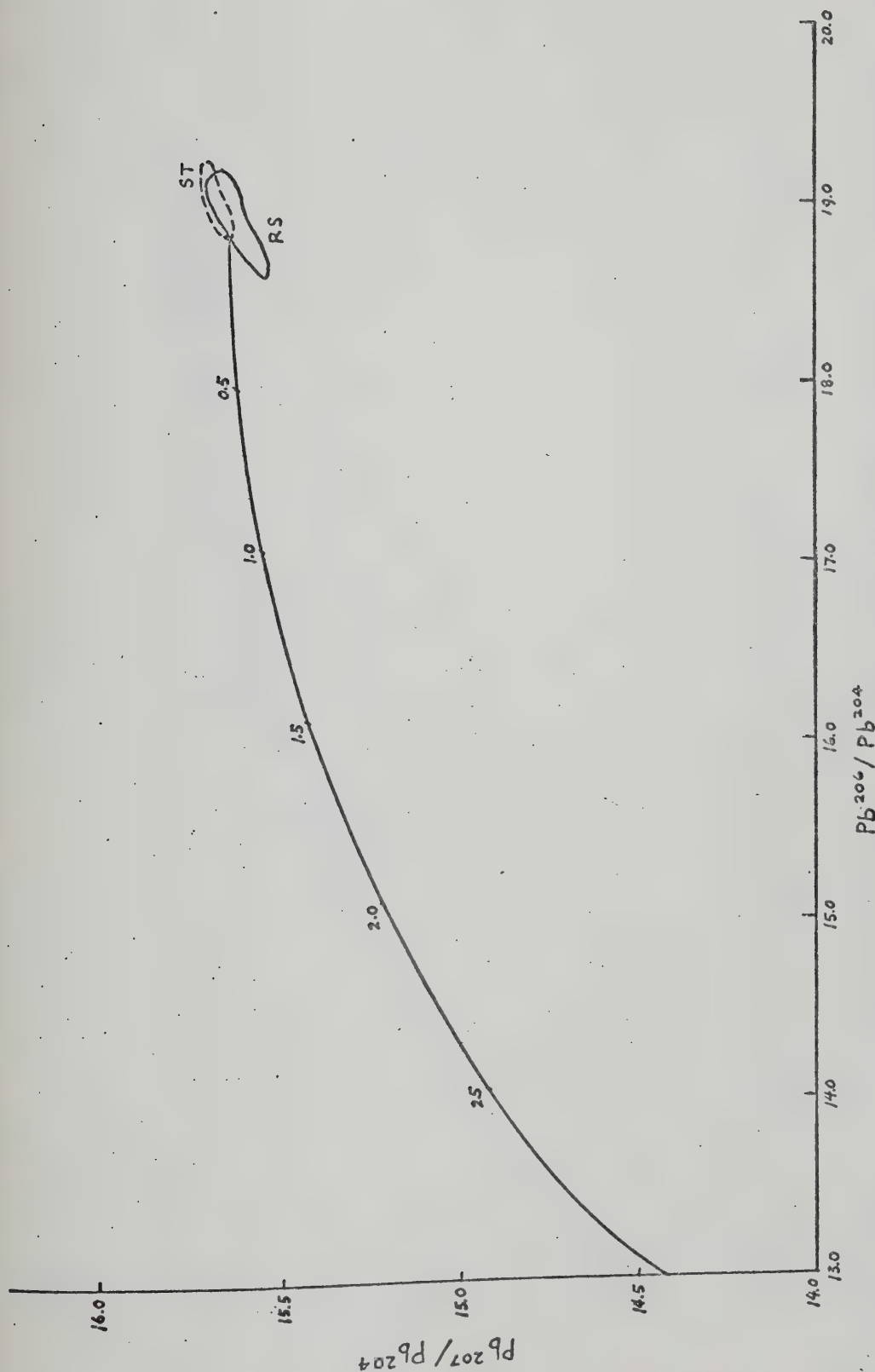


Fig. VII-16. Modern and ancient stratiform ore deposits as examples of anomalous leads or isotope heterogeneities. Evolution curve is that of Cumming and Richards (1975).
 a) ST: Chloride brine, Salton Trough geothermal area, California; RS: Chloride brine and metalliferous sediments, Red Sea.

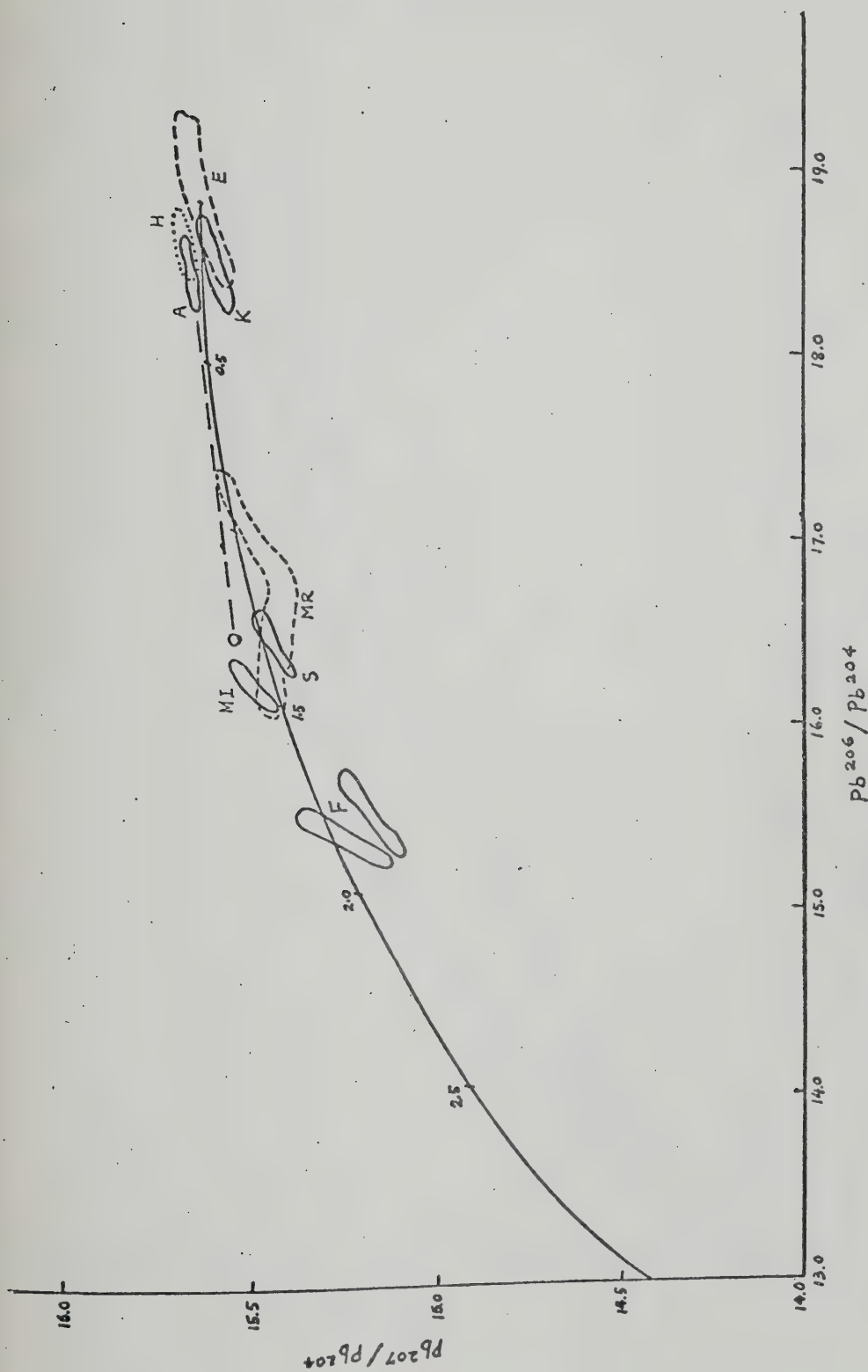


Fig. VII-16. b) A: Anvil deposits, Yukon. H: Howard's Pass deposits, Y.T.-N.W.T. K: Kuroko deposits, Japan. E: Um Gheig and related deposits, Egypt. MI: Mount Isa, Australia. MR: McArthur River (H.Y.C.) deposits, Australia. S: Sullivan and related deposits in Aldridge Formation, B.C. F: Flin Flon and related deposits, Manitoba.

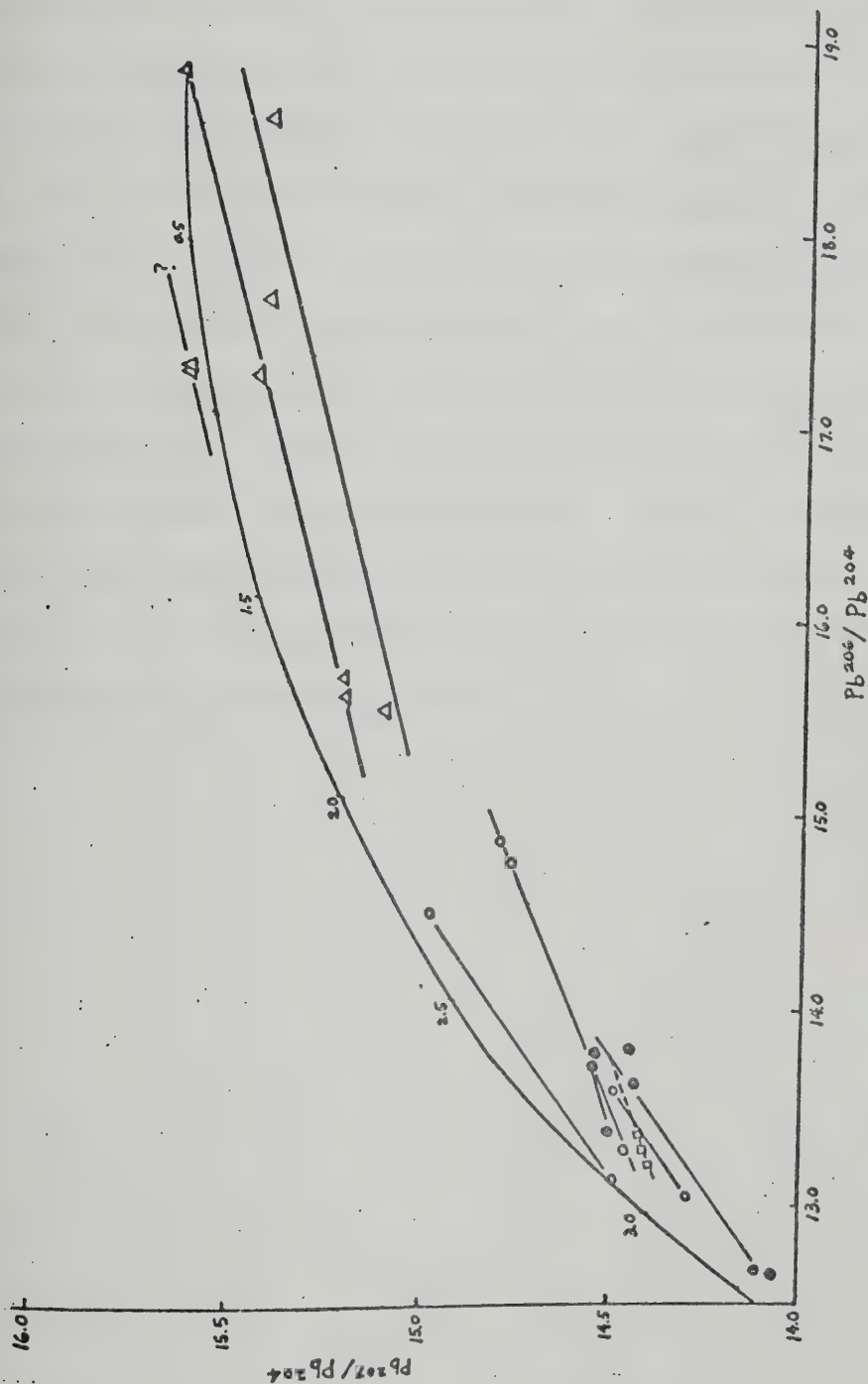


Fig. VII-16. c) Triangles: Ruttan Lake deposit, Manitoba.
 Squares: Manitowadge deposits, Ontario.
 Open Circles: Sheba Queen and related deposits, Barberton Mountain Land, South Africa.
 Solid Circles: Letaba and related deposits, Murchison Range, South Africa.

The list is undoubtedly longer. The writer believes that as more lead isotope studies are carried out on the major stratiform deposits, especially on other major mineral components of the deposits, more complex and heterogeneous isotope patterns will be encountered and deviation from the "single-stage" growth curve will become a common feature rather than an exception. Extensive analyses of major geological/mineralogical units within and around a stratiform deposit should be made in order to make useful interpretations of lead isotope data.

It is proposed here that anomalous leads or isotope heterogeneity should be frequently found in stratiform deposits in regions of oceanic ridges or continental rifts, primitive island arcs of strong oceanic affinity (e.g. Tonga-Kermadec), enclosed sedimentary basins, and continental or marine regions where shallow hydrothermal circulation or lateral secretion processes are active.

Chapter VIII

CHEMICAL COMPOSITION OF ORE SOLUTIONS

A. INTRODUCTION

This chapter presents an estimation of initial concentrations of metallic elements and major dissolved species in ore solutions responsible for the formation of the Anvil ore deposits and the Thompson Creek ore deposits, by making certain reasonable assumptions and using physico-chemical factors deduced from previous chapters. Discussion of the possible types of complex ions of metals in the solutions prior to ore deposition is also briefly made in conjunction with the estimation.

Estimation of diagenetic interstitial metal-bearing brines in Howard's Pass district is not made because of great difficulty and insufficient knowledge in considering complex processes in addition to the known physico-chemical factors. The processes include diffusion of dissolved ions, pore fluid convection, diagenetic changes involving carbonate equilibria, sulfate reduction by bacteria, uptake of cations in alumino-silicate minerals, and ion exchange between pore fluids and sediments.

B. ANVIL ORE DEPOSITS

Solubility of metallic ions in aqueous sodium chloride solutions has been evaluated both theoretically and experimentally by Helgeson (1969), Melent'yev et al. (1968), Hennig (1971), Nriagu (1970, 1971a,b), Hinners (1963) and others. The general expression is the molarity of total dissolved ions, which can be defined if the temperature, ionic strength (molarity of alkali chloride), pH of the solutions and some other pertinent

ent parameters such as stoichiometric individual ion activity coefficient (γ) and total dissolved sulfur ($m_{\Sigma S}$) are known. There are different approaches in estimating the solubility data.

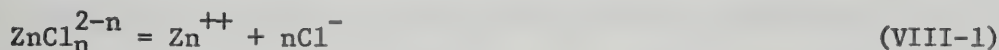
One can assume the metallic ions in original solutions are precipitated as solid phases now observed and set up equilibrium chemical reactions between these phases and the solutions and calculate molarities of the ions concerned; or one can set up equilibrium chemical reactions between one or two major phases and the solutions, calculate molarities of these ions, and estimate the solubility of other ions by using the atomic ratio among them as deduced from the metallic compositions now observed in a deposit. The former approach relies entirely on ideal chemical equilibria and estimate of optimum saturation equilibrium for each ion (or phase) and disregard the complicated relations of partitioning among different ion-complexes. The latter approach also assumes chemical equilibria but takes into account the interrelation of phases and the overall ratio of these phases in a large and essentially chemically constant reservoir (deposit); certain reasonable assumptions are necessary in this approach. The writer adopts the second approach and makes the following assumptions for estimating solubility in the Anvil ore solutions:

(i) All the heavy metals dissolved initially in the ore solution were precipitated and fixed in the deposits, i.e. the relative abundance of initially dissolved heavy metals was the same with that fixed in the present deposits as minerals.

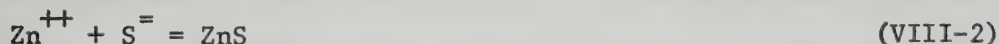
(ii) The chemical compositions and physico-chemical conditions of the ore solution prior to and during ore deposition remained largely constant.

(iii) The dissolved sulfur in the solution is sufficient to precipitate all the dissolved heavy metals.

Since sphalerite is a major ore sulfide in the Anvil ore deposits, and because chemical equilibrium appears to have been established between sphalerite and other metal sulfides on the one hand and ore solution on the other hand, estimate of initial concentration of total dissolved zinc ion (Zn^{++}) in ore solutions is made and used to estimate solubility of other metal ions. Theoretical and experimental data on the solubility of zinc and its complex ions in sodium chloride solution were given by Helgeson (1969), Melent'yev (1968) and Hennig (1971). Assuming the principal chemical equilibrium reactions describing the dissolution of ZnS in the lower pH region ($2 \sim 6$) to be:



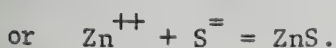
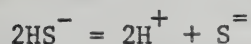
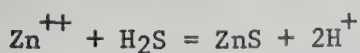
$$(n = 1 \sim 4)$$



The solubility of Zn^{++} at a given temperature (Equation VIII-2) is given by:

$$m_{\text{Zn}^{++}} = \frac{K}{\gamma_{\text{Zn}^{++}} \gamma_{\text{S}^{=}} m_{\text{S}^{=}}} \quad (\text{VIII-3})$$

Here $m_{\text{S}^{=}}$ can be approximated by total dissolved reduced sulfur ($m_{\Sigma\text{S}}$) since Equation VIII-2 is obtained by combining the reactions:



Using the thermodynamic constants given by Helgeson (1969), the molarity of zinc in 1 mole NaCl solution (average salinity of Anvil ore solution as deduced from fluid inclusion study) with total dissolved

sulfur (m_{S}) of 0.001 mole (lower limit of concentration in Anvil ore solution, see Chapter VII) can be calculated as functions of temperatures, pH, and dominant types of complex ions. The calculated results are shown graphically in Fig. VIII-1a and the experimental results by Hennig (1971) in Fig. VIII-1b. Experimental results given by Melent'yev (1968) were used by Mercer (1975, personal communication) to calculate a non-charged neutral complex $\text{Zn}(\text{HS})_2^0$, which is also shown in Fig. VIII-1a. This complex is found to be an insignificant contributor to the observed ZnS solubility. Over the temperature range ($200\sim 250^\circ\text{C}$) and pH range ($4.5\sim 5.5$), the major zinc "carriers" are probably zinc-chlorides (ZnCl^- , ZnCl_2 , ZnCl_3^- , ZnCl_4^{--}) and to a much lesser extent $\text{Zn}(\text{HS})_2$ and $\text{Zn}(\text{HS})_3^-$ (i.e. $\text{ZnS-H}_2\text{S-HS}^-$). Most of the sulfur, however, is provided by hydrothermal reduction of dissolved sulfate through mixing with seawater upon discharge of ore solution (see Chapter VII). Initial condition of ore solution was characterized by higher temperature (250°C) and lower pH ($4.5\sim 5.5$). At these conditions, the concentration of zinc calculated from Equation VIII-3 ranges from 0.1 to 6.7 ppm and averages about 3.4 ppm. The experimental data of Hennig (Fig. VIII-1b) give a concentration of zinc of 2.9 ppm at a pH of about 5.5. The two estimates by both theoretical and experimental data thus agree well. As a first approximation, initial concentration of total dissolved zinc ion in Anvil ore solution is estimated to be about 3 ppm. The initial concentrations of other metal ions in the ore solution can then be calculated by using the atomic ratio of metals to zinc. The results are given in Table VIII-1. Estimation of Ba^{++} concentration (which was precipitated as sulfate and not sulfide) by assuming equilibrium conditions with other metal ions such as Zn^{++} is valid if the three assumptions are satisfied.

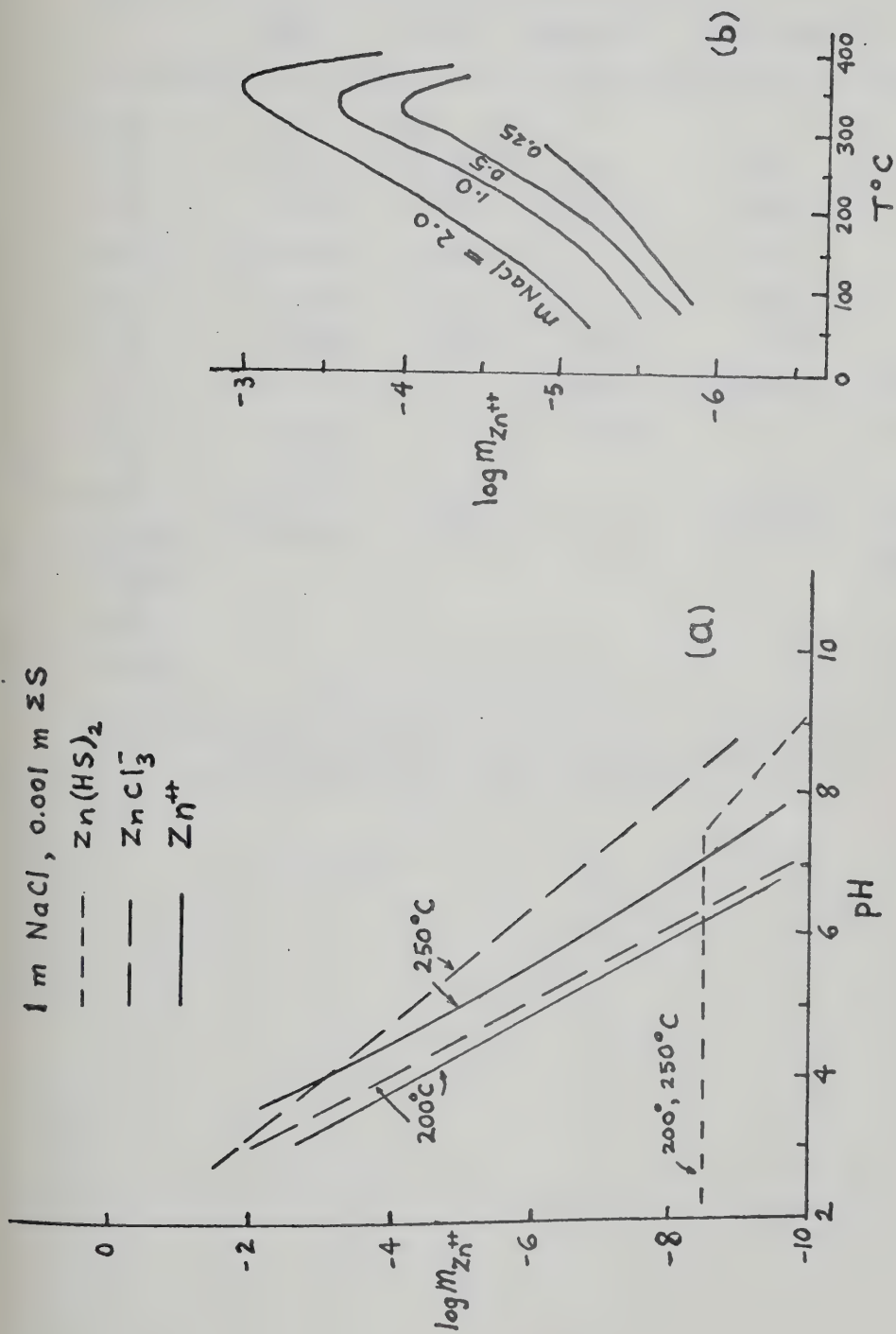


Fig. VIII-1. (a) Calculated solubility of complex ions of zinc as a function of T° and pH at 1 m NaCl and 0.001 m ΣS . (b) Experimental solubility of ZnS as a function of T° and $mNaCl$ at a pH of 5.5 (after Hennig, 1971).

TABLE VIII-1

Initial Concentrations of Major Ions in
Anvil Ore Solutions (ppm)

	Faro	Grum	Vangorda	Swim Lakes	Mean
Zn	3	3	3	3	3
Fe	22.7	16.0	20.8	17.9	19.4
Pb	0.6	0.6	00.6	0.6	0.6
Ba	0.12	0.06	-	0.2	0.13
Cu	0.08	0.12	0.17	0.09	0.12
Ag	0.001	0.002	0.002	0.002	0.002
Au	-	-	0.00001	0.00001	0.00001
As	0.01	-	0.98?	-	~ 0.01
Mn	0.07	-	-	-	0.07
NaCl	83,300	59,300	-	51,500	64,700
H ₂ S					10 ~ 30
HS ⁻					1.7
SO ₄ ⁼					10 ~ 60

-: no estimation made due to lack of information.

The solubility of H_2S , $\text{SO}_4^{=}$ and HS^- can be calculated from mole fractions of dissolved sulfur species at given temperature and pH. A total dissolved sulfur concentration of 0.001 mole/kg H_2O has been previously derived. The concentrations of three sulfur species in ore solution are calculated over the temperature of 200~250°C and pH of 4.5~5.5. The results are also shown in Table VIII-1.

For comparison, chemical compositions of ore solution estimated for Kuroko ore deposits of Japan and Red Sea Hot brines are listed in Table VIII-2 together with the mean chemical composition of the Anvil ore solution. The concentration level of $\text{SO}_4^{=}$, H_2S , Pb, Zn in Anvil and Kuroko ore solutions is strikingly similar, whereas Red Sea Hot Brine shows a similar level of concentration of Fe, Ba and Cu with that of the Anvil ore solution.

C. THOMPSON CREEK ORE DEPOSIT

Using an approach similar to the above, the initial concentration of zinc in the ore solution responsible for the formation of the Thompson Creek ore deposit is estimated and the concentrations of other elements are estimated by using the atomic ratios among metals observed presently in the deposit.

Conditions for the formation of Thompson Creek deposit are: average temperature = 250°C, pH = 5.5~7.5, average NaCl wt.% = 12 (equivalent to 2 mole NaCl). Taking an average pH of 6 and a minimum total dissolved sulfur content of 0.001 mole/kg H_2O , the initial concentration of zinc can be calculated from Equation VIII-3 using thermodynamic constants given by Helgeson (1969), and this results in a molarity of 10^{-6} or about 0.07 ppm zinc. From this value the concentrations of other metallic ions in

TABLE VIII-2

Comparison of Chemical Composition of
Kuroko Ore Solution, Red Sea Brines and
Anvil Ore Solution (ppm)

	Kuroko*1	Anvil	Red Sea*2
Salinity	31,000	64,700	257,600
SO ₄	100	10~60	770
H ₂ S	>20	10~30	?
Ca	400	-	5135
Fe	?	19.4	80
Zn	2	3	5
Pb	0.5	0.6	0.6
Ba	20	0.13	0.9*3
Cu	1	0.12	0.3

*1: Estimates are taken from Ichikuni (1975)
at T > 250°C, pH < 5.

*2: Estimates summarized in Emery *et al.* (1969)
for Atlantis II and Discovery Deeps (T°C =
45 ~ 57).

*3: Craig (1969), for Atlantis II Deep.

the Thompson Creek ore solution can be estimated. The results are given in Table VIII-3. Also shown are the concentration of H_2S and HS^- in the ore solution as estimated from a total dissolved sulfur content of 0.001 mole/kg H_2O and $X_{\text{H}_2\text{S}} = 0.7$ and $X_{\text{HS}} = 0.3$ (see Chapter VII). Data on the concentration of dissolved ions in solutions directly or indirectly responsible for some basemetal replacement type deposits in Tertiary (e.g. Toyoha Pb-Zn deposit, Japan, Miocene in age; East Tintic Pb-Zn-Ag deposits, Utah, Early Tertiary in age) and Recent (e.g. Broadland Geothermal area, New Zealand) settings are also shown in Table VIII-3. These deposits were formed mainly in a subaerial to terrestrial environment. Comparison of the table shows that Thompson Creek ore solution generally has comparable concentration of metallic ions but higher salinity as compared with those in the ore solution or thermal effluent associated with the other deposits mentioned.

The composition estimate made for the Thompson Creek ore solution should be considered as a rough approximation only, because immature cessation of boiling or termination of sulfur generation or supply might have occurred (see Chapter VII) and therefore either assumption (i) or (iii) may not have been entirely satisfied.

TABLE VIII-3

Chemical Composition of the Thompson Creek Ore Solution as Compared with other Replacement Type Deposits (unit in p.p.m.)

	Fe	Zn	Pb	Sb	Ag	Mn	Cu	H ₂ S	HS ⁻	NaCl
Thompson Creek	0.07	0.07	0.02	0.002	0.005	0.003	0.001	23.8	10.2	~120,000
Toyoha*1	-	0.01	-	-	-	-	-	(> 300)	-	27,000
E. Tintic*2	1.0	0.1	present	0.15	0.007	0.6	0.07	0.3	-	6,170
Broadland*3	-	0.015	0.005	-	0.002	-	0.012	64.0	?	5,500

*1: Shikazono (1974)

*2: White (1967)

*3: Browne (1971)

Chapter IX

CONCLUSIONS

Detailed studies have been carried out on the geology and geochemistry of ore deposits in the Anvil Range, Frances Lake, and Howard's Pass districts in the southern Yukon and southwestern District of Mackenzie, N.W.T.. Six deposits have been included in the studies. The deposits are all interpreted to be lower Paleozoic in age, covering a time span of less than 50 million years from Middle-Upper Cambrian to Middle-Upper Ordovician. They are therefore essentially coeval deposits forming in three unique geological environments in a region best interpreted as a continental margin geosyncline. From a reinterpretation of the regional geological setting in southern Yukon and southwestern District of Mackenzie, coupled with chemical evidence on some conformable volcanic sequences in the western part of the region, it is concluded that there existed a passive (e.g. Atlantic-type) continental margin geosyncline in which initial continental separation occurred over an extended period of time from Late Proterozoic to Lower Paleozoic in the western part of the geosyncline. From the margin oceanward (westward), the geosyncline was characterized by a sedimentary complex of carbonate-orthoquartzite sequences on the shelf, with lutite and turbidite forming above subsided escarpment or basin on the continental rise and abyssal plain beyond the slope, with the latter transitional to an "outer ridge" or oceanic rise with accumulation of fine-grained turbidites, clastics and oceanic tholeiites to island tholeiites. Interruption or termination of initial continental separation took place in the lower Paleozoic while the Atlantic type geosyncline continued to develop with a prograding sedimentary wedge building oceanwards. Major subsidence of the buried marginal escarpments or basins beyond the slope occurred during this period.

The ore deposits forming on or below seafloor in each distinctive sedimentary-tectonic setting across the continental margin geosyncline have been shown to display unique features reflecting variations in geological environment, pattern and nature of ore fluid generation, physico-chemical conditions and properties of ore fluids, and mode of deposition. These variations are summarized as follows:

(i) The deposits forming in "outer ridge", i.e. the outer part of the geosyncline where oceanic tholeiites were extruded are typically stratiform, massive sulfides; the seawater depth was generally moderate to deep, confining pressure was also moderate; the seafloor topography was probably quite rugged with abundant basinal depressions and "ridges"; ore fluid was mostly circulating heated connate brine (recycled seawater) through hot rock-seawater interaction with significant leaching of acid-volatile metals and adsorption from various sources such as clays, hydroxides, carbonaceous matter, silicate minerals in sediments and volcanics; heat source was probably furnished by volcanic activity but could be due also to contemporaneous sub-seafloor geothermal metamorphism; temperature, salinity, density, pH and other physico-chemical properties of the ore fluid were to a large extent controlled or influenced by the mixing process with overlying seawater upon discharging; ore deposition occurred in favorable depressions forming either stratified or unstratified brine pools and seawater sulfate provides most of the dissolved sulfur for metal chlorides to precipitate sulfides. Mixing could also have occurred in vents from which ascending brines discharged.

(ii) The deposits forming in the region of "central" deeper basin or escarpment are mainly replacement type sulfide layers or masses with limited extent of mineralization; confining pressure on these deposits was

slightly greater than in the first case and probably due to some lithostatic load pressure since these deposits were formed as replacements below the seafloor; ore fluid was mainly derived from heated formation water due to burial and/or sub-seafloor geothermal metamorphism and apparently boiled before reaching sediment-water interface; cooling, dilution and some other causes such as seal-off of open spaces, etc. might terminate prematurely the replacement process and limit the extent of mineralization. In a sense these are stratabound replacement deposits which can be classified broadly as Mississippi Valley type deposits; sulfur source in these deposits was mostly in-situ sedimentary sulfide.

(iii) The deposits forming in near shelf region are typically well-laminated to disseminated, very fine-grained sulfides in silty calcareous clastic sediments; the confining pressure and depth of seawater on the sediments were generally moderate and shallow; the deposits occur over a wide area; metal-bearing fluids were most probably derived from updip migration of intraformational brines from adjacent basins or from a compaction dewatering process, but also through thermal spring activity; the depositional environment was probably a restricted shallow marine basin with relatively quiet deposition in an anaerobic, iron oxide, carbonate and inert sediment-bearing system; ore deposition took place at lower hydrothermal temperatures ($60\sim 150^{\circ}\text{C}$) through mainly non-biological, chemical reduction of dissolved sulfate in seawater or pore fluids without significant isotope fractionation due to "closed system" effect or complete sulfate reduction.

The above characteristic features of ore deposits forming in distinctive sedimentary-tectonic settings across a passive continental margin geosyncline may be significant and have general application in similar geo-

logical settings in both ancient and modern environments. Minor variation or even omission of certain types of deposits may occur in other regions of similar geological settings, but the general distribution and type of deposits should be the same.

Occurrence of massive sulfides in sediments in hot brine areas of the Red Sea rift valleys and "Mississippi Valley type" stratabound deposits of Um Gheig, Bir Ranga, Um Ans and Zur Bahar along Red Sea coast of Egypt may be cited as good Recent analogies to the present model. It is speculated that modern regions that might show similar distribution of deposits include Kuroko deposits-Japan Sea-Asiatic continental margin, Juan de Fuca Ridge and northwestern U.S.A. continental margin, most of Atlantic ridges and the Atlantic continental margins.

BIBLIOGRAPHY

- Ackermann, D. and Morteani, G., 1973: Occurrence and breakdown of paragonite and margarite in the Greiner Schiefer Series Zillerthal Alps, Tyrol. Contr. Mineral. Petrol., 40: 293-304.
- Aitken, J.D., 1959: Atlin map-area, B.C.. Geol. Surv. Can., Memoir 307.
- Amagat, E.H., 1892: Sur la détermination de la densité des gaz liquéfiés et de leurs vapeurs saturées. Compt. rend., 114: 1093-1098.
- Arden, J.W. and Gale, N.H., 1974: New electrochemical technique for the separation of lead at trace levels from natural silicates. Anal. Chem., 46: 1-9.
- Armstrong, R.L., 1968: A model for the evolution of strontium and lead isotopes in a dynamic earth. Rev. Geophys., 6: 175-199.
- Arnold, R.G., 1967: Range in composition and structure of 82 natural terrestrial pyrrhotites. Can. Mineral., 9: 31-50.
- 1969: Pyrrhotite phase relations below $304 \pm 6^\circ\text{C}$ at <1 atm total pressure. Econ. Geol., 64: 405-419.
- 1971: Evidence for liquid immiscibility in the system FeS-S. Econ. Geol., 66: 1121-1130.
- Aston, F.W., 1927: The constitution of ordinary lead. Nature, 120: 224.
- Aumento, F., 1967: Magmatic evolution on the mid-Atlantic Ridge. Earth Planet. Sci. Lett., 2: 225-230.
- 1968: The mid-Atlantic Ridge near 45°N . II: Basalts from the area of Confederation Peak. Can. Jour. Earth Sci., 5: 1-21.
- 1971: Uranium content of mid-oceanic basalts. Earth Planet. Sci. Lett., 11(2): 90-94.
- Aymé, J.M., 1965: The Senegal Salt Basin. In: Salt Basins Around Africa. London Inst. Petrol.: 83-90.
- Baadsgaard, H., Folinsbee, R.E. and Lipson, J., 1961: Potassium-argon dates of biotite from Cordilleran granites. Geol. Soc. Amer., Bull. 72: 689.
- Bachinski, D.J., 1969: Bond strength and sulfur isotopic fractionation in coexisting sulfides. Econ. Geol., 64: 56-65.
- Banno, S., 1959: Aegerinaugites from crystalline schists in Shikoku. Geol. Soc. Japan. Jour., 65: 652-657.
- 1964: Petrologic studies on Sanbagawa crystalline schists in the Beeshi-Ino district, central Shikoku, Japan. Jour. Fac. Sci., Univ. Tokyo, Sect. V, 15: 203-319.

-
- 1966: Eclogite and eclogite facies. Japan Jour. Geol. Geogr., 37: 101-122.
-
- 1970: Classification of eclogites in terms of physical conditions of their origin. Phys. Earth Planet. Interiors, 3: 405-421.
- Banno, S. and Matsui, Y., 1965: Eclogite types and partition of Mg, Fe and Mn between clinopyroxene and garnet. Japan Acad. Proc., 41: 716-721.
- Barnes, I.L., Murphy, T.J., Gramlich, J.W. and Shields, W.R., 1973: Lead separation by anodic deposition and isotope ratio mass spectrometry of microgram and smaller samples. Anal. Chem., 45: 1881-1884.
- Barton, P.B., 1970: Sulfide petrology. Mineral. Soc. Amer., Spec. Paper 3: 187-198.
- Barton, P.B. and Skinner, B.J., 1967: Sulfide mineral stabilities. In: H.L. Barnes, Ed., Geochemistry of Hydrothermal Ore Deposits. Holt, Reinhart and Winston, Inc., New York: 236-333.
- Barton, P.B. and Toulmin, P., 1964: Experimental determination of the reaction chalcopyrite + sulfur = pyrite + bornite from 350° to 500°C. Econ. Geol., 59: 747-752.
-
- 1966: Phase relations involving sphalerite in the Fe-Zn-S system. Econ. Geol., 61: 815-849.
- Battey, M.H., 1974: Spilites as weakly metamorphosed tholeiites. Ibid., 365-372.
- Beeson, M.H. and Jackson, E.D., 1970: Origin of the garnet pyroxenite xenoliths at Salt Lake Crater, Oahu. Mineral. Soc. Amer., Spec. Paper 3: 95-112.
- Bell, R.T., 1968: Proterozoic stratigraphy of northeastern B.C.. Geol. Surv. Can., Paper 67-68.
- Bence, A.E., Papike, J.J. and Ayuso, R.A., 1975: Petrology of submarine basalts from the central Caribbean: DSDP Leg 15. Jour. Geophys. Res., 80(35): 4775-4804.
- Ben-Yaakov, S., 1973: pH buffering of pore water of recent anoxic marine sediments. Limnol. Oceanogr., quoted in Goldhaber and Kaplan, 1974.
- Berner, R.A., 1964: Distribution and diagenesis of sulfur in some sediments from the Gulf of California. Marine Geol., 1: 117-140.
-
- 1969: The synthesis of framboidal pyrite. Econ. Geol., 64: 383-384.
-
- 1970: Sedimentary pyrite formation. Amer. Jour. Sci., 268: 1-23.

- Berner, R.A., Scott, M.R. and Thomlinson, C., 1970: Carbonate alkalinity in the pore waters of anoxic marine sediments. *Limnol. Oceanogr.*, 15: 544-549.
- Bertine, K.K. and Keene, J.B., 1974: Submarine barite-opal rocks of hydrothermal origin. *Science*, 188: 150-152.
- Blanchard, R. and Hall, G., 1942: Rock deformation and mineralization at Mount Isa. *Aust. Inst. Min. Metall., Proc.*, 125: 1-60.
- Blusson, S.L., 1966: Frances Lake, Y.T.. *Geol. Surv. Can.*, Map 6-1966.
- 1967: Nahanni, District of Mackenzie and Y.T.. *Geol. Surv. Can.*, Map 8-1967.
- 1968: Geology and tungsten deposits near the headwaters of Flat River, Y.T. and southwestern District of Mackenzie. *Geol. Surv. Can.*, Paper 67-22.
- Bostock, H.S., 1948: Physiography of the Canadian Cordillera with special reference to the area north of the 55th parallel. *Geol. Surv. Can.*, Memoir 247.
- 1970: Physiographic subdivision of Canada. *In*: *Geology and Economic Minerals of Canada*, Chapter 2. *Geol. Surv. Can.*, *Econ. Geol. Rept. No. 1*: 11-30.
- Bostrom, K., Frazer, J. and Blankenburg, J., 1967: The solid solution series in the PbSO_4 - BaSO_4 system. *Arkansas Mineral. Geol.*, Paper 27, 4(6): 477-485.
- Bottinga, Y. and Craig, H., 1969: Oxygen isotope fractionation between CO_2 and water and the isotopic composition of marine atmospheric CO_2 . *Earth Planet. Sci. Lett.*, 5: 285.
- Boyle, R.W., Wanless, R.K. and Stevens, R.D., 1970: Sulfur isotope investigation of the lead-zinc-silver-cadmium deposits of the Keno Hill-Galena Hill area, Yukon, Canada. *Econ. Geol.*, 65: 1-10.
- Brathwaite, R.L., 1969: The geology of the Rosebery ore deposits. Unpub. Ph.D. thesis, Univ. Tasmania.
- Brew, D.A., Loney, R.A. and Muffler, L.J.P., 1966: Tectonic history of southeastern Alaska. *Can. Inst. Min. Metall., Spec. vol.* 8: 149-170.
- Brown, G.C. and Fyfe, W.S., 1972: The transition from metamorphism to melting: status of the granulite and eclogite facies. *Internat. Geol. Congr.*, 24th session, Sect. 2: Petrology: 27-34.
- Brown, J.S., 1965: Oceanic lead isotopes and ore genesis. *Econ. Geol.*, 60: 47-68.

- Browne, P.R.L., 1971: Mineralization in the Broadland geothermal field, Taupo volcanic zone, New Zealand. Proc. IMA-IAGOD Meetings, Joint Symp. Vol.: 64-75.
- Browne, P.R.L. and Lovering, J.F., 1973: Composition of sphalerites from the Broadlands geothermal field and their significance to sphalerite geothermometry and geobarometry. Econ. Geol., 68: 381-387.
- Cameron, A.E., Smith, D.H. and Walker, R.L., 1969: Mass spectrometry of nanogram-size samples of lead. Anal. Chem., 41: 525-526.
- Campbell, F.A. and Ethier, V.G., 1973: Sulfur isotopes, iron content of sphalerites and ore textures in the Anvil ore body, Canada. Econ. Geol., 69: 482-493.
- Campsie, J., Bailey, J.C., Rasmussen, M. and Ditter, F., 1973: Chemistry of tholeiites from the Reykjanes Ridge and Charlie Gibbs fracture zone. Nature Phys. Sci., 244: 71-73.
- Cann, J.R., 1969: Spillites from the Carlsberg Ridge, Indian Ocean. Jour. Petrol., 10: 1-19.
- 1970: Rb, Sr, Y, Zr and Nb in some ocean floor basaltic rocks. Earth Planet. Sci. Lett., 10: 7-11.
- Carmichael, I.S.E., Turner, F.J. and Verhougen, J., 1974: Igneous Petrology. McGraw-Hill Book Co., New York.
- Catanzaro, E.J., 1967: Triple-filament method for solid-sample lead isotope analysis. Jour. Geophys. Res., 72: 1325-1327.
- Chase, R.L., 1969: Basalt from the axial trough of the Red Sea. In: E.T. Degens and D.A. Ross, Eds., Hot Brines and Recent Heavy Metal Deposits in the Red Sea. Springer-Verlag, New York: 122-128.
- Chatterjee, N.D., 1970: Synthesis and upper stability of paragonite. Contr. Mineral. Petrol., 27: 244-257.
- 1971: Preliminary results on the synthesis and upper stability limit of margarite. Naturwissenschaften, 58: 147.
- 1972: The upper stability limit of the assemblage paragonite + quartz and its natural occurrence. Contr. Mineral. Petrol., 34: 288-303.
- Chisholm, E.O., 1957: Geophysical exploration of a lead-zinc deposit in Yukon Territory: methods and case histories in mining geophysics. 6th Commonwealth Min. Metall. Congr.: 269-277.
- Chow, T.J., 1968: Lead isotopes of the Red Sea region. Earth Planet. Sci. Lett., 5: 143-147.

- Chow, T.J. and Patterson, C.C., 1962: The occurrence and significance of lead isotopes in pelagic sediments. *Geochim. Cosmochim. Acta*, 26: 263-308.
- Chukrov, F.V., Yermilova, L.P., Churikov, V.S. and Nossik, L.P., 1975: Regeneration of sulfate and their isotopic composition of natural sulfur. *Chem. Geol.*, 16: 39-51.
- Church, T., 1970: Unpub. thesis, Univ. California, San Diego.
- Clark, J.R. and Papike, J.J., 1968: Crystal-chemical characterization of omphacites. *Amer. Mineral.*, 53: 840-868.
- Clayton, R.N. and Epstein, S., 1958: The relationship between O^{18}/O^{16} ratios in coexisting quartz, carbonate and iron oxides from various geologic deposits. *Jour. Geol.*, 66: 352-373.
- Clayton, R.N., O'Neil, J.R. and Mayeda, T.K., 1972: Oxygen isotope exchange between quartz and water. *Jour. Geophys. Res.*, 77: 3057-3067.
- Coleman, R.G., 1967: Low-temperature reaction zones and alpine ultramafic rocks of California, Oregon and Washington. *U.S. Geol. Surv., Bull.* 1247.
- Coleman, R.G. and Lee, D.E., 1963: Glaucophane-bearing metamorphic rock types of the Cazadero area, California. *Jour. Petrol.*, 4: 260-301.
- Coleman, R.G., Lee, D.E., Beatty, L.B. and Brannock, W.W., 1965: Eclogites and eclogites: their differences and similarities. *Geol. Soc. Amer., Bull.*, 76: 483-508.
- Coleman, R.G., Tatsumoto, M., Coles, D.G., Hedge, C.E. and Mays, R.E.: 1973: Red Sea basalts. *Trans., Amer. Geophys. Union*, 54(11): 1001-1002.
- Compston, W. and Oversby, V.M., 1969: Lead isotopic analysis using a double spike. *Jour. Geophys. Res.*, 74: 4338-4348.
- Coombs, P.S., 1974: On the mineral facies of spilitic rocks and their genesis. *In*: G.C. Amstutz, Ed., *Spilites and Spilitic Rocks*. Springer-Verlag, New York: 373-386.
- Cooper, J.A. and Richards, J.R., 1966: Lead isotopes and volcanic magmas. *Earth Planet. Sci. Lett.*, 1: 259-269.
-
- 1969a: Lead isotope measurements on sediments from Atlantis II and Discovery Deep areas. *In*: E.T. Degens and D.A. Ross, Eds., *Hot Brines and Recent Heavy Metal Deposits in the Red Sea*. Springer-Verlag, New York: 499-511.
-
- 1969b: Lead isotope measurements on volcanics and associated galenas from the Coromandel-TeAroha region, New Zealand. *Geochem. Jour.*, 3: 1-14.

- Cooper, J.A., Reynolds, P.H. and Richards, J.R., 1969: Double-spike calibration of the Broken Hill standard lead. *Earth Planet. Sci. Lett.*, 6: 467-478.
- Cornwall, H.R. and Rose, H.J., 1957: Minor elements in Keweenaw lavas, Michigan. *Geochim. Cosmochim. Acta*, 12: 209-224.
- Craig, H., 1961: Standards for reporting concentrations of deuterium and oxygen-18 in natural waters. *Science*, 133: 1833-1834.
- 1963: The isotopic geochemistry of water and carbon in geothermal areas. Conf. on Nuclear Geology in Geothermal Areas, Spoleto, Italy: 17-53.
- 1969: Geochemistry and origin of the Red Sea brines. In: E.T. Degens and D.A. Ross, Eds., *Hot Brines and Recent Heavy Metal Deposits in the Red Sea*. Springer-Verlag, New York: 208-242.
- Craig, H., Boato, G. and White, D.E., 1956: Isotopic geochemistry of thermal waters. Proc., 2nd Conf. on Nuclear Processes in Geologic Settings, Natl. Res. Council, Nuclear Sci. Ser. Rept. 19: 29-38.
- Craig, J.R. and Barton, P.B., 1973: Thermochemical approximations for sulfosalts. *Econ. Geol.*, 68: 493-506.
- Croxford, N.J.W. and Jephcott, S., 1972: The McArthur lead-zinc-silver deposit, N.T. *Aust. Inst. Min. Metall., Proc.*, 243: 1-26.
- Cumming, G.L., 1976: Lead isotope ratios in DSDP Leg 7 basalts. *Geol. Assoc. Can./Mineral. Assoc. Can., Ann. Meeting, Program with Abst.*, 1: 68.
- Cumming, G.L. and Richards, J.R., 1975: Ore lead isotope ratios in a continuously changing earth. *Earth Planet. Sci. Lett.*, 28: 155-171.
- Cumming, G.L., Burke, M.D., Tsong, F. and McCullough, H., 1971: A digital mass spectrometer. *Can. Jour. Phys.*, 49: 956.
- Czamanske, G.K. and Rye, R.O., 1974: Experimentally determined sulfur isotope fractionations between sphalerite and galena in the temperature range 600°C to 275°C. *Econ. Geol.*, 69: 17-25.
- Dallmeyer, R.D., 1974: Eclogite inclusions in an alpine peridotite sill, Georgia-North Carolina: their chemistry and petrogenetic evolution. *Amer. Jour. Sci.*, 274: 356-377.
- Davidson, D.F. and Lakin, H.W., 1961: Metal content of some black shales of the western United States. In: *Short Papers in the Geologic and Hydrologic Sciences*. U.S. Geol. Surv., Prof. Paper 424-C: C329-C331.
- 1962: Metal content of some black shales of the western conterminous United States. In: *Short Papers in the Geologic and Hydrologic Sciences*. U.S. Geol. Surv., Prof. Paper 450-C: C74.

- Davies, G.R. and Krouse, H.R., 1975: Sulfur isotope distribution in Paleozoic sulfate evaporites, Canadian Arctic Archipelago. Geol. Surv. Can., Paper 75-1, Part B: 221-225.
- Delevaux, M.H. and Doe, B.R., 1974: Preliminary report on uranium, thorium, and lead contents and lead isotopic composition in sediment samples from the Red Sea. Initial Reports of the DSDP: 943-946.
- Delevaux, M.H., Doe, B.R. and Brown, G.F., 1967: Preliminary lead isotope investigations of brine from the Red Sea, galena from the Kingdom of Saudi Arabia and galena from the United Arab Republic (Egypt). Earth Planet. Sci. Lett., 3: 139-144.
- Devereux, I., 1968: Oxygen isotope ratios of minerals from the regionally metamorphosed schists of Otago, New Zealand. N.Z. Jour. Sci., 11: 526-548.
- Dewey, J.F., 1971: Origin and emplacement of the ophiolite suite, Appalachian ophiolites in Newfoundland. Jour. Geophys. Res., 76: 3179-3206.
- Dewey, J.F. and Bird, J.M., 1970: Lithosphere plate-continental margin tectonics and the evolution of the Appalachian orogen. Geol. Surv. Can., Bull. 81: 1031-1060.
- Doe, B.R., 1967: The bearing of lead isotopes on the source of granitic magma. Jour. Petrol., 8: 51-83.
- 1970: Lead isotopes. In: Minerals, Rocks and Inorganic Materials, 3. Springer-Verlag, Berlin: 137 pp.
- Doe, B.R. and Zartman, R.E., 1975: Plumbotectonics I, The Phanerozoic. Preprint.
- Doe, B.R., Hedge, C.E. and White, D.E., 1966: Preliminary investigation of the source of lead and strontium in deep geothermal brines underlying the Salton Sea geothermal area. Econ. Geol., 61: 462-483.
- Douglas, R.J.W. and Gabrielse, H., 1970: Fig. VIII-4. In: Geology and Economic Minerals of Canada. Geol. Surv. Can., Econ. Geol. Rept. No. 1.
- Douglas, R.J.W. and Norris, D.K., 1961: Camsell Bend and Root River map-areas, District of Mackenzie, N.W.T.. Geol. Surv. Can., Paper 61-13.
- Douglas, R.J.W., Gabrielse, H., Wheeler, J.O., Stott, D.F. and Belyea, H.R., 1970: Geology of Western Canada. In: Geology and Economic Minerals of Canada, Chapter 7. Geol. Surv. Can., Econ. Geol. Rept. No. 1: 367-488.
- Dudley, P.P., 1969: Electron microprobe analyses of garnet in glaucophane schists and associated eclogites. Amer. Mineral., 54: 1139-1150.

- Ellis, A.J. and Golding, R.M., 1963: The solubility of carbon dioxide above 100°C in water and in sodium chloride solutions. *Amer. Jour. Sci.*, 261: 47-60.
- Emery, K.O., Hunt, J.M. and Hays, E.E., 1969: Summary of hot brines and heavy metal deposits in the Red Sea. *In*: E.T. Degens and D.A. Ross, Eds., *Hot Brines and Recent Heavy Metal Deposits in the Red Sea*. Springer-Verlag, New York: 557-571.
- Engel, A.E.J., Engel, C.G. and Havens, R.G., 1965: Chemical characteristics of oceanic basalts and the upper mantle. *Geol. Soc. Amer., Bull.*, 76: 719-734.
- Ernst, W.G., 1965: Mineral parageneses in Franciscan metamorphic rocks, Panoche Pass, California. *Geol. Soc. Amer., Bull.*, 76: 879-914.
- 1968: *Amphiboles*. Springer-Verlag, New York.
- Essene, E.J. and Fyfe, W.S., 1967: Omphacite in Californian metamorphic rocks. *Contr. Mineral. Petrol.*, 15: 1-23.
- Ewing, J.I., Worzel, J.L. and Ewing, M., 1962: Sediments and oceanic structural history of the Gulf of Mexico. *Jour. Geophys. Res.*, 67(6): 2509-2527.
- Ewing, M. and Antoine, J.W., 1966: New seismic data concerning sediments and diapiric structures in Sigsbee Deep and continental slope, Gulf of Mexico. *Amer. Assoc. Petrol. Geol., Bull* 50(3), Part 1: 479-504.
- Ewing, M., Brune, J. and Kuo, J., 1962: Surface-wave studies of the Pacific crust and mantle. *Aust. Natl. Univ., Geophys. Mono. No.* 6: 30-40.
- Farkas, A., 1973: A trace element study of the Texas Gulf orebody, Timmins, Ontario. Unpub. M.Sc. thesis, Univ. Alberta.
- Farrand, M., 1970: Framboidal sulfides precipitated synthetically. *Mineral. Deposita.*, 5: 237-247.
- Findlay, P.C., 1967: The mineral history of Yukon Territory and southwestern District of Mackenzie. *Geol. Surv. Can.*, Paper 67-40.
- French, B.M. and Rosenberg, P.E., 1965: Siderite (FeCO₃): thermal decomposition in equilibrium with graphite. *Science*, 147: 1283-1284.
- Frey, F.A., 1970: Rare earth and potassium abundances in St. Paul's rocks. *Earth Planet. Sci. Lett.*, 7: 351-360.
- Frey, F.A., Bryan, W.B. and Thompson, G., 1974: Atlantic Ocean floor: geochemistry and petrology of basalts from Legs 2 and 3 of the Deep-Sea Drilling Project. *Jour. Geophys. Res.*, 79(35): 5507-5528.

- Fritz, W.H., 1975: Broad correlations of some Lower and Middle Cambrian strata in the North American Cordillera. Geol. Surv. Can., Paper 75-1, Part A: 533-539.
- Fry, N. and Fyfe, W.S., 1969: Eclogites and water pressure. Contr. Mineral. Petrol., 24: 1-6.
- Gabrielse, H., 1963: McDame map-area, B.C.. Geol. Surv. Can., Memoir 319.
- 1967a: Watson Lake, Yukon Territory. Geol. Surv. Can., Map 19-1966.
- 1967b: Tectonic evolution of the northern Canadian Cordillera. Can. Jour. Earth Sci., 4(2): 271-298.
- 1972: Younger Precambrian of the Canadian Cordillera. Amer. Jour. Sci., 272: 521-536.
- Gabrielse, H. and Blusson, S.L., 1969: Coal River map-area, Yukon Territory and District of Mackenzie. Geol. Surv. Can., Paper 68-38.
- Gabrielse, H. and Wheeler, J.O., 1961: Tectonic framework of southern Yukon and northwestern B.C.. Geol. Surv. Can., Paper 60-24.
- 1970: Western Canadian Cordillera. In: Geology and Economic Minerals of Canada, Chapter 8. Geol. Surv. Can., Econ. Geol., Rept. No. 1.
- 1972: The Cordilleran structural province: island arc - ocean basin regime. In: Variations in Tectonic Styles in Canada. Geol. Assoc. Can., Spec. Paper 2: 19-25.
- Gabrielse, H., Blusson, S.L. and Roddick, J.A., 1973: Geology of Flat River, Glacier Lake and Wrigley Lake map-areas, District of Mackenzie and Yukon Territory. Geol. Surv. Can., Memoir 366.
- Gabrielse, H., Roddick, J.A. and Blusson, S.L., 1965: Flat River, Glacier Lake and Wrigley Lake, District of Mackenzie and Yukon Territory. Geol. Surv. Can., Paper 64-52.
- Gale, H.N. and Mussett, A.E., 1973: Episodic uranium-lead models and the interpretation of variations in the isotopic compositions of lead in rocks. Rev. Geophys. Space Phys., 11: 37-86.
- Gardner, L.B., 1973: Chemical models for sulfate reduction in closed anaerobic marine environments. Geochim. Cosmochim. Acta, 37: 53-68.
- Garlick, G.D. and Epstein, S., 1967: Oxygen isotope ratios in coexisting minerals of regionally metamorphosed rocks. Geochim. Cosmochim. Acta, 31: 181-214.
- Garvin, P.L., 1973: Phase relations in the Pb-Sb-S system. N. Jb. Min. Abh., 118(3): 235-267.

- Gast, P.W., 1967: Isotope geochemistry of volcanic rocks. *In*: H.H. Hess and A. Poldervaart, Eds., *Basalts*. Interscience Publishers, New York: 325-358.
- Gast, P.W., Tilton, G.R. and Hedge, C.E., 1964: Isotopic composition of lead and strontium from Ascension and Gough Islands. *Science*, 145: 1181-1185.
- Ghent, E.D. and Coleman, R.G., 1973: Eclogites from southwestern Oregon. *Geol. Soc. Amer., Bull.* 84: 2471-2488.
- Gold, C.M. and Smith, D.G.W., 1975: EDATA - a FORTRAN IV program for calculation of chemical compositions from spectra obtained by Energy Dispersive Microbeam Analysis. Preprint.
- Goldhaber, M.B., 1974: Equilibrium and dynamic aspects of the marine geochemistry of sulfur. *Dissert. Abst. B* (1974), Ph.D. thesis, Univ. California, Los Angeles: 6055-6056.
- Goldhaber, M.B. and Kaplan, I.R., 1974: The sulfur cycle. *In*: E.D. Goldberg, Ed., *The Sea. Marine Chem.*: 569-656.
- Gondi, J., 1972: Geology of the Anvil Mine. *In*: D.J. Glass, Ed., *Major Lead-Zinc Deposits of Western Canada*. *Internat. Geol. Congr.*, 14th session, Guidebook.
- Graeser, S., 1969: Isotopic composition of lead in some basic and ultra-basic rocks from the Alps. *Earth Planet. Sci. Lett.*, 6: 491-497.
- Green, D.H., 1970: The origin of basaltic and nephelinitic magmas. *Trans., Leicester Lit. Phil. Soc.*, 64: 26-54.
- Green, D.H. and Ringwood, A.E., 1967: The genesis of basaltic magmas. *Contr. Mineral. Petrol.*, 15: 103.
- Green, L.H. and Godwin, C.I., 1963: Mineral industry of Yukon Territory and southwestern District of Mackenzie. *Geol. Surv. Can.*, Paper 63-38.
- _____ 1964: Mineral industry of Yukon Territory and southwestern District of Mackenzie. *Geol. Surv. Can.*, Paper 64-36.
- Green, L.H. and Roddick, J.A., 1961: Nahanni, Yukon Territory and District of Mackenzie. *Geol. Surv. Can.*, Map 14-1961.
- _____ 1962: Dawson, Larsen Creek and Nash Creek map-areas, Yukon Territory. *Geol. Surv. Can.*, Paper 62-7.
- Green, L.H., Roddick, J.A. and Wheeler, J.O., 1960: Finlayson Lake map-area, Yukon Territory. *Geol. Surv. Can.*, Map 8-1960.
- Grinenko, V.A., Grinenko, L.N. and Zagryazhskaya, G.D., 1969: Kinetic isotope effect in high temperature reduction of sulfate. *Geochem. Internat.* (1969): 370-376.

- Grootenboer, J. and Schwartz, H.P., 1969: Experimentally determined sulfur isotope fractionations between sulfide minerals. *Earth Planet. Sci. Lett.*, 7: 162-166.
- Groves, D.I. and Solomon, M., 1969: Fluid inclusion studies at Mount Bischoff, Tasmania. *Aust. Inst. Min. Metall., Bull.*, 747, Sect. B, 78: B1-B11.
- Gulson, B.L., 1975: Differences in lead isotope composition in the stratiform McArthur zinc-lead-silver deposit. *Mineral. Deposita.*, 10: 277-286.
- Haas, J.L., Jr., 1971: The effect of salinity on the maximum thermal gradient of a hydrothermal system at hydrostatic pressure. *Econ. Geol.*, 66: 940-946.
- Hamilton, E.I., 1965: *Applied Geochronology*. Academic Press, London: 267 pp.
- Haranczyk, C., 1970: Zechstein lead-bearing shales in the Fore-Sudetic monocline in Poland. *Econ. Geol.*, 65: 481-495.
- Hart, R., 1970: Chemical exchange between sea water and deep ocean basalts. *Earth Planet. Sci. Lett.*, 9: 269-279.
- Hartmann, U.M. and Nielson, H., 1969: δS^{34} werte in rezentein meeres-sedimenten und ihre deutung am beispiel einiger sedimentprofile ans der west lichen ostsee. *Geol. Runds.*, 58: 612-655.
- Hattori, H., Sugisaki, R. and Tanaka, T., 1972: Nature of hydration in Japanese Paleozoic geosynclinal basalt. *Earth Planet. Sci. Lett.*, 15: 271-285.
- Haverslew, R.E., 1976: *Geology and genesis of the Ruttan Lake deposit, Manitoba*. Unpub. M.Sc. thesis, Univ. Alberta, Canada: 149 pp.
- Hawley, J.E. and Nicol, I., 1961: Trace elements in pyrite and pyrrhotite. *Econ. Geol.*, 56: 467-487.
- Hedge, C.E., 1966: Variations in radiogenic strontium found in volcanic rocks. *Jour. Geophys. Res.*, 71: 6119-6126.
- Hedge, C.E. and Peterman, Z.E., 1970: The strontium isotopic composition of basalts from the Gordo and Juan de Fuca Rises, northeastern Pacific Ocean. *Contr. Mineral. Petrol.*, 27: 114-120.
- Helgeson, H.C., 1969: Thermodynamics of hydrothermal systems at elevated temperatures and pressures. *Amer. Jour. Sci.*, 267: 729-804.
- Hemley, J.J., 1959: Some mineralogical equilibria in the system $K_2O-Al_2O_3-SiO_2-H_2O$. *Amer. Jour. Sci.*, 257: 241-270.
- Hennig, W., 1971: Löslichkeit von Zinkblende unter hydrothermalen Bedingungen im System $ZnS-NaCl-H_2O$. *N. Jb. Min. Abh.*, 116: 61-79.

- Hinners, N.W., 1963: The solubility of sphalerite in aqueous solutions at 80°C. Unpub. Ph.D. thesis, Princeton Univ., N.J.: 111 pp.
- Hoda, S.N. and Chang, L.L.Y., 1975: Phase relations in the pseudoternary system $\text{PbS-Cu}_2\text{S-Sb}_2\text{S}_3$ and the synthesis of meneghinite. *Can. Mineral.*, 13: 388-393.
- Holland, H.D., 1959: Some applications of thermochemical data to problems of ore deposits. I: Stability relations among the oxides, sulfides, sulfates, and carbonates of ore and gangue metals. *Econ. Geol.*, 54: 184-233.
- 1965a: Some applications of thermochemical data to problems of ore deposits. II: Mineral assemblages and the composition of ore-forming fluids. *Econ. Geol.*, 60: 1101-1166.
- 1965b: The history of ocean water and its effects on the chemistry of the atmosphere. *Proc., Natl. Acad. Sci.*, 53: 1173-1183.
- Hollister, L.S., 1966: Garnet zoning: an interpretation based on the Rayleigh fractionation model. *Science*, 154: 1647-1651.
- Holmes, A., 1937: The origin of primary lead ores. *Econ. Geol.*, 32: 763-782.
- Hyndman, D.W., 1972: *Petrology of Igneous and Metamorphic Rocks*. McGraw-Hill Book Co., New York: 171 pp.
- Ichikuni, M., 1975: A chemical model for black ore-forming solution. *Jour. Japan Assoc. Mineral. Petrol. Econ. Geol.*, 70: 71 (in Japanese).
- Irvine, W.T., 1972: An outline of the geology of the Sullivan Mine, Kimberley, B.C.. In: D.J. Glass, Ed., *Major Lead-Zinc Deposits of Western Canada*. Internat. Geol. Congr., 24th session, Guide-books A24 and C24: 26-34.
- Jaffey, A.H., Flynn, K.F., Glendenin, L.E., Bentley, W.C. and Essling, A.M., 1971: Precision measurement of half-lives and specific activities of U^{235} and U^{238} . *Phys. Rev.*, C4: 1889-1906.
- James, H.L. and Clayton, R.N., 1962: Oxygen isotope fractionation in metamorphosed iron formations of the Lake Superior region and in other iron-rich rocks. *Geol. Soc. Amer., Buddington Vol.*: 217-232.
- Jensen, M.L., 1957: Sulfur isotopes and mineral paragenesis. *Econ. Geol.*, 52: 269-281.
- 1959: Sulfur isotopes and hydrothermal mineral deposits. *Econ. Geol.*, 54: 374-394.
- 1967: Sulfur isotope and mineral genesis. In: H.L. Barnes, Ed., *Geochemistry of Hydrothermal Ore Deposits*. Holt, Reinhart and Winston, Inc., New York: 143-165.

- Kajiwarra, Y., 1971: Sulfur isotope study of the Kuroko ores of the Shakanai No. 1 deposit: Akita Prefecture, Japan. *Geochem. Jour.*, 4: 157-181.
- 1973a: Chemical composition of ore-forming solution responsible for the Kuroko type mineralization in Japan. *Geochem. Jour.*, 6: 141-149.
- 1973b: A simulation of the Kuroko type mineralization in Japan. *Geochem. Jour.*, 6: 193-209.
- 1973c: Significance of cyclic seawater as a possible determinant of rock alteration facies in the earth's crust. *Geochem. Jour.*, 7: 23-36.
- Kajiwarra, Y. and Honma, H., 1972: Lead content of barite coexisting with galena - an indicator of oxygen fugacity during ore formation. *Min. Geol.*, 22: 457-465.
- Kajiwarra, Y. and Krouse, H.R., 1971: Sulfur isotope partitioning in metallic sulfide systems. *Can. Jour. Earth Sci.*, 8: 1397-1408.
- Kajiwarra, Y., Krouse, H.R. and Sasaki, A., 1969: Experimental study of sulfur isotope fractionation between coexisting sulfide minerals. *Earth Planet. Sci. Lett.*, 7: 271-277.
- Kanasewich, E.R., 1962: Quantitative interpretations of anomalous lead isotope abundances. Ph.D. thesis, Univ. British Columbia: 187 pp.
- 1968: The interpretation of lead isotopes and their geological significance. *In*: Radiometric Dating for Geologists. Interscience Publishers, London: 147-223.
- Kaplan, I.R., Emery, K.O. and Rittenberg, S.C., 1963: The distribution and isotopic abundance of sulfur in recent marine sediments off southern California. *Geochim. Cosmochim. Acta*, 27: 297-331.
- Kawabe, I., 1974: Transition metal contents of Paleozoic geosynclinal basalts in southwest Japan and their geological significance. *Jour. Geol. (Chishitzugaku-Zasshi)*, 80(11): 539-554 (in Japanese with English abstract).
- Kay, M., 1951: North American geosynclines. *Geol. Soc. Amer., Memoir* 48.
- Kay, R., Hubbard, N.J. and Gast, P.W., 1970: Chemical characteristics and origin of oceanic ridge volcanic rocks. *Jour. Geophys. Res.*, 75(8): 1585-1613.
- Keevil, N.B., 1942: Vapor pressures of aqueous solutions at high temperatures. *Jour. Amer. Chem. Soc.*, 64: 841-850.
- Kelly, W.C. and Turneure, F.S., 1970: Mineralogy, paragenesis and geothermometry of the tin and tungsten deposits of the eastern Andes, Bolivia. *Econ. Geol.*, 65: 609-680.

- Kempe, D.R.C., 1973: Basalts from the southern Indian Ocean: DSDP Leg 26. Trans., Amer. Geophys. Union, 54(11): 1008-1011.
- Kissin, S.A., 1974: Relations in a portion of the Fe-S system. Unpub. Ph.D. thesis, Univ. Toronto.
- Kissin, S.A. and Scott, S.D., 1972: Phase relations of intermediate pyrrhotites. Abstract, Econ. Geol., 67: 1007.
- Kiyosu, Y., 1973: Sulfur isotopic fractionation among sphalerite, galena and sulfide iron. Geochem. Jour., 7: 191-199.
- Klevtsov, P.V. and Lemmlein, G.G., 1959: Pressure corrections for the homogenization temperatures of aqueous NaCl solutions. USSR Acad. Sci., Doklady, 128(1-6): 995-997.
- Kolfun, L.I., 1965: Application of mineralothermometric analysis in studies of origins of certain gold ore deposits in Ural. In: Research on the Nature of Mineral-Forming Solutions. Pergamon Press, New York: 743 pp.
- Krauskopf, K.B., 1955: Sedimentary deposits of rare metals. In: A.M. Bateman, Ed., Econ. Geol. 50th Anniversary Volume 1905-1955, Part 1. Econ. Geol. Publishing Co., Urbana, Ill.: 411-463.
- 1967: Introduction to Geochemistry, Chapter 20. McGraw-Hill Book Co., New York.
- Kretz, R., 1961: Some applications of thermodynamics to coexisting minerals of variable composition. Examples: orthopyroxene-clinopyroxenes and orthopyroxene-garnet. Jour. Geol., 69: 361-387.
- 1963: Distribution of magnesium and iron between orthopyroxene and calcic pyroxene in natural mineral assemblages. Jour. Geol., 71: 773-785.
- Kullerud, G., 1953: The FeS-ZnS system, a geological thermometer. Norsk Geol. Tidss., 32: 61-147.
- 1967: Sulfide studies. In: P.H. Abelson, Ed., Researches in Geochemistry, 2. John Wiley & Sons: 286-321.
- Kulp, J.L., Ault, W.U. and Feeby, H.W., 1956: Sulfur isotope abundances in sulfide minerals. Econ. Geol., 51: 139-149.
- Kuo, S.L. and Folinsbee, R.E., 1974: Lead isotope geology of mineral deposits spatially related to the Tintina Trench, Yukon Territory. Econ. Geol., 69: 806-813.
- Kuo, S.L. and Greig, J., 1973: Geology and geochemical survey of the Anvil Range and Lapie Lake area, Yukon. Report for Vestor Explorations and Cream Silver Mines Ltd..

- Kuo, S.L. and Thalenhorst, H., 1972: Geology of the Frances Lake (east arm) area. Joint Venture Report for Canico-Metallgesellschaft Canada-Matt Berry Mines Ltd., Toronto.
- Kushiro, I., 1973: Origin of some magmas in oceanic and circum-oceanic regions. *Tectonophysics*, 17(3): 211-222.
- Lambert, I.B. and Sato, T., 1974: The Kuroko and associated ore deposits of Japan: a review of their features and metallogenesis. *Econ. Geol.*, 69: 1215-1236.
- Lambert, I.B. and Scott, K.M., 1973: Implications of geochemical investigations of sedimentary rocks within and around the McArthur zinc-lead-silver deposit, northern Territory. *Jour. Geochem. Expl.*, 2: 307-330.
- Lanphere, M.A., MacKevitt, E.M. and Stern, T.W., 1964: Potassium-argon and lead-alpha ages of plutonic rocks, Bogan Mountain area, Alaska. *Science*, 145(3633): 705-707.
- Larson, S.D., 1956: Phase studies of the two component carbon dioxide - water system involving the carbon dioxide hydrate. *Dissert. Abst.*, 16, Univ. microfilm no. 15235, Ann Arbor, Michigan: 248.
- LeCouteur, P., 1973: A lead isotope study of ore deposits from the East Kootenay district, B.C., and the Anvil district, Y.T.. Unpub. Ph.D. thesis, Univ. British Columbia, Canada.
- Leech, G.B. and Wanless, R.K., 1962: Lead isotope and potassium-argon studies in the East Kootenay district of British Columbia. *Geol. Soc. Amer.*, *Buddington Vol.*: 241-279.
- Lemmler, G.G. and Klevtsov, P.V., 1961: Relations among the principal thermodynamic parameters in a part of the system $H_2O-NaCl$. *Geochem.*, 2: 148-158.
- LeRoux, L.J. and Glendenin, L.E., 1963: Half-life of thorium-232. *Proc., Natl. Conf. on Nuclear Energy*, Pretoria: 83-94.
- Love, L.G., 1965: Micro-organic material with diagenetic pyrite from the Lower Proterozoic Mount Isa shale and a carboniferous shale. *Proc., Yorkshire Geol. Soc.*, 35: 187-202.
- Lusk, J., 1972: Examination of volcanic-exhalative and biogenic origins for sulfur in the stratiform massive sulfide deposits of New Brunswick. *Econ. Geol.*, 67: 169-183.
- MacKevitt, E.M. and Blake, M.C., 1964: Geology of the north Bradfield River iron prospect, southeastern Alaska. *U.S. Geol. Surv., Bull.* 1103-D: D1-D21.
- Malinin, S.D. and Khitarov, N.I., 1969: Reduction of sulfate sulfur by hydrogen under hydrothermal conditions. *Geochem. Internat.* (1969): 1022-1027.

- Manheim, F.T. and Sayles, F.L., 1971: Interstitial water studies on small core samples, DSDP Leg 37. Initial Reports of the DSDP, 6: 811-821.
-
- 1974: Composition and origin of interstitial waters of marine sediments, based on deep-sea drill cores. In: E.D. Goldberg, Ed., The Sea, 5. Marine Chem.: 527-568.
- Manheim, F.T., Chan, K.M. and Sayles, F.L., 1970: Interstitial water studies on small core samples: Deep Sea Drilling Project Leg 5. Initial Reports of the DSDP, 5: 501-511.
- Manson, V., 1967: Geochemistry of basaltic rocks: major elements. In: H.H. Hess, Ed., Basalts, 1. Interscience Publishers, New York.
- Matsukuma, T., Nitsuma, H., Yui, S. and Wada, F., 1974: Rare minerals from Kuroko ores of the Uwamuki deposits of the Kosaka Mine, Akita Prefecture. In: S. Ishihara, Ed., Geology of Kuroko Deposits. Min. Geol., Spec. Issue 6, Soc. Min. Geol. Japan: 349-362.
- McBirney, A.R. and Gass, I.G., 1967: Relations of oceanic volcanic rocks to mid-oceanic rises and heat flow. Earth Planet. Sci. Lett., 2: 265.
- McDougall, I. and Compston, W., 1965: Strontium isotope composition and potassium-rubidium ratios in some rocks from Reunion and Rodriguez, Indian Ocean. Nature, 207: 252-253.
- McKinney, C.R., McCrea, J.M., Epstein, S., Allen, H.A. and Urey, H.C., 1950: Improvements in mass spectrometer for measurement of small differences in isotope abundance ratios. Rev. Sci. Instr., 21: 724-730.
- Melent'yev, B.N., Ivanenko, V.V. and Pamfilova, L.A., 1968: Solubility of some ore-bearing sulfides under hydrothermal conditions. 416-460.
- Melson, W.G. and Van Andel, T.H., 1966: Metamorphism in the mid-Atlantic Ridge, 22°N latitude. Marine Geol., 4: 165-186.
- Melson, W.G., Thompson, G. and Van Andel, T.H., 1968: Volcanism and metamorphism in the mid-Atlantic Ridge, 22°N latitude. Jour. Geophys. Res., 73: 5925-5941.
- Mitchell, A.H. and Reading, H.G., 1969: Continental margins, geosynclines, and oceanfloor spreading. Jour. Geol., 77: 629-646.
- Miyashiro, A., 1973: The Troodos ophiolitic complex was probably formed in an island arc. Earth Planet. Sci. Lett., 19: 218-224.
-
- 1974: Volcanic rock series in island arcs and active continental margins. Amer. Jour. Sci., 274: 321-355.
- Miyashiro, A. and Shido, F., 1975: Tholeiitic and calc-alkalic series in relation to the behaviors of titanium, vanadium, chromium and nickel. Amer. Jour. Sci., 275: 265-277.

- Miyashiro, A., Shido, F. and Ewing, M., 1970: Crystallization and differentiation in abyssal tholeiites and gabbros from mid-oceanic ridges. *Earth Planet. Sci. Lett.*, 7: 361-365.
- Mohr, P.A., 1963: The Ethiopian Cenozoic lavas: a preliminary study of some trends: spatial, temporal and chemical. *Bull. Geophys. Obs. of Haile Selassie I Univ., Addis Araba No. 6*: 103.
- Monger, J.W.H. and Hutchison, W.W., 1971: Metamorphic map of the Canadian Cordillera. *Geol. Surv. Can.*, Paper 70-33.
- Monger, J.W.H., Souther, J.G. and Gabrielse, H., 1972: Evolution of the Canadian Cordillera: a plate tectonic model. *Amer. Jour. Sci.*, 272: 577-602.
- Moorbath, S. and Walker, G.P.L., 1965: Strontium isotope investigations of igneous rocks from Iceland. *Nature*, 207: 837-840.
- Mori, T. and Banno, S., 1973: Petrology of peridotite and garnet clinopyroxenite of the Mt. Higashi-Alaishi Mass, central Shikoku, Japan - subsolidus relation of anhydrous phases. *Contr. Mineral. Petrol.*, 41: 301-323.
- Muehlenbachs, K. and Clayton, R.N., 1976: Oxygen isotope composition of the oceanic crust and its bearing on sea water. Preprint.
- Nakai, N., 1967: Isotopic ratios of sulfur compounds in sulfide ore deposits. Abstract, Annual Meeting Geol. Soc. Japan (in Japanese).
- Nakai, N. and Jensen, M.L., 1964: The kinetic isotope effect in the bacterial reduction and oxidation of sulfur. *Geochim. Cosmochim. Acta*, 28: 1893-1912.
- Nakazawa, H. and Morimoto, N., 1971: Phase relations and superstructures of pyrrhotite, Fe_{1-x}S . *Mater. Res. Bull.*, 6: 345-358.
- Nicolas, A., 1966: Le complexe ophiolite schistes lustrés entre Dora Maira et Grand Paradis (Alpes Piedmontaises) tectonique et métamorphisme. D.Sc. thesis, 2, Univ. Nantes, France.
- Nier, A.O., 1938: Variations in the relative abundances of the isotopes of common lead from various sources. *Amer. Chem. Soc. Jour.*, 60: 1571-1576.
- 1947: A mass spectrometer for isotope and gas analysis. *Rev. Sci. Instr.*, 18: 398-411.
- Nissenbaum, A., Presley, B.J. and Kaplan, I.R., 1972: Early diagenesis in reducing fjord, Saanich Inlet, B.C.. I: Chemical and isotopic changes in major components of interstitial water. *Geochim. Cosmochim. Acta*, 36: 1007-1027.

- Nriagu, J.O., 1970: Solubility of galena under hydrothermal conditions. Unpub. Ph.D. thesis, Univ. Toronto: 133 pp.
- 1971a: Experimental investigation of a portion of the system $\text{PbS-NaCl-HCl-H}_2\text{O}$ at elevated temperatures. *Amer. Jour. Sci.*, 271: 157-169.
- 1971b: Studies in the system $\text{PbS-NaCl-H}_2\text{S-H}_2\text{O}$: stability of lead (II) thiocomplexes at 90°C . *Chem. Geol.*, 8: 299-310.
- Oana, S. and Ishikawa, H., 1965: Sulfur isotopic fractionation between sulfur and sulfuric acid in the hydrothermal solution of sulfur dioxide. *Geochem. Jour.*, 1: 45-50.
- O'Hara, M.J., 1968: The bearing of phase equilibria studies in synthetic and natural systems on the origin and evolution of basic and ultra-basic rocks. *Earth Sci. Rev.*, 4: 69-133.
- 1973: Non-primary magmas and dubious mantle plume beneath Iceland. *Nature*, 243: 507-508.
- O'Hara, M.J. and Mercy, E.L.P., 1963: Petrology and petrogenesis of some garnetiferous peridotites. *Trans., Roy. Soc. Edinburgh*, 65(12): 251-314.
- Ohmoto, H., 1972: Systematics of sulfur and carbon isotopes in hydrothermal ore deposits. *Econ. Geol.*, 67: 551-578.
- Ohmoto, H. and Rye, R.O., 1970: The Bluebell Mine, British Columbia. I: Mineralogy, paragenesis, fluid inclusions and the isotopes of hydrogen, oxygen, and carbon. *Econ. Geol.*, 65: 417-437.
- Ohmoto, H., Cole, D.R. and Mottl, M.J., 1976: Experimental basalt-seawater interaction: sulfur and oxygen isotope studies. *Trans., Amer. Geophys. Union (Abst.)*, 57: 342.
- Ohmoto, H., Kajiwarra, Y. and Date, J., 1970: The Kuroko ores in Japan: products of seawater. *Geol. Soc. Amer., Ann. Meeting, Milwaukee (Abst.)*: 640.
- Orr, W.L., 1974: Changes in sulfur content and isotopic ratios of sulfur during petroleum maturation - a study of Big Horn Basin Paleozoic oils. *Amer. Assoc. Petrol. Geol.*: 2295-2318.
- Osmaston, M.F., 1971: Genesis of ocean ridge median valleys and continental rift valleys. *Tectonophysics*, 11: 387-405.
- Ostic, R.G., 1963: Isotopic investigation of conformable lead deposits. Unpub. Ph.D. thesis, Univ. British Columbia: 124 pp.
- Ostic, R.G., Russell, R.D. and Stanton, R.L., 1967: Additional measurements of the isotope of lead from stratiform deposits. *Can. Jour. Earth Sci.*, 4: 245-269.

- Oversby, V.M., 1971: Lead in oceanic islands: Faial, Azores and Trindade. *Earth Planet. Sci. Lett.*, 11: 401-408.
- 1972: Genetic relations among the volcanic rocks of Reunion: chemical and lead isotopic evidence. *Geochim. Cosmochim. Acta*, 36: 1167-1179.
- 1973: New look at the lead isotope growth curve. *Nature*, 248: 132-133.
- Oversby, V.M. and Gast, P.W., 1970: Lead from oceanic islands. *Jour. Geophys. Res.*, 75: 2097-2114.
- Palache, C., Berman, H. and Frondel, C., 1951: Sulfates: the system of mineralogy, vol. II. John Wiley & Sons, New York.
- Patterson, C.C. and Duffield, B., 1963: The isotopic composition of lead in Easter Island rhyolite. *Geochim. Cosmochim. Acta*, 27: 1180-1182.
- Pearce, J.A., 1975: Basalt geochemistry used to investigate past tectonic environments on Cyprus. *Tectonophysics*, 25: 41-67.
- Pearce, J.A. and Cann, J.R., 1973: Tectonic setting of basic volcanic rocks determined using trace element analyses. *Earth Planet. Sci. Lett.*, 19: 290-300.
- Pearce, T.H., Gorman, B.E. and Birkett, T.C., 1975: The TiO_2 - K_2O - P_2O_5 diagram: a method of discriminating between oceanic and non-oceanic basalts. *Earth Planet. Sci. Lett.*, 24: 419-426.
- Peterman, Z.E. and Hedge, C.E., 1971: Related strontium isotopic and chemical variations in oceanic basalts. *Geol. Soc. Amer., Bull.*, 82: 493-500.
- Poole, W.H., 1956: Geology of the Cassiar Mountains in the vicinity of the Yukon-British Columbia boundary. Ph.D. thesis, Princeton Univ., N.J.
- Presley, B.J., Goldhaber, M.B. and Kaplan, I.R., 1970: Interstitial water chemistry: DSDP Leg 5. Initial Reports of the DSDP, 5: 513-522.
- Price, R.A., 1964: The Precambrian Purcell system in the Rocky Mountains of southern Alberta and B.C.. *Can. Soc. Petrol. Geol., Bull.* 12: 399-426.
- Prinz, M., 1967: Geochemistry of basaltic rocks: trace elements. In: H.H. Hess, Ed., *Basalts*, 1. Interscience Publishers, New York: 271-324.
- Puchelt, H., 1967: Sulfur isotope fractionation in minerals. *Carnegie Inst. Geophys. Lab., Ann. Rept. 1967-1968*: 192-197.
- Puchelt, H. and Kullerud, G., 1969: Sulfur fractionation in the Pb-S system. *Earth Planet. Sci. Lett.*, 7: 301-306.

- Ramdohr, P., 1950: Die Lagerstätte von Broken Hill in New South Wales in Lichte der neuen geologischen Erkenntnisse und erzmikroskopischer Untersuchungen. Heidelberg. Beitr. Mineral. Petrog., 2: 291-333.
- 1969: The Ore Minerals and Their Intergrowths. Pergamon Press, Oxford.
- Rhodes, J.M., 1973: Major and trace element chemistry of basalts from Leg 9 of the Deep Sea Drilling Project. Trans., Amer. Geophys. Union, 54(11): 1014-1015.
- Richards, J.R., 1971: Major lead orebodies - mantle origin? Econ. Geol., 66: 425-434.
- 1975: Lead isotope data on three north Australian galena localities. Mineral. Deposita., 10: 287-301.
- 1977: Some thoughts on the time-dependence of lead isotope ratios. Contr. Tugarinov volume.
- Richards, J.R., Page, R.W. and Black, L.P., 1976: Age and isotopic studies in economic geology. Reprinted from Econ. Geol. of Australia and Papua New Guinea, 1. Metals. Aust. Inst. Min. Metall.: 15-25.
- Rickard, D.T., 1969: The chemistry of iron sulfide formation at low temperatures. Stockholm Contr. Geol., 20: 67-95.
- 1970: The origin of framboids. Lithos., 3: 269-293.
- Ridge, J.D., 1973: Volcanic exhalations and ore deposition in the vicinity of the seafloor. Mineral. Deposita., 8: 332-348.
- Roberts, W.M.B., Walker, A.L. and Buchanan, A.S., 1969: The chemistry of pyrite formation in aqueous solution and its relation to the depositional environment. Mineral. Deposita., 4: 18-29.
- Roddick, J.A., 1967: Tintina Trench. Jour. Geol., 75: 23-33.
- Roddick, J.A. and Green, L.H., 1961a: Sheldon Lake, Yukon Territory. Geol. Surv. Can., Map 12-1961.
- 1961b: Tay River, Yukon Territory. Geol. Surv. Can., Map 13-1961.
- Roddick, J.A., Wheeler, J.O., Gabrielse, H. and Souther, J.G., 1967: Age and nature of the Canadian part of the circum-Pacific orogenic belt. Tectonophysics, 4(4-6): 319-337.
- Roedder, E., 1962: Studies of fluid inclusions. I: Low temperature application of a dual-purpose freezing and heating stage. Econ. Geol., 57: 1045-1061.
- 1963: Studies of fluid inclusions. II: Freezing data and their interpretation. Econ. Geol., 58: 167-211.

- _____ 1967: Fluid inclusions as samples of ore fluids. In: H.L. Barnes, Ed., *Geochemistry of Hydrothermal Ore Deposits*. Holt, Reinhart & Winston Inc., New York: 515-574.
- _____ 1970: Application of an improved crushing microscope stage to studies of the gases in fluid inclusions. *Schweizer. Min. U. Petrog. Mitt.*, Part 1, 50: 41-58.
- _____ 1972: Data of Geochemistry Chapter JJ. Composition of fluid inclusions. *U.S. Geol. Surv., Prof. Paper* 440-JJ.
- Roedder, E. and Coombs, D.S., 1967: Immiscibility in granitic melts, indicated by fluid inclusions in ejected granitic blocks from Ascension Island volcanic breccias. *Jour. Petrol.*, 8: 417-451.
- Roedder, E. and Skinner, B.J., 1968: Experimental evidence that fluid inclusions do not leak. *Econ. Geol.*, 63: 715-730.
- Rogers, J.J.W. and Adams, J.A.S., 1969: Thorium. In: *Handbook of Geochemistry*, II-1, 90-B-1 to 90-N-1. Springer-Verlag, Berlin.
- Roots, E.F., 1954: Geology and mineral deposits of Aitken Lake map-area, B.C.. *Geol. Surv. Can., Memoir* 274.
- Roscoe, S.M., 1965: Geochemical and isotopic studies, Noranda and Mattagami. *Can. Inst. Min. Metall., Trans.* LXVIII: 279-285.
- Rosenberg, P.E., 1967: Subsolidus relations in the system $\text{CaCO}_3\text{-MgCO}_3\text{-FeCO}_3$ between 350° and 550°C. *Amer. Mineral.*, 52: 787-796.
- Russell, R.D., 1956: Interpretation of lead isotope abundances. In: *Nuclear Processes in Geologic Settings*. *Proc. 2nd Conf., NAS-NRC Publ.* 400: 68-78.
- _____ 1972: Evolutionary model for lead isotopes in conformable ores and in ocean volcanics. *Rev. Geophys. Space Phys.*, 10: 529-549.
- Russell, R.D. and Farquhar, R.M., 1960: *Lead Isotopes in Geology*. Interscience Publishers, New York: 243 pp.
- Rye, R.O., 1966: The carbon, hydrogen, and oxygen isotopic composition of the hydrothermal fluids responsible for the lead-zinc deposits at Providencia, Zacatecas, Mexico. *Econ. Geol.*, 61: 1399-1427.
- Rye, R.O. and Czamanske, G.K., 1969: Experimental determination of sphalerite-galena sulfur isotope fractionation and application to the ores at Providencia, Mexico. *Geol. Soc. Amer., Ann. Meeting, Milwaukee (Abst.)*: 195-196.
- Rye, R.O. and Ohmoto, H., 1974: Sulfur and carbon isotopes and ore genesis: a review. *Econ. Geol.*, 69: 826-842.

- Rye, R.O., Hall, W.E. and Ohmoto, H., 1974: Carbon, hydrogen, oxygen and sulfur isotope study of the Darwin lead-silver-zinc deposit, southern California. *Econ. Geol.*, 69: 468-481.
- Saager, R. and Koeppel, V.H., 1976: Lead isotopes and trace elements from sulfides of Archean greenstone belts in South Africa - a contribution to the knowledge of the oldest known mineralizations. *Econ. Geol.*, 71: 44-57.
- Saagerson, E.P. and Williams, L.A.J., 1964: Ngummanite from southern Kenya and its bearing on the origin of rocks in the northern Tanganyika alkaline district. *Jour. Petrol.*, 5: 40.
- Sakai, H., 1957: Fractionation of sulfur isotopes in nature. *Geochim. Cosmochim. Acta*, 12: 150-169.
- 1968: Isotopic properties of sulfur compounds in hydrothermal processes. *Geochem. Jour.*, 2: 29-49.
- 1971: Sulfur and oxygen isotopic study of barite concretions from banks in the Japan Sea off the Northeast Honshu, Japan. *Geochem. Jour.*, 5: 79-93.
- Sakai, H., Osaki, S. and Tsukagishi, M., 1970: Sulfur and oxygen isotopic geochemistry of sulfate in the black ore deposits of Japan. *Geochem. Jour.*, 4: 27-39.
- Sangster, D.F., 1968: Relative sulfur isotope abundances of ancient seas and stratabound sulfide deposits. *Geol. Assoc. Can., Proc.*, 19: 79-91.
- 1971: Sulfur isotopes, stratabound sulfide deposits, and ancient seas. *Proc., IMA-IAGOD Meetings, 1970, IAGOD Volume*: 295-299.
- Sasaki, A., 1970: Seawater sulfate as a possible determinant for sulfur isotopic compositions of some stratabound sulfide ores. *Geochem. Jour.*, 4: 41-51.
- Sasaki, A. and Kajiwar, Y., 1971: Evidence of isotopic exchange between seawater sulfate and some syngenetic sulfide ores. *Proc., IMA-IAGOD Meetings, 1970, IAGOD Volume 1*: 289-294.
- Sato, K. and Sasaki, A., 1973: Lead isotopes of the Black Ore ("Kuroko") deposits from Japan. *Econ. Geol.*, 68: 547-552.
- Sato, K., Slawson, W.F. and Kanasevich, E.R., 1973: Additional isotopic measurements on Japanese ore leads. *Geochem. Jour.*, 7: 115-122.
- Saxena, S.K., 1971: Mg^{2+} - Fe^{2+} order-disorder in orthopyroxene and the Mg^{2+} - Fe^{2+} distribution between coexisting minerals. *Lithos.*, 4: 345-356.

- Saxena, S.K. and Ghose, S., 1971: $Mg^{2+} - Fe^{2+}$ order-disorder and the thermodynamics of the orthopyroxene-crystalline solution. *Amer. Mineral.*, 56: 532-559.
- Sayles, F.L., Manheim, F.T. and Waterman, L.S., 1971: Interstitial water studies on small core samples: DSDP Leg 7. Initial Reports of the DSDP, 7: 871-881.
- Schiller, W.R., Gehlen, K.V. and Nilsen, H., 1970: Hydrothermal exchange and fractionation of sulfur isotopes in synthesized ZnS and PbS. *Econ. Geol.*, 65: 350-351.
- Schilling, J.G., 1973: Iceland mantle plume: geochemical evidence along Reykjanes Ridge. *Nature*, 242: 565-571.
- Schneiderhohn, H., 1923: Chalkoeraphische untersuchung des mansfelder cupferschiefers. *N. Jb. Min. Geol. Paleon.*, Beilage-B, 47: 1-38.
- Schouten, A., 1946: The role of sulfur bacteria in the formation of the so-called sedimentary copper ores and pyritic ore bodies. *Econ. Geol.*, 41: 517-538.
- Schwartz, H.P. and Burnie, S.W., 1973: Influence of sedimentary environments on sulfur isotope ratios in clastic rocks: a review. *Mineral. Deposita.*, 8: 264-277.
- Scott, S.D., 1973: Experimental calibration of the sphalerite geobarometer. *Econ. Geol.*, 68: 466-474.
- 1974: The Fe-S system: sulfide phase equilibria. In: P.H. Ribbe, Ed., *Sulfide Mineralogy*. Min. Soc. Amer., Short Course Notes, 1: 21-40.
- Scott, S.D. and Barnes, H.L., 1971: Sphalerite geothermometry and geobarometry. *Econ. Geol.*, 66: 653-669.
- Scott, S.D. and Kissin, S.A., 1973: Sphalerite composition in the Zn-Fe-S system below 300°C. *Econ. Geol.*, 68: 475-479.
- Seguín, M.K., 1965: The system Fe-C-O-S-H₂O. Unpub. Ph.D. thesis, McGill Univ.
- 1971: Phase relations in the Fe-C-O-S-H₂O system and its geological application. *Chem. Geol.*, 7: 5-18.
- Shido, F., Miyashiro, A. and Ewing, M., 1971: Crystallization of abyssal tholeiites. *Contr. Mineral. Petrol.*, 31: 251-266.
- Shikazono, N., 1973: Sphalerite-carbonate-pyrite assemblage in hydrothermal veins and its bearing on limiting the environment of their deposition. *Geochem. Jour.*, 7: 97-114.
- 1974: Physico-chemical properties of ore-forming solution responsible for the formation of Toyaha Pb-Zn deposits, Hokkaido, Japan. *Geochem. Jour.*, 8: 37-46.

- Shiskina, O.V., 1958: On the salt composition of the interstitial waters of the far eastern seas and the adjacent part of the Pacific. *Trans., Inst. Okeanologii Akad. Nauk. USSR*, 27: 109-180.
- Sinha, A.K., 1970: Model lead and radiometric ages from the Churchill Province, Canadian Shield. *Geochim. Cosmochim. Acta*, 34: 1089-1106.
- Sinha, A.K. and Tilton, G.R., 1973: Isotopic evolution of common lead. *Geochim. Cosmochim. Acta*, 37: 1823-1849.
- Skinner, R., 1962: Mineral industry of Yukon Territory and southwestern District of Mackenzie. *Geol. Surv. Can.*, Paper 62-27.
- Slawson, W.F. and Russell, R.D., 1973: A multistage history for Flin Flon lead. *Can. Jour. Earth Sci.*, 10: 582-583.
- Smith, F.G. and Little, W.M., 1959: Filling temperatures of H₂O-CO₂ fluid inclusions and their significance in geothermometry. *Can. Mineral.*, 6: 380-388.
- Sourirajan, S. and Kennedy, G.C., 1962: The system H₂O-NaCl at elevated temperatures and pressures. *Amer. Jour. Sci.*, 260: 115-141.
- Spooner, E.T.C. and Fyfe, W.S., 1973: Sub-seafloor metamorphism, heat and mass transfer. *Contr. Mineral. Petrol.*, 42: 287-304.
- Stacey, J.S. and Kramers, J.D., 1975: Approximation of terrestrial lead isotope evolution by a two-stage model. *Earth Planet. Sci. Lett.*, 26: 207-221.
- Stacey, J.S., Delevaux, M.E. and Ulrych, T.K., 1969: Some triple-filament lead isotope ratio measurements and an absolute growth curve for single-stage leads. *Earth Planet. Sci. Lett.*, 6: 15-25.
- Stanton, R.L., 1960: The application of sulfur isotope studies in ore genesis theory - a suggested model. *N.Z. Jour. Geol. Geophys.*, 3: 375-389.
-
- 1962: Elemental constitution of the Black Star orebodies, Mount Isa, and its interpretation. *Trans., Inst. Min. Metall.*, 72: 69-124.
- Stanton, R.L. and Russell, R.D., 1959: Anomalous leads and the emplacement of lead sulfide ores. *Econ. Geol.*, 54: 588-607.
- Stewart, J.H., 1972: Initial deposits in the Cordilleran geosyncline: evidence of a Late Precambrian (<850 m.y.) continental separation. *Geol. Soc. Amer., Bull.* 83: 1345-1360.
- Stillwell, F.L., 1926: Observations on the mineral constitution of the Broken Hill lode. *Aust. Inst. Min. Metall., Proc.*, 64: 1-76.

- Stockwell, C.H. (Ed.), 1968: Tectonic Map of Canada. Geol. Surv. Can., Map 1251A.
- Sugisaki, R. and Jensen, M.L., 1971: Oxygen isotopic studies of silicate minerals with special reference to hydrothermal mineral deposits. *Geochem. Jour.*, 5: 7-21.
- Sugisaki, R., Mizutani, S., Hattori, H., Adachi, M. and Tanaka, T., 1972: Late Paleozoic geosynclinal basalt and tectonism in the Japanese Islands. *Tectonophysics*, 14: 35-56.
- Sugitani, Y., Hanasawa, N., Horada, K. and Nagashima, K., 1969: Variations of lattice constants and refractive indices in the (Ba,Pb)SO₄ solid solutions. *Kobutsugaku-Zasshi (Jour. Min. Soc. Japan)*, 9: 266-273 (in Japanese).
- Sun, S.S. and Hanson, G.N., 1975: Evolution of the mantle: geochemical evidence from alkali basalt. *Geology*, 3: 297-302.
- Sun, S.S. and Jahn, B.M., 1975: Lead and strontium isotopes in postglacial basalts from Iceland. *Nature*, 255: 527-530.
- Sunagawa, I., Endo, Y. and Nakai, N., 1971: Hydrothermal synthesis of framboidal pyrite. *Japan Soc. Min. Geol., Spec. Issue* 2: 10-14.
- Sweeney, R.E. and Kaplan, I.R., 1973: Pyrite framboid formation: laboratory synthesis and marine sediments. *Econ. Geol.*, quoted in Goldhaber and Kaplan, 1974.
- Sweeney, R.E., Goldhaber, M.B. and Kaplan, I.R., 1973: Isotopic fractionation of sulfur during sulfate reduction in marine sediments. Quoted in Goldhaber and Kaplan, 1974.
- Takano, B. and Watanuki, K., 1974: Geochemical implications of the lead content of barite from various origins. *Geochem. Jour.*, 8: 87-95.
- Takano, B., Yanagisawa, M. and Watanuki, K., 1969: Structure gap in the BaSO₄-PbSO₄ solid solution series. *Mineral. Jour.*, 6: 159-171.
- Takeuchi, S., 1971: Study of CO₂-Bearing fluid inclusions by means of a freezing stage microscope. *Min. Geol.*, 21: 286-300 (in Japanese with English abstract).
- Takeuchi, S. and Kennedy, G.C., 1965a: Dissociation pressures of the phase CO₂ 5 3/4 H₂O. *Jour. Geol.*, 73: 383-390.
-
- 1965b: The solubility of carbon dioxide in NaCl solutions at high temperatures and pressures. *Amer. Jour. Sci.*, 263: 445-454.
- Takiyama, K., 1967: On the BaSO₄-PbSO₄ system. *Proc., 16th Ann. Meeting, Japan Soc. Anal. Chem.*

- Talwani, M. and Eldholm, O., 1973: Boundary between continental and oceanic crust at the margin of rifted continents. *Nature*, 241: 325-330.
- Tatsumi, T., 1965: Sulfur isotope fractionation between coexisting sulfide minerals from some Japanese ore deposits. *Econ. Geol.*, 60: 1645.
- Tatsumi, T. and Oshima, T., 1966: Mineralogical composition of ores from "black ore deposits" of the Kosaka and Hanaoka Mines. *Jour. Japan Min. Metall. Inst.*, 82: 1008-1014 (in Japanese).
- Tatsumoto, M., 1966a: Genetic relations of oceanic basalts as indicated by lead isotopes. *Science*, 153: 1094-1101.
- 1966b: Isotopic composition of lead in volcanic rocks from Hawaii, Iwo Jima and Japan. *Jour. Geophys. Res.*, 71: 1721-1733.
- Tatsumoto, M., Knight, R.J. and Allegre, C.J., 1973: Time differences in the formation of meteorites as determined from the ratio of lead-207 to lead-206. *Science*, 180: 1279-1283.
- Tatsumoto, M., Knight, R.J. and Delevaux, M.H., 1972: Uranium, thorium, and lead concentrations in three silicate standards and a method of lead isotopic analysis. *U.S. Geol. Surv., Prof. Paper 800-D*: D111-D115.
- Taylor, H.P., 1974: The application of oxygen and hydrogen isotope studies to problems of hydrothermal alteration and ore deposition. *Econ. Geol.*, 69: 843-883.
- Taylor, H.P. and Coleman, R.G., 1968: O^{18}/O^{16} ratios of coexisting minerals in glaucophane-bearing metamorphic rocks. *Geol. Soc. Amer., Bull.*, 79: 1727-1756.
- Taylor, H.P., Albee, A.L. and Epstein, S., 1963: O^{18}/O^{16} ratios of coexisting minerals in three mineral assemblages of kyanite-zone pelitic schist. *Jour. Geol.*, 71: 513-522.
- Templeman-Kluit, D.J., 1968: Geological setting of the Faro, Vangorda and Swim base metal deposits, Yukon Territory. *Geol. Surv. Can., Paper 68-1, Part A*: 43-52.
- 1970a: The relationship between sulfide grain size and metamorphic grade of host rocks in some stratabound pyritic ores. *Can. Jour. Earth Sci.*, 7: 1339-1345.
- 1970b: An occurrence of eclogite near Tintina Trench, Yukon. *Geol. Surv. Can., Paper 70-1b*: 19-22.
- 1972: Geology and origin of the Faro, Vangorda and Swim concordant zinc-lead deposits, central Yukon Territory. *Geol. Surv. Can., Bull.* 208.

- Templeman-Kluit, D.J., Abbot, G., Gordey, S. and Read, B., 1975: Stratigraphic and structural studies in the Pelly Mountains, Yukon Territory. Geol. Surv. Can., Paper 75-1, Part A: 45-48.
- Thode, H.G. and Monster, J., 1965: Sulfur-isotope geochemistry of petroleum evaporites, and ancient seas. Amer. Assoc. Petrol. Geol., Memoir 4: 367-377.
- Thompson, G., 1973: A geochemical study of the low-temperature interaction of seawater and oceanic igneous rocks. Trans., Amer. Geophys. Res., 54(11): 1015-1018.
- Tilton, G.R., 1973: Isotopic lead ages of chondritic meteorites. Earth Planet. Sci. Lett., 19: 321-329.
- Toland, W.G., 1960: Oxidation of organic compounds with aqueous sulfate. Jour. Amer. Chem. Soc., 82: 1911-1916.
- Tomlinson, M.C. and Smith, D.G.W., 1970: PROBEDATA - an APL language computer program for the use in electron microprobe analysis. Computer Contr. 45, State Geol. Surv., Univ. Kansas, Lawrence.
- Toulmin, P. and Barton, P.B., 1964: A thermodynamic study of pyrite and pyrrhotite. Geochim. Cosmochim. Acta, 28: 641-671.
- Tupper, W.M., 1960: Sulfur isotopes and the origin of the sulfide deposits of the Bathurst-Newcastle area of northern New Brunswick. Econ. Geol., 55: 1676-1707.
- Urabe, T., 1974: Iron content of sphalerite coexisting with pyrite from some Kuroko deposits. In: S. Ishihara, Ed., Geology of Kuroko Deposits. Min. Geol., Spec. Issue No. 6, Soc. Min. Geol. Japan: 377-384.
- Vine, J.D., 1966: Element distribution in some shelf and eugeosynclinal black shales. U.S. Geol. Surv., Bull. 1214-E: E1-E31.
- 1969: Element distribution in some Paleozoic black shales and associated rocks. U.S. Geol. Surv., Bull. 1214-G: G1-G32.
- Vine, J.D. and Tourtelot, E.B., 1969: Geochemical investigations of some black shales and associated rocks. U.S. Geol. Surv., Bull. 1314-A: A1-A43.
- 1970: Geochemistry of black shale deposits - a summary report. Econ. Geol., 65: 253-272.
- Vinogradov, A.P., Chupakhin, M.S. and Grinenko, V.A., 1956: Isotope ratios S^{32}/S^{34} in sulfides. Geochem. Jour., 4: 331-338.
- Vogel, D.E. and Garlick, G.D., 1970: Oxygen isotope ratios in metamorphic eclogites. Contr. Mineral. Petrol., 48: 183-191.

- Wanless, R.K., Stevens, R.D., Lachance, G.R. and Reinsalte, J.Y.H., 1965: Age determinations and geological studies: report 6. Geol. Surv. Can., Paper 65-17.
- Wedepohl, K.H., 1964: Untersuchungen am Kupferschiefer in Nordwestdeutschland. Ein Beitrag zur Deutung der Genese bitumioser Sedimente. *Geochim. Cosmochim. Acta*, 28: 305-364.
- 1971: "Kupferschiefer" as a prototype of syngenetic sedimentary ore deposits. In: Y. Takeuchi, Ed., Proc., IMA-IAGOD Meetings 1970, IAGOD Volume, Soc. Min. Geol. Japan, Spec. Issue No. 3: 268-273.
- Wheeler, J.O., 1959: Mesozoic tectonics of central southern Yukon. *Geol. Assoc. Can., Proc.* 11: 23-43.
- Wheeler, J.O., Green, L.H. and Roddick, J.A., 1960a: Quiet Lake, Yukon Territory. *Geol. Surv. Can., Map* 7-1960.
- 1960b: Finlayson Lake, Yukon Territory. *Geol. Surv. Can., Map* 8-1960.
- White, D.E., 1967: Mercury and basemetal deposits associated with thermal and mineral waters. In: H.L. Barnes, Ed., *Geochemistry of Hydrothermal Ore Deposits*. Holt, Reinhart and Winston Inc., New York: 575-631.
- Whitehead, R.E., 1973: Environment of stratiform sulfide deposition, variation in Mn:Fe ratio in host rocks at Heath Steel Mine, New Brunswick, Canada. *Mineral. Deposita.*, 8: 148-160.
- Wikstrom, A., 1970: Hydrothermal experiments in the system jadeite-diopside. *Norsk. Geol. Tidss.*, 50: 1-14.
- Williams, K.L., 1974: Compositions of sphalerites from the zoned hydrothermal lead-zinc deposits at Zeeham, Tasmania. *Econ. Geol.*, 69: 657-672.
- Winkler, H.G.F., 1967: *Die Genese der metamorphen Gesteine*, 2, Auflage. Springer-Verlag, Berlin; Heidelberg, New York.
- Woodward, O.H., 1965: A review of the Broken Hill lead-silver-zinc industry. K.P.W. Parsons, Ed. 2nd Edition, West Publishing Corp., Sydney.
- Yoder, H.S.Jr., 1967: Spillites and serpentinites. *Carnegie Inst. Ann. Rept. Director Geophys. Lab.* 1965-1966: 269-279.
- Yoder, H.S. and Tilley, C.E., 1962: Origin of basaltic magmas: an experimental study of natural and synthetic rock systems. *Jour. Petrol.*, 3: 342-532.
- Yui, S., 1966a: Stability relations among iron oxide, sulfide, and carbonate minerals during magmatic ore deposition with special reference to the role of graphite. *Min. Geol.*, 16: 16-27 (in Japanese).

- 1966b: Decomposition of siderite to magnetite at lower oxygen fugacities: a thermochemical interpretation and geological implications. *Econ. Geol.*, 61: 768-776.
- Yund, R.A. and Hall, H.T., 1969: Hexagonal and monoclinic pyrrhotites. *Econ. Geol.*, 64: 420-423.
- Zartman, R.E. and Stacy, J.S., 1971: Lead isotopes and mineralization ages in Belt Supergroup rocks, northwestern Montana and northern Idaho. *Econ. Geol.*, 66: 849-860.
- Zartman, R.E. and Tera, F., 1973: Lead concentration and isotopic composition in five peridotite inclusions of probably mantle origin. *Earth Planet. Sci. Lett.*, 20: 54-66.
- Zen, E-An and Albee, A.L., 1964: Coexistent muscovite and paragonite in pelitic schists. *Amer. Mineral.*, 49: 904-923.
- Ziegler, P.A., 1959: Frühpaläozoische tillite im östlichen Yukon Territorium (Kanada). *Eclogae Geol. Helv.*, 52(2): 735-741.

APPENDIX II-1

GENERAL FACIES DISTRIBUTION OF PALEOZOIC STRATA IN THE SELWYN FOLD BELT AND RELATED AREAS

Lower Cambrian strata are underlain by the Grit unit in the southeastern region of Selwyn Fold Belt as well as in the map-areas to the east flank of the region (Gabrielse et al., 1973; Gabrielse, 1967b) and to the west of the region (Tempelman-Kluit et al., 1974). The base of the strata is generally believed to be unconformable, but local conformity further to the east and northeast of the region is observed (Gabrielse et al., 1973). Generally speaking, the strata display a marked facies change westward from the eastern flank (the Redstone Arch) of the Selwyn Fold Belt, possibly indicating a basinal environment to the west. Three distinct facies of the strata are observed (Gabrielse, 1967b; Gabrielse et al., 1973) in the southern Mackenzie Mountains and the South Nahanni River areas (Fig. II-4) - an eastern belt dominated by sandstones and minor conglomerates, a central belt characterized by varicolored sandy carbonates and siltstones, and a western belt consisting of fine clastic sediments (shales, siltstones and limestones). The thickness of the strata is greatest (6,000 feet) at the eastern flank of the Selwyn Fold Belt and decreases rapidly westward (2,500 feet). Locally minor basic volcanic flows and/or breccias occur in the upper part of the strata. The facies distribution indicates an easterly source for the clastic sediments - a situation that appears applicable to Lower Cambrian deposition the entire length of the Cordillera (Kay, 1951). Field measurement data on cross bedding and ripple marks obtained from Lower Cambrian strata in the central Redstone Plateau, north of Redstone

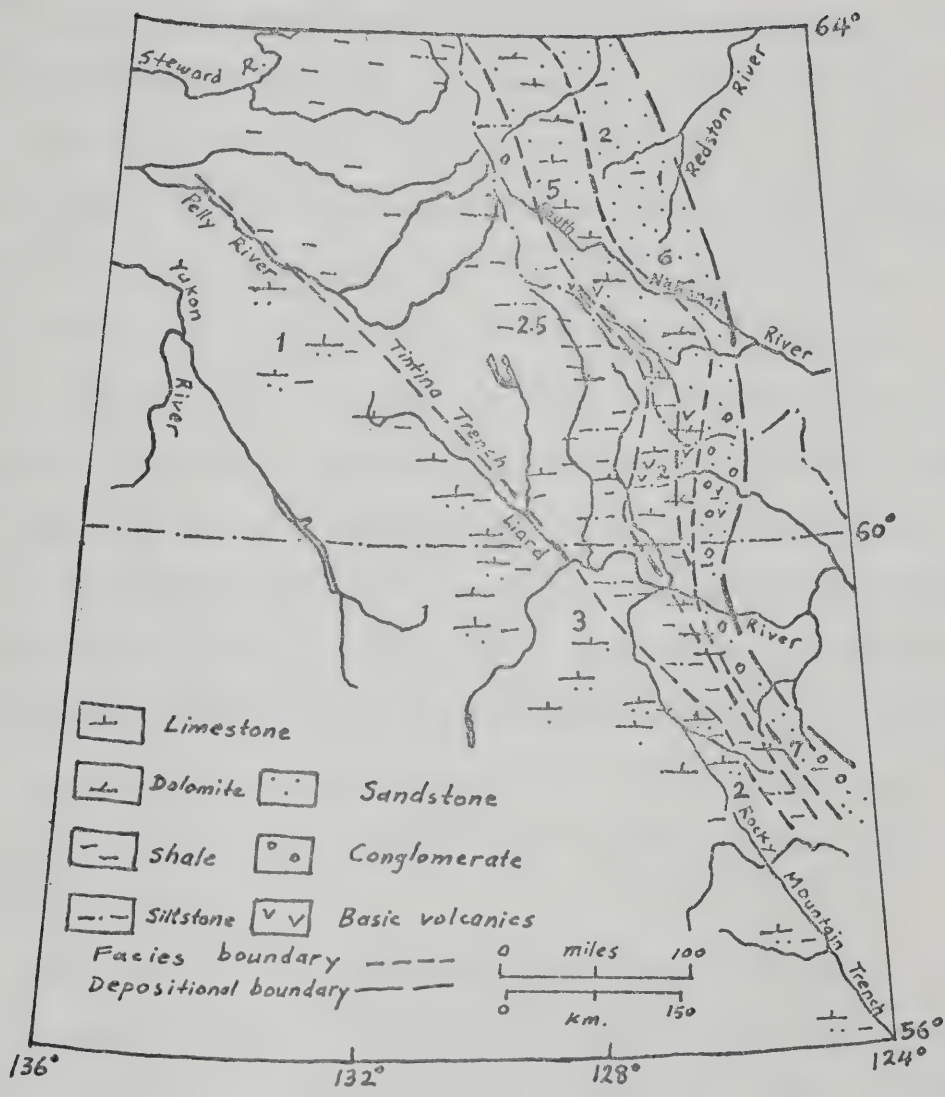


Fig. II-4. Distribution of Lower Cambrian rocks in the northern Canadian Cordillera.

River, also indicate a southwesterly current direction (Gabrielse et al., 1973).

Middle Cambrian strata appear to be absent in many parts of the Mackenzie Mountains and are generally thin (1000 - 1500 feet) where observed. The strata vary in thickness from place to place and appear to be truncated above by an angular unconformity. Judging from the unique type sections observed in the areas east and northeast of the region by Gabrielse (1967b) and Gabrielse et al. (1973), the strata apparently consisting of carbonates and minor fine clastics, were deposited in a shallow-water, near-shore environment (as carbonate bank ?) on a regional disconformity over the Lower Cambrian strata; the general absence or thinness of the Middle Cambrian strata south of the Redstone Arch and in the Selwyn Fold Belt could be due to either non-deposition or major erosion. The source and polarity of sedimentation during Middle Cambrian time were essentially the same as those in the Lower Cambrian time. A facies distribution map for the Middle Cambrian strata in the region is shown in Fig. II-5.

The Upper Cambrian and Lower-Middle Ordovician strata appear to form a conformable sequence* (Gabrielse and Wheeler, 1970; Gabrielse et al., 1973), but lie on a widespread angular unconformity above the Middle Cambrian in the region and adjacent areas. This major unconformity is believed to have resulted from Late Cambrian (Pre-Franconian) regional uplift and erosion. The facies distribution maps for the Upper Cambrian and the Lower-Middle Ordovician strata are shown in Fig. II-6 and Fig. II-7, respectively. Generally speaking, the sequence represents prograding

*There is, however, evidence for local unconformity between Upper Cambrian and Lower-Middle Ordovician strata in some localities (Blusson, 1966; Tempelman-Kluit, 1972).

LEGENDS FOR FIGS. II-5, II-6, II-7 AND II-8



Sandstone



Gypsum, Anhydrite



Siltstone



Volcanics



Shale



Conglomerate



Limestone



Chert



Dolomite



Salt

R

Red beds



Truncated limit

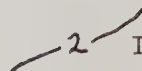
S: Silurian
 UO: Upper Ordovician
 Ra: Road River, Ashgillian
 Rl: Road River, Llandoveryian
 D: Delorme
 W: Whittaker



Facies boundary



Outcrop limit



Isopach (thousands of feet)

1.5 Thickness (thousands of feet)

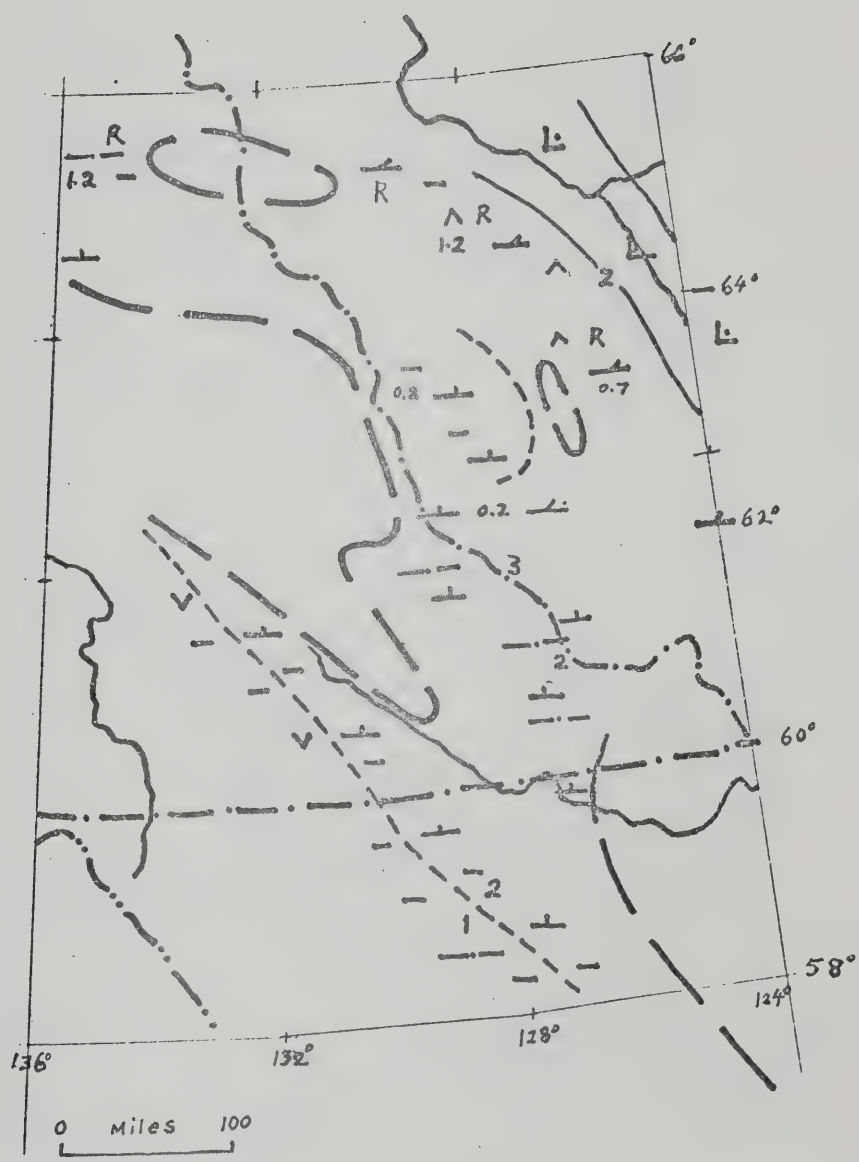


Fig. II-5. Facies distribution of Middle Cambrian rocks in the northern Canadian Cordillera.

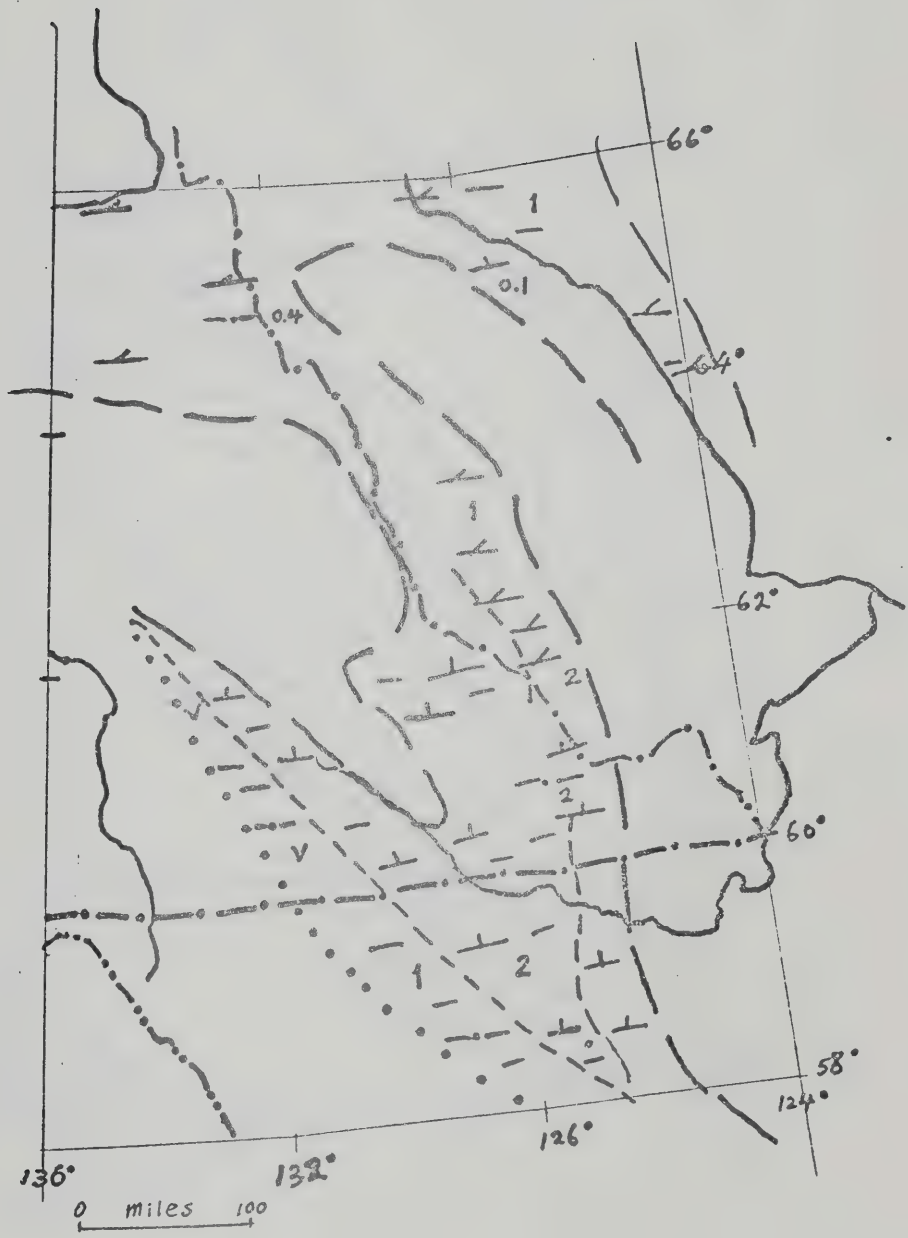


Fig. II-6. Facies distribution of Upper Cambrian rocks in the northern Canadian Cordillera.

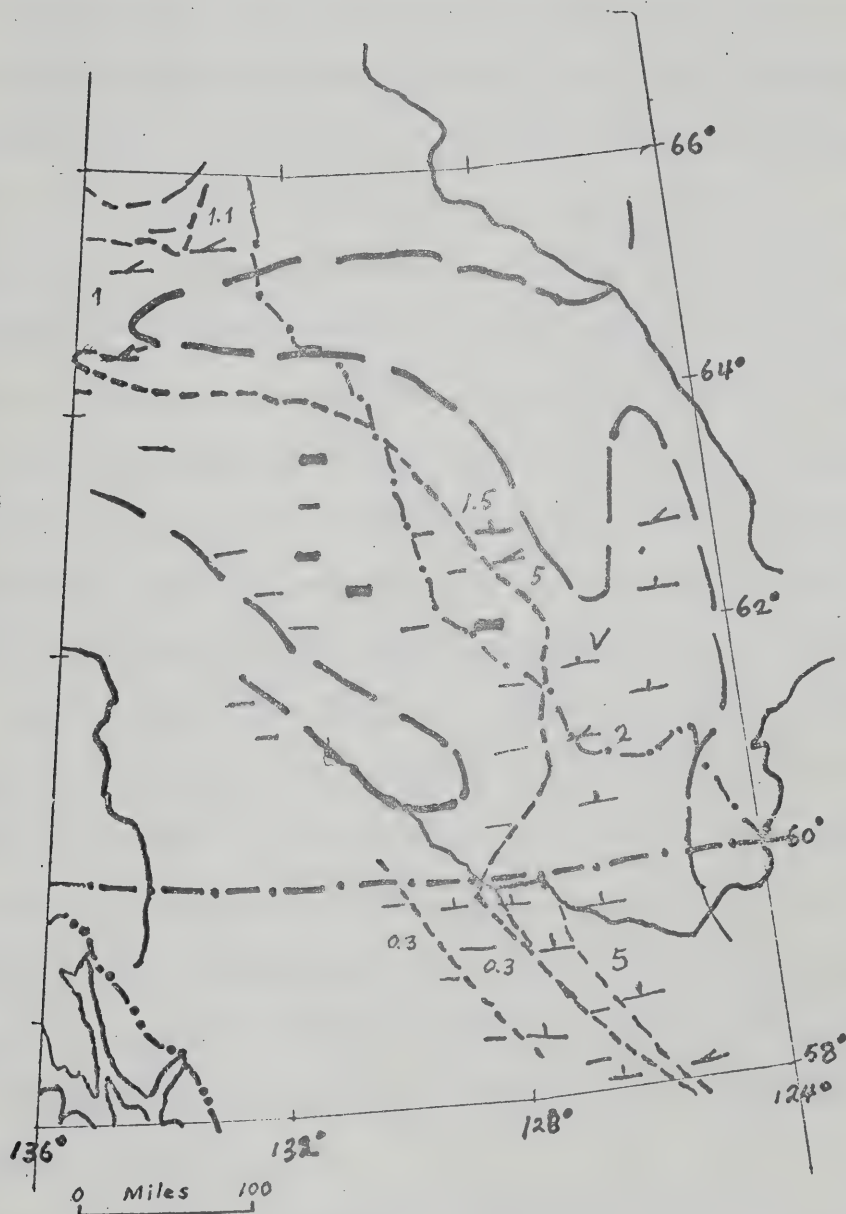


Fig. II-7. Facies distribution of Lower and Middle Ordovician rocks in the northern Canadian Cordillera.

sedimentation on a continental margin with distinct facies boundaries separating depositional environments representing shelf and deep basins (see next section and Chapter III for a more detailed account). To the east and northeast near South Nahanni River and southern Mackenzie Mountains, the Upper Cambrian-Lower Ordovician strata are shallow-water, shelf-type carbonates with near-shore sandy-silty facies near the base (Gabrielse et al., 1973); to the southeast in the Flat River area, a similar facies is predominant (ditto; Blusson, 1968); in the Howard's Pass district, detailed stratigraphic construction shows that there existed a shelf-edge and/or off-slope type environment with euxinic and closed basins and a transitional sedimentation zone characterized by carbonate-fine clastic-chert deposition. In the Frances Lake district, the Upper Cambrian-Lower Ordovician strata represent essentially a deeper water sequence comprising fine clastics and impure carbonates with minor chert and tuff. The strata in the Anvil Range district are believed to be essentially a mixed sequence of fine clastic sediments and volcanic tuff with some lava flows near the upper part (Tempelman-Kluit, 1972). The environment in which these sediments and volcanics were deposited is probably around a relatively shallow marine, oceanic rise or "miogeanticline" the origin of which will be postulated in the final section of Chapter II.

In between the Middle and Upper Ordovician, there appears to exist a regional unconformity which separates latest Ordovician and Silurian rocks from Middle Ordovician and older strata throughout the northern Canadian Cordillera, except possibly in Richardson Trough and Selwyn Fold Belt (Gabrielse, 1967b; Gabrielse and Wheeler, 1970). An orogeny centered in the westernmost part of the northern Canadian Cordillera is

believed to have been accompanied by regional uplift extended far to the east. In the Upper Ordovician the craton was generally uniformly depressed, the sea transgressing the truncated margin of earlier Paleozoic rocks and the Precambrian Shield (Fig. II-8). Gabrielse and Wheeler (1970) stressed that facies relationships of the Upper Ordovician and Silurian in the northern Canadian Cordillera (especially in the western Selwyn Fold Belt) are similar to those of the Lower-Middle Ordovician rocks with which Upper Ordovician and Silurian carbonates, shales and minor pyroclastics form a conformable sequence. They believed that the differences are mainly in the greater extent of graptolitic shale facies in the latter. During Upper Ordovician to Lower Devonian time, remarkably abrupt facies changes occur along the northeastern and eastern margins of the Selwyn Fold Belt where carbonate assemblages commonly reach their maximum thickness just east of the facies boundary which maintained an almost constant position throughout the interval (Fig. II-9; see also Fig. II-12a).

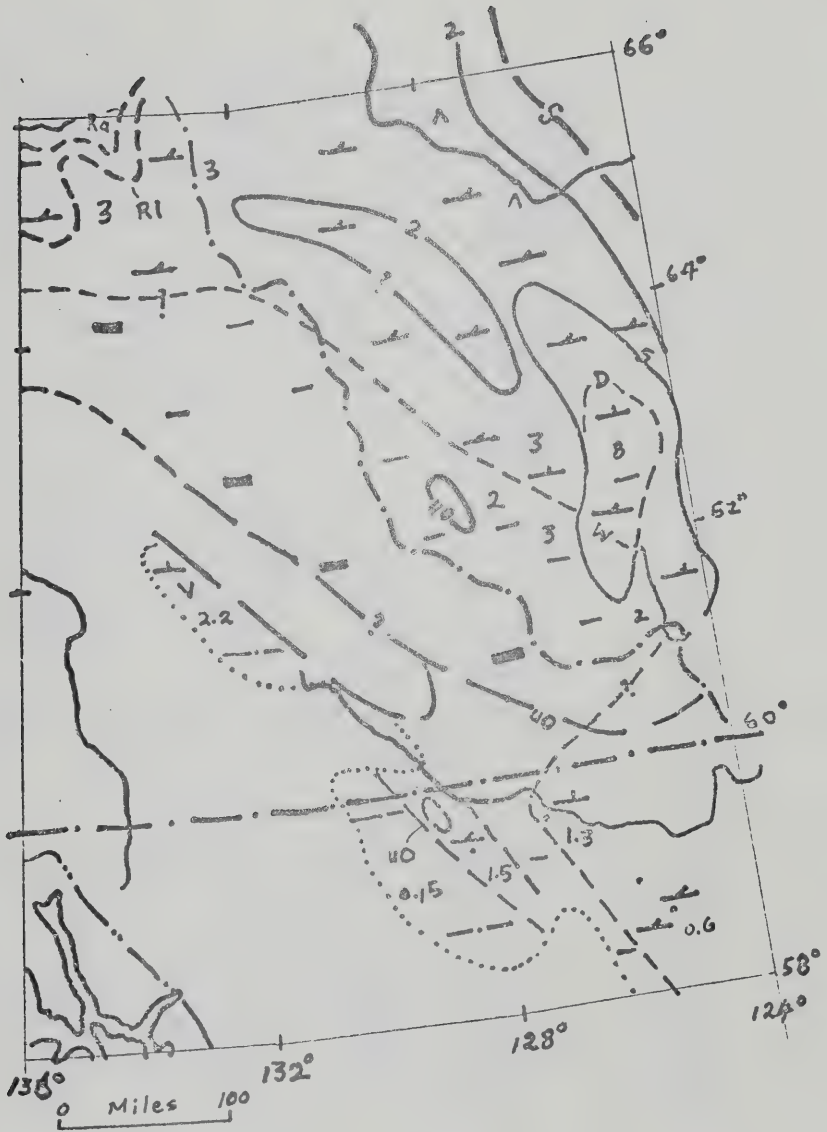


Fig. II-8. Facies distribution of Upper Ordovician and Silurian rocks in the northern Canadian Cordillera.

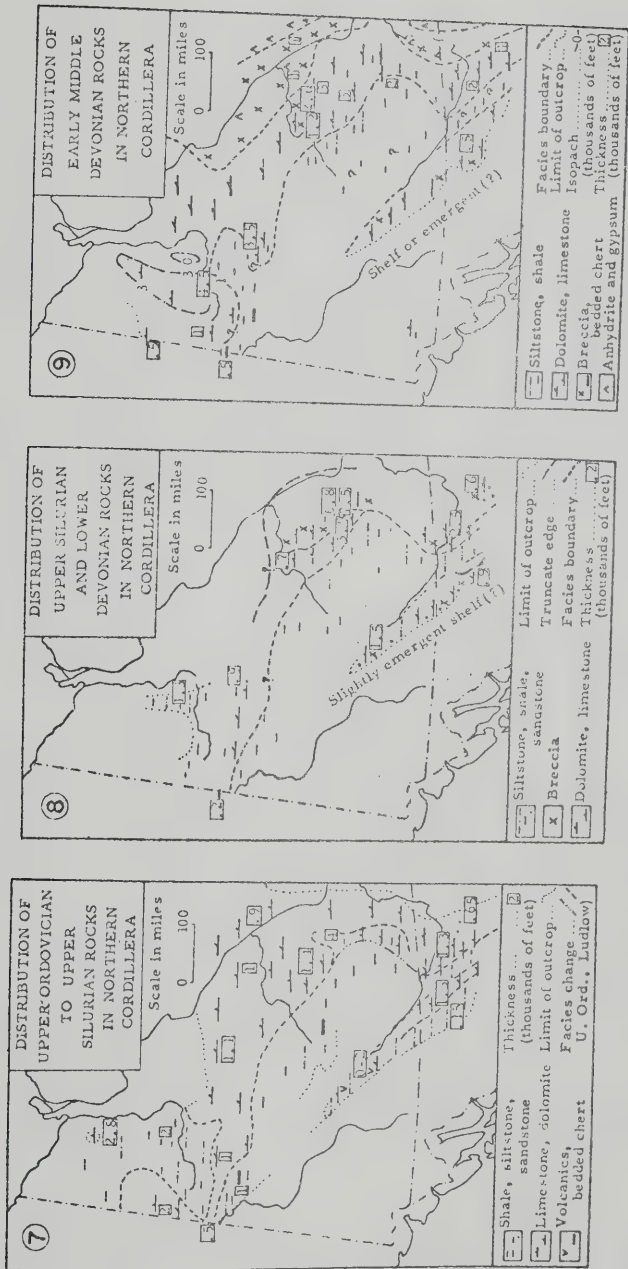


Fig. II-9. Distribution of Upper Ordovician to early Middle Devonian rocks in the northern Canadian Cordillera.

APPENDIX II-2

IGNEOUS ACTIVITY, METAMORPHISM AND TECTONISM IN THE SELWYN FOLD BELT AND RELATED AREAS

1. Volcanic Rocks

Minor and scattered occurrences of basic volcanic flow rocks are found in the early Paleozoic (Cambro-Ordovician) strata within most of the southeastern Selwyn Fold Belt. Notable locations are:

(a) upper part of unit 6 (Sekwi Formation) of Blusson (1968) at North Pyramid Mountain, 10 miles southeast of Cantung.

(b) two locations of basic volcanic flows and tuffaceous rocks in the upper part of the "Swiss Cheese" limestone unit of the Sekwi Formation, at southwest and north of the headwaters of Rabbitkettle River (Gabrielse et al., 1973).

(c) a basic flow (150 feet thick) in the upper part of Sunblood Formation northeast of Clearwater Creek, near Sunblood Mountain, South Nahanni River area (Gabrielse et al., 1973).

(d) several composite basic volcanic flows intercalated in Lower-Middle Cambrian calcareous shale and slate sequence in the western Frances Lake map-area (see Chapter III).

(e) "greenstone" or basic flow rocks in unit 2 of Wheeler et al. (1960) in the northeastern Finlayson map-area.

(f) basaltic flows and tuffs in unit 3 of Tempelman-Kluit (1972) in the Anvil Range district.

(g) andesite flows (?) in unit 1c of Roddick and Green (1961) in the Sheldon Lake map-area.

Upper Paleozoic (Pennsylvanian and Permian) alkali basalt flows and pyroclastics with associated radiolarian chert, clastic sediments

(with associated Permo-Triassic ultramafic intrusions) described as unit 8 in Tempelman-Kluit (1972) occur in Anvil Range district, north-eastern Finlayson Lake map-area, and western Frances Lake map-area (see Chapter III for detail). In fact, these great volumes (~4,000 feet) of volcanics probably extruded in the whole southwestern part of Selwyn Fold Belt, and extended an unknown distance southwest of Tintina Trench. Poole (1956) and Gabrielse (1963) considered that the volcanism began somewhat earlier to the southwest.

In summary, basic volcanic rocks were minor during Lower-Middle Paleozoic period; towards the later part of Paleozoic, much more intensive and extensive basic volcanism with closely associated ultramafic intrusion took place in the western part of the Selwyn Fold Belt.

2. Plutonic Rocks

The oldest dated granitic rocks are coarse porphyritic granites in Brooks Range Geoanticline, northwestern Yukon. A date of post-Early Devonian was recorded (Baadsgaard et al., 1961; Wanless et al., 1965). No plutonic rocks of Paleozoic age was ever recorded within the Selwyn Fold Belt. Most of the typical post-tectonic intrusions in the Fold Belt seem to be about Middle Cretaceous (Baadsgaard et al., 1961; Gabrielse, 1967b; Blusson, 1968; Tempelman-Kluit, 1972; Gabrielse et al., 1973).

Minor gabbroic dikes, sills and dioritic intrusives cutting Lower Cambrian and older strata are found in the vicinity of Cantung, Anvil Range, and various other localities. The age of these intrusives is unknown but it seems certain that they were not related to Middle Cretaceous plutons. Alpine-type ultramafic intrusives (serpentinized

peridotite, and minor dunite) of possibly Permo-Triassic age occur in the Anvil Range district, Finlayson map-area northeast of Tintina Trench, and southwestern Frances Lake map-area. Outside the Selwyn Fold Belt, these intrusives are found southwest of Tintina Trench, extending from Dawson district down to northern B.C.. They are considered to have been emplaced essentially coeval to the Late Paleozoic basic volcanic rocks (Aitken, 1959; Gabrielse and Wheeler, 1961), but also to have been tectonically emplaced as "cold" intrusions into their present positions during later deformation (Gabrielse, 1967b).

3. Metamorphism

Regional metamorphism that is recognizable in the Selwyn Fold Belt is considered to have occurred in two widely separated intervals: Lower Paleozoic (Cambro-Ordovician) and Mesozoic (Middle Cretaceous). The Cambro-Ordovician metamorphism has been observed in the Anvil Range district, Frances Lake map-area, and possibly northeastern Finlayson Lake map-area. In these areas, low-grade greenschist facies rocks are overlain by unmetamorphosed Ordovician and/or Silurian-Devonian sediments. In the eastern margin of the Selwyn Fold Belt, particularly in the Nahanni and Flat River map-areas, latest Hadrynian to Lower Cambrian rocks were weakly metamorphosed and some phyllitic rocks developed (Blusson, 1967, 1968; Gabrielse et al., 1973). This sequence is overlain by late Lower Cambrian unmetamorphosed sediments.

No known occurrence of Lower Paleozoic plutonic rocks has been reported in the region, even though metamorphosed volcanic and sedimentary rocks with related plutonic rocks of Ordovician or older age (?) have been reported in southeasternmost Alaska (Lanphere et al., 1964; Mac-

kevitt, 1963; Brew et al., 1966). The cause of the low-grade metamorphism in latest Hadrynian to Cambro-Ordovician could be due to deep burial of a thick sedimentary pile in the eugeosyncline with progressively younger burial metamorphism taking place towards the oceanic side.

The Middle Cretaceous metamorphism is well explained by the coeval plutonic activity which was related to a subduction developed further to the west during this time (Monger et al., 1972).

Eclogite and blue-amphibole (?) rocks were found along Tintina fault zone south of Anvil Range by Tempelman-Kluit (1970b, 1972; personal communication, 1973). Another occurrence of in situ (?) boulders of eclogite a few miles southeast of the eclogite outcrop was found by the writer in 1973. A more detailed account of these rocks is given in Chapter III.

4. Structural Style

The region north and east of the Selwyn Fold Belt displays simple and continuous structures reflecting deformation of relatively uniform, layered sediments (Fig. II-13), although in detail certain incompetent units are complexly folded near faults and in syncline along and west of Redstone Arch and Root Basin to the southeast. The Selwyn Fold Belt, on the other hand, displays very complex structures resulting from discordant granitic intrusions, complex structures developed in regionally metamorphosed terrains, and the overlapping of several phases of deformation. A structural cross section from the Redstone Arch to the Selwyn Mountains (A-B in Fig. II-13) is shown in Fig. II-14. Many folds within the region of Redstone Arch and Root Basin have been modified by

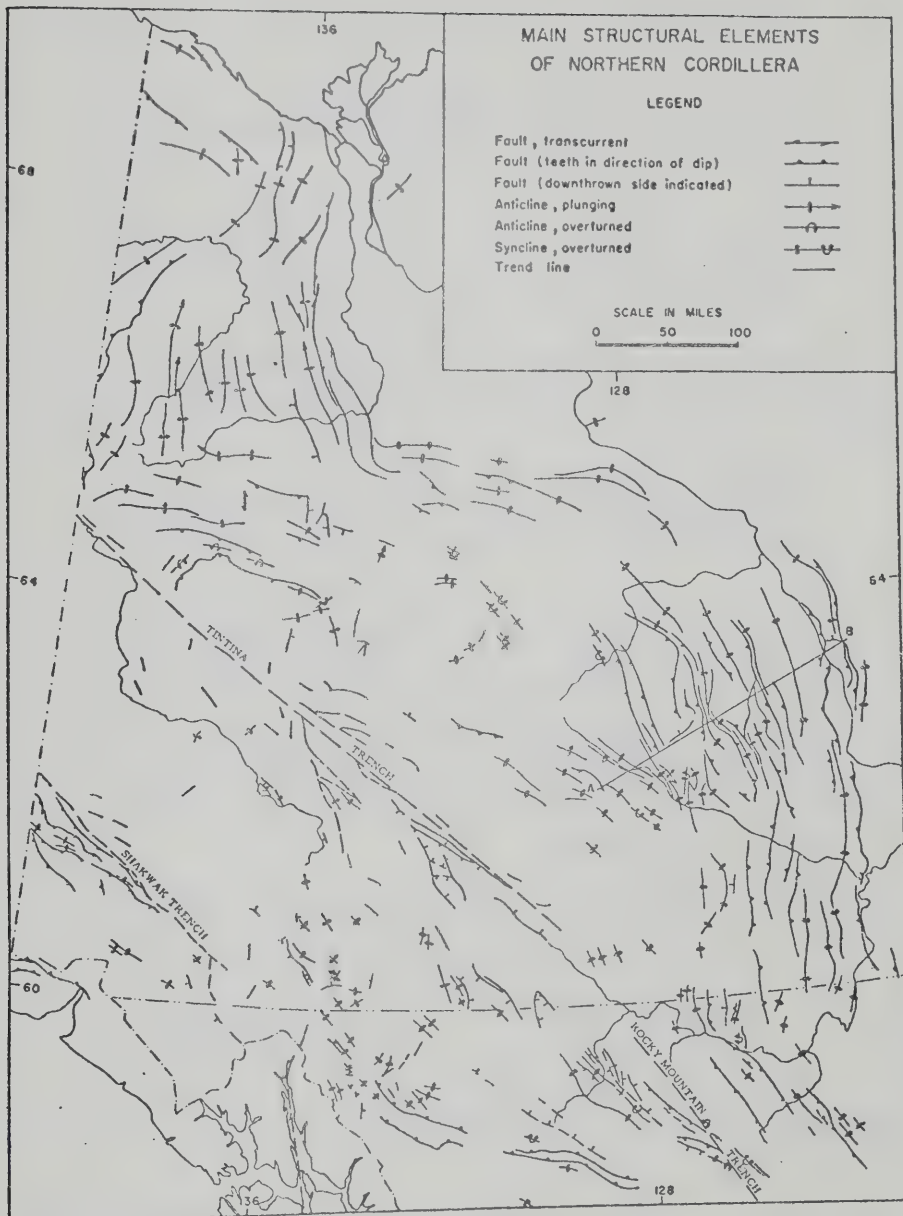


Fig. II-13. Main structural elements of the northern Canadian Cordillera (after Gabrielse, 1967b).

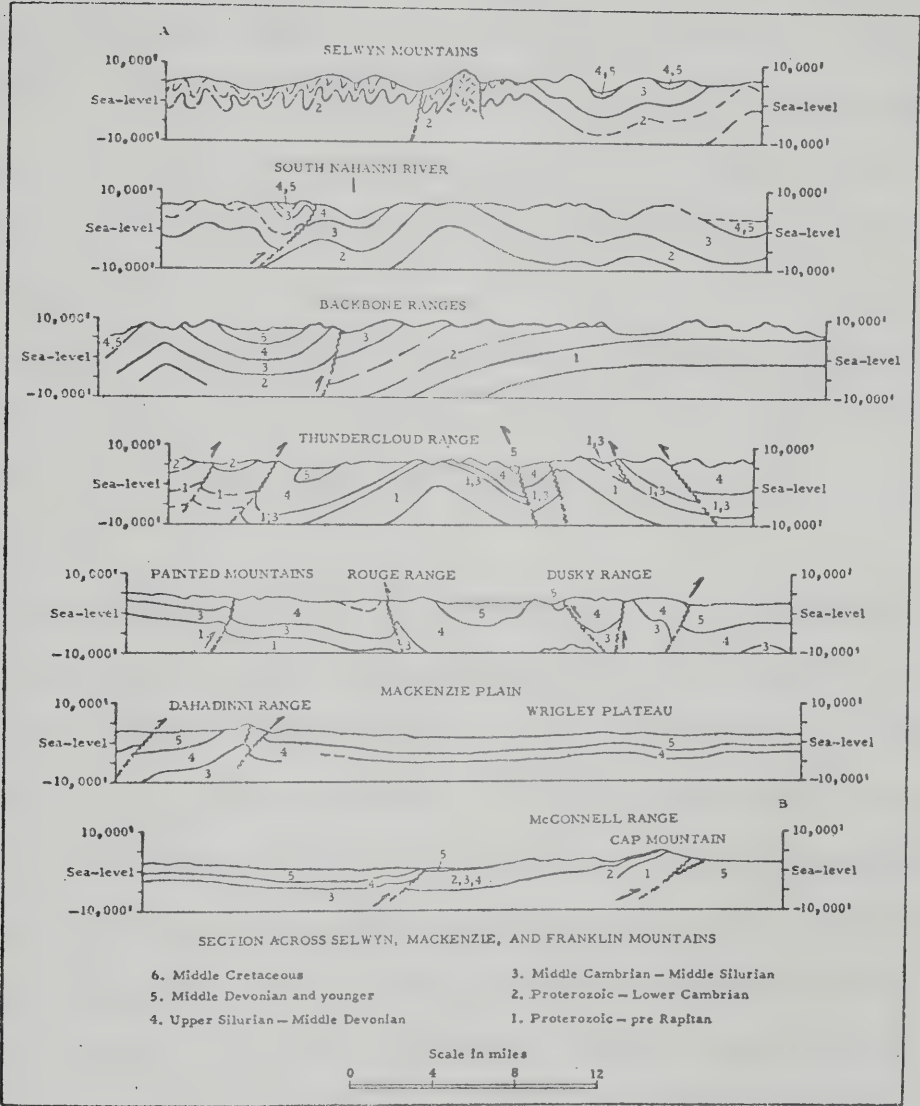


Fig. II-14. Structural section across Selwyn, Mackenzie, and Franklin Mountains (after Gabrielse, 1967b).

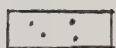
faults, some of which may be basement controlled (Gabrielse, 1967b). Locally, folds and thrust faults end abruptly against NE-trending faults along which transcurrent movement may have taken place (Douglas and Norris, 1961). Further to the east in the eastern ranges of Mackenzie Mountains and Franklin Mountains, westerly as well as fewer easterly-dipping thrust faults do occur, but they are different from the southern Canadian Rocky Mountains which are characterized by a frontal belt of thrust faults of an easterly directed asymmetry. Generally speaking, the eastern part of northern Canadian Cordillera displays more widely-spaced thrust faults, more open folds, and varying directions of structural asymmetry.

In the southeastern part of the Selwyn Fold Belt, structures of a northeasterly-directed asymmetry is prevalent (Green and Roddick, 1961; Blusson, 1968). Tight, upright to strongly overturned folds are common, particularly in the incompetent strata. The highly deformed incompetent strata of the southeastern part of the Selwyn Fold Belt were apparently pushed against the relatively competent strata of the western flank of Redstone Arch (Gabrielse, 1967b). The contrast in tectonic style between Mackenzie Mountains and northern Rocky Mountains may be partly related to the ability of a great volume of incompetent sediments in the Selwyn Fold Belt to accommodate compressive stress.

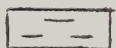
In the Tectonic Map of Canada (Stockwell, 1968) there are four major periods of deformation in this region (Fig. II-15):

(i) Late Hadrynian to Middle Devonian rocks in the northern and eastern parts of the Fold Belt were subjected to deformation by Ellesmerian Orogeny (Devonian to Viséan) of the Arctic Islands; a small region in the central Finlayson Lake map-area and the northwestern Watson

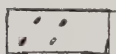
LEGENDS FOR FIG. II-15



Cover of unfolded and gently folded rocks



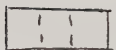
Laramide Orogeny



Lower Hadrynian and Older - folded during the East Kootenay Orogeny and refolded during the Laramide Orogeny



Mississippian and Older gneiss and schist - folded during the Tahltanian Orogeny and modified during younger orogenies



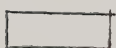
Permian and Older - folded during the Tahltanian Orogeny and refolded during the Nassian Orogeny



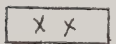
Early Mesozoic - folded during the Tahltanian Orogeny and refolded during the Columbian Orogeny



Mississippian and Permian - folded during the Tahltanian Orogeny and refolded during the Columbian Orogeny



Upper Hadrynian-Devonian - folded during the Ellesmerian Orogeny and refolded during the Columbian Orogeny



Granitic intrusions - ages undifferentiated, including Tahltanian, Columbian and Laramide

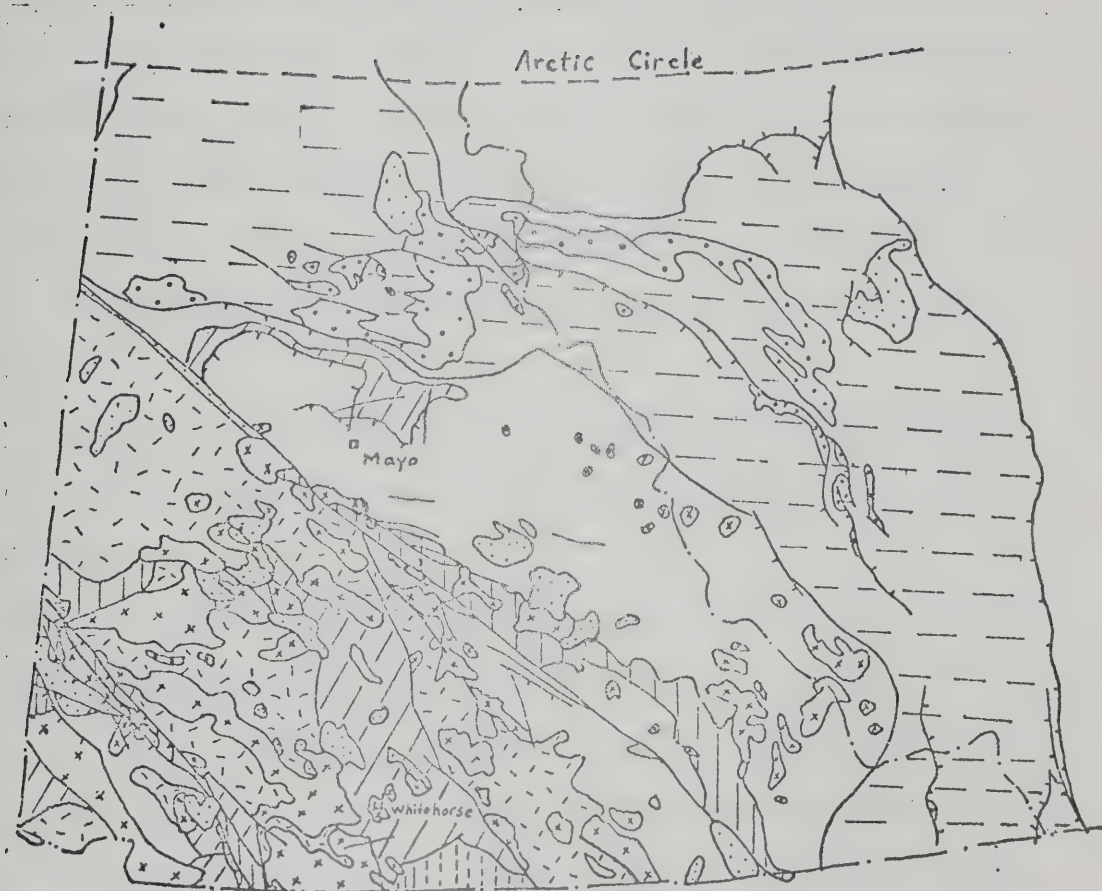


Fig. II-15. Tectonic map of northern Canadian Cordillera.

Lake map-area (northeast of Tintina Trench) is also shown to have been subjected to the same deformation.

(ii) Upper Paleozoic rocks in an arcuate region in the "core" of the Fold Belt are shown to have been subjected to deformation by the Tahltanian Orogeny (Middle Triassic) of the Coast Geanticline (extended from southwestern Yukon to southwestern B.C.) and Omineca Geanticline (southwest of Tintina Trench, from Pelly Mountains to north-central B.C.).

(iii) All the above rocks in the Fold Belt were subjected to deformation by Columbian Orogeny (Middle Cretaceous) with accompanying plutons.

(iv) Rocks of different ages in the eastern and northern flanks of the Fold Belt were subjected to Laramide Orogeny (Late Cretaceous-Early Tertiary).

Detailed field information revealed that, except for the Columbian and Laramide deformations, absence of deformations belonging to the Ellesmerian and/or Tahltanian Orogenies is quite common in particular areas. The Ellesmerian Orogeny probably resulted in deformation of the rocks of Late Hadrynian-Middle Devonian in the northwesternmost Yukon, and that Tahltanian Orogeny in deformation of Upper Paleozoic rocks in Coast Geoanticline and Omineca Geoanticline. In Anvil Range district, except the Late Cambrian-Early Ordovician deformation, all stratayounger than the Cambrian are thought to have been deformed only during Columbian Orogeny (Tempelman-Kluit, 1972). In Frances Lake map-area, post-Late Ordovician but pre-Cretaceous deformation was observed in rocks older than Ordovician (Blusson, 1966). In the Nahanni map-area, post-Devonian but pre-Cretaceous deformation was observed in rocks older than Silurian (Blusson, 1967). In the Selwyn Mountains and Watson Lake map areas, a

pronounced deformation of Upper Cambrian-Lower Ordovician was observed in the Upper Proterozoic and Lower Cambrian rocks (Gabrielse et al., 1973).

APPENDIX III-1

GENERAL GEOLOGY, ANVIL RANGE DISTRICT

1. Hadrynian

Rocks considered to be of this age are exposed only in a NW-trending zone just north of Pelly River. They form relatively good outcrops along creeks north of Faro town, and along the central reaches of Vangorda Creek. They are in fault or unconformable contact with younger strata wherever seen, and their base or older rocks are unknown. No bedding was recognized in these rocks, thus no estimate of thickness can be made.

The rocks consist largely of muscovite-quartz schist and micaceous quartzite, and in smaller amount, graphite-rich micaceous quartzite. The muscovite quartzite rocks are medium to dark grey, massive, medium- to fine-grained and strongly recrystallized. Locally color-banded, medium-grained (2mm in diameter) bluish-strained quartz and altered K-feldspar are seen. Chlorite, tourmaline and carbonate are minor constituents locally. Muscovite occurs as ragged small flakes throughout the rocks. Graphite quartzite is generally dark grey, micaceous, and interfoliated with muscovitic quartzite and is particularly common along Vangorda Creek and Pelly River.

The rock unit has been named "Grit unit" and correlated with the Proterozoic "Grit unit" of similar lithology occurring in other areas in the Selwyn Fold Belt.

An outcrop of eclogite has been noted by Tempelman-Kluit (1970b, 1972) along Tintina Fault zone. Another occurrence of large boulders of eclogite probably locally derived (in situ ?) was found by the writer in outcrops of Proterozoic rocks about 1.5 miles north of Faro town (Fig. III-2). A probable blue-amphibole (?) rock occurrence in Proterozoic

rocks is exposed along the north bank of Pelly River, about 4 miles south of Orchary Lakes.

The eclogite outcrop is apparently interfoliated with micaceous quartzite where seen and a serpentinite outcrop occurs just 50 feet northeast. No direct contact between the serpentinite and eclogite can be observed. The outcrop occurs on ridge top and has a surface extension of 10 feet x 20 feet. The contact with micaceous quartzite is not distinct but may be transitional. The eclogite is a medium green, dense, medium- to fine-grained foliated rock containing porphyroblasts of pink garnet, fine-grained apple green omphacite, prismatic grains of green amphibole, and other minor fine-grained epidote (clinozoisite), chlorite, muscovite (phengite), plagioclase, etc.. Photomicrographs of the two occurrences of eclogite are shown in Plate III-1.

The "blue-amphibole" rock occurs on a scree slope mapped as a Proterozoic unit by Tempelman-Kluit (1972). The rock is a light bluish to greenish schist rich in quartz interfolded in a greyish micaceous quartz schist. Petrographical observations of this bluish schist showed that it contains minute crystals of bluish green amphibole (generally chloritized) and some very small pale blue minerals, possibly crossite (?). Rocks containing glaucophane and crossites are best developed in the Upper Paleozoic rocks west of Pinchi fault and in the western part of the Cascade Fold Belt (Monger and Hutchison, 1971; Misch, unpublished information, see p. 58 in Price and Douglas, 1972).

Chemical analyses have been made on both whole rocks and individual minerals (garnet, omphacite, amphibole, muscovite, chlorite) of eclogite samples and are reported in a later chapter.

2. Lower Cambrian

Rocks of this age abut the northern and southern margins of the Anvil batholith, particularly in the vicinity (NW and SE) of Faro deposit. Their exposure is good on ridge tops. The stratigraphic relations of these rocks are uncertain, especially with regards to the adjacent rock units (unit 3) considered to be younger by Tempelman-Kluit (1972). Original bedding cannot be recognized in outcrops due to the development of a strong crenulation foliation (see "Structural Geology"). Their stratigraphic thickness has been estimated to be more than 2,000 feet (Tempelman-Kluit, 1972).

The base of these rocks was not observed. The rocks are composed largely of muscovite-biotite-quartz schist, phyllite, calc-silicate hornfels, and minor amounts of marble and amphibolite. The muscovite-biotite-quartz schist is well-foliated, containing commonly equigranular anhedral quartz, scattered subhedral biotite and muscovite, euhedral crystals (1-5 mm long) of staurolite, large prismatic subhedral grains of andalusite. Penninite, after biotite, is rarely present. Locally the schist grades into phyllite. The calc-silicate hornfels rocks are pale green to purple brown, consisting of alternating laminae of two components: (a) fine-grained diopside-quartz skarn with calcite, amphibole, and minor grossularite, and (b) biotite-quartz schist. Compositional layering probably is the cause of alternating laminae; foliation is present throughout. The marble is white to pale grey, coarsely crystalline, interfoliated with biotite schist and occurs only in a 300 foot-wide zone in the upper part of the unit as discontinuous lenses. Amphibolite occurs in lenses of various thickness throughout the unit; it consists of green tremolite-actinolite intergrown with andesine and minor quartz.

The original rocks are considered to be thin-bedded, fine-grained siltstone and shale, partly calcareous, with minor intercalated lenses of volcanic flows or sills (?).

The age of these rocks has been inferred from indirect stratigraphic evidence (metamorphism and deformation) and correlated with other Lower Cambrian strata of similar lithology in other areas, (see Chapter II) by Tempelman-Kluit (1972).

The writer considers that these rocks might be a time equivalent component of the rocks of probable Middle-Upper Cambrian and/or Lower Ordovician age (unit 3) and probably represents a more strongly contact metamorphosed phase. David Jennings (personal communication, 1974) showed that calc-silicate rocks that belong to this rock unit are gradational to and overlying the rock unit (unit 3) hosting the Faro deposit. However, until more detailed structural and geochronological work is done, nothing conclusive can be said.

3. Cambro-Ordovician

Phyllitic rocks of this age occur extensively in the district, particularly north and south of the Anvil batholith. The rocks weather recessively and the exposure is generally poor, but good outcrops are seen along Vangorda Creek, on lower hills north of Mount Mye, and along some creeks. The rock unit is overlain unconformably by Upper Paleozoic volcanic rocks along its northern and southern contacts, and by Middle Devonian carbonate south of Swim Lakes deposit (Tempelman-Kluit, 1972). An unconformable contact between Upper Paleozoic volcanic rocks and this rock unit has also been observed by the writer in localities north of Mount Mye and north of Swim Lakes (Kuo and Greig, 1973). The strati-

graphic thickness of this rock unit is unknown, but a thickness of about 4,000 feet is estimated.

The rock unit is subdivided into Upper and Lower members: the lower member, about 1,000 feet thick, consists of phyllites and locally schists that are enriched in quartz, graphite and chlorite, and generally lack volcanic flow through tuffaceous sediments might be present; the upper member, about 3,000 feet thick, consists of phyllites containing less quartz, numerous large volcanic flows and tuff beds, and are generally not graphitic. A thinly laminated silty limestone with phyllitic partings occurs commonly in the upper 1,500 feet of the upper member. Gondi (1972) gave a thickness of at least 2,000 feet for the Lower Cambrian strata hosting Faro deposit. The common rock types of the lower member include well-foliated, lustrous silvery grey to greenish grey chlorite-muscovite-quartz phyllite and biotite-muscovite-quartz phyllite and graphite phyllite. The former two phyllitic rocks contain more than 50% quartz, with variable proportions of chlorite, biotite, and muscovite. Alternating layers of quartz and mica are common. Within Faro deposit, proportion of quartz in some phyllites becomes so significant that they are classified as "quartzite". The graphitic phyllite generally contain 25% or more graphite with quartz and muscovite, but biotite and chlorite are absent. The phyllites of the upper member commonly contain about 20% quartz, and are hard and massive. The uppermost silty limestone consists of alternating laminae of phyllite and slightly silty, micritic to very fine crystalline grey limestone.

Volcanic rocks in the upper member include greenstone and metatuff of basalt to basaltic andesite composition. They form lenses several ten to several hundred feet thick and several hundred to several thousand

feet long. The greenstone is a fine-grained amphibolite, well-foliated near the margin of its bodies but internally lacks foliation and is generally coarser-grained. Metatuff is generally pale green laminated, cherty tuffite intimately associated with massive greenstone. Two gradational contacts observed by the writer are, from top to base, as follows:

(i) greenish laminated chert and tuffite → quartz-rich fine-grained chert → fine-grained tuffaceous greenstone → massive greenish grey volcanic (north of Swim Lakes, $62^{\circ}13.5'N$, $132^{\circ}52'W$).

(ii) weakly folded, greenish banded chert and tuffite (~100 feet thick) → massive pyritic greenstone (3-5 feet, locally 10 feet thick) → dark grey quartz phyllite - well-foliated quartz mica phyllite ($62^{\circ}26'N$, $133^{\circ}10'W$, 8 miles NNW of Mount Mye).

Photomicrographs of some greenstone volcanic, and tuffaceous rocks, and some chert and quartz mica schists are shown in Plate III-1 and Plate III-2, respectively.

Original rocks of this unit were probably fine-grained clastics, mainly siltstone and shale; volcanic flows and tuffs of oceanic tholeiite composition (see later: geochemistry of volcanic rocks) and minor deep-water carbonates occur in the upper portion of the sedimentary pile.

The age of this unit is considered by Tempelman-Kluit (1972) to be pre-Ordovician on the grounds that a graptolitic slate sequence of Middle Ordovician or younger age displays negligible deformation and metamorphism, and therefore must post-date the regional metamorphism so extensively affecting this and the previous units. Correlation of this unit with other Middle-Upper Cambrian strata has already been made (see Chapter II).

4. Middle Ordovician

A thin sequence of graptolitic shale occurs locally in the NE end of the district. The extent of the exposure is uncertain due to poor exposure and excessive weathering. A minimum thickness of 400 feet has been given (Tempelman-Kluit, 1972).

The rock is a graptolite-bearing, black to dark grey slate and silty shale containing in part thin-bedded black dense chert with thin carbonaceous partings. The rock is commonly pyritic and carbonaceous. A weak slaty cleavage intersects a faint lamination (original bedding) at very slight angles.

The age of the rock has been determined as Middle Ordovician to Early Silurian by means of graptolites (B.S. Norford, see Appendix III-2). Correlation of the rock with similar sequences in other areas is therefore very well-established (see Chapter II).

5. Silurian-Devonian

Scattered occurrences of quartzite can be seen at the NE edge of the district. The rock forms good exposures and is generally thick-bedded and massive. No internal structure can be seen although occasionally bedding (slight color banding) is measurable. Abundant quartz streaks and drusey-quartz crystals with inclusions occur locally. The contact of quartzite with graptolite slate is apparently conformable, although it may not necessarily overlie the latter. It is possible that the quartzite occupies the upper part of the graptolite shale sequence. A maximum thickness of 100 feet is estimated.

The quartzite is medium to dark grey dense rock composed of rounded, medium- to coarse-grained crystalline quartz with minor amounts of inter-

granular graphite. The rock is thus a mature sandstone formed under stable sedimentary conditions; it is best termed an orthoquartzite. In thin section, the quartz grains show uniform extinction under crossed nicols and trace amounts of tourmaline are present (Tempelman-Kluit, 1972).

The age is estimated to be Silurian-Devonian on the basis of conformable (overlying ?) contact with Ordovician-Silurian graptolite slate and possibly underlying contact with carbonate rocks of Middle Devonian age. Correlation of the unit with similar strata in other areas has been made in Chapter II.

6. Middle Devonian

Three occurrences of carbonate rocks were found. Generally speaking, the rocks form very small outcrops and no bedding planes were visible. The thickness averages 100 feet, and stratigraphically the rocks appear to overlies orthoquartzite sequence with conformity.

The rocks include limestone and dolomite and are generally light to dark grey, thin-bedded to platy, in part graphitic and bioclastic, and fetid. Diagnostic "two-hole" crinoids were observed at two localities by Tempelman-Kluit (1972).

Conodonts from the rocks have been dated by Uyeno (Appendix III-2) as Middle Devonian.

The carbonates and orthoquartzite sequence can be correlated to similar strata in other areas, but it is much thinner in the Anvil district.

7. Upper Devonian and Mississippian

The rocks form good exposures along ridges at the northwest and northeast margin of Anvil Range. The thickness of the unit has not been estimated but its correlative in other areas has a thickness of 10,000 feet. The unit was observed to be resting unconformably on a sequence of volcanic rocks.

The rocks are mainly dark grey to black, massive to thick-bedded, graphitic chert locally associated with lamination of graphitic cherty siltstone and argillaceous siltstone. Minor interbedded medium grey silty limestone, lenticular beds of gritty greywacke, chert-and-quartz pebble conglomerate are found locally.

Brachiopods from this unit were dated by Bamber (Appendix III-2) to be Carboniferous or Permian; Roddick and Green (1961) also found Late Devonian and Mississippian fossils in the same unit.

8. Pennsylvanian and Permian (Anvil Range Group)

Volcanic rocks with associated chert and limestone occur extensively north and south of Anvil Range (Fig. III-2). Volcanic rocks form resistant outcrops and underlie the more rugged peaks in the area whereas the cherty rocks weather more recessively; limestones occur only in a sinuous zone near faults south of Pelly River. The rock unit rests on all the above rock units and an unconformity at its base has been postulated. A regional unconformity beneath this unit has also been recognized in Finlayson Lake and Frances Lake map-areas. A total thickness of close to 3,000 feet has been estimated.

The unit is subdivided into three members: the lower cherty and tuffaceous sequence (2,000 feet thick); the middle basalt flow and pyro-

clastic sequence (1,500 feet thick); and the upper limestone with minor tuff sequence of uncertain thickness.

(i) The lower chert member is composed largely of varicolored, massive to laminated, silty and tuffaceous chert. Jaspers (hematitic) chert is common especially near transition contact with the middle volcanic sequence. Relict "radiolarian" spherulites (0.1-0.2 mm across) and tiny pyrite cubes are common throughout the cherty rocks. Massive angular chert breccia in graphitic matrix constitutes a minor part of the member. A sequence of laminated green chert and siliceous tuff with abundant K-feldspar crystal fragments occurs extensively in Tintina Trench, south of Pelly River. Its stratigraphic relations are uncertain but it has been tentatively correlated with the lower member by Tempelman-Kluit (1972).

(ii) The middle volcanic member includes massive amygdaloidal flow rocks, pyroclastic tuffs, and pillowed basalt. The former two are most common whereas the latter is abundant north of the Anvil Batholith. Typical flows observed by the writer range from dark grey, dense pillow basalt through greenish medium-grained massive basalt to reddish amygdaloidal basalt. Pyroclastics range from lapilli tuff breccia, through medium-grained agglomeratic tuff to brick-red thin-bedded sandy tuff to fine-grained cherty tuff. Detailed petrographic description of this unit has been given by Tempelman-Kluit (1972). Photomicrographs of typical flow rocks are shown in Plate III-3. Generally speaking, certain features observed in the field characterize this volcanic member and distinguish it from the Lower Cambrian volcanics:

(a) The Upper Paleozoic volcanics are generally fresh, show no visible foliation and have locally well-developed pillow and columnar (?) structures; tuffs occur as large layers or lenses traceable for a long

distance, and are thin-bedded and enriched in siliceous tuff fragments and graded layers of sandy, silty to cherty tuff. The rocks show a great variety of colors.

(b) Cambrian volcanics are generally well foliated, lack gross structures such as pillows or columns, commonly contain actinolite and pyrite, and occur with banded to laminated green chert; tuffs are metamorphosed and occur only as very thin layers with massive greenstone volcanics, and are lustrous and deformed (folded, contorted) wherever observed.

(iii) The upper limestone member is dense and massive, finely recrystallized, containing probably crinoid columnals, and is commonly dolomitized along fractures. Some chlorite-rich horizons of tuffaceous origin occur locally. Bedding is only recognizable in some places. Minimum thickness is about 300 feet.

Thin limestone lenses within the lower chert member and the upper limestone member yield foraminifera which were dated as latest Pennsylvanian to earliest Permian and as Late Permian, respectively (Ross, Appendix III-2). The lowest fossils are about 1,500 feet above the base of the lower member. Therefore the rock unit as a whole probably ranges in age from Pennsylvanian to Upper Permian.

This unit is correlative with similar cherty and volcanic rocks in many areas in the Selwyn Fold Belt, notably, NE Finlayson Lake, western Frances Lake, and northwesternmost Watson Lake.

9. Upper Permian and Lower Triassic

Ultramafic rocks occur in a narrow continuous belt along Vangorda fault north of Pelly River. They weather recessively but form relatively

good exposures. The belt is outlined very well by aeromagnetic anomalies in the district (see G.S.C. map 7839G). The rocks are generally fault bounded at contacts with other rocks, but transgressive contact with the Anvil Range Group are observed in some locations.

The rocks are mainly dark green to black serpentinite and serpentized peridotite. Petrographically, the serpentinite consists mostly of antigorite pseudomorph after olivine and pyroxene; the serpentized peridotite contains mainly weakly serpentized olivine and minor basitized enstite and accessory magnetite and perovskite. Talc-carbonate (ankerite ?) rocks containing minor fuchsite occur in the altered margin of the serpentinite belt (Tempelman-Kluit, 1972).

The age of the rocks probably is Upper Permian and Lower Triassic and pre-dates an Upper to Middle Triassic coarse clastic sequence (flysch) which contains serpentine pebbles. The rocks are closely associated especially with the middle volcanic member of Pennsylvanian and Permian (Fig. III-2). Similar association of basaltic and ultramafic rocks can be found in many areas NE and SW of Tintina Trench, and in other parts of southern Yukon and northern British Columbia.

10. Middle and Upper Triassic

Elongated bodies of coarse clastic rocks occur along the northern side of Tintina Trench, and form good outcrops near ridge tops. They rest unconformably on "grit unit" of Proterozoic age and occur immediately SW of Vangorda fault zone and probably accumulated along fault scarp. No bedding or foliation can be recognized. Locally the rocks are strongly fractured and steeply dipping slickensided joint planes are common. The thickness is estimated to be 2,000 feet.

The rocks consist mainly of cobble and pebble conglomerate and minor siltstone; slate and limestone occur in the upper part. The conglomerate contains coarse- to medium-grained (6" to 1/2") pebbles of most of the local older rocks, including serpentinite, cemented by fine-grained matrix of muscovite, quartz and other rock particles. It is interpreted as a typical "post-orogenic" flysch-type sediment, if not a wild flysch. The slate is thin-bedded, platy, medium grey, silty to calcareous, locally with interbedded grey, fine-grained silty limestone. A minimum thickness of 300 feet is estimated. Conodonts from this sequence were dated to be Middle or Upper Triassic by Cameron (see Appendix III-2).

The unit is correlative with similar lithology in Finlayson Lake map-area (Roddick and Green, 1961).

11. Middle Cretaceous

Granitic intrusives (Anvil Batholith) form the core of the Anvil Range. They are resistant and outcrop strongly.

The granitic rocks range from biotite-quartz monzonite to biotite-granodiorite, but most are quartz monzonites. No significant compositional variation is evident within the batholith. The rocks are generally medium grey and medium-grained rocks with equigranular texture, but porphyritic and foliated textures were also observed. Petrographic details of these rocks have been presented by Tempelman-Kluit (1972).

K-Ar dating on biotite and muscovite from the granitic rocks yield ages with a range of 79 to 99 m.y. with an average of 91 ± 5 m.y. (7 samples). Similar ages have been obtained for granitic batholiths in the southern and central Yukon, including the Selwyn Fold Belt.

12. Age Unknown (Permo-Triassic ? Tertiary ?)

Small plugs and sills of pyroxenite and gabbro occur in rock units of Lower Paleozoic.

Pyroxenite is generally dark grey, medium- to coarse-grained and equigranular, containing pyroxene altered to amphibole, calcite, serpentine and magnetite or hematite. Locally (e.g., north of Mount Mye) the rock grades to medium-grained gabbro which contains plagioclase (andesine) with lesser hornblende (some actinolite), epidote and quartz. All these rocks were serpentinized to varying degrees.

The age of the rocks is not clear but may be coeval with ultramafic intrusives and Anvil Range Group volcanics. The rocks might, however, be related to a younger, Tertiary-Cretaceous intrusive.

13. Tertiary or Cretaceous

Very small dikes and plugs of saussuritized, medium grey diorite are found at various localities within and at the margin of Anvil Batholith. They cut the batholith on Mount Mye and Lower Cambrian metasediments at many localities, some in the Faro deposit area (see later section on mine geology).

The rocks contain quartz in groundmass of fine-grained sericite, chlorite, epidote, calcite with rare epidotized or chloritized hornblende and plagioclase. The original rock was probably a porphyritic hornblende diorite.

The rocks may be a later phase apophysis of Anvil Batholith but might also be younger (Tertiary) intrusives.

14. Upper Cretaceous and Tertiary

Several occurrences of acid porphyries and tuffs are found and scattered widely in the district; one north of Mount Mye, and one more widespread south of Pelly River. They cut Anvil Batholith rocks and overlie graptolite slate of Ordovician and Anvil Range Group volcanics north of Mount Mye.

The rocks occurring north of Mount Mye are rhyolitic ignimbrites ranging from light greenish, aphanitic cherty rhyolite to rhyolitic tuff breccia and agglomerate. They weather and form a rubble of small fragments on hill slopes. Faint color lamination can be recognized occasionally.

The acid rocks south of Pelly River include quartz-feldspar granite porphyries and crystal tuffs. The former are light grey to pinkish rocks containing in most cases quartz and feldspar phenocrysts set in a fine-grained matrix of the two minerals. The crystal tuffs are thinly laminated, light colored and flinty. They contain partly devitrified glass shards and tiny quartz fragments under thin section.

The ignimbrite sequence can be correlated with acid volcanic flows and pyroclastics extensively occurring in South Fork Range, about 25 miles NE of Mount Mye, and extending some 100 miles SE to the western part of Sheldon Lake map-area. Two K-Ar age determinations of the latter volcanic rocks gave 100 and 117 m.y.. Therefore the ignimbrite sequence could be contemporaneous to the Anvil Batholith and a date of Late Cretaceous and Early Tertiary is assigned.

Tempelman-Kluit (1972) related the acid porphyries and tuffs south of Pelly River to the ignimbrites and a similar age was assigned. Acid porphyries closely associated with South Fork volcanics in the eastern

Tay River map-area and western Sheldon Lake map-area are considered to be either feeders to or intrusive equivalents of the volcanics (Roddick and Green, 1961a,b). A total thickness of 5,000 feet for South Fork volcanics was given (Roddick and Green, 1961a,b).

15. Tertiary

A unit of poorly consolidated clastic rocks and associated basalt occurs south of Pelly River. At one location (Grew Creek) conglomerate bed contains some basaltic boulders in a basalt sand matrix and therefore the basalt has been considered to be older than the clastic rocks.

The clastic rocks include thick-bedded sandstone and conglomerate containing angular fragments of chert, slate, schist, quartz and granite loosely cemented by hematite and quartz. Locally these rocks grade into brownish siltstone and silty shale containing plant remains dated as Paleocene (Roddick and Green, 1961a).

The basaltic rock is a dark green, fine-grained, porphyritic and strongly fractured rock consisting of olivine, sanidine, augite in a groundmass of plagioclase and epidote.

APPENDIX III-2

IDENTIFICATION AND DATING OF FOSSILS

Anvil Range District (after Tempelman-Kluit, 1972)

<u>Locality</u>	<u>Fauna and Age</u>
1. Graptolites collected from "unit 4" identified by B.S. Norford.	
62°27.3'N, 133°02.0'W	inarticulate brachiopod ? CARYOCARIS sp. ? CLIMACOGRAPTUS sp. GLOSSOGRAPTUS sp. age: Ordovician, Llanvirn to Caradoc
2. Conodonts collected from "unit 6" identified by T.T. Uyeno.	
62°22.8'N, 132°59.1'W	POLYGNATHUS LINGUIFORMIS LINGUIFORMIS Hinde P. VARCUS Stauffer P. sp. (probably n. sp.) approaching SCHMIDTOGNATHUS in the size of basal cavity age: probably Late Middle Devonian (P. VARCUS - zone, or the lower part of the S. HERMANNI-P. CRISTATUS- zone)
3. Brachiopods collected from "unit 7" identified by E.W. Bamber.	
62°32.9'N, 133°08.2'W	Orthotetid brachiopod ? MICHELINIA sp. ? EKVASOPHYLLUM sp. - possibly E. PROTEUS Sutherland age: Osagian or Early Meramerician. This is a tentative age determina- tion. The material is poorly pre- served.
62°32.9'N, 133°08.4'W	spiriferid, orthotetid, and choretid brachiopods (too poorly preserved for identification) age: Carboniferous or Permian

APPENDIX III-2 (cont'd)

- | <u>Locality</u> | <u>Fauna and Age</u> |
|---|---|
| 4. Fusulinids collected from Anvil Range Group identified by C.A. Ross. | |
| 62°20'N, 133°33'W | TRITICITES sp. advanced form
PSEUDOFUSULINELLA sp.
SCHUBERTELLA sp.
THOMPSONELLA sp.
age: latest Pennsylvanian to Early Permian |
| 62°02'30"N, 132°47'W | SCHWAGERINA sp. (very large)
age: Permian, could be wolfcampian to Wordian |
| 5. Conodonts collected from "unit 10a" identified by B.E.B. Cameron. | |
| 62°21'N, 133°42'W | GONDOLELLA sp. A
GONDOLELLA sp. B
GONDOLELLA aff. MILLERI Miller |
| 62°21'N, 133°42'W | GONDOLELLA aff. MILLERI Miller
GONDOLELLA sp. B
GONDOLELLA sp. B
age: Middle or Upper Triassic |

Frances Lake District

Brachiopods collected from a limestone bed W of the East Arm identified by J.B. Waterhouse.

61°27.9'N, 129°30.9'W	RETCHONETES ? ATHYRIS
-----------------------	--------------------------

Both are most characteristic of the Devonian period, but the full permissible range is from Upper Silurian to Carboniferous. RETCHONETES especially resembles Middle Devonian species R. SUBCANCEL-LATUS (Reed) from the Shan States, Asia and R. MINUTUS (Von Buch) from the Middle Devonian species. R. MARYLANDICUS (Prosser) from the Romney Formation of Maryland is also close in shape, but has finer ribs and longer ventral septum. R. VICINUS Castelnau from the Hamilton Group is more quadrate in shape. A Middle Devonian age seems likely.

APPENDIX III-3

STRUCTURAL GEOLOGY, ANVIL RANGE DISTRICT

1. Internal Structures

Rock units in the district are internally deformed to various degrees and in different styles, and are fairly complex. Most of this internal deformation was produced by an older event, presumably in Lower Paleozoic, because rocks younger than Cambro-Ordovician display negligible and different deformation styles.

A well developed crenulation foliation (F_2) characterizes the structures of rocks older than Cambro-Ordovician. F_2 transposes partly or completely an older planar structure (F_1) which forms small folds between F_2 planes. F_2 is axial planar to these small folds in most cases. Sometimes F_2 is so penetrative that remnants of earlier foliation are completely lacking and thus F_1 may be considered to be completely transposed to F_2 . The intersection of F_1 and F_2 defines a lineation (L_2) which sometimes coincides with the fold axis of F_1 . F_1 results from parallel alignment of micas and by segregation of quartz and mica which forms compositional layering; F_1 might be original bedding. F_2 is sometimes folded in small amplitude and the fold axis thus defines a kinked cleavage (F_3) and the intersection of the two foliations defines a coarse wrinkle lineation (L_3). L_2 is generally masked by L_3 . Besides these two lineations, one or more very fine wrinkle lineations are observed on F_2 in rare cases; these fine wrinkles may be a complex set of different lineations, some must have post-dated L_3 .*

*In a detailed investigation, up to 6 generations of foliations have been defined in the Faro deposit, and anticline structures in Vangorda deposit define 4 foliations (Jennings, Personal Communication, 1974).

Folds in Cambro-Ordovician and older rocks are generally quite tight, subisoclinal slip folds with axial angles of 30-40° plunging NW. They occur on all scales, from thin section to large outcrop. Small-and-intermediate-scale folds are outlined by F_1 and locally by bedding, and the large-scale folds by contact between greenstone and phyllitic rocks.

For a more detailed account of internal structures in the Lower Paleozoic rock units, see Tempelman-Kluit (1972).

Rock units younger than Ordovician show weak to minor deformation with development of foliation in incompetent members. Ordovician graptolite slate shows a cleavage plane developed at a very slight angle to bedding; the cleavage may be the result of slight pervasive recrystallization. Slate in the Upper Devonian and Mississippian strata shows only a cleavage plane probably resulting from weak pervasive recrystallization. The lower cherty member of the Anvil Range Group shows local transposition of the bedding plane outlined by compositional layering and development of a weak crenulation foliation which transects the bedding at various angles and defines a weak lineation. A very fine wrinkle lineation forms locally at various angles to the intersection of bedding and foliation. No large-scale or minor folds were seen, but the weak pervasive foliation may be an axial plane or slaty cleavage related to the development of unrecognized folds in these rocks.

Most internal structures except L_3 are not observed in Middle Ordovician slate and shale unit, suggesting that the older deformation occurred before Middle Ordovician. Alternatively, different structural styles may be stratigraphically controlled and deformation was weaker in higher stratigraphic units than in lower strata; if so then the older deformation is pre-Middle Devonian because strata of that age overlie folded rocks of Cambro-Ordovician with marked angular unconformity

(Tempelman-Kluit, 1972). Minor structures in the cherty member of Anvil Range Group may have been formed during early Cretaceous, a time of widespread deformation in much of the northern Canadian Cordillera. The deformation may have accompanied or preceded the intrusion of the Anvil Batholith and consequent doming. Incidentally, the lineation in cherty member of Anvil Range Group is parallel to the wrinkle lineation (L_3) in Cambro-Ordovician strata and the two might be coeval and syngenetic; thus the latter were also affected by the Early Cretaceous Orogeny.

2. Doming of Anvil Batholith

Intrusion and doming of Anvil Batholith resulted in an anticlinal cumulation about 40 miles long; 15 miles wide, with an amplitude of about 2 miles. The dome or arch trends NW roughly parallel to Tintina Trench. It has a gently-dipping NE limb and a more steeply-dipping SW limb. Rocks on the flanks of the arch are repeated and dip away from it.

To the NW and SE, the arch plunges beneath its cover and terminates probably by other structures.

Minor elevation and tilting in the district probably occurred in Late Mississippian or Early Pennsylvanian time because the unconformity beneath the Anvil Range Group overlies progressively older rocks southward. Some steepening of the southeastern limb of the arch may have occurred during movement of Vangorda Fault.

3. Faults

General NW-trending, steeply-dipping, subparallel normal faults occur along the valley of Pelly River and define the Tintina fault zone. They separate rocks of different ages and some of the appear to be deep-seated. Roddick (1967) and Tempelman-Kluit (1970a) postulated that

the fault system was strike-slip transcurrent faulting with a right lateral displacement of about 250 miles.

The northern faults (Rose Creek fault, Vangorda Creek faults, and Lapie River fault) dip to the SW and are closely associated with ultramafic intrusions and local occurrences of eclogite. These faults may have been deep-seated and perhaps extended down to lower crust or upper mantle (?) (Tempelman-Kluit, 1972). Their displacement probably occurred in Early Triassic time, but renewed movement of Vangorda faults probably took place after Anvil Batholith intrusion because the intrusive is truncated by the faults at their eastern end (see Fig. III-2).

The southern faults (Buttle Creek fault, Grew Creek fault, and Danger Creek fault) probably dip vertically or to the NE. They are not considered to be deep-seated. Offset of these faults probably began in Late Cretaceous, perhaps after some of the northern faults ceased movement.

Small-scale subsidiary faults, too numerous and small to map, occur locally in many places, especially in the southern flank of Anvil Range near Faro deposit.

APPENDIX III-4

GENERAL GEOLOGY, FRANCES LAKE DISTRICT

1. Middle and Upper Cambrian

The Cambrian rocks can be conveniently divided into two members: the lower member consisting of calcareous phyllite and slate with thin-bedded dolomite and limestone; the upper member is mainly graphitic to chloritic quartz sericite phyllite and silty shale. The lowermost rocks of the lower member are generally light-colored, soft phyllites containing abundant quartz-carbonate (ankerite to siderite) probably derived from metamorphic mobilization, and grade upwards into intercalated calcareous and silty phyllites and phyllitic limestones. These are usually well-banded rocks, the bands being between a half and one inch thick. An apparent thickness of at least 1,500 feet is estimated. Two layers of foliated, chloritized, leucoxene-bearing metavolcanic flows and tuffs, about 150 to 200 feet thick, occur in the middle to upper part of the lower member. The metavolcanics typically contain major plagioclase (sometimes hornblende), chlorite, and minor quartz, ilmenite or leucoxene, sphene, carbonate, opaque minerals (sulfides and oxides), rarely biotite and volcanic glass.

At the northeastern corner of the district, a sequence of light to medium grey, calcareous to silty, thin-bedded to laminated shales and phyllites is exposed. These resemble in lithology the calcareous phyllite sequence at the western side of the East Arm. The former has been assigned a Middle to Upper Cambrian age (Blusson, 1966).

The lower member probably underlies conformably or grades into the upper member even though their contact has not been observed. They may be entirely coeval. The upper member is well-exposed at the eastern

side of the East Arm and along Anderson Creek, and is host to the Thompson Creek deposit. The rocks are dark grey to black, partly banded, siliceous phyllites and slates. Graphitic and chloritic layers are locally abundant, especially in the drill cores in the vicinity of the deposit. Foliation is always present and mostly at angles to bedding planes wherever seen. At about the middle part of the sequence, a 150 foot layer of quartz-sericite-chlorite schist has been observed in the drill cores as well as in the outcrops extending to the SE of the deposit. Total thickness for the upper member is estimated to be about 4,500 feet.

The following is a summary of petrographic observations made on the major rock types of the Cambrian strata:

(a) Calcareous Phyllite. Consists mainly of carbonate, quartz, biotite and sericite, with minor opaque minerals and siderite. In some specimens, quartz together with graphite is present in minor amounts. A compositional banding (F_1) is commonly observed; it is outlined by changing ratios of carbonates and quartz, sometimes also by grain size difference in quartz. A foliation (F_2) outlined by biotite forms sub-parallel with F_1 . A younger foliation (F_3) shows rather widely-spaced planes intersect F_1 and F_2 at about $30-40^\circ$, and causes boudinage in harder beds of the rocks. The rocks can be best termed quartzose, phyllitic metalimestones (see Plate III-3 and Plate III-13).

(b) Quartz Sericite Phyllite. Major minerals are quartz, sericite, chlorite with minor graphite, carbonate and opaque minerals. Andalusite and thin needles of tourmaline have been observed in some core specimens in the upper sequence of the host rocks to the Thompson Creek deposit (see section on "Ore Deposits", for detailed subdivision of host units). Generally speaking, relationships among F_1 , F_2 and F_3 foliations

are grossly similar to those in the calcareous phyllite except that F_2 is oblique to F_1 and F_3 intersects F_1 and F_2 at almost vertical angles.

(c) Quartz-Sericite-Chlorite Schist. The rock contains clasts or "phenocrysts" of quartz (1 to 3 mm across) wrapped or interfoliated in sericite and chlorite layers. Minor recrystallized carbonate, epidote and opaque minerals (mostly porphyroblastic pyrite) and relict grains of plagioclase and perhaps some epidotized pyroxene were observed. Thalenhorst (personal communication, 1971) reported in one outcrop an intercalated massive porphyritic rock composed mainly of plagioclase and minor sericite, opaque minerals, zircon and leucoxene. Flow banding of sericite and chlorite around quartz is common and the rock has an apparent pyroclastic texture indicating a tuffaceous origin.

The Cambrian strata is correlative with a similar sequence in the adjacent areas, notably, units 9 and 10 of Blusson (1966) in the general Frances Lake map-area and Flat River map-area, and unit 2 in the Finlayson Lake map-area (Wheeler et al., 1960b) and the Quiet Lake map-area (Wheeler et al., 1960a).

No fossils have been found in the Cambrian strata, but the above correlation places the strata in Middle to Upper Cambrian.

2. Middle Ordovician and Silurian

A sequence of black shale and slate occurs above the Cambrian strata with an apparent unconformity or disconformity at the western side of the East Arm. The rocks are generally thick-bedded, banding is lacking or very rare, and the rocks grade into a more calcareous facies with thin layers of dark grey to black impure limestones to the NW. The total apparent thickness of the sequence is estimated to be about 1,500 to 2,000 feet.

A black slate and shale sequence with dark impure limestone occurring in the upper part was also observed in the southeastern and the northeastern parts of the district near the presumed boundary of the two members of Cambrian strata; these two occurrences of black slate and shale may or may not be correlative with the western occurrence.

The sequence lacks fossils but it grossly resembles unit 11 of Blusson (1966), which bears graptolites of Middle Ordovician to Silurian age and occurs about 50 miles E of the district along Flat River valleys. An Ordovician to Silurian age is thus tentatively assigned to the black shale and slate sequence in the district.

3. Silurian and Devonian

A sequence of carbonate and coarse clastic sediments accumulated above the Ordovician-Silurian strata in apparent conformity and occupies most of the western part of the district.

The sequence consists of interfingering or intercalated quartzite, dolomite and dolomitic slate and limestone. The quartzite is generally fine-grained, white to light grey, massive and partly banded, locally containing cross-bedded facies, and forms interfingers laterally and vertically with a light colored to brownish dolomite and dolomitic phyllite (siltstone) and minor thin-bedded limestone layers or lenses. Facies change is common both locally and aurally. The area was probably the site of active deposition with a landmass not too far away. The thickness of the member is estimated to be about 1,000 feet. To the south, it becomes much thinner and may eventually taper out with the disappearance of quartzite; on the other hand, the underlying black slate and phyllite increase in thickness indicating that both units may be in part lateral facies equivalents of each other. Deposition here

was obviously quieter, and no influence of a landmass can be detected. At the western margin of the district, dark grey thick-bedded dolomite with a few intercalations of thick-bedded, dark colored quartzite are exposed. Facies change probably did occur but appear to be less than those to the east. Fossils found in a limestone bed in the upper part of the sequence have been dated as Middle Devonian (range: Upper Silurian to Carboniferous) by J.B. Waterhouse (Appendix III-2).

The sequence is correlative with unit 12 in the general Frances Lake map-area (Blusson, 1966), unit 4 in the northeastern Finlayson Lake map-area (Wheeler *et al.*, 1960b), unit 6 in the Watson Lake map-area (Gabrielse, 1967a) and units 5 and 6 in the Anvil Range district (Tempelman-Kluit, 1972).

4. Devonian and Younger

A sequence of dark grey to black slate and shale with intercalated thick-bedded greywacke is exposed in the western part of the district. The slate or shale is a dark grey mica-rich, non-calcareous rock with abundant mobilized quartz layers or bands up to 1 foot wide, occurring along foliation planes; sometimes the bands are so well-developed that they form white and black "gneisses". On the surface the micaceous lineations commonly display crenulation or "fish-bone" structure. The greywacke is a medium- to coarse-grained (1 to 5 mm across) rock containing rounded to angular clastic grains of quartz, small chips of chert and a few grains of plagioclase, zircon and opaque minerals set in a groundmass of sericite and fine-grained interlocked quartz in about equal amounts. Sometimes pieces of folded graphite biotite-sericite phyllite derived from phyllites of the lower sequence were observed. Locally the

greywacke contains some layers of soft, dark grey dolomitic limestone in the upper part. An average thickness of 4,000 feet is estimated for the sequence.

The sequence is correlative with unit 13 of Blusson (1966) in the general Frances Lake map-area, unit 5 and perhaps part of unit 6 of Wheeler et al. (1960b) in the Finlayson Lake map-area, unit 7 and perhaps part of unit 8 in the Anvil Range district (Tempelman-Kluit, 1972), unit 5 in the Sheldon Lake map-area (Roddick and Green, 1961b), and unit 7 in the northwestern Watson Lake map-area (Gabrielse, 1967a). An age of Upper Devonian to possibly Upper Mississippian is tentatively assigned to this sequence.

The contact between this sequence and the Silurian-Devonian strata appears to be a minor disconformity; however, Blusson (1966) reported a pronounced unconformity at the base of the Devonian-Mississippian strata in the general Frances Lake map-area.

5. Hornfels

Rocks around batholith of Mount Hunt and those bounded by smaller batholith bodies at Simpson Tower are collectively classified as hornfels. These rocks display a series of lithological variations corresponding to their original compositions.

Hornfels surrounding Mount Hunt batholith are mostly non-calcareous silicate rocks and can be subdivided into a spotted hornfels abutting the batholith at its northeastern margin and an unspotted massive hornfels extending at least 1 mile from the batholith contact. The spotted hornfels is a medium-grained, dark grey to black rock containing 5-10% iron sulfides, which commonly weathers rusty brown. The original rock might have been a slightly graphitic shale. The unspotted

hornfels is generally very fine-grained, massive, light to dark grey, containing mobilized quartz layers; the original bedding is still recognizable and foliation seems to have been reduced if not eliminated during contact metamorphism. With increasing distance from the intrusive contact, the hornfels becomes more slaty and less siliceous.

Both these spotted and unspotted hornfeldes are considered to be the contact metamorphic equivalent of the quartz sericite phyllite of the Cambrian sequence.

Limited petrographic observations indicate that hornfels nearer to the intrusive contact (600 feet or less) is characterized by minerals typical of hornblende hornfels facies (major: muscovite, biotite, andalusite; minor: plagioclase, quartz, opaque minerals, graphite, sometimes rare tourmaline); and hornfels further from the intrusive contact (1,500 feet or more) shows minerals typical of albite-epidote hornfels facies (major: plagioclase, quartz, biotite, muscovite; and minor: spessartite (?), pyrite, graphite, amphibole, tourmaline, chlorite, apatite).

Hornfeldes adjacent to and bounded by several medium to small intrusive bodies in the Simpson Tower area can also be divided into two types, a spotted biotite hornfels and a mixed sequence of calc-silicate hornfeldes. The spotted biotite hornfels is a coarse-grained, massive to slightly foliated, dark grey rock containing mobilized quartz layers. It occurs along the western contact of a more easterly intrusive body and a gradational "mixed" zone of biotite hornfels and intrusive rock can be observed at their mutual contact. The biotite hornfels appears to be the contact metamorphic equivalent of the black slate and phyllite sequence. The calc-silicate hornfeldes occur extensively over the more northern side of the Simpson Tower area. They are generally very

fine-grained, unspotted, and can be subdivided into a more siliceous unit and a more calcareous unit. Lithological gradation both between and within these two units occurs laterally as well as across strike. Generally speaking, siliceous calc-silicate hornfels is light grey to greenish grey, contains about 2/3 or more silicate and very little or no carbonate, and is hard, flinty, clearly banded and in part somewhat slaty; whereas the calcareous calc-silicate hornfels is dull light grey to dark grey, containing abundant carbonate and is softer and less well banded. A thin layer (30 feet) of spotted, slightly foliated and porphyritic hornfelsed tuff occur above the calcareous calc-silicate hornfels; an unconformity appears to exist at the base of the tuff.

The calc-silicate hornfelses are probably contact metamorphic equivalents of Devono-Mississippian and part of the Siluro-Devonian strata. However, stratigraphic relations are obscured due to strong tectonic deformation and lithological modification.

6. Middle Cretaceous

The big batholith of Mount Hunt and several medium to small intrusive bodies at Simpson Tower are petrologically biotite quartz monzonites in composition. These intrusive rocks, together with a large area of similar rocks in the northern Canadian Cordillera, have been dated as Middle Cretaceous.

Typical rock type of the Mount Hunt batholith is an equigranular, medium- to coarse-grained, light colored rock commonly containing zoned plagioclase, quartz, biotite, chlorite, opaque minerals (pyrite, etc.), sphene, epidote, zircon, apatite, and rutile. Amphibole was probably altered to chlorite, epidote and sphene. Zoned plagioclase is generally about 30% richer in An content in the core.

Intrusive rocks at the Simpson Tower area are similar in mineralogy except that they contain a higher amount of quartz, somewhat finer-grained than the Mount Hunt intrusive. It is possible that the former rocks occurred at a higher level of intrusion than those at Mount Hunt.

Small aplite dikes were observed in the vicinity of the batholith in the hornfelses; they are commonly associated with quartz veins and fissures and in part seem to occupy fault planes. They are apophyses of the Middle Cretaceous batholiths.

APPENDIX III-5

GENERAL GEOLOGY, HOWARD'S PASS DISTRICT

1. Lower Cambrian and Older

This rock unit though not exposed in the Howard's Pass district outcrops further to the S and SE. It is believed to be the oldest unit exposed in the Nahanni map-area and consists of a lower "grit unit" and an upper slate and phyllite sequence. The grit unit is more than 10,000 feet thick made up of a lower sandy to pebbly sequence and an upper shaly sequence; the lower sequence consists of calcareous, gritty, feldspathic sandstone, pebble conglomerate and silty shale and slate, locally containing thin beds of dark grey, fine-grained impure limestone; the upper sequence is mainly maroon and green shale totalling about 3,000 feet in thickness. The upper unit is estimated to have a minimum thickness of 8,000 feet at the southeastern part of Nahanni map-area (Blusson, 1967); it consists dominantly of brown to red-brown weathering, varicolored slates, siltstones and phyllites. The contact between this upper unit and the grit unit appears to be conformable.

The age is tentatively assigned to the Lower Cambrian and older; judging from the Early Cambrian trilobites occurring in strata 5,000 feet above this unit, its age could possibly be Late Hadrynian.

The unit is correlative with similar sequences in adjacent map-areas. "Grit unit" and "phyllite unit" of Gabrielse et al. (1973) to the E in the Flat River, Glacier Lake and Wrigley Lake map-areas; unit 1 in the Frances Lake map-area (Blusson, 1966); units 1d and 1c in the Sheldon Lake map-area (Roddick and Green, 1961a) and the "grit unit" in the southeastern Finlayson Lake and Ketra River area (Tempelman-Kluit et al., 1974).

2. Upper Cambrian and Lower Ordovician

The rock unit forms the base of the Howard's Pass district wherever seen and can be subdivided into three subunits: a lower massive carbonate and siltstone member, a central wavy banded silty limestone member and an upper "transition"zone" limestone and dolomite member.

The lower member consists of massive, buff grey and brown silty and sandy limestone and dolomite locally showing calcareous "nodules" or lenses; a sequence of light orange, massive siltstone which is locally calcareous occurs in the lower part of the member. In the southwestern part of the Summit Lake region about 8 miles SE of Placer's main zone, a sequence of red bed about 500 feet thick is exposed; it consists of red, orange weathering sandstone, sandy dolomite and cross-bedded, ripple marked orthoquartzite. This red bed is believed to be the base of the rock unit and represents recycled Lower Cambrian arenites (Blusson, 1967). The base of the rock unit has not been observed in the district, but further to the E in the eastern side of South Nahanni River, an angular unconformity exists at the base of the unit which has been dated as pre-Upper Cambrian in the Glacier Lake and Wrigley Lake map-areas further to the E.

The central member consists of interbedded and thin-bedded (1/2 to 1 inch) grey limestone and dolomite; locally containing thin shaly interbeds or partings which are displayed by widely-spaced cleavage giving a wavy banding appearance. Dolomite beds locally form discrete lenses containing fine-grained limestone squeezed up between them.

The upper transition zone member occurs gradationally above the wavy banded limestone and consists of thin-bedded limestone and dolomite laterally changing into massive calcareous siltstone. The gradation probably reflects a facies change that occurs with the deepening of a lagoonal or back-reef shelf facies to a deeper water environment.

The rock unit is estimated to be more than 1,000 feet thick, the lower member varies in thickness and is not always present. The rock unit is correlative with the Rabbitkettle Formation and part of the Broken Skull Formation in the southwestern Glacier Lake map-area and in Flat River map-area (Blusson, 1966). Fossils from these strata indicate an age of Upper Cambrian to Lower Ordovician.

3. Ordovician

The rock unit probably represents a period of uninterrupted cyclic sedimentation in closed, euxinic basins of relatively deep-water environment over a considerable period of time. It is exposed as a narrow sinuous belt in most parts of the district. The base of the unit is a calcareous siltstone sequence very similar to the underlying transition zone rocks, but it is believed that some discontinuity in sedimentation between the contact existed (House, personal communication, 1975). The thickness of the unit varies in places, but an estimate from two sections in the southern and northwestern parts of the district (see Fig. III-16 and Fig. III-17) and one section at Placer's main zone (see Fig. III-18) yield a thickness of 500 to 600 feet. In the Nahanni anticline northeast of South Nahanni River, a maximum thickness of less than 1,000 feet has been estimated by Blusson (1967).

The rock unit can be subdivided into four members, from base to top:

(a) Lower Siltstone Member. The rocks are generally very fine-grained to black, graphitic and graptolitic siltstone with a lower calcareous sequence and an upper pyritic graphitic or siliceous sequence. *Diplograptid* sp. graptolites found in the Placer's main zone indicate an age of Lower to Middle Ordovician (House, personal communication, 1975).

The thickness of this member is very thin, probably in the order of 50 feet or less.

(b) Cherty Limestone Member. The rocks are dark grey to black, fine-grained cherty siltstones containing abundant large clasts and lenses of crystalline limestone in highly varying sizes (1 to 5 feet in diameter); in Placer's main zone, thinly interbedded cherty and limy siltstones are tightly folded and appear to be an integral part of the sedimentary sequence.

(c) Cherty Siltstone Member. This member probably represents a continuing sedimentation of chert and silt in a siliceous environment without a calcareous component. The rock is a massive, dark grey to black, very hard and fine-grained cherty siltstone with abundant siliceous shale partings between beds. Pyrite occurs sporadically in places. In most of the outcrop the rock is tightly folded without axial plane cleavage developed, and without thickening of the fold axis, indicating that the folding took place before the consolidation or lithification of the rock. Under the microscope, the rock consists of abundant cryptograined and interlocking quartz crystals set in a siliceous and silty groundmass. Lead-zinc mineralization occurs mainly in this member, and also in part of the underlying cherty limestone member.

(d) Siliceous Siltstone Member. The upper part of cherty siltstone member grades into a cherty rock with abundant siliceous shale interbeds and into an entirely siliceous shale or siltstone sequence which appears to occupy the major section of the Ordovician strata, as evidenced by its abundance in Placer's main zone (see Fig. III-18). The rock is a very fine-grained, light grey siliceous to shaly siltstone, partly pyritic along laminations; massive beds of black chert as well as isolated limestone clasts occur throughout this member. The

regional axial plane cleavage affects the member to a great extent and abundant slaty cleavages were developed. Minor amounts of sphalerite and galena have been seen in some of the limestone clasts.

The rock unit is correlative with similar sequences in many regions of the northern Canadian Cordillera, notably: unit 10 in the general Nahanni map-area (Blusson, 1967); Road River and part of Whittaker Formations in the Glacier Lake and Wrigley Lake map-areas (Gabrielse *et al.*, 1973); unit 11 in the Frances Lake map-area (Blusson, 1966), and unit 4 in the Anvil Range district (Tempelman-Kluit, 1972). The rock unit is therefore assigned an age of Lower Ordovician to possibly Lower Silurian.

4. Silurian

This rock unit overlies the Ordovician strata with apparent conformity and probably represents an environment of submarine channel turbidity current sedimentation. It can be divided into a lower flaggy dolomitic siltstone member and an upper siliceous siltstone member. A total thickness of about 600 feet for this unit is estimated from available geological sections.

The lower member consists of buff weathering, fine-grained, pyritic and partly graphitic grey dolomitic siltstone characterized by dissemination of clasts or flakes of clay or carbonaceous material and is flaggy in outcrop occurrence; the lower part is generally enriched in graphite and massive to disseminated pyrite, towards the upper part a fairly massive bed of more siliceous dolomitic siltstone occurs.

Overlying the lower member in conformable sequence is a siliceous, dark grey, thinly laminated siltstone with bedded pyrite in the more shaly parts. Minor massive chert beds and limestone clasts occur in this upper member. In several locations the member contains barite as

brecciated clasts or as disseminations and laminations in the matrix of the siltstone. The uppermost part has more sandstone interbeds and is very siliceous: grading, ripple-marks, cross-bedding, scouring and loading are the common features observed and the rocks probably represent a turbidite sequence. Very small-scale Bouma sequences are commonly observed and thus the rocks are interpreted as distal turbidites.

The rock unit is correlative with the upper part of unit 10 in the general Nahanni map-area (Blusson, 1967) and upper Road River Formation in the Glacier Lake and Wrigley Lake map-areas (Gabrielse et al., 1973). Tentatively, a Silurian age is assigned.

5. Devonian and Mississippian

Unconformably overlying the Silurian strata is a cyclic sequence of conglomerates interbedded with sandstones, siltstones or grits. Each cycle starts with conglomerate overlain by interbedded sandstone and siltstone. In the northwestern part of the district (see Fig. III-17) as much as eleven cycles were mapped by the writer. The conglomerate usually contain rounded chert pebbles and shale fragments in a matrix of black shale or siltstone; angular fragments or chips of shale, sandstone boulders and large clasts of black shale or interbedded shale and sandstone were also observed in the conglomerate. Contacts between individual conglomerate, sandstone and shale beds are sharp; they are overlain by either alternating sandstone and shale or by sandstones. The sandstones vary in grain size and texture and generally resemble greywacke; cross-bedding and ripple-mark were observed locally; the bases are generally sharp and often scour underlying beds and the tops are normally sharp. Sandstones occur as massive beds as much as 10 feet thick or interbeds (few inches

to 2 feet thick) with shale which is weakly graphitic and strongly cleaved. Locally near the upper part of the unit, red hematitic liesegang rings or bandings were observed in some sandstone and siltstone beds and these resemble red-bed rocks; it is possible that these features merely reflect the weathering of pyrite commonly observed in the unit.

Channel fill and scouring erosion are commonly observed in outcrops of conglomerate and interbedded sandstones and siltstones, and the whole unit probably represents a slump turbidite flow facies in a deltaic to near-shore environment with a low-lying source area for the detritus as indicated by the occurrence of hard chert pebbles which were derived from the underlying cherty siltstone. A few beds of highly contorted black shale containing scattered rounded boulders (up to 3 feet across) of underlying sandstone were found and are good evidence for the slump hypothesis.

The thickness of the rock unit has not been estimated but probably is several thousand feet thick in the region W of South Nahanni River (Blusson, 1967). The unit is correlative with unit 18 in the Nahanni map-area and an age of Devonian and Mississippian is assigned.

APPENDIX IV-1

ECLOGITES AND THEIR MINERALS, ANVIL RANGE DISTRICT

Eclogites occurring in late Proterozoic micaceous quartzite and as one insitu (?) boulder were collected by the writer in the Anvil district in 1973. Five whole rock analyses by XRF and eighteen analyses on garnet, omphacite, amphibole, muscovite and chlorite from these rocks by electron microprobe were made. Analyses of whole rock, garnet, omphacite and amphibole from a single specimen of eclogite were previously published (Tempelman-Kluit, 1970) and are used in the present study. Mineral analyses were made on an A.R.L. EMX electron microprobe analyser using an Energy Dispersive detector. The analyses quoted represent the averages of 10 to 20 spot analyses per sample.

Whole rock analyses of eclogite with normative compositions and some trace elements concentrations are given in Table IV-4. Electron probe analyses of garnet, omphacite, amphibole, muscovite and chlorite, together with the calculated structural formula and end-member proportions are presented in Tables IV-5a, b, c, d, and e, respectively.

1. Introduction

Eclogites are actually a class of high pressure metamorphic rocks forming over a wide temperature range starting perhaps as low as 300°C (in the glaucophane-lawsonite schist facies) and ranging up to the temperatures of migmatite or those of the upper mantle. Literature on eclogites is enormous and it is not the purpose of this section to make a review; equally vast are the proposed origins for eclogitic rocks. The popular view is that eclogites form from a combination of the following processes:

TABLE IV-4

Chemical and Normative* Compositions of Eclogites, Anvil Range District.

	TK-1**	K31-1A	HHA13-1	KWA13-5	A13-7	A13-12
SiO ₂	51.82	49.30	49.30	50.36	47.32	48.51
Al ₂ O ₃	11.88	13.80	15.15	14.31	12.82	13.80
Fe ₂ O ₃	1.90	2.74	2.50	2.48	3.28	2.53
FeO	7.69	8.37	7.65	7.58	10.01	7.71
CaO	7.89	8.74	9.20	9.48	9.45	9.41
MgO	11.58	13.88	12.48	12.19	13.74	14.28
Na ₂ O	2.00	1.83	2.23	2.39	1.62	2.33
K ₂ O	0.60	0.51	0.53	0.34	0.08	0.51
TiO ₂	0.82	0.50	0.66	0.55	1.24	0.60
P ₂ O ₅	-	0.12	0.17	0.16	0.27	0.15
MnO	0.24	0.19	0.15	0.14	0.18	0.16
CO ₂	-	-	-	-	-	-
H ₂ O	3.59	-	-	-	-	-
S	-	0.01	-	-	-	-

* Normative compositions - first column: CIPW norms, second column in parenthesis: molecular norms (Niggli and Barth).

** Tempelman-Kluit (1970).

TABLE IV-4 (cont'd)

	TK-1**	K31-1A		HHA13-1		KWA13-5		A13-7		A13-12	
Q	2.28 (2.09)	0	(0)	0	(0)	0	(0)	0	(0)	0	(0)
Or	3.68 (3.65)	3.02	(2.97)	3.13	(3.09)	2.01	(1.98)	0.47	(0.47)	3.02	(2.95)
Ab	17.55 (18.49)	15.50	(16.20)	18.87	(19.71)	20.23	(21.16)	13.71	(14.48)	19.72	(20.46)
An	22.47 (22.31)	27.96	(27.56)	29.77	(29.31)	27.33	(26.94)	27.49	(27.36)	25.70	(25.14)
Di	14.59 (14.40)	17.42	(11.55)	11.88	(11.63)	15.04	(14.73)	14.25	(14.06)	16.06	(15.66)
Hy	34.96 (35.83)	22.54	(22.88)	16.56	(16.13)	19.49	(19.83)	22.69	(23.19)	6.95	(7.07)
Ol	0 (0)	15.02	(15.84)	15.02	(15.92)	11.50	(12.16)	14.43	(15.30)	24.01	(25.45)
Mt	2.86 (2.05)	2.90	(2.06)	3.13	(2.22)	2.97	(2.11)	3.97	(2.85)	3.05	(2.15)
Il	1.61 (1.18)	0.95	(0.69)	1.25	(0.91)	1.05	(0.76)	2.36	(1.72)	1.14	(0.82)
Ap	0 (0)	0.28	(0.25)	0.39	(0.35)	0.37	(0.33)	0.63	(0.56)	0.35	(0.31)
Po	0 (0)	0.03	(0.03)	0	(0)	0	(0)	0	(0)	0	(0)

TABLE IV-5a
Electron Microprobe Analyses of Garnets

	A13-4	HHA-13	31-1A	A13-6
SiO ₂	37.47	37.74	37.36	37.75
Al ₂ O ₃	21.59	21.85	21.47	21.71
TiO ₂	-	-	0.06	0.10
FeO	27.97	27.20	28.55	27.33
MnO	0.65	0.36	1.15	0.43
MgO	4.55	5.38	3.42	4.72
CaO	<u>7.71</u>	<u>7.43</u>	<u>7.93</u>	<u>7.90</u>
	100.21	99.96	99.94	99.94

Structural Formula on the Basis of 12 Oxygens

Si	2.97	2.957	2.965	2.965
Al	2.015	2.018	2.009	2.010
Ti	-	-	0.003	0.006
Fe	1.853	1.782	1.895	1.796
Mn	0.044	0.024	0.077	0.029
Mg	0.537	0.628	0.404	0.553
Ca	0.606	0.624	0.674	0.665

End-member Proportions Calculated for all
Iron in Ferrous State

Almandine	60.95	58.27	62.13	59.02
Spessartite	1.45	0.79	2.52	0.953
Pyrope	17.66	20.54	13.25	18.17
Grossular	19.93	20.41	22.10	21.85

TABLE IV-5b

Electron Microprobe Analyses of Omphacites

	A13-4	HHa-13	31-1A	A13-6
SiO ₂	56.12	56.35	57.73	56.15
Al ₂ O ₃	10.31	10.38	10.28	10.59
TiO ₂	0.07	-	-	0.15
Fe ₂ O ₃	0.43	0.04	0	0.34
FeO	3.30	4.05	2.78	3.18
MgO	9.16	9.11	9.07	9.08
CaO	14.08	13.63	13.94	13.97
Na ₂ O	6.28	6.27	5.85	6.24
K ₂ O	<u>0.05</u>	<u>-</u>	<u>0.05</u>	<u>0.05</u>
	99.80	99.83	99.70	99.75

Structural Formula on the Basis of 6 Oxygens
and Cations Normalized to 4

Si	1.998	$\left. \begin{array}{l} 0.002 \\ 0.431 \end{array} \right\} 2.0$	2.0	2.0	1.996	$\left. \begin{array}{l} 0.004 \\ 0.440 \end{array} \right\} 2.0$
Al	0.433		0.435	0.427	0.444	
Ti	0.002		-	-	0.004	
Fe ⁺³	0.011		0.001	0	0.009	
Fe ⁺²	0.098		0.124	0.082	0.102	
Mg	0.486		0.483	0.477	0.481	
Ca	0.537		0.519	0.527	0.532	
Na	0.434		0.432	0.400	0.430	
K	0.002		-	0.002	0.002	

TABLE IV-5b (cont'd)

End-member Proportions Calculated After Method of
Banno (1959) and Essene and Fyfe (1967)

	(1)	(2)	(1)	(2)	(1)	(2)	(1)	(2)
Cats	-	0.2	-	0	-	0	-	0.4
Jadeite	42.64	43.1	45.12	43.5	47.3	42.7	46.8	44.0
Acmite	3.66	1.1	2.88	0.1	0	0	3.48	0.9
Diopside + Hedenbergite	53.7	55.6	52.0	56.4	52.7	57.3	53.2	54.7
Jd/Cats	-	215.5	-	∞	-	∞	-	110.0

(1) Banno (1959): $0.757 \times \text{Fe}^{+++} + 0.028 = \text{Ac}\%$

(2) Essene and Fyfe (1967): $\text{Jadeite \%} = \text{Al}^{\text{VI}} - \text{Al}^{\text{IV}}$
 $\text{Acmite \%} = \text{Fe}^{+++}$

TABLE IV-5c

Electron Microprobe Analyses of Amphiboles

	A13-4	HHA-13	31-1A	A13-6
SiO ₂	54.57	54.61	54.93	54.53
Al ₂ O ₃	8.01	8.22	5.30	7.68
TiO ₂	0.09	0.12	-	0.14
FeO	5.17	4.73	7.71	4.81
MgO	17.76	17.68	17.49	18.41
Na ₂ O	3.04	3.07	1.75	2.53
K ₂ O	0.22	0.18	0.12	0.22
CaO	9.01	9.19	10.29	9.45
V ₂ O ₅	0.11	0.09	0.15	0.07
Cr ₂ O ₅	0.07	0.06	0.10	0.12
NiO	-	-	0.08	-
BaO	-	-	0.08	-
H ₂ O*	<u>2.00</u>	<u>2.00</u>	<u>2.00</u>	<u>2.00</u>
	100.05	100.03	100.05	100.05

* Assumed content, based on data in literature.

TABLE IV-5c (cont'd)

Structural Formula on the Basis of 23 Oxygens**

Si	7.22	8	7.21	8	7.36	8	7.21	8
Al	1.25	{ 0.78 }	1.28	{ 0.79 }	0.84	{ 0.64 }	1.20	{ 0.79 }
Ti	0.01	{ 0.47 }	0.01	{ 0.49 }	-	{ 0.20 }	0.01	{ 0.41 }
Fe	0.57		0.52		0.86		0.53	
Mg	3.50		3.48		3.49		3.63	
Ni	-		4.57		4.53		0.01	4.61
Cr	0.01		0.01		0.01		0.01	
V	0.01		0.01		0.01		0.01	
Mn	-		-		0.01		-	
Ba	-		-		0.00		-	
Na	0.78		0.79		0.46		0.65	
K	0.04		0.03		0.02		0.04	
Ca	1.28		1.30		1.48		1.34	
OH	1.76		1.76		1.79		1.76	
F, Cl*	0.13		0.13		0.12		0.13	

$$(K, Ca, Na) 2.05^{(Ti, Fe, Mg, Al)} 4.58^{(Al)} 0.75^{Si} 7.25^{O} 22^{(F, Cl, OH)} 1.89$$

* F+Cl = 0; (OH) = OH+F+Cl

**Miyashiro (1957), Borg (1967).

TABLE IV-5d

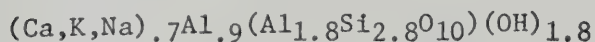
Electron Microprobe Analyses
of White Micas

	HHA-13	A13-6
SiO ₂	46.76	47.76
Al ₂ O ₃	39.62	38.64
TiO ₂	0.07	0.10
FeO	0.30	1.41
MgO	-	1.40
CaO	0.45	0.31
Na ₂ O	4.96	3.98
K ₂ O	3.15	1.66
Cr ₂ O ₃	0.06	0.09
F*	0.10	0.10
H ₂ O*	<u>4.50</u>	<u>4.50</u>
	99.94	99.95

Structural Formula Calculated
on the Basis of 11 Oxygens

Si	2.761	2.801
Al	2.758	2.670
Ti	.003	.004
Fe	.015	.069
Mg	-	.122
Cr	.003	.004
Ca	.029	.019
Na	.568	.452
K	.237	.124
OH	1.77	1.76

Margarite	3.48%	2.42%
Paragonite	68.10%	57.50%
Phengite	28.42%	40.08%



*Assumed content, based on data in literature.

TABLE IV-5e

Electron Microprobe Analyses of Chlorites (Retrogressed from Garnet)

	Al3-4	HHA-13	31-1A	Al3-6
SiO ₂	26.67	26.64	27.31	26.73
Al ₂ O ₃	20.20	20.41	20.18	20.05
FeO	22.90	22.28	19.46	22.28
MgO	17.84	18.32	20.50	18.53
CaO	0.11	0.09	0.12	0.10
MnO	0.18	0.19	0.26	0.21
NiO	0.09	0.06	0.08	0.10
Cr ₂ O ₃	-	-	0.08	-
F*	0.10	0.10	0.10	0.10
H ₂ O*	<u>12.00</u>	<u>12.00</u>	<u>12.00</u>	<u>12.00</u>
	100.09	100.09	100.09	100.10

* Assumed content, based on data in literature.

TABLE IV-5e (cont'd)

Structural Formula Calculated on the Basis of 18 Oxygens

Si	2.74	$\left. \begin{array}{c} \{ \\ 1.26 \\ \} \end{array} \right\} 4$	2.73	$\left. \begin{array}{c} \{ \\ 1.27 \\ \} \end{array} \right\} 4$	2.77	$\left. \begin{array}{c} \{ \\ 1.23 \\ \} \end{array} \right\} 4$	2.74	$\left. \begin{array}{c} \{ \\ 1.26 \\ \} \end{array} \right\} 4$
Al	2.45	$\left. \begin{array}{c} \{ \\ 1.19 \\ \} \end{array} \right\}$	2.47	$\left. \begin{array}{c} \{ \\ 1.20 \\ \} \end{array} \right\}$	2.41	$\left. \begin{array}{c} \{ \\ 1.18 \\ \} \end{array} \right\}$	2.42	$\left. \begin{array}{c} \{ \\ 1.16 \\ \} \end{array} \right\}$
Fe	1.97	} 5.94						
Mg	2.73							
Ca	0.01							
Mn	0.02							
Ni	0.01							
Cr	-							
OH	8.23		8.20		8.11		-	8.21

$$(\text{Mg, Fe, Al, Mn, Ca, Ni, Cr})_{5.95} (\text{Si, Al})_4 \text{O}_{10} (\text{F, OH})_{8.19}$$

(a) high lithostatic pressure, low water pressure ("dry") metamorphism of basaltic rocks via solid-state reaction.

(b) concurrent higher water pressure ("wet" or hydrous) metamorphism of the enclosing rocks gives rise to glaucophane schist or the high pressure parts of the greenschist, amphibolite or granulite facies.

(c) small slices or "tectonic inclusions" incorporated in basic to ultrabasic rocks (lower continental crust) such as basanites, peridotites or kimberlite during tectonic deformation ("eclogite facies" sensu stricto).

Therefore, as pointed out by Brown and Fyfe (1972), if "dry" basaltic material is buried along with "wet" basaltic material, during prograde metamorphism, one would expect at deep levels to find:

glaucophane schist + the eclogite assemblage →

greenschist + less eclogite →

amphibolite + even less eclogite.

The amount of eclogite would diminish as the wet component releases water, i.e. eclogite becomes unstable relative to other facies if water becomes a significant component and lithostatic pressure approaches water pressure (Fry and Fyfe, 1969).

On the basis of mode of occurrence, eclogites are conveniently divided into different groups (Banno, 1966, 1970; Coleman et al., 1965). According to the nomenclature proposed by Coleman et al., the division of eclogites is as follows:

(a) Group A Eclogites. Inclusions in kimberlites, basalts or layers in ultrabasic rocks; often contain diamond, orthopyroxene, or olivine and appear to have a deep-seated igneous or metamorphic origin.

(b) Group B Eclogites. Bands or lenses within migmatitic gneissic terrains. These are surrounded by amphibolite and show retrograde

metamorphism (including granulite facies eclogite or garnet-clinopyroxene granulite).

(c) Group C Eclogites. Bands or lenses within the metamorphic rocks of the alpine-type orogenic zones, locally forming isolated blocks when associated with glaucophane schists.

2. Whole Rocks

Petrography of the Anvil eclogites (see Chapter III) indicates that they are amphibole eclogites in the broad sense since they contain the primary minerals garnet, omphacite, amphibole and accessory minerals rutile, sphene (?), clinozoisite, chlorite, muscovite, quartz, apatite, plagioclase (albite), saponite, and opaque minerals (pyrite, chalcopyrite).

Chemical analyses of the eclogites reveal that they are tholeiitic basalts (Fig. IV-10a) and their compositions overlap Group A and Group B eclogites but are different from Group C eclogites on an A-F-M diagram (Fig. IV-10b). For comparison within the Canadian Cordillera, two glaucophane-rich eclogite samples from the Pinchi Lake Mercury Mine area near Fort St. James, B.C. were analyzed by the writer and plotted in Fig. IV-10a and b.

The Pinchi eclogites clearly belong to Group C and are distinctly different from the Anvil eclogites. Normative compositions of the Anvil eclogites again indicate their tholeiitic character and distinction from most of the Group C eclogites which are generally nepheline normative (Fig. IV-10c). One analysis by Tempelman-Kluit (1970) is slightly quartz-normative. Since serpentized peridotite at Vangorda Fault occurs very close to the eclogite outcrop, it is tempting to relate the formation of the eclogites to crystallization in an environment in-

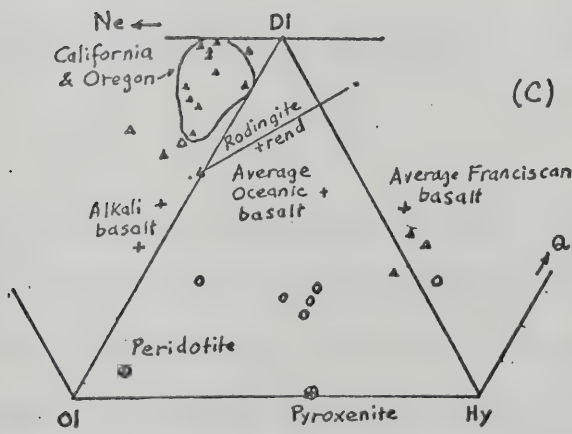
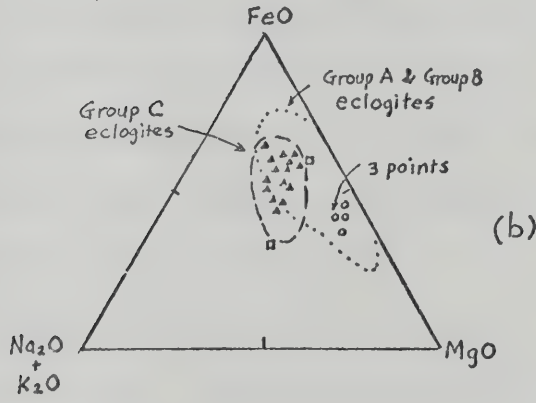
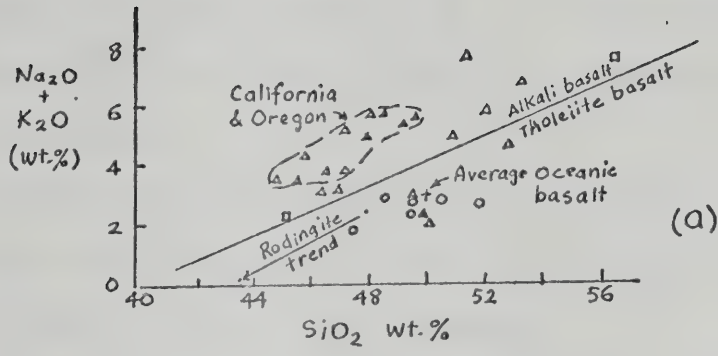


Fig. IV-10. Comparison of Anvil eclogites with other rocks.

- o: Anvil eclogites
- Δ : Eclogites from glaucophane schist terranes
- \square : Pinchi Lake eclogites

fluenced by the ultrabasic rocks. Serpentinization has been shown to be related to metasomatic production of rodingite (Coleman, 1967) which is depleted in SiO_2 and enriched in Ca. It seems unlikely, however, that eclogitization is related in anyway to serpentinization of ultrabasic rocks because:

1. chemical trends of rodingite indicated in Fig. IV-10a and c do not show any plausible process by which a peridotite or pyroxenite from the same district can give rise to eclogite.

2. water vapour pressure of serpentinization at approximate temperature range of eclogitization ($400\text{--}500^\circ\text{C}$) is too high to stabilize eclogite relative to other facies (Ghent and Coleman, 1973).

Comparison of average composition of eclogites and Cambro-Ordovician greenstones indicate that eclogites have higher MgO , TiO_2 , SiO_2 , and lower Al_2O_3 , in the rest they are similar. The eclogites therefore are apparently different in bulk composition from the basic volcanic rocks of lower Paleozoic age. Foliated amphibolite occurs in the lower Cambrian unit just above the "grit unit" in which eclogites occur; however, there is no data on amphibolite to make any comparison.

3. Minerals

The end-member molecular proportions or certain cation proportions of primary minerals garnet, omphacite and amphibole have been used by Coleman et al. (1965), Banno (1965, 1970), Mori and Banno (1973), Essene and Fyfe (1967), Ghent and Coleman (1973), Dallmeyer (1974) and many others to characterize or distinguish different groups of eclogites of the world. Likewise, white mica and chlorite structural formula and molecular proportions can be used in elucidating retrogressive conditions in certain cases.

Analyses of garnet (Table IV-5a) show compositional overlap with those from eclogites in glaucophane schist, amphibolite and granulite rocks (Fig. IV-11a, b). The garnet is distinctly zoned, with Ca and Mn enrichment in cores and Fe and Mg enrichment in the rims of grains. Similar zoning patterns have been observed in garnet from metamorphic rocks as well as eclogite (Hollister, 1966; Dudley, 1969; Ghent and Coleman, 1973).

Microprobe analyses of omphacite were recalculated to estimate ferrous-ferric ratio (after the method outlined by Ghent and Coleman, 1973) and the end-member molecules computed following the procedures given by Essene and Fyfe (1967) and Banno (1959) (Table IV-5b). The end-member proportions calculated by these two procedures show some differences. For reason of consistency with the literature, the former results are preferred. Clark and Papike (1968) report that an omphacite having a P2 space-group symmetry and a restricted compositional range of (jadeite + aegirine)/total pyroxene molecules of about 0.5. This lower symmetry is interpreted to be the result of cation ordering, whereas other omphacite of C2/c space-group symmetry is interpreted to be disordered. Ordered omphacite occurs in Group C eclogite, and disordered omphacite occurs in eclogite inferred to be of higher temperature origin (Ghent and Coleman, 1973). The (jadeite + aegirine)/total pyroxene molecular ratios of omphacite from Anvil eclogite are about 0.43-0.44 (Essene and Fyfe's procedure) or about 0.46-0.53 (Banno's procedure), suggesting an omphacite approaching an ordered variety. Therefore, Group C eclogites are generally enriched in jadeite and aegirine, whereas Group A and Group B eclogites are enriched in diopside, hedenbergite and Ca-Tschermak's molecule (Cats). Molecular proportions of omphacite from Anvil eclogite show a transitional nature between different groups,

Figure IV-11

Composition diagrams of garnets, omphacites and amphiboles from
Anvil eclogites

- (a) Ca-Mg-Fe compositions of garnets from Anvil eclogites.



Blueschist metamorphic terrane



Amphibolite facies terrane

(after Banno, 1967)

- (b) Garnet end-members grossular + andradite (Gr + Ad), pyrope (pyr), and almandine + spessartine (Alm + Spess).



Blueschist terrane

1: in amphibolite; 2: in charnockite and granulite; 3: Group B eclogite; 4: in dunite and peridotite; 5: in kimberlite pipes.
(after Coleman et al., 1965).

- (c) Omphacite end-members diopside + hedenbergite (Di + He), jadeite (Jd) and aegirine (Ae).

o: Group A eclogites

Δ: Group B eclogites



Group C eclogites

(after Coleman et al., 1965)

- (d) Distribution of amphiboles in the composition range: tremolite-ferrotremolite-edenite-ferroedenite.

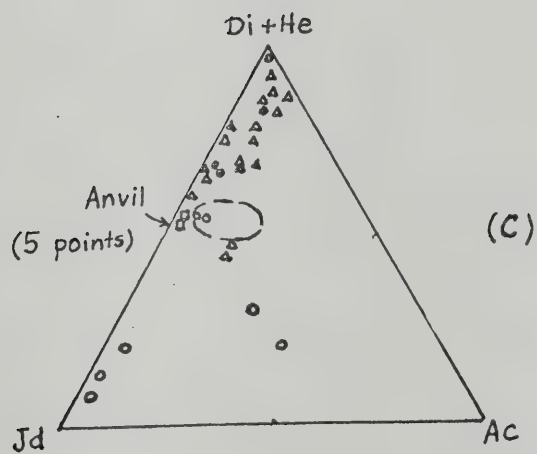
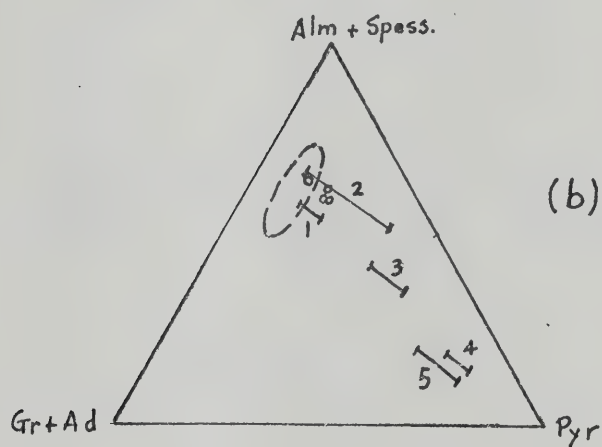
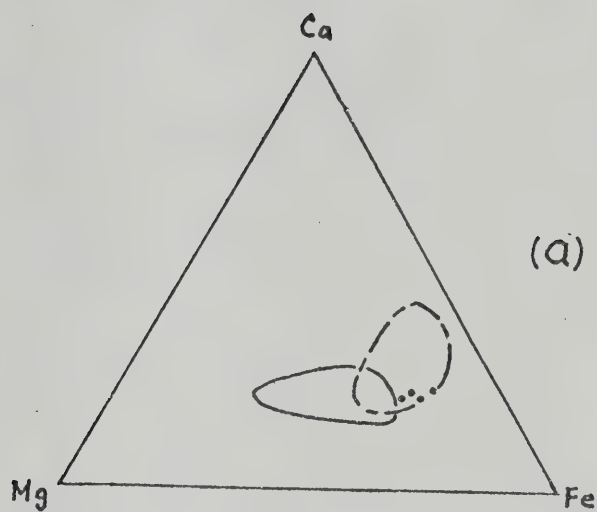


Figure IV-11.

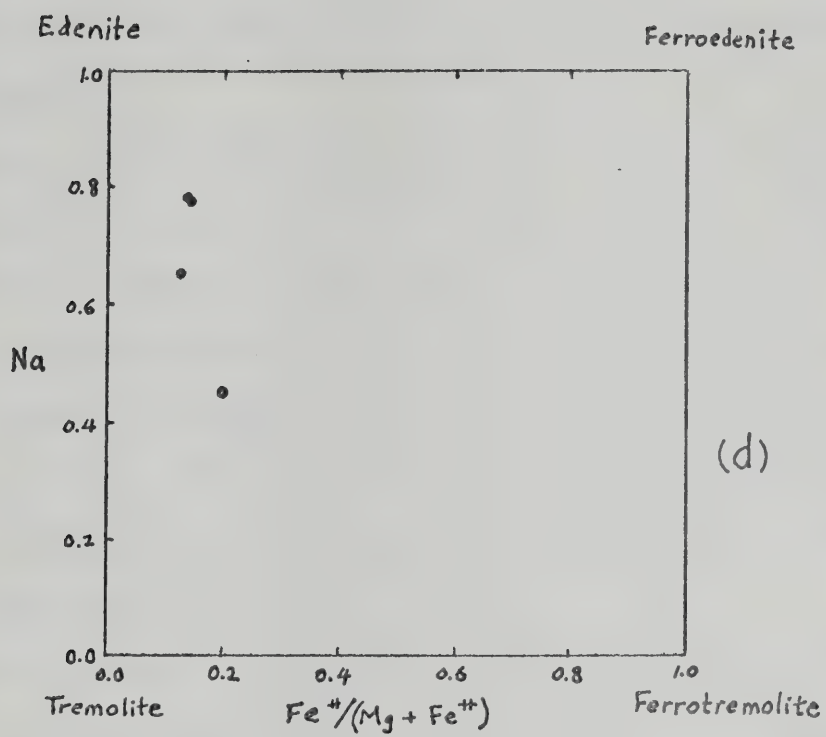


Figure IV-11.

or alternatively, lie close to the composition of Group C omphacite (Fig. IV-11c).

Analyses of green amphibole (Table IV-5c) reveal a composition of calcic amphibole with molecular end-members of edenite, tremolite and some ferrous components like ferro-edenite and ferro-tremolite (Fig. IV-11d). Calcic amphiboles are members of complicated solid solution series, and are most abundant in greenschist facies basic rocks or amphibolites (Ernst, 1968), although calcic amphiboles have also been described from glaucophane schists of Japan and California (Banno, 1964; Coleman and Lee, 1963; Ernst, 1965).

Chlorite rimming or retrogressed from garnet has a constant range of Si, Al, Ca, Mn concentration and a higher Mg/Fe ratio than that of chlorite in eclogites from blueschist terrain. A notable feature of the Anvil chlorite is the high Mg and Ni contents (Table IV-5d).

Analyses of white mica from 2 samples (Table IV-5e) indicate that the mica is mainly paragonite with solid solutions of muscovite or phengite and minor margarite. The maximum solid solution of paragonite in mica from eclogites in blueschist terrain is 8 mole % (Ghent and Coleman, 1973), whereas the Anvil eclogite mica contains more than 50 mole % paragonite. Coexistence of paragonite and muscovite in pelitic schists (Zen and Albee, 1964) and paragonite and margarite in amphibolites (Ackermann and Morteani, 1973) have been reported. Pressure-temperature stability limits of paragonite, margarite, paragonite + quartz have been studied and appear to be stable under intermediate temperatures ($>650^{\circ}\text{C}$) and intermediate-high pressures ($<8\text{ Kb}$) conditions (Chatterjee, 1970, 1971, 1972).

Geometric comparison of tie lines of garnet and omphacite from different groups of eclogites in a CaO-FeO+MnO-MgO diagram is presented

in Fig. IV-12. Temperature-pressure variations and geological occurrences of Groups A, B, and C can be differentiated in this diagram. Tie lines for garnet and omphacite pairs from Anvil eclogite are also shown. Continuous (parallel to subparallel) sweep across the diagram has been taken to indicate that eclogites of varying bulk composition formed under similar temperature-pressure conditions (Yoder and Tilley, 1962). Conversely, crossing of tie lines must indicate that the T-P conditions were different for the eclogites under consideration. Tie lines of Anvil garnet and omphacite can be seen to cross those of Group C eclogite whereas they are parallel to those of Group B, forming a more or less continuous sweep. Thus Anvil eclogites show an affinity to Group B eclogites insofar as the partition of Fe(Mn)-Mg-Ca between coexisting garnet and pyroxene is concerned.

Subparallelism within the separate eclogite groups and nonparallelism from group to group is probably significant; but the partition of Ca, Fe+Mn, Mg between garnet-pyroxene pairs is evidently not quite similar within the eclogite facies, strongly suggesting that eclogites must form under a wide range of temperature-pressure conditions.

4. Metamorphic Conditions

Estimation of lithostatic pressure, temperature and fluid pressure conditions of eclogite formation in natural rocks has been attempted by various authors (Banno, 1970; Mori and Banno, 1973; Ghent and Coleman, 1973; Taylor and Coleman, 1968; Vogel and Garlick, 1970). Procedures adopted for estimation include consideration of subsolidus equilibrium (e.g. compositional range of solid solutions, and element partition among coexisting minerals), phase equilibria of hydrous and anhydrous minerals, and oxygen isotope fractionation among coexisting minerals.

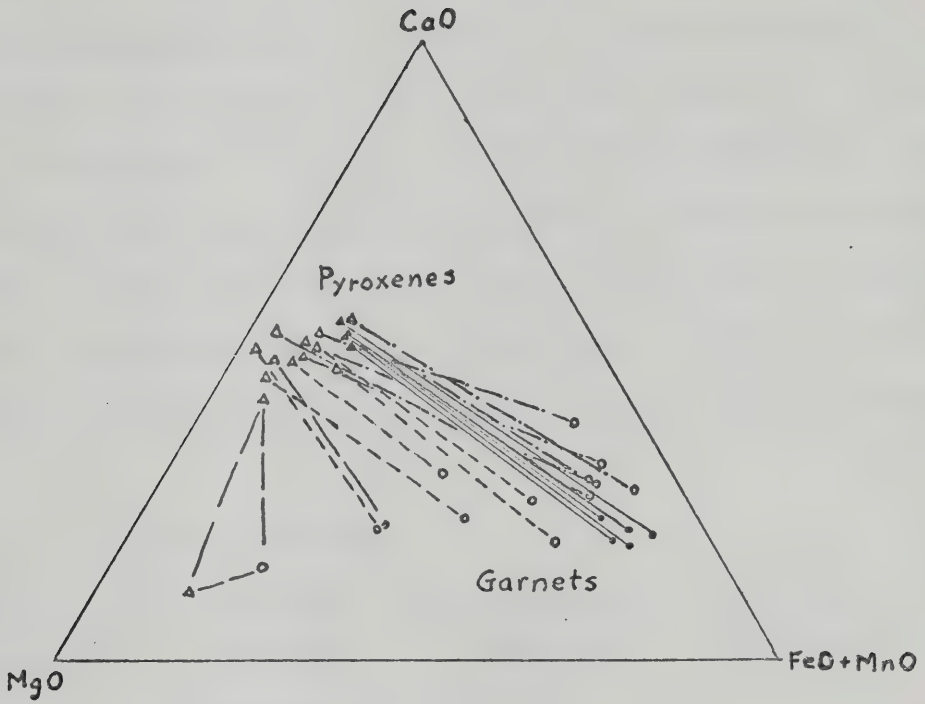
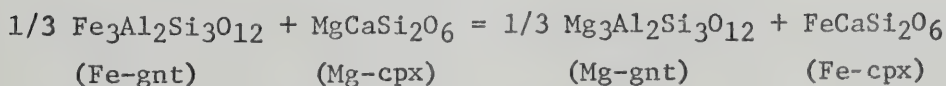


Figure IV-12. CFM plots of coexisting garnet-pyroxene pairs from eclogites. Tie lines connect these pairs. Long dashed line: Group A eclogites; short dashed line: Group B eclogites; dash-dotted line: Group C eclogites; solid line: Anvil eclogites (diagram after Coleman et al., 1965).

The latter can be a useful geothermometer if a quartz-rutile pair is available; whereas measurements on omphacite, garnet and rutile do not provide good geothermometers (Ghent and Coleman, 1973).

(a) Formation Temperature. Fe^{+2} and Mg^{+2} partition between co-existing primary minerals garnet and clinopyroxene omphacite or between ortho- and clinopyroxene pairs as a function of temperatures has been studied by Banno and Matsui (1965), Banno (1970), Mori and Banno (1973), Saxena (1971), Saxena and Ghose (1971), Kretz (1961, 1963). In this study, atomic proportion of Fe in garnet has been assumed to be Fe^{+2} since most of the iron in the eclogite (Table IV-4) is in the ferrous state.

For the ion exchange reaction:



the distribution coefficient K_D is defined as:

$$K_D = \frac{\left(\frac{X_{\text{Fe}}}{X_{\text{Mg}}}\right)_{\text{gnt}}}{\left(\frac{X_{\text{Fe}}}{X_{\text{Mg}}}\right)_{\text{cpx}}}$$

where X_{Fe} and X_{Mg} are mole fractions of Fe^{+2} and Mg^{+2} , respectively.

Logarithms of K_D for all eclogites are approximately linear against the reciprocal of absolute temperatures (Fig. IV-13a), that is, highest temperature eclogite has the smallest K_D values. Inspection of Fig. IV-13a reveals that Anvil eclogites represent the lowest temperature among the data quoted. It is also clear from the figure that eclogitic rocks from Hawaii ($K_D = 1.6$) represent one of the highest temperature varieties, and those from Norway ($K_D = 4.5$) and Shikoku ($K_D = 7.88$) intermediate temperature range varieties. Since formation temperatures of these rocks have also been established (Beason and Jackson, 1970; Mori and Banno, 1973), the formation temperature of Anvil eclogites can be calculated from the following equation (Mori and Banno, 1973):

Figure IV-13

Comparison of Fe^{2+}/Mg ratios in garnets and pyroxenes in
eclogites and temperature estimates

(a) Fe^{2+}/Mg ratios of garnet and pyroxene.

o: Anvil eclogites

I: eclogites in glaucophane schist

II: eclogites in amphibolite-granulite

III: eclogites in kimberlite

IV: Hawaiian-type eclogites

(b) Temperatures of eclogites from Shikoku and Anvil Range, Yukon.

(c) Temperatures of eclogites from Norway and Anvil Range, Yukon.

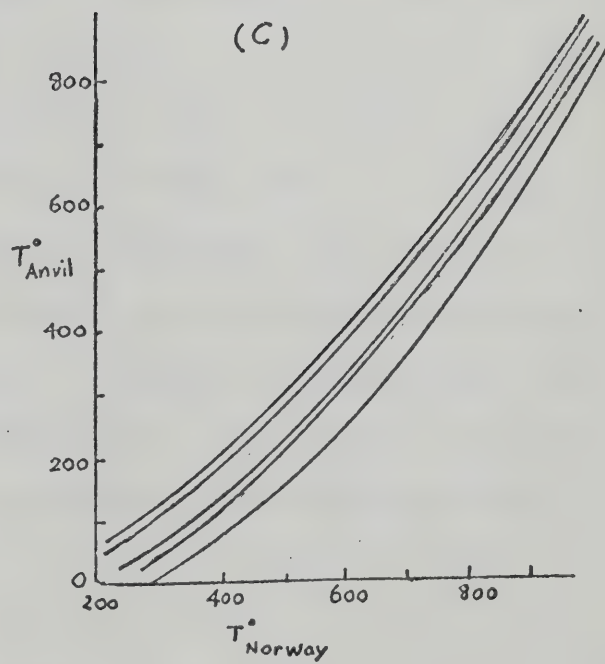
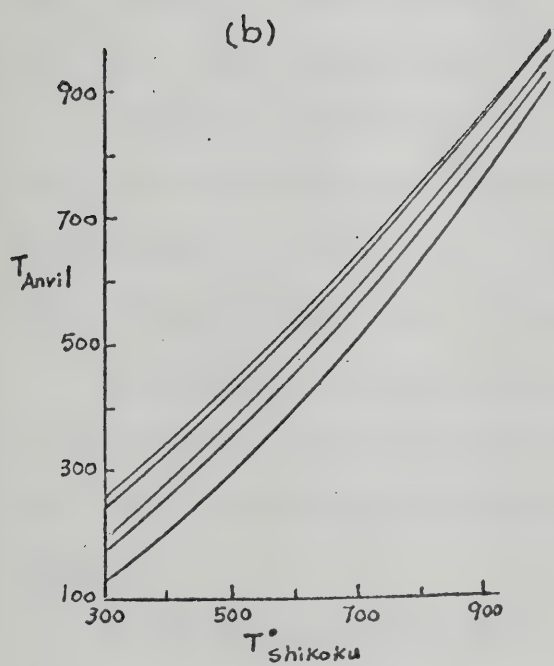
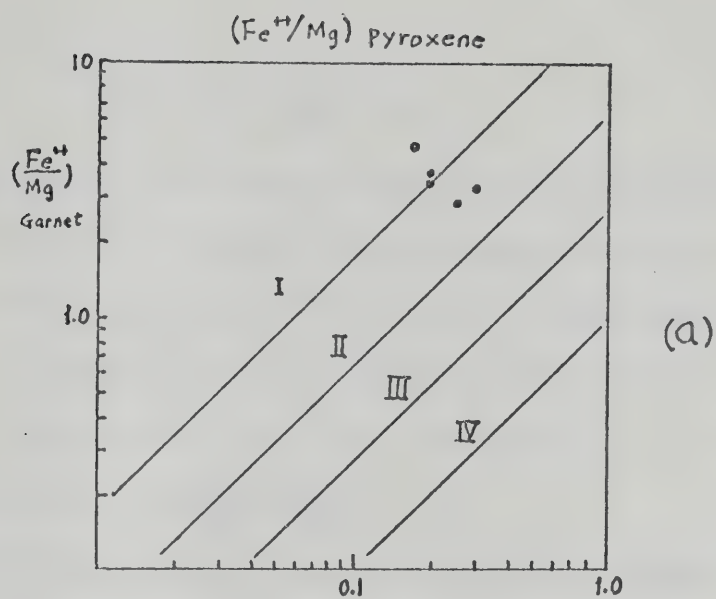


Figure IV-13.

$$\ln\left(\frac{K_1}{K_0}\right)/\ln\left(\frac{K_2}{K_0}\right) = \left(\frac{1}{T_1} - \frac{1}{T_0}\right)/\left(\frac{1}{T_2} - \frac{1}{T_0}\right)$$

or

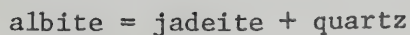
$$\frac{1}{T_2} = \alpha\left(\frac{1}{T_1} - \frac{1}{T_0}\right) + \frac{1}{T_0}$$

where $K_0 = K_D$ of highest temperature eclogite (e.g. Hawaii); $K_1 = K_D$ of intermediate temperature eclogite (e.g., Norway or Shikoku); $K_2 = K_D$ of eclogite in the question; $T_0 = T$ of highest temperature eclogite (e.g. Hawaii, $T = 1150^\circ\text{C}$); $T_1 = T$ of intermediate temperature eclogite (e.g. Norway, $T = 650\text{--}700^\circ\text{C}$; Shikoku, $T = 550\text{--}600^\circ\text{C}$); $T_2 = T$ of eclogite in question; and $\alpha = \ln\left(\frac{K_2}{K_0}\right)/\ln\left(\frac{K_1}{K_0}\right)$.

A T_1 vs. T_2 diagram can be constructed for a given temperature range, e.g. 300 to 1000°C . From the known temperatures of Norway and Shikoku eclogitic rocks, the formation temperatures of Anvil eclogites are estimated to have an average range of 380 to 480°C (see Figs. IV-13b and c) with a full range of 300° to 550°C .

(b) Formation Lithostatic Pressure. Estimation of formation pressures of eclogites has been made by Mori and Banno (1973) by the use of Al_2O_3 content of orthopyroxene coexisting with garnet. There are no other independent estimates of formation pressure for high-grade eclogites.

The presence of quartz and albite in the Anvil eclogites allows one to consider the stability relation of omphacite in equilibrium with albite and quartz and estimate equilibrium pressure of the following two reactions:



Essene and Fyfe (1967) have constructed a diagram depicting pressure- X_{Jd} (jadeite mole fraction in omphacite) relationship using an ideal solid

solution model assuming that omphacite can be described in terms of the components jadeite, acmite, and diopside-hedenbergite with mixing of cations on two sites (X and Y in $X Y Z_2O_6$ where $X = Na, Ca$; $Y = Fe^{+3}, Al, Mg, Fe^{+2}$; $Z = Si$). Mole fraction of jadeite in omphacite from Anvil eclogites (Table IV-5b) and a temperature range of 380° - $480^{\circ}C$ correspond to a pressure range of about 8 to 10 Kb on a pressure- X_{Jd} diagram (Fig. IV-14) using the diopside-jadeite curve (diopside and jadeite are the two predominant components in omphacite).

(c) Fluid Pressure. Fluid pressure in metamorphic conditions can be approximated by water fugacity (f_{H_2O}) since composition of metamorphic fluid indicates that water is by far the most significant component whereas CO_2 , CH_4 , $NaCl-KCl$ are either minor or unlikely.

The range of water fugacities can be estimated from phase equilibria of hydrous minerals (amphibole, chlorite, clinozoisite, mica) in equilibrium with primary minerals garnet and omphacite at given temperatures and pressures. At maximum pressure and temperature conditions during eclogite crystallization, epidote-rutile was stable and its phase relation constituted the maximum limit of water fugacity; minimum water fugacity at which hydrous minerals remain stable or crystallize in equilibrium with primary minerals can be estimated from the retrogressive reaction of chlorite from garnet.

A series of reactions involving hydrous and anhydrous minerals and their calculated water fugacity estimates for given temperatures and pressures are listed in Table IV-6. Inspection of the table indicates that the hydrous minerals (chlorite, tremolite, epidote, mica) are stable at values of X_{H_2O} (ratio of water fugacities for reaction and for pure water at given temperatures and pressures) = 0.14 or less (minimum limit of X_{H_2O}) over a full range of 300 - $550^{\circ}C$ and 8-10 Kb (refer to

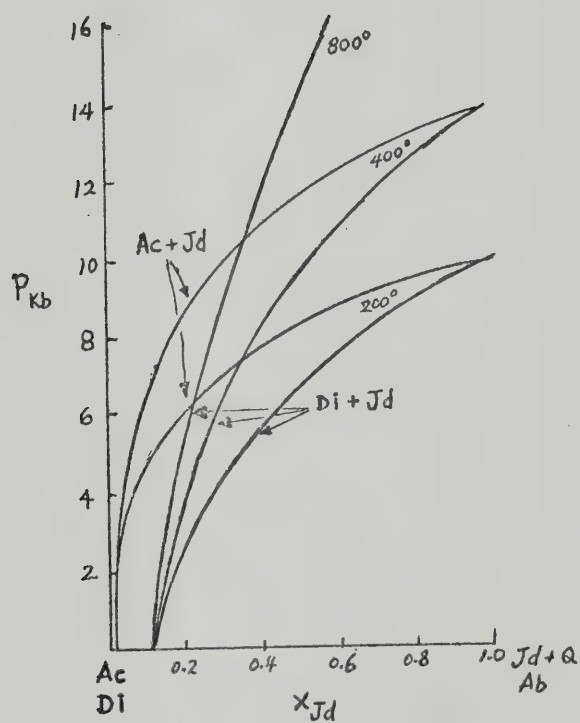


Figure IV-14. Pressure - X_{Jd} diagram for Di-Ac-Jd pyroxenes (after Essene and Fyfe, 1967).

TABLE IV-6

Estimation of Minimum and Maximum X_{H_2O} in Fluid Based on
Calculations from Experimental Phase Equilibria

Reaction	(Kb)	Temperature (°C)					
	Pressure	300	350	400	450	500	550
1	7	≥.002	≥.012	≥.027	≥.051	≥.088	≥.150
	8	"	"	≥.026	≥.049	≥.084	≥.140
	9	"	"	≥.025	≥.046	≥.080	≥.130
	10	"	"	≥.024	≥.044	≥.076	≥.120
2	7	≥.0002	≥.0005	≥.001	≥.0022	≥.0050	≥.0120
	8	"	"	"	≥.0023	≥.0053	≥.0127
	9	"	"	"	≥.0024	≥.0056	≥.0133
	10	"	"	"	≥.0025	≥.0060	≥.0140
3	7	"	"	≥.0010	≥.0032	≥.013	≥.044
	8	"	"	≥.0008	≥.0023	≥.009	≥.031
	9	"	"	≥.0007	≥.0015	≥.005	≥.017
	10	"	"	≥.0005	≥.0006	≥.001	≥.004
4	7	≥.0020	≥.0140	≥.031	≥.059	≥.100	≥.170
	8	≥.0013	≥.0110	≥.026	≥.050	≥.085	≥.143
	9	≥.0006	≥.0077	≥.020	≥.041	≥.069	≥.116
	10	0	≥.0045	≥.015	≥.032	≥.054	≥.089
5	7	≤.300	≤.557	≤.853	n.s.	n.s.	n.s.
	8	≤.205	≤.452	≤.748	n.s.	n.s.	n.s.
	9	≤.110	≤.346	≤.642	≤.960	n.s.	n.s.
	10	≤.015	≤.241	≤.537	≤.855	n.s.	n.s.
6	7	-	-	≤.0060	≤.040	≤.1260	≤.447
	8	-	-	≤.0053	≤.034	≤.1107	≤.393
	9	-	-	≤.0047	≤.028	≤.0950	≤.340
	10	-	-	≤.0040	≤.022	≤.0800	≤.286

Reaction (1): Mg-chlorite = Forsterite + 2 Enstatite + Spinel + 4H₂O

Reaction (2): Tremolite = 2 Diopside + 3 Enstatite + Quartz + H₂O

Reaction (3): 4 Zoisite + Quartz = 5 Anorthite + grossular + 2H₂O

Reaction (4): Muscovite + Quartz = K-feldspar + sillimanite + H₂O

Reaction (5): 3 Lawsonite + Sphene = 2 Zoisite + Rutile + Quartz + 5H₂O

Reaction (6): 2 Fe-chlorite + 4 Quartz = 3 Almandine + 18H₂O

n.s. = not stable.

reactions (1) to (4)). A full possible range of temperatures and pressures was investigated in order to detect the upper limit of a minimum X_{H_2O} for the Anvil eclogites.

Lawsonite is not stable at temperatures of 450°C and above for any reasonable water fugacity (Reaction 5, Table IV-6; also Ghent and Coleman, 1973); absence of lawsonite in Anvil eclogites suggests that X_{H_2O} is less than 0.6 if temperature is around 400°C and pressure 9Kb. On the other hand, the presence of garnet sets a maximum limit on X_{H_2O} for given temperatures and pressures. The garnet in Anvil eclogites is dominantly almandine, therefore for reaction 6, almandine is stable at X_{H_2O} of 0.3 or less at the peak of temperatures and pressures during eclogite crystallization. Spessartite and grossular might stabilize garnet at slightly higher X_{H_2O} limit (Nicolas, 1966) but spessartite only constitutes 2 mole % or less of the garnet solid solutions and the effect of pyrope is difficult to predict (Ghent and Coleman, 1973).

Omphacite is necessarily stable at the relatively low temperature range (300–550°C) in the presence of a H₂O-rich phase. Evidence for this stability was given by Essene and Fyfe (1967) and Wikstrom (1970).

From the above phase equilibria considerations, the most likely X_{H_2O} range over which most of the hydrous and primary minerals would be stable is in the order of $X_{H_2O} = 0.14-0.30$. It seems probable that during eclogite crystallization, no or a very low fluid phase (i.e. low water fugacity) was present. The hydrous-anhydrous solid phases in the assemblage may be due to buffering water fugacity at low value.

5. Discussion

The Anvil eclogites, as stated before, occur as small lenses interfoliated with muscovite quartzite of probable Hadrynian age. Occurrence

of paragonite, green amphibole, zoisite and plagioclase has been taken as the characteristic assemblage of eclogites in greenschist-amphibolite facies (Hyndman, 1972).

The close relation of eclogites to the Vangorda Fault has led Tempelman-Kluit (1970) to propose that local build-up of high vapour pressure near the fault existed long enough to allow transformation of some Permo-Triassic basalts to eclogites. He cited occurrence of blue amphibole rock near this fault at another locality as supporting evidence. However, as discussed before, eclogites are not stable relative to other facies if water becomes a significant component and lithostatic pressure approaches water pressure. Furthermore, eclogitization of basaltic rocks in contact with ultrabasic rocks is usually accompanied by loss of silica and alkali and enrichment in Ca (Coleman *et al.*, 1965; Ghent and Coleman, 1973). Neither Permo-Triassic basalts nor ultrabasic rocks (peridotite, pyroxenite) could have been transformed to eclogites by this process (see Fig. IV-10b).

It is proposed here that, in accordance with chemical data and field association, the Anvil eclogites must have been formed by a dry metamorphism of some "basaltic" rocks or amphibolites in the clastic sediments which were subjected to a precedent "wet" metamorphism during prograde metamorphism upon burial. This assemblage of greenschist + few eclogite is in agreement with the proposal of Brown and Fyfe (1972). Erratic and limited occurrence of eclogites in the muscovite quartzite suggests that the formation of eclogites is localized and perhaps resulted from "tectonic overpressure" during metamorphism (Coleman and Lee, 1962), for example, by tectonic overpressure related to ultrabasic intrusion but prior to serpentinization. Eclogite lenses in metamorphic terrains may have been introduced as crystalline mass by tectonic action (O'Hara and

Mercy, 1963). Overthrust or obduction of slices of oceanic crust onto the western edge of a continental margin geosyncline during Upper Paleozoic and Triassic may have facilitated the metamorphism of the eclogites.

APPENDIX V-1

EXPERIMENTAL CONDITION AND RELATED DETAILS OF ELECTRON MICROPROBE ANALYSES OF SULFIDES, CARBONATES AND SULFOSALTS

Polished sections were prepared from drill core to allow study with an electron microprobe as well as by conventional microscopy.

Chemical analyses of pyrrhotites, sphalerites, carbonates and sulfosalts were made using an Applied Research Laboratory EMX 1967 electron microprobe at the Department of Geology, University of Alberta. Analyses of pyrrhotites, sphalerites and carbonates using a Silicon-Lithium Energy Dispersive Detector were made at an accelerating voltage of 15 kV, a microbeam current of 300 nano-amperes and a specimen current of 25~30 nano-amperes. Analyses of Mn, Cd in sphalerites and Pb, Sb, Bi and Cu in sulfosalt minerals were made by Wavelength Dispersive Detectors at an accelerating voltage of 25 kV (except for Cu and Mn where 15 kV was used), and a microbeam current of 100 nano-amperes. The crystal Ammonium Dihydrogen Phosphate (ADP) was used for X-ray detection of Sb, Bi and Cd, and the crystal Lithium Fluoride (LiF) for the detection of Pb, Cu and Mn. Analytical sequence in Wavelength Dispersive Analysis was: upper-background readings for samples and standards, followed by peaks of standards and samples, then standard peaks were repeated after the sample peaks (in order to account for any instrumental drift over time), and finally the readings for lower-backgrounds for standards and samples. A total of 500 counts with 50 counts on each sample point was made on at least three grains of a mineral specimen.

Standards used in the analyses of the minerals are for pyrrhotites - native Fe, Ni and Co; for sphalerites - willemite, pyrite, native Cd and Mn; for carbonates - calcite, pyrite, native Mn and Mg; for sulfosalts - galena, native Sb, Cu and Bi.

Reduction and correction of data obtained by Energy Dispersive Analysis was performed using a FORTRAN IV computer program EDATA written by C.M. Gold and D.G.W. Smith (1975). Data reduction of analytical results obtained by Wavelength Dispersive Analysis was processed by an APL computer program PROBADATA written by M.C. Tomlinson and D.G.W. Smith (1970).

APPENDIX V-2

APL COMPUTER PROGRAM MOL FOR ESTIMATING MOLE PERCENTS OF SOLID SOLUTIONS IN SULFIDES, CARBONATES AND SULFOSALTS

A. COMPUTATIONAL PROCEDURE

The analytical results of elements in sulfides, carbonates or sulfosalts by electron microprobe are rounded off to 100% and each element percentage is divided by the atomic weight of the element. Each ratio is then divided by the sum of the ratios and the atomic proportion is multiplied by the anion percentage and the "anion proportion" is added to each element percentage. This is the weight percent of each element solid solution. The element solid solution weight percent is divided by molecular weight of the element solid solution to give mole percent of the element solid solution.

B. INPUTS

The element percentages from the analytical results are given as an assymmetric matrix X of N rows and J columns. Atomic weights of the elements are given as a vector Y, the last scalar being the atomic weight of the anion (S in sulfides and sulfosalts, and CO₃ in carbonates).

C. APL PROGRAMS MOL

1. MOL for Pyrrhotites

```
V MOL;A;B;B1;C;C1;C2;D;D1;J;Z;ZZ
[1] J+0
[2] J+J+1
[3] Z+X[J;J]+Y
[4] ZZ+ 1 1 1 1 1 0 /4
[5] A+ZZ+ /ZZ
[6] J+A×X[J;6]
[7] B1+ 1 1 1 1 1 0 /X[J;]
[8] C+B+D1
[9] C1+ 1 1 1 1 1 0 /Y
[10] C2+C1+32.064
[11] D+C+C2
[12] D1+100×D+ /D
[13] 'SAMPLE ' ;J;':(ORDER: PES NIS COS CUS MNS)'
[14] 'MOLE PERCENT: ' ;D1
[15] 'WT. PERCENT: ' ;C
[16] 'STOICHIOMETRIC CHECK:'
[17] 'TOTAL CATIONS: ' ;ZZ; ' = ' ;+ /ZZ
[18] ' SULFUR: ' ;Z16]
[19] '
[20] V +(J<N)/2
V
```


2. Output Example

SAMPLE 1:(ORDER: FES NIS COS CUS MNS)

MOLE PERCENT: 68.91643958 26.80503015 3.8999247 0.3786055684 0

WT. PERCENT: 68.20485572 27.39220639 3.995452256 0.4074856341 0

STOICHIOMETRIC CHECK:

TOTAL CATIONS: 0.8045194908 0.3125532277 0.04546996946 0.004406672962 0 = 1.166949361

SULFUR: 1.052894212

SAMPLE 2:(ORDER: FES NIS COS CUS MNS)

MOLE PERCENT: 98.60227899 0.8579333989 0.142448541 0.3973390672 0

WT. PERCENT: 98.43701233 0.8843889325 0.1472131948 0.4313855385 0

STOICHIOMETRIC CHECK:

TOTAL CATIONS: 1.176428456 0.01021972407 0.001696640652 0.004721435316 0 = 1.193066256

SULFUR: 1.035429142

3. MOL for Sphalerites

```
V MOL;A;B;B1;C;C1;C2;D;D1;J;Z;ZZ
[1] J+0
[2] J+J+1
[3] Z+X[J;]+Y
[4] ZZ+ 1 1 1 1 0 /Z
[5] A+ZZ+ /ZZ
[6] B+A*X[J;6]
[7] B1+ 1 1 1 1 0 /X[J;]
[8] C+B+B1
[9] C1+ 1 1 1 1 0 /Y
[10] C2+C1+32.064
[11] D+C+C2
[12] D1+100*D+ /D
[13] 'SAMPLE ':J;':(ORDER: ZNS FES MNS CDS CUS)'
[14] 'MOLE PERCENT: ':D1
[15] 'WT. PERCENT: ':C
[16] 'STOICHIOMETRIC CHECK:'
[17] 'TOTAL CATIONS: ':ZZ;' = ':+/ZZ
[18] '      SULFUR: ':Z[6]
[19] '
[20] -(J<N)/2
V
```

4. Output Example

MOL

SAMPLE 1:(ORDER: ZNS FES MNS COS CUS)

MOLE PERCENT: 85.04501977 14.20981984 0 0.07987167074 0.6652887254

WT. PERCENT: 86.25747136 13.0037645 0 0.0756642192 0.6620999129

STOICHIOMETRIC CHECK:

TOTAL CATIONS: 0.8852072816 0.1479040951 0 0.0008313539192 0.006924771797 = 1.040867502

SULFUR: 1.041167665

SAMPLE 2:(ORDER: ZNS FES MNS COS CUS)

MOLE PERCENT: 91.86383791 8.047962905 0 0.08819918478 0

WT. PERCENT: 92.59759235 7.319371036 0 0.08303661364 0

STOICHIOMETRIC CHECK:

TOTAL CATIONS: 0.9374789659 0.08200977671 0 0.0008992195453 0 = 1.020387962

SULFUR: 1.062999002

5. MOL for Sb-Pb-Cu Sulfosalts

```

      V MOL[ ] V
V MOL;A;B;B1;C;C1;D;D1;J;Z;ZZ;Z1
[1] J+0
[2] J+J+1
[3] Z+X[J;]+Y
[4] ZZ+ 1 1 1 0 /Z
[5] Z1+ 1 1.5 0.5 *ZZ
[6] A+Z1+;/Z1
[7] B+A*X[J;4]
[8] B1+ 1 1 1 0 /X[J;]
[9] C+B+B1
[10] C1+ 239.254 339.692 159.144
[11] D+C+C1
[12] D1+100*D+;/D
[13] 'SAMPLE ';J;':(ORDER: PBS SB2S3 CU2S)'
[14] 'MOLE PERCENT: ';D1
[15] 'WT. PERCENT: ';C
[16] 'STOICHIOMETRIC CHECK:'
[17] 'TOTAL CATIONS: ';ZZ;' = ';/ZZ
[18] '          SULFUR: ';Z[4]
[19] ' '
[20] + (J<N)/2
V

```

6. Output Example

MOL

```

SAMPLE 1:(ORDER: PBS SB2S3 CU2S)
MOLE PERCENT: 76.39094037 21.70672831 1.902330826
WT. PERCENT: 70.4230368 28.41144908 1.166514121
STOICHIOMETRIC CHECK:
TOTAL CATIONS: 0.2975867561 0.1712197125 0.01490399748 = 0.4837104661
SULFUR: 0.5161863772

```

```

SAMPLE 2:(ORDER: PBS SB2S3 CU2S)
MOLE PERCENT: 76.52271145 21.0448264 2.432462151
WT. PERCENT: 70.84119258 27.66094244 1.497864981
STOICHIOMETRIC CHECK:
TOTAL CATIONS: 0.3000048265 0.1674743326 0.01920050362 = 0.4866796628
SULFUR: 0.506237525

```

7. MOL for Carbonates

```

V MOL;A;B;B1;C;C1;C2;D;D1;J;Z;ZZ
[1] J+0
[2] J+J+1
[3] Z+X[J;]+Y
[4] ZZ+ 1 1 1 1 1 0 /Z
[5] A+ZZ+;/ZZ
[6] B+A*X[J;6]
[7] B1+ 1 1 1 1 1 0 /X[J;]
[8] C+B+B1
[9] C1+ 1 1 1 1 1 0 /Y
[10] C2+C1+60.00935
[11] D+C+C2
[12] D1+100*D+;/D
[13] 'SAMPLE ';J;':(ORDER: FECO3 MNCO3 CAPO3 MGCO3 ZNCO3)'
[14] 'MOLE PERCENT: ';D1
[15] 'WT. PERCENT: ';C
[16] 'STOICHIOMETRIC CHECK:'
[17] 'TOTAL CATIONS: ';ZZ;' = ';/ZZ
[18] '          CO3: ';Z[6]
[19] 'ATOMIC PROPORTIONS OF CATIONS (ORDER: FE MN CA MG ZN)'
[20] Z
[21] ' '
[22] + (J<N)/2
V

```


8. Output Example

SAMPLE 1:(ORDER: FECCO3 HFCO3 CACCO3 HCCO3 ZHCO3)

MOLE PERCENT: 85.8416693 2.45529921 2.708171534 8.306066539 0.6287930178

WT. PERCENT: 88.14512386 2.501403098 2.402094903 6.252790685 0.6987374496

STOICHIOMETRIC CHARGE:

TOTAL CATIONS: 0.760809943 0.0217608941 0.02400199601 0.07414651201 0.005572892764 = 0.886282337

CO3: 0.8863135495

ATOMIC PROPORTIONS OF CATIONS (ORDER: FE HFC CA HC ZH)

0.760809943 0.0217608941 0.02400199601 0.07414651201 0.005572892764 0.8863135495

SAMPLE 2:(ORDER: FECCO3 HFCO3 CACCO3 HCCO3 ZHCO3)

MOLE PERCENT: 65.7783198 20.23860005 4.406073208 8.743283943 0.8337170042

WT. PERCENT: 67.86146207 20.71573202 3.926994579 6.564971602 0.9708133383

STOICHIOMETRIC CHARGE:

TOTAL CATIONS: 0.5857270758 0.1802158797 0.03923403194 0.07785455742 0.007423894753 = 0.80045543

CO3: 0.800487899

ATOMIC PROPORTIONS OF CATIONS (ORDER: FE HFC CA HC ZH)

0.5857270758 0.1802158797 0.03923403194 0.07785455742 0.007423894753 0.800487899

APPENDIX VII-1

PREFERENTIAL CHEMICAL DISSOLUTION AND PURIFICATION PROCEDURE FOR SULFIDE AND SULFATE MINERALS

A. SULFIDE MINERALS

Conventional heavy liquid and magnetic separation procedures should help obtaining relatively pure sulfide mineral separates. However, galena and sphalerite are sometimes so intricately associated that chemical procedure is required to purify one of the two minerals.

The following procedure is employed to purify fine-grained separates (mesh size = 200~270) of lead-zinc sulfides.

(a) Boiling in 50% acetic acid to remove trace impurities of carbonates mixed with the sulfides.

(b) Cold 3N HCl or lukewarm 1N HCl with constant nitrogen bubbling in the presence of a chip of Sn or SiC slowly dissolve galena while sphalerite is only negligibly leached or dissolved. This technique is used to obtain sulfur from galena in a fine galena separate with minor sphalerite mixture. Pyrite or pyrrhotite is unaffected.

(c) Boiling in 3N HCl with constant nitrogen bubbling in the presence of Sn or SiC chip dissolves the remaining sphalerite while any mixture of pyrite is unaffected.

B. BARITE

Pure barite separate can be obtained normally by conventional heavy liquid and magnetic separation procedures, but sometimes trace mixture of sulfides (galena, sphalerite or pyrite) cannot be removed satisfactorily by the physical procedure. The following procedure is employed to purify barite separate.

(a) Boiling in 3N HCl should dissolve all lead-zinc sulfide mixture in barite separate.

(b) In case of pyrite impurity in barite separate, roast the separate to about 900°C for one hour in a porcelain cup; pyrite is then oxidized to iron oxide and can be easily dissolved in HCl. Barite is unaffected.

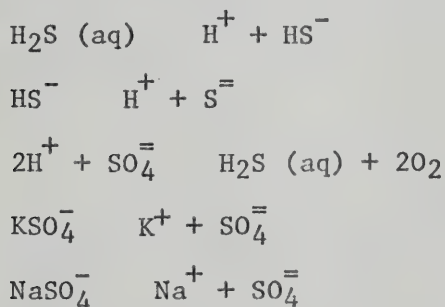
(c) In case of barite impurity in pyrite separate, boil the separate in HI-H₃PO₄-HCl reduction solution with constant nitrogen bubbling and barite should be readily dissolved while pyrite is not affected (minor leaching might occur).

APPENDIX VII-2

APL COMPUTER PROGRAM XS1 FOR ESTIMATING MOLE FRACTIONS OF AQUEOUS SULFUR SPECIES

A. BASIS AND FORMULAE USED FOR THE COMPUTATION

As demonstrated by Ohmoto (1972), if chemical equilibrium is established in a hydrothermal system, the mole fractions of aqueous sulfur species relative to total sulfur content X_i can be evaluated from the following reactions:



Expressing the equilibrium constants for the above chemical reactions in terms of $K_{\text{H}_2\text{S}}$, $K_{\text{SO}_4^{=2}}$, $K_{\text{HSO}_4^-}$, $K_{\text{KSO}_4^-}$ and $K_{\text{NaSO}_4^-}$, respectively, we can write the mole fractions of sulfur species as (equations 17 to 24, Ohmoto, 1972):

$$X_{\text{H}_2\text{S}} = \frac{1}{C}$$

$$X_{\text{HS}^-} = \frac{K_{\text{H}_2\text{S}} \cdot \gamma_{\text{H}_2\text{S}}}{C \cdot a_{\text{H}^+} \cdot \gamma_{\text{HS}^-}}$$

$$X_{\text{S}^{=2}} = \frac{K_{\text{H}_2\text{S}} \cdot K_{\text{HS}^-} \cdot \gamma_{\text{H}_2\text{S}}}{C \cdot (a_{\text{H}^+})^2 \cdot \gamma_{\text{S}^{=2}}}$$

$$X_{\text{SO}_4^{=2}} = \frac{A_1 \cdot \gamma_{\text{H}_2\text{S}}}{C \cdot \gamma_{\text{SO}_4^{=2}}} \quad \text{where } A_1 = \frac{(f_{\text{O}_2})^2}{K_{\text{SO}_4^{=2}} \cdot (a_{\text{H}^+})^2}$$

$$X_{\text{HSO}_4^-} = \frac{A_2 \cdot \gamma_{\text{H}_2\text{S}}}{C \cdot K_{\text{HSO}_4^-} \cdot \gamma_{\text{HSO}_4^-}} \quad \text{where } A_2 = \frac{(f_{\text{O}_2})^2}{K_{\text{SO}_4^{=2}} \cdot a_{\text{H}^+}}$$

$$X_{\text{KSO}_4^-} = \frac{A_1 \cdot M_{\text{K}^+} \cdot \gamma_{\text{K}^+} \cdot \gamma_{\text{H}_2\text{S}}}{C \cdot K_{\text{KSO}_4^-} \cdot \gamma_{\text{KSO}_4^-}}$$

$$X_{\text{NaSO}_4} = \frac{A_1 \cdot M_{\text{Na}^+} \cdot \gamma_{\text{Na}^+} \cdot \gamma_{\text{H}_2\text{S}}}{C \cdot K_{\text{NaSO}_4} \cdot \gamma_{\text{NaSO}_4}}$$

in which

$$C = 1 + \left(\frac{K_{\text{H}_2\text{S}} \cdot \gamma_{\text{H}_2\text{S}}}{a_{\text{H}^+} \cdot \gamma_{\text{HS}^-}} \right) \cdot \left(1 + \frac{K_{\text{HS}^-} \cdot \gamma_{\text{HS}^-}}{a_{\text{H}^+} \cdot \gamma_{\text{S}^{2-}}} \right) + \left(\frac{(f_{\text{O}_2})^2 \cdot \gamma_{\text{H}_2\text{S}}}{K_{\text{SO}_4} \cdot (a_{\text{H}^+})^2} \right) \cdot \left(\frac{1}{\gamma_{\text{SO}_4}} + \frac{a_{\text{H}^+}}{K_{\text{HSO}_4} \cdot \gamma_{\text{HSO}_4}} + \frac{M_{\text{K}^+} \cdot \gamma_{\text{K}^+}}{K_{\text{KSO}_4} \cdot \gamma_{\text{KSO}_4}} + \frac{M_{\text{Na}^+} \cdot \gamma_{\text{Na}^+}}{K_{\text{NaSO}_4} \cdot \gamma_{\text{NaSO}_4}} \right)$$

M_i and γ_i in the above equations are, respectively, the molality and activity coefficient of a species i . Values for K_i , M_i and γ_i (i denotes aqueous sulfur species) from 150° to 350°C have been compiled and given by Ohmoto (1972).

B. INPUTS

Inputs for the APL program XS1 are either given values or separately calculated; they are: C , $K_{\text{H}_2\text{S}}$, $\gamma_{\text{H}_2\text{S}}$, K_{HS^-} , γ_{HS^-} , $\gamma_{\text{S}^{2-}}$, A_1 , γ_{SO_4} , A_2 , K_{HSO_4} , γ_{HSO_4} , M_{K^+} , γ_{K^+} , K_{KSO_4} , γ_{KSO_4} , M_{Na^+} , γ_{Na^+} , K_{NaSO_4} , γ_{NaSO_4} , at given pH, T°C, ionic strength I , and f_{O_2} range.

C. APL PROGRAM XS1

```

V XS1;XH2S;XHS;XS2;XKSO4;XHSO4;XNASO4;AH
[1] AH←10*(-PH)
[2] XH2S←1+C
[3] XHS←(KH2S×PH2S)+C×AH×RHS
[4] XS2←(KP2S×KHS×PH2S)+C×(AH*2)×RS2
[5] XSO4←A1×RH2S+C×RSO4
[6] XHSO4←A2×PH2S+C×XHSO4×RPSO4
[7] XKSO4←A1×(MK×RK×PH2S)+C×KKSO4×RKS04
[8] XNASO4←A1×(MNA×PNA×PH2S)+C×KNASO4×RNASO4
[9] 'THE MOLE FRACTION OF EACH SULFUR SPECIES OVER THE DESIRED FO2 RANGE IS : '
[10] 'PH= ':PH;' T°C= ':T;' IONIC STRENGTH = ':I
[11] 'XH2S : ':3 5 ρXH2S
[12] 'XHS : ':3 5 ρXHS
[13] 'XS2 : ':3 5 ρXS2
[14] 'XSO4 : ':3 5 ρXSO4
[15] 'XHSO4 : ':3 5 ρXHSO4
[16] 'XKSO4 : ':3 5 ρXKSO4
[17] 'XNASO4 : ':3 5 ρXNASO4
[18] ' '
[19] ' '
V

```


D. OUTPUT EXAMPLE

(for f_{O_2} range 10^{-34} to 10^{-48})

THE MOLE FRACTION OF EACH SULFUR SPECIES OVER THE DESIRED f_{O_2} RANGE IS :									
PH= 2 T°C= 200 IONIC STRENGTH = 1									
XS1									
XF2S :									
9.200901688E-7	9.200026338E-5	9.116983664E-3	4.791842368F-1	9.892273145E-1					
9.998660180E-1	9.999732007E-1	9.999742907E-1	9.999743007F-1	9.999743007E-1					
9.999743007E-1	9.999743007E-1	9.999743007F-1	9.999743007F-1	9.999743007E-1					
XHS :									
2.364995890E-11	2.364770890E-9	2.343425636E-7	1.231693141E-5	2.542705718E-5					
2.570051396E-5	2.570326898E-5	2.570329700E-5	2.570329725E-5	2.570329725E-5					
2.570329725F-5	2.570329725E-5	2.570329725F-5	2.570329725F-5	2.570329725E-5					
XS2 :									
3.924916215E-18	3.924542808E-16	3.889118504F-14	2.044101811E-12	4.219841118E-12					
4.265223648E-12	4.265680868F-12	4.265685517F-12	4.265685560E-12	4.265685560F-12					
4.265685560E-12	4.265685560E-12	4.265685560E-12	4.265685560F-12	4.265685560F-12					
XS04 :									
2.653569067E-2	2.653316613F-2	2.629366844E-2	1.381982452F-2	2.852962776E-4					
2.883645132E-6	2.883954250E-8	2.883957394E-10	2.883957423F-12	2.883957423F-14					
2.883957423F-16	2.883957423F-18	2.883957423F-20	2.883957423E-22	2.883957423E-24					
XHSO4 :									
8.391322180E-1	8.390523851F-1	8.314788031E-1	4.370212236E-1	9.021860451E-3					
9.11886580E-5	9.119864099F-7	9.119874039F-9	9.119874130F-11	9.119874130E-13					
9.119874130E-15	9.119874130E-17	9.119874130F-19	9.119874130F-21	9.119874130E-23					
XKSO4 :									
1.185305763E-2	1.185192996E-2	1.174495027E-2	6.173088861E-3	1.274371661E-4					
1.288076966F-6	1.288215044F-8	1.288216448F-10	1.288216461F-12	1.288216461E-14					
1.288216461E-16	1.288216461E-18	1.288216461F-20	1.288216461E-22	1.288216461F-24					
XNASO4 :									
1.224821794F-1	1.224705267E-1	1.213650647F-1	6.378888899E-2	1.316856994E-3					
1.331019210E-5	1.331161891E-7	1.331163342E-9	1.331163356F-11	1.331163356E-13					
1.331163356E-15	1.331163356F-17	1.331163356F-19	1.331163356E-21	1.331163356F-23					

THE MOLE FRACTION OF EACH SULFUR SPECIES OVER THE DESIRED FO2 RANGE IS :

PH= 3 T°C= 200 IONIC STRENGTH = 1

XH2S :

3.75877674E-8	3.758767560E-6	3.757368670E-4	3.622584642E-2	7.897022822E-1
9.970885016E-1	9.997430660E-1	9.997430660E-1	9.997430660E-1	9.997430660E-1
9.997430660E-1	9.997430660E-1	9.997430660E-1	9.997430660E-1	9.997430660E-1

XHS :

9.661543890E-12	9.661520285E-10	9.657924583E-8	9.311476288E-6	2.029847416E-4
2.562912079E-4	2.569735361E-4	2.569735361E-4	2.569735361E-4	2.569735361E-4
2.569735361E-4	2.569735361E-4	2.569735361E-4	2.569735361E-4	2.569735361E-4

XS2 :

1.603417175E-17	1.603413257E-15	1.602816519E-13	1.545320413E-11	3.368708196E-10
4.253375332E-10	4.264699160E-10	4.264699160E-10	4.264699160E-10	4.264699160E-10
4.264699160E-10	4.264699160E-10	4.264699160E-10	4.264699160E-10	4.264699160E-10

XSO4 :

1.084043068E-1	1.084040420E-1	1.083636975E-1	1.044764836E-1	2.277526289E-2
2.875634687E-4	2.883290535E-6	2.883290535E-8	2.883290535E-10	2.883290535E-12
2.883290535E-14	2.883290535E-16	2.883290535E-18	2.883290535E-20	2.883290535E-22

XHSO4 :

3.428045177E-1	3.428036802E-1	3.426760998E-1	3.303836502E-1	7.202170506E-2
9.093555330E-4	9.117765246E-6	9.117765246E-8	9.117765246E-10	9.117765246E-12
9.117765246E-14	9.117765246E-16	9.117765246E-18	9.117765246E-20	9.117765246E-22

XKSO4 :

4.842242517E-2	4.842230687E-2	4.840428567E-2	4.666793101E-2	1.017333624E-2
1.284498832E-4	1.287918573E-6	1.287918573E-8	1.287918573E-10	1.287918573E-12
1.287918573E-14	1.287918573E-16	1.287918573E-18	1.287918573E-20	1.287918573E-22

XNASO4 :

5.003674454E-1	5.003662229E-1	5.001800030E-1	4.822375860E-1	1.051249756E-1
1.327321787E-3	1.330855537E-5	1.330855537E-7	1.330855537E-9	1.330855537E-11
1.330855537E-13	1.330855537E-15	1.330855537E-17	1.330855537E-19	1.330855537E-21

APPENDIX VII-2

APL COMPUTER PROGRAM DSI FOR ESTIMATING ISOTOPE COMPOSITION OF AQUEOUS SULFUR SPECIES

A. BASIS OF COMPUTATION (see Ohmoto, 1972, p. 552-553)

The mean isotopic composition of sulfur in ore solutions, $\delta S_{\Sigma S}^{34}$, can be closely approximated by:

$$\begin{aligned} \delta S_{\Sigma S}^{34} = & (\delta S_{H_2S}^{34} \cdot X_{H_2S}) + (\delta S_{HS^-}^{34} \cdot X_{HS^-}) + (\delta S_{S^{=}}^{34} \cdot X_{S^{=}}) + \\ & (\delta S_{SO_4^{=}}^{34} \cdot X_{SO_4^{=}}) + (\delta S_{HSO_4^-}^{34} \cdot X_{HSO_4^-}) + (\delta S_{KSO_4^-}^{34} \cdot X_{KSO_4^-}) + \\ & (\delta S_{NaSO_4^-}^{34} \cdot X_{NaSO_4^-}) \end{aligned}$$

in which δS_i^{34} is the isotopic composition of a sulfur species i and X_i is the mole fraction of the sulfur species.

When the $\delta S_{H_2S}^{34}$ value is taken as a reference, δS^{34} values of other sulfur species in the solutions and of minerals which precipitate from the same solutions at the same temperature can be expressed as:

$$\delta S_i^{34} = \delta S_{H_2S}^{34} + \Delta_i$$

where Δ_i is the relative isotopic enrichment factor between a sulfur species i and H_2S . The above two equations can be rewritten as:

$$\begin{aligned} \delta S_i^{34} = & \delta S_{\Sigma S}^{34} + \Delta_i - [(\Delta_{HS^-} \cdot X_{HS^-}) + (\Delta_{S^{=}} \cdot X_{S^{=}}) + (\Delta_{SO_4^{=}} \cdot X_{SO_4^{=}}) + \\ & (\Delta_{HSO_4^-} \cdot X_{HSO_4^-}) + (\Delta_{KSO_4^-} \cdot X_{KSO_4^-}) + (\Delta_{NaSO_4^-} \cdot X_{NaSO_4^-}) \end{aligned}$$

Values for Δ_i over temperature range 150° to 350°C have been compiled and given by Ohmoto (1972).

The computer program is written for the last equation for ZnS (sphalerite), FeS₂ (pyrite), PbS (galena), and sulfate (as BaSO₄).

B. IMPUTS

Imputs for the program XSI are δS_{Σ}^{34} (DTS), δS_i^{34} (DI), $\Delta_S=$, $\Delta_{SO_4}^=$, $\Delta_{HSO_4}^-$, $\Delta_{KSO_4}^-$, $\Delta_{NaSO_4}^-$, X_{HS}^- , $X_S=$, $X_{SO_4}^=$, $X_{KSO_4}^-$, and $X_{NaSO_4}^-$ at given pH, $T^\circ C$, I and f_{O_2} range.

```

L←'SPHLRTPYRITEGALENABARITE'
L
SPHLRTPYRITEGALENABARITE
L←+ 6pL
L
SPHLRT
PYRITE
GALENA
BARITE

```

C. APL PROGRAM DSI

```

V DSI;J;DS
[1] J←0
[2] J←J+1
[3] DS←(DTS+DI[J]-((DHS×XHS)+(DS2×XS2)+(DSO4×XSO4)+(DHSO4×XHSO4)+(DKSO4×XKSO4)+DNASO4×XNASO4))
[4] 'THE CALCULATED DS34 VALUES FOR 'L[J;]' OVER THE DESIRED FO2 RANGE AT'
[5] 'PH=';PH;' DS34(TOTAL SULFUR)=';DTS;' T°C=';T;' IONIC STRENGTH=1'; ARE:'
[6] 3 5 pDS
[7] +(J<4)/2
[8] ' '
V

```

D. OUTPUT EXAMPLE

DSI

```

THE CALCULATED DS34 VALUES FOR SPHLRT OVER THE DESIRED FO2 RANGE AT
PH=10 DS34(TOTAL SULFUR)=25 T°C=200 IONIC STRENGTH=1 ARE:
-8.200481669 -8.200481669 -8.200481669 -8.200481669 -8.200481652
-8.200479913 -8.200306089 -8.182923654 -0.2288573262 29.14368142
30.56870116 30.5870983 30.58729176 30.58729299 30.587293
THE CALCULATED DS34 VALUES FOR PYRITE OVER THE DESIRED FO2 RANGE AT
PH=10 DS34(TOTAL SULFUR)=25 T°C=200 IONIC STRENGTH=1 ARE:
-6.900481669 -6.900481669 -6.900481669 -6.900481669 -6.900481652
-6.900479913 -6.900306089 -6.882923654 1.071142674 30.44368142
31.86870116 31.8870983 31.88729176 31.88729299 31.887293
THE CALCULATED DS34 VALUES FOR GALENA OVER THE DESIRED FO2 RANGE AT
PH=10 DS34(TOTAL SULFUR)=25 T°C=200 IONIC STRENGTH=1 ARE:
-11.33048167 -11.33048167 -11.33048167 -11.33048167 -11.33048165
-11.33047991 -11.33030609 -11.31292365 -3.358857326 26.01368142
27.43870116 27.4570983 27.45729176 27.45729299 27.457293
THE CALCULATED DS34 VALUES FOR BARITE OVER THE DESIRED FO2 RANGE AT
PH=10 DS34(TOTAL SULFUR)=25 T°C=200 IONIC STRENGTH=1 ARE:
24.99951833 24.99951833 24.99951833 24.99951833 24.99951835
24.99952009 24.99969391 25.01707635 32.97114267 62.34368142
63.76870116 63.7870983 63.78729176 63.78729299 63.787293

```


APPENDIX VII-3

LABORATORY PROCEDURES FOR LEAD ISOTOPE WORKS

A. SEPARATION AND EXTRACTION OF LEAD FROM SULFIDE AND SULFATE MINERALS

1. Iron and Copper Sulfides

Metallic sulfides such as pyrite, pyrrhotite, chalcopyrite, chalcocite, bornite always contain at least microgram traces of lead.

The following chemical separation and extraction procedure is employed to obtain lead from a relatively small amount of sulfide:

(a) Add 10 cc of double-distilled 8N HNO_3 to dissolve 50~100 mg sulfides; slowly evaporate to dryness on a teflon-covered hot plate (this may take several hours); repeat.

(b) Add 4 cc of double-distilled 8N HCl ; again evaporate to dryness; repeat this step with 2 cc of double-distilled 8N HCl .

(c) Add 3 cc of double-distilled 1.5N HCl to dissolve evaporate.

(d) Filter-pour (or centrifuge beforehand) the sample solution into an ion-exchange resin column (3 cc of Dowex 1-8 resin in 8 mm diameter x 15 cm length teflon column) preset in double-distilled 1.5N HCl ; discard the eluate; wash column with 3 cc of double-distilled 1.5N HCl .

(e) Elute column with 10 cc of double-distilled 1.5N HCl .

(f) Strip lead from the column by adding 10 cc of triple-distilled water; collect the eluate in a cleaned beaker.

(g) Evaporate the eluate to dryness.

(h) Convert the evaporate to nitrate form by adding 2 cc of double-distilled 8N HNO_3 ; evaporate to dryness again; and add 10 cc of double-distilled 2% HNO_3 .

(i) Transfer the sample solution to a cleaned extraction funnel; extract lead by cleaned dithiocarbozone (dithiozone) reagent in the presence of 10 cc of cleaned ammonia citrate and 5 cc of cleaned KCN; pH of the extraction solution is adjusted to about 8.5.

(j) Obtain about one or two cc of sample solution (in double-distilled 2% HNO_3) containing lead in a cleaned beaker; evaporate to dryness; and seal the beaker with parafilm wrap.

2. Galena and Sphalerite

The separation and extraction procedure of lead for galena and sphalerite is the same as that for iron and copper sulfides except that step (a) is skipped, and that step (i) is modified somewhat for sphalerite as follows. Extract zinc by cleaned dithiozone in the presence of cleaned ammonia citrate and KCN at a pH of about 6; repeat several times (impossible to isolate completely zinc from lead); and extract lead by the same reagent mixture at a pH of 8.5.

3. Sulfate (Barite)

Decomposition and dissolution procedure step (a) for barite is as follows. Add 20~30 cc of double-distilled 8N HNO_3 and 8N HCl (mixing proportion of $\text{HNO}_3:\text{HCl} = 2:1$) to slowly leach and dissolve 10~20 mg of finely ground barite powder on a teflon-covered hot plate (this may take one day). Add a few drops of cleaned HBr. After most or all barite powder has been dissolved, evaporate the solution to dryness. Continue with step (b) to step (j).

B. MOUNTING OF LEAD SAMPLE ON RHENIUM FILAMENT FOR
MASS SPECTROMETRY ANALYSIS

(a) Place one drop of silica-gel solution on an outgassed sample (Re) filament and evaporate slowly to dryness with an overhead (8 inches above the filament) ultraviolet heat lamp.

(b) Place one drop of purified 0.75N phosphoric acid on the previously evaporated lead sample (as lead nitrate); warm the drop under the heat lamp until it is barely wet.

(c) Pick up the lead-nitrate-phosphate solution with an acid-cleaned capillary tube and mount one drop of the solution on the dried silica-gel in the center of the filament; warm with the heat lamp for about 5 minutes; then turn off heat lamp.

(d) Switch on electric current passing through the filament and turn up to 0.7 or 0.8 amps; hold there for 15 to 20 minutes.

(e) Increase filament current slowly up to about 1.4~1.5 amps; phosphate should start to fume off.

(f) Increase current steadily to 1.6~1.7 amps; remaining phosphate should fume off.

(g) Turn up the current to about 2 amps or more when the filament glows dull red; leave it for a few seconds.

(h) Turn down the current and then up again to above 2 amps; repeat two to three times.

(i) Turn off the current. Mounted sample should be in the center of the filament and appears pure white.

(j) Store the sample filament for mass spectrometry analysis.

B30164